THE UNIVERSITY
of EDINBURGH

AMPK and the hypoxic ventilatory response: signal integration at an oxygen-sensing nucleus within the brainstem respiratory network?

By

Sandy MacMillan

Thesis submitted for the degree of doctor of philosophy at the University of Edinburgh

2019

Declaration

I, Sandy MacMillan, declare that this thesis was composed by myself and that the experimental work contained herein is my own unless otherwise explicitly stated in the text. No part of this work has been or is being submitted for any other degree or qualification. Any included published data are my own work, except where indicated throughout the thesis and cited appropriately.

Signature:

Date:

Acknowledgements

“No man is an island” – John Donne

Indeed, it took an entire continent for me to achieve everything I have accomplished over the past few years and to write this thesis. Therefore, I would like to begin by expressing my gratitude to the people who helped me along the way, and without whom I never would have got this far.

First of all, I would like to thank Prof A. Mark Evans for his continuous supervision, guidance and support throughout the past 4.5 years and for not giving up when I – once again – took forever to make sense of the data or connect the relevant dots.

A big thanks to my thesis committee: Dr Peter Flatman for all his emotional support and putting my world back into the context of the real world, and Dr Dawn Livingstone for her insightful perspectives, support and being a wonderful role-model (the “Carole to my Kirsten”) for many aspects of life.

I also wish to thank Javier Moral-Sanz and Oluseye Ogunbayo for their continuous scientific guidance, insights and help in the lab as well as the office, Amira Mahmoud for setting the bar high and being such an inspiration, both in regard to work ethic and sheer persistence. So far you are also the only person who got me back into exercising! Ryan Lewis, thank you for being such a wonderful friend and full of genius ideas. I look up to you and the wealth of knowledge and wisdom you continue to offer. Sarah Tennant, thank you for your guidance, pep talks, general mental health support and advice that you have given me, particularly during my last year.

A big thanks to Chris Wilson, Iain McCall and Dan McGurk from the 5th floor for keeping me sane with their banter. You guys made even the bad days in the unit worthwhile.

Catherine Hume and Luis Paiva, I am eternally indebted to you. You taught me almost everything I currently know about immunohistochemistry. Without you, there would have only been half a thesis. Also thanks to Crispin Jordan for his patience and perseverance in analysing my rather large datasets, helping me understand them and finding out more about my numbers.

My lovely Jingxian Duan. Thank you for being my friend, for going through each of the steps with me, for preparing me for what was still to come and for lending me an ear at any time. I think you may have helped me more than you might realise.

I also need to thank all my other friends: Amy Warnock, Katherine Bonnycastle, Catherine Hume (whoop whoop, second mention), Kirsten Wilson and all the other night owls for making life worth living and drowning our problems in dancing juice yet again and again and again… Having people like you in my life brought back the joy during the darkest of times.

I must also not forget the freelance emotional supporters, which were appointed by me without any prior consultation: my Mum, who comforted me time and time again when it all got too much, my Dad and Oma Gina (I miss you all so much!) for making adult life a little easier, Jenny (aka Jendawg, aka Hnnj) with her nuggets of wisdom at only 16/17 years of age and for bringing music and singing back into my life, Conny Rösl for letting me moan and complain and then cheering me up with baby stories, and Paul Skehel for always taking the time and giving me some informal advice. Also a big thanks to the lunchtime crew (aka Chocolate Thieves) for giving me a daily break filled with the latest news, jokes, and upcoming events.

Finally, I could never forget to thank my dearest Ash. You have been making so many sacrifices for me by moving again and again and agreeing to travel long distances to your own work place. Thank you so much for looking after me, for feeding me, keeping me healthy, listening to my endless complaints, holding me when I once again hit rock bottom, and simply being my better half in all aspects of life. You are my rock, my inspiration, my reason. Your sacrifices have allowed me to follow this path and you never once complained. I can never repay you, but I will do my best to give you a happy, long, and fulfilled life ♥

Table of Contents

Abstract

The capacity for mammals to regulate breathing is critical to match ventilation to changes in oxygen availability and demand, for example during sleep or ascent to altitude. Acute falls in arterial PO_2 activate specialised oxygen-sensing chemoreceptors, which relay this information to the cardiorespiratory centre of the brainstem, which then acts to restore blood gas homeostasis. While the role of the carotid bodies as peripheral chemoreceptors is undisputed, it has been proposed that a central oxygen sensor may exist. However, this view remains controversial.

The work in this thesis built on recent findings which showed that the AMP-activated protein kinase (AMPK), a ubiquitously expressed cellular energy sensor, within catecholaminergic (tyrosine hydroxylase (TH)-expressing) cells is critical to the proper regulation of breathing during acute hypoxia. It was found that targeted deletion of AMPK within this subpopulation of respiratory neurons of the mouse brainstem led to decreases in ventilation and more frequent and prolonged apnoeas. The fact that this ventilatory deficit was hypoxia-specific and rescued by addition of hypercapnia showed that the capacity for neuronal activation was not affected *per se*, because central and peripheral chemosensors contributing to the hypercapnic response also express TH. Importantly, the activity of the carotid bodies in response to hypoxia remained fully intact, indicating that the respiratory deficits originated centrally.

In light of these findings, the experiments carried out in this thesis further investigated how the deletion of both AMPK catalytic subunits in catecholaminergic cells (TH AMPK-α1/α2 dKO) impacts on hypoxic ventilation and where within the brainstem neuronal activation may be affected. By using whole-body plethysmography, I show that AMPK within the brainstem respiratory network is not only critical for appropriate ventilatory adjustments during acute hypoxia, but also during prolonged periods of low oxygen availability. Following the severe hypoventilation observed at the onset of hypoxia, ventilation remained attenuated relative to controls, even during periods lasting up to an hour. Moreover, some TH AMPK-α1/α2 dKO mice lost all respiratory rhythmogenesis after 20-30min

of hypoxia. In those mice where respiratory rhythmogenesis was retained, it was found to be interrupted at regular intervals by high frequency periods of spontaneous apnoeas. Immunohistochemical analyses of the brainstems of TH AMPK-α1/α2 dKO mice revealed a comparable number of catecholaminergic cells relative to controls, supporting the conclusion of a functional deficit within these neurons rather than hypo- or hyperplasia. This was further corroborated by the identification of a specific area within the brainstem that showed significant reductions in immediate early gene expression (cFos) and thus neuronal activation during hypoxia. Importantly, cardiovascular responses to hypoxia were unaltered in TH AMPK-α1/α2 dKO mice relative to controls, indicating that this identified brainstem nucleus may separately control the respiratory and the cardiovascular responses to hypoxia through AMPK-dependent pathways. Finally, directing AMPK deletion to the adrenergic subset of catecholaminergic neurons revealed that the ventilatory deficit originated within the noradrenergic cells of the caudal brainstem, consistent with the location of the identified area of cFos deficiency.

In summary, AMPK-dependent signalling is required within a specific group of noradrenergic neurons within the caudal brainstem to ensure appropriate signal integration and transduction during hypoxia in order to appropriately regulate ventilatory adaptations and protect from hypoventilation and respiratory instability. Therefore, AMPK may be a potential new therapeutic target to protect from sleep-disordered breathing associated with metabolic syndrome-related disorders and ascent to altitude.

Lay summary

A reduction in available oxygen increases breathing frequency to supply more oxygen to our lungs. It is therefore crucial for mammals to be able to regulate breathing, for example during sleep or ascent to altitude. When blood oxygen levels fall, sensory organs within the carotid arteries – called the carotid bodies – detect these changes and relay signals to the brainstem. From there, the modulation of heart rate, blood pressure and more importantly increases in the drive to breathe are aimed to restore blood oxygen levels.

Recent work demonstrated that the proper regulation of breathing during acute periods of low oxygen availability (hypoxia) is supported by a protein called AMP-activated protein kinase (AMPK). My studies support these findings and show that reduced levels of AMPK trigger conditions symptomatic of altitude sickness, namely sleep disordered breathing and apnoea. Importantly, I have shown that these symptoms can last for prolonged periods of hypoxia, with very little, if any, signs of recovery.

Because the drive to breathe is generated within the brainstem I sought to explore how the activation of neurons during hypoxia is affected in the absence of AMPK. While the activation of the majority of respiratory neurons was unaltered, I found that a particular area within the brainstem showed a reduction in neuronal activity. It is therefore likely that this area controls the appropriate respiratory adaptations during periods of low oxygen availability.

Obesity and type-2 diabetes also lower AMPK levels and are, like altitude sickness, strongly associated with sleep disordered breathing (1-3 million people in the UK). I therefore propose that AMPK deficiency within the brainstem causes these respiratory diseases and that it may also contribute to sudden infant death syndrome (cot death, 1 in 3200 UK births), which is associated with maternal obesity. These studies could lead to new therapeutic strategies for those who suffer from sleep apnoea and may help reduce cot deaths.

Allgemeinverständliche Zusammenfassung

Eine Verringerung des verfügbaren Sauerstoffs erhöht die Atemfrequenz um mehr Sauerstoff in unsere Lungen zu bringen. Daher ist es für Säugetiere entscheidend dass die Atmung reguliert werden kann, zum Beispiel während des Schlafes oder beim Aufstieg in die Höhe. Wenn der Blutsauerstoffspiegel sinkt erkennen Sinnesorgane in den Halsschlagadern - die so genannten Karotiskörper - diese Veränderungen und leiten diese Informationen an den Hirnstamm weiter. Von dort aus zielt die Modulation der Herzfrequenz, des Blutdrucks und vor allem die Steigerung des Atemtriebs darauf ab, den Blutsauerstoffspiegel wieder herzustellen.

Jüngste Arbeiten haben gezeigt dass die richtige Atmungsregulierung während akuter Perioden mit geringer Sauerstoffverfügbarkeit (Hypoxie) von einem Protein namens AMP-aktivierte Proteinkinase (AMPK) unterstützt wird. Meine Studien belegen diese Befunde und zeigen, dass reduzierte Proteinexpression von AMPK den Symptomen der Höhenkrankheit ähnelt, nämlich schlafbezogene Atmungsstörung und Apnoe. Wichtig ist dass ich gezeigt habe, dass diese Symptome über längere Zeiträume von Hypoxie anhalten, mit sehr wenigen, wenn überhaupt, Zeichen der Genesung.

Da der Antrieb zum Atmen im Hirnstamm erzeugt wird wollte ich untersuchen, wie die Aktivierung von Neuronen während der Hypoxie in Abwesenheit von AMPK beeinflusst wird. Während die Aktivierung der Mehrheit der Atmungsneuronen unverändert war, fand ich dass ein bestimmter Bereich innerhalb des Hirnstamms eine Verringerung der neuronalen Aktivität zeigte. Es ist daher wahrscheinlich, dass dieser Bereich in Zeiten geringer Sauerstoffverfügbarkeit die entsprechenden Anpassungen der Atmung steuert.

Adipositas und Typ-2-Diabetes senken auch den AMPK-Spiegel und sind, wie die Höhenkrankheit, stark mit schlafbezogenen Atmungsstörungen verbunden (1-3 Millionen Menschen in Großbritannien). Daher ist meine Annahme dass ein AMPK-Mangel im Hirnstamm diese Atemwegserkrankungen verursacht und dass er auch zum plötzlichen

Kindstod beitragen kann (1 von 3200 Geburten im Vereinigten Königreich), der mit mütterlicher Fettleibigkeit einhergeht. Diese Studien könnten zu neuen therapeutischen Strategien für diejenigen führen, die an Schlafapnoe leiden und dazu könnte dazu beitragen, die Zahl der plötzlichen Kindstode zu reduzieren.

List of Abbreviations

7N	Parafacial nucleus
10N	Dorsal motor nucleus of the vagus
A1	A1 noradrenergic cells
A2	A2 noradrenergic cells
AI	Apnoeic index
ADI	Apnoea-duration index
ADP	Adenosine diphosphate
AMP	Adenosine monophosphate
AMPK	AMP-activated protein kinase
AP	Area postrema
ATP	Adenosine triphosphate
BB_n	Inter-breath interval
BötC	Bötzinger complex
C1	C1 adrenergic cells
C2	C2 adrenergic cells
CB	Carotid body
Cre	Causes recombination events
CVL	Caudal ventrolateral medulla
cVRG	Caudal ventral respiratory group
DAR	Dorsal active region
fMRI	Functional magnetic resonance imaging
Fq	Frequency

Flx	Floxed
HVD	Hypoxic ventilatory depression/decline
HVR	Hypoxic ventilatory response
KF	Kölliker-Fuse nucleus
KO	Knock-out
LKB1	Liver kinase beta 1
Mv	Minute ventilation
NA	Nucleus ambiguus
NTS	Nucleus tractus solitarius
pFRG	Parafacial respiratory group
PiCo	Post-inspiratory complex
PNMT	Phenylethanolamine N-methyltransferase
preBötC	pre-Bötzinger complex
PRG	Pontine respiratory group
PSA	Post-sigh apnoea
rCPG	Respiratory central pattern generators
RVL	Rostral ventrolateral medulla
rVRG	Rostral ventral respiratory group
RTN	Retrotrapezoid nucleus
SA	Spontaneous apnoea
SD	Standard deviation
SEM	Standard error of the mean
SM	Smooth muscle
SolC	Commissural subnucleus of the NTS

SolCe	Central subnucleus of the NTS
SolDL	Dorsolateral subnucleus of the NTS
SolDM	Dorsomedial subnucleus of the NTS
SolI	Interstitial subnucleus of the NTS
SolIM	Intermediate subnucleus of the NTS
SolL	Lateral subnucleus of the NTS
SolM	Medial subnucleus of the NTS
SolV	Ventral subnucleus of the NTS
SolVL	Ventrolateral subnucleus of the NTS
SubP	Sub-postrema
Te	Expiration time
TH	Tyrosine hydroxylase
Thr	Threonine
Ti	Inspiration time
To	Total breath time
Tv	Tidal volume
VAR	Ventral active region
VLM	Ventrolateral medulla
VRC	Ventral respiratory column

List of Figures

List of Tables

Chapter 1: General Introduction

1.1 The mammalian respiratory network

Vertebrates have a very low capacity to store oxygen (Endeward *et al.*, 2010; Gros *et al.*, 2010), which means a constant oxygen (O_2) supply is paramount for survival. Adequate delivery of O_2 to all tissues in mammals is achieved by the periodic intake of air and exchange of O_2 and carbon dioxide (CO_2) between the lung alveoli and the blood stream, which carries them to and from all cells in the organism. In order to facilitate an appropriate degree of gas exchange, muscles of the ribcage and diaphragm need to be rhythmically activated in order to contract. This contraction increases the pleural cavity, which leads to lung inflation and air intake. Relaxation of these muscles is then followed by lung recoil and air outflow (Seeley, 2011).

1.1.1 The anatomy of the brainstem respiratory network

The mammalian drive to breathe is primarily generated in the pons and medulla oblongata of the brainstem, where several functionally distinct neuronal compartments form two bilaterally distributed ventral respiratory columns (VRC) that are necessary to generate respiratory rhythm (Figure 1.1).

In a caudal to rostral order, the medullary VRCs comprise the caudal and rostral ventral respiratory groups (cVRG and rVRG, respectively), the pre Bötzinger complex (preBötC), the Bötzinger complex (BötC), the post-inspiratory complex (PiCo), and the retrotrapezoid nucleus/parafacial respiratory group complex (RTN/pFRG). Within the pons, the bilateral pontine respiratory groups (PRG) consist of the Kölliker-Fuse nucleus (KF) and the dorsally adjacent lateral parabrachial region (LPBr) (Alheid & McCrimmon, 2008; Smith *et al.*, 2013).

The neural machinery that the VRCs form is robust, yet flexible, and integrates and coordinates physiology and behaviour based on modulations by neuronal inputs from the area postrema (AP) and the nucleus tractus solitarius (NTS), which are located medially and bilaterally in the dorsal medulla oblongata, respectively, as well as other supra-brainstem structures such as the hypothalamus, cortex, or thalamus (Pattinson *et al.*, 2009a;

Pattinson *et al.*, 2009b; King *et al.*, 2013). Collectively, the VRC and its interneuron populations are known as the respiratory central pattern generators (rCPGs).

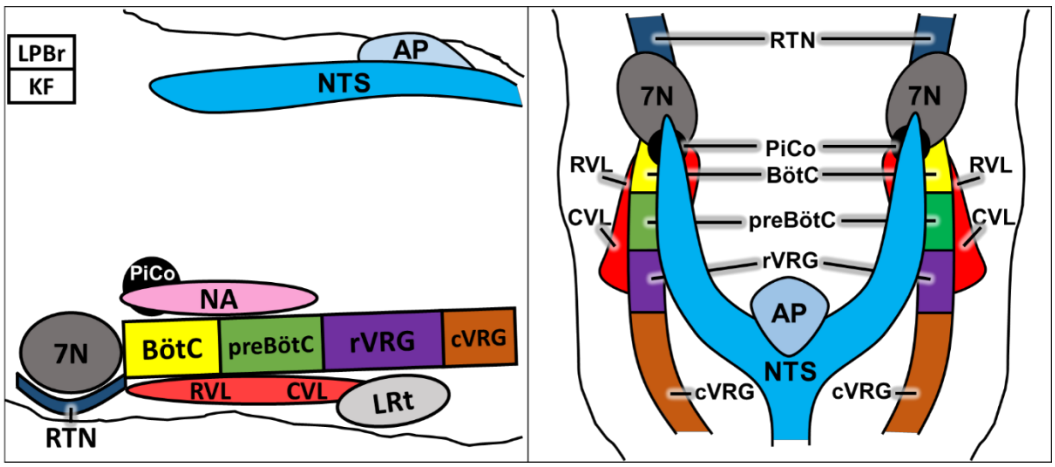

Figure 1.1: The anatomy of the brainstem respiratory network.

Side view (left) and top view (right) of the brainstem showing the compartments of the respiratory centres in the dorsal (AP, NTS) and ventral medulla. LPBr: lateral parabrachial region, KF: Kölliker-Fuse nucleus, AP: area postrema, NTS: Nucleus tractus solitarius, 7N: facial nucleus, RTN: retrotrapezoid nucleus, PiCo: post-inspiratory complex, NA: nucleus ambiguus, BötC: Bötzinger complex, preBötC: pre-Bötzinger complex, rVRG: rostral ventral respiratory group, cVRG: caudal ventral respiratory group, RVL: rostral ventrolateral medulla, CVL: caudal ventrolateral medulla, LRt: lateral reticular nucleus. Figure adapted from Alheid et. al. (2011) and Anderson et. al. (2016).

1.1.2 Functionality of individual compartments within the brainstem respiratory network

As mentioned above, each compartment of the VRCs serves a functionally distinct role in respiratory pattern generation, which in concert shape respiration. Eupneic breathing consists of three phases: (1) inspiration, (2) post-inspiration and (3) late expiration. During inspiration, the lungs inflate due to contraction of the diaphragm, which receives innervation from the rVRG. At the same time, motor output from the preBötC coordinates muscles that open up the oropharyngeal airway to allow for airflow. Inspiration is terminated during post-inspiration, where the airflow is stopped by adduction of the larynx to allow for longer gas exchange in the lungs. Subsequent abduction of the larynx marks the beginning of exhalation, which is completed by minor innervation of intercostal and abdominal muscles from the BötC and the cVRG (Smith *et al.*, 2013). The synaptic network of these respiratory neurons is a complex and delicate interplay of excitatory and inhibitory propriobulbar (projecting to medullary respiratory neurons) and bulbospinal (projecting to spinal motoneurons) interneurons (Horner, 2009) (Figure 1.2):

(1) Breathing commences with the preBötC, which is densely populated by glutamatergic neurons that provide an excitatory inspiratory drive (Koizumi *et al.*, 2013). Additionally, a subset of preBötC neurons have been found to have intrinsic bursting properties, similar to a pacemaker, *in vitro* and *in situ* (Koizumi & Smith, 2008; St-John *et al.*, 2009). The neurons within the preBötC are highly interconnected and also project to other structures such as the PiCo and the BötC, where some glycinergic and GABAergic neurons have been suggested to inhibit post-inspiratory and expiratory neurons during inspiration. In concert with the preBötC works the rVRG, which contains the main cluster of glutamatergic bulbospinal inspiratory premotor neurons that lead to innervation of the diaphragm (Dobbins & Feldman, 1994; Guyenet *et al.*, 2002). Activity of the rVRG is determined by excitatory innervations from the inspiratory preBötC neurons, and the rVRG is later inhibited by the expiratory BötC neurons.

(2) Following inspiration, post-inspiration is initiated by an increase in the bursting activity within the PiCo, which like the preBötC exhibits autonomous rhythm-generating properties that are necessary and sufficient for *in vivo* post-inspiratory activity. Post-inspiration is tightly coupled to occur immediately after inspiration, and the absence of GABAergic inhibitory input from the preBötC to the PiCo leads to synchronisation of bursting from both of these oscillators. This in turn disrupts the appropriate sequential phases that determine eupneic breathing and can lead to aspiration pneumonia (Anderson *et al.*, 2016). The overall signalling output from the PiCo is glutamatergic and hence excitatory, and this excitatory output appears to be increased by noradrenergic input from the pons. That said, the pontine respiratory structures appear to also deliver an additional inhibitory input to ventilation through noradrenergic A5 neurons, because transection studies have demonstrated increased phrenic nerve activity associated with increased respiratory frequency in the absence of the pons (Hilaire *et al.*, 1989).

(3) The transition from post-inspiration to expiration is primarily driven by glycinergic and GABAergic inhibitory projections from the BötC to the preBötC and rVRG, but also by excitatory inputs from the PRG to the BötC and pFRG/RTN (Ezure *et al.*, 2003; Dutschmann & Herbert, 2006). The pFRG/RTN is an interesting structure, which contains glutamatergic neurons expressing the transcription factor paired-like homeobox 2b (Phox2b), the mutation of which leads to congenital central hypoventilation syndrome that can lead to fatal respiratory arrest during sleep if left untreated (Weese-Mayer *et al.*, 2005; Stornetta *et al.*, 2006; Abbott *et al.*, 2009). The pFRG/RTN is initially rhythmically active in perinatal rodents and at this point called the pFRG. Following developmental transformation the pFRG becomes tonically active and respiratory-modulated in adults, at which point it is referred to as the RTN (Thoby-Brisson *et al.*, 2009; Abbott *et al.*, 2011; Depuy *et al.*, 2011). Importantly, the RTN has been under intense investigation for its central chemoreceptor activity, as its modulation of respiration is regulated by changes in central CO_2 and

pH (Kumar *et al.*, 2015; Guyenet *et al.*, 2016; Souza *et al.*, 2018). Lastly, it has also been suggested to contribute to abdominal muscle contraction during active expiration (Feldman & Del Negro, 2006). Following the transition from post-inspiration, expiration is carried out through excitation of bulbospinal expiratory premotor neurons from the cVRG that receive innervations from BötC and pFRG/RTN (Smith *et al.*, 2013).

In addition to the respiratory modulation by the rCPGs of the brainstem, an essential contribution to the patterning of eupneic breathing also comes from the mechanoreceptors located in the lungs. Particularly in small mammals with high breathing frequencies, such as mice, feedback from slowly adapting mechanoreceptors is crucial in the modulation of respiratory rhythm (Milsom, 1990). During inspiration, mechanical feedback occurs when the lung volume exceedes the functional residual capacity during expansion of the pleural cavity. Afferent output by pulmonary mechanoreceptors travels via the vagus nerve and is conveyed to the rCPGs via so-called Pump cells of the NTS. These Pump cells excite post-inspiratory neurons and inhibit early-inspiratory neurons within the rCPGs, thereby advancing the termination of the inspiratory phase of eupneic breathing and allowing for the high respiratory frequencies observed in small mammals (Molkov *et al.*, 2017).

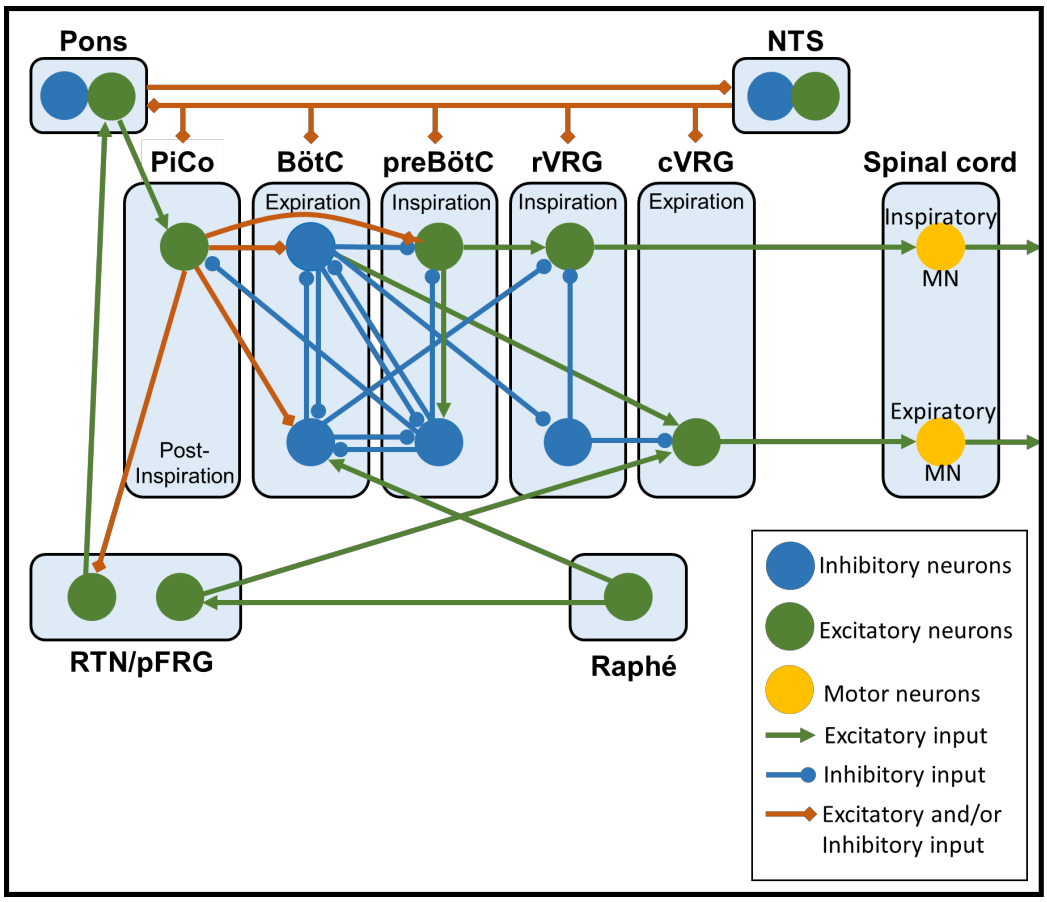

Figure 1.2: Microcircuits that shape respiratory rhythm and pattern generation.

The Post-inspiratoy complex (PiCo), Bötzinger complex (BötC) and pre-Bötzinger complex (preBötC) have been proposed to contain autonomic rhythmogenic properties. These circuits involve populations of excitatory (green) pre-inspiratory, inspiratory and inhibitory (blue) expiratory neurons. The inhibitory populations not only project to the excitatory population within the PreBötC, but also mutually inhibit each other via an 'inhibitory ring'. Projections are also made from the rhythmogenic microcircuits to the transmission circuits, which contain the rostral and caudal ventral respiratory group (rVRG and cVRG, respectively). These premotor neurons then project to inspiratory or expiratory motor neurons (MN) within the spinal cord. Furthermore, all compartments receive tonic, phasic, or rhythmic input from the pons, nucleus tractus solitarius (NTS), and the retrotrapezoid nucleus/parafacial respiratory group (RTN/pFRG). Figure adapted from Smith et. al. (2013) and Anderson et. al. (2016).

1.2 Oxygen-sensing by peripheral catecholaminergic cells

The evolution of a respiratory system that was able to provide a continuous supply and delivery of O_2 allowed for the development and maintenance of large, diverse, and complex animals, because respiration and mitochondrial oxidative phosphorylation sufficiently and consistently provided enough O_2 and energy, respectively. Nevertheless, the evolution of a monitor with the capacity to detect changes in O_2 supply and the ability to respond accordingly in a manner that maintains O_2 homeostasis, and thus mitochondrial function and energy supply, at a whole-body level was required. This was achieved by the development of specialised chemoreceptors, which have the ability to sense acute reductions in O_2 supply and trigger a respiratory response that acts to re-establish O_2 levels. Interestingly, the location of the primary peripheral arterial chemoreceptors has changed throughout evolution from being dispersed amongst all respiratory passages (i.e. gills) in fish, to multiple sites within the carotid arteries in amphibians and reptiles, and finally to a single dominant receptor site at each carotid artery in mammals and birds called the carotid body (CB) (Milsom & Burleson, 2007). That said, other O_2-sensitive sites also exist within mammals, which are able to trigger responses to hypoxia that maintain whole-body O_2 supply in the absence of fully a functional CB.

1.2.1 Neonatal adrenomedullary chromaffin cells

Newborn mammals have a poorly developed respiratory network at birth (Lavezzi & Matturri, 2008) and in humans the proper drive to breathe only commences at around 6 months of age (Kinney *et al.*, 1992). In addition, the environment in which the CB develops *in utero* is relatively hypoxic, which means that after birth the comparatively hyperoxic environment leads to initial silencing of the CB-mediated stimulation of breathing (Wasicko *et al.*, 1999; Donnelly, 2000). This leaves newborn infants vulnerable to ventilatory deficits, especially during periods of hypoxia, for example when the infant is asleep.

Maturation of the peripheral and central respiratory network starts at birth and is hypothesised to be triggered by a surge of catecholamines released from neonatal adrenal medullary chromaffin cells (nAMCs) as a response to the severe hypoxia experienced during birth (Lagercrantz & Bistoletti, 1977; Faxelius *et al.*, 1983; Lagercrantz, 1996). nAMCs are derived from the neural crest and during the early postnatal life they are able to respond to reductions in O_2 through inhibition of O_2-sensitive K^+ channels (for example large-conductance Ca^{2+}-dependent K^+ (BK) channels and delayed-rectifier type Kv channels), which leads to membrane depolarisation and voltage-gated Ca^{2+} entry via L-type and T-type Ca^{2+} channels. The increases in intracellular Ca^{2+} trigger the release of catecholamines into the blood stream (Mochizuki-Oda *et al.*, 1997; Thompson *et al.*, 1997; Thompson *et al.*, 2002; Levitsky & López-Barneo, 2009; Nurse *et al.*, 2018). The secretion of catecholamines, particularly noradrenaline, activates the sympathetic nervous system to increase heart rate and facilitate O_2 delivery to the tissues (Ream *et al.*, 2008). Therefore, the O_2 sensitivity of nAMCs partly overcomes the lack of chemosensitivity of the CB (Donnelly, 2000).

The non-neurogenic and direct O_2 sensitivity of nAMCs is lost during postnatal development at a time that roughly coincides with the sympathetic innervation of the adrenal gland by the splanchnic nerve (for example 1-2 weeks for rodents, 24 hours for sheep) (Comline & Silver, 1961; Seidler & Slotkin, 1985; Slotkin & Seidler, 1988; Nurse *et al.*, 2009). It is likely that cholinergic signalling from the splanchnic nerve is the underlying cause of this, as activation of α7 nicotinic acetycholine receptors has been shown to lead to upregulation K_{ATP} channels and membrane hyperpolarisation (Buttigieg *et al.*, 2008; Nurse *et al.*, 2009). It is therefore not surprising that denervation of the splanchnic nerve in adults has been shown to recover the direct hypoxia-sensing mechanism of chromaffin cells (Seidler & Slotkin, 1986; Levitsky & López-Barneo, 2009).

It should be mentioned at this point that the non-neurogenic O_2 sensitivity of nAMCs may not be the only neonatal response system to hypoxia. At birth, so-called neuroepithelial bodies (NEBs) which are innervated cell clusters found throughout the airway epithelium (Lauweryns & Cokelaere, 1973),

have also been suggested to act as peripheral hypoxia-sensitive airway sensors due to the following set of characteristics (Lauweryns & Cokelaere, 1973; Lauweryns *et al.*, 1977; Lauweryns *et al.*, 1985; Cutz & Jackson, 1999):

- They are preferentially located at airway branching points and therefore strategically placed to directly monitor inspired O_2 levels
- They contain microvilli that are in direct contact with the airway lumen
- They are in close proximity to blood capillaries
- Their cellular content includes cytoplasmic neurosecretory granules that contain serotonin and other neuropeptides
- They are innervated by afferent nerve fibres from the dorsal root and nodose ganglion

Studies have shown that during airway hypoxia, but not blood hypoxaemia, NEBs release serotonin, which shunts blood flow from poorly to better ventilated areas of the lung (Lauweryns & Cokelaere, 1973; Lauweryns *et al.*, 1978). The cellular signalling pathway that mediates release of serotonin is similar, but not identical, to other O_2-sensing cells. In response to hypoxia, closure of K^+ channels and subsequent membrane depolarisation leads to activation of voltage-gated Ca^{2+} channels, influx of extracellular Ca^{2+}, and neurotransmitter secretion via exocytosis (Youngson *et al.*, 1993). The cellular O_2 sensor in the case of NEBs appears to be NADPH oxidase, which during hypoxia fails to maintain superoxide and hence hydrogen peroxide production. This leads to reductions in the oxidised redox state of a cysteine residue in the H_2O_2-sensitive K^+ channel subunit, which triggers a conformational change that closes the channel and in the end results in neurotransmitter release (Ruppersberg *et al.*, 1991). Importantly, the fact that both spinal and vagal afferent nerves arborise on NEBs highlights their potential to send afferent information to the central nervous system during periods of hypoxia (Kemp *et al.*, 2003). Therefore, although not catecholaminergic, NEBs may also have a function in the control of respiration during the transition from the intrauterine environment to air breathing and thus complement CB activity during the neonatal period (Cutz & Jackson, 1999).

1.2.2 Carotid body type I cells

As mentioned earlier, the CBs have evolved as the primary mammalian peripheral arterial chemoreceptors, which are located at the bifurcation of the carotid artery in the neck (Figure 1.3 A). The CB is one of the most highly vascularised organs in the body and consists of two cell types: clusters of catecholaminergic O_2-sensing glomus (type I) cells and more glial-like sustentacular (type II) cells, which associate with type I cells in an approximate ratio of 1:4 (Nurse, 2014). The glomus cells are highly fenestrated and receive their blood supply from a branch off the carotid artery, which allows them to sense even minor changes in the blood gas composition (Kumar, 2007; López-Barneo *et al.*, 2008). In addition, a series of nerve innervations allow for rapid communication between the periphery and the central nervous system. Afferent sympathetic nerves from the CB petrosal ganglia join the carotid sinus branch of the glossopharyngeal nerve, which innervates the breathing centres located in the medulla oblongata (Mifflin, 1992; Gonzalez *et al.*, 1994) to prompt ventilatory adjustments by increased afferent fibre discharge in response to even minor reductions in O_2 availability, which, for other non-O_2-sensing cells, would still lie within the "normal" physiological range of PO_2 (Mills, 1972; Erickson & Millhorn, 1994; Donnelly, 2000; López-Barneo *et al.*, 2008; Buckler & Turner, 2015).

While eupneic breathing during normoxia is stable and rhythmic with a very low frequency of basal CB chemoafferent fibre discharge (Kumar & Prabhakar, 2012), exposures to hypoxia increase respiratory drive and precipitate a biphasic hypoxic ventilatory response (HVR). The first part of the response to an acute fall in arterial PO_2 is a rapid and robust increase in ventilation, which is driven by increases in breathing frequency and tidal volume and termed the "Augmenting phase". The Augmenting phase occurs within seconds of the onset of hypoxia, and, as mentioned above, is primarily driven by peripheral chemoreceptor afferent fibre discharge to the respiratory centres of the brainstem (Ramirez *et al.*, 1998; Palmer *et al.*, 2013; Pamenter & Powell, 2016). Within the brainstem, CB afferents terminate and activate specific nuclei in the caudal portion of the NTS, as well as the ventrolateral medulla (a detailed description of the CB

innervations of the NTS will be provided in the introduction to Chapter 4) (Finley & Katz, 1992). Furthermore, catecholaminergic neurons within the NTS provide additional afferent inputs to ventral catecholaminergic cells and the rCPGs of the ventrolateral medulla (Ross *et al.*, 1985; Koshiya & Guyenet, 1996), which provides an opportunity for signal amplification. Importantly, due to the immediate nature of this response, the Augmenting phase is determined by neurotransmitter release (predominantly glutamate) and enhanced synaptic transmission mediated by the effects of excitatory amino acids, rather than *de novo* protein synthesis (Gozal *et al.*, 2000; Pamenter & Powell, 2016). Thereafter, within seconds to minutes, the central effect of hypoxia leads to the second phase of the ventilatory response, which manifests as a reduction in ventilation called “Roll-Off”. This ventilatory decline is primarily driven by reductions in breathing frequency with a lesser degree of reductions in tidal volume (Palmer *et al.*, 2013). Given the continuous chemoafferent fibre discharge that is maintained throughout the hypoxic period, ventilatory “Roll-Off” may be mediated downstream of the CB chemoafferent input by changes in neurochemical signalling pathways secondary to receptor activation during the Augmenting phase (Gozal *et al.*, 2000), as well as due to the declining metabolic rates of non-O_2 sensitive neurons and activation of central chemosensitive sites within the brainstem that respond to the decreasing levels of CO_2 subsequent to the hyperventilation that occurred during the Augmenting phase (Neubauer *et al.*, 1990; LaManna *et al.*, 1996). However, the fact that ventilatory “Roll-Off” is proportional to the degree of the Augmenting phase, and that “Roll-Off” does not occur following peripheral chemodenervation or blockage indicates that the CBs may still play a pivotal role in the development of both phases of the HVR (Teppema & Dahan, 2010).

Historically, the first direct evidence for a role of the CB in mediating cardiorespiratory homeostasis was obtained in the late 1920’s, when hyperventilation was triggered in response to decreases in arterial PO_2 of vascularly isolated carotid bifurcations from dogs (Heymans & Heymans, 1927). Since then, several studies across species have corroborated the pivotal role of the CB in the control of ventilatory responses and blood

pressure (Lahiri *et al.*, 1981; Timmers *et al.*, 2003; Izumizaki *et al.*, 2004; Mouradian *et al.*, 2012; McBryde *et al.*, 2016), as well as determining the morphology and proposing stimulus-response mechanisms that underlie chemoafferent fibre discharge (Biscoe & Silver, 1966; Biscoe & Stehbens, 1966; Biscoe & Duchen, 1990b, a; Buckler, 1997; Buckler *et al.*, 2000; Campanucci *et al.*, 2006; Buckler & Turner, 2013; Murali & Nurse, 2016).

1.2.2.1 Hypoxia-response coupling within the carotid bodies

It is now understood that within type I cells, inhibition of TASK1/3 potassium (K^+) channels leads to cell depolarisation and voltage-gated calcium (Ca^{2+}) entry (Figure 1.3 B) (Buckler, 2015), which triggers the release of various neurotransmitter and neuromodulators that shape the subsequent afferent discharge (Gonzalez *et al.*, 1994; Peers & Buckler, 1995; López-Barneo *et al.*, 2008; Nurse, 2010; Kumar & Prabhakar, 2012; Nurse & Piskuric, 2013). The key neurotransmitter in this pathway is likely ATP, which has been shown to activate post-synaptic ionotropic P2X2/3 receptors on afferent nerve terminals (Nurse, 2010, 2014). Recently, evidence of 'ATP-induced ATP release' has emerged, which allows for signal amplification through the expression of purinergic P2Y2 receptors on type II cells. Within these cells, receptor activation by ATP has been shown to trigger increases in intracellular Ca^{2+}, leading to further release of ATP via Panx-1 channels into the synaptic cleft. There, ATP from both type I and type II cells is broken down by extracellular 5'-ectonucleases into adenosine, triggering an additional activation of type I cells via adenosine A_{2A} receptors on the presynaptic type I cells (Conde & Monteiro, 2004; Conde *et al.*, 2009; Conde *et al.*, 2012) leading to a secondary rise of Ca^{2+} within type I cells and, therefore, release of ATP (Xu *et al.*, 2006).

In addition to the ATP-dependent excitation of chemoafferent fibre discharge, acetylcholine (Ach) has also been proposed to be a major excitatory neurotransmitter within the CB (Nurse & Zhang, 1999; Fitzgerald, 2000; Iturriaga & Alcayaga, 2004). Various nicotinic and muscarinic ACh receptors (AChR) are expressed in the CB of several species, and the release of ACh in response to hypoxia has been shown in intact CBs from

cats, rabbits, and humans (Fitzgerald *et al.*, 2000; Shirahata *et al.*, 2007; Kahlin *et al.*, 2014). Furthermore, the blockage of both nicotinic and purinergic receptors was needed in order to inhibit the postsynaptic response to hypoxia in co-cultures of rat CB and petrosal ganglia (Zhang *et al.*, 2000), and dual blockage of these receptors resulted in inhibition of respiration in neonatal rats (Niane *et al.*, 2012). As mentioned above, ATP release from type I cells induces increases in intracellular Ca^{2+} and Panx-1 channel activation on CB type II cells. This effect has also been observed after application of ACh to CB cell cultures, which induced Ca^{2+} increases with similar potency and also activated Panx-1 channels on the same type II cells (Tse *et al.*, 2012; Murali *et al.*, 2015). However, whether or not these neuroactive agents functionally combine to enhance Ca^{2+} signalling within type II cells during CB stimulation remains to be determined (Leonard *et al.*, 2018).

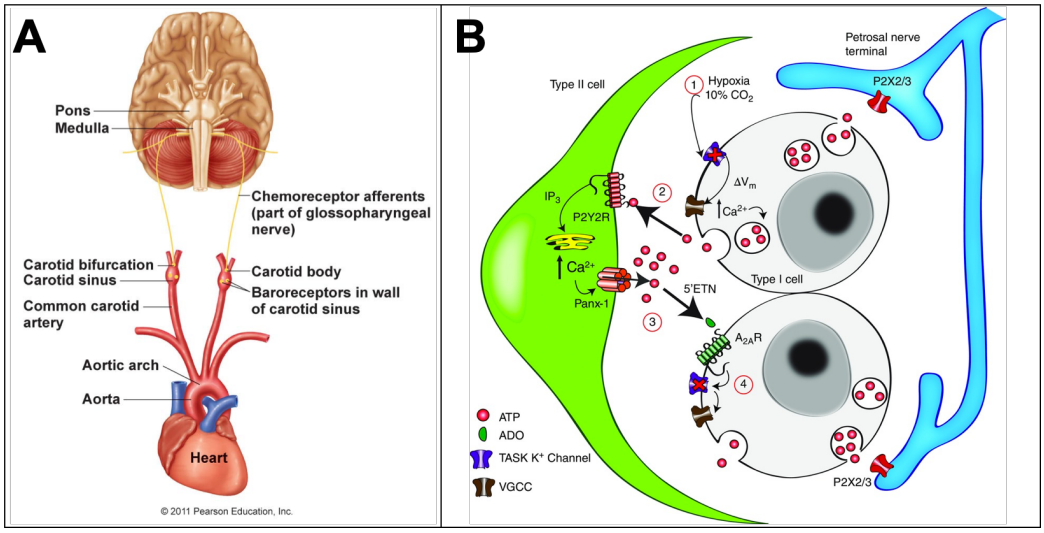

Figure 1.3: Chemosensing and signalling at the carotid body tripartite synapse.

(**A**) The anatomical location of the carotid body at the bifurcation of the common carotid arteries, which relays chemosensory information to the brainstem via afferent projections of the glossopharyngeal nerve. (**B**) The 'tripartite' synapse of the carotid body is made up of type I glomus cells (white), type II sustentacular cells (green) and terminals of the petrosal nerve (blue). During hypoxia, inhibition of TASK1/3 K^+ channels ([1], dark blue) depolarises the type I cell membrane, which leads to increases in intracellular Ca^{2+} via voltage-gated Ca^{2+} channels (VGCC, brown) and exocytotic release of ATP (red circles) into the synaptic cleft [2]. ATP then activates postsynaptic P2X2/3 receptors found on the petrosal nerve terminals causing excitation and action potential firing, as well as P2Y2 receptors found on type II cells, where subsequent increases in intracellular Ca^{2+} activate signalling inositol triphosphase (IP_3) pathways that release further ATP into the synaptic cleft. There, ATP is broken down into adenosine ([3], ADO, green half circle) by extracellular 5′-ectonucleotidase (5′ENT). ADO in turn activates A_{2A} receptors ($A_{2A}R$) located on type I cells and further inhibits TASK1/3 channels to enhance type I cell depolarization [4] and ATP release (ATP-dependent ATP release). Panel A adapted from Pearson Education, Inc (2011), panel B from Murali & Nurse (2016).

1.2.2.2 O_2-sensing mechanisms within the carotid bodies

While the hypoxia-response pathways leading to chemoafferent discharge have been largely determined, the O_2-sensing pathways within the CB still remain under debate. There are, however, several hypotheses that aimed to identify the ultimate O_2-sensor of the CB, which could either be a single sensor, or multiple sensors with varying affinities for O_2 and thresholds for activation. The most favourable hypotheses are the *Mitochondrial Hypothesis* and the *Membrane Hypothesis* (Figure 1.4).

The *Mitochondrial Hypothesis* (Figure 1.4 A) is based on the assumption that K^+ channel closure is secondary to the effect of hypoxia, with the primary effector being the mitochondria. This theory was first postulated when mitochondrial NAD(P)H:NA(P)D^+ ratios increased with decreasing PO_2, which triggered afferent fibre discharges over the range of physiological O_2 levels (Mills & Jobsis, 1970, 1972). In support of this, inhibitors of the mitochondrial electron transport chain in type I cells were later shown to increase afferent fibre discharge (Mulligan *et al.*, 1981; Wilson *et al.*, 1994; Ortega-Saenz *et al.*, 2003). Therefore, mitochondria of O_2-sensing cells appear to be unusually sensitive to even minor fluctuations in O_2, which allows them to trigger chemoafferent fibre discharge during exposures to mild hypoxia.

The primary candidate of the mitochondrial respiratory chain that determines O_2 sensitivity was proposed to be the expression of a specific form of cytochrome a_3 with an unusually low affinity for O_2 (Mills & Jobsis, 1972). More recently, the constitutive expressions of NADH dehydrogenase (ubiquinone) 1 alpha subcomplex 4-like 2 (NDUFA4L2) and cytochrome C oxidase (COX) subunit 4 isoform 2 (COX4I2) have been demonstrated in CB type I cells, which in non-specialised cells have an ordinarily low expression profile, but may be increased during prolonged hypoxia (Huttemann *et al.*, 2001; Fukuda *et al.*, 2007; Tello *et al.*, 2011; Zhou *et al.*, 2016). Important in the context of O_2-sensing, ATP confers allosteric COX inhibition via COX4I1, but not COX4I2 (Huttemann *et al.*, 2001; Horvat *et al.*, 2006), which creates an unusually high rate of mitochondrial O_2 consumption near maximal

capacity in the CB during normoxia (Mills & Jobsis, 1972; Duchen & Biscoe, 1992). Therefore, the COX4I2-dependent activity of COX may determine, at least in part, the capacity of O_2-sensing cells to monitor and quickly respond to even minor reductions in arterial PO_2 (Evans *et al.*, 2016; Evans, 2018). In non-O_2-sensing cells on the other hand, reductions in ATP supply during hypoxia would relieve COX4I1 inhibition, leading to increases in O_2 consumption to maintain ATP levels within the cell until mitochondrial oxidative phosphorylation is finally inhibited by a PO_2 of <5mmHg (0-1% O_2) (Duchen & Biscoe, 1992). By contrast, an acute fall in O_2 availability would not be able to trigger increases in O_2 consumption and ATP supply of O_2-sensing cells, leading to the rapid induction of signalling pathways that will aim to restore tissue O_2 homeostasis, namely CB afferent fibre discharge that mediates increases in ventilation to maximise O_2 uptake. In addition, the high expression of NDUFA4L2 was shown to limit the production of mitochondrial reactive oxygen species (ROS) during hypoxia through reductions in the activity of the mitochondrial complex I (Tello *et al.*, 2011), thereby further reducing the capacity for increases in mitochondrial oxygen consumption of O_2-sensing cells during hypoxia. Overall, the constitutive expression of these two complexes in CB type I cells might thus determine the mitochondrial affinity for O_2 and confer, at least in part, the capacity to monitor and respond to even minor reductions in arterial PO_2.

Finally, the signalling cascade that links mitochondrial inhibition to closure of K^+ channels within the CB type I cells is still controversial, but several pathways have been suggested that include signalling via hydrogen sulfide, reactive oxygen species, lactate, or adenosine nucleotides (Buckler & Turner, 2013; Chang *et al.*, 2015; Fernandez-Aguera *et al.*, 2015; Chang, 2017):

Hydrogen sulfide production CB type I cell activation has been suggested to occur consequent to fall in carbon monoxide (CO) synthesis during hypoxia, which ultimately leads to the production of hydrogen sulfide (H_2S) and activation of redox-sensitive L-type Ca^{2+} channels (Peng *et al.*, 2010; Yuan *et al.*, 2015). However, the action of H_2S may lie upstream of the mitochondria, as application of exogenous H_2S was shown to activate

type I cells through direct inhibition of mitochondrial oxidative phosphorylation (Buckler, 2012). Additionally, mouse CB type I cell transcriptome analysis revealed few to no reads of haem oxygenase-2, or cystathionine-γ-lyase and cystathionine-β-synthase, which are responsible for the generation of CO and H_2S, respectively (Zhou *et al.*, 2016).

Reactive oxygen species The incomplete transfer of electrons following hypoxia-mediated inhibition of the mitochondrial electron transport chain has been linked to increases in the concentration of reactive oxygen species (ROS) (Turrens, 2003; Gonzalez *et al.*, 2007), which may directly or indirectly affect K^+ channel function (Wyatt & Buckler, 2004). However, their functional role in hypoxia-response coupling of type I cells is still not well established and as mentioned above, the constitutive expression of NDUFA4L2 and COX4I2 by CB type I cells act to limit mitochondrial ROS production during hypoxia (Huttemann *et al.*, 2001; Fukuda *et al.*, 2007).

ATP A direct role for ATP regulation of TASK1/3 channel activity within CB type I cells came from the observation that upon patch excision, channel activity ceased rapidly unless physiologically relevant concentrations of MgATP were supplied to the inside of the patch (Varas *et al.*, 2007). Therefore, MgATP levels could, directly or indirectly, regulate channel activity, which close during hypoxia subsequent to falls in ATP supply. However, there are currently no identified ATP-binding domains in either TASK1 or TASK3 channels, and other cytosolic signalling compounds may be required to recover loss of channel activity caused by patch excision even after MgATP supplementation (Buckler & Turner, 2015).

Lactate-dependent activation of olfactory receptor 78 Most recently, activation of the G-protein coupled olfactory receptor 78 (Olfr78) has been proposed to underpin CB type I cell activation following increases in lactate production subsequent to anaerobic glycolysis during hypoxia (Chang *et al.*, 2015). While this mechanism supports the mitochondrial hypothesis, it does not appear to comply with a role of TASK K^+ channel inhibition in the determination of type I cell activation. Furthermore, the expression of Olfr78 is not limited to CB type I cells and the study undertaken here utilised a global knockout model of *Olfr78* (Chang *et al.*, 2015). A more precise

identification of the cellular transduction pathways along with a targeted deletion strategy would be required to further substantiate the proposed role of lactate in the O_2-sensing signalling cascade, especially because serious doubt for a role of Olfr78 in CB activity arose after a follow-up study was unable to replicate these findings and showed no differences in the ventilatory and CB responses to hypoxia between wild-type mice and those with deletion of Olfr78 (Torres-Torrelo *et al.*, 2018).

Clearly, the precise O_2-sensing mechanism(s) within CB type I cells have still not been fully elucidated. However, an alternative hypothesis predicts K^+ channels to be the ultimate O_2 sensor within the type I cells. It is indisputable that closure of selective K^+ channels is critical for the signal transduction process during hypoxia, which has been proven in a variety of species (Lopez-Barneo *et al.*, 1988; Chou & Shirahata, 1996; Buckler, 1997; Yamaguchi *et al.*, 2004). However, the expression patterns of K^+ channel subtypes are highly variable within and between species, as well as between different developmental stages, making one type of channel as the ultimate O_2 sensor unlikely. That said, several different channel types may depolarise the membrane equally, provided they are either directly or indirectly inhibited by hypoxia. The finding that hypoxia decreased – reversibly and selectively – a small conductance, fast inactivating delayed rectifier K^+ current in the rabbit type I cells ultimately coined the *Membrane Hypothesis* (Figure 1.4 B) and the existence of so-called K_{O_2} channels (Lopez-Barneo *et al.*, 1988; Lopez-Lopez *et al.*, 1989; Lopez-Lopez *et al.*, 1993), which have also been suggested to exist in the rat (Peers, 1990; Buckler, 1997; Buckler *et al.*, 2000) and mouse (Perez-Garcia *et al.*, 2004). However, despite their subtype variability within and between species, some limitations of this hypothesis arose when direct K^+ channel blockers failed to induce afferent fibre discharge or neurotransmitter release under basal conditions (Donnelly, 1997; Osanai *et al.*, 1997), which led to speculations that closure of K^+ channels was indirect and subsequent to another primary O_2 sensing mechanism. The more recent findings on COX4I2 expression further opposed considerations on the *Membrane Hypothesis*, as they confirmed

the predictions of Mills and Jobsis regarding both the site and mechanism of O_2 sensing within the CB type I cells.

Generating further controversy within the field, the most recent studies from our laboratory have now questioned the view that the HVR is entirely driven by the peripheral chemoreceptors, i.e. increases in the CB chemoafferent fibre discharge frequency in response to a fall in arterial PO_2. Acutely, a fall in ATP supply will be partially compensated for by the adenylate kinase reaction, which increases the cellular AMP:ATP ratio by converting two molecules of ADP into one molecule of AMP and one molecule of ATP (Dzeja & Terzic, 2009). AMP is a potent activator of the AMP-activated protein kinase (AMPK) (Hardie *et al.*, 2016), so a role for AMPK in hypoxia-response coupling seemed highly plausible. Accordingly, deletion of both AMPK catalytic subunits in catecholaminergic cells blocked the HVR and precipitated hypoventilation and apnoea. However, it did so without affecting CB type I cells and chemoafferent input responses during hypoxia. Moreover, the degree of the ventilatory deficit precipitated by loss of AMPK was more severe than when conditional deletion of an AMPK upstream kinase completely blocked CB chemoafferent fibre discharge (Mahmoud *et al.*, 2016). Therefore, these observations suggest that in addition to the peripheral control by the CB, a component of the HVR arises centrally and that the latter is determined by AMPK-dependent signalling pathways within the catecholaminergic respiratory network of the brainstem.

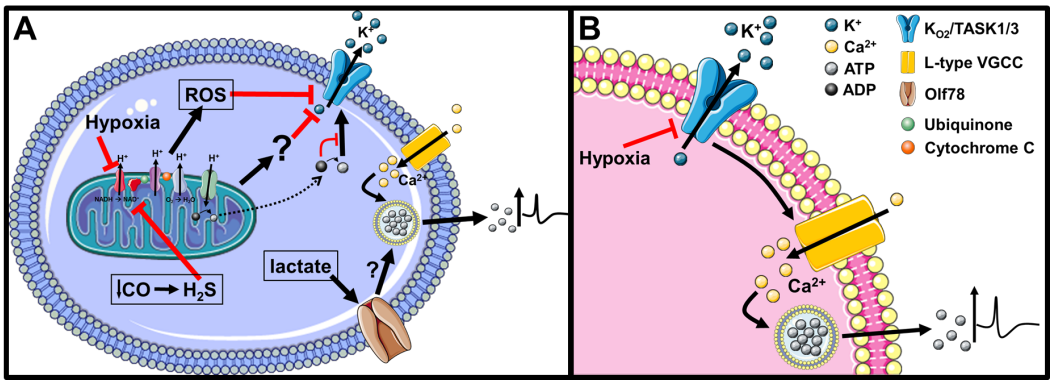

Figure 1.4: Hypotheses of acute O_2 sensing in the carotid body type I cell.

(**A**) The *Mitochondrial Hypothesis* proposes that inhibition of TASK1/3 K^+ channels is subsequent to hypoxia-induced inhibition of mitochondrial oxidative phosphorylation. In this case, O_2-sensitivity is determined by the expression of specific isoforms and subtypes of the NADH dehydrogenase and cytochrome c complexes of the respiratory chain. Downstream of the mitochondria, several pathways have been proposed to lead to afferent fibre discharge, for example increases in hydrogen sulfide (H_2S) production subsequent to decreases in carbon monoxide (CO) levels, increases in the production of reactive oxygen species (ROS) due to the incomplete electron transfer of the respiratory chain, closure of K^+ channels due to reductions in ATP levels, or production of lactate by anaerobic glycolysis and activation of the olfactory receptor 78 (Olfr78). (**B**) The *Membrane Hypothesis* proposes that O_2-sensitivity is conferred by O_2-sensitive K_{O2} K^+ channels, which depolarise the membrane, leading to opening of voltage-gated Ca^{2+} channel (VGCC) and the release of neurotransmitter that increase afferent fibre discharge.

1.3 The AMP-activated protein kinase

As mentioned above, a reduction of ATP supply during hypoxia with a subsequent increase in the AMP/ATP ratios via the adenylate kinase reaction creates the possibility of a role for adenosine mono-/diphosphates and the ubiquitously expressed cellular energy sensor AMPK in mediating hypoxia-response coupling. Classically, AMPK monitors cellular adenosine phosphates (AMP, ADP and ATP) and prompts metabolic adjustments with the goal to maintain energy homeostasis during cellular stress (Hardie *et al.*, 2006; Hardie *et al.*, 2011; Gowans *et al.*, 2013; Hardie *et al.*, 2016).

1.3.1 The structure of AMPK

AMPK is a ubiquitously expressed heterotrimeric serine/threonine kinase consisting of one catalytic (α) and two regulatory (β and γ) subunits. Each of these subunits has multiple isoforms encoded by distinct genes: two for the α-subunit, (α1 and α2), two for the β-subunit (β1 and β2), and three for the γ-subunit (γ1, γ2 and γ3) (Stapleton *et al.*, 1996; Thornton *et al.*, 1998; Cheung *et al.*, 2000). Although each heterotrimeric AMPK complex only contains one of each subunits, the expression of these seven isoforms can result in at least 12 different combinations into which AMPK can assemble (Ross *et al.*, 2016). As such, certain subunit combinations are expressed in a tissue-specific manner. For example, skeletal muscle predominantly expresses the catalytic α2 subunit, whereas adipose tissue mainly expresses the α1 subunit. Other tissues, for example in the liver, have been found to express α subunits with no particular preference (Stapleton *et al.*, 1996; Woods *et al.*, 1996; Daval *et al.*, 2006). Importantly, recent findings suggest that different subunit combinations could also be targeted to different subcellular localisations, have different sensitivities to metabolic stress (i.e. changes in the AMP, ADP and ATP levels), and create specificity regarding differential phosphorylation of downstream targets and thus signalling outputs (Ross *et al.*, 2016).

<u>The α-subunits</u> Encoded within the α-subunit are three key structures (Figure 1.5). At the N-terminus, the serine/threonine kinase domain (KD) is

found, whose activation loop contains a highly conserved threonine residue at position 172 (Thr172). Phosphorylation of Thr172 by an upstream kinase leads to increased AMPK activity (see section 1.3.2 below) (Hawley *et al.*, 1996). The KD is followed by an auto-inhibitory domain (AID), which can determine the activity of the KD through conformational changes and binding to the opposite side of the active site (Pang *et al.*, 2007; Chen *et al.*, 2009; Ross *et al.*, 2016). Lastly, a linker domain connects the AID to the globular C-terminal domain (CTD), which is important in the regulation of activity via adenine nucleotides (Ross *et al.*, 2016).

The β-subunits The N-terminal region of the β-subunit contains a carbohydrate-binding module (CBM), which participates in glycogen binding and may thus co-localise AMPK with glycogen synthase (Koay *et al.*, 2007; Bultot *et al.*, 2012). The C-terminal domain (CTD) on the other hand forms the core of the heterotrimeric complex by binding to both the CTD of the α-subunit, as well as the γ-subunit (Iseli *et al.*, 2005).

The γ-subunits The majority of the γ-subunit is made up of four tandem repeats of cystathionine β-synthase (CBS) motifs (CBS1-CBS4). The assembly of these CBS repeats creates a disk-like shape with one repeat in each quadrant, thereby forming four pseudosymmetrical clefts that create adenine nucleotide (AMP, ADP, ATP) binding sites (Scott *et al.*, 2004). However, not all of these binding sites participate in nucleotide exchange. Within the mammalian γ1 subunit, site 2 appears to be always empty, whereas sites 1, 3 and 4 competitively bind to the adenosine nucleotides based on the metabolic status of the cell (Xiao *et al.*, 2007; Xiao *et al.*, 2011; Xiao *et al.*, 2013). This way, AMPK is able to monitor and respond to metabolic stresses that affect the cellular AMP:ADP:ATP ratios.

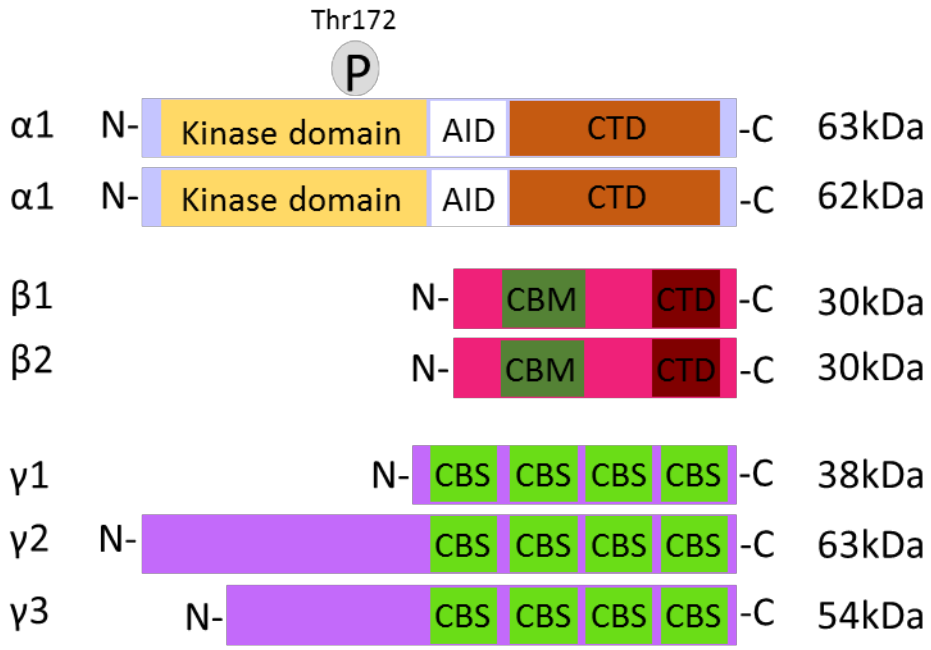

Figure 1.5: The structure of the AMPK subunits.

The catalytic α-subunits contain a serine/threonine kinase domain within their N-terminus. This part contains the threonine residue at position 172 (Thr172), which is phosphorylated by upstream kinases. The kinase domain is followed by an auto-inhibitory domain (AID) and lastly a C-terminal domain (CTD) for binding of the β-subunit. The β-subunits contain two conserved binding domains: a carbohydrate-binding module (CBM) in the N-terminus, and CTD that links the α-subunit with the γ-subunit. The γ-subunits' corresponding binding domain lies within its N-terminus and is followed by four tandem repeats of cystathionine-β-synthase (CBS) motifs that act in pairs to form binding pockets for the adenine nucleotides. Figure adapted from Ross & Hardie (2016).

1.3.2 The regulation of AMPK

The regulation of AMPK occurs via three key mechanisms that can act individually or simultaneously: (1) allosteric activation by adenosine nucleotide-binding to the γ subunit, which is closely linked to (2) inhibition of dephosphorylation of Thr172, and (3) direct activation via phosphorylation of Thr172 (Figure 1.6).

Metabolic stress increases the cellular AMP:ATP ratio through activity of the adenylate kinase reaction, which converts two molecules of ADP into one molecule of AMP and one molecule of ATP (Dzeja & Terzic, 2009). Under normal homeostatic conditions, ATP prevails in the cell and competitively occupies all the binding sites within the γ subunit. Therefore, AMPK is subjected to dephosphorylation at Thr172 and thus inactivation. During metabolic stress, allosteric activation of AMPK is mediated by displacement of ATP and binding of the more abundant nucleotide AMP to the high-affinity domain of site 1 within CBS repeats of the γ subunit, which induces a 10-fold increase in activity. Additionally, binding of either AMP or ADP to the low-affinity site 3 of the γ subunit results in a conformational change of the heterotrimer that hinders phosphatases, for example protein phosphatase 2A (PP2A), from dephosphorylating AMPK at Thr172 (Hardie, 2007; Wu *et al.*, 2007; Hardie *et al.*, 2011; Ross *et al.*, 2016). This allows for an additional 100-fold activation by phosphorylation, which is facilitated by the main upstream tumour suppressor kinase Liver Kinase B1 (LKB1) (Hawley *et al.*, 2003; Woods *et al.*, 2003). Notably, LKB1 constitutively phosphorylates AMPK at Thr172 even during normal metabolic homeostasis, but inhibition of dephosphorylation leads to a more rapid and maintained phosphorylation of Thr172 (Sakamoto *et al.*, 2004). Alternatively, a cytosolic increase in Ca^{2+} mediated by cellular activity, but not a reduction in ATP, activates the upstream Calcium^{2+}/calmodulin-dependent protein kinase kinase 2 (CaMKK2), which also acts to phosphorylate and activate AMPK (Hawley *et al.*, 2005; Woods *et al.*, 2005).

As indicated above, ADP does not bind to the high affinity site 1 within the γ subunit and therefore cannot activate AMPK allosterically (Xiao *et al.*, 2007). This means that during mild conditions of metabolic stress, AMPK responds

to increases in ADP:ATP ratio with a >100-fold activation, whereas during more severe conditions of metabolic stress, additional increases of the AMP:ATP ratio and allosteric activation by AMP-binding to site 1 are able to increase the total activity of AMPK by >1000-fold. This shows how AMPK is able to monitor the cellular ADP:ATP and AMP:ATP ratios and prompt appropriate cellular responses that aim to increase ATP production and at the same time reduce ATP consumption. For example, AMPK-dependent signalling pathways increase glucose uptake via translocation of the glucose transporter type 4 (GLUT4) (Pehmoller *et al.*, 2009), glycolysis and fatty acid oxidation via mitochondrial β-oxidation (Hardie *et al.*, 2012), mitochondrial biogenesis via activation of the peroxisome proliferator-activated receptor-γ co-activator 1α (PGC1α) (Jager *et al.*, 2007), and clearance of non-functional mitochondria via UNC-51-like kinase 1 (ULK1)-dependent mitophagy (Egan *et al.*, 2011). On the other hand, AMPK-dependent signalling pathways decrease gluconeogenesis, lipogenesis, and fatty acid, cholesterol, and protein synthesis (Carling, 2004; Daval *et al.*, 2006; Hardie *et al.*, 2012) via phosphorylation of, for example, Acetyl-CoA carboxylase (ACC) (Davies *et al.*, 1992) glycogen synthase (Jorgensen *et al.*, 2004a), and regulatory associated protein of the mammalian target of rapamycin (RAPTOR) (Gwinn *et al.*, 2008).

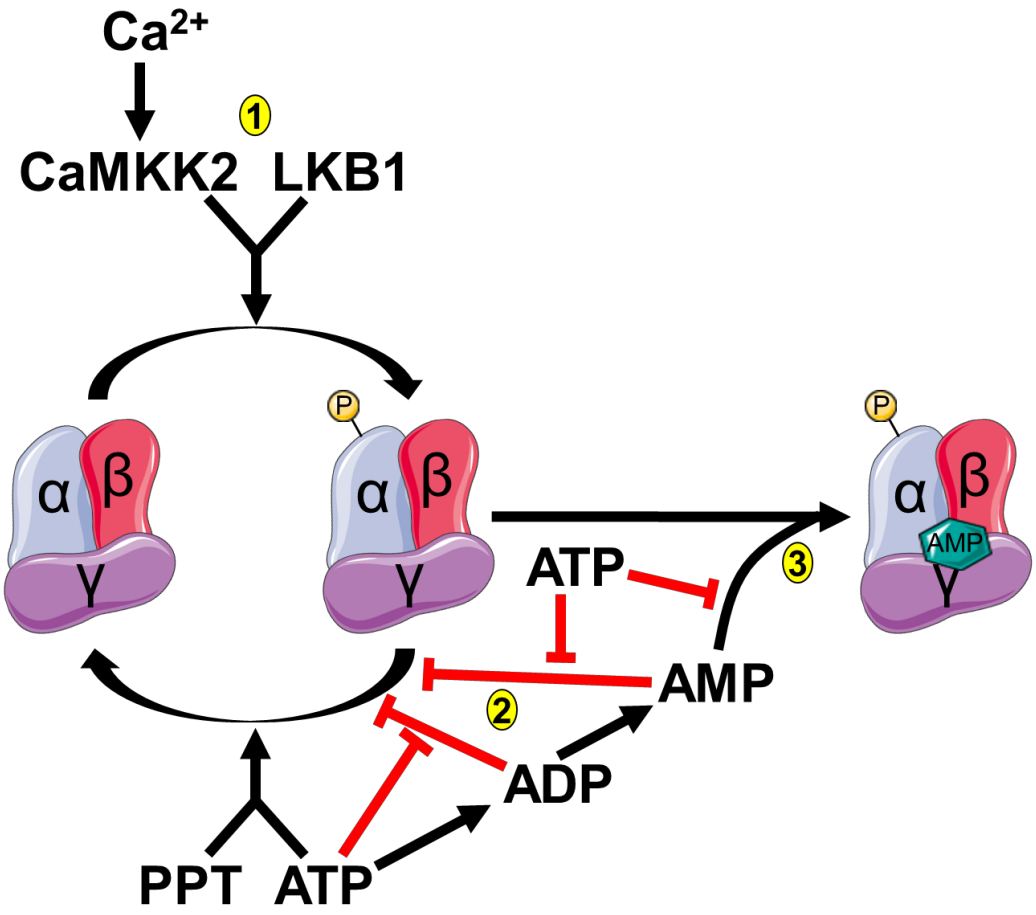

Figure 1.6: The regulation of AMPK by adenosine nucleotides and upstream kinases.

(**1**) AMPK is activated by phosphorylation via the upstream kinases Liver kinase beta 1 (LKB1), or Calcium/Calmodulin Dependent Protein Kinase Kinase 2 (CaMKK2). (**2**) During metabolic stress-induced depletion of ATP, the ratios of ADP:ATP and AMP:ATP increase. Inhibitory binding of ATP is displaced by AMP or ADP, which changes the conformation of the heterotrimers and protects the Thr172 residue from dephosphorylation by protein phosphatases (PPT). (**3**) Binding of AMP to the high affinity site in the γ-subunit also activates AMPK allosterically. Figure adapted from (Hardie & Ashford, 2014).

1.4 AMPK and the hypoxic ventilatory response

As highlighted earlier, the cellular mechanisms of hypoxia-response coupling in the CB are still a highly controversial topic with no definite consensus. Moreover, the expression of COX4I2 likely leads to quick reductions of ATP levels during hypoxia, which would increase the AMP:ATP ratio subsequent to the activity of adenylate kinase (Dzeja & Terzic, 2003; Panayiotou *et al.*, 2014). Given that activation of AMPK is tightly coupled to mitochondrial metabolism via increases in the AM(D)P:ATP ratio, the possibility of a connection between AMPK activity and hypoxia-response coupling in O_2-sensing cells emerged. In this regard, being a serine/threonine kinase, AMPK may have the capacity for the regulation of processes outside of metabolic control. Indeed, AMPK may phosphorylate and thus regulate the activity of several ion channels, such as the Ca^{2+}-activated potassium channels $K_{Ca}1.1$ and $K_{Ca}3.1$ (Klein *et al.*, 2009; Ross *et al.*, 2011), the voltage-gated K^+ channels Kv1.5 and Kv2.1 (Ikematsu *et al.*, 2011; Mia *et al.*, 2012; Andersen *et al.*, 2015; Moral-Sanz *et al.*, 2016), or the ATP-inhibited K_{ATP} channel Kir6.2 (Chang *et al.*, 2009). In addition, an emerging role for AMPK in the regulation of enzymes involved in transmitter biosynthesis (Zhang *et al.*, 2018), receptors (Ahmadi & Roy, 2016), and pumps and transporters (Schneider *et al.*, 2015) further suggests that AMPK may have a crucial function in determining cell excitability and signal transduction.

A pivotal role for AMPK in mediating the HVR was first suggested in 2005, when activators of AMPK were able to activate isolated CB type I cells and increase afferent fibre discharge, whereas AMPK inhibitors blocked these actions (Evans *et al.*, 2005a; Wyatt *et al.*, 2007). Additionally, conditional genetic deletion strategies of the upstream kinase LKB1 in the catecholaminergic cells of mice further supported these findings, in that the capacity for type I cell activation during hypoxia was virtually abolished following conditional LKB1 deletion, as were increases in afferent fibre discharge. Consistent with this, the HVR of these mice was significantly attenuated (Evans, 2012; Mahmoud *et al.*, 2015). However, when another genetic deletion strategy was employed that directed the deletion of both

AMPK catalytic subunits to catecholaminergic cells, the off-target effects of the previously used pharmacological agents were uncovered, because against expectation, conditional deletion of AMPK in CB type I cells failed to attenuate CB afferent fibre discharge in response to hypoxia (Mahmoud *et al.*, 2016).

It is now clear that the initial outcomes were due to the off-target effects of, for example, the AMPK antagonist Compound C, which was found to inhibit at least 10 other kinases more potently than AMPK (Bain *et al.*, 2007). The responses to the AMPK activator AICAR were also attributable to off-target effects, such as the AICAR-mediated inhibition of adenosine transporters which are key modulators of type I cell activity, and/or reductions in the adenylate pool and ATP (Gadalla *et al.*, 2004; Hasenour *et al.*, 2014; Lantier *et al.*, 2014; Murali & Nurse, 2016). Therefore, it appears that unlike LKB1, AMPK activity is clearly not necessary for CB type I cell activation during hypoxia, which has since been corroborated by the pharmacological and genetic modulation of AMPK activity (Kim *et al.*, 2014; Buckler, 2015; Mahmoud *et al.*, 2016).

That said, despite showing no effect on the chemoafferent discharge response of CB type I cells, targeted deletion of AMPK in catecholaminergic cells did precipitate a more severe attenuation of the HVR than targeted deletion of LKB1 did (Mahmoud *et al.*, 2016). These findings therefore uncovered a split in the dependency of LKB1 and AMPK on the activation of the carotid body on one side, and the HVR or the other. In this regard, type I cell activation could be regulated in an LKB1-dependent manner by activation of one or more of the 12 AMPK-related kinases (Lizcano *et al.*, 2004; Evans *et al.*, 2016; Evans, 2018). However, regardless of the LKB1-dependent signalling pathways that determine type I cell afferent discharge, AMPK activity clearly seems to serve a crucial function in facilitating appropriate ventilatory adjustments that shape the HVR, a component of which, according to these findings, must originate centrally within the brainstem respiratory network. Indeed, by using functional magnetic resonance imaging (fMRI), two well defined regions within the mouse caudal brainstem were identified to exhibit significantly reduced

neuronal activity upon AMPK deletion in catecholaminergic cells relative to controls (Mahmoud *et al.*, 2016), which were termed the 'dorsal active region' (DAR) and 'ventral active region' (VAR). Importantly, their anatomical locations were consistent with those of the dorsal nucleus tractus solitarius (NTS) and the ventrolateral medulla, respectively, which receive CB chemoafferent fibre inputs and harbour the dorsal catecholaminergic A2 and C2 cell groups and the ventral catecholaminergic A1 and C1 cell groups (Finley & Katz, 1992; Erickson & Millhorn, 1994; Li *et al.*, 2008; Kline *et al.*, 2010). Therefore, the question arose whether specific brainstem catecholaminergic cells may be able to respond to hypoxia centrally and thus support the HVR in a manner that is dependent on AMPK activity.

1.4.1 Central oxygen-responsive neurons of the brainstem

Dominating within both the scientific and educational literature is the commonly held view that the central nervous system lacks a defined O_2 sensor capable of stimulating ventilation during periods of hypoxia. This may be the case for humans, as there appears to be no documented case of a retained HVR following bilateral carotid body resection (Timmers *et al.*, 2003; Gourine & Funk, 2017). By contrast, a variety of mammalian animal studies have demonstrated that the HVR can be partially or completely restored after either denervation or surgical removal of the CB (Davenport *et al.*, 1947; Miller & Tenney, 1975; Bisgard *et al.*, 1980; Martin-Body *et al.*, 1986; Daristotle *et al.*, 1991; Roux *et al.*, 2000a). Therefore, the existence of a central respiratory O_2-sensitive network seems likely after all and, given that larger mammals appeared to require a considerably longer time period to recover evidence of a HVR, the possibility remains that due to the small number of cases and lack of long-term follow-up studies any degree of restoration of a HVR in humans may have simply remained undetected.

Indeed, several hypoxia-responsive sites have been identified within the rodent brain, some of which were inhibitory and related to hypoxic ventilatory depression (thalamus and pons) (Martin-Body, 1988; Kramer *et al.*, 1999), while others were excitatory and related to increased respiratory activity (hypothalamus, dorsal and ventral medulla oblongata) (Sun & Reis, 1994b;

Horn & Waldrop, 1997; Pascual *et al.*, 2002). Of these excitatory networks that increase ventilation, catecholaminergic neurons seem to be the likely candidate to modulate the ventilatory response to hypoxia. Catecholamines, in particular noradrenaline, often have a stimulating effect on the respiratory network and several studies have linked the activity of catecholaminergic A1/C1 neurons of the ventral medulla and A2/C2 neurons of the dorsal medulla to increases of ventilation (Teppema *et al.*, 1997; Zanella *et al.*, 2006; Viemari, 2008; King *et al.*, 2012; King *et al.*, 2013; Burke *et al.*, 2014; King *et al.*, 2015). Furthermore, genetic mutations within catecholaminergic neurons have been related to mortality due to respiratory diseases such as Rett syndrome (Ide *et al.*, 2005; Viemari *et al.*, 2005; Weese-Mayer *et al.*, 2006; Roux *et al.*, 2010) . Therefore, the catecholaminergic neurons of the medulla oblongata are attractive candidates for conferring an O_2-sensing, hypoxia-responsive network within the brainstem.

1.4.2 AMPK within the catecholaminergic cells of the brainstem

If such a brainstem catecholaminergic network with central O_2-sensitivity truly existed, then it may offer an explanation of how the deletion of AMPK could have had a more severe impact on the HVR than deletion of LKB1, while retaining a completely normal afferent discharge from the carotid bodies that was abolished upon LKB1 deletion. If the HVR was not solely determined by chemoafferent inputs to the respiratory centres of the brainstem, but also by the activity of a central hypoxia-sensitive network within the brainstem, then their coordinated action could determine its full extent. In support of this view, the HVR of amphibians is modulated by O_2-sensing cells within the caudal brainstem while the role and the anatomical location of the peripheral chemoreceptors changes during the metamorphosis from the gill breathing tadpole to the lung-assisted, air breathing adult (Jia & Burggren, 1997; Porteus *et al.*, 2011). It seems therefore entirely possible that throughout evolution the peripheral chemoreceptor inputs may have been periodically reconfigured about a common ancestral hypoxia sensor located within the caudal brainstem, which ultimately underpins signal integration and thus acts as a “gatekeeper”

of respiratory adjustments during hypoxia (Evans *et al.*, 2016; Evans, 2018). Further support for this view comes from the fact that brainstem hypoxia alone may initiate increases in ventilation, given that there is continuous basal afferent input from the carotid bodies (Smith *et al.*, 1993; Curran *et al.*, 2000). In addition, different aspects of the brainstem respiratory network may have different hypoxic sensitivities (Hill *et al.*, 2011), and partial recovery of the HVR following CB resection may be derived from hypoxia-sensitive catecholaminergic neurons of the caudal brainstem in some animals (Smith & Mills, 1980; Roux *et al.*, 2000a; Roux *et al.*, 2000b). Furthermore, dysfunction of these catecholaminergic neurons has been shown to precipitate hypoventilation and apnoea associated with Rett syndrome, which worsens under hypoxic conditions (Roux & Villard, 2010).

The evidence for a role of AMPK signalling in the central response to hypoxia came from the genetic deletion strategy which targeted AMPK deletion to catecholaminergic cells. As mentioned earlier, CB afferent discharge was retained during hypoxia, yet the HVR was severely attenuated. Furthermore, fMRI studies on these knockout mice revealed a reduction in activity of discrete dorsal and ventral nuclei of the caudal brainstem during hypoxia which matched the location of catecholaminergic neurons within the NTS (A2 and C2 neuronal groups) and VLM (A1 and C1 neuronal groups), which also represent the primary site of CB afferent input (Finley & Katz, 1992; Koshiya & Guyenet, 1996; Guyenet, 2000; Teppema & Dahan, 2010; Mahmoud *et al.*, 2016).

Therefore, these findings support a model of AMPK-dependent modulation of discrete nuclei within the caudal brainstem called DAR and VAR, which during hypoxia deliver increases in the drive to breathe via afferent projections to neural networks that modulate the ventral rCPG (see also section 1.5 below) (Guyenet, 2014; Evans *et al.*, 2016; Evans, 2018).

1.5 Hypothesis

Based on the assumption that a cluster of hypoxia-responsive neurons proximal to the NTS may form a nucleus that acts as a 'gatekeeper' of the HVR, I hypothesise that the LKB1-AMPK signalling pathway supports coincidence detection at either a single node or possibly multiple nodes within, and thus activation of, a hypoxia-responsive circuit that encompasses, at the very least, dorsal A2/C2 neurons of the NTS as suggested by the DAR, and ventrolateral A1 neurons as suggested by the VAR (Figure 1.7) (Evans *et al.*, 2016; Mahmoud *et al.*, 2016; Evans, 2018). Within this circuit, the capacity of AMPK activation may be determined by the co-action of 'local hypoxic stress' within the brainstem that increases the AM(D)P:ATP ratio via decreases in ATP supply (Hardie, 2014), coupled to 'applied metabolic stress' via neuronal activation following afferent inputs from peripheral chemoreceptors and thus increases in ATP usage. Activation of AMPK, and thus the brainstem respiratory network, may therefore be determined by the coupling of chemoafferent fibre input and brainstem hypoxia. Thereafter, efferent output and increases in the drive to breathe may be facilitated by AMPK-dependent modulation of cellular metabolism, ion channel activity, neuronal firing frequency and/or neurotransmitter release in a manner that may be attenuated or augmented via regulation of AMPK expression (Lipton *et al.*, 2001; Murphy *et al.*, 2009; Ikematsu *et al.*, 2011; Hardie, 2014).

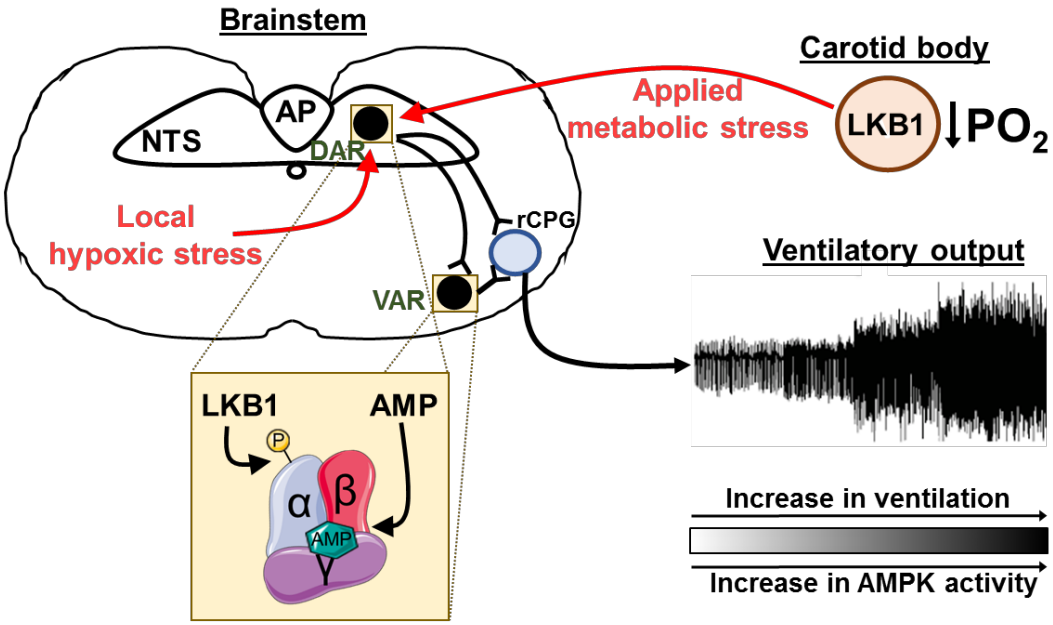

Figure 1.7: Schematic model of the AMPK-dependent integration of local hypoxic and applied metabolic stress that together determine the hypoxic ventilatory response.

Activation of AMPK within brainstem catecholaminergic A1 and C1 neurons corresponding to the ventral active region (VAR), as well as A2 and C2 neurons corresponding to the dorsal active region (DAR), is determined by the synergistic effects of 'local hypoxic stress' (decreases in ATP supply) caused by brain hypoxaemia and 'applied metabolic stress' (increases in ATP usage) caused by increased neuronal activity subsequent to carotid body chemoafferent fibre input. AP: area postrema; NTS: nucleus tractus solitarius; rCPG: respiratory central pattern generators; LKB1: liver kinase β1; AMP: adenosine monophosphate. Figure adapted from Mahmoud et. al. (2016).

1.6 Aims of the Thesis

The studies performed in this thesis aimed to investigate whether AMPK-dependent signalling pathways originating within the DAR and VAR could modulate the HVR centrally. Given the retained CB chemoafferent fibre discharge, this involved utilising the mouse model of targeted dual deletion of the AMPK-α1 and -α2 catalytic subunits in catecholaminergic cells in order to:

1) Investigate the effect of AMPK deletion in catecholaminergic cells on the ventilatory responses during acute and more prolonged exposures to mild and severe hypoxia by unrestrained whole-body plethysmography.
2) Investigate the effect of AMPK deletion in catecholaminergic cells on the dorsal brainstem respiratory network activity by immunohistochemical staining for nuclear cFos expression as an index of neuronal activation following exposures to hypoxia.
3) Investigate the effect of AMPK deletion in catecholaminergic cells on the apnoeic phenotype, with particular focus on the separation of spontaneous and post-sigh apnoeas.
4) Investigate the effect of AMPK deletion in catecholaminergic cells on the ventilatory duty cycle during exposures to mild and severe hypoxia by using unrestrained whole-body plethysmography.
5) Investigate the effect of AMPK deletion in catecholaminergic cells on the cardiovascular responses to hypoxia by tail cuff and pulse oximetry and comparing the hypoxia-induced cardiovascular responses of mice with AMPK deletion in catecholaminergic cells to those of mice with AMPK deletion in arterial smooth muscle cells.
6) Compare the ventilatory responses during acute exposures to severe hypoxia of mice with AMPK deletion in catecholaminergic cells to those of mice with AMPK deletion in adrenergic cells by unrestrained whole-body plethysmography.

Chapter 2: Materials and Methods

2.1 Mouse models and colony management

All experiments were performed in accordance with the regulations of the United Kingdom Animals (Scientific Procedures) Act of 1986. All studies and breeding schemes were approved by the University of Edinburgh and performed under UK Home Office project and personal licenses. Both adult male and female mice were used, and all were bred on a C57/Bl6 background unless stated otherwise. Numbers of mice (≥3 per measure) used are indicated for each experiment.

2.1.1 Mice containing transgenic loxP sites surrounding the catalytic α1 and α2 subunits of AMPK

The foundation of the research undertaken for this thesis was based on transgenic mice carrying loxP sites which flank both of the AMPK catalytic α-subunits (Viollet *et al.*, 2003; Jorgensen *et al.*, 2004b). These genetic modifications were global, which means every cell of the entire organism carried a homozygously "floxed" AMPK-α1 and -α2 subunit.

Because loxP sites were strategically placed in the introns surrounding the coding exons, the transcription and translation of the α-subunits was not disturbed, thus giving rise to phenotypically wild-type mice which throughout this thesis were used as genetic "wild-type" controls.

2.1.2 Targeted deletion of AMPK-α1 and -α2 subunits by transgenic expression of Cre recombinase under the reporter of tyrosine hydroxylase

In order to target AMPK-α1 and -α2 subunit deletion to only catecholaminergic cells, Cre recombinase was conditionally expressed under the promoter for tyrosine hydroxylase (TH), the rate-limiting enzyme in catecholamine biosynthesis which converts Tyrosine to L-DOPA (Karobath, 1971). Thus, all dopaminergic, noradrenergic, and adrenergic cells of the organism were targeted. Cre insertion into the 3' UTR of the gene for TH was achieved by genetic knock-in of a vector encoding for an encephalomyocarditis virus internal ribosome entry site (IRES) together with

the gene for Cre recombinase (Lindeberg *et al.*, 2004), thereby creating a bicistronic mRNA strand that allows for co-expression of both tyrosine hydroxylase and Cre recombinase.

Repeated crossing of TH-Cre mice with AMPK-α1/α2 homozygous floxed (AMPK-α1/α2 Flx) mice resulted in offspring that carried heterozygous TH-driven Cre recombinase and global homozygous loxP sites for the AMPK catalytic α-subunits, thereby generating cell type-specific AMPK-α1/α2 double knock-out (TH AMPK-α1/α2 dKO) mice. Confirmation of the presence of all target transgenes was done by genotyping, as described in section 2.1.6.

Using this approach meant that conditional AMPK-α1/α2 deletion will occur from the first time expression of TH, and hence Cre, is initiated during development, even if this expression is only transient. Therefore, loss of AMPK activity in the adult could be, at least partially, compensated for by alternative metabolic coping strategies, which may extend to the way targeted cells respond to a hypoxic stimulus. One possibility to circumvent cellular compensatory mechanisms would be to utilise ligand-dependent chimeric Cre recombinases (CreER recombinases), which are inherently inactive but activated by administration (e.g. oral, intraperitoneal, intravascular) of tamoxifen (Feil *et al.*, 2009). This method would therefore not only allow for spatial control of gene knockout, but also temporal. Moreover, it would allow us to test whether cellular mechanisms are engaged that could compensate for AMPK-α1/α2 subunit deletion.

2.1.3 Targeted deletion of AMPK-α1 and -α2 subunits by transgenic expression of Cre recombinase under the reporter of Phenylethanolamine N-methyltransferase

I also wished to further investigate the requirement of AMPK in catecholaminergic cells and sought to compare the phenotype of catecholaminergic AMPK-α1/α2 dKO mice to that of adrenergic AMPK-α1/α2 dKO mice.

This was achieved by utilising a transgenic mouse model whereby the gene encoding for Cre recombinase was inserted into exon 1 of the Phenylethanolamine N-methyltransferase (PNMT) gene (Ebert *et al.*, 2004). PNMT is the final rate-limiting enzyme of catecholamine synthesis, which transfers a methyl-group from S-adenosyl-L-methionine onto noradrenaline, thereby converting it to adrenaline. By using this strategy, Cre was exclusively expressed in adrenergic cells.

Once again, PNMT-Cre mice were crossed with AMPK-α1/α2 Flx mice, resulting in offspring that carried a heterozygous PNMT-driven Cre recombinase and global homozygous loxP sites for the AMPK catalytic α-subunits, thus generating adrenergic cell type-specific AMPK-α1/α2 double knock-out (PNMT AMPKα1+α2 dKO) mice.

Confirmation of the presence of all target transgenes was done by genotyping, as described in section 2.1.6.

2.1.4 Targeted deletion of AMPK-α1 and -α2 subunits by transgenic expression of Cre recombinase under the reporter of transgelin

Given the distinct possibility of Cre-leakage and ectopic expression of TH in the developing heart (Lindeberg *et al.*, 2004), I also sought to assess the effects of AMPK deletion in the cardiovasculature. This was achieved by crossing AMPK-α1/α2 Flx mice with mice expressing Cre recombinase under the control of the SM22 promoter (Holtwick *et al.*, 2002), a smooth muscle-specific gene encoding for transgelin. Because viability of mice with dual deletion of AMPK catalytic subunits in smooth muscle (Sm) cells is compromised (Moral-Sanz, J., awaiting publication), colonies were maintained as Sm AMPK-α1 KO and Sm AMPK-α2 KO, or as precursory breeders for Sm AMPK-α1/α2 dKO, whose AMPK catalytic subunits were heterozygously floxed and therefore retained a low level of AMPK-α1 and AMPK-α2 expression.

Confirmation of the presence of all target transgenes was done by genotyping, as described in section 2.1.6.

2.1.5 Breeding plan

To maintain colonies, one male and two female AMPK-α1/α2 Flx mice were continuously crossed with each other. For the knockout lines, virgin AMPK-α1/α2 Flx mice were mated with either TH AMPK-α1/α2 dKO or PNMT AMPK-α1/α2 dKO mice. Although in-breeding of the mouse lines could not be circumvented, brother-sister matings were avoided by mating cousins. No fertility or viability problems were recorded.

Breeding for the Sm AMPK-α1 KO, Sm AMPK-α2 KO, and Sm AMPKα1+α2 dKO mice was carried out and managed by Dr Oluseye Ogunbayo independently of the other three colonies mentioned above.

Pups were ear notched by the technicians within the animal facility for genotyping and identification at 14 days of age and weaned at 21 days of age. Whenever possible, male mice were kept alongside littermates and females in company of up to 5 other mice, which has been shown to promote well-being and reduce stress (Deacon, 2006).

2.1.6 Genotype analysis

Ear notch samples, between 1 to 3 pieces of approximately 4mm^2 from each animal, were stored in DNAse free 1.5ml Eppendorf tubes at -20°C until addition of 120µl Direct PCR lysis buffer (Viagen Biotech, Inc.) and 6µl of 20mg/ml Proteinase K (Thermo Fisher). Samples were incubated overnight at 55°C in a rotating hybridisation oven (Thermo Hybrid) and the activity of Proteinase K stopped by moving the samples into a waterbath at 85°C for 45min. This step is crucial to ensure proper activity of Taq polymerase during the subsequent PCR.

For the PCR reaction, a total reaction volume of 26µl per sample was used. Each reaction mix consisted of 2µl of sample lysate, 12.5µl of 2xGoTaq® Polymerase Green Master Mix (Promega), 1.6µl from a 10µM stock of each primer, as well as nuclease-free water to the final volume. All primers used for genotyping are presented in Table 2.1.

The PCR was carried out using a SimpliAmp™ Thermal Cycler (Applied Biosystems) under the conditions illustrated in Table 2.2. 10µl of PCR products were run on a 2% agarose gel made with 10% SYBR®Safe DNA gel stain (Invitrogen) to visualise DNA bands, and a 100bp DNA Ladder (Promega). Each gel was run in a Sub-cell GT gel tank with a PowerPac™ Basic Power Supply (Bio-Rad) for 35-45min and imaged using a Genius Bio Imaging System and GeneSnap Software 7.12 (SynGene).

Table 2.1: Primers used for genotyping of transgenic mice.

Target Gene	Primer Sequence	Expected Length
PRKAA-1 (AMPK-α1)	α1-FWD: 5’ TATTGCTGCCATTAGGCTAC 3’ α1-REV: 5’ GACCTGACAGAATAGGATATGCCCAACCTC 3’	WT: 588bp Floxed: 682bp
PRKAA-2 (AMPK-α2)	α2-FWD: 5’ GCTTAGCACGTTACCCTGGATGG 3’ α2-REV: 5’ GTTATCAGCCCAACTAATTACAC 3’	WT: 204bp Floxed: 250bp
TH Cre	TH-FWD: 5’ CACCCTGACCCAAGCACT 3’ TH-REV: 5’ CTTTCCTTCCTTTATTGAGAT 3’ Cre-UD: 5’ GATACCTGGCCTGGTCTCG 3’	WT: 290bp Cre: 390bp
PNMT Cre	21: 5’ CAGGCGCCTCATCCCTCAGCAGCC 3’ 22: 5’ CTGGCCAGCGTCGGAGTCAGGGTC 3’ 23: 5’ GGTGTACGGTCAGTAAATTGGACACCGTCCTC 3’	WT: 190bp Cre: 300bp
Sm Cre	78: 5’ GCGGTCTGGCAGTAAAAACTATC 3’ 79: 5’ GTGAAACAGCATTGCTGTCACTT 3’ 80: 5’ CTAGGCCACAGAATTGAAAGATCT 3’ 81: 5’ GTAGGTGGAAATTCTAGCATCATCC 3’	WT: 320bp Cre: 100bp

Table 2.2: PCR protocols used for genotyping of transgenic mice.

Gene	Denaturing	Annealing	Extending	Cycles	Holding
PRKAA-1 PRKAA-2 TH Cre	94ºC, 5min 94ºC, 45sec	56ºC, 40sec	72ºC, 60sec 72ºC, 10min	35x	4ºC
PNMT Cre	94ºC, 5min 94ºC, 15sec	70ºC, 30sec	72ºC, 30sec 72ºC, 2min	35x	4ºC
Sm Cre	94ºC, 5min 94ºC, 15sec	65ºC, 30sec	72ºC, 30sec 72ºC, 2min	35x	4ºC

2.2 Unrestrained whole-body plethysmography

To study ventilation during various degrees of hypoxia in conscious mice, an unrestrained whole-body plethysmography chamber (Buxco) was used. The advantages of this method are that each animal can be habituated to the environment, which on experimental days reduces stress levels and animals are generally calmer sooner. In addition, the animal can roam freely within a confined space and is allowed to explore and groom naturally until it has settled. The high sensitivity of the transducer to detect pressure differences during respiration ensures a high degree of accuracy for the measurements obtained.

2.2.1 System setup

The plethysmograph itself is made of Plexiglas and consists of a 450ml mouse chamber and a 100ml reference chamber (Figure 2.1). Linked to both chambers is a differential pressure transducer on one side, which is connected to a preamplifier, and a Halycon^{TM} low noise pneumotachograph on the other side. Room air is drawn in through the pneumotachograph and is withdrawn at the bottom of the mouse chamber by the bias flow outlet at a rate of 1l/min. The gas inlet, which feeds into the mouse chamber and is connected to the transducer and pneumotachograph, is regulated by a valve at the top of the plethysmograph. An inlet rate greater than 1l/min (rate of bias flow outlet) must be ensured to avoid drawing in room air during gas challenges. A direct supply of gas was used which originated from a pre-mixed gas cylinder (BOC). Each cylinder was composed of 0.05% CO_2 (500ppm) and 12% or 8% O_2 balanced in N_2. The gas supply and flow were regulated via a pressure gauge on the gas cylinder, as well as a second distribution reservoir fitted with a pressure gauge (Buxco) to ensure air flow was constant. A gas flow of 2l/min was chosen for all experiments, including exposures for cFos expression, blood pressure and SpO_2 measurements.

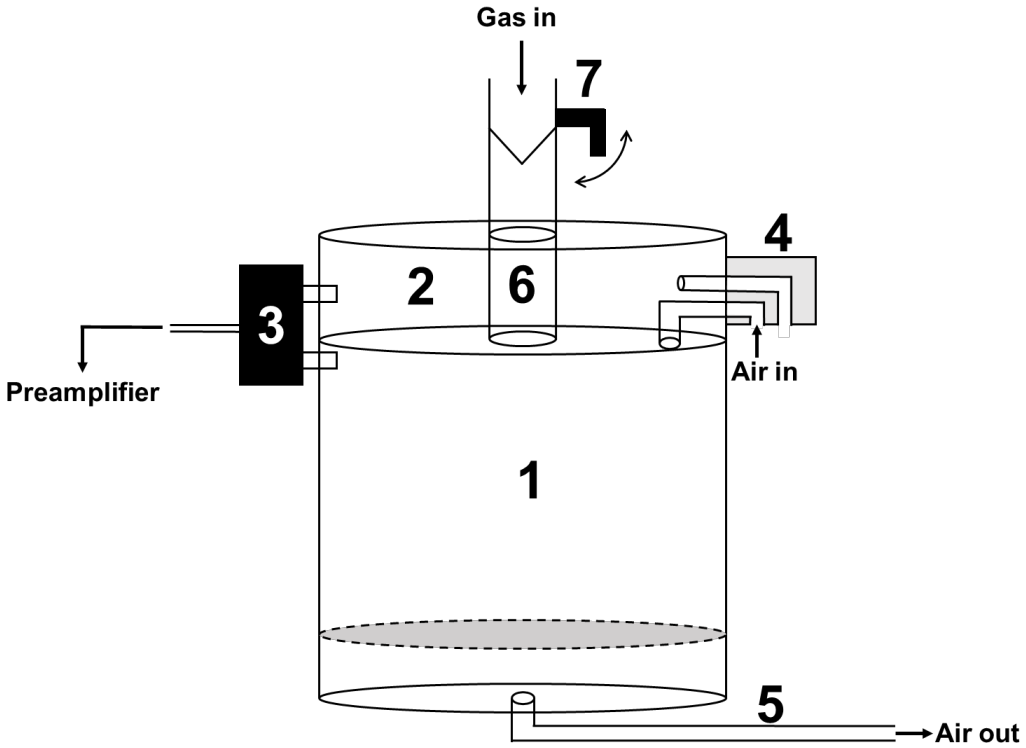

Figure 2.1: Schematic of the mouse whole-body plethysmography apparatus.

During normoxia, air is drawn out of the mouse chamber (**1**) from the bias flow outlet (**5**). The negative pressure thereby created results in room air being drawn into the chamber via the pneumotachograph (**4**) air inlet. During experiments a single mouse would be placed on the platform (grey dashed lines) and the chamber closed. During animal ventilation within the sealed chamber, a pressure transducer (**3**) monitors the pressure changes that occur in the mouse chamber relative to the reference chamber (**2**) and relays the information to a preamplifier for subsequent analysis. Hypoxia is introduced by opening a valve (**7**) at the gas inlet (**6**) ensuring that the gas flow rate is greater than the bias flow outlet rate.

2.2.2 FinePointe acquisition software

The foundation of data acquisition by this method is the occurrence of pressure changes during inhalation and exhalation within an enclosed environment (Chapin, 1954). During inhalation, the air becomes humidified and warmed by the animal's lungs, thereby expanding in volume. This expansion within the lungs means the volume within the thorax is larger than the initially inspired volume, which increases the overall pressure in the sealed mouse chamber relative to the reference chamber that retains a constant pressure. During exhalation, air cools again and water vapor condensates, whereby the pressure decreases again. These pressure differences in relation to the reference chamber are measured by the transducer, which relays them to the acquisition software as a 'box flow' graph with a sampling frequency of 1kHz.

The FinePointe software (DSI, version 2.4.6.9414) computes the received signals and displays the outcomes graphically and numerically. For the graphical box flow, a value of zero indicates no pressure differences between the mouse and reference chamber due to no respiratory activity. During inspiration the box flow crosses into negative pressure, whereas expiration is determined by positive pressures. Because the box flow is plotted over time, the data is displayed as a waveform from which several parameters are calculated. The duration of inspiration (Ti) and expiration (Te) are calculated as the time taken to cross the zero point, and the total breath duration (To) can be computed. From this, respiratory frequency per minute (60/To) can be deducted. A little more complex is the determination of the tidal volume, which takes into consideration the pressure changes within the chamber and the box flow amplitudes according to the formula by Drorbaugh and Fenn (Drorbaugh & Fenn, 1955). This formula accounts for body and ambient temperatures, humidity, and their subsequent influence on the pressure changes. Finally, the product of respiratory frequency and tidal volume allows for calculation of minute ventilation. Because pressure changes are also very sensitive to movement artefacts the software also incorporates a series of algorithms to reject periods that were considered non-ventilatory, such as gross body movements, sniffing, or grooming.

Numerical data was acquired as averages of 2sec intervals, for which the software automatically computed the above mentioned values.

2.2.3 Experimental protocols

Prior to experimental procedures, naïve mice were habituated to the chamber environment on 5 consecutive days for 30 minutes (Plethysmography) or 60 minutes (cFOS expression analysis) at room air.

2.2.3.1 Plethysmography measurements

Following habituation, mice were placed in the plethysmography chamber and allowed to settle for 5 minutes before commencing measurements at room air. The duration of room air exposure would last until at least 3 or 4 baseline measurements were obtained (see section 2.2.4.1). Room air exposures were followed by flushing and maintaining delivery of 12% or 8% O_2 into the chamber. The FinePointe system automatically includes a 30s "washing" period, after which the 10min experimental period began. At the end of the hypoxic exposures, a 5min recovery period was recorded during which animals were breathing room air again. A full recovery indicated by activity, grooming, or sniffing must have been observed before the mice were placed back in their home cage and allowed to rest for at least 48 hours.

2.2.3.2 cFos expression analysis

As described above, following habituation mice were placed in the plethysmography chamber and allowed to settle for 5 minutes before commencing measurements at room air. The duration of room air exposure would last for 15min, regardless of whether a baseline record has been obtained or not. Room air exposures were either maintained at 21% O_2 for controls, or followed by flushing and maintaining delivery of 12% or 8% O_2 into the chamber for 60min. At the end of the 60min period, room air was returned to the chamber for a 10min recovery period, after which the mice

were injected intraperitoneally with 2000mg/kg Pentobarbital Sodium (Merial) within a 5min period and immediately perfused thereafter (see section 2.5.1).

2.2.4 Respiratory analysis

In order to assess the ventilatory phenotypes of the genetic mouse models described above, ventilatory parameters such as respiratory frequency, tidal volume, minute ventilation, inspiration time and expiration time were computed by the FinePointe software over a 2s period and analysed for control and knockout mice according to the criteria described below.

2.2.4.1 Baseline measurements

Each experiment of hypoxic exposures was preceded by a period of normoxic recordings. This period aimed to collect samples of baseline breathing, which were required to compute the percentage changes of breathing parameters during hypoxia. Baseline records were selected following a strict set of criteria: 1 – the animal had to be sitting quietly in the chamber without grooming, sniffing, or eating; 2 – the box flow pattern had to be regular and at least 4 breaths in length; 3 – the respiratory frequency and tidal volume should have been within the range of 150-250 breaths/min and 0.2-0.35ml, respectively (Palmer *et al.*, 2013), even though subconscious bias often lead to a selection of baselines with frequencies close to 200 breaths/min and tidal volumes around 0.3ml. Example traces of selected baseline records can be seen in Figure 2.2.

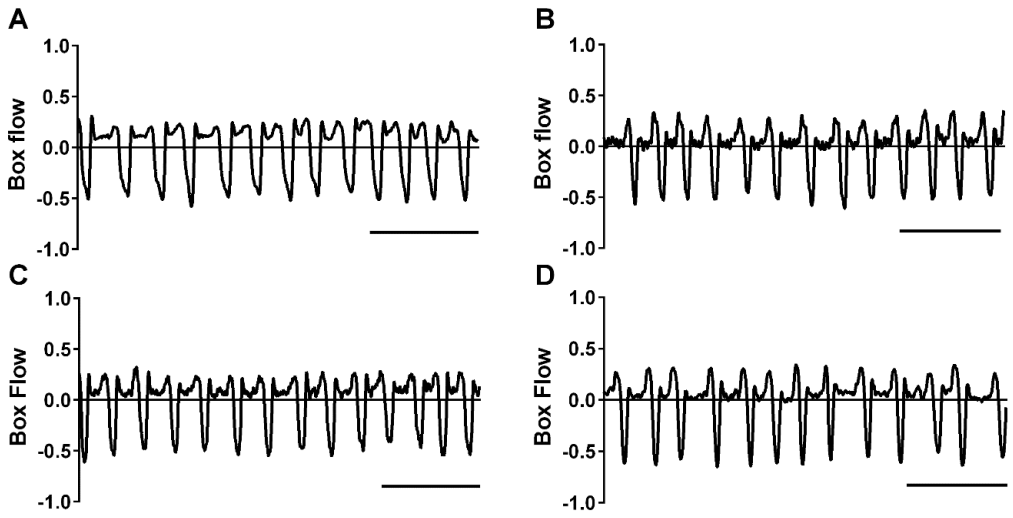

Figure 2.2 Exemplary box flow records of baseline breathing.

Raw box flow traces show exemplary periods selected as baselines. Respiratory values computed by the FinePointe software for these periods were: **(A)** 205.2breaths/min, 0.33ml, 68.91ml/min; **(B)** 209breaths/min, 0.26ml, 55.2ml/min; **(C)** 202.42breaths/min, 0.30ml, 62.14ml/min; **(D)** 195.9breaths/min, 0.3ml, 58.9ml/min. Scale bar 1s.

2.2.4.2 Hypoxic ventilatory response during 5min exposures

In order to assess the HVR during 5min exposures, the following points were chosen for analysis: 1 – the peak of the Augmenting phase (around 30s), 2 – the nadir of the "Roll-Off", (around 100s), and 3 – the plateau of the Sustained phase (around 300s). At or closest to each time point, a 2-8s period of ventilation was selected which was free of sighs, apnoeas, and movement.

2.2.4.3 Minute-by-minute ventilatory response

Respiratory frequency, tidal volume and minute ventilation were also analysed after every whole minute of hypoxia (i.e. in 60s intervals). The start point of hypoxia was chosen as the time point of the gas exchange, and not following the 30s "washing period" included by the FinePointe software. A 6s breathing period was selected with the following criteria: 1 – free of sighs, 2 – free of apnoeas unless unavoidable, 3 – free of movement artefacts, and 4 – as close to the intended time point as possible. Occasionally, only a 2s or 4s period could be used.

2.2.4.4 Whole minute ventilatory response

For AMPK-α1/α2 Flx and TH AMPK-α1/α2 dKO mice respiratory data was also analysed as whole-minute averages (see Appendix 1). As above, the hypoxic start point was the moment of gas exchange and averages were taken for each full minute. For the first minute, however, values were only used for analysis once the animal started to respond to the hypoxic stimulus, which was evident by a cessation of sniffing and presentation of a more regular breathing pattern that usually occurred 25-35s after the onset of hypoxia. Thereafter, any occurrences of sighs, apnoeas, movements, or sniffs were included in the analysis.

2.2.4.5 Duty cycle analysis

In order to assess the time course of the ventilatory duty cycle in control and knockout mice, the values acquired by the FinePointe software for inspiration time (Ti), expiration time (Te), and total breath time (To, manually calculated as Ti+Te) were displayed as the ratiometric changes of hypoxia:normoxia. Each hypoxic value, starting 30s after the gas exchange, was divided by the total average of normoxic values, which were taken from the same time points as the baseline measurements described above. In addition, the ratios of tidal volume to inspiration time (Tv/Ti), expiration time (Tv/Te), and total breath time (Tv/To) were analysed in relation to normoxia.

2.2.5 Apnoea and sigh analysis

The raw box flow data from the point of gas exchange was extracted into CSV files and run through a Python script designed by Prof Mayank Dutia (University of Edinburgh). This script detects apnoeas as cessations of breathing that were greater than the average duration, including the interval, of 2 successive breaths (600ms) during normoxia, with a detection threshold of 0.25mmHg (SD of noise). Apnoeas were also separated manually based on whether or not they were immediately preceded by a sigh. All apnoeas were analysed in terms of frequency (apnoeic index, AI), duration, and the product of frequency and duration (apnoea-duration index, ADI). Sighs, regardless of whether they were accompanied by an apnoea or not, were also analysed, but only in terms of their frequency (sigh index, SI).

2.3 Blood pressure

Given that a subset of the catecholaminergic neurons targeted by our conditional AMPK deletion strategy employed have been heavily implicated in the control of the baroreflex, (Ross *et al.*, 1984; Dampney *et al.*, 2002; Guyenet, 2006; Guyenet *et al.*, 2013), measurements of blood pressure and heart rate during exposures to hypoxia have been carried out by tail cuff and pulse oximetry, respectively.

2.3.1 Kent CODA tail cuff system

To measure blood pressure under normoxic and hypoxic conditions, the tail cuff method was chosen. The CODA™ Non-Invasive Blood Pressure System (Kent) works on the principle of volume pressure recording (VPR), whereby a VPR sensor measures the characteristics of returning blood flow from an occluded tail artery during deflation of an occlusion cuff (O-cuff). First, the VPR cuff inflates to push blood out of the tail. Immediately following this the O-cuff inflates to a maximum occlusion pressure of 250mmHg, which stops the flow of blood back into the tail. The O-cuff is then slowly deflated over a pre-set 20s period. Once blood flows back into the tail the VPR cuff senses the pulsations of the returning blood flow, and hence the "swelling" of the tail.

On the graphic display, the returning blood flow can be seen as an increase in the VPR graph and at the first sign of "swelling" the systolic blood pressure (SBP) is measured (Figure 2.3 A). Diastolic blood pressure (DBP) is determined once the increasing rate of swelling first starts to cease. Once blood flow has been fully restored the graph on the monitor peaks and then declines as the cuff finishes its deflation.

Mean blood pressure (MBP) is then calculated by the following formula:

$$\mathrm{MBP} = \mathrm{DBP} + \frac{\mathrm{SBP}-\mathrm{DBP}}{3}.$$

An advantage of this method is that direct pressure changes are measured in the tail, as opposed to light emission and absorption, which is limited in animals with dark pigmentation such as our genetic background of C57BL/6J mice.

The software also includes several exclusion criteria by which it assesses each measured cycle. The most commonly encountered reasons for exclusion were "wrong shape", which was usually caused by animal movements that created dramatic artefacts in the graphs (Figure 2.3 B), and "no tail volume", which meant blood flow in the tail could not be detected and the VPR graph was largely a straight line (Figure 2.3 C). Occasionally, the system critiqued "too short" when SBP and DBP were too close to be

physiologically possible. However, subjective exclusion needed to also be applied in some cases, for example when sighs obviously influenced the results (Figure 2.3 D).

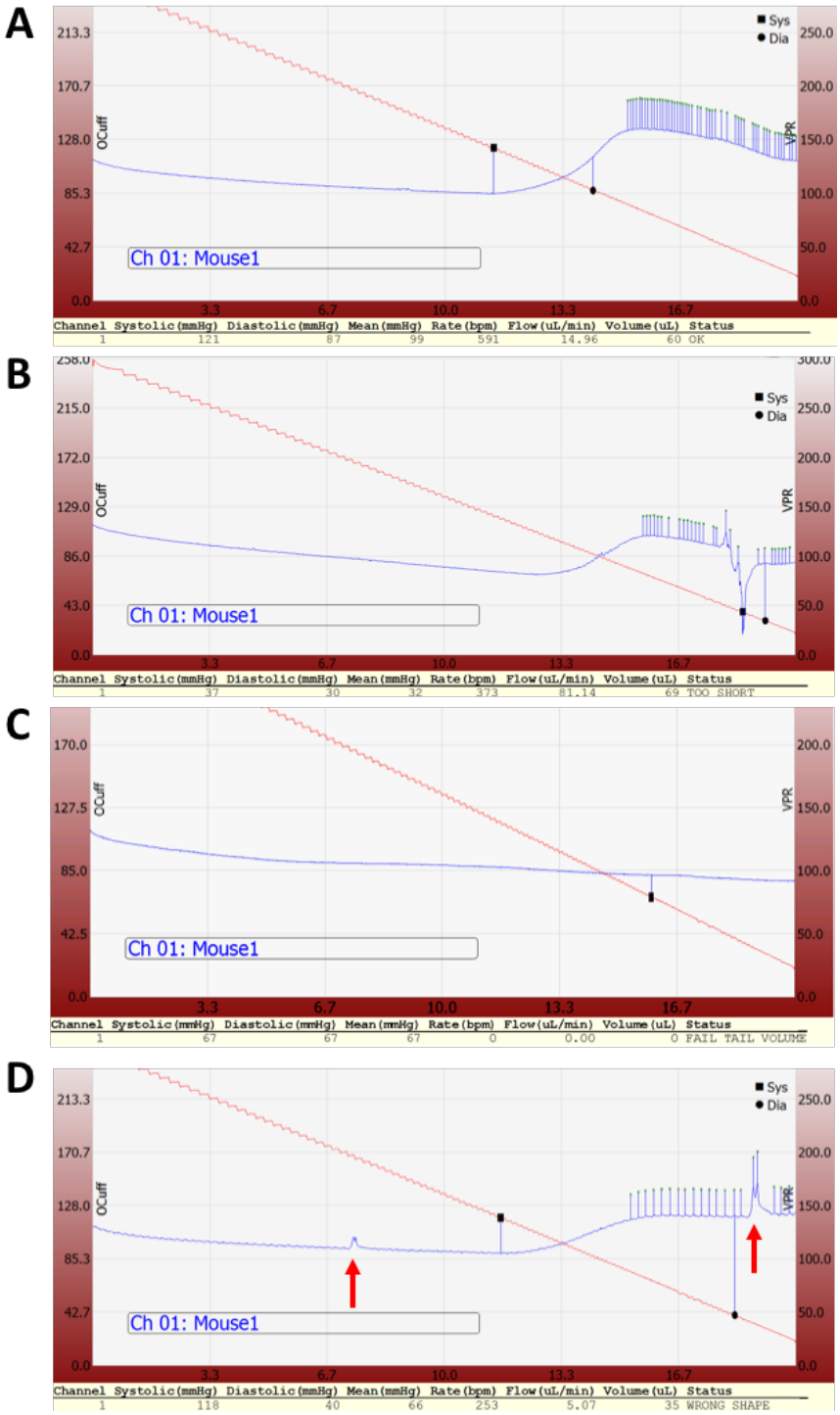

Figure 2.3 Example records obtained during blood pressure measurements.

Panels show examples of **(A)** a good cycle, where measurements for systolic (square) and diastolic (circle) pressures were obtained accurately; **(B)** a cycle that was affected by mouse movement; **(C)** a cycle where no blood flow was detected; **(D)** and a cycle where the detection of diastolic blood pressure was influenced by sighs (red arrows).

2.3.2 Experimental protocols

Before commencing blood pressure experiments, all mice were habituated to the restraint of a mouse holder (Kent) to reduce stress-induced blood pressure responses. For this, mice were placed in the pre-warmed holder for 30mins on 5 consecutive days.

On the day(s) of the experiment, each mouse was placed in the pre-warmed mouse holder and allowed to settle for 5mins with the cuffs attached to the tail.

The first objective was to obtain measurements of resting blood pressure while breathing room air. For this, blood pressure was taken in 32 cycles with a 5s pause between each cycle, until 3 good records have been obtained (see section 2.3.3 for definition of “good records”).

Blood pressure during hypoxia was measured on separate days after completion of all resting blood pressure measurements. For this protocol, 13 cycles of measurements were taken during room air, which served as a baseline, followed by 16 cycles of hypoxia (12% or 8% O_2 in 0.05% CO_2, balanced in N_2) and 8 cycles of recovery at room air. The durations of these cycles correspond to approximately 8mins room air, 10mins hypoxia, 5mins recovery. Hypoxic gas originated from a pre-mixed gas cylinder (BOC) and was delivered at a flow rate of 2l/min via a head cone that inserted into the mouse holder.

2.3.3 Blood pressure analysis

The tail cuff measurements are extremely sensitive to disturbances, such as animal movements or respiratory sighs. Such disturbances create artefacts in the VPR graph that interfere with appropriate detection of SBP and DBP points. Cycles that contained interferences were excluded from the analysis. If the disturbance only interfered with one of the measurements, then this value plus the mean blood pressure value were omitted from the analysis. The exclusion of cycles and data ultimately lead to a reduction in available information about the blood pressure. I therefore decided that at least 50%

of the data needed to be retained during hypoxic exposures in order for the experiment to be considered for group analyses.

2.4 Peripheral arterial oxygen saturation and heart rate

In order to measure peripheral arterial oxygen saturation (SpO_2) and heart rate (HR) in mice during hypoxia, the PhysioSuite® MouseSTAT™ module (Kent) was used, which uses pulse oximetry for its measurements.

2.4.1 Kent PhysioSuite® system

The pulse oximeter is a Y-clip, which is attached to the tail of the mouse and contains a sensor that measures SpO_2 and HR. One side of the sensor emits light at two different wavelengths – red and infrared. On the other side of the clip is a photosensor, which detects the light signals that have passed through the body tissue. Several factors influence the detection of light, such as tissue thickness, appropriate placement of the sensor, and, of course, the O_2 content of arterial and venous blood, because the absorption rate is higher in O_2-depleted blood than in O_2-rich. It is very important to avoid restriction of blood flow, as the measurements depend on a pulsating vascular bed. It has previously been observed that measuring SpO_2 in the tail is quite challenging and often leads to inaccurate readings. It was found that the perfusion rate varies greatly along the length of the tail, and warming of the animal increases perfusion rates at different degrees on the base, middle, and tip of the tail (Wu *et al.*, 1995). Therefore, in order to ensure adequate blood flow and reproducibility, each animal was pre-warmed on a heating platform and the clip always placed at or as close as possible to the base of the tail. The sampling rate of the sensor was set to 0.5Hz.

2.4.2 Experimental protocol

As described in section 2.3.2, all animals were pre-habituated to the mouse holder for 30min on 5 consecutive days unless habituation had already occurred.

Following 5min acclimation in the mouse holder, the tail clip was attached and repositioned until the SpO_2 levels read between 95-99% (Ceylan *et al.*, 2016). After a 2min baseline, hypoxia (12% or 8% O_2, 0.05% CO_2, balanced in N_2) was introduced via a head cone with an air flow of 2l/min for a duration of 10min. Exposures were then terminated and the animals allowed to recover for 3-5mins before being returned to their home cages.

2.4.3 SpO_2 and HR analysis

The analysis for both SpO_2 and HR was carried out identically, in that a total average was taken of the 2min baseline, the 10min exposure to hypoxia, and the entire recovery period.

2.5 Brainstem immunohistochemistry

In order to evaluate the activation of brainstem neurons after exposures to hypoxia, control and knockout mice were culled at the end of the experiment by an overdose of anaesthesia and the brains fixed for immunohistochemical processing.

2.5.1 Perfusion, fixation and cryoprotection

Following administration of an overdose of sodium pentobarbital as described in section 2.2.3.2, mice were checked for the absence of signs of breathing and withdrawal to pain by squeezing the paw with forceps. Once confirmed, the thoracic cavity was opened and the ribcage clamped back. The exposed heart, which at this point was still beating, was freed of the pericardium and any fat obstructing access before inserting the tip of a 25mm Sterican® 26-gauge needle (Braun) into the left ventricle. The needle had been previously attached to the tubing of an Autoclude peristaltic infusion pump (Verder) and filled with ice-cold heparinised saline (Table 2.3). Immediately after switching on the peristaltic pump an incision was made to the right atrium of the heart to drain the fluid that flowed through the systemic circulation while avoiding the pulmonary circulation. Approximately

80-100ml of heparinised saline were passed before infusing approximately 50-100ml of 4% paraformaldehyde (Table 2.3). A good perfusion resulted in the immediate and full clearance of the liver, no inflation of the lungs, no dripping of fluid from the mouth or nose, a robust ‘formalin dance’ and muscle twitching, and finally overall stiffness of the entire body of the mouse.

Following transcardial perfusion and fixation, brains were carefully removed from the skull and placed overnight into Post-Fix solution (Table 2.3) at 4°C. Once sunken to the bottom of the vessel, brains were transferred into a 30% sucrose solution and stored at 4°C. For longer-term storage (several months), 0.01-0.05% sodium azide was added to the 30% sucrose solution to prevent fungal and bacterial growth.

2.5.2 Sectioning of the brainstem

To prepare for cryosectioning, brains were blotted dry on tissue paper and the brainstem separated from the forebrain roughly at the point of the optic chiasm using a sharp razor blade. A further incision was made to the right side of the brainstem in order to differentiate left and right sides during mounting. Brainstems were wrapped in aluminium foil and flash frozen in ground dry ice. Frozen brainstems were then mounted caudal side up onto a Frigomobil freezing microtome (Leica) set to -17°C to -18°C, covered in Cryo-M-Bed embedding compound (Bright) and allowed to freeze again.

Sections were cut with a 33° blade at a thickness of 30µm and collection started as soon as the cerebellum became visible. Per vial, a series of 7 alternating sections (A’s and B’s), each separated by 60µm, were collected in 0.1M phosphate buffer (PB) and later transferred into cryoprotecant (see Table 2.3) for storage at -20°C.

One of the major problems arising with this procedure was that the brain would almost certainly be mounted at an angle onto the cryostat platform, which resultes in sections at slightly different anatomical planes (‘dorsoventral tilt’). Another challenge was the fragility of the sections during the cutting, as improper fixation, storage, or freezing could lead to tissue damage. This often presented as torn or frayed sections which during

handling often tore apart. Fragility also arose from the thickness of the sections, as most commonly brains were cut at 40-44µm thick. However, I was unable to obtain double staining at this thickness and changes in the staining protocol did not overcome this issue. Only once I reduced the thickness to 30µm the double labelling was successful.

2.5.3 Immunohistochemistry – fluorescence

For immunostaining, several vials per animal from the same alternation (either all A's or all B's per animal) were used. All procedures were carried out at room temperature on a shaker.

All sections per vial were drained into Falcon™ Cell Strainers (Fisher) with 100µm pores and washed four times in a 6-well plate filled with 0.1M phosphate buffered saline (PBS, Table 2.3) for 10min each. To block non-specific binding sites for secondary antibodies, sections were then incubated in blocking solution (Table 2.3) for 2hr. The addition of Triton X-100 (Sigma) results in disruption of cell membranes, which allows for easier penetration of antibodies.

Following a 10min rinse in 0.1M PBS, the sections were incubated overnight in primary antibodies prepared in a carrier solution (Table 2.3). The concentration of each primary antibodies needed to be tested upon first time use. All information on antibody origin and dilution can be found in Table 2.4.

On the second day, primary antibodies were rinsed off by washing 10mins for four times in 0.1M PBS and secondary antibodies diluted in carrier solution were applied. Once again, sections were left overnight, but this time the incubation was covered to ensure dark conditions and avoid unnecessary photobleaching of the fluorophores on the secondary antibodies.

Finally, on the third day all sections were washed in darkness four times for 10min in 0.1M PBS and mounted on microscope slides (Fisher) in a caudo-rostral order. After a brief moment of air drying, Vision™ PermaFluor™ Aqueous Mounting Medium (Thermo Fisher) was added to

the slide and a coverslip carefully dropped. Slides were then stored in darkness at 4°C.

2.5.4 Immunohistochemistry – Diaminobezidine staining

As with fluorescent immunostaining, several vials from the same alternation were used for each animal undergoing Diaminobezidine (DAB) staining. All procedures were carried out on a shaker.

Sections from each vial were drained into cell strainers and washed four times for 10min at room temperature in 0.1M phosphate buffered triton (PBT, Table 2.3). A 20min incubation in hydrogen peroxide immediately followed, which is important to block endogenous activity of neuronal peroxidase enzymes that can increase false positives during DAB staining. After another four 10min washes in 0.1M PBT, sections were incubated in blocking buffer (Table 2.3) for 30-60min. This step was immediately followed by incubation of sections in primary antibodies diluted in blocking buffer. It is important to note at this stage, that due to the cellular localisations and the nature of the colour development, primary antibodies targeting cFos (Table 2.4) were applied first. Sections were left to incubate for an initial 30-60min at room temperature before being transferred to 4°C for at least 36-48hr.

After six 5min washes in 0.1M PBT to remove excess primary antibodies, a biotinylated IgG horse anti-rabbit secondary antibody diluted in blocking buffer was applied for 1hr at room temperature. The excess secondary antibodies were removed in four 5min washes, and an avidin-biotin complex (ABC; Vector Laboratories) applied to the sections for 1hr at room temperature. Avidin has an extremely high affinity for biotin and forms an incredibly strong non-covalent bond. The additional formation of complexes between avidin and horseradish peroxidase targets this construct to the antigen of interest. Following two 10min washes with 0.1M PB and one wash in 0.05M Tris buffer (Table 2.3), sections were incubated in a solution comprising 0.05M Tris buffer, DAB, Nickel II sulfate, ammonium chloride and hydrogen peroxide. Hydrogen peroxide is required for the oxidation of DAB into a water insoluble brown precipitant at sites where horseradish

peroxidase is present also. The addition of metallic ions such as nickel will turn a brown precipitant into a dark purple to black colour. For cFos visualisation, sections were incubated for 8min and the reaction stopped by washing in 0.05M Tris buffer for 5min. Longer incubations result in higher background precipitation of DAB, so for each staining a “test section” was incubated first and great care was taken that each sample was not incubated for longer periods. At the end, sections were washed in 0.1M PB twice for 5min and once for 10min.

At this point a single staining protocol would be completed, but because double labelling for cFos and TH was desired the protocol was immediately repeated, starting with four 10min washes in 0.1M PBT. This time, a mouse anti-TH primary antibody and biotinylated IgG horse anti-mouse (Table 2.4) were used. For the DAB colour development, the use of nickel II sulphate and ammonium chloride were omitted, so that cell bodies were stained in a brown precipitant, whereas cFos-positive cell nuclei were black in colour. For each primary and secondary antibody, negative controls were carried out by omission of said antibody in order to ensure binding specificity. None of the controls showed any immunoreactivity. In addition, incubations with pre-immunised serums specific for each primary antibody, and pre-absorbed cFos primary antibodies incubated with purified cFos peptide also showed no immunoreactivity (Hume, 2017; Hume *et al.*, 2017).

Once the immunohistochemistry had been completed, all sections were mounted on gelatine-coated glass microscope slides (Fisher) in a caudo-rostral order and air dried in a sealed container to protect from dust overnight. On the next day, the dried sections were dehydrated by submerging them in solutions of increasing concentrations of ethanol, namely 70% v/v, 90% v/v and 95% v/v for 5mins each, followed by three times 10mins at 100% v/v and finally two 10mins steps in xylene. A glass coverslip was quickly applied to the slides before the xylene had evaporated using DPX Mountant for histology (Sigma) and all slides were left to dry in a fume hood for 48hrs before storage at 4°C and microscopy.

Table 2.3: Solutions used for immunohistochemistry.

Immunofluorescence Solutions	**Ingredients**
Heparinised Saline	0.9% w/v sodium chloride (VWR International) 0.012% w/v heparin sodium salt from porcine intestinal mucosa (Sigma)
Phosphate Buffer (PB), 1M	11.5% w/v sodium phosphate dibasic dehydrate (Sigma) 2.72% w/v sodium phosphate monobasic monohydrate (Sigma) pH 7.4
4% Paraformaldehyde (PAF)	4% paraformaldehyde (Sigma) in 0.1M PB pH 7.4
Post-Fix solution	15% w/v sucrose (Fisher) in 4% PAF
Cryoprotectant	20% v/v glycerol 30% v/v ethylene glycol 50% v/v 0.2M PBS
Phosphate buffered saline (PBS), 1M	0.9% w/v sodium chloride in 1M PB pH 7.4
Blocking solution	10% v/v normal serum in PBT
Carrier solution	2% v/v normal serum in PBT
DAB staining Solutions	**Ingredients**
Phosphate buffered triton (PBT)	0.3% v/v Triton™ X-100 (Sigma) in 0.1M PB pH7.4
Hydrogen peroxide	0.3% v/v hydrogen peroxide (Sigma) in PBT
Blocking buffer	3% v/v normal horse serum in PBT
Avidin-biotin complex	0.2% v/v avidin 0.2% v/v peroxidase in PBT
Tris buffer, 0.5M	6.1% w/v Trizma® base (Sigma) pH 7.6
Diaminobenzidine tetrachloride solution with nickel, ammonium chloride and hydrogen peroxide	0.025% w/v diaminobenzidine tetrachloride (Sigma) 2.5% w/v nickel II sulphate hexahydrate (Sigma) 0.08% w/v ammonium chloride (Fisher) 0.05% v/v hydrogen peroxide in 0.01M Tris buffer

Table 2.4: Antibodies used for immunohistochemistry.

Immunofluorescence antibodies	**Host species**	**Dilution**	**Supplier**
Anti-cFos	rabbit	1/5000 in carrier solution	226 003, Synaptic Systems
Anti-Tyrosine Hydroxylase	mouse	1/1000 in carrier solution	MAB318, Merck Millipore
Anti-rabbit IgG secondary, Alexa Fluor® 488	goat	1/750 in blocking buffer	A-11034, Thermo Fisher Scientific
Anti-mouse IgG secondary, Cy3	goat	1/750 in blocking buffer	A10521, Thermo Fisher Scientific
DAB staining antibodies	**Host species**	**Dilution**	**Supplier**
Anti-cFos	rabbit	1/50,000 in blocking buffer	226 003, Synaptic Systems
Anti-Tyrosine Hydroxylase	mouse	1/2000 in blocking buffer	MAB318, Merck Millipore
Anti-rabbit IgG secondary, biotinylated	horse	1/500 in blocking buffer	BA-1100, Vector Laboratories
Anti-mouse IgG secondary, biotinylated	horse	1/500 in blocking buffer	BA2000, Vector Laboratories

2.5.5 Image acquisition

Images of each brainstem section were captured using a Leica DMR reflected light microscope and LAS V4.5.0 imaging software (Leica). A x5 magnification was used to capture an overview the entire section, whereas a x20 magnification was used to capture images of the dorsal nucleus tractus solitarius (NTS) and area postrema (AP), and the ventrolateral regions that showed TH-positive cell bodies.

For the dorsal regions of interest, three images were stitched together using the LAS imaging software in order to retain the original pixilation for subsequent image analysis.

2.5.6 Image analysis

Using an online tool, regions of the NTS present in the mouse brain atlas (Franklin & Paxinos, 2008) were selected and the background made transparent (Figure 2.4). These “templates” were then overlaid onto each immunohistochemical image using Inkscape version 0.48.2. The template with the best fit for the AP as a landmark was chosen, whereby the size of the template was increased or decreased proportionally to fit the underlying image (Figure 2.5 A). Templates were created for each brain map in the mouse brain atlas that included the AP, which encompassed the following Bregmas: -7.76mm, -7.64mm, -7.56mm, and -7.48mm (Figure 2.4). Any sections that could not be clearly allocated to a specific Bregma from the brain atlas – due to smaller distances between sections cut (60µm) than those illustrated in the atlas (80µm) – were labelled as -7.70mm, -7.60mm, -7.52mm, -7.44mm.

The images with the templates were then further analysed using (FIJI Is Just) ImageJ version 2.0.0-rc-43/1.51s. To measure the surface area for each subnucleus of the NTS, a global scale was set for each image according to the LAS specifications for x20 magnifications. Using the “ROI” plugin and a free-hand drawing tool, each NTS subnucleus and the AP were traced along the template lines and the surface areas measured. Each of the measurements was then multiplied by 30 to account for the 30µm

thickness of each section. Cell counting was done with the help of the “Cell Counter” plugin and each subnucleus was counted manually by clicking on each target with a different corresponding number, and thus colour, for each subnucleus. Each target, be it a cFos-positive nucleus or a cFos-negative/TH-positive cell body, was confirmed by looking directly through the microscope, as this allowed for greater differentiation of background versus true staining and it enabled me to clearly visualise nuclei and cells at different depths of the sections by adjusting the focus. Staining was counted in the dorsal brainstem for total cFos per subnucleus (Figure 2.5 Bi), TH-positive/cFos-negative, and TH-positive/cFos-positive cells (Figure 2.5 Bii). For the ventral brainstem only TH-positive cells were counted and separated for cFos-positive or cFos-negative labelling (Figure 2.5 Biii).

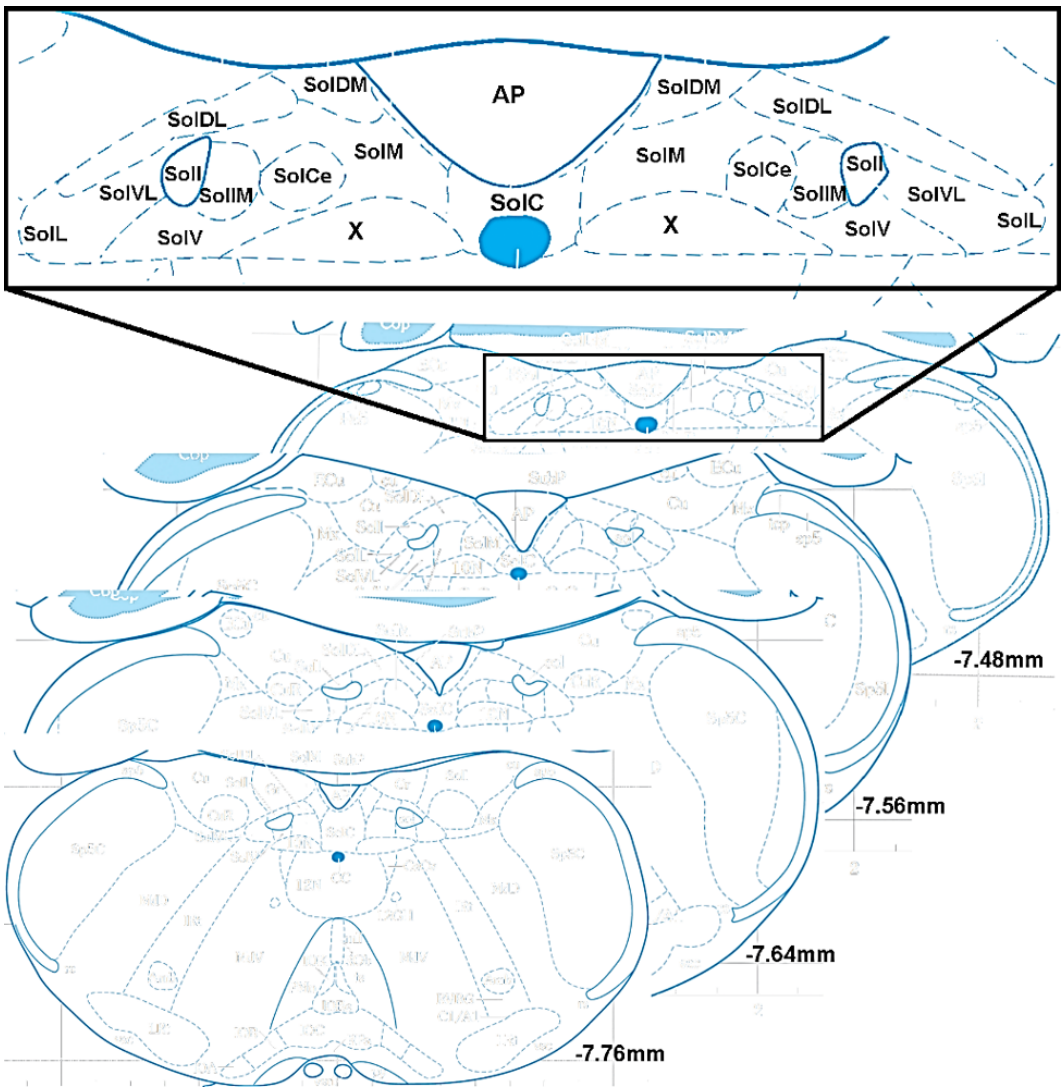

Figure 2.4 Template maps from the Mouse Brain Atlas used to identify subnuclei of the NTS.

Four maps from the Franklin & Paxinos (2008) mouse brain atlas were used to identify regions of interest within the caudal nucleus tractus solitarius at Bregmas that encompassed the area postrema (AP). The individual nuclei that were used for Immunohistochemical studies are shown in the magnified top image. X = Dorsal motor nucleus of the vagus; SolC = commissural nucleus; SolM = medial nucleus; SolDM = dorsomedial nucleus; SolDL = dorsolateral nucleus; SolCe = central nucleus; SolIM = intermediate nucleus; SolI = interstitial nucleus; SolV = ventral nucleus; SolVL = ventrolateral nucleus; SolL = lateral nucleus

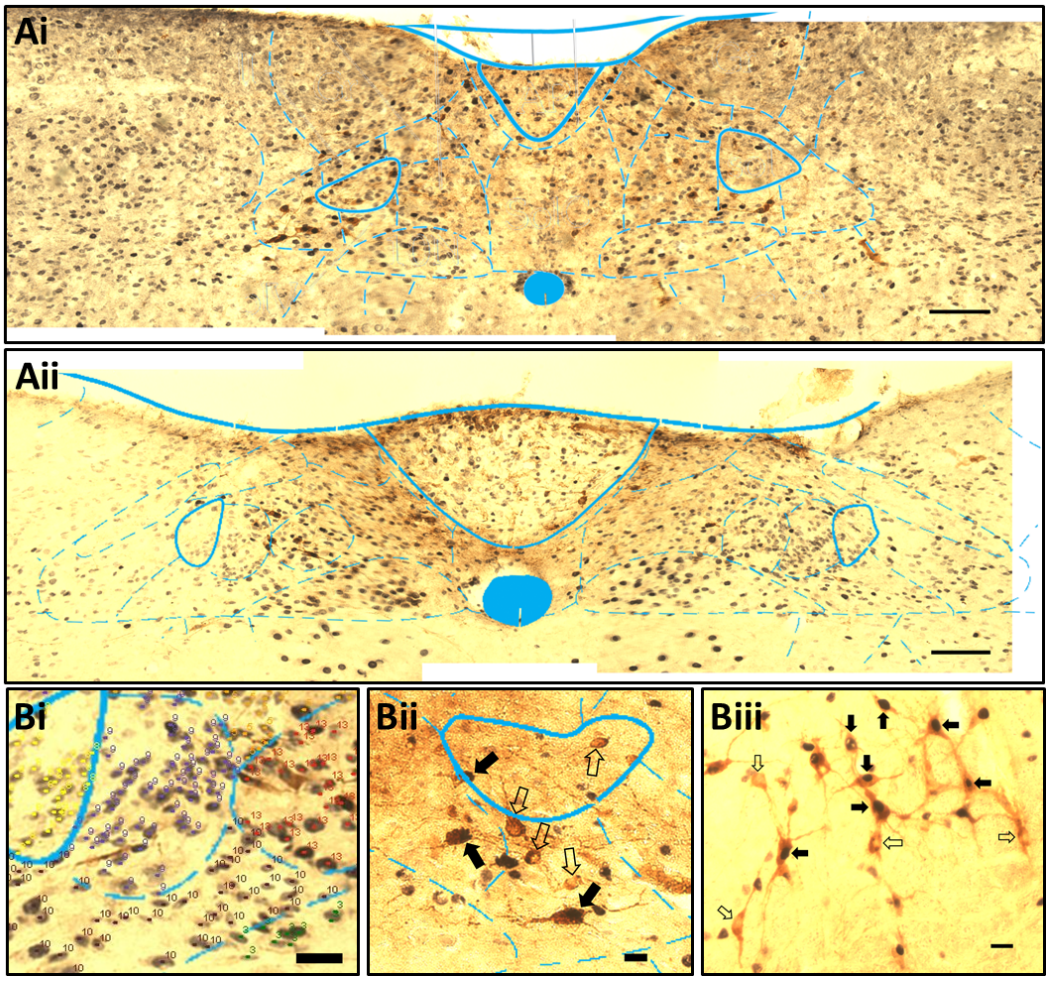

Figure 2.5 Representative immunohistochemistry photomicrographs for double labelling of cFos and tyrosine hydroxylase.

(A) shows exemplary templates from the mouse brain atlas superimposed onto acquired photomicrographs for approximate Bregmas -7.76mm **(Ai)** and -7.48mm **(Aii)**; **(B)** shows an example of how each subregion of the NTS was counted using the Cell Counter plugin in FIJI **(Bi)**, and the counting of TH-positive cell bodies classified into cFOS-positive (black arrows) and cFOS-negative (clear arrows) for the dorsal catecholaminergic A2 **(Bii)** and ventral catecholaminergic A1 **(Biii)** neurons. Scale bars are 100μm for **(A)** and 20μm for **(B)**.

2.6 Metabolic measurements

To confirm ventilatory outcomes, metabolic measurements of O_2 consumption ($\dot{V}O_2$) and CO_2 production ($\dot{V}CO_2$) were carried out independently by David Burns at the University of Cork, Ireland.

Naïve and untrained mice undergoing metabolic measurements were placed in a whole-body plethysmography chamber as described above (Buxco, USA). Airflow through the chamber was maintained at 1l/min. Fractional concentrations of O_2 and CO_2 were measured in air entering and exiting the plethysmography chamber by an O_2 and CO_2 analyser (ADInstruments, Colorado Springs, CO,USA) and transmitted to a computer software with a frequency of 0.1Hz.

Two hypoxic protocols were used for each mouse – a step challenge and a graded hypoxia challenge. The step challenge introduced 8% O_2 (0.05% CO_2, balanced in N_2) immediately following a 5min baseline period at 21% O_2 (0.05% CO_2, balanced in N_2) and lasted for a total of 10min. The graded hypoxia challenge involved a 5min baseline period at 21% O_2 (0.05% CO_2, balanced in N_2), which was then followed by 5min of decreasing O_2 concentrations (18% O_2, 15% O_2, 12% O_2, 10% O_2, 8% O_2, all in 0.05% CO_2, balanced in N_2).

For the hypoxic step challenge data are shown normalised for body mass (g) after 5min of hypoxia and presented in a minute-by-minute basis thereafter. For the graded hypoxic challenge, measurements were taken during the fifth minute of each given O_2 concentration.

2.7 Bioamine High Performance Liquid Chromatography

Finally, the effect of AMPK deletion in catecholaminergic cells on the brainstem bioamine content was assessed by High Performance Liquid Chromatography (HPLC), which was carried out independently by David Burns at the University of Cork, Ireland.

Following completion of all metabolic measurements, experimental mice were returned to their holding cages and allowed to recover and settle for a

minimum of 60min. Mice were culled by dislocation of the neck and trunk blood was collected immediately and placed on ice. In addition, the brainstems and part of the spinal cords were dissected. Samples were then analysed by HPLC at an independent facility within the University of Cork.

2.8 Statistical analyses

All data were presented as the mean±SEM for 'N' exposures and 'n' mice. The analyses, comparisons and generation of Figures were carried out using GraphPad Prism for Windows, Version 6.05 (US). If only two datasets were compared, an unpaired two-tailed t-test was conducted. If comparing between three or more groups of data, the analysis of variance (ANOVA) was tested. For the comparison of data sets with only one independent variable, for example across regions of interest, the analysis was carried out using a one-way ANOVA followed by a post-hoc Tukey multiple comparisons test. If the data set that had two independent variables, for example time and genotype, the comparisons between the groups were carried out using a two-way ANOVA followed by a post-hoc Sidak multiple comparisons test. Probability values less than 0.05 were considered to be statistically significant, whereby * = $p<0.05$, **= $p<0.01$, ***= $p<0.001$ and ****= $p<0.0001$.

Chapter 3: Characterisation of the hypoxic ventilatory response in mice with AMPK deficiency in catecholaminergic cells

3.1 Introduction

3.1.1 AMPK deficiency blocks the hypoxic ventilatory response and thus precipitates hypoventilation

Recent studies have established that deletion of AMPK-α1 and -α2 catalytic subunits in tyrosine hydroxylase (TH)-positive cells (TH AMPK-α1/α2 dKO) attenuates the acute HVR to mild and severe hypoxia (Mahmoud *et al.*, 2016). Rather than hyperventilating, mice lacking AMPK-α1 and -α2 subunits exhibited hypoventilation and more frequent, prolonged apnoeas during hypoxia. In fact, the HVR in response to 8% O_2 was virtually abolished, and anaesthesia further exacerbated ventilatory depression observed during hypoxia. It was found that loss of AMPK-α1 expression was the primary precipitant of the phenotype. Deletion of AMPK-α2 appeared to have little effect, although the AMPK-α1/α2 dKO exhibited a more severe hypoxic phenotype than AMPK-α1 knockouts. Interestingly though, the carotid bodies of TH AMPK-α1/α2 dKO mice – which were also targeted by the conditional knockout – remained exquisitely sensitive to hypoxia, contrary to the view that the HVR is determined solely by increased carotid body afferent input to the brainstem. It was therefore concluded that, at least in this context, deficits in the drive to breathe during hypoxia arose at the level of the brainstem. Importantly, dual deletion of AMPK-α1 and -α2 catalytic subunits had no effect on the hypercapnic ventilatory response. In fact, the hypoxic phenotype of TH AMPK-α1/α2 dKO mice was completely rescued upon exposure to hypoxic hypercapnia, which highlights that AMPK deletion did not compromise the capacity for increased ventilation during hypoxia per se, but rather that AMPK deficiency specifically affects the HVR. AMPK activation may therefore selectively support hyperventilation and protect against hypoxia-induced ventilatory instability that can occur during sleep or ascent to altitude (Ainslie *et al.*, 2013; Panossian & Daley, 2013).

The proposed mechanism suggests a role for AMPK to support coincidence detection and signal integration within a subset of hypoxia-sensitive catecholaminergic neurons of the brainstem. In this setting, AMPK activation may be determined by ‘local hypoxic stress’ subsequent to hypoxic inhibition

of mitochondrial oxidative phosphorylation and thus decreased ATP supply, and 'applied metabolic stress' delivered via increased ATP usage subsequent to peripheral chemoafferent input and neuronal activation (Evans *et al.*, 2016; Mahmoud *et al.*, 2016). Together, the sum of these two pathways may determine the magnitude of activation of AMPK and the brainstem respiratory network during hypoxia due to AMPK-related modulation of cell metabolism, ion channel activity, neuronal firing frequency and/or release of neurotransmitters (Lipton *et al.*, 2001; Murphy *et al.*, 2009; Ikematsu *et al.*, 2011).

3.1.2 The hypoxic ventilatory response is supported by the activation of LKB1-AMPK signalling pathways downstream of the carotid bodies

As mentioned in Chapter 1, AMPK activation can occur through two distinct pathways, involving the upstream kinases LKB1 or Ca^{2+}/CaMKK2 (Hardie *et al.*, 2016). Our most recent investigations therefore considered the role of the LKB1-AMPK pathway and the Ca^{2+}/CaMKKβ-AMPK pathway in mediating the HVR (Evans, 2012; Mahmoud *et al.*, 2015). It was found that global deletion of *Camkk2* was without effect on the HVR. By contrast, in mice with conditional deletion of *Stk11* (the gene encoding LKB1) in catecholaminergic cells, inclusive of carotid body type I cells and brainstem respiratory network, outcomes were similar to those observed in TH AMPK-α1/α2 dKO mice, where hypoxia evoked hypoventilation and apnoea rather than hyperventilation. Furthermore, attenuation of the HVR, albeit less severe, was also conferred in mice carrying ~90% knockdown of LKB1. However, while *Stk11* deletion markedly attenuated carotid body afferent discharge during normoxia, hypoxia, and hypercapnia, afferent input responses were retained following either ~90% knockdown of LKB1 or AMPK-α1/α2 deletion. Therefore, it seems that the LKB1-AMPK pathway, but not the Ca^{2+}/CaMKK2-AMPK pathway, supports the HVR and that it does so as previously proposed (Mahmoud *et al.*, 2016), by acting at a site downstream of the carotid body within brainstem catecholaminergic cells of the respiratory network.

3.1.3 Aims

Given the outcomes from the studies above I sought to test the hypothesis that AMPK activity in catecholaminergic cells continuously supports ventilation during hypoxia beyond the manifestation of the initial sustained phase of the HVR observed at 5min. Accordingly, mice with dual deletion of the AMPK-α1/α2 catalytic subunits in TH-expressing cells (as described in Chapter 2) were exposed to mild (12% O_2, 10min) and severe (8% O_2, 10min and 60min) hypoxia, and their ventilatory phenotype assessed using whole-body plethysmography.

3.2 Results

3.2.1 AMPK deletion in catecholaminergic cells attenuates ventilation throughout 10min exposures to hypoxia

Consistent with previous studies (Mahmoud *et al.*, 2016), deletion of AMPK-α1/α2 catalytic subunits in catecholaminergic cells was found to have no effect on normoxic baseline breathing (Appendix 1.1), but markedly attenuated the HVR during mild and severe hypoxia. However, the data presented here also show that this attenuation continues beyond 5min with no evidence of delayed compensation. Example records of changes in breathing frequency (Figure 3.1 Ai), tidal volume (Figure 3.3 Ai) and minute ventilation (Figure 3.4 Ai) illustrate the difference between AMPK-α1/α2 Flx and TH AMPK-α1/α2 dKO mice in response to 10min exposures to 12% O_2 or 8% O_2. Whereas control AMPK-α1/α2 Flx mice responded to hypoxia with robust increases in ventilation which later stayed slightly above or returned to baseline values, TH AMPK-α1/α2 dKO mice were unable to maintain an equivalent level of ventilation. Notably, the severity of ventilatory depression observed in TH AMPK-α1/α2 dKO mice was PO_2-dependent.

3.2.1.1 Breathing frequency

5min exposures to mild hypoxia As depicted in Figure 3.1 Ai, control AMPK-α1/α2 Flx mice responded to mild hypoxia (12% O_2) with increases in breathing frequency. Following the onset of hypoxia, values reached 57.4 ± 3.9% relative to normoxia (n = 37 exposures from 14 mice) during the peak of the Augmenting phase (A) and then declined during ventilatory Roll-Off (RO) to 27.5 ± 2.4%. On average, this level of ventilation was maintained during the Sustained Phase (SP), where breathing frequency measured 27.2 ± 3%.

TH AMPK-α1/α2 dKO mice displayed a comparable response during the Augmenting phase, increasing breathing frequency by 47.9 ± 3.5% relative to normoxia (n = 28 exposures from 11 mice). However, thereafter frequency

was significantly decreased during the RO (14.5 ± 3.1%, $p<0.05$) and SP (14.2 ± 2.8%, $p<0.05$).

5min exposures to severe hypoxia During severe hypoxia (8% O_2, Figure 3.1 Bii), more pronounced differences were observed between genotypes. Both AMPK-α1/α2 Flx and TH AMPK-α1/α2 dKO mice increased their breathing frequency during the Augmenting phase. However, while control AMPK-α1/α2 Flx mice responded with an increase of 63.8 ± 4% (n = 54 exposures from 21 mice), TH AMPK-α1/α2 dKO mice had a significantly attenuated augmenting phase, reaching only 47.1 ± 3.3% (n = 49 exposures from 21 mice, $p<0.001$). Thereafter, respiratory depression reduced breathing frequency in AMPK-α1/α2 Flx mice to 9.5 ± 2.4%, a level of ventilation that was maintained during the SP (11.9 ± 2.4%). In marked contrast, TH AMPK-α1/α2 dKO mice fell into hypoventilation relative to normoxia during RO (-15.8 ± 2.8%), where breathing frequency was significantly lower than for control AMPK-α1/α2 Flx mice ($p<0.0001$). This significant attenuation was still evident during the SP, when breathing frequency measured -9 ± 2.2% ($p<0.0001$ relative to AMPK-α1/α2 Flx).

10min exposures to mild hypoxia Differences between genotypes in the HVR were also evident during more prolonged 10min exposures to hypoxia (Figure 3.2 A). Measurements taken at each full minute of hypoxia showed that breathing frequencies during mild hypoxia were higher for control AMPK-α1/α2 Flx mice than TH AMPK-α1/α2 dKO mice (Figure 3.2 Ai; controls n = 37 exposures from 14 mice, knockouts n = 28 exposures from 11 mice). Although only statistically significant during the first half of the response (controls versus knockouts – at 1min: 49.6 ± 3.1% versus 24.7 ± 2.3%, $p<0.0001$; at 5min: 26.3 ± 3.1% versus 12.6 ± 2.8%, $p<0.01$), average frequencies of TH AMPK-α1/α2 dKO mice remained attenuated throughout the exposure (controls versus knockouts – at 6min: 26.6 ± 2.8% versus 15.9 ± 2.9%, not significant; at 10min: 22.2 ± 2.8% versus 11.9 ± 2.5%, not significant).

10min exposures to severe hypoxia During severe hypoxia, breathing frequencies of TH AMPK-α1/α2 dKO mice were significantly attenuated relative to controls at each minute measured throughout the exposure (Figure 3.2 Aii; controls: n = 55 exposures from 21 mice versus knockouts: n = 40 exposures from 18 mice – at 1min: 28.4 ± 2.5% versus 0.9 ± 4.1%, $p<0.0001$; at 5min: 11.4 ± 2.4% versus -11.8 ± 2.7%, $p<0.0001$; at 10min: 6.9 ± 2.4% versus -10.6 ± 3.3%, $p<0.0001$).

These outcomes suggest that while TH AMPK-α1/α2 dKO mice are initially able to produce an, albeit reduced, augmentation of breathing frequency during hypoxia, they are unable to maintain normal hyperventilatory activity during severe hypoxia with breathing frequency very quickly dropping below normoxic baseline measurements throughout the remainder of the hypoxic period.

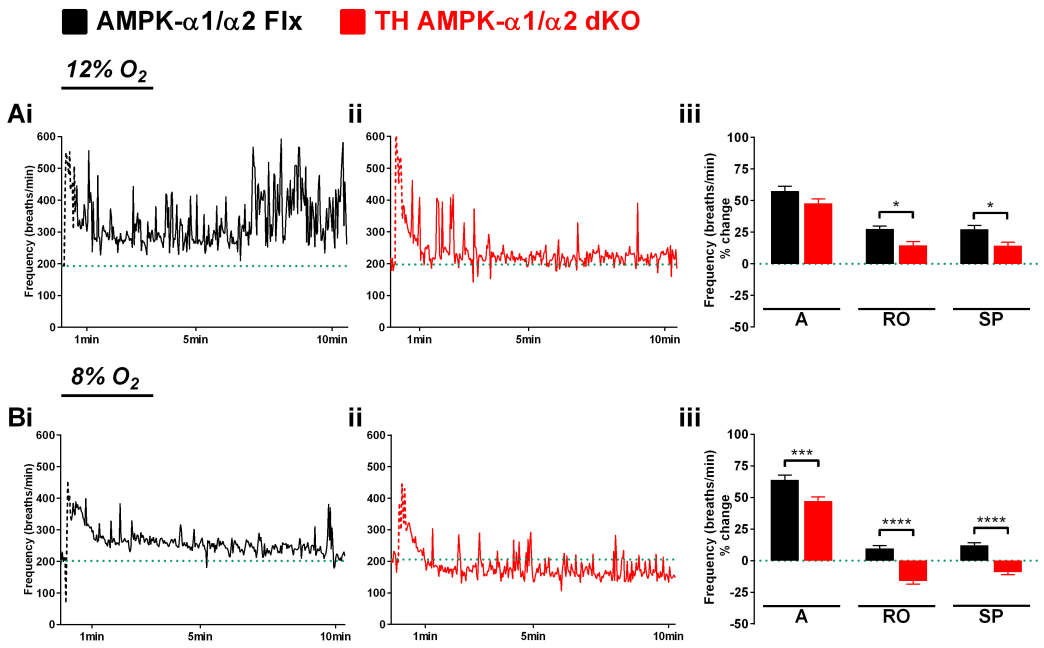

Figure 3.1: The breathing frequency of TH AMPK-α1/α2 dKO mice is attenuated during acute hypoxia in a PO_2-dependent manner.

Left and middle panels show raw example records of breathing frequencies (breaths/min) during 10 minute exposures to **(A)** mild hypoxia (12% O_2) and **(B)** severe hypoxia (8% O_2) of **(i)** AMPK-α1 and -α2 floxed (AMPK-α1/α2 Flx, black) and **(ii)** TH-driven AMPK-α1 and -α2 double knockout (TH AMPK-α1/α2 dKO, red) mice with a 2s sampling frequency. Dotted green lines indicate pre-hypoxic baseline frequencies, dashed lines the artefacts induced by gas exchange. Right panels **(iii)** show means ± SEM for percentage changes of breathing frequency during the peak of the Augmenting phase (A, approximately 30s), the nadir of the Roll-Off (RO, approximately 100s), and the plateau of the sustained phase (SP, at 300s) of the HVR in AMPK-α1/α2 Flx (12% O_2: n = 37 exposures from 14 mice, 8% O_2: n = 54 exposures from 21 mice) and TH AMPK-α1/α2 dKO mice (12% O_2: n = 28 exposures from 11 mice, 8% O_2: n = 49 exposures from 21 mice). * = $p<0.05$, *** = $p<0.001$, **** = $p<0.0001$. Significance tested by two-way ANOVA with Sidak post-hoc tests.

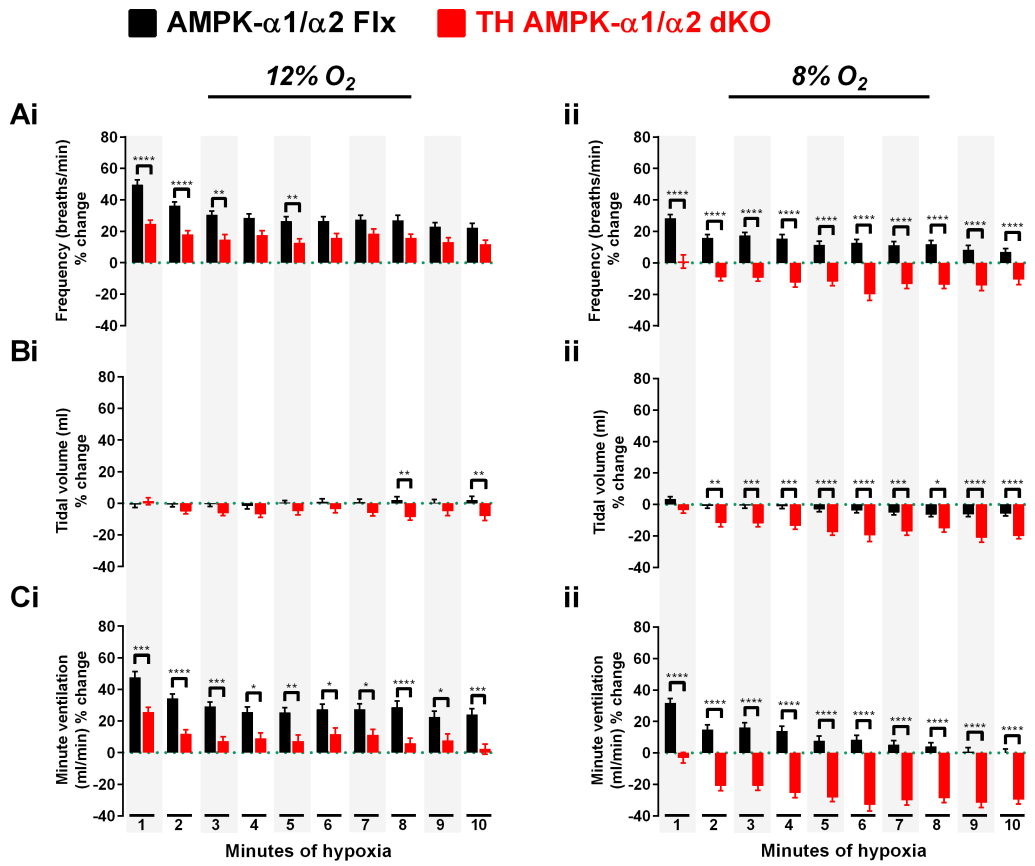

Figure 3.2: The PO_2-dependent attenuation of breathing frequency, tidal volume, and minute ventilation in TH-driven AMPK-α1/α2 knockout mice persists beyond the early hypoxic ventilatory response. Means ± SEM for percentage changes of **(A)** breathing frequency (breaths/min), **(B)** tidal volume (ml), and **(C)** minute ventilation (ml/min) during 10 minute exposures to **(i)** mild hypoxia (12% O_2) and **(ii)** severe hypoxia (8% O_2) in AMPK-α1 and -α2 floxed mice (AMPK-α1/α2 Flx, black, 12% O_2: n = 37 exposures from 14 mice, 8% O_2: n = 55 exposures from 21 mice) and TH-driven AMPK-α1 and -α2 double knockout mice (TH AMPK-α1/α2 dKO, red, 12% O_2: n = 28 exposures from 11 mice, 8% O_2: n = 40 exposures from 18 mice) measured at each full minute of hypoxia. * = p<0.05, ** = p<0.01, *** = p<0.001, **** = p<0.0001. Significance tested by two-way ANOVA with Sidak post-hoc tests.

3.2.1.2 Tidal volume

5min exposures to mild hypoxia In marked contrast to the hypoxia-induced increases in breathing frequency, only marginal changes in tidal volume were observed. During mild (12% O_2) hypoxia (Figure 3.3 Aii), measurements for AMPK-α1/α2 Flx mice were 1.9 ± 2.5% relative to normoxia during the Augmenting phase, -1.7 ± 2% for RO, and 0.1 ± 1.7% during the SP. Interestingly, for TH AMPK-α1/α2 dKO mice measures (relative to normoxia) of tidal volume during hypoxia were lower at -3.1 ± 1.6% during the Augmenting phase, -4.2 ± 2.3% for RO, and -5.3 ± 2.4% during the SP, but these differences did not reach significance relative to controls at any stage during 5 min exposures.

5min exposures to severe hypoxia Changes in tidal volume of control AMPK-α1/α2 Flx mice during severe hypoxia (Figure 3.3 Bii) were comparable to those during mild hypoxia, with measurements of -2.1 ± 1.5% during the Augmenting phase, 1.2 ± 1.8% for RO, and -1.8 ± 1.7% during the SP. However, in TH AMPK-α1/α2 dKO mice measures of tidal volume during severe hypoxia were attenuated when compared to controls. Despite being more than twice the deficit, the reduction in tidal volume relative to normoxia during the Augmenting phase was not significantly different in TH AMPK-α1/α2 dKO mice compared to AMPK-α1/α2 Flx mice (-5.4 ± 1.4%, not significant). Following this, however, measurements during RO and the SP were significantly attenuated compared to controls (RO: -5.0 ± 2.1%, $p<0.05$; SP: -14.6 ± 1.9%, $p<0.0001$).

10min exposures to mild hypoxia During slightly longer exposures to mild hypoxia, the changes in tidal volume of control AMPK-α1/α2 Flx mice were minimal compared to measures obtained during normoxia (Figure 3.2 Bi; at 1min: -0.7 ± 2.1%; at 5min: 0.4 ± 1.5%; at 10min: 2 ± 2.4%). Despite being on average lower at each time point, the changes in tidal volume in TH AMPK-α1/α2 dKO mice during mild hypoxia were comparable to controls, but reached significance by the eighth and tenth minute of 10min exposures (Figure 3.4 Bi; at 1min: 1.3 ± 2.2%, not significant; at 5min: -4.9 ± 2.4%, not significant; at 10min: -8 ± 2.9%, $p<0.01$).

10min exposures to severe hypoxia During severe hypoxia, differences between genotypes were much more evident (Figure 3.2 Bii). Similar to outcomes for 5min exposures, increases in tidal volume in TH AMPK-α1/α2 dKO mice were attenuated after 1min of hypoxia, although no significant different was apparent at this point between controls (3.3 ± 1.8%) and knockouts (-3.3 ± 2.2%). Thereafter, significant attenuation of tidal volume in TH AMPK-α1/α2 dKO mice compared to controls was observed for the remainder of the exposure (controls versus knockouts – at 2min: -0.8 ± 1.6% versus -11.6 ± 2.5%, $p<0.01$; at 5min: -2.9 ± 1.6% versus -17.6 ± 1.9%, $p<0.0001$; at 10min: -5.8 ± 1.5% versus -19.9 ± 1.8%, $p<0.0001$).

From this, it would appear that TH AMPK-α1/α2 dKO mice do not only breathe slower, but also take smaller breaths during severe hypoxia than control mice.

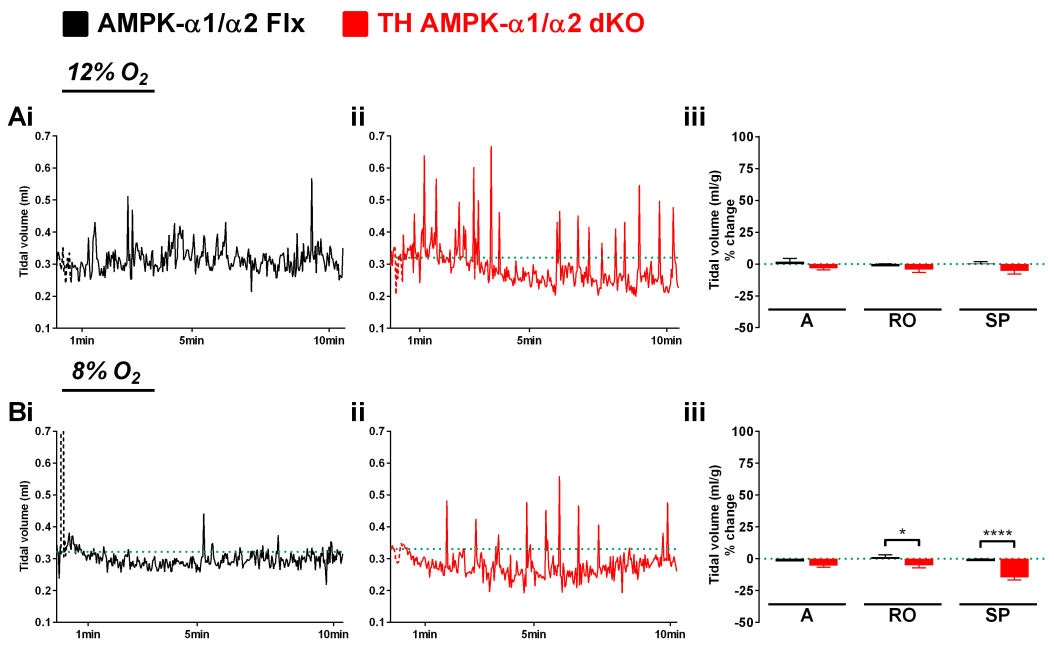

Figure 3.3: The tidal volume of TH AMPK-α1/α2 dKO mice is attenuated during acute hypoxia in a PO_2-dependent manner.

Left and middle panels show raw example records of tidal volumes (ml) during 10 minute exposures to **(A)** mild hypoxia (12% O_2) and **(B)** severe hypoxia (8% O_2) of **(i)** AMPK-α1 and -α2 floxed (AMPK-α1/α2 Flx, black) and **(ii)** TH-driven AMPK-α1 and -α2 double knockout (TH AMPK-α1/α2 dKO, red) mice with a 2s sampling frequency. Dotted green lines indicate pre-hypoxic baseline tidal volume, dashed lines the artefacts induced by gas exchange. Right panels **(iii)** show means ± SEM for percentage changes of tidal volume during the peak of the Augmenting phase (A, approximately 30s), the nadir of the Roll-Off (RO, approximately 100s), and the plateau of the sustained phase (SP, at 300s) of HVR in AMPK-α1/α2 Flx (12% O_2: n = 37 exposures from 14 mice, 8% O_2: n = 54 exposures from 21 mice) and TH AMPK-α1/α2 dKO mice (12% O_2: n = 28 exposures from 11 mice, 8% O_2: n = 49 exposures from 21 mice). * = $p<0.05$, **** = $p<0.0001$. Significance tested by two-way ANOVA with Sidak post-hoc tests.

3.2.1.3 Minute ventilation

5min exposures to mild hypoxia Adjustments of minute ventilation followed a similar trend to breathing frequency. During mild hypoxia (Figure 3.4 Aii), control AMPK-α1/α2 Flx mice responded with an increase of 58 ± 4% relative to normoxia during the Augmenting phase, which then declined to 23.5 ± 2.8% during RO and 26.1 ± 3.5% for the SP. Compared to this, each of these measurements was significantly attenuated in TH AMPK-α1/α2 dKO mice, measuring 42.9 ± 3.8% during the augmenting phase ($p<0.05$), 8.6 ± 3% during RO ($p<0.05$) and 8.3 ± 4.1% for the SP ($p<0.01$).

5min exposures to severe hypoxia During severe hypoxia (Figure 3.4 Bii), control AMPK-α1/α2 Flx mice responded with a similar initial augmentation to mild hypoxia, increasing minute ventilation to 58.8 ± 3.8% relative to normoxia. Thereafter, however, minute ventilation was slightly more depressed during severe hypoxia, reaching 10.5 ± 3.3% during RO and 9.2 ± 3% for the SP. As would be expected given the outcomes for frequency and tidal volume, minute ventilation was significantly attenuated in TH AMPK-α1/α2 dKO compared to control mice at each point measured (A: 38.2 ± 3.4%, $p<0.0001$; RO: -22 ± 2.8%, $p<0.0001$; SP: -23.8 ± 2.1%, $p<0.0001$).

10min exposures to mild hypoxia In stark contrast to breathing frequency and tidal volume, each measurement of minute ventilation during 10min exposures to mild hypoxia was significantly attenuated in TH AMPK-α1/α2 dKO mice compared to control AMPK-α1/α2 Flx mice (Figure 3.2 Ci; controls versus knockouts – at 1min: 47.5 ± 3.7% versus 25.7 ± 3%, $p<0.001$; at 5min: 25.3 ± 3.1% versus 7.2 ± 3.9%, $p<0.01$; at 10min: 24 ± 3.8% versus 2.3 ± 3.2%, $p<0.001$).

10min exposures to severe hypoxia Not surprisingly, however, given the 10min outcomes for breathing frequency and tidal volume during severe hypoxia described above, minute ventilation was also significantly attenuated in TH AMPK-α1/α2 dKO mice at every time point measured during exposures to severe hypoxia (8% O_2, Figure 3.2 Cii; controls versus knockouts – at 1min: 31.8 ± 2.9% versus -3.1 ± 3.3%, $p<0.0001$; at 5min: 7.8 ± 3% versus -28.2 ± 2.7%, $p<0.0001$; at 10min: 0 ± 2.4% versus -29.4 ± 3%, $p<0.0001$).

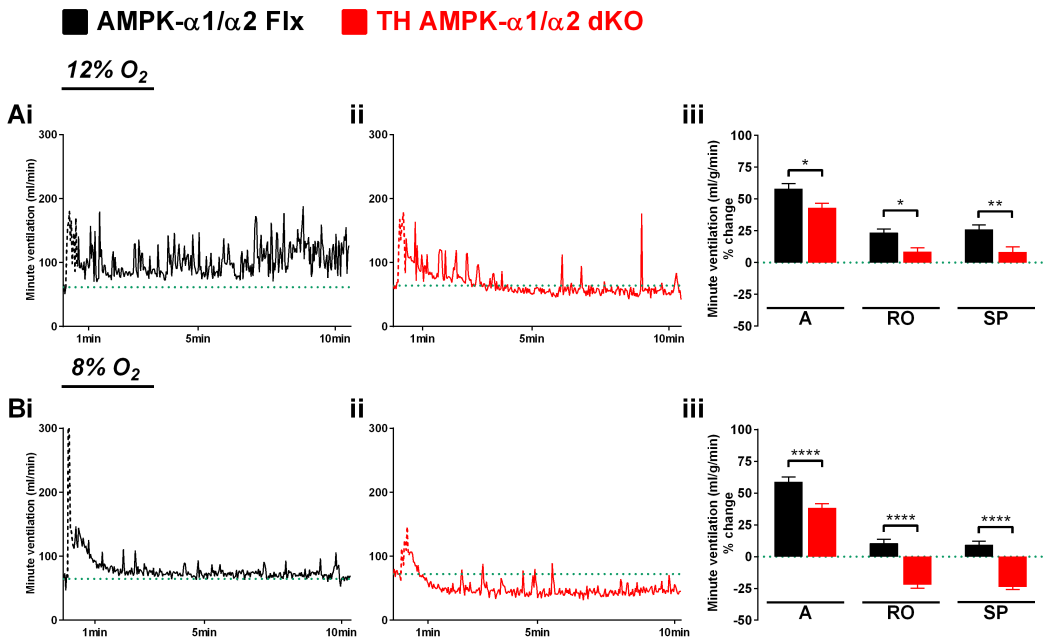

Figure 3.4: The minute ventilation of TH AMPK-α1/α2 dKO mice is attenuated during acute hypoxia in a PO_2-dependent manner.

Left and middle panels show raw example records of minute ventilation (ml/min) during 10 minute exposures to **(A)** mild hypoxia (12% O_2) and **(B)** severe hypoxia (8% O_2) of **(i)** AMPK-α1 and -α2 floxed (AMPK-α1/α2 Flx, black) and **(ii)** TH-driven AMPK-α1 and -α2 double knockout (TH AMPK-α1/α2 dKO, red) mice with a 2s sampling frequency. Dotted green lines indicate pre-hypoxic baseline minute ventilation, dashed lines the artefacts induced by gas exchange. Right panels **(iii)** show means ± SEM for percentage changes of minute ventilation during the peak of the Augmenting phase (A, approximately 30s), the nadir of the Roll-Off (RO, approximately 100s), and the plateau of the sustained phase (SP, at 300s) of the HVR in AMPK-α1/α2 Flx (12% O_2: n = 37 exposures from 14 mice, 8% O_2: n = 54 exposures from 21 mice) and TH AMPK-α1/α2 dKO mice (12% O_2: n = 28 exposures from 11 mice, 8% O_2: n = 49 exposures from 21 mice). * = $p<0.05$, ** = $p<0.01$, **** = $p<0.0001$. Significance tested by two-way ANOVA with Sidak post-hoc tests.

3.2.2 The attenuation of hypoxic ventilation in mice with deletion of AMPK in catecholaminergic cells is not compensated for by changes in metabolism

The fact that TH AMPK-α1/α2 dKO mice enter a torpor-like state during hypoxia (Mahmoud *et al.*, 2016) along with the observed ventilatory depression of TH AMPK-α1/α2 dKO mice described above could be indicative of a hypometabolic response (Guppy & Withers, 1999). It was therefore of interest to assess the metabolic responses of control AMPK-α1/α2 Flx and TH AMPK-α1/α2 dKO mice during hypoxia, the experiments of which were carried out by Mr David Burns at the University of Cork (Prof Ken O'Halloran's group).

Metabolic rates during normoxia (21% O_2) were comparable between control AMPK-α1/α2 Flx and TH AMPK-α1/α2 dKO mice, measuring 0.07 ± 0.03ml/g/min (n = 11 mice) and 0.08 ± 0.02ml/g/min (n = 12 mice), respectively, for oxygen consumption (VO_2), and 0.03 ± 0.009ml/g/min and 0.03 ± 0.001ml/g/min, respectively, for carbon dioxide production (VCO_2) (Figure 3.5 Ai and Bi).

During 10min exposures to 8% O_2 (Figure 3.5 Aii and Bii), control AMPK-α1/α2 Flx mice displayed a reduction of VO_2 relative to normoxia which measured 0.038 ± 0.03ml/g/min (n = 9 mice) by 5min, and 0.038 ± 0.02ml/g/min by 10min. Likewise, VCO_2 was reduced relative to normoxia in control mice, measuring 0.028 ± 0.02ml/g/min by 5min, and 0.024 ± 0.01ml/g/min at 10min. Compared to this, the VO_2 of TH AMPK-α1/α2 dKO mice displayed minimal differences relative to controls, measuring 0.028 ± 0.03ml/g/min (n = 10 mice) by 5min (not significant) and 0.027 ± 0.02ml/g/min (not significant) at 10min. Similarly, VCO_2 was not significantly different compared to control mice, measuring 0.022 ± 0.03ml/g/min by 5min (not significant) and 0.017 ± 0.02ml/g/min (not significant) by 10min. This shows that TH AMPK-α1/α2 dKO mice do not alter their metabolic rates relative to controls during sudden 10min exposures of 8% O_2.

Furthermore, O_2 consumption and CO_2 production were assessed during 5min exposures to graded hypoxia (5min, each, of 21% O_2, 18% O_2, 15% O_2, 12% O_2, 10% O_2, 8% O_2; Figure 3.5 Aiii and Biii). A progressive reduction

in O_2 availability that lasted for a total of 25min also revealed no differences between control (n = 11 mice) and TH AMPK-α1/α2 dKO mice (n = 12) with respect to the gradual reductions of VO_2 and VCO_2, respectively (Figure 3.5 Aiii and Biii).

Collectively, the data above show that the depressed ventilatory phenotype of TH AMPK-α1/α2 dKO mice during hypoxia is not compensated for by entering into a hypometabolic state. This therefore indicates that deletion of AMPK-α1 and -α2 catalytic subunits in catecholaminergic cells results in true hypoventilation during hypoxia.

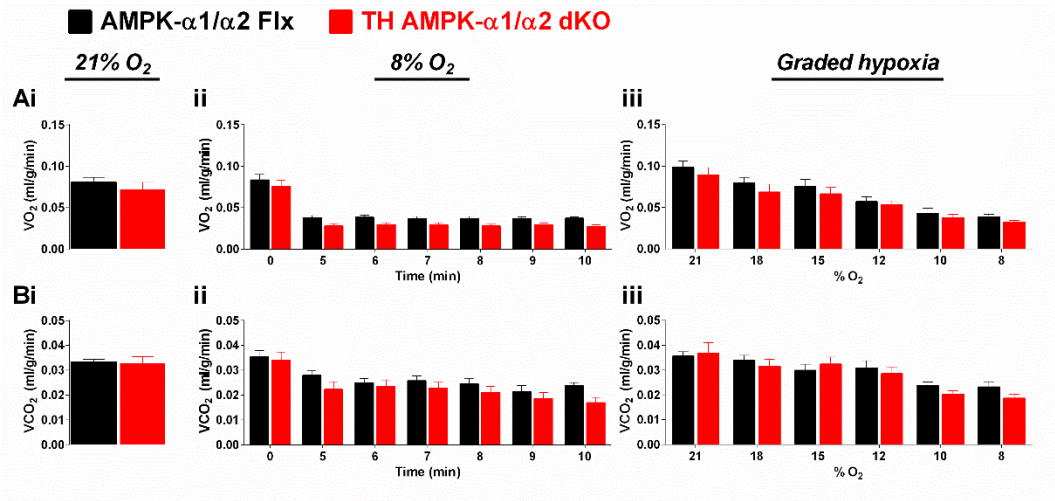

Figure 3.5: Metabolic responses during hypoxia are unaffected in TH-driven AMPK-α1/α2 knockout mice.

Means ± SEM for **(A)** oxygen consumption (VO_2) and **(B)** carbon dioxide production (VCO_2) during **(i)** normoxia (21% O_2), **(ii)** 10min of 8% O2, and **(iii)** 5min exposures to graded hypoxia (21% O_2, 18% O_2, 15% O_2, 12% O_2, 10% O_2, 8% O_2) in AMPK-α1 and -α2 floxed mice (AMPK-α1/α2 Flx, black, 21% O_2: n = 11 mice; 8% O_2: n = 9 mice; graded hypoxia: n = 11 mice) and TH-driven AMPK-α1 and -α2 double knockout mice (TH AMPK-α1/α2 dKO, red, 21% O_2: n = 12 mice; 8% O_2: n =10 mice; graded hypoxia: n = 12 mice). Significance tested by t-test for **(i)** and two-way ANOVA with Sidak post-hoc tests for **(ii)** and **(iii)**.

Collection of metabolic data was performed in collaboration with David Burns at the University of Cork and analysed by me.

3.2.3 AMPK deletion in catecholaminergic cells attenuates ventilation throughout 60min exposures to hypoxia

More prolonged 60min exposures to severe hypoxia (8% O_2) were used to assess whether the ventilatory deficit of TH AMPK-α1/α2 dKO mice observed during 5min and 10min exposures to hypoxia in naïve mice might continue during longer exposures or show a delayed recovery during later phases of the HVR. During the experiments it quickly became obvious that a subset of experimental TH AMPK-α1/α2 dKO mice (3 out of 7, Figure 3.6 Bi-iii)) had to be excluded from the group analysis due to their highly disordered breathing patterns, as shown in Figures 3.6 B and 3.7 B. The raw box flow records showed that the respiratory pattern in these mice started to become increasingly disordered around 20-30min of hypoxia, indicated by failure to clearly identify inspiratory and expiratory peaks in the box flow traces (Figure 3.7). Moreover, by the end of the exposure these mice had lost all ventilatory rhythmicity, whereas all of the control AMPK-α1/α2 Flx mice (6 out of 6) retained rhythmicity until the end of the 60min exposure. Furthermore, observations of the animal behaviour (chest movements) during the experiment did not match the ventilatory values computed by the FinePointe plethysmography software. For example, breathing frequencies for the raw box flow record shown in Figure 3.7 B were computed as an average of 356 ± 92 breaths per minute, which is in the range of breathing frequencies obtained during periods of sniffing or grooming. Yet all TH AMPK-α1/α2 dKO mice were observed to be exquisitely quiet throughout the exposures with minimal movements sparsely scattered throughout the hypoxic period. In the end, 4 out of 7 TH AMPK-α1/α2 dKO mice could be analysed for their ventilatory phenotype during 60min of 8% O_2 and were compared to 5 control AMPK-α1/α2 Flx mice (one control mouse did not produce a useable baseline to measure % change during hypoxia).

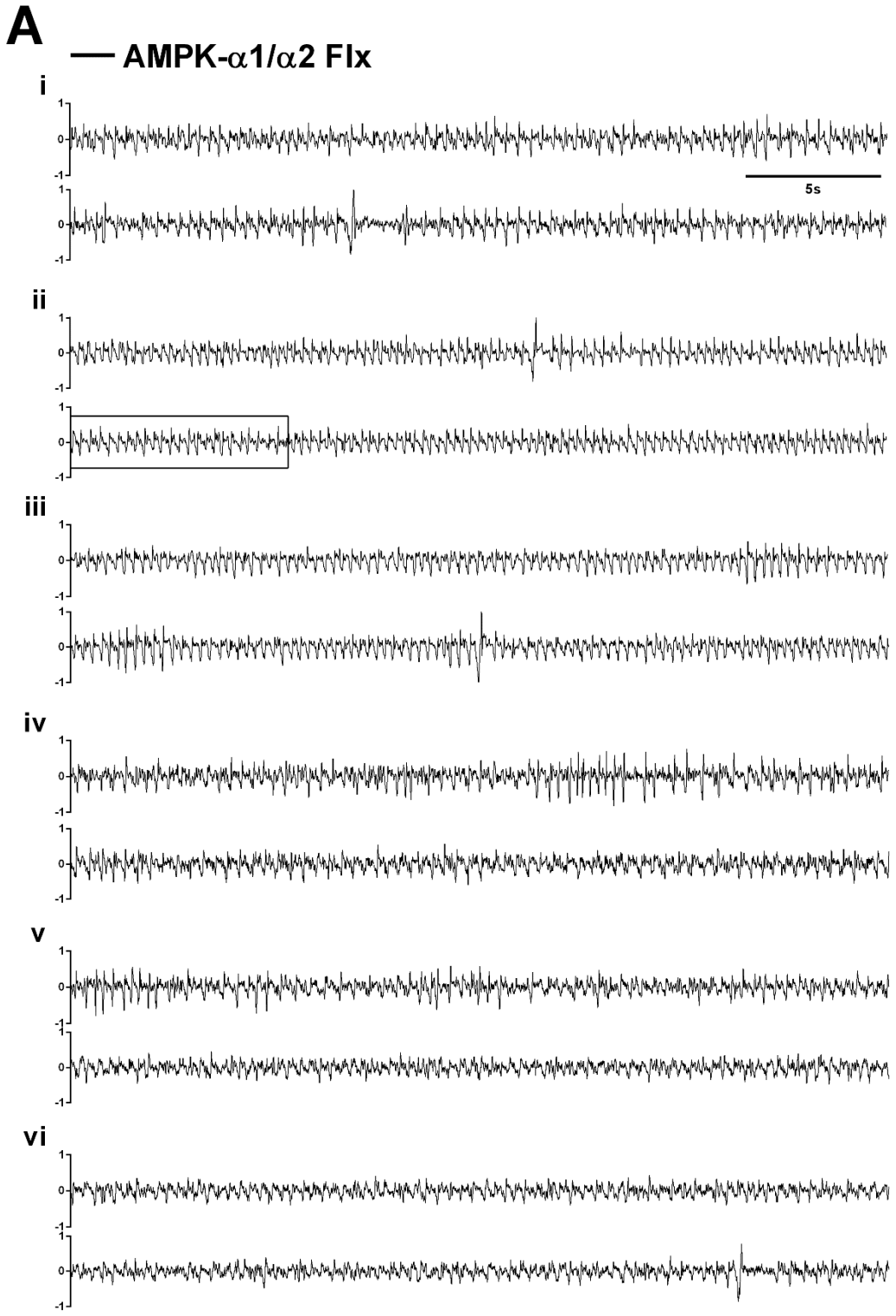

Figure continued overleaf, legend on page 91.

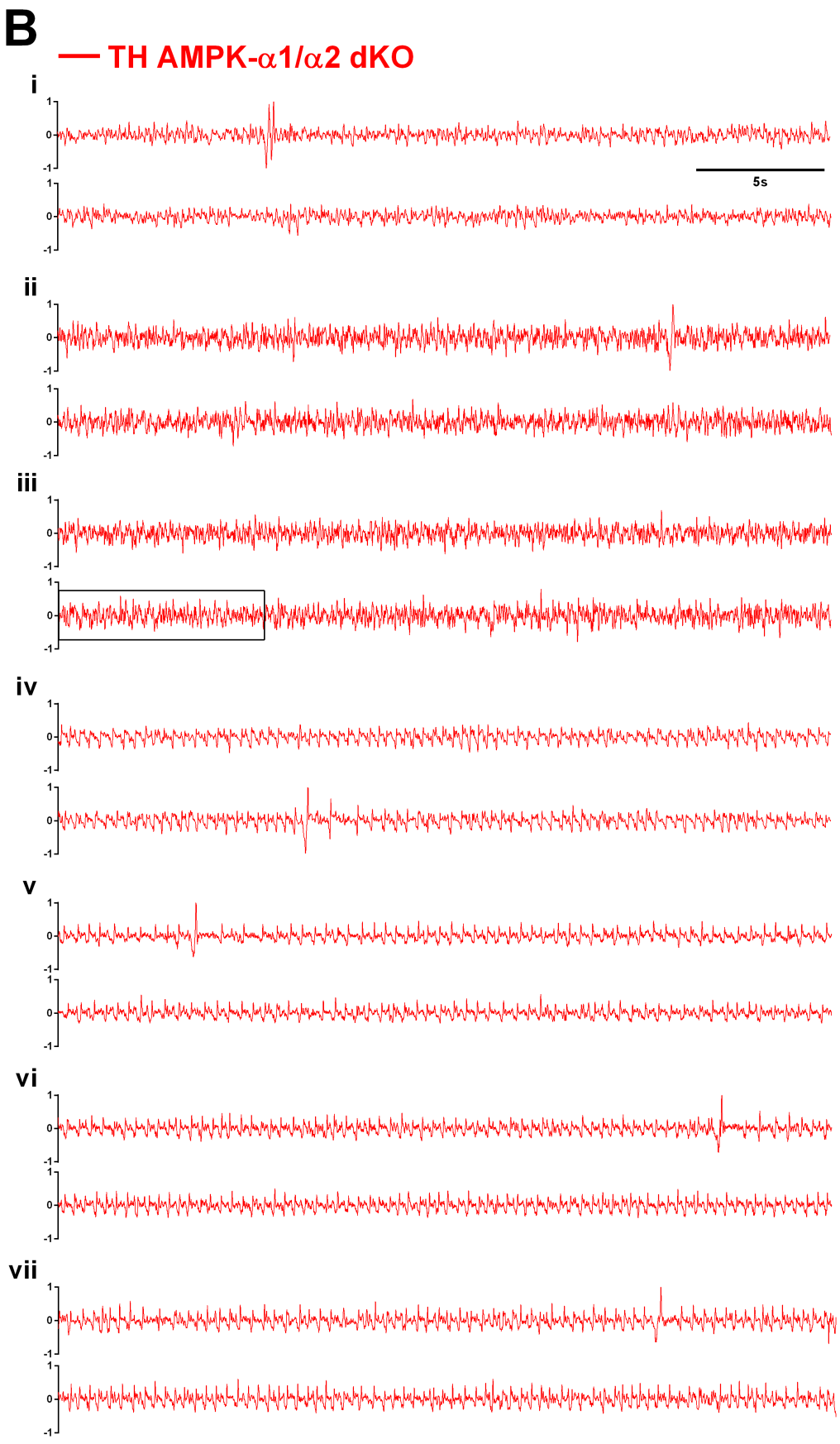
B
— TH AMPK-α1/α2 dKO
i
ii
iii
iv
v
vi
vii
5s

Figure 3.6: Example records showing the breathing patterns of control and TH-driven AMPK-α1/α2 knockout mice during prolonged exposures to severe hypoxia.

Raw box flow traces of ventilatory activity in **(A)** six (**i** – **vi**) AMPK-α1 and -α2 floxed (AMPK-α1/α2 Flx, black) and **(B)** seven (**i** – **vii**) TH-driven AMPK-α1 and -α2 double knockout (TH AMPK-α1/α2 dKO, red) mice during the 60th minute of severe hypoxia (8% O_2). Boxed regions in records Aii and Biii were magnified and displayed in Figure 3.7.

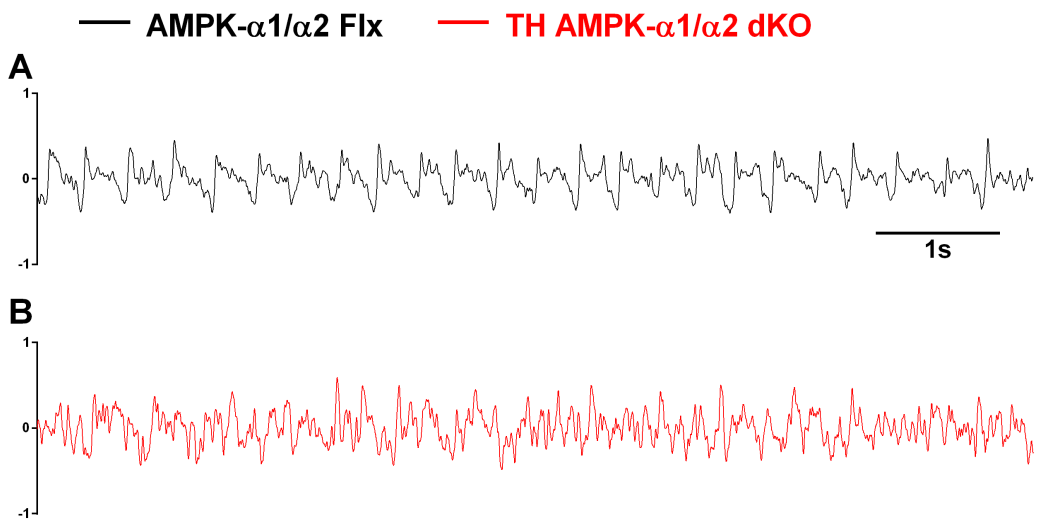

Figure 3.7: Expanded view of the disordered breathing pattern in TH-driven AMPK-α1/α2 knockout mice during prolonged exposures to severe hypoxia.

Expanded box flow traces from boxed-in records in Figure 3.6 showing the individual breaths of one **(A)** AMPK-α1 and -α2 floxed (AMPK-α1/α2 Flx, black, Figure 3.6 Aii) and one **(B)** TH-driven AMPK-α1 and -α2 double knockout (TH AMPK-α1/α2 dKO, red, Figure 3.6 Biii) mouse during the 60th minute of severe hypoxia (8% O_2).

3.2.3.1 Breathing frequency

As shown in Figure 3.8 A, the sustained phase of breathing frequencies in naïve AMPK-α1/α2 Flx (n = 5) mice appeared to only last for 10min. Thereafter, frequency declined slightly but remained augmented relative to normoxia. Importantly, breathing frequencies remained stable from 10min until the end of the exposure at 60min, measuring 6.1 ± 0.9% by 10-15min, 8.4 ± 1.1% by 30-35min, and 7.6 ± 1.6% by 55-60min.

Compared to controls, the breathing frequencies of naïve TH AMPK-α1/α2 dKO mice (n = 4) were significantly attenuated throughout the entire 60min period. That said, the most severe ventilatory deficiency appeared to occur during the first 10-15min of hypoxia, where breathing frequencies in TH AMPK-α1/α2 dKO mice declined to -21.4 ± 1.7% by 5-10min ($p<0.01$ compared to controls) and -19.5 ± 0.7% by 10-15min ($p<0.001$ compared to controls). Curiously, a recovery of frequency occurred after 10-15min of hypoxia, whereby values slowly increased for approximately 20min and then plateaued slightly below normoxic values (30-35min: -6.1 ± 1.2%, $p<0.001$ compared to controls; 55-60min: -3.4 ± 0.7%, $p<0.01$ compared to controls).

Overall, however, TH AMPK-α1/α2 dKO mice did not recover their respiratory frequency to the level observed for controls and instead continued to display an attenuated breathing frequency and hypoventilation for the entire duration of the hypoxic exposure.

3.2.3.2 Tidal volume

Measurements for control AMPK-α1/α2 Flx mice showed a time-dependent reduction in tidal volume (Figure 3.8 B). Consistent with outcomes from 10min exposures, tidal volume fell below normoxic values within 5-10min (-10.5 ± 0.8%), but then continued to decline to -20.9 ± 1.2% by 15-20min before decreasing at a slower rate for the remainder of the 60min exposure (30-35min: -24.5 ± 0.2%; 55-60min: -29.4 ± 1.1%).

The tidal volume response of TH AMPK-α1/α2 dKO mice from these experiments was somewhat unexpected. Unlike outcomes from previous experiments, for the first 20min of the exposure the changes in tidal volume

for this cohort of mice were comparable to the response of controls (0-5min: 3.9 ± 1.5%, not significant; 15-20min: -25.3 ± 2.1%, not significant). Even more surprising was the fact that, although reduced relative to normoxia, the tidal volume of these TH AMPK-α1/α2 dKO mice was significantly higher compared to controls between 5-10min (-4.3 ± 2%, $p<0.05$). Following this period, however, TH AMPK-α1/α2 dKO mice exhibited a faster decline of tidal volume which slowed around 25mins of hypoxia and thereafter remained significantly lower than that of control mice (30-35min: -31 ± 1.3%, $p<0.01$; 55-60min: -37.9 ± 0.6%, $p<0.001$).

Therefore, the overall attenuation of tidal volume in TH AMPK-α1/α2 dKO mice that has been described previously (Mahmoud *et al.*, 2016) and during 5min and 10min exposures described above remained exacerbated relative to controls during prolonged 60min exposures to 8% O_2 without any signs of recovery.

3.2.3.3 Minute ventilation

Changes in breathing frequency and tidal volume of control AMPK-α1/α2 Flx mice translated into a time-dependent reduction in minute ventilation that fell below normoxic values after 10min of 8% O_2 (10-15min: -13 ± 0.8%). From then on, minute ventilation continued to decline at a very low rate, measuring -21.3 ± 0.5% by 30-35min and -28.5 ± 1.9% by 55-60min (Figure 3.8 C).

As expected, minute ventilation of TH AMPK-α1/α2 dKO mice was significantly attenuated compared to controls throughout the entire 60min period. Following the onset of hypoxia, minute ventilation fell below normoxic values within 5min and continued to rapidly decrease until the 15min mark (10-15min: -34.1 ± 2.4%, $p<0.001$ compared to controls). However, unlike controls the minute ventilation of TH AMPK-α1/α2 dKO mice plateaued at this point and while it did not decline much further until the end of the exposure, it remained significantly attenuated relative to controls (15-20min: -39.9 ± 0.8%, $p<0.0001$; 30-35min: -37.9 ± 1.6%, $p<0.001$; 55-60min: -42.4 ± 0.4%, $p<0.001$).

Collectively, these data strongly suggest that deletion of AMPK-α1 and -α2 catalytic subunits in catecholaminergic cells results in a PO_2-dependent ventilatory depression during hypoxia that extends beyond the 5min period measured previously. Notably, deficits observed in exposures to severe hypoxia lasting up to 60min showed no delayed recovery of ventilation and that the degree of hypoxic ventilatory depression observed in control mice is further exacerbated. Therefore, AMPK activity is required in catecholaminergic cells to support ventilation throughout the entire hypoxic period.

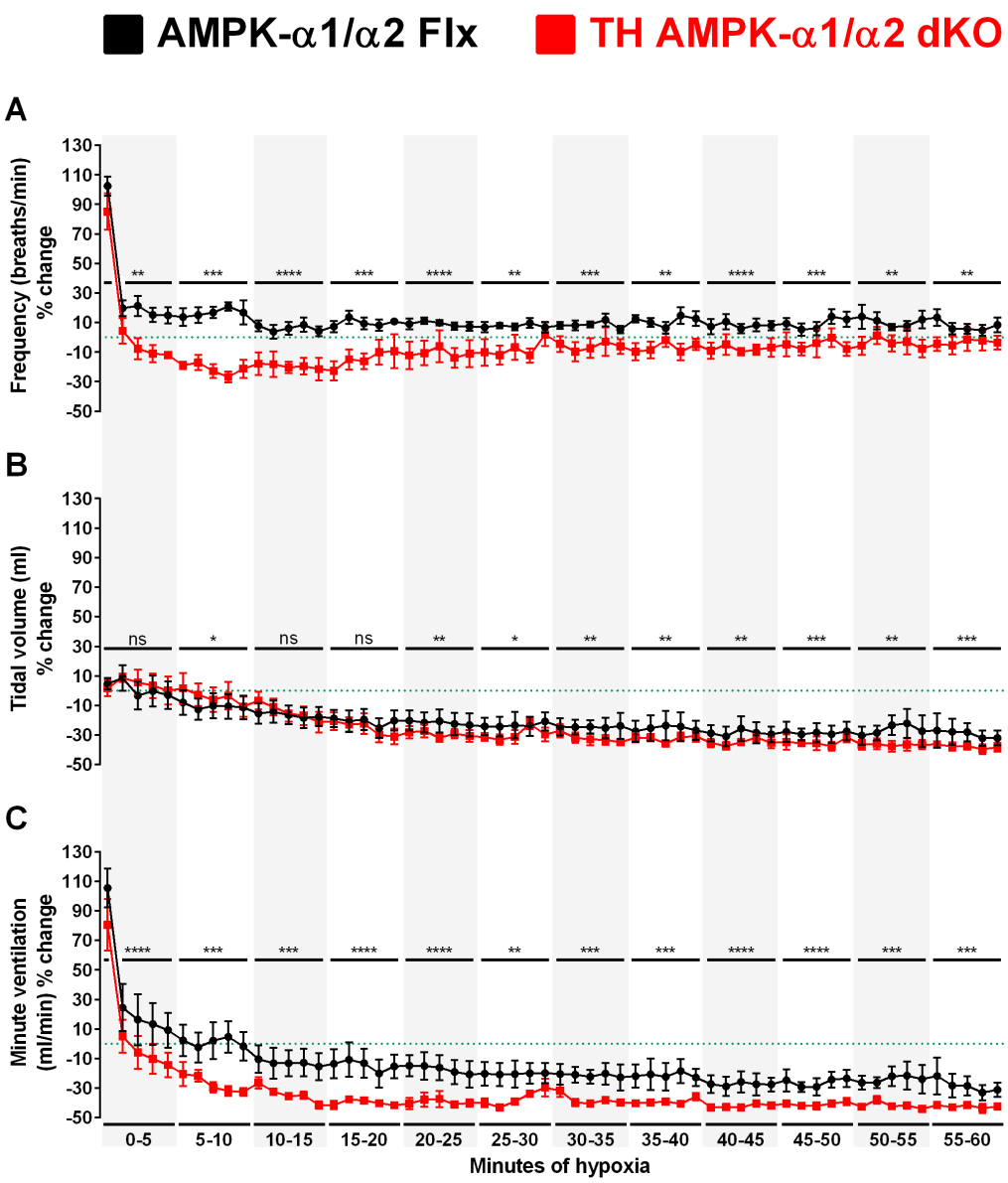

Figure 3.8: Deletion of AMPK-α1/α2 catalytic subunits in catecholaminergic cells attenuated breathing frequency, tidal volume, and minute ventilation over a 60min period of severe hypoxia.

Means ± SEM for the % change relative to normoxia (green dotted line) in **(A)** breathing frequency, **(B)** tidal volume, and **(C)** minute ventilation during 60min exposures to severe hypoxia (8% O_2) for whole minute averages in AMPK-α1 and -α2 floxed mice (AMPK-α1/α2 Flx, black, n = 5 mice) and TH-driven AMPK-α1 and -α2 double knockout mice (TH AMPK-α1/α2 dKO, red, n = 4 mice). ns = not significant, * = p<0.05, ** = p<0.01, *** = p<0.001, **** = p<0.0001. Significance tested for each 5min block by Student's paired t-test between genotypes.

3.3 Discussion

3.3.1 Summary of findings

Chapter 3 shows that the appropriate modulation of the respiratory response to hypoxia requires AMPK activity in catecholaminergic cells regardless of the duration of exposure to hypoxia, highlighted by the fact that there was no time-dependent or delayed compensation for the ventilatory deficiency reported previously. Importantly, the hypoxic respiratory depression triggered by AMPK deficiency was not only sustained, but increased in a manner proportional to the severity of hypoxia. During prolonged 60min exposures to severe hypoxia, the loss of both AMPK-α1 and -α2 catalytic subunits attenuated the ventilatory response to hypoxia and further exacerbated the hypoxic ventilatory decline observed in controls. Therefore, AMPK activity in catecholaminergic cells governs the maintenance of whole-body O_2 supply throughout periods of acute hypoxia by continuously supporting appropriate ventilatory adjustments.

3.3.2 AMPK activity in brainstem catecholaminergic cells supports increases in ventilation during hypoxia

Firstly, and consistent with previous reports, deletion of AMPK-α1 and -α2 catalytic subunits in catecholaminergic cells did not affect breathing during normoxia. In contrast, upon exposure to mild and severe hypoxic gas, increases in the drive to breathe were significantly attenuated (see also Appendices 1.2 to 1.4).

By extending the duration of hypoxic exposures from 5min to 10min and then up to 60min, it became apparent that AMPK activity is not only required to support modulation of ventilation during the initial phases of the HVR, but also beyond and throughout more prolonged exposures to hypoxia. Classically, the HVR of mice and other mammals is biphasic. The first response to an acute fall in PO_2 is a rapid and robust increase in ventilation, which is termed the “Augmenting phase” and primarily driven by carotid body chemoafferent fibre discharge to the respiratory centres of the brainstem

(Ramirez *et al.*, 1998; Palmer *et al.*, 2013; Pamenter & Powell, 2016). Thereafter, the central effect of hypoxia leads to a reduction in ventilation called “Roll-Off”, which may be partially driven by declining metabolic rates of non-O_2 sensitive neurons, as well as activation of central chemosensitive sites within the brainstem in response to increasing levels of hypocapnia subsequent to hyperventilation during the Augmenting phase. As has been demonstrated before (Mahmoud, 2014; Mahmoud *et al.*, 2016), components of the classical biphasic HVR were retained in TH AMPK-α1/α2 dKO mice, albeit in an attenuated manner. These outcomes are entirely consistent with the view that – despite the fact that carotid body chemoafferent input responses remained unaffected – AMPK-α1/α2 deletion in catecholaminergic neurons blocked the HVR beyond the initial ventilatory augmentation during hypoxia for which afferent inputs may be responsible (Teppema & Dahan, 2010; Mahmoud *et al.*, 2016; Wilson & Teppema, 2016). That said, the attenuation of the Augmenting phase, particularly at 8% O_2, indicates that while chemoafferent inputs were most likely received within the brainstem, the appropriate physiological responses could not be executed sufficiently in the absence of AMPK activity within central catecholaminergic cells. This is entirely consistent with the proposal that AMPK-dependent signalling pathways within brainstem catecholaminergic cells support signal integration and thus modulation of ventilatory output via the respiratory central pattern generators (rCPGs) (Evans *et al.*, 2016; Mahmoud *et al.*, 2016; Evans, 2018). The rCPGs adjust ventilation by coordinating the rhythmic patterns of motor activity for the diaphragm, ribcage, and upper airway muscles (von Euler, 1983; Dobbins & Feldman, 1994; Guyenet *et al.*, 2002). During hypoxia, motor output from the rCPGs is modulated by signals from peripheral and central O_2-sensing cells, which increase ventilation and thus protect against metabolic stress and tissue hypoxaemia at the whole-body level. It is now apparent that such modulation of rCPGs is reliant on AMPK-dependent signalling pathways for the entire duration of a hypoxic exposure, because significant deficits in ventilatory drive within TH AMPK-α1/α2 dKO mice were observed during exposures to severe hypoxia that lasted as long as 60 minutes.

The fact that AMPK-dependent signalling pathways are continuously required to support ventilatory drive became especially apparent during the acute hypoxic ventilatory decline, or “Roll-Off”, which was significantly attenuated in TH AMPK-α1/α2 dKO mice to the point where these mice entered a state of hypoventilation during severe hypoxia. Similar to the findings of others (Palmer *et al.*, 2013), ventilatory efforts of control AMPK-α1/α2 Flx mice declined progressively until ventilatory activity approximated that observed during normoxia at the end of the 10 minute exposure. By contrast, TH AMPK-α1/α2 dKO mice maintained a fairly stable level of hypoventilation between 6 to 10 minutes of hypoxia. It may be possible for these mice to have reached a “minimum of ventilation”, not too dissimilar to patients suffering from central congenital hypoventilation syndrome (Healy & Marcus, 2011). Indeed, outcomes from hypoxic exposures lasting 60 minutes revealed no further decreases in ventilation of TH AMPK-α1/α2 dKO mice after approximately 15 minutes of severe hypoxia, whereas control AMPK-α1/α2 Flx mice still exhibited a minor decline in ventilation. This decline was mostly driven by continuous time-dependent reductions in tidal volume, consistent with the manifestation of hypoxic ventilatory depression/decline (HVD) (Pamenter & Powell, 2016). That said, control AMPK-α1/α2 Flx mice continued to maintain an augmented breathing frequency relative to normoxia throughout the 60min exposures, whereas breathing frequencies of TH AMPK-α1/α2 dKO mice remained attenuated relative to both controls and normoxia.

Similar to the ventilatory phenotype of TH AMPK-α1/α2 dKO mice, a marked HVD has also been observed in neonatal mammals, whose oxygen-sensing network comprising the catecholaminergic cells of the peripheral carotid body and central nucleus tractus solitarius (NTS) are still immature at birth (Bissonnette, 2000; Teppema & Dahan, 2010; Koos & Rajaee, 2014). The neonatal response to hypoxia is characterised by a reduced augmentation phase and a quick decline into hypoventilation, which is, at least partially, equalised by a decrease in metabolism and hence O_2 demand (Mortola & Maskrey, 2011). Given that catecholaminergic deletion of AMPK-α1 and -α2 catalytic subunits produced a similar ventilatory pattern during hypoxia, an

index of the metabolic status relative to controls was required to determine whether these mice compensated their minimal ventilatory output by decreases in metabolic demand, or whether they truly entered a hypoventilatory state. Neither an immediate exposure to severe hypoxia, nor graded intensities of increasing environmental hypoxia revealed any differences in the metabolic rates of TH AMPK-α1/α2 dKO mice relative to controls, confirming that deletion of AMPK-α1 and -α2 catalytic subunits in catecholaminergic cells results in true hypoventilation during hypoxia with no compensatory reductions in metabolism.

On the whole, these findings add further weight to the hypothesis that AMPK-dependent signalling pathways have been adapted to regulate O_2 supply, and thus energy homeostasis, at the whole-body level. Deficiencies in AMPK expression may therefore compromise the appropriate modulation of breathing during hypoxic stress, for example during sleep or ascent to altitude (Ainslie *et al.*, 2013; Panossian & Daley, 2013).

3.3.3 Conclusion

In conclusion, mice with dual deletion of the AMPK-α1 and -α2 catalytic subunits in catecholaminergic cells are unable to sustain an increase in ventilation during hypoxia and exhibit a severely disordered ventilatory phenotype during prolonged exposures. Given the normal increases of carotid body chemoafferent input and yet an attenuated HVR, AMPK-dependent signalling pathways are critical within the brainstem catecholaminergic network for signal integration and coordination of the appropriate ventilatory responses to hypoxia, which are modulated via afferent projections to the rCPGs within the ventral medulla. Therefore, in addition to the primary peripheral chemosensors of the carotid body, it seems quite plausible that AMPK-dependent modulation of a group of central oxygen-sensing catecholaminergic cells within the caudal brainstem may determine the overall degree of the ventilatory responses to hypoxia and whose role is to maintain O_2 supply, and hence energy homeostasis, at the whole-body level

Chapter 4: Characterisation of the neuronal activation within the caudal brainstem following exposures to hypoxia and the effect of AMPK deletion in catecholaminergic neurons

4.1 Introduction

The nucleus tractus solitarius (NTS), located bilaterally within the dorsal medulla oblongata, contains undoubtedly one of the most complex neuronal aggregates of the brainstem. The NTS has been implicated in the control of a variety of respiratory, autonomic, emotional, volitional, appetitive, and gustatory functions (Geerling *et al.*, 2006; Rinaman, 2010; Roussin *et al.*, 2012; Zoccal *et al.*, 2014; Hume, 2017; Venkatraman *et al.*, 2017). It is therefore not surprising that the NTS is the subject of a wide range of afferent innervations from the periphery and forms a vast network of neuronal projections within the brainstem, and to the spinal cord and forebrain (Andresen & Kunze, 1994; Horner, 2009; Kline *et al.*, 2010; King *et al.*, 2012; Zoccal *et al.*, 2014; King *et al.*, 2015).

Important in the context of this thesis, sensory afferent innervations from the carotid bodies (chemoreceptors), pulmonary stretch receptors (mechanoreceptors) and arterial baroreceptors innervate the caudal portions of the NTS (Finley & Katz, 1992; Mendelowitz *et al.*, 1992; Kubin *et al.*, 2006) and mediate, through innervation of the ventrolateral medulla (VLM), cardiorespiratory changes in response to homeostatic threats such as hypoxia.

4.1.1 The functional compartmentalisation of the NTS

Several studies have sought to determine the precise neuronal connections between the NTS and VLM that modulate the control of breathing, and to separate innervations from specific compartments (subnuclei) of the NTS to the individual compartments of the VLM that form the ventral respiratory central pattern generators (rCPGs [bilateral symmetry]) (Ellenberger & Feldman, 1990; Nunez-Abades *et al.*, 1993; Ellenberger & Feldman, 1994; Rosin *et al.*, 2006; Alheid *et al.*, 2011). Using retrograde tracer injections into individual compartments of the rCPGs, it was found that particular subnuclei of the NTS differentially innervate the VLM (Ross *et al.*, 1985; Alheid *et al.*, 2011). Figure 4.1 illustrates these findings schematically, whereby projections from specific NTS subnuclei to the VLM are colour-coded on the

left, and the cardiorespiratory (hearts and lungs, respectively) functions and carotid body afferent innervations (arteries) are illustrated on the right. Within the NTS, carotid body afferent inputs terminate within the portions that are mostly caudal to the level of the area postrema (AP), but also at the level of the AP (Finley & Katz, 1992), where afferent inputs from the baroreceptors and mechanoreceptors mostly terminate as well (Kubin *et al.*, 2006). With respect to the individual subnuclei of the NTS that receive these innervations, the most prominent afferent chemoreceptor projections were found to terminate within the commissural (SolC) and medial (SolM) subnuclei, while less prominent projections arrive at the interstitial (SolI), intermediate (SolIM), dorsolateral (SolDL), and ventrolateral (SolVL) subnuclei (Figure 4.1, right). In addition, few terminals also terminated in the area postrema (AP) and the dorsal motor nucleus of the vagus (10N), the latter of which contains parasympathetic preganglionic neurons that innervate the thorax and abdomen (Finley & Katz, 1992; Watson *et al.*, 2012). Vagal afferents arising from the pulmonary stretch receptors, on the other hand, were found to terminate within the NTS subnuclei of SolIM, SolI, SolV (ventral subnucleus), and SolVL (Kubin *et al.*, 2006). Finally, densely projecting baroreceptor afferent terminals project to the SolM, caudal to and at the level of the AP, coinciding with the afferent innervations from the chemoreceptors (Mendelowitz *et al.*, 1992).

A picture began to emerge whereby the regulation of the respiratory and cardiovascular systems appeared to be synergistic. In support of this view, the majority of NTS neurons that project to the VLM were found to simultaneously innervate compartments of rCPG and the rostral and caudal ventrolateral medulla (Figure 4.1 left; RVL and CVL, respectively, red), which contain pre-sympathetic catecholaminergic C1 neurons (Alheid *et al.*, 2011). Therefore, it appears that within the NTS, networks that control cardiovascular responses are closely linked with those that modulate the respiratory responses. Nonetheless, there appears to also be a degree of selectivity with respect to the afferent innervation from the NTS subnuclei to the rCPGs. For example, while most subnuclei project broadly to each of the respiratory compartments of the VLM, the midline nuclei of AP and SolC, as

well as the bilaterally located SolM were found to completely avoid innervations of the inspiratory pre-Bötzinger complex (preBötC, green) and expiratory Bötzinger complex (BötC, yellow). Therefore, at least some of the reflex pathways that shape cardiorespiratory responses via caudal NTS nuclei appear to do so by directly innervating motor pattern forming compartments of the VLM (such as the rostral ventral respiratory group; Figure 4.1 left, purple), while indirectly acting on compartments that generate respiratory rhythm (such as the preBötC, and the BötC).

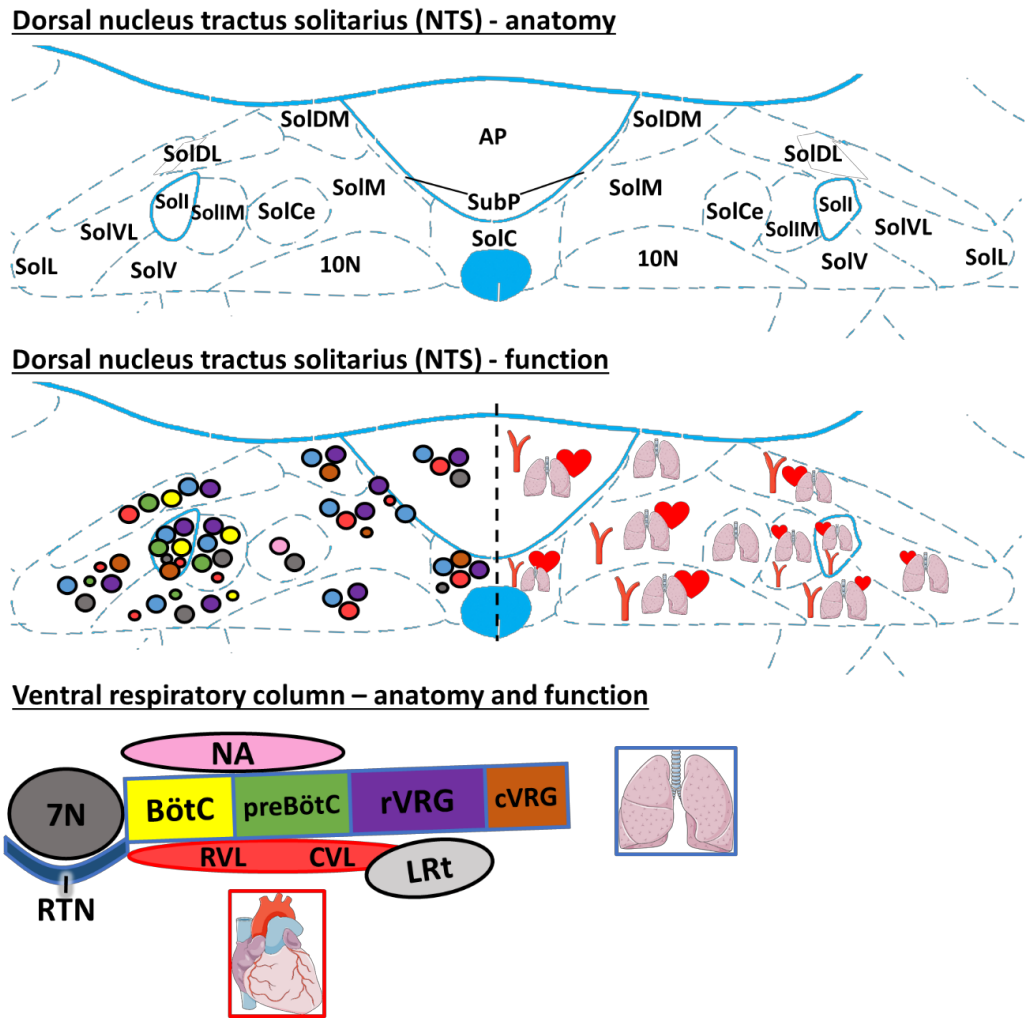

Figure 4.1: Schematic of the projections from the nucleus tractus solitarius to the ventral respiratory column.

Top panel shows the anatomical organisation of the nucleus tractus solitarius (NTS) according to the Mouse Brain Atlas (Franklin & Paxinos, 2008) at Bregma -7.48mm. *Middle panel* shows the functional organisation of the NTS according to findings from Alheid et. al. (2011) with respect to their afferent innervations to the ventral medulla (left) and their physiological control (right). *Lower panel* shows the compartmentalisation of the ventral respiratory column (VRC), which is colour coded according to the physiological function of each compartment (border colour – respiratory: blue, cardiovascular: red) and the connection to each NTS subnucleus (fill colours). Larger circles within the NTS subnuclei indicate strong innervation of each colour coded compartment of the VRC, smaller circles indicate weaker innervation. Schematic based on the findings of Alheid et. al. (2011). Abbreviations listed overleaf…

Abbreviations for Figure 4.1:

Lungs: respiratory control, heart: cardiovascular control, artery: received afferent input from carotid bodies, AP: = area postrema; SubP: sub-postrema; 10N = dorsal motor nucleus of the vagus; SolC = commissural nucleus; SolM = medial nucleus; SolDM = dorsomedial nucleus; SolDL = dorsolateral nucleus; SolCe = central nucleus; SolIM = intermediate nucleus; SolI = interstitial nucleus; SolV = ventral nucleus; SolVL = ventrolateral nucleus; SolL = lateral nucleus 7N: facial nucleus, RTN: retrotrapezoid nucleus, NA: nucleus ambiguus, BötC: Bötzinger complex, preBötC: pre-Bötzinger complex, rVRG: rostral ventral respiratory group, cVRG: caudal ventral respiratory group, RVL: rostral ventrolateral medulla, CVL: caudal ventrolateral medulla, LRt: lateral reticular nucleus.

4.1.2 cFos as a marker for neuronal activation

In order to study the stimulus-dependent activation of particular neurons of the central nervous system *in vivo*, the use of cFos labelling became highly popular. Being part of the immediate-early gene family, the expression of the proto-oncogene cFos is rapidly activated and/or increased in response to a variety of extracellular stimuli and subsequent cellular activation, including the firing of action potentials within neurons of the central nervous system (Dragunow & Faull, 1989). Following membrane depolarisation and entry of extracellular Ca^{2+} via voltage-gated Ca^{2+}-channels, activation of the Ca^{2+}/calmodulin-dependent protein kinase (CaMK) allows for phosphorylation of the cyclic AMP response element binding protein (CREB) at Ser133, which induces its activity as a transcription factor for immediate-early genes such as cFos (Sheng *et al.*, 1990). Therefore, any increases in cFos expression relative to unstimulated controls can be related back to any given stimulus-induced strong neuronal activation.

Its latency of maximal expression after 20-90 minutes and long half-life made the cFos protein an ideal target for immunohistochemical experiments (Morgan *et al.*, 1987; Johnstone *et al.*, 2006; Perrin-Terrin *et al.*, 2016). In addition, due to its functional role in regulating gene expression, cFos is localised to the nucleus (Sambucetti & Curran, 1986) and therefore allows for co-labelling of cytoplasmic structures in order to distinguish between activated cell types.

Using this technique, a number of studies have aimed to identify the central respiratory network involved in the ventilatory responses to hypoxia. Invariably, systemic hypoxia was found to induce cFos expression bilaterally within the NTS and defined regions of the rCPG in the cat (Larnicol *et al.*, 1994), rabbit (Hirooka *et al.*, 1997), rat (Erickson & Millhorn, 1994; Smith *et al.*, 1995; Teppema *et al.*, 1997; Bodineau & Larnicol, 2001; Cruz Jde *et al.*, 2010; Kline *et al.*, 2010; King *et al.*, 2012; King *et al.*, 2013; Wakai *et al.*, 2015), and the neonatal mouse (Joubert *et al.*, 2016). Importantly, increasing intensities of the hypoxic stimulus resulted in increased cFos expression within these animal models. Therefore, cFos expression is a highly useful tool to identify the neural components that drive the HVR and

to study alterations within the central respiratory network activity following a variety of pharmacological treatments or genetic modifications.

4.1.3 AMPK deletion in catecholaminergic cells led to attenuations in brainstem cFos expression

As described in Chapter 3, mice with dual deletion of AMPK-α1 and -α2 catalytic subunits in tyrosine hydroxylase-expressing cells (TH AMPK-α1/α2 dKO mice) exhibited marked hypoventilation during acute and prolonged periods of hypoxia. Functional magnetic resonance imaging (fMRI) revealed that during hypoxic exposures, TH AMPK-α1/α2 dKO mice also displayed reduced neuronal activity relative to controls within particular areas of the NTS and the VLM, which aligned well with the anatomical location of dorsal catecholaminergic A2/C2 and ventral A1/C2 neurons that were targeted by the TH-driven deletion of AMPK (Mahmoud *et al.*, 2016). These regions were termed the “dorsal active region” (DAR) and “ventral active region” (VAR), respectively, and their anatomical location within the brainstem was found to span across several Bregma along the neuraxis. Analysis of cFos expression was subsequently used to identify the subpopulations of cells within the brainstems of TH AMPK-α1/α2 dKO mice that exhibited *in vivo* deficits of neuronal activation during hypoxia. A significant reduction in hypoxia-induced cFos expression was proposed to occur within the dorsal NTS subnuclei of SolM and SubP (sub-postrema), as well as the more rostrally located catecholaminergic C2 cell group. Significant reductions in cFos expression within TH-positive cells targeted by AMPK deletion were also observed within the dorsal catecholaminergic A2 neurons confined to the SubP, the dorsal C2 cell group, and the ventral A1 cell group. By contrast, significant increases in cFos expression were found within TH-positive cells of NTS subnuclei SolC, SolV, and SolVL, as well as the ventral catecholaminergic C1 cells.

4.1.4 Aims

From the findings in the study described above, it was unclear whether AMPK-dependent reductions in the hypoxia-induced cFos expression spanned the entire neuraxis of the NTS or whether the deficits were confined to a particular rostrocaudal region as indicated by fMRI. Furthermore, the number and size of individual subnuclei of the NTS changes throughout its rostrocaudal length, and not all subnuclei were included in the cFos counts. I therefore sought to re-visit these outcomes and to provide a more detailed analysis by assessing the cFos expression in response to hypoxia within all subnuclei of the NTS, and to additionally separate my counts by individual Bregmas along the neuraxis of the caudal mouse brainstem.

Accordingly, mice with dual deletion of the AMPK-α1 and -α2 catalytic subunits were exposed to hypoxia and their neuronal activation analysed by immunohistochemical labelling for cFos and TH.

4.2 Results

4.2.1 Ventilatory outcomes of experimental animals

As shown in Figure 4.2 A, control AMPK-α1/α2 Flx mice used for analysis of cFos expression displayed a typical HVR, presenting as robust increases in ventilation at the onset of hypoxia, followed by a time-dependent roll-off until a sustained plateau was reached. Consistent with my previous studies (Chapter 3), analysis of TH AMPK-α1/α2 dKO mice used to compare cFos expression demonstrated that increases in minute ventilation during hypoxia were attenuated compared to controls (Figure 4.2 B, $p<0.01$), thereby confirming that ventilatory outcomes described in Chapter 3 were also observed in single exposures of naïve mice used for experiments carried out in this chapter.

4.2.2 Immunohistochemical co-staining for the expression of cFos and tyrosine hydroxylase

Fluorescence-based immunohistochemistry Previously published data on the expression of cFos and tyrosine hydroxylase (TH) within AMPK-α1/α2 Flx and TH AMPK-α1/α2 mice utilised a fluorescence approach (Mahmoud *et al.*, 2016), which I sought to emulate in order to confirm proof of principle by directly comparing outcomes from my experiments with those carried out by others and to ultimately analyse the data in more detail. Unfortunately, I found that the use of fluorescent secondary antibodies did not produce the desired qualitative outcomes during imaging. The staining of catecholaminergic (TH-positive) cell bodies was poor to absent for ventral A1/C1 neurons, and indistinguishable between individual cell bodies for dorsal A2/C2 neurons due to high background fluorescence proximal to the area postrema (Figure 4.3). Furthermore, labelling of cFos-positive nuclei resulted in a high degree of overall background fluorescence and additional unexpected labelling of cell bodies. Due to these technical difficulties an alternative method of immunohistochemical staining was employed that would provide a higher quality of image analysis.

3,3'-Diaminobenzidine (DAB)-based immunohistochemistry The chosen alternative approach was to use DAB staining, a technique commonly used and described within the literature on cFos expression within the central nervous system following exposures to hypoxia (Erickson & Millhorn, 1994; Smith *et al.*, 1995; Hirooka *et al.*, 1997; King *et al.*, 2012; Wakai *et al.*, 2015). It was an immediate success regarding the specific detection of nuclear cFos expression. However, in initial trials TH labelling appeared entirely absent regardless of the primary and secondary antibody concentration used for incubations. In the end, reducing the section thickness from 40µm to 30µm finally allowed for visualisation of brown cell bodies of TH-positive neurons (see Figure 4.9). That said, the final working concentration for the anti-TH antibodies was 1/2,000 whereas the anti-cFos antibodies were used at a final concentration of 1/100,000. Therefore, there is a strong possibility that using a mouse primary antibody with an anti-mouse secondary antibody on mouse tissue may have resulted in non-specific detection of endogenous mouse immunoglobulin within the sections. However, this should have resulted in increased background levels, rather than poor overall staining.

One way to resolve this issue would be to use a genetic reporter, such as LacZ or tdTomato fluorescent protein fused to Cre. This way, any cells that conditionally express Cre leading to AMPK-α1 and -α2 catalytic subunit deletion would co-express one of these two markers. In the end, this method does not only provide more specificity regarding identification of the target cells, but would also reduce the need for dual labelling procedures.

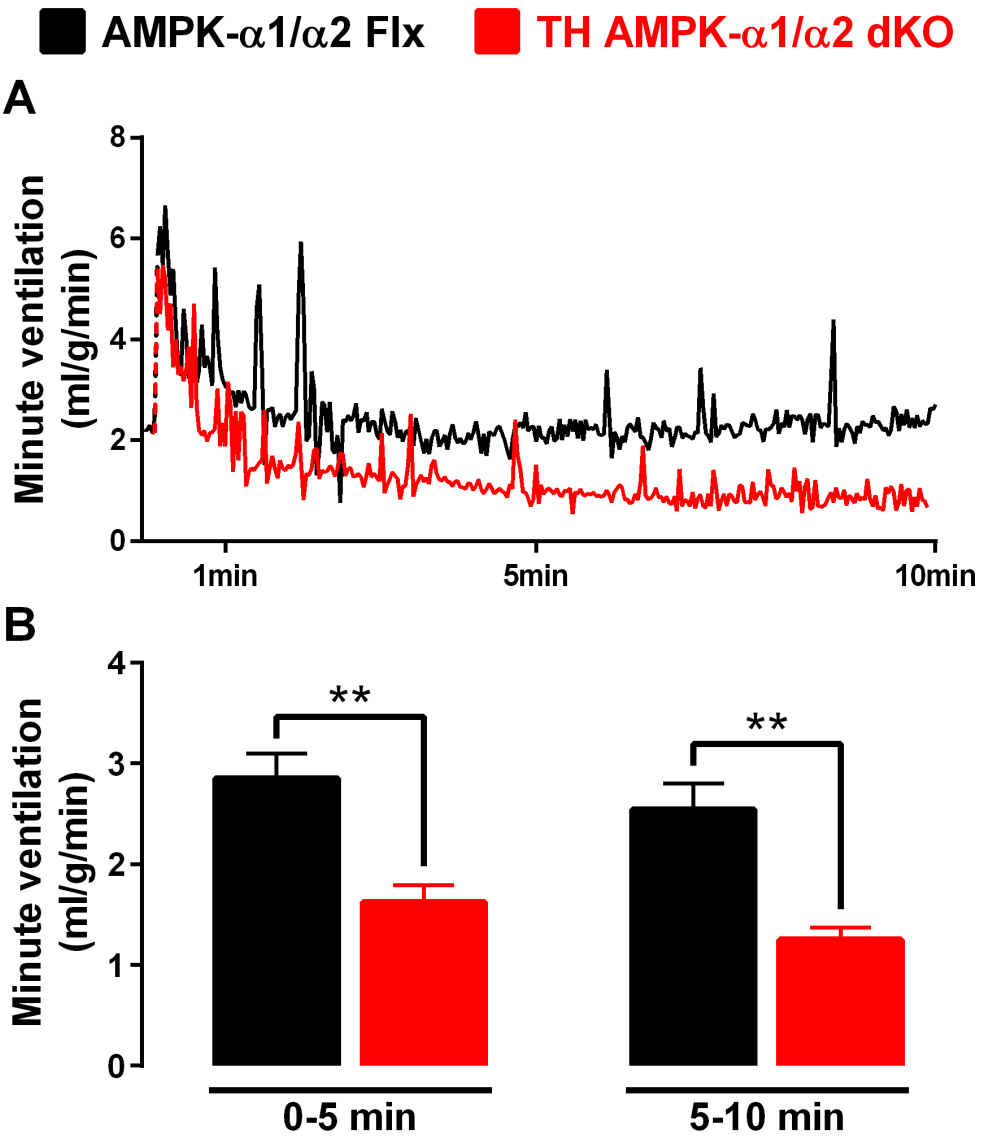

Figure 4.2: Attenuations of minute ventilation were confirmed in TH-driven AMPK-α1/α2 knockout mice used for analysis of cFos expression.

(A) Example 10min records of minute ventilation (ml/g/min) for one AMPK-α1 and -α2 floxed mouse (AMPK-α1/α2 Flx, black) and one TH-driven AMPK-α1 and -α2 double knockout mouse (TH AMPK-α1/α2 dKO, red) used for cFos analysis after exposure to severe hypoxia (8% O_2). **(B)** Means ± SEM for minute ventilation during both halves of the 10min exposures to 8% O_2 in AMPK-α1/α2 Flx (n = 7) and TH AMPK-α1/α2 dKO mice (n = 5). ** = $p<0.01$. Significance tested by two-way ANOVA with Sidak post-hoc tests.

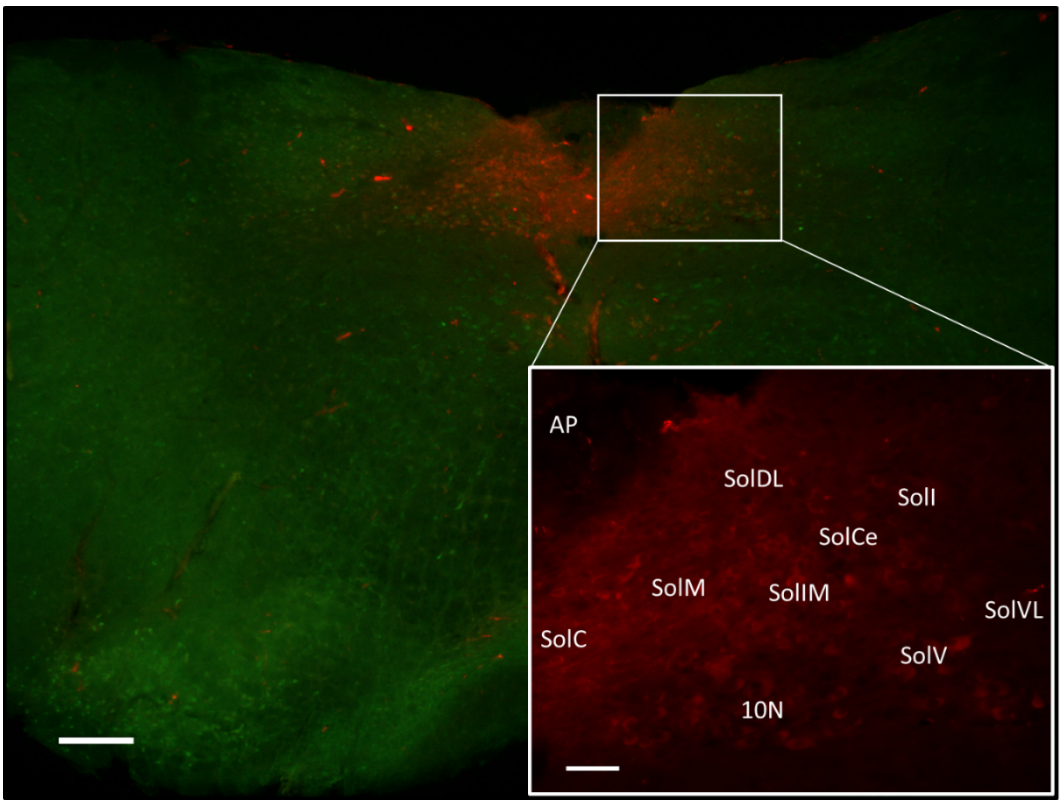

Figure 4.3: Fluorescence photomicrographs following a 10min exposure to severe hypoxia.

Representative photomicrographs of tyrosine hydroxylase (TH)-positive (red) cell bodies and cFos-positive (green) nuclei in the caudal brainstem of an AMPK-α1 and -α2 floxed (AMPK-α1/α2 Flx) mouse following 10min exposures to 8% O_2. Approximate Bregma -7.64mm; scale bar = 200μm, inset 50μm.

4.2.3 Assessment of catecholaminergic cell numbers following deletion of AMPK-α1 and -α2 catalytic subunits

Within different systems and pathologies, AMPK has been shown to either promote or protect from cell death (Mihaylova & Shaw, 2011; Merlen *et al.*, 2014; Evans *et al.*, 2015; Hardie, 2015). Importantly, neuronal AMPK has been proposed to be required within the rodent brain to promote survival following metabolic stress (Culmsee *et al.*, 2001) and reductions in brainstem catecholaminergic neurotransmission may underlie, at least in part, the hypoventilatory and apnoeic phenotypes associated with Rett Syndrome (Ide *et al.*, 2005; Viemari *et al.*, 2005; Stettner *et al.*, 2007; Katz *et al.*, 2009; Roux & Villard, 2010). On the other hand, breathing irregularities and apnoeas during hypoxia have also been shown to be triggered by increases in catecholaminergic neurotransmission (Zanella *et al.*, 2014).

Therefore, it was important to firstly assess whether the deletion of AMPK-α1 and -α2 catalytic subunits in TH-positive cells may have affected ventilatory stability during hypoxia through alterations in the overall number of brainstem catecholaminergic cells or the total bioamine content.

4.2.3.1 Deletion of AMPK-α1 and -α2 catalytic subunits does not alter the number of TH-positive cells in the brainstem

Total counts – dorsal and ventral As can be seen in Figure 4.4, counts for TH-labelled cells revealed no differences in the total number of catecholaminergic neurons within the dorsal (left panels) or ventral (right panels) brainstems of AMPK-α1/α2 Flx (n = 16) and TH AMPK-α1/α2 dKO (n = 11) mice. These outcomes were retained regardless of whether the counts were grouped into total counts for both hemispheres (Figure 4.4 A), or separated into the right side (Figure 4.4 B) and left side (Figure 4.4 C) of the brainstem (see Appendix 2.1 for data tables).

Dorsal counts per Bregma Comparable counts between controls and TH AMPK-α1/α2 dKO mice were also obtained when separating the number of catecholaminergic neurons within the dorsal NTS by each identified Bregma, irrespective of whether the counts were grouped together or separated into

the right and left divisions of the NTS (Figure 4.5, Appendix 2.2). Notably, the number of TH-positive cells decreased slightly in a caudo-rostral direction, consistent with the reported location and density of the catecholaminergic A2 cell group that is primarily located in the caudal and medial portions of the NTS (Rinaman, 2011).

Dorsal counts per subnucleus Additionally, no differences in TH cell counts between controls and TH AMPK-α1/α2 dKO mice were found when comparing the total, right-, and left-sided numbers of TH-positive cells found within each subnucleus of the NTS spanning the entire length of the caudal brainstem (Figure 4.6, Appendix 2.3). Notably, the highest density of TH-labelling following DAB staining was obtained within the mediolateral parts of the NTS (SolIM, SolV, SolVL, SolCe), however the presence of TH-positive cells was observed in every subnucleus.

Ventral counts per cell group Total counts for TH labelled cells within the ventral medulla were also comparable between AMPK-α1/α2 Flx and TH AMPK-α1/α2 dKO mice after separation of ventral catecholaminergic cells into their neuronal cell groups, namely A1 cells at the level of the area postrema, C1 cells at the level of the 4th ventricle, and the mixed population of A1/C1 cells at the level of the obex (Figure 4.7, Appendix 2.4). That said, cell counts indicated a significant increase in the number of TH labelled neurons in the rostral ventrolateral medulla following AMPK deletion ($p<0.05$), where C1 neurons are predominant. However, this was only evident on the right side of the brainstem, with counts comparable for TH AMPK-α1/α2 dKO mice and controls for the left side alone and when both sides were added together. Separation of the more caudally located A1/C1 and A1 neurons into the right and left sides of the ventrolateral medulla did not reveal any changes in the number of TH-positive cells following deletion of AMPK-α1 and -α2 catalytic subunits.

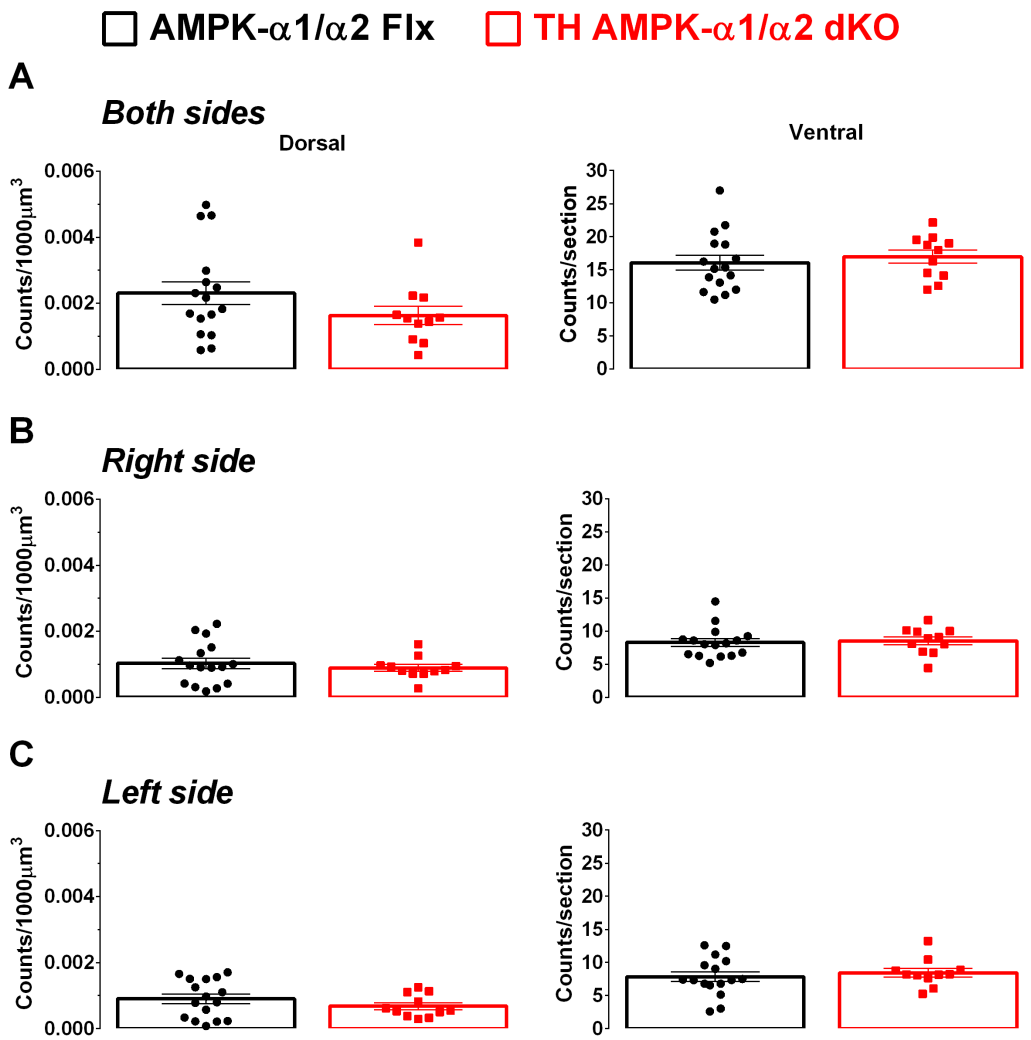

Figure 4.4: Targeted deletion of AMPK-α1/-α2 catalytic subunits in catecholaminergic cells did not alter total brainstem catecholaminergic cell counts.

Means ± SEM of tyrosine hydroxylase-positive cell counts (per 1000µm^3) for all identified Bregma within the **(A)** total, **(B)** right side, and **(C)** left side of the dorsal brainstem within the nucleus tractus solitarius (left panels) and ventral brainstem (right panels) of AMPK-α1 and -α2 floxed mice (AMPK-α1/α2 Flx, black, n = 16 mice) and TH-driven AMPK-α1 and -α2 double knockout mice (TH AMPK-α1/α2 dKO, red, n = 11 mice). Significance tested by Student's t-test between genotypes.

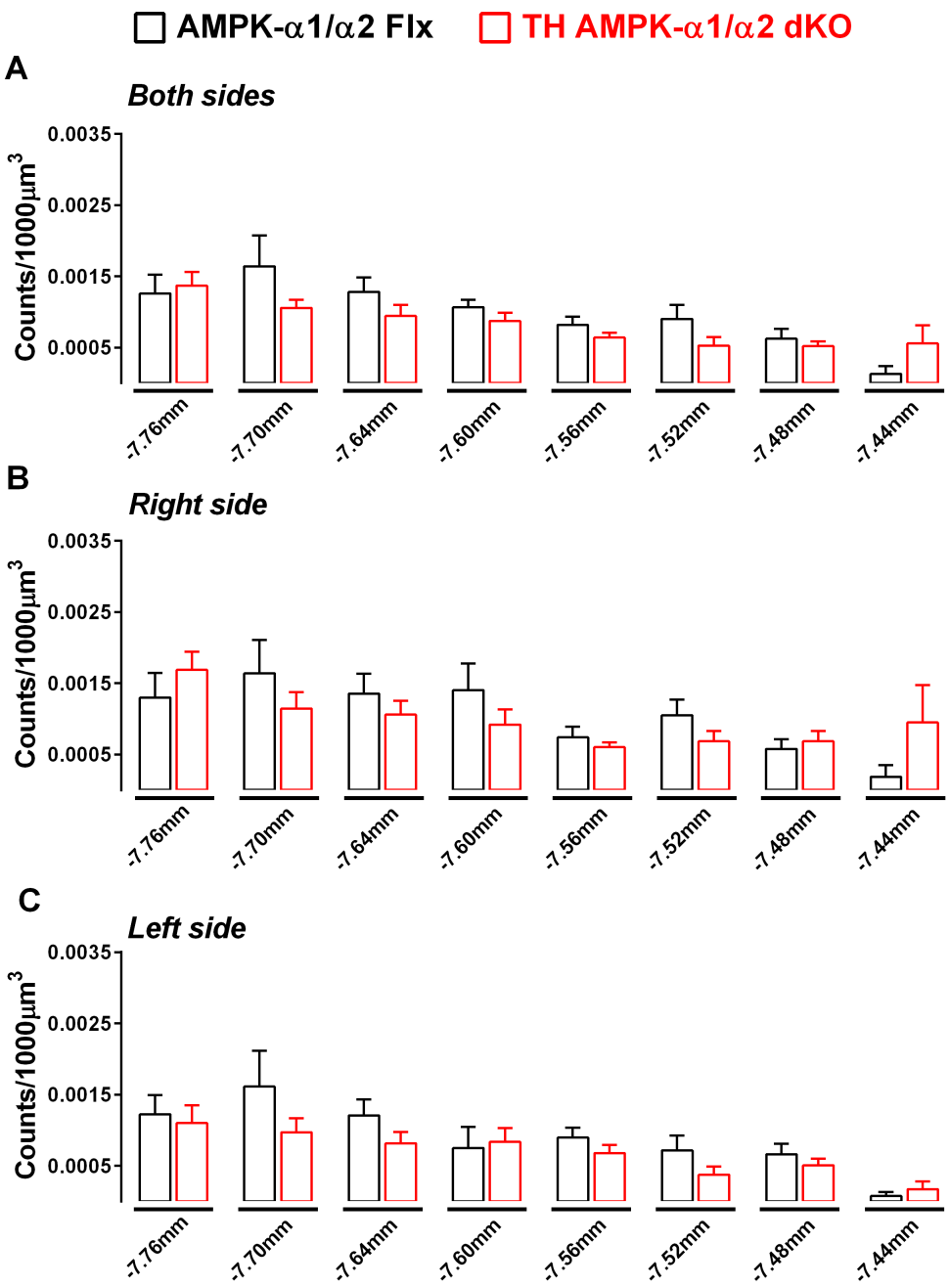

Figure 4.5: Targeted deletion of AMPK-α1/α2 catalytic subunits in catecholaminergic cells did not alter dorsal brainstem catecholaminergic cell counts within any Bregma.

Means ± SEM of tyrosine hydroxylase-positive cell counts (per 1000µm^3) for all identified Bregma within the **(A)** total, **(B)** right-sided, and **(C)** left-sided nucleus tractus solitarius of AMPK-α1/α2 floxed (AMPK-α1/α2 Flx, black, n = 16 mice) and TH-driven AMPK-α1 and -α2 double knockout mice (TH AMPK-α1/α2 dKO, red, n = 11 mice). Significance tested by Student's t-test between genotypes for each Bregma.

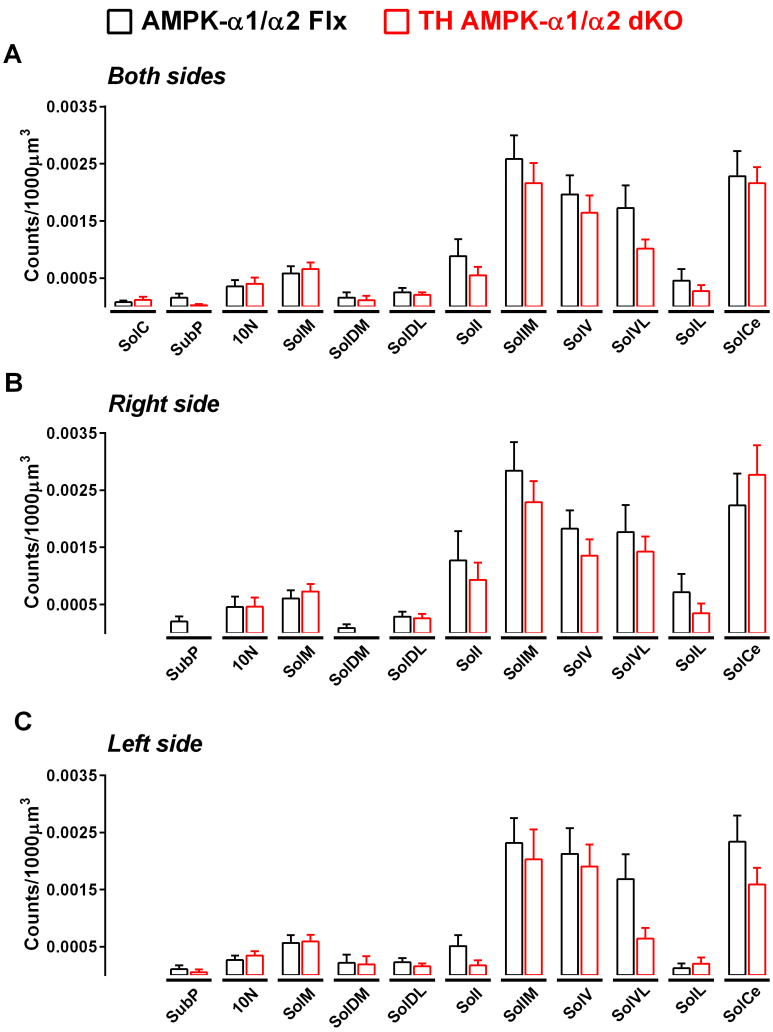

Figure 4.6: Targeted deletion of AMPK-α1/α2 catalytic subunits in catecholaminergic cells did not alter dorsal brainstem catecholaminergic cell counts within any region of interest.

Means ± SEM of tyrosine hydroxylase-positive cell counts (per 1000µm^3) for each subnucleus of the **(A)** total, **(B)** right-sided, and **(C)** left-sided nucleus tractus solitarius of AMPK-α1/α2 floxed (AMPK-α1/α2 Flx, black, n = 16 mice) and TH-driven AMPK-α1 and -α2 double knockout mice (TH AMPK-α1/α2 dKO, red, n = 11 mice). SolC = commissural nucleus, SubP = sub-postrema, 10N = hypoglossal nucleus, SolM = medial nucleus, SolDM = dorsomedial nucleus, SolDL = dorsolateral nucleus, SolI = interstitial nucleus, SolIM = intermediate nucleus, SolV = ventral nucleus, SolVL = ventrolateral nucleus, SolL lateral nucleus, SolCe = central nucleus. Significance tested by Student's t-test between genotypes for each region of interest.

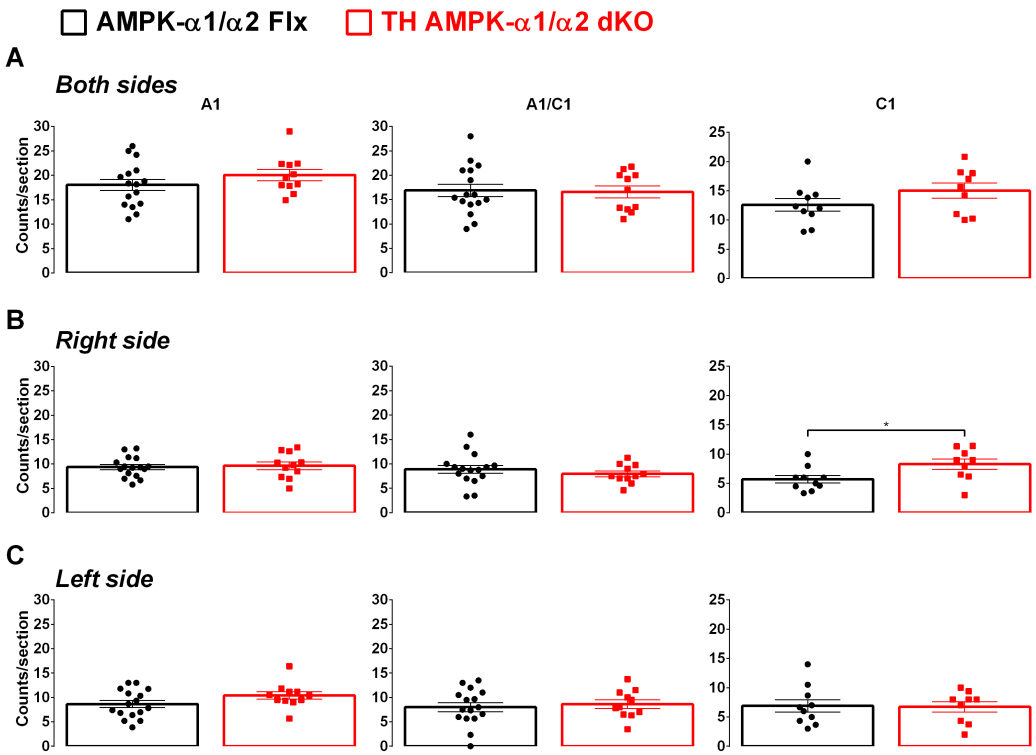

Figure 4.7: Targeted deletion of AMPK-α1/α2 catalytic subunits in catecholaminergic cells did not alter ventral brainstem catecholaminergic cell counts.

Means ± SEM of tyrosine hydroxylase-positive cell counts (per 1000µm^3) for all identified Bregma within the **(A)** total, **(B)** right-sided, and **(C)** left-sided ventral brainstem corresponding to the catecholaminergic A1 neurons (left panels), A1/C1 neurons (middle panels), and C1 neurons (right panels) in AMPK-α1/α2 floxed (AMPK-α1/α2 Flx, black, n = 16 mice) and TH-driven AMPK-α1 and -α2 double knockout mice (TH AMPK-α1/α2 dKO, red, n = 11 mice). * = $p<0.05$. Significance tested by Student's t-test between genotypes for each population of neurons.

4.2.3.2 Deletion of AMPK-α1 and -α2 catalytic subunits does not alter brainstem bioamine content

Consistent with the outcomes for TH-positive cell counts, measurements of bioamine levels within the brainstems (Figure 4.8 A) and spinal cords (Figure 4.8 B) of control AMPK-α1/α2 Flx (n = 11) and TH AMPK-α1/α2 dKO (n = 12) mice carried out by David Burns at the University of Cork revealed no differences in the amounts of catecholamines (noradrenaline and serotonin), the catecholamine precursor L-DOPA, or the serotonin metabolite 5-hydroxyindoleacetic acid (5-HIAA; see Appendix 2.5 for data tables).

It would appear, therefore, that deletion of AMPK-α1 and -α2 catalytic subunits in catecholaminergic neurons did not result in any hyper- or hypoplasia of TH-positive cells and did not alter the catecholamine content within the brainstem. Therefore, the breathing irregularities, hypoventilation and apnoeas observed in TH AMPK-α1/α2 dKO mice during hypoxia were unlikely to be due to aberrant catecholaminergic biosynthesis and availability. It seems most likely, therefore, that ventilatory dysfunction resulted from inappropriate signal integration and transduction within the catecholaminergic respiratory network of the brainstem, ultimately leading to a *functional* deficit as suggested by previous fMRI analysis (Mahmoud *et al.*, 2016).

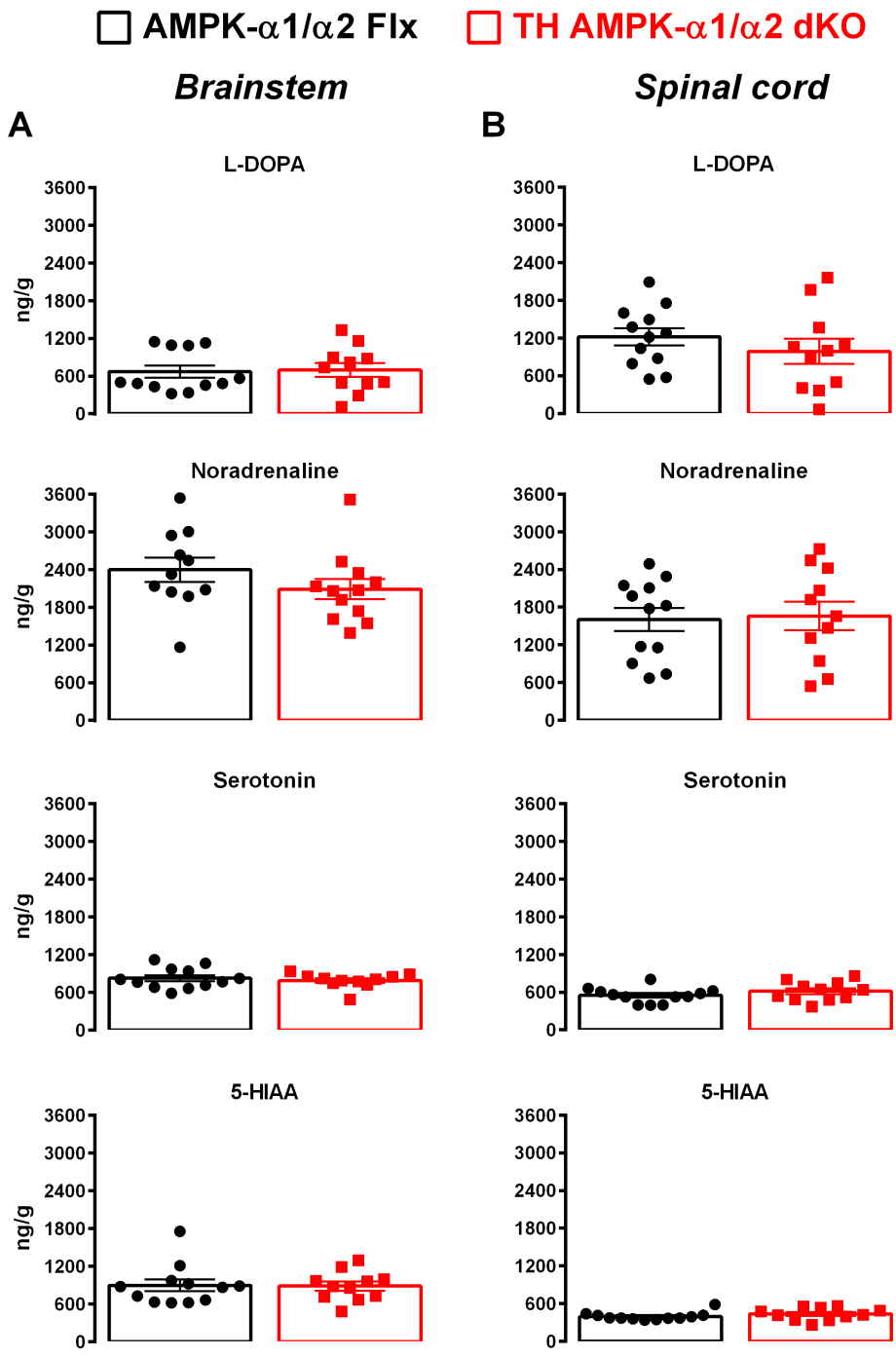

Figure 4.8: Deletion of AMPK-α1/α2 catalytic subunits in catecholaminergic cells did not alter bioamine content.

Means ± SEM of bioamine levels within the **(A)** brainstems and **(B)** spinal cords of AMPK-α1/α2 floxed (AMPK-α1/α2 Flx, black, n = 11 mice) and TH-driven AMPK-α1 and -α2 double knockout mice (TH AMPK-α1/α2 dKO, red, n = 12 mice). 5-HIAA = 5-hydroxyindoleacetic acid. Significance tested by Student's t-test between genotypes for each bioamine.

4.2.4 The expression of nuclear cFos following 10min exposures to severe hypoxia

In order to match experimental outcomes to plethysmography experiments described in Chapter 3 and to previously published data (Sunday Udoh, 2015; Mahmoud *et al.*, 2016), naïve mice were exposed to 10min of severe hypoxia (8% O_2) and sacrificed 90min later to study the cFos expression within the brainstem.

4.2.4.1 10min exposures to severe hypoxia are not sufficient to evoke hypoxia-dependent increases in cFos expression

cFos expression in control mice Analysis of cFos expression in control AMPK-α1/α2 Flx mice following 10min exposures to 8% O_2 showed a highly variable expression profile between animals, both with respect to the number of cFos-positive nuclei stained and their distribution within the NTS (Figure 4.9). These observations were further corroborated by the fact that there was no significant increase in the number of cFos-positive cells compared to mice exposed to room air (Figure 4.10; 21% O_2: 0.007 ± 0.0005 nuclei/1000μm^3, 8% O_2: 0.0186 ± 0.003 nuclei/1000μm^3). This finding was contrary to outcomes described previously, which suggested that increasing intensities of hypoxia evoke increased expression of cFos within the rodent brainstem (Erickson & Millhorn, 1994; Smith *et al.*, 1995; Hirooka *et al.*, 1997; King *et al.*, 2012; Wakai *et al.*, 2015). However, these previous studies of others generally used a much longer stimulus protocol, whereby hypoxia was administered for at least 60min and up to 3 hours.

Considering the various methods described in the literature and following very kind guidance and advice from Prof Roger Dampney (University of Sydney), another stimulus protocol was tested where hypoxia (8% O_2) was given for a period of 60min, with mice sacrificed after a 15min recovery period. This prolonged stimulus resulted in significant increases in cFos expression within the NTS of control mice (0.0624 ± 0.006 nuclei/1000μm^3) when compared to either 21% O_2 ($p<0.0001$) or 10min exposures to 8% O_2 ($p<0.0001$). Therefore, the exposure of mice to prolonged (60min) of severe

hypoxia (8% O_2) increased cFos expression within the NTS consistent with previously reported outcomes, while 10min exposures appeared to be of insufficient duration to do so.

The effect of AMPK deletion on cFos expression Counts for cFos expression in TH AMPK-α1/α2 dKO mice following 10min hypoxia followed the same trend as control AMPK-α1/α2 Flx mice. There was no significant increase in the number of cFos-positive nuclei in TH AMPK-α1/α2 dKO mice exposed to severe hypoxia (8%O_2) when compared to TH AMPK-α1/α2 dKO mice exposed to room air (Figure 4.10; 21% O_2: 0.009 ± 0.002 nuclei/1000μm^3, 8% O_2: 0.0182 ± 0.007 nuclei/1000μm^3). Furthermore, the average expression of cFos following 10min hypoxia was almost identical within the NTS of TH AMPK-α1/α2 dKO mice compared to control AMPK-α1/α2 Flx mice exposed to 10min of 8% O_2 ($p=0.999$).

By contrast, and consistent with outcomes for control mice, prolonged 60min exposures to 8% O_2 significantly increased the number of cFos-positive nuclei in TH AMPK-α1/α2 dKO mice compared to TH AMPK-α1/α2 dKO mice exposed to room air (0.0469 ± 0.0086 nuclei/1000μm^3; $p<0.05$). Importantly, average counts revealed a small reduction in the total number of cFos positive nuclei when compared to control AMPK-α1/α2 Flx mice that were also exposed to 60min of 8% O_2 ($p=0.336$).

These findings highlight that 60min of hypoxia is an appropriate stimulus, which was therefore used for further, more detailed analyses of cFos expression in response to hypoxia.

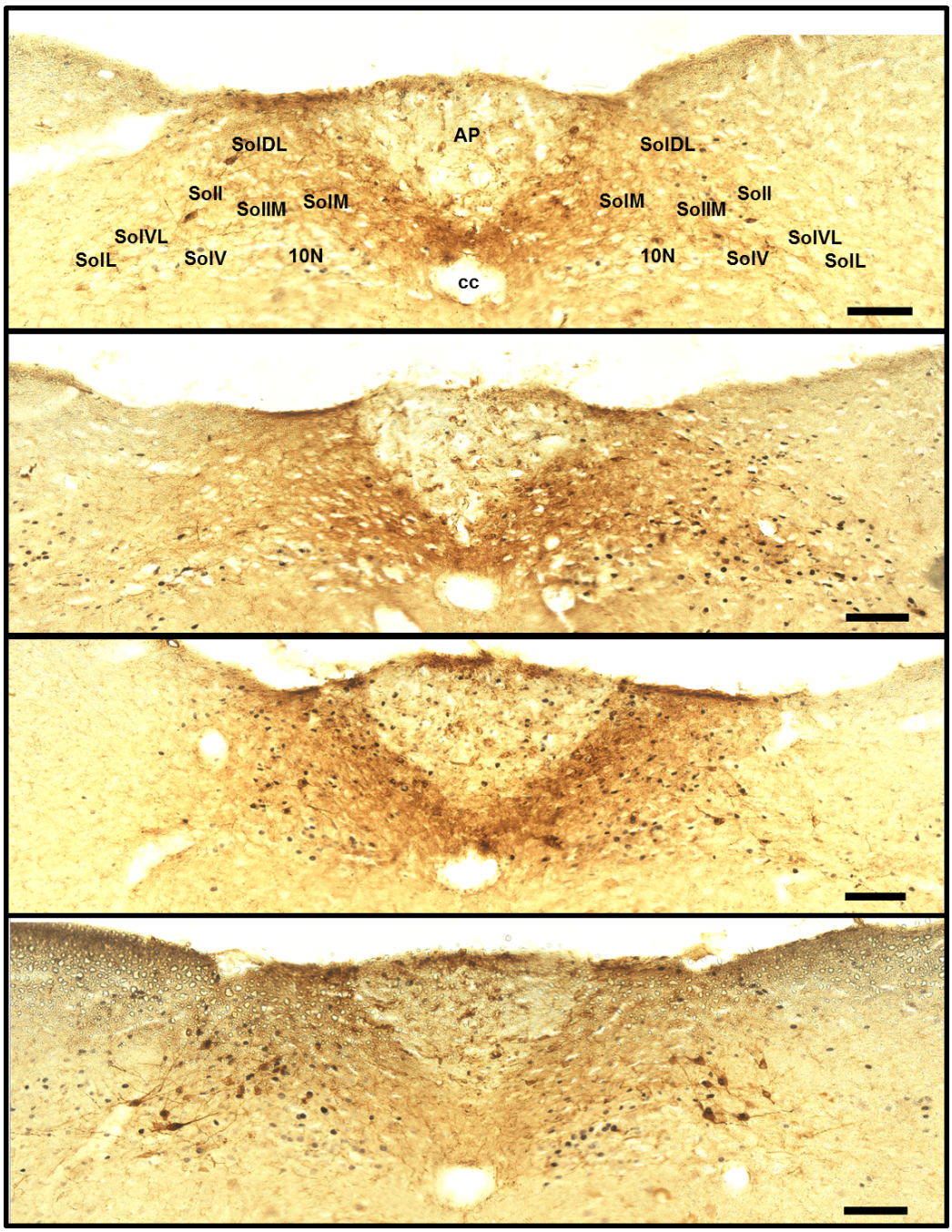

Figure 4.9: 10min exposures to severe hypoxia resulted in highly variable expression of cFos within the dorsal brainstem.

Representative photomicrographs of tyrosine hydroxylase (TH)-positive (brown) cell bodies and cFos-positive (black) nuclei in the caudal brainstem of four different AMPK-α1 and -α2 floxed mice following 10min exposures to 8% O_2. Approximate Bregma -7.56mm. AP = area postrema, cc = central canal, SolM = medial nucleus, SolDL = dorsolateral nucleus, SolIM = intermediate nucleus, SolI = interstitial nucleus, SolV = ventral nucleus, SolVL = ventrolateral nucleus, SolL = lateral nucleus. Scale bar = 100μm.

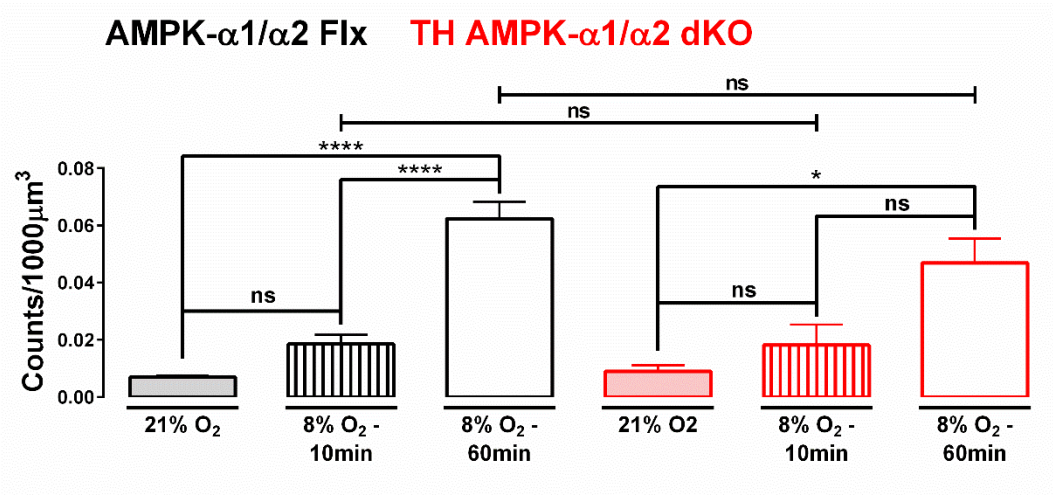

Figure 4.10: 60min of severe hypoxia are required to evoke PO_2-dependent changes in total dorsal brainstem cFos expression.

Means ± SEM for changes in whole NTS cFos counts (per 1000µm^3) in AMPK-α1 and -α2 floxed (AMPK-α1/α2 Flx, black) and TH-driven AMPK-α1 and -α2 double knockout mice (TH AMPK-α1/α2 dKO, red) exposed to room air (21% O_2, shaded bars; controls: n = 4, knockouts: n = 4), 10min of 8% O_2 (lined bars; controls: n = 7, knockouts: n = 4), or 60min of 8% O_2 (empty bars; controls: n = 6, knockouts: n = 7). ns = not significant, * = p<0.05, **** = p<0.0001. Significance tested by one-way ANOVA with Sidak post-hoc tests.

4.2.5 PO_2-dependent increases in cFos expression of control AMPK-α1/α2 Flx mice following 60min exposures to hypoxia

From this point forward, cFos expression was assessed as an index of neuronal activation following 60min exposures to hypoxia.

As illustrated in Figure 4.11, the overall intensity of cFos expression in control AMPK-α1/α2 Flx mice increased with decreasing PO_2, consistent with outcomes previously described in the adult rabbit and rat (Erickson & Millhorn, 1994; Hirooka *et al.*, 1997; King *et al.*, 2012), as well as neonatal mice (Joubert *et al.*, 2016).

My further analyses incorporated subdivisions of brainstem regions by Bregma, given that previous studies have assessed cFos expression per Bregma (Erickson & Millhorn, 1994; Smith *et al.*, 1995; Hirooka *et al.*, 1997; King *et al.*, 2012; King *et al.*, 2015; Joubert *et al.*, 2016). However, in my opinion this is not an ideal method of analysis, because for each experimental animal a number of sections could not be precisely allocated to one or the other of the 'major' Bregma presented in the brain atlas (-7.76mm, -7.64mm, -7.56mm, -7.48mm) and were therefore classified as sections of 'minor' or 'intermediate' Bregma (-7.70mm, -7.60mm, -7.52mm, -7.44mm). This means that ultimately the total number of counted sections varied for each Bregma within each O_2 concentration and genotype, and therefore resulted in an unbalanced dataset. One way to circumvent this issue was to summarise cFos outcomes for each subnucleus of the NTS across all Bregmas. This way, the number of counted sections per group remained consistent, as each subnucleus was present in at least one identified Bregma per animal. Normalisation of cFos counts by surface area and section thickness ensured that differences in subnuclei spanning multiple Bregmas were accounted for. In order to take the most thorough approach possible, however, outcomes were assessed using both approaches and presented throughout this chapter. Finally, in order to assess the bilaterality of hypoxia-induced cFos expression, counts will be presented as the total counts of cFos-positive nuclei (per 1000μm^3) for both sides of the NTS combined, and with the NTS separated into right and left subdivisions. That said, exceptions were made for the AP and SolC,

which in rodents and lagomorphs are midline structures and therefore were only analysed as a whole (Brizzee & Klara, 1984; Franklin & Paxinos, 2008; Low, 2016).

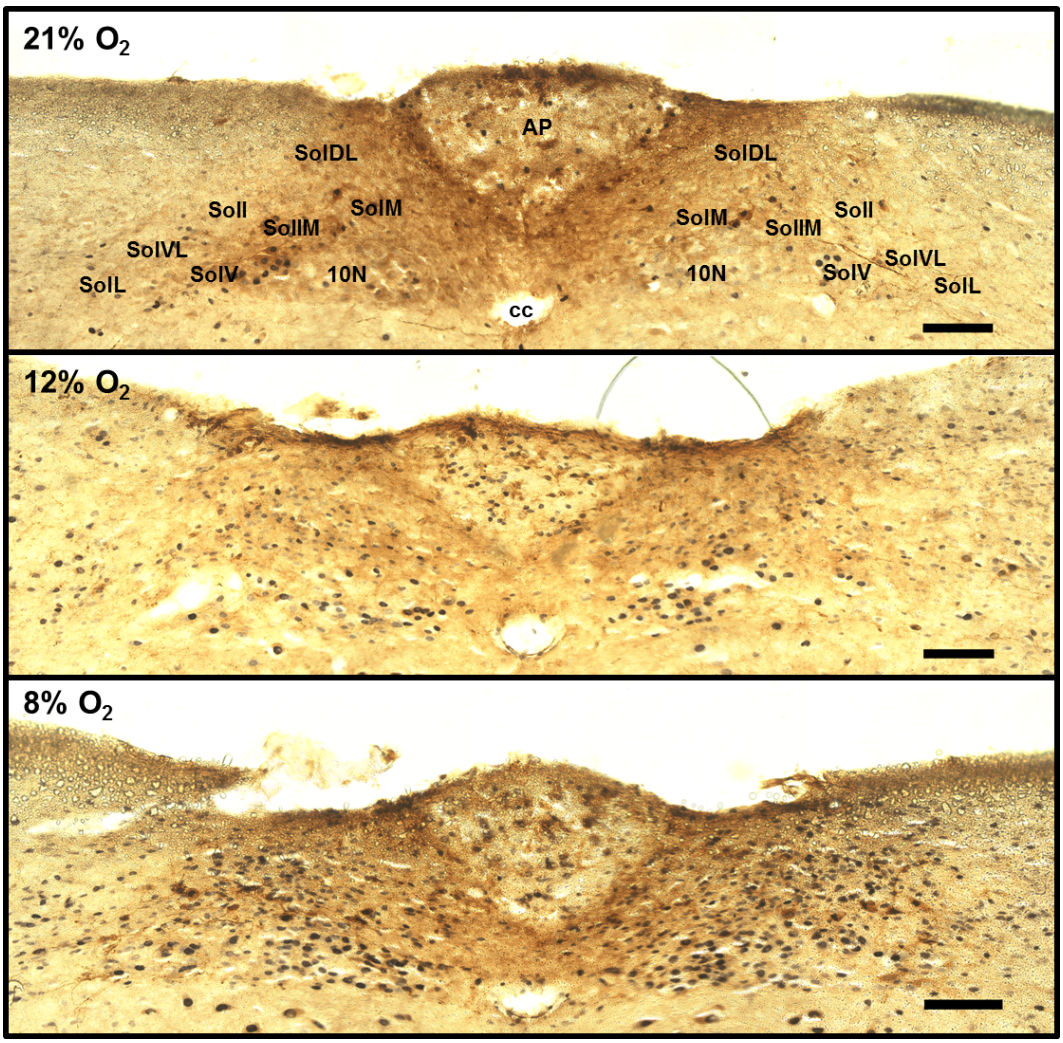

Figure 4.11: 60min exposures to hypoxia increased dorsal brainstem cFos expression in a PO_2-dependent manner.

Representative photomicrographs of tyrosine hydroxylase-positive (brown) and cFos-positive (black) cells in the caudal brainstem of AMPK-α1 and -α2 floxed mice following 60min exposures to 21% O_2 (top panel), 12% O_2 (middle panel), and 8% O_2 (bottom panel). Approximate Bregma -7.56mm. AP = area postrema, cc = central canal, SolM = medial nucleus, SolDL = dorsolateral nucleus, SolIM = intermediate nucleus, SolI = interstitial nucleus, SolV = ventral nucleus, SolVL = ventrolateral nucleus, SolL = lateral nucleus. Scale bar = 100μm.

4.2.5.1 PO_2-dependent increases in cFos expression of control AMPK-α1/α2 Flx mice within each Bregma

Mild hypoxia Consistent with observations made by others (Hirooka *et al.*, 1997; King *et al.*, 2012), 60min exposures to 12% O_2 increased the average expression of cFos in control AMPK-α1/α2 Flx mice relative to room air (21% O_2). These increases in cFos expression from 21% O_2 to 12% O_2 reached significance within the right and left side of the NTS at Bregma -7.56mm, and when both sides of the NTS were added together (Figure 4.12, Table 4.1 and Appendix 2.6; $p<0.05$ for each grouping). In addition, the NTS at the more rostrally located Bregma -7.48mm also displayed a significant increase in cFos expression ($p<0.05$), but only on the right side, with non-significant increases on the left side and when both sides were added together. These outcomes were slightly surprising, given that chemoafferent discharge from the carotid body increases during periods of mild hypoxia (Kumar, 2007). Therefore, afferent chemoreceptor discharge during exposures to 12% O_2 was expected to preferentially increase the activation of brainstem neurons within the caudal portions of the NTS, rather than the rostral portions. However, these Bregma align well with the rostrocaudal extent of the DAR, the area of the brainstem which, compared to controls, exhibited reduced activity during hypoxia following deletion of AMPK-α1/α2 catalytic subunits in catecholaminergic cells.

Table 4.1: Bregma-specific responses of neuronal activation of AMPK-α1/α2 Flx mice following exposures to 12% O_2.

	- 7.76 mm	- 7.70 mm	- 7.64 mm	- 7.60 mm	- 7.56 mm	- 7.52 mm	- 7.48 mm	- 7.44 mm
Both sides	✕	✕	✕	✕	✓	✕	✕	✕
Right side	✕	✕	✕	✕	✓	✕	✓	✕
Left side	✕	✕	✕	✕	✓	✕	✕	✕

✕ = no activation, ✓ = mild activation

Severe hypoxia In contrast to mild hypoxia, significant increases in cFos expression from 21% O_2 to 8% O_2 were observed for both sides of the NTS

in all clearly identified 'major' Bregma along the caudo-rostral axis (Figure 4.10 A, Table 4.2 and Appendix 2.6; Bregma: -7.76mm, $p<0.05$; -7.64mm, $p<0.05$; -7.56mm, $p<0.01$; -7.48mm, $p<0.001$). Importantly, a similar level of cFos expression after exposures to 8% O_2 was also obtained in sections that fell between two of the major Bregma ('minor' Bregma: -7.70mm, -7.60mm, -7.52mm, and -7.44mm), but the numbers of sections per minor Bregma were too low to test for or reach statistical significance. That aside, the degree of activation during 8% O_2 was clearly strongest in more rostral Bregma of the caudal brainstem, which may point to activation of these regions as being critical in the response to hypoxia.

Analysis of the right side of the brainstem alone revealed that significant increases from 21% O_2 to 8% O_2 were retained in all major Bregmas (Figure 4.10 B, Appendix 2.6; -7.76mm, $p<0.05$; -7.64mm, $p<0.05$; -7.56mm, $p<0.01$; -7.48mm, $p<0.001$). In addition, significance was reached at Bregma -7.52mm ($p<0.05$), while the level of cFos expression in all other 'minor' Bregmas after exposures to 8% O_2 was comparable to those obtained in 'major' Bregmas.

Outcomes for cFos expression within the left side of the brainstem alone revealed that the increase of cFos expression from 21% O_2 to 8% O_2 did not quite reach significance at Bregma -7.76mm (Figure 4.10 C; $p=0.0536$). In all other Bregmas, however, outcomes were identical to those of the right side alone and when both sides were added together (-7.64mm, $p<0.05$; -7.56mm, $p<0.01$; -7.48mm, $p<0.001$).

Table 4.2: Bregma-specific responses of neuronal activation in AMPK-α1/α2 Flx mice following exposure to 8% O_2.

	- 7.76 mm	- 7.70 mm	- 7.64 mm	- 7.60 mm	- 7.56 mm	- 7.52 mm	- 7.48 mm	- 7.44 mm
Both sides	✓	✕	✓	✕	✓✓	✕	✓✓✓	✕
Right side	✓	✕	✓	✕	✓✓	✓	✓✓✓	✕
Left side	✕	✕	✓	✕	✓✓	✕	✓✓✓	✕

✕ = no activation, ✓ = mild activation, ✓✓ = moderate activation, ✓✓✓ = strong activation

Mild versus severe hypoxia Increases in the average cFos expression of control mice were also observed between 12% O_2 and 8% O_2 (Table 4.3), but once again these only reached significance within both sides of the NTS at the more rostral Bregma, namely -7.48mm ($p<0.05$), and -7.44mm ($p<0.001$). Significant increases in cFos expression at Bregma -7.48mm and -7.44mm were also retained when cFos-positive counts were separated into the right side (-7.48mm: $p<0.05$; -7.44mm: $p<0.001$) and left side (-7.48mm: $p<0.05$; -7.44mm: $p<0.01$) of the NTS.

Table 4.3: Bregma-specific responses of neuronal activation in AMPK-α1/α2 Flx mice between exposures to 12% O_2 and 8% O_2.

	- 7.76 mm	- 7.70 mm	- 7.64 mm	- 7.60 mm	- 7.56 mm	- 7.52 mm	- 7.48 mm	- 7.44 mm
Both sides	✕	✕	✕	✕	✕	✕	✓	✓✓✓
Right side	✕	✕	✕	✕	✕	✕	✓	✓✓✓
Left side	✕	✕	✕	✕	✕	✕	✓	✓✓

✕ = no activation, ✓ = mild activation, ✓✓ = moderate activation, ✓✓✓ = strong activation

As described above, the significant increases in rostral, but not caudal, parts of the NTS were unexpected, given the termination of carotid body afferent innervations within the caudal portions of the NTS. However, the possibility remains that the rostral portions of the caudal NTS may contain a central O_2-responsive neuronal network, which determines – in concert with CB afferent fibre input – the overall degree of respiratory drive during hypoxia.

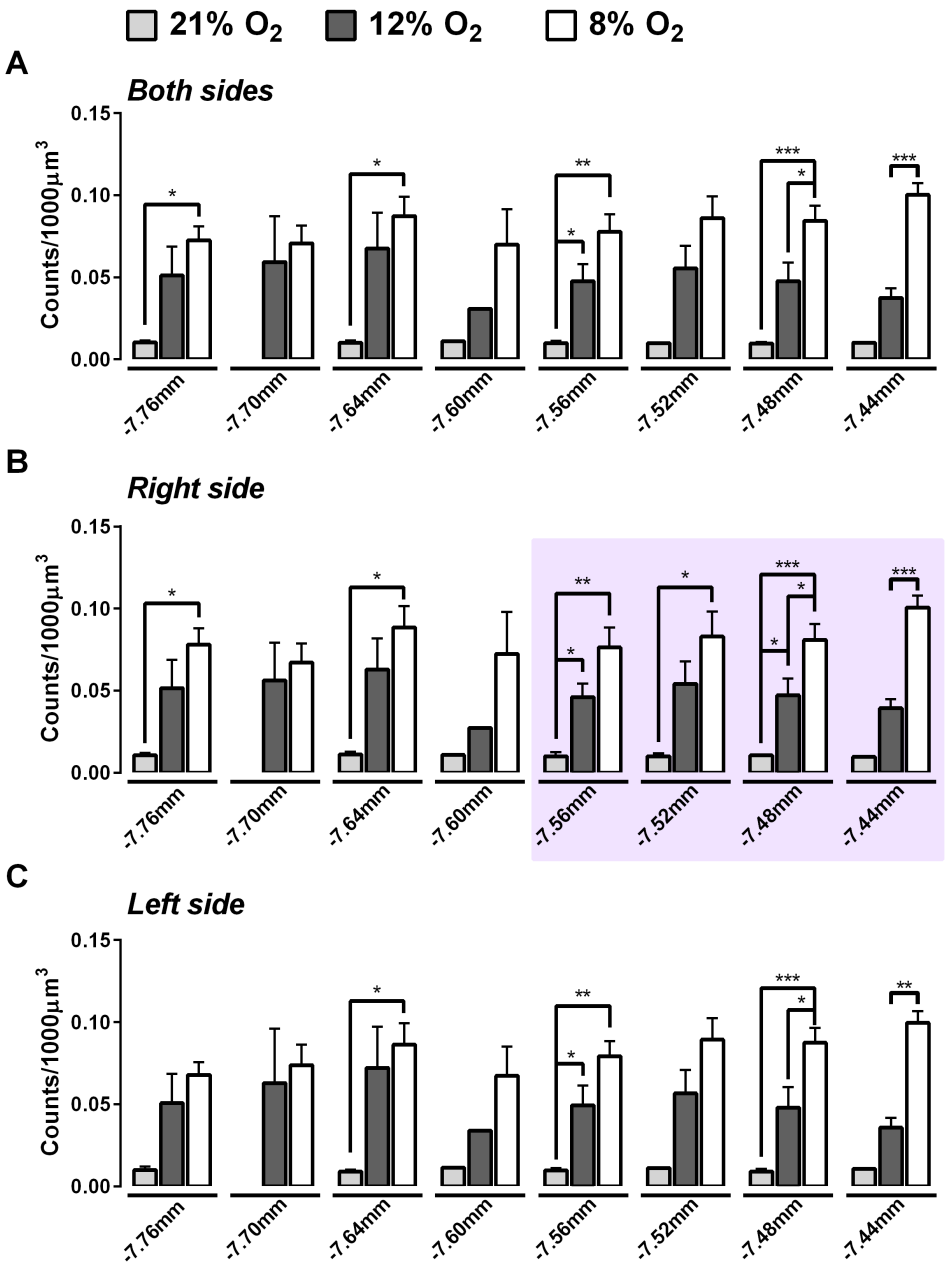

Figure 4.12: 60min exposures to hypoxia increased brainstem cFos expression in a PO_2-dependent manner in every identified Bregma.
Means ± SEM of cFos-positive cell counts per 1000µm^3 in identified Bregma of the **(A)** total, **(B)** right-sided, and **(C)** left-sided nucleus tractus solitarius of AMPK-α1/α2 floxed mice after 60min exposures to 21% O_2 (n = 4 mice), 12% O_2 (n = 6 mice), or 8% O_2 (n = 6 mice). * = p<0.05, ** = p<0.01, *** = p<0.001, **** = p<0.0001. Significance tested by one-way ANOVA with Tukey post-hoc tests (long brackets) and Student's t-test (short brackets). Highlighted in purple is the approximate location of the DAR (Mahmoud *et al.*, 2016).

4.2.5.2 PO_2-dependent increases in cFos expression of control AMPK-α1/α2 Flx mice within each subnucleus of the NTS

Mild hypoxia Analyses of both sides of the NTS as a whole revealed that 60min exposures of control AMPK-α1/α2 Flx mice to 12% O_2 increased the average cFos expression relative to room air (21% O_2) in every subnucleus of the NTS (Figure 4.13 A, Appendix 2.7). These increases reached significance within the medioventral subnuclei 10N ($p<0.01$), SolC ($p<0.05$), SolM ($p<0.05$), and SolCe ($p<0.05$) (Table 4.4). While the afferent projections from SolCe to the ventral medulla were found to be restricted to the facial nucleus (7N) and the nucleus ambiguus (NA), 10N, SolC, and SolM have been implicated in the control of cardiorespiratory responses due to their afferent projections to the rostral and caudal ventral respiratory groups (rVRG and cVRG, respectively), and the rostral and caudal ventrolateral medulla (RVL and CVL, respectively; see also Figure 4.1) (Alheid *et al.*, 2011). Therefore, these nuclei might be primarily implicated in delivering the mild increases in ventilation described in Chapter 3.

Considering the right side of the NTS alone (Figure 4.13 B, Appendix 2.7), 12% O_2 still induced significant increases in cFos expression relative to room air within 10N ($p<0.01$) SolM ($p<0.05$) and SolCe ($p<0.05$), consistent with outcomes for both sides together. Although findings so far have consistently demonstrated bilateral increases in cFos expression within the NTS following hypoxic stimulation (Erickson & Millhorn, 1994; Hirooka *et al.*, 1997; Teppema *et al.*, 1997), additional significance within the right NTS was reached within the mediolateral NTS subnuclei SolDM ($p<0.05$) and SolIM ($p<0.05$). Both SolDM and SolIM were found to have prominent ipsilateral afferent projections to the respiratory compartments of the cVRG, rVRG and the retrotrapezoid nucleus (RTN), and SolIM also weakly projects to the cardiovascular compartments of the RVL and CVL (Alheid *et al.*, 2011).

Within the left side of the NTS (Figure 4.13 C, Appendix 2.7), significant increases in cFos expression from 21% O_2 to 12% O_2 were retained within 10N ($p<0.05$) and SolCe ($p<0.05$), consistent with outcomes for both sides together. Unlike outcomes for the right side alone, however, no additional

significance was reached within any other subnuclei on the left side of the NTS, and significance was lost within SolM (p=0.0519).

It is possible, therefore, that the drive to breathe during mild hypoxia is modulated by a hemisphere-specific activation of specific NTS subnuclei.

Table 4.4: NTS subnucleus-specific neuronal activation in AMPK-α1/α2 Flx mice following exposure to 12% O_2.

	AP	SubP	10N	SolC	SolM	SolDM	SolDL	SolI	SolIM	SolV	SolVL	SolL	SolCe
Both sides	✕	✕	✓✓	✓	✓	✕	✕	✕	✕	✕	✕	✕	✓
Right side	/	✕	✓✓	/	✓	✓	✕	✕	✓	✕	✕	✕	✓
Left side	/	✕	✓	/	✕	✕	✕	✕	✕	✕	✕	✕	✓

✕ = no activation, ✓ = mild activation, ✓✓ = moderate activation

Severe hypoxia Robust increases in cFos expression were observed following exposures to 8% O_2, which significantly augmented cFos expression in every single subnucleus of the NTS relative to 21% O_2, irrespective of whether the counts were grouped together for both sides of the NTS, or separated into its right and left divisions (Figure 4.13, Appendix 2.7).

Table 4.5: NTS subnucleus-specific neuronal activation of AMPK-α1/α2 Flx mice following exposure to 8% O_2.

	AP	SubP	10N	SolC	SolM	SolDM	SolDL	SolI	SolIM	SolV	SolVL	SolL	SolCe
Both sides	✓✓	✓✓✓	✓✓✓✓	✓✓✓	✓✓	✓✓	✓✓✓	✓✓	✓✓✓	✓✓✓	✓✓✓	✓✓	✓✓✓
Right side	/	✓✓	✓✓✓✓	/	✓✓	✓✓	✓✓✓	✓✓	✓✓✓	✓✓	✓✓	✓✓✓	✓✓✓
Left side	/	✓✓	✓✓✓	/	✓✓	✓✓	✓✓	✓✓✓	✓✓	✓✓✓✓	✓✓✓	✓	✓✓

✕ = no activation, ✓ = mild activation, ✓✓ = moderate activation, ✓✓✓ = strong activation, ✓✓✓✓ = very strong activation

Mild versus severe hypoxia Within both sides of the NTS of control AMPK-α1/α2 Flx mice, further hypoxia-dependent increases were observed between 12% O_2 and 8% O_2 within the majority of cardiorespiratory NTS

subnuclei (Table 4.6; SubP: $p<0.05$; 10N: $p<0.05$; SolC: $p<0.05$; SolDL: $p<0.05$; SolI: $p<0.05$; SolV: $p<0.01$; SolVL: $p<0.05$; SolL: $p<0.05$).

Consistent with these outcomes, significant increases within the right side of the NTS alone were also observed within SubP ($p<0.05$), SolC ($p<0.05$), SolDL ($p<0.05$), SolI ($p<0.05$), SolV ($p<0.05$), SolVL ($p<0.05$), and SolL ($p<0.01$), but almost within 10N ($p=0.0549$). However, additional significance was gained within SolIM ($p<0.05$) and SolCe ($p<0.05$).

Considering the left side of the NTS alone, the significant differences observed for both sides of the NTS combined were retained at 10N ($p<0.05$), SolC ($p<0.05$), SolI ($p<0.05$), SolV ($p<0.001$) and SolVL ($p<0.05$), whereas SubP ($p=0.07$), SolDL ($p=0.156$) and SolL ($p=0.0816$) did no longer show a significant increase in cFos expression between 12% O_2 and 8% O_2.

Table 4.6: NTS subnucleus-specific responses of neuronal activation of AMPK-α1/α2 Flx mice between exposures to 12% O_2 and 8% O_2.

	AP	SubP	10N	SolC	SolM	SolDM	SolDL	SolI	SolIM	SolV	SolVL	SolL	SolCe
Both sides	✕	✓	✓	✓	✕	✕	✓	✓	✕	✓✓	✓	✓	✕
Right side	/	✓	✕	/	✕	✕	✓	✓	✓	✓	✓	✓	✓
Left side	/	✕	✓	/	✕	✕	✕	✓	✕	✓✓✓	✓	✕	✕

✕ = no activation, ✓ = mild activation, ✓✓ = moderate activation, ✓✓✓ = strong activation

Overall, the three-point assay described above showed that 60min of hypoxia was of sufficient duration to induce PO_2-dependent increases in cFos expression within the caudal brainstems of AMPK-α1/α2 Flx mice, regardless of whether the data were presented for the entire brainstem (Figure 4.10), categorised as the whole NTS per Bregma (Figure 4.12), each NTS subnucleus in entirety along the full length of the caudal brainstem (Figure 4.13), as the total for both sides of the NTS, or divided into bilateral components of the NTS found within the right and left sides of the brainstem. Additionally, further separating these categories into outcomes for each subnucleus at each Bregma (see Appendices 2.8-2.11) also supported the above described findings. Therefore, although only more rostral Bregma of

the caudal brainstem were primarily activated in a PO_2-dependent manner, each nucleus within the NTS of AMPK-α1/α2 Flx mice was responsive to hypoxia with robust increases in cFos expression during severe hypoxia. These outcomes are consistent with the PO_2-dependent increases in ventilation of control mice described in Chapter 3, as well as the PO_2-dependent attenuation of the HVR observed in TH AMPK-α1/α2 dKO mice. Therefore, a subset of neurons within NTS subnuclei may form a central hypoxia-responsive neural circuit within the rostral portion of the caudal brainstem that determines the degree of ventilatory drive. Additionally, the findings described above indicate for the first time that separation of the NTS into its individual subnuclei may have revealed a degree of specificity for some subnuclei to be differentially activated in a PO_2- and hemisphere-dependent manner during milder exposures to hypoxia.

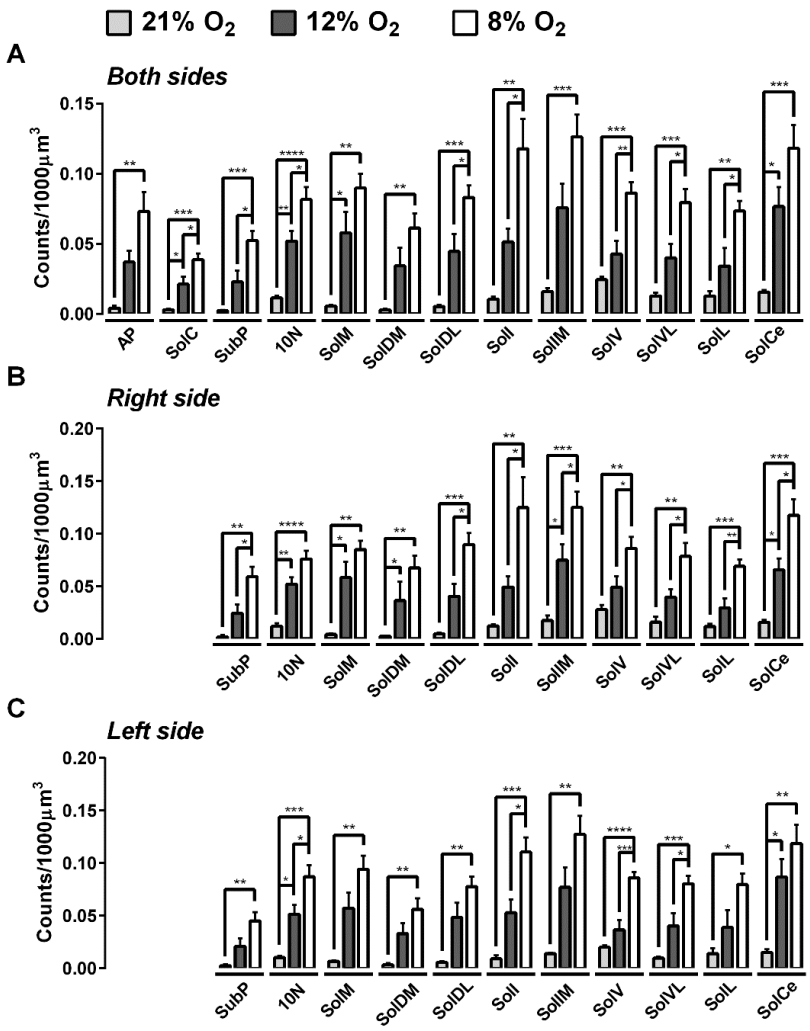

Figure 4.13: 60min exposures to hypoxia increased brainstem cFos expression in a PO_2-dependent manner in every subnucleus of the NTS.

Means ± SEM of cFos-positive cell counts per 1000µm^3 in specific regions of interest over all identified Bregma of the **(A)** total, **(B)** right-sided, and **(C)** left-sided nucleus tractus solitarius of AMPK-α1/α2 floxed mice after 60min exposures to 21% O_2 (n = 4 mice), 12% O_2 (n = 6 mice), or 8% O_2 (n = 6 mice). AP = area postrema, SolC = commissural nucleus, SubP = sub-postrema, 10N = hypoglossal nucleus, SolM = medial nucleus, SolDM = dorsomedial nucleus, SolDL = dorsolateral nucleus, SolI = interstitial nucleus, SolIM = intermediate nucleus, SolV = ventral nucleus, SolVL = ventrolateral nucleus, SolL lateral nucleus, SolCe = central nucleus. * = p<0.05, ** = p<0.01, *** = p<0.001, **** = p<0.0001. Significance tested by one-way ANOVA with Tukey post-hoc tests.

4.2.6 The impact of AMPK-α1 and -α2 catalytic subunit deletion in catecholaminergic cells on the cFos expression in response to 60min of severe hypoxia

Given the fact that the ventilatory deficit in mice with TH-driven deletion of AMPK-α1 and -α2 catalytic subunits appeared to be due to a functional deficit rather than alterations in catecholaminergic cell numbers or bioamine content, the expression of cFos in TH AMPK-α1/α2 dKO mice was compared to control AMPK-α1/α2 Flx mice following 60min exposures to severe hypoxia. A stimulus of 8% O_2 was chosen for this comparison because it induced significant increases in cFos expression within every Bregma and every subnucleus of AMPK-α1/α2 Flx mice and also precipitated the most severe ventilatory deficit within TH AMPK-α1/α2 dKO mice relative to controls.

The effect of AMPK deletion on NTS cFos expression within each Bregma

Analyses of both sides of the NTS at any given Bregma as a whole revealed no significant changes in cFos expression (normalised as counts per 1000μm^3) following 60min exposures to 8% O_2 in TH AMPK-α1/α2 dKO mice relative to controls, even though on average cFos expression was mildly reduced in the more rostral parts of the caudal brainstem (Figure 4.14 A, Appendix 2.12; Bregmas -7.56mm to -7.44mm). A non-significant reduction in cFos expression within the rostral Bregma of TH AMPK-α1/α2 dKO mice relative to controls was also observed when the NTS was separated into its right and left divisions (Figure 4.14 B and C, respectively).

It would therefore appear that any reductions in cFos expression that might have occurred arose within more rostral regions of the NTS and not the caudal portion, which is the primary site of carotid body afferent innervation (Finley & Katz, 1992). In support of this, deficits within the more rostral Bregma of TH AMPK-α1/α2 dKO mice would be consistent with the anatomical location of the DAR, the decrease in neuronal “activity” during severe hypoxia that was identified by fMRI, and the unaltered response of increased carotid body chemoafferent discharge during exposure to hypoxia (Mahmoud *et al.*, 2016).

The effect of AMPK deletion on cFos expression within each NTS subnucleus When considering each subnucleus from both sides of the NTS along their entire length, TH AMPK-α1/α2 dKO mice had, on average, fewer cFos counts per 1000μm^3 than control AMPK-α1/α2 Flx mice did (Figure 4.15 A). However, as shown in Figure 4.10, these individual reductions did not reach significance relative to controls when all subnuclei were added together. Furthermore, none of the individual subnuclei on their own revealed a significant reduction in cFos expression for TH AMPK-α1/α2 dKO mice relative to controls (Appendix 2.13), regardless of whether each subnucleus of the NTS was taken as a total of both sides, or divided into its bilateral components (Figure 4.15 B and C, respectively).

From these data it seemed that deletion of AMPK-α1 and -α2 catalytic subunits in catecholaminergic cells did not have an impact on neuronal activation sufficient enough to explain the severe ventilatory deficits described in Chapter 3. That said, outcomes from our previous fMRI study (Mahmoud *et al.*, 2016) revealed that the functional deficit in neuronal activity (measured via decreases in O_2 consumption) during hypoxia was confined to a few Bregma and did not span the entire caudal brainstem. This area, i.e. the DAR, and its location could be consistent with the average, albeit non-significant, reductions in cFos expression observed in more rostral, but not caudal Bregma of TH AMPK-α1/α2 dKO brainstems. If true, this would suggest that the analyses of cFos-positive counts per subnucleus for the entire length of the NTS may have diluted any Bregma-specific differences within the more rostral portions. Therefore, these data were reanalysed to compare the cFos responses after 60min of 8% O_2 in AMPK-α1/α2 Flx and TH AMPK-α1/α2 dKO for each subnucleus at each identified Bregma.

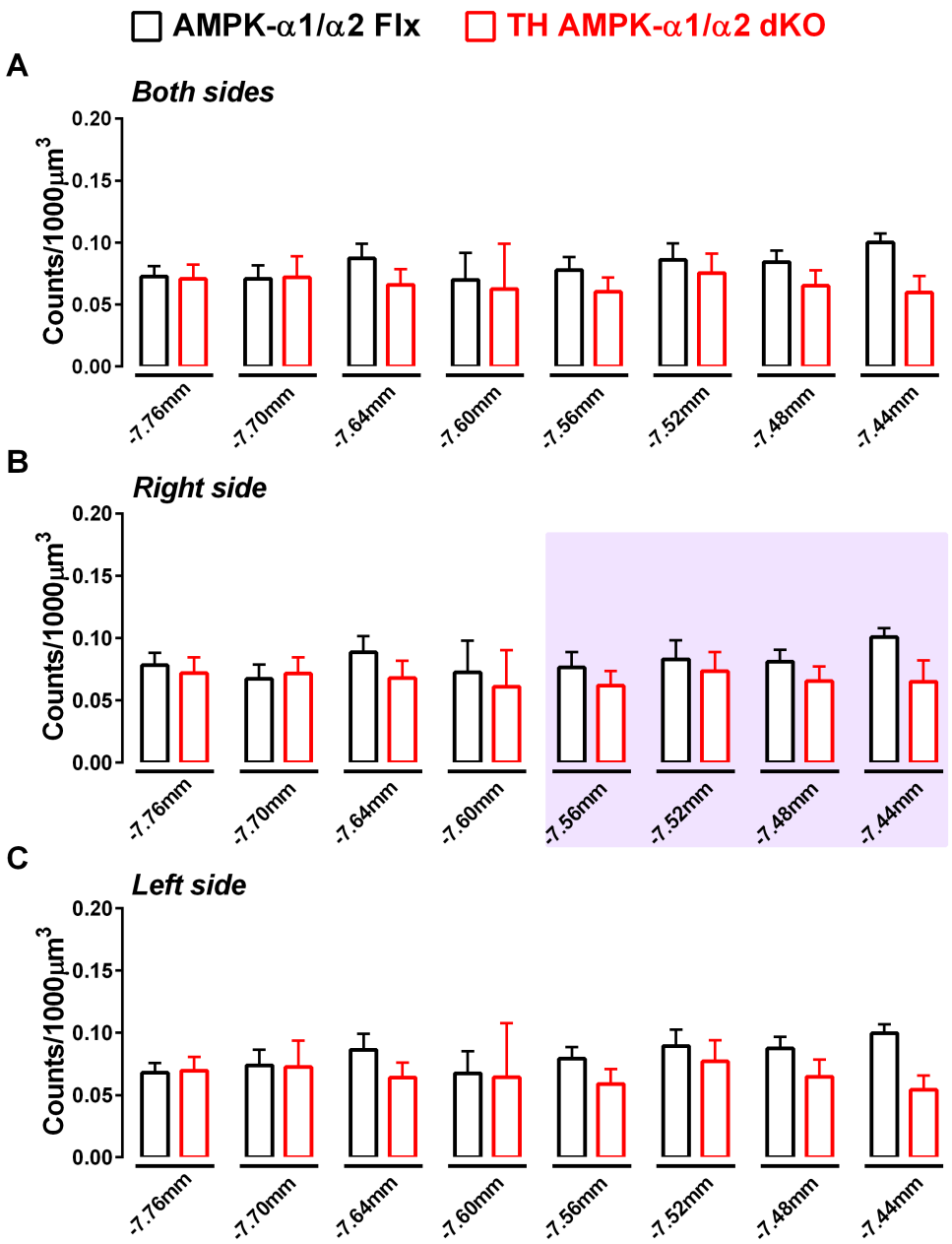

Figure 4.14: Targeted deletion of AMPK-α1/α2 catalytic subunits in catecholaminergic cells did not alter dorsal brainstem cFos counts within any Bregma.

Means ± SEM of cFos counts (per 1000µm^3) for all identified Bregma within the **(A)** total, **(B)** right-sided, and **(C)** left-sided nucleus tractus solitarius of AMPK-α1/α2 floxed (AMPK-α1/α2 Flx, black, n = 16 mice) and TH-driven AMPK-α1 and -α2 double knockout mice (TH AMPK-α1/α2 dKO, red, n = 11 mice). Significance tested by one-way ANOVA with Tukey post-hoc test. Highlighted in purple is the approximate location of the DAR (Mahmoud *et al.*, 2016).

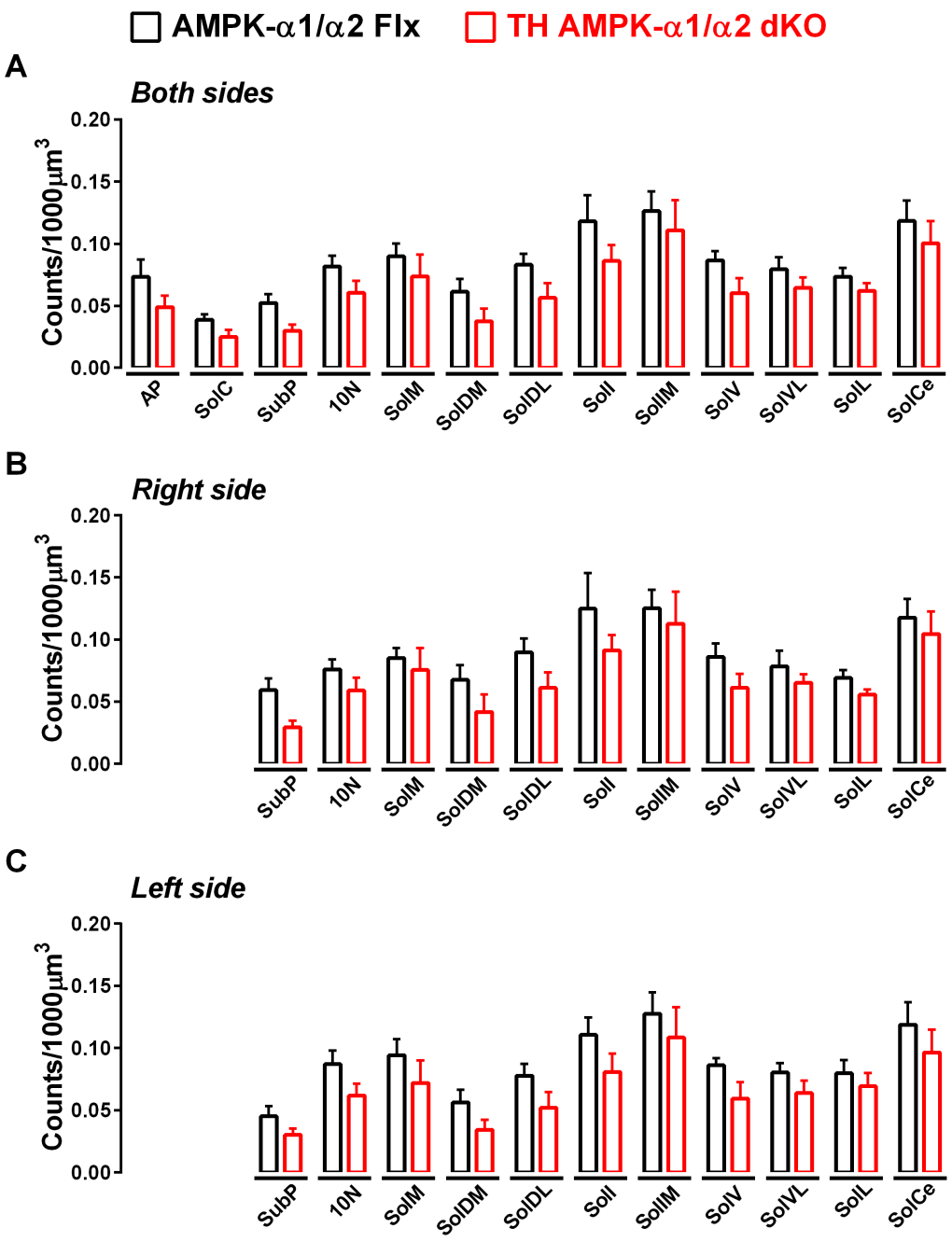

Figure 4.15: Targeted deletion of AMPK-α1/α2 catalytic subunits in catecholaminergic cells did not alter dorsal brainstem cFos counts within any subnuclei of the NTS.

Means ± SEM of cFos counts (per 1000µm^3) for each subnucleus within the **(A)** total, **(B)** right-sided, and **(C)** left-sided nucleus tractus solitarius of AMPK-α1/α2 floxed (AMPK-α1/α2 Flx, black, n = 6 mice) and TH-driven AMPK-α1 and -α2 double knockout mice (TH AMPK-α1/α2 dKO, red, n = 7 mice). Significance tested by one-way ANOVA with Tukey post-hoc test.

4.2.6.1 Identification of a Bregma- and subnucleus-specific deficit in cFos expression following deletion of AMPK-α1 and -α2 catalytic subunits in catecholaminergic cells

As mentioned above, the region of the DAR appeared in more rostral regions within the right side of the NTS and its overall shape suggested that several anatomical subnuclei could be affected by the targeted deletion of AMPK in the catecholaminergic cells within them. Surprisingly, however, given the afferent innervations of both cardiovascular and respiratory compartments in the ventral medulla that originate from the vast majority of NTS subnuclei (see Figure 4.1), AMPK deletion and subsequent reductions in neuronal activity within the DAR only precipitated deficits in the respiratory response and did not impact on the cardiovascular responses to hypoxia (Mahmoud *et al.*, 2016). Therefore, elucidating the precise subnuclear location of the DAR along the neuraxis of TH AMPK-α1/α2 dKO mice could lead to a better understanding of why only the respiratory, but not the cardiovascular response was affected.

Overall, separating the comparisons of cFos expression between AMPK-α1/α2 Flx and TH AMPK-α1/α2 dKO mice by subnucleus of the NTS at each identified Bregma revealed no significant differences between genotypes within caudal Bregma ranging from -7.76mm to -7.60mm. However, excitement was sparked when significant reductions in the cFos expression of TH AMPK-α1/α2 dKO mice were identified relative to controls within specific subnuclei of the NTS located within the more rostral Bregma, consistent with the indications from the outcomes above (Figure 4.16, Appendix 2.14). Furthermore, even more thrilling was the fact that two of these subnuclei (hereon referred to as Nucleus A and Nucleus B) coincided with the approximate anatomical location of the DAR within the NTS. Both subnuclei showed a significant reduction within the right side of the brainstem ($p<0.05$ for Nucleus A and Nucleus B, respectively, relative to controls), but not the left, entirely consistent with the observed right-side dominance of the DAR (Figure 4.17 A, Appendix 2.15). Like most other NTS subnuclei, both Nucleus A and B were proposed to innervate respiratory and

cardiovascular compartments of the VLM. However, Nucleus A appears to also innervate compartments of the ventral medulla responsible for the generation of respiratory rhythmogenesis, which could, at least in part, explain the disordered ventilatory phenotype observed in TH AMPK-α1/α2 dKO mice, which will be further discussed in Chapter 5.

Curiously, Nucleus A and Nucleus B were not anatomically adjacent to each other, so the relationship between them and the DAR was in question (Figure 4.17 B). In addition, a reduction in the average density of cFos-positive nuclei in TH AMPK-α1/α2 dKO mice was observed relative to controls within all of the DAR-spanning Bregma. Therefore, in order to determine the Bregma-specific contributions of each Nucleus to the formation of the DAR, various combinations of multiple Bregmas that might link these nuclei together were tested to see how the statistical difference between controls and TH AMPK-α1/α2 dKO mice changes.

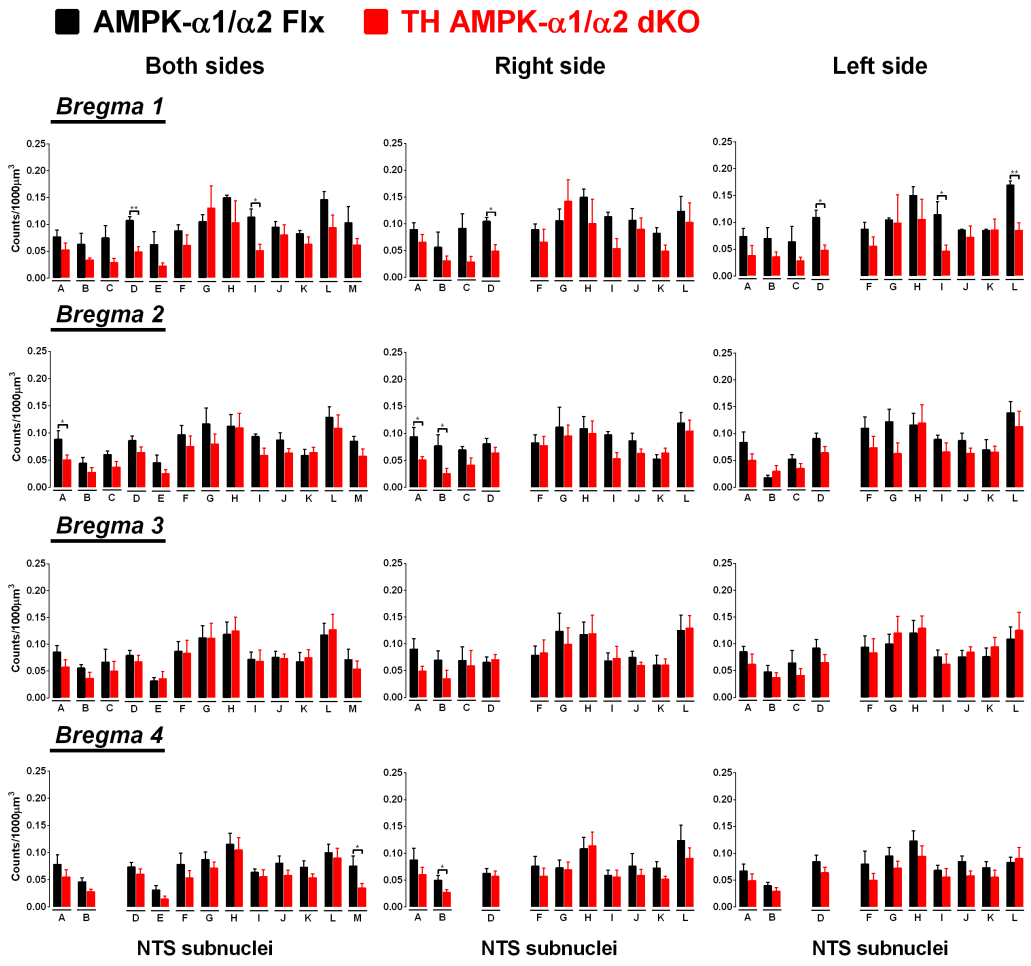

Figure 4.16: Separation of Bregma and subnuclei revealed significant, right-side dominant attenuation of cFos expression following AMPK-α1/α2 catalytic subunit deletion in catecholaminergic cells.

Means ± SEM of cFos counts (per 1000µm^3) for the total (*left panels*), right (*middle panels*), and left (*right panels*) sides of all subnuclei (encrypted A to M) within the nucleus tractus solitarius (NTS) in four caudal brainstem Bregmas (encrypted Bregma 1 to 4) of AMPK-α1/α2 floxed (AMPK-α1/α2 Flx, black) and TH-driven AMPK-α1 and -α2 double knockout mice (TH AMPK-α1/α2 dKO, red). * = $p<0.05$, ** = $p<0.01$; significance tested by Student's t-test between genotypes for each grouping.

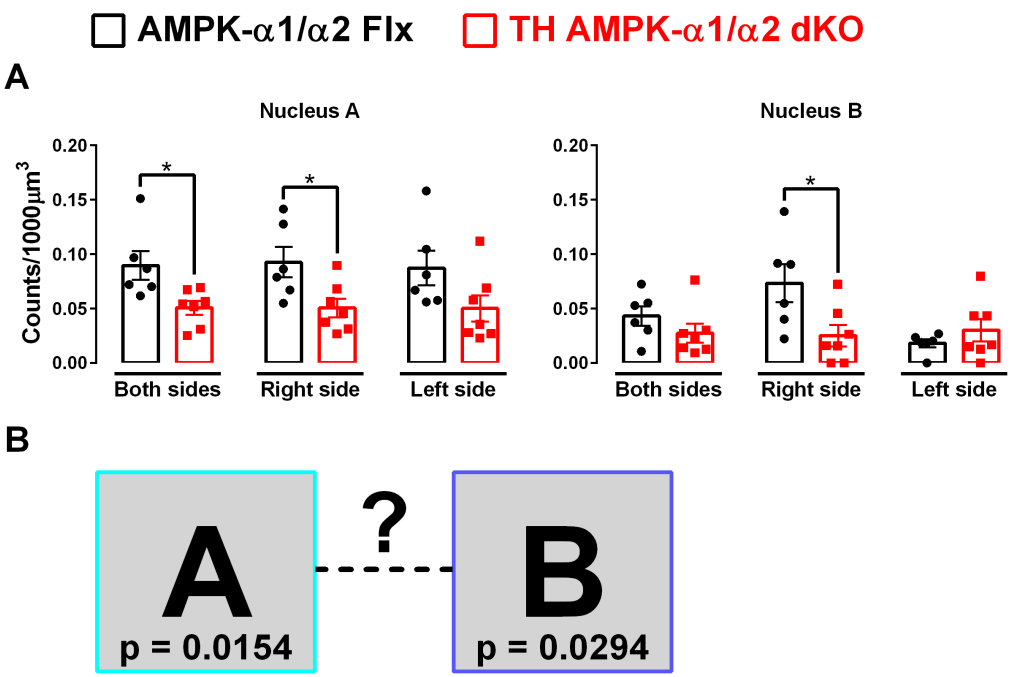

Figure 4.17: A Bregma- and subnucleus-specific deficiency in cFos expression was revealed by deletion of AMPK-α1 and -α2 catalytic subunits in catecholaminergic cells.

(A) Means ± SEM of cFos counts (per 1000µm^3) of two specific subnuclei within the nucleus tractus solitarius of AMPK-α1/α2 floxed (AMPK-α1/α2 Flx, black, n = 6 mice) and TH-driven AMPK-α1 and -α2 double knockout mice (TH AMPK-α1/α2 dKO, red, n = 7 mice). **(B)** Schematic representing the relationship of the two identified nuclei to each other and the p-values obtained. * = $p<0.05$; significance tested by Student's t-test between genotypes for each grouping.

Combinations of Nucleus A and Nucleus B across Bregma The first approach was to identify whether the deficit within each of the two nuclei within the right side of the NTS spanned more than one Bregma, as was suggested by the DAR. As described above, cFos expression in Nucleus A and Nucleus B were significantly attenuated in TH AMPK-α1/α2 dKO mice relative to controls in Bregma 2 (Figure 4.18 Ai, Aiv, Bi, Biv and Appendix 2.15; Nucleus A: p=0.0154, Nucleus B: p=0.0294), but not in the next more caudal or rostral Bregma (Nucleus A – Bregma 1: p=0.2895, Bregma 3: p=0.1321, Bregma 4: p=0.2928; Nucleus B – Bregma 1: p=0.3767, Bregma 3: p=0.1787). However, Nucleus B also exhibited significant reductions in cFos expression at Bregma 4 (p=0.0355), which sits at the caudal-most edge of the DAR-spanning Bregma along this neuraxis.

Connecting the cFos densities across two of the four adjacent Bregma retained significance for Nucleus A at the rostral end (Figure 4.18 Aii, Bii and Appendix 2.15; Bregma 1+2: p=0.0113), but not at the others (Bregma 2+3: p=0.1034, Bregma 3+4: p=0.2536). However, connecting up three of the 4 adjacent Bregmas almost retained significance in each combination (Figure 4.18 Aiii, Biii; Bregma 1-3: p=0.042, Bregma 2-4: p=0.0508). Finally, the connection of all 4 identified Bregmas retained significance for the decrease in TH AMPK-α1/α2 dKO mice relative to controls (Bregma 1-4: p=0.0417), although the difference was smaller than for Bregma 2 and the combination of Bregma 1+2.

For Nucleus B, combining two adjacent Bregma only retained significance at the caudal end, but not at the others (Figure 4.18 Av, Bv and Appendix 2.15; Bregma 1+2: p=0.0543, Bregma 2+3: p=0.0719, Bregma 3+4: p=0.038). Furthermore, connecting up three of the 4 adjacent Bregmas revealed significance in both combinations (Figure 4.18 Avi, Bvi; Bregma 1-3: p=0.0394, Bregma 2-4: p=0.0178), as did the combination of Nucleus B across all four Bregmas (Bregma 1-4: p=0.0232). Therefore, Nucleus B showed the greatest significant attenuation of cFos expression in TH AMPK-α1/α2 dKO mice when Bregmas 2-4 and possibly Bregmas 1-4 were grouped together.

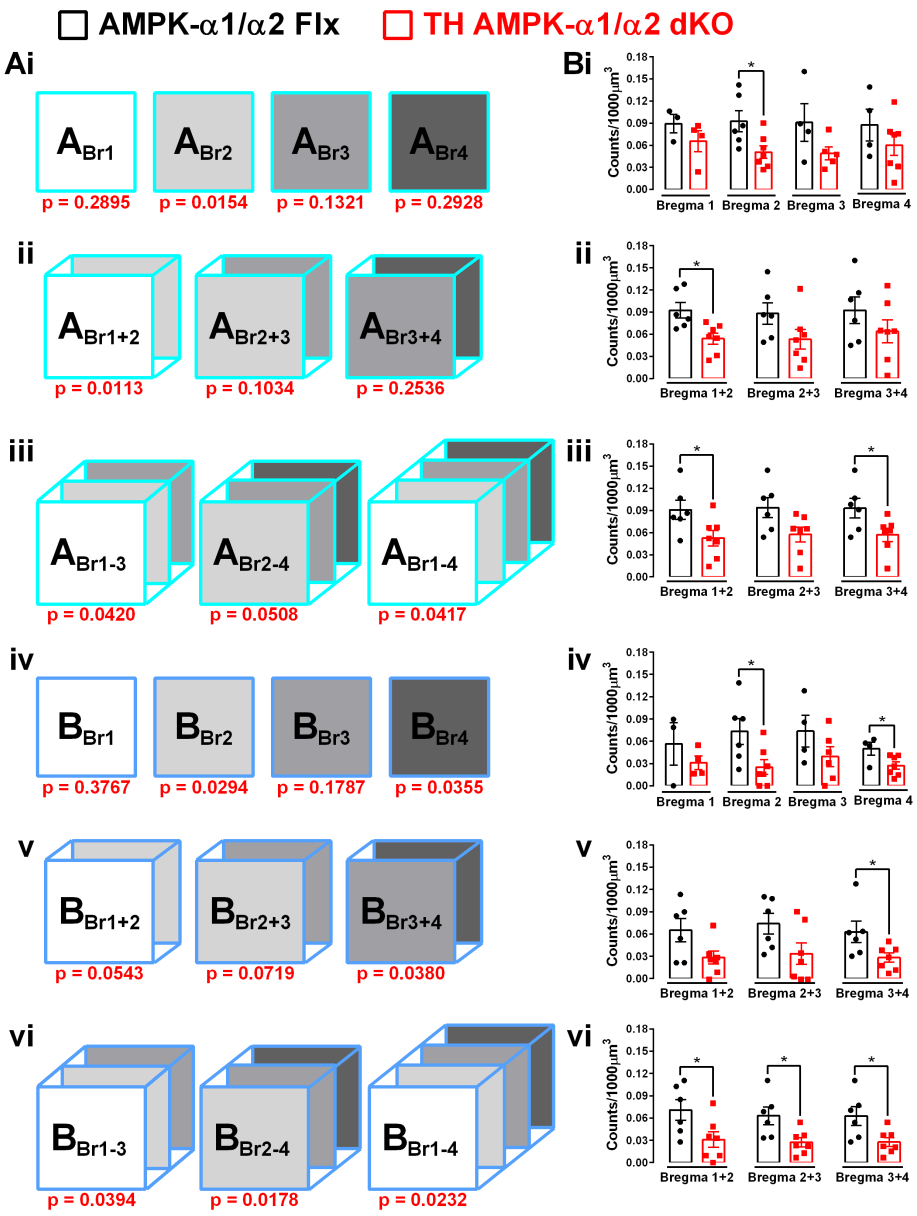

Figure 4.18: The deficiency of cFos expression in mice with targeted deletion of AMPK-α1 and -α2 catalytic subunits spans multiple Bregma at each identified subnucleus.

(A) Schematics representing which combination of the two identified nuclei in relation to the Bregma and each other has been tested, and the p-values (red) that were obtained. **(B)** Means ± SEM of cFos counts (per 1000µm^3) for each Bregma combination of the two identified subnuclei within the nucleus tractus solitarius of AMPK-α1/α2 floxed (AMPK-α1/α2 Flx, black, n = 3-6 mice) and TH-driven AMPK-α1 and -α2 double knockout mice (TH AMPK-α1/α2 dKO, red, n = 4-7 mice). * = p<0.05; significance tested by Student's t-test between genotypes for each grouping.

Additional consideration of a 'linker nucleus' As mentioned earlier, Nucleus A and B were not anatomically adjacent to each other. Therefore, the possibility was considered that they might be connected, on the right side of the NTS, by a subnucleus that sits in-between them, hereon referred to as Nucleus C. Nucleus C was found to span a distance that ranged from Bregma 1 to 3, but exhibited no statistical differences within any of these Bregma in its own right when TH AMPK-α1/α2 dKO mice were compared to controls (Figure 4.19 Ai and Bi, Appendix 2.15). However, a significant reduction in cFos expression in TH AMPK-α1/α2 dKO mice relative to controls was almost reached at Bregma 1, where p=0.056, but not at Bregma 2 (p=0.2139) or Bregma 3 (p=0.5727), although in each case there was a trend towards a reduction in cFOS expression for AMPK-α1/α2 dKO mice. Furthermore, linking these adjacent Bregma together did not yield any significant differences, regardless of whether the combinations spanned two Bregma (Figure 4.19 Aii, Bii; Bregma 1+2: p=0.1423, Bregma 2+3: p=0.2056), or all three Bregma (Bregma 1-3: p=0.2008). Unfortunately, there is currently no information available within the literature regarding the afferent innervation(s) from Nucleus C to the VLM.

Overall, outcomes from these three nuclei would suggest that:

1) Nucleus A showed the most severe deficit across Bregmas 1 and 2,
2) Nucleus B showed the most severe deficit across Bregmas 2 to 4, and
3) Nucleus C showed the most severe deficit across Bregma 1 alone.

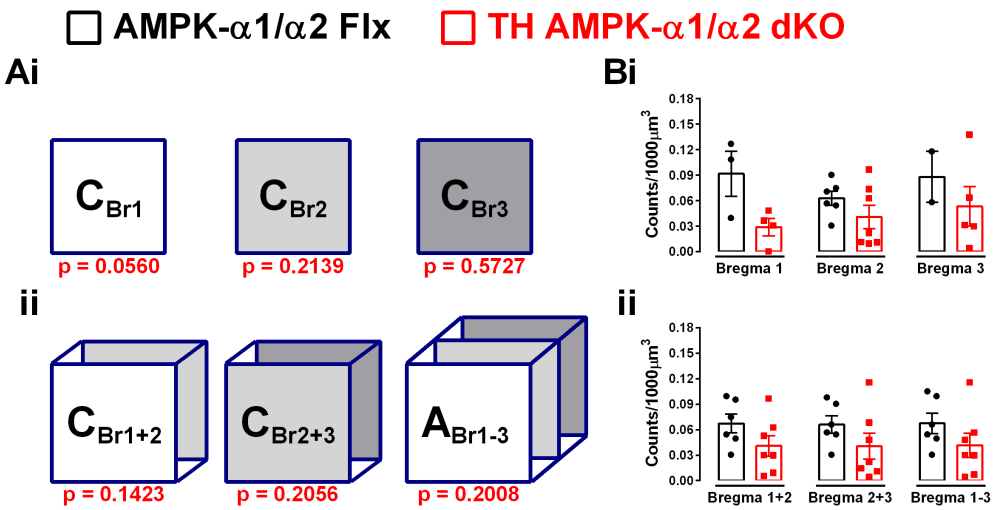

Figure 4.19: Assessment of the degrees of significance in attenuated cFos expression between genotypes within a third 'linker' nucleus at multiple Bregma.

(A) Schematics representing which combination of the 'linker' subnucleus (Nucleus C) in relation to the Bregma has been tested, and the p-values that were obtained. **(B)** Means ± SEM of cFos counts (per 1000μm^3) for each combination from (A) of AMPK-α1/α2 floxed (AMPK-α1/α2 Flx, black, n = 2-6 mice) and TH-driven AMPK-α1 and -α2 double knockout mice (TH AMPK-α1/α2 dKO, red, n = 4-7 mice). Significance tested by Student's t-test between genotypes for each grouping.

From these findings a schematic could be predicted that is illustrated in Figure 4.20 Ai. While the joint combination of Nucleus A, B and C across the above listed Bregma resulted in a very strong statistical difference (Figure 4.20 B, Appendix 2.15; p=0.0043), there was no anatomical connection apparent between Nucleus B and C that could link the DAR together. Therefore, another model with the addition of Nucleus B at Bregma 1 was considered (Figure 4.20 Aii, B). Surprisingly, this second model did not appear to affect the statistical differences of the first model. If anything, the p-value was reduced even further (p=0.0042). Finally, in order to see whether the anatomical connection(s) between these nuclei could be strengthened any further, Nucleus C at Bregma 2 was incorporated into a third model (Figure 4.20 Aiii, B). Despite having retained a high degree of statistical significance, the inclusion of Nucleus C at Bregma 2 slightly reduced the p-value obtained (p=0.007). This finding was unsurprising, given the high p-values obtained from Nucleus C alone following Bregma-specific combinations that included Bregma 2 (see Figure 4.19).

Therefore, it would appear that the model that most likely corresponds to the area of functional neuronal deficit in TH AMPK-α1/α2 dKO mice – and therefore predicts the location of the DAR – is made of neurons located within three subnuclei of the NTS, which are highly co-localised at Bregma 1 and span up to 4 additional Bregma, as we move caudal from Bregma 1 (Figure 4.20 Aii).

In summary, deficits in hypoxia-induced cFos expression in TH AMPK-α1/α2 dKO mice revealed the location of a right-side dominant and hypoxia-responsive nucleus within the caudal brainstem, which is anatomically consistent with the location of the DAR identified by fMRI and shows reduced hypoxia-induced neuronal activation following deletion of AMPK-α1 and -α2 catalytic subunits in catecholaminergic cells. Therefore, this nucleus might support signal integration and thus ventilatory adjustments during hypoxia through AMPK-dependent pathways and thus protect against hypoventilation and apnoea. Moreover, it appears that the hypoxia-responsive neurons that shape this nucleus are interspersed throughout and thus couple three anatomically defined nuclei (A-C).

Additional experiments are now required to elucidate the precise cellular characteristics of these neurons, and to confirm whether the deficit in cFos expression does indeed reflect a functional deficit driven by AMPK deficiency, through direct measurements from live preparations *in vitro* and *in vivo*.

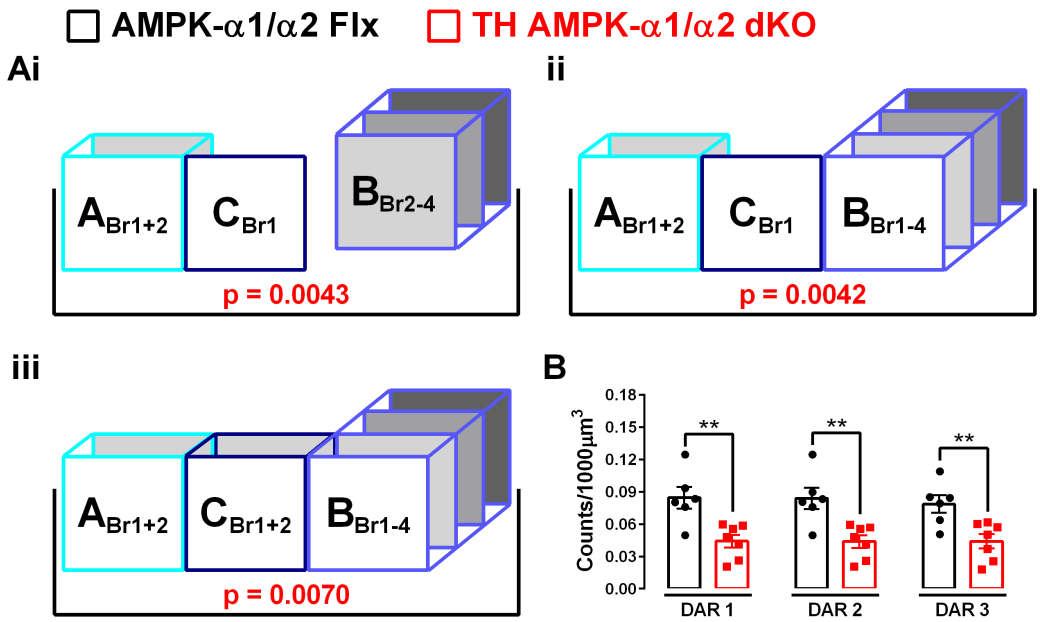

Figure 4.20: Remodelling cFos deficient areas by degree of significance predicts the extent to which the DAR spans across the four identified nuclei.

(A) Schematics representing combinations of the three nuclei across Bregmas that may shape the DAR, and the p-values that were obtained. **(B)** Means ± SEM of cFos counts (per 1000µm^3) for each combination of the two identified subnuclei within the nucleus tractus solitarius of AMPK-α1/α2 floxed (AMPK-α1/α2 Flx, black, n = 6 mice) and TH-driven AMPK-α1 and -α2 double knockout mice (TH AMPK-α1/α2 dKO, red, n = 7 mice). ** = p<0.01; significance tested by Student's t-test between genotypes for each grouping.

4.2.6.2 Additional nuclei with hypoxia-induced cFos deficits in mice with AMPK-α1 and -α2 catalytic subunit deletion in catecholaminergic cells

In addition to the nuclei identified above, a few more subnuclei of the NTS displayed a significant Bregma-specific reduction in hypoxia-induced cFos expression following deletion of AMPK-α1 and -α2 catalytic subunits in catecholaminergic cells relative to controls (Figure 4.21, Appendix 2.14). However, it seemed unlikely that these nuclei form part of the DAR.

Firstly, a deficit in cFos expression was observed within the area postrema (AP), but this was only apparent at one Bregma with no convincing trend towards a significant reduction of cFos expression in TH AMPK-α1/α2 dKO mice relative to controls at any other Bregma along the neuraxis (Figure 4.21 A). It seems unlikely, therefore, that this reflects a true contribution to the DAR, even though it is within the range of Bregma that encompass the DAR.

Secondly, attenuations within additional NTS subnuclei were identified, which were either left-side dominant (Figure 4.21 B; SolV at Bregma -7.64mm: $p<0.05$ for both sides, $p<0.01$ for left side alone; SolV at Bregma -7.44mm: $p<0.05$ for both sides and left side alone, but with a trend towards a reduction on the right side alone; SolCe: $p<0.01$ for the left side alone, with a minor trend towards a reduction for both sides together), or bilateral (Figure 4.21 C; 10N: $p<0.01$ for both sides, $p<0.05$ for the right and left sides alone), which is inconsistent with the right-side dominance observed for the DAR. Furthermore, the left-side dominant reductions of cFos expression within SolV at two spatially separated Bregmas were not retained throughout the neuraxis, because statistical significance was lost after combining cFos-positive cell counts from Bregma -7.64mm to -7.44mm and resulted in a comparable degree of cFos expression between genotypes ($p=0.1257$ for both sides, $p=0.1941$ for the right side, $p=0.106$ for the left side). However, the data for SolV and SolCe at Bregma -7.44mm should be interpreted with caution due to the small number of sections obtained for control AMPK-α1/α2 Flx (n=3) and TH AMPK-α1/α2 dKO mice (n=4). If the observed trend was true, the addition of further cFos-positive cell counts at Bregma -7.44mm could reveal a statistical significance between

AMPK-α1/α2 Flx and TH AMPK-α1/α2 dKO mice within SolV and possibly SolCe on the right side of the NTS, therefore resulting in a bilateral deficit. Either way, a contribution of the DAR remains unlikely.

Thirdly, the anatomical location of SolV, SolCe and 10N was too lateral and/or ventral relative to the location of the DAR.

All that said, the possibility that these nuclei do indeed form part of the hypoxia-sensitive area compromised by deletion of AMPK-α1 and -α2 catalytic subunits cannot be excluded at this point. It is possible that activation of these nuclei may lie downstream of the O_2-responsive nucleus identified above and that therefore the fMRI was unable to detect a significant reduction in O_2 consumption during hypoxia relative to controls, i.e. they are not intrinsically O_2-sensitive but rather they are activated following signal integration at DAR. Further electrophysiological *in vivo* and *in vitro* experiments are required in order to determine their functional role in response to hypoxia within control mice and those with AMPK-α1 and -α2 catalytic subunits in catecholaminergic cells (see also Discussion section 4.3).

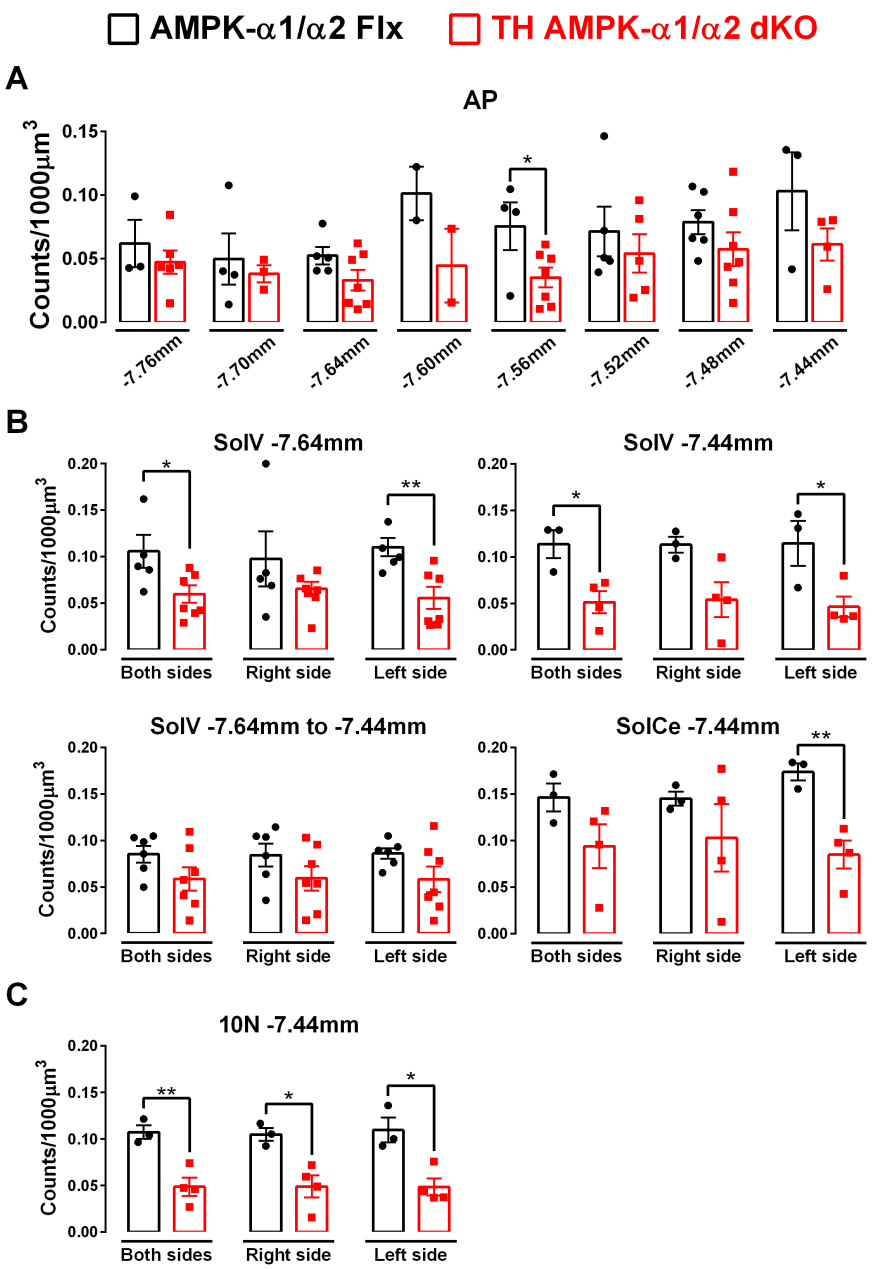

Figure 4.21: Additional deficiencies of cFos expression were identified in mice with targeted deletion of AMPK-α1 and -α2 catalytic subunits in a Bregma- and subnucleus-specific manner.

Means ± SEM of cFos counts (per 1000µm^3) of additional subnuclei within the nucleus tractus solitarius of AMPK-α1/α2 floxed (AMPK-α1/α2 Flx, black) and TH-driven AMPK-α1 and -α2 double knockout mice (TH AMPK-α1/α2 dKO, red). AP = area postrema; SolV = ventral subnucleus; SolCe = central subnucleus; 10N = dorsal motornucleus of the vagus. * = $p<0.05$, ** = $p<0.01$; significance tested by Student's t-test between genotypes for each grouping.

4.2.7 Hypoxia-induced cFos expression within catecholaminergic cells of the caudal brainstem

The outcomes for cFos expression described above were assessed in terms of total cFos-positive counts, regardless of whether the cells were TH-positive or TH-negative. Because AMPK-α1 and -α2 catalytic subunit deletion was targeted only to catecholaminergic cells, it was important to identify whether hypoxic activation of these neurons specifically was affected in this transgenic mouse model.

Activation of TH-positive cells in controls after exposures to severe hypoxia

On average, approximately 70-80% of the identified TH-positive cells per Bregma within the NTS of control AMPK-α1/α2 Flx mice were also cFos-positive following exposures to 8% O_2 (Figure 4.22 A, Appendix 2.16). This was surprising, given that such a high degree of catecholaminergic cell activation following hypoxia had not been previously described. Table 4.1 directly compared outcomes from various publications regarding the brainstem catecholaminergic cell activation following exposures to similar degrees of hypoxia. A maximum of 70% activation of TH-positive cells was reported by Erickson & Millhorn (1994), whereas all other published reports suggest a drastically lower percentage. However, the total number of TH-positive cells counted in control AMPK-α1/α2 Flx mice was comparable to those obtained by others (Figure 4.22 B, Table 4.7, Appendix 2.16), indicating that it was unlikely that discrepancies in the number of catecholaminergic neurons would account for such differences.

While variations between species and between protocols for the hypoxic stimulus and immunohistochemistry may explain some discrepancies between studies, there remains the possibility that the total number of catecholaminergic neurons within the rodent brainstem may have been grossly underestimated. In a recent study, single immunohistochemical staining using the DAB method aimed to simply evaluate the total numbers of TH-positive cells within specific parts of the brainstem, and was the first to date to do so in the adult mouse (Bucci *et al.*, 2017). According to the authors, the total number of TH cells within the NTS was higher than any other reports by one to two orders of magnitude. If one accepts the outcomes

of this study, then it suggests that counts of TH-positive cells from previous studies and the amount of TH-positively labelled cells obtained in AMPK-α1/α2 Flx mice from my study were a gross underestimate of the true number of catecholaminergic cells.

Because calculating the percentage activation of any given cell type depends on the successful labelling of all cells present within a given structure, it seems entirely possible that the high degree of TH+cFos co-staining observed in AMPK-α1/α2 Flx mice after exposures to 8% O_2 was likely due to chance, given the high possibility that many cFos-negative (and cFos-positive, for that matter) cells remained unlabelled for TH. This suspicion was further strengthened by the fact that cFos expression within catecholaminergic cells of AMPK-α1/α2 Flx mice was also observed at an extremely high level after exposures to 21% and 12% O_2 (Figure 4.23, Appendix 2.17). In fact, some Bregma revealed an up to 80% activation of catecholaminergic cells, which is highly inconsistent with previously reported findings, whereby almost none of the TH-positive cells were found to co-express nuclear cFos after continuously breathing room air (Smith *et al.*, 1995; King *et al.*, 2012). Furthermore, no PO_2-dependent increases in catecholaminergic cell activation were observed. Rather, the percentage of activated cells often appeared to slightly decrease following exposures to hypoxia relative to 21% O_2. On the contrary, in the sections above a clear PO_2-dependent increase of <u>total</u> cFos expression in AMPK-α1/α2 Flx mice was demonstrated, highlighting that cFos expression likely occurred in cells that were not labelled for TH.

Therefore,

1) A vast number of cFos-negative cells are expected to be TH-positive following exposures to 21% O_2, with some, perhaps random, degree of TH-positive/cFos-negative labelling expected after exposures to 8% O_2, and
2) The number of TH-positive/cFos-negative cells are expected to decrease following exposures to increasing intensities of hypoxia, whereas the number of TH-positive/cFos-positive cells is expected to increase without any change in the TH-positive cell numbers.

Overall, however, it is clear that the TH-labelling achieved for AMPK-α1/α2 Flx (and TH AMPK-α1/α2 dKO) mice was too poor to draw any conclusions regarding the activation of catecholaminergic cells during hypoxia and to subsequently assess any impact of AMPK-α1 and -α2 catalytic subunit deletion. That said, TH-labelling could still be used to confirm the presence of catecholaminergic neurons within each subnucleus of the NTS, which for the time being shall be the sole purpose of TH-labelling in regards to the conclusions drawn for these experiments.

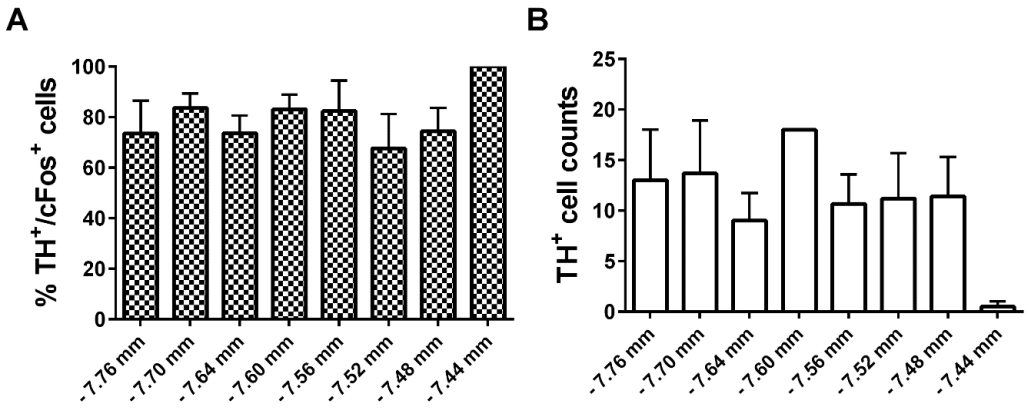

Figure 4.22: The activation of catecholaminergic cells following exposures to 8% O_2 was very high.

Means ± SEM of **(A)** the percentage of catecholaminergic cells at each identified Bregma that co-expressed cFos ($TH^+/cFos^+$) and **(B)** total counts of catecholaminergic cells within each identified Bregma of AMPK-α1/α2 floxed (AMPK-α1/α2 Flx) mice.

Table 4.7: Comparison of TH-positive and cFos-positive cell counts following exposures to hypoxia within the literature.

Species	PO_2	Duration of hypoxia	Number of TH-positive cells	Number of cFos-positive cells	% activation of TH-positive cells	Reference
Rat	8% O_2	3h	50-80 per section	90-100 per section	20-70%	Erickson & Millhorn, 1994
Rat	9% O_2	2h	25 per section per side	60-90 per section per side	14-22%	Teppema et. al., 1997
Rabbit	10% O_2	60min	20 per section	70 per section	25-30%	Hirooka et. al., 1997
Rat	8% O_2	3h	n.d.	180-190 (30-20 per Bregma)	45-50%	King et. al., 2012
Rat	8% O_2	3h	150 (15-30 per section; PVN-projecting)	n.d.	n.d.	King et. al., 2015
Mouse	21% O_2	NA	673 ± 59 per side	n.d.	n.d.	Bucci et. al., 2017

'Section' refers to the counts per coronal slice, 'side' refers to the unilateral counts per brainstem hemisphere. NA = not applicable; n.d. = not determined. 'PVN-projecting' refers to the authors' approach to identify TH-positive cells within the dorsal brainstem by means of injecting a retrogradely labelled dye into the hypothalamic paraventricular nucleus (PVN).

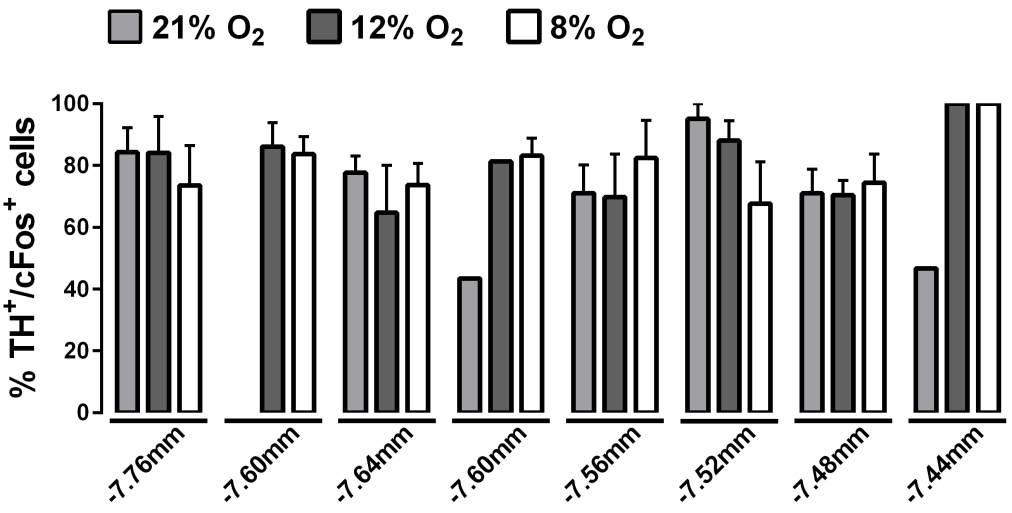

Figure 4.23: Decreasing PO_2 did not result in clear increases of catecholaminergic cell activation.

Means ± SEM of the percentage of catecholaminergic cells at each identified Bregma that co-expressed cFos ($TH^+/cFos^+$) in AMPK-α1/α2 floxed (AMPK-α1/α2 Flx) mice following 60min exposures to 21% O_2 (light grey), 12% O_2 (dark grey)and 8% O_2 (white). Significance tested by two-way ANOVA with Sidak post-hoc test.

4.2.8 Predictive outcomes for TH-positive cell activation in control mice and those with AMPK-α1 and -α2 catalytic subunit deletion in catecholaminergic cells

Given the large number of TH-positive cells reported by Bucci et. al. (2017), it seems reasonable to conclude that a significant number of the cFos-positive nuclei in AMPK-α1/α2 Flx mice represented unlabelled TH-positive neurons. Indeed, the total number of cFos-positive nuclei that were counted within the NTS of AMPK-α1/α2 Flx mice after exposures to 8% O_2 were 2-3 times higher than the total number of TH-positive cells reported by Bucci et. al. (2017) (Table 4.8). Therefore, a large proportion of these cFos-positive nuclei counted by me could likely belong to the catecholaminergic neuronal group, if one accepts the findings of Bucci et. al. (2017). These outcomes provided an opportunity for me to mathematically predict the percentages of catecholaminergic cell activation.

However, before any outcomes could be predicted, a couple of assumptions needed to be made:

- Firstly, it was not clear whether the numbers reported by the authors encompassed catecholaminergic cells of both hemispheres, or whether they were unilateral counts. Given that all representative images within the report were unilateral, my first assumption was that **the reported cell counts were for one side of the brainstem only**.
- My second assumption was that all of the TH-positive cells identified by Bucci et. al. (2017) would have been co-labelled for cFos, given the up to 3-times higher cFos-positive cell counts per side in control AMPK-α1/α2 Flx mice. In other words, **exposures to 8% O_2 led to an activation of 100% of catecholaminergic neurons**.

Given these assumptions, in response to 60min exposures to 8% O_2 a cFos count of 1691 ± 350 nuclei activated 100% of 673 ± 59 TH-positive cells (Bucci *et al.*, 2017) (Table 4.8).

During 60min exposures to 12% O_2, a total of 979 ± 270 cFos-positive nuclei was obtained. Relative to the number cFos-positive nuclei obtained during 8% O_2, the number of cFos counts during mild hypoxia would have led to a

mathematical activation of 57.9% of all catecholaminergic neurons reported by Bucci et. al. (2017).

Finally, during exposures to room air (21% O_2), only 196 ± 40 cFos-positive nuclei were detected, which would have accounted for a mathematical activation of approximately 11.6% of the total number of TH-positive cells.

Given that all samples underwent the exact same staining protocol and that the number of TH-positive cells seemed to be unaffected upon AMPK-α1 and -α2 catalytic subunit deletion, the same assumptions as above were applied to the cFos-positive cell counts obtained from TH AMPK dKO mice. In this case, following exposures to 8% O_2 a total cFos count of 1447 ± 314 nuclei was obtained. Applying the same calculations as above, this would mean that within TH AMPK-α1/α2 dKO mice a total of 85.6% of all catecholaminergic neurons would have been activated (Table 4.8). Considering the Bregma- and subnucleus-specific reductions in cFos expression relative to controls, a large proportion of these putative non-activated catecholaminergic neurons are hypothesised to lie within the subnuclei identified above that form part of the DAR.

Table 4.8: Mathematical prediction of catecholaminergic cell activation following exposures to hypoxia.

	PO_2	Number of mice	Total cell counts	Percentage of total
TH (C57Bl6)	/	9	673 ± 59	/
cFos (AMPK-α1/α2 Flx)	8% O_2	6	1691 ± 350	100%
	12% O_2	6	979 ± 270	57.9%
	21% O_2	4	196 ± 40	11.6%
cFos (TH AMPK-α1/α2 dKO)	8% O_2	7	1447 ± 314	85.6%

Total catecholaminergic (TH) cell counts obtained from adult wild-type C57Bl6 mice (Bucci *et al.*, 2017) were compared to the total dorsal brainstem cFos-positive cell counts per hemisphere and the percentage of activation calculated under the assumption that 8% O_2 activated all TH-positive cells in control AMPK-α1/α2 Flx mice.

4.3 Discussion

4.3.1 Summary of findings

Chapter 4 revealed that dual deletion of AMPK-α1 and -α2 catalytic subunits in catecholaminergic (TH-positive) cells resulted in significant reductions in cFos expression within specific areas of the caudal brainstem. Importantly, the locations of these cFos-deficient areas were consistent with the anatomical location of the DAR, which was previously identified by fMRI and revealed a right-side dominant area with significantly attenuated neuronal activity during hypoxia in TH AMPK-α1/α2 dKO mice relative to controls. Combining these identified areas of attenuated cFos expression across several Bregma revealed the shape of a putative O_2-responsive neuronal circuit whose activity is dependent on AMPK expression in catecholaminergic cells. Importantly, there was no evidence indicating loss of TH-positive cell numbers upon AMPK-α1/α2 deletion relative to controls, which was further supported by an unaltered brainstem bioamine content. Contrary to previous findings (Sunday Udoh, 2015; Mahmoud *et al.*, 2016), I found that 10min exposures to hypoxia were of insufficient duration to consistently increase cFos expression within the mouse brainstem. Therefore the hypoxic stimulus was extended to 60min, which robustly induced cFos expression throughout the caudal brainstems of control AMPK-α1/α2 Flx mice.

4.3.2 Exposures to mild and severe hypoxia preferentially induce increases in cFos expression of control AMPK-α1/α2 Flx mice within more rostral Bregma of the caudal brainstem

My analyses of brainstem cFos expression in response to hypoxia were centred on the NTS because of the anatomical location of the DAR, and therefore the putative O_2-responsive neuronal circuit. Firstly, I have shown that the expression of nuclear cFos within the NTS of mice increased in a manner proportional to the severity of hypoxia (see Figure 4.10), consistent with previous findings in the cat (Larnicol *et al.*, 1994), rabbit (Hirooka *et al.*,

1997) and rat (Erickson & Millhorn, 1994; Smith *et al.*, 1995; Teppema *et al.*, 1997; Bodineau & Larnicol, 2001; Cruz Jde *et al.*, 2010; Kline *et al.*, 2010; King *et al.*, 2012; King *et al.*, 2013; Wakai *et al.*, 2015).

Surprisingly, however, while the average cFos expression of controls in response to exposures to mild hypoxia (12% O_2) increased throughout the caudal brainstem, significance was only reached in the more rostral Bregma of the caudal NTS. This was unexpected, given the termination of carotid body (CB) afferent innervations within the caudal-most portions of the NTS (Finley & Katz, 1992). If anything, the increased afferent discharge frequency associated with increasing severities of hypoxia was therefore expected to have preferentially activated neurons at caudal Bregmas. One possible explanation for the lack of significant activation within the caudal Bregmas of the NTS could be the high degree of variability of cFos expression obtained following exposures to 12% O_2. The sigmoidal nature of the CB discharge frequency in response to reductions of arterial PO_2 results in only moderate increases of the chemoafferent activation slope in response to mild hypoxia, whereas more severe reductions of arterial PO_2 lead to an abrupt increase in the slope and a high afferent discharge frequency (Kumar, 2007). Therefore, variations in the afferent discharge frequency during exposures to 12% O_2 could have resulted in a greater variability of cFos expression across animals that subsequently failed to identify statistically significant changes in caudal Bregmas, while relay pathways within the NTS may have led to a more consistent activation of second-order neurons in more rostral Bregmas (Andresen *et al.*, 2004). By contrast, the entire caudal brainstem exhibited significant activation in response to 8% O_2, yet it appeared that once again the strongest activation was found within more rostral Bregma.

Similar to the PO_2-dependent increases in cFos expression across Bregmas, exposures to mild hypoxia appeared to increase the average expression of cFos in every subnucleus of the NTS, yet significance was only reached within the mediolateral subset of 10N, SolC, SolM, and SolCe. Moreover, differences were also observed in a hemisphere-specific manner, whereby SolDM and SolIM exhibited additional significant increases on the

right side of the NTS only. These findings have not been documented or discussed in the literature before, so they provide the first insight into the response of these subnuclei to hypoxia in the mouse. Importantly, all of these subnuclei are known to receive afferent inputs from the CB, and in turn deliver inputs to the ventrolateral medulla that modulates cardiorespiratory responses (see Figure 4.1) (Finley & Katz, 1992; Alheid *et al.*, 2011). The question remains why these specific subnuclei were preferentially activated in response to mild hypoxia, and whether it truly is a hemisphere-specific activation that occurs in the mouse, but not in other rodents who have shown a bilateral activation of the NTS in response to mild hypoxia (Smith *et al.*, 1995; Hirooka *et al.*, 1997; King *et al.*, 2012).

Exposures to severe hypoxia, on the other hand, robustly activated all subnuclei of the NTS in a bilateral manner. Therefore, irrespective of Bregma and subnucleus, severe hypoxia increases neuronal activity across the entire caudal brainstem, which is consistent with the findings of others (Erickson & Millhorn, 1994; Hirooka *et al.*, 1997; Teppema *et al.*, 1997; King *et al.*, 2012; Joubert *et al.*, 2016) and the robust PO_2-dependent increases in ventilation observed in control AMPK-α1/α2 Flx and wild-type mice (Palmer *et al.*, 2013; Getsy *et al.*, 2014; Mahmoud *et al.*, 2016).

4.3.3 Ventilatory deficits of TH AMPK-α1/α2 dKO mice were not precipitated by reductions or loss of TH-positive neurons following AMPK deletion in catecholaminergic cells

The expression and activity of AMPK is not limited to the modulation of metabolic homeostasis within the cell, but also extends to the cell's fate of survival versus apoptosis (Mihaylova & Shaw, 2011; Merlen *et al.*, 2014; Evans *et al.*, 2015; Hardie, 2015). Importantly, AMPK activity within neurons has been proposed to promote survival following metabolic stress (Culmsee *et al.*, 2001), and progressive loss of catecholaminergic neurons within the brainstem, as occurs in patients suffering from Rett syndrome, results in hypoventilation and apnoea which are exacerbated during hypoxia (Ide *et al.*, 2005; Viemari *et al.*, 2005; Weese-Mayer *et al.*, 2006; Stettner *et al.*, 2007; Katz *et al.*, 2009; Roux *et al.*, 2010; Roux & Villard, 2010).

Despite the fact that mice with dual deletion of the AMPK-α1 and -α2 catalytic subunits in catecholaminergic cells exhibited striking similarities to mouse models of Rett syndrome, i.e. pronounced hypoventilation which worsens with decreasing PO_2, no deficits in the numbers of identified TH-positive cells were found relative to controls. Although staining for TH-positive cells was clearly poor and likely grossly underrepresented the total catecholaminergic cell population of the mouse brainstem, all samples for controls and TH AMPK-α1/α2 dKO mice were processed equally with strict adherence to the immunohistochemical protocol. This means that the overall ratio of TH-positive cells stained should be equal between the two genotypes and any significant increases or decreases in the total TH-positive cell numbers should have been reflected in the subsets of catecholaminergic cells that were positively stained. Clearly, this was not the case. Therefore, unlike the ventilatory deficits associated with Rett syndrome (Viemari *et al.*, 2005; Stettner *et al.*, 2007), hypoxic hypoventilation in TH AMPK-α1/α2 dKO mice was not precipitated by loss of TH-positive neurons.

Further support for no alterations of TH-positive cell numbers came from measurements of the total brainstem and spinal cord bioamine content. Once again, the fact that no changes were found between TH AMPK-α1/α2 dKO mice and controls highlights that the phenotype observed in our mouse model is determined by a functional deficit, rather than loss of catecholaminergic neurotransmission or hypoplasia. It is likely, therefore, that AMPK-dependent pathways within TH-positive cells of the brainstem coordinate appropriate signal integration and transduction to prompt ventilatory adjustments that increase the drive to breathe and retain ventilatory stability during periods of hypoxia.

4.3.4 O_2-sensitivity within the DAR is conferred by AMPK activity in rostral noradrenergic A2 cells

It is important to note at this stage that the DAR was identified in our previous fMRI studies by way of a reductions in O_2 consumption within this region of the NTS in TH AMPK-α1/α2 dKO mice when compared to controls. The

rationale for this investigation was two-fold: (1) In other specialised O_2-sensing tissues, cellular O_2-sensitivity is conferred, at least in part, by the mitochondrial electron transport chain protein cytochrome C oxidase subunit 4 isoform 2 (COX4I2) (Fukuda *et al.*, 2007; Zhou *et al.*, 2016), which renders mitochondria exquisitely sensitive to even minor changes in O_2 supply, because COX4I2 is not inhibited by ATP and thus O_2 consumption will not increase as ATP levels fall. Rather, in these cells O_2 consumption is maintained during hypoxia, leading to a fall in ATP supply and activation of onward signalling pathways. We hypothesised that O_2-sensing cells within the NTS would respond in a similar way; (2) Changes in the fMRI Blood-oxygen-level dependent (BOLD) signal induced by peripheral pain are lost at ≤9% O_2 (Sicard & Duong, 2005), thus removing confounding inputs due to vasodilation and only revealing differences in signal changes due to alterations in O_2 consumption and hence neuronal activity.

Given that a hypoxic stimulus of 8% O_2 was used in previous experiments and mine, I followed up the fMRI study by using the expression of nuclear cFos protein as a marker for neuronal activity (Dragunow & Faull, 1989) and assessed differences in neuronal activation between AMPK-α1/α2 Flx and TH AMPK-α1/α2 dKO mice. More specifically, I sought to determine whether cFos expression was reduced in any of the hypoxia-responsive NTS subnuclei described for controls above.

At first, no overall differences in cFos expression within the NTS ranging from Bregma -7.76mm to -7.44mm were identified between controls and TH AMPK-α1/α2 dKO mice, either when taken as a whole, or separated by each Bregma or subnucleus. I therefore also investigated whether there was bilateral asymmetry with a right-sided deficit to the cFos response of TH AMPK-α1/α2 dKO mice, as suggested by the fMRI. Once again, this revealed no differences in the total cFos counts of the right and left sides of the NTS per Bregma or subnucleus between TH AMPK-α1/α2 dKO mice and controls. However, separation of cFos counts by anatomical subnuclei of the NTS per Bregma identified 3 regions of significantly attenuated cFos expression, which were herein named nuclei A, B and C. More significant still, I demonstrated that these nuclei were linked together both anatomically

and by significant difference with respect to cFos expression relative to controls and the left-hand side of the brainstem. Aided by a subnucleus combination/exclusion strategy across Bregma and based on the degree of statistical significance by component of subnucleus included, I also demonstrated that the combination of nuclei A, B and C exhibited an overall shape that was very similar to that of the DAR across the NTS. Moreover, the Bregma which exhibited significant PO_2-dependent increases in cFos expression in controls also aligned well with the rostrocaudal extent of the DAR (Mahmoud *et al.*, 2016). Therefore, I predict that this identified neural network which spans multiple subnuclei could likely form an O_2-responsive neuronal circuit within the dorsal medulla and through which ventilatory drive may be increased during hypoxia in an AMPK-dependent manner. Consistent with this view, the identified nuclei incorporate catecholaminergic neurons that receive inputs from the carotid body and project themselves to the ventrolateral medulla and thus the respiratory central pattern generators (rCPGs) (Finley & Katz, 1992; Alheid *et al.*, 2011). However, future analyses of responses to hypoxia in TH AMPK-α1/α2 dKO mice and COX4I2 expression within the NTS will be required to confirm the nature and capacity for O_2-sensing by the DAR, and the role of signal integration by these neurons in mediating the HVR and apnoea genesis.

The location of the DAR and the neural ciruit identified here is consistent with the location of the more rostral portion of the noradrenergic A2 cell group. Caudally, the A2 neurons receive the carotid body chemoafferent input and relay these information to other brain regions that are involved in the control of breathing (Andresen & Kunze, 1994; Andresen & Mendelowitz, 1996; King *et al.*, 2015). However, the neurons of the A2 cell group themselves were also reported to be hypoxia-sensitive and able to potently modulate ventilation during hypoxia (Buller *et al.*, 2008; Li *et al.*, 2008; Soliz *et al.*, 2008; McGinnis *et al.*, 2013). In light of the findings presented in this chapter, it may be possible that these two functions are carried out by spatially divided subsets of dorsal noradrenergic neurons within the NTS that span nuclei A, B and C. Within this subset, AMPK activity may be required within these rostral noradrenergic A2 cells for the modulation of

cellular metabolism, ion channel activity, neuronal firing frequency and/or neurotransmitter release (Lipton *et al.*, 2001; Murphy *et al.*, 2009; Ikematsu *et al.*, 2011; Hardie, 2014), which defines a central O_2-responsive neuronal circuit that determines – in concert with CB afferent fibre input – the overall degree of respiratory drive during hypoxia. Moreover, given the proposed hypoxia-sensitive nature of A2 cells (Andresen & Kunze, 1994; Andresen & Mendelowitz, 1996), one could even speculate that this O_2-responsive circuit does not only determine the degree of the HVR, but may also underpin, at least partially, the ability to restore components of the HVR following CB resection (Davenport *et al.*, 1947; Miller & Tenney, 1975; Bisgard *et al.*, 1980; Martin-Body *et al.*, 1986; Daristotle *et al.*, 1991; Roux *et al.*, 2000a).

In addition to this aforementioned proposal, the anatomical location of the DAR, and therefore the putative O_2-responsive neuronal circuit, lies in close proximity to the area postrema (AP). Being the caudal-most circumventricular organ of the brain, the AP is a highly vascularised structure containing mostly fenestrated capillaries (Price *et al.*, 2008). Moreover, the position outside of the blood-brain-barrier allows the AP to share blood-borne signals with the NTS via its unusual blood supply. Its fenestrated capillaries form short connecting vessels within the sub-postrema (SubP), which then break up again into 'normal' capillaries that supply the rest of the medulla. In this respect, fenestrations allow for re-entrant of venous blood into the capillary bed, which results in a relatively low O_2 saturation within the surrounding tissue (Fodor *et al.*, 2007; McGinnis *et al.*, 2013). This already mildly hypoxic environment in turn could lead to an increased sensitivity to further reductions in the arterial O_2 saturation, as would occur during periods of hypoxia, perhaps rendering a subpopulation of neurons sensitive to local PO_2 due to COX4I2 expression, consequent susceptibility to deficits in mitochondrial ATP production during hypoxia, and thus activation of AMPK-dependent signalling pathways.

Therefore, these findings provide further support to our hypothesis that the DAR is most likely made up of, at the very least, rostrally located and hypoxia-responsive noradrenergic cells, within which AMPK activity is determined by:

1) ‘applied metabolic stress’ (increased neuronal activity which is triggered by increased carotid body chemoafferent discharge that may be received by caudal A2 neurons, but is integrated and relayed by rostral A2 neurons within the DAR), and
2) ‘local hypoxic stress’ (increased sensitivity of the neurons within the DAR to even minor decreases in arterial O_2 saturation due to the already mildly hypoxic environment created by the fenestrated capillaries of the AP)

4.3.5 Activity of additional putative non-O_2-sensing regions of the dorsal medulla require AMPK expression in catecholaminergic cells

All other nuclei within the caudal brainstem of TH AMPK-α1/α2 dKO mice exhibited cFos responses comparable to controls, with key exceptions. Against expectations, a significant reduction in cFos expression following AMPK deletion in catecholaminergic cells was identified within the AP (albeit within only a single Bregma), 10N and SolV. Importantly, their anatomical location within the brainstem was not consistent with the location of the DAR.

It is possible that activity of 10N lies downstream of the O_2-sensitive network that encompasses catecholaminergic neurons, as it has been shown to receive afferent inputs from the adrenergic C1 cells, which sit in the ventrolateral medulla and are likely candidates for VAR (see section 1.3.7 below), as well as the dorsal C2 and C3 neurons (Hokfelt *et al.*, 1973; Abbott *et al.*, 2013; DePuy *et al.*, 2013; Guyenet *et al.*, 2013). 10N contains parasympathetic preganglionic neurons that innervate the thorax and abdomen (Watson *et al.*, 2012), and bilateral projections from the 10N were proposed to contribute to the bradycardia and mild hypertension associated with the diving reflex (Panneton *et al.*, 2014). Therefore, the cardiovascular regulation during periods of apnoea could be determined via motor output from the 10N, which in turn could be subjected to modulation via AMPK-dependent signalling pathways from adrenergic neurons. SolV, on the other hand, is one of the NTS subnuclei whose bilateral activation was reported to contribute to the laryngeal closure reflex associated with

swallowing (Wang *et al.*, 2015). In this regard, loss of AMPK-dependent signalling pathways from within this subnucleus could underlie the pathogenesis of obstructive sleep apnoea, during which the airflow is obstructed by loss of laryngeal muscle tone (Panossian & Daley, 2013). However, further experiments are required to substantiate these suggestions. Either way, a contribution of these two nuclei to the O_2-sensitivity of the DAR and modulation of ventilation seems unlikely, but cannot be excluded at this point.

A very small subsection of the AP at Bregma -7.56mm also exhibited a marginally significant reduction of cFos expression in TH AMPK-α1/α2 dKO mice relative to controls. A contribution of the AP to the central O_2-sensing neural network is plausible, because the anatomical location of the DAR, and therefore the putative O_2-responsive neuronal circuit, lies in close proximity to the AP. Furthermore, noradrenergic cell bodies are also found within the central zone of the AP (Hermann *et al.*, 2005), which would be affected by our targeted AMPK deletion strategy. As mentioned earlier, the AP is the caudal-most circumventricular organ of the brain and has a highly vascularised structure containing mostly fenestrated capillaries (Price *et al.*, 2008), which means it is well placed to monitor arterial PO_2 centrally. In addition, it contains bidirectional projections to the dorsal portions of the NTS (van der Kooy & Koda, 1983; Shapiro & Miselis, 1985; Hermann *et al.*, 2005), thus allowing for rapid communication between the AP, NTS, and VLM to modulate ventilation in response to changes in arterial PO_2. However, a marginally significant reduction in cFos expression within the AP of TH AMPK-α1/α2 dKO mice relative to controls was only identified at one particular Bregma (-7.56mm). If the AP was to truly contribute to the DAR, then a significant attenuation of cFos expression would have been expected to occur at more than just one Bregma, given that the approximately 300µm rostrocaudal extend of the AP spans all of the analysed Bregma of the NTS (-7.76mm to -7.44mm), and a rostrocaudal structural subdivision of the AP has not been described within the literature. In fact, none of the other surrounding Bregma even revealed a clear trend towards a reduction in nuclear cFos expression (see Figure 4.21), even though the identified

Bregma were only 40μm apart. Therefore, a contribution of the AP to the formation of the O_2-sensitive neuronal circuit would be surprising, but cannot be ruled out at this point.

4.3.6 Conclusion

In conclusion, AMPK-dependent signalling pathways prompt increases in ventilation during hypoxia through the modulation of a putative hypoxia-responsive noradrenergic neuronal circuit located in the dorsal medulla oblongata in a region of close proximity to the DAR previously identified by fMRI. This suggests that in response to a fall in PO_2, activation of AMPK supports increases the drive to breathe via afferent projections from the DAR to the respiratory network of the ventrolateral medulla, with AMPK activity being determined by the synergistic effects of 'local hypoxic stress' subsequent to reductions in the arterial O_2 concentrations within the brainstem, and 'applied metabolic stress' subsequent to increased neuronal activity elicited by carotid body chemoafferent inputs. Therefore, it seems all the more likely that AMPK-dependent signalling pathways support coincidence detection and thus signal integration within a hypoxia-responsive circuit of the brainstem that delivers increases in the drive to breathe during hypoxia and therefore regulates whole-body O_2 supply.

4.3.7 Limitations and future directions

As highlighted in section 4.2.5, not all sections could be reliable allocated to the 'major' Bregma presented in the Mouse Brain Atlas (Franklin & Paxinos, 2008). This problem is not uncommon and has been described by others who also did not use a matrix to block the brains, which can result in a dorsoventral tilt during sectioning (Llewellyn-Smith *et al.*, 2013). However, creating transparent overlays of the Mouse Brain atlas which could be superimposed onto the photomicrographs allowed for the identification of the closest Bregma that would fit each individual section. Therefore, the data obtained for each of the 'minor' Bregma, which did not fit a specific brain

map and sat in-between two of the transparent overlays, need to be assessed with caution, not at least because very few numbers of sections were allocated to them.

The small number of sections within the minor Bregma also limited the statistical analyses that could be carried out. This was particularly true for controls that were exposed to room air, where the total number of mice used was n = 4. Therefore, while sections of each major Bregma could be allocated for each animal, it often happened that ≤2 animals had sections allocated to minor Bregma, which means statistical differences could not be determined throughout the rostrocaudal extend.

Lastly, the experiments presented in this Chapter focussed on the expression of cFos within the dorsal medulla at the level of the area postrema. However, it is entirely possible that the DAR extends more rostrally to the location of the adrenergic C2 and C3 cells. In addition, the fMRI study also revealed the existence of an area with deficiency of neuronal activity in TH AMPK-α1/α2 dKO mice relative to controls within the ventral medulla, which was termed the VAR (Mahmoud *et al.*, 2016). Additional counts of cFos-positive cells are now required within the ventral medulla in order to determine whether the VAR is located within the anatomical region of the noradrenergic A1 and/or adrenergic C1 cells, and whether the DAR stretches further rostrally to encompass dorsal adrenergic C2 and C3 cells.

Chapter 5: Characterisation of the hypoxic apnoeic response in mice with AMPK deficiency in catecholaminergic cells

5.1 Introduction

5.1.1 Sighs, post-sigh apnoeas, and spontaneous apnoeas

In mammals, eupneic breathing is periodically interrupted by the occurrence of augmented breaths (sighs), which are characterised by their large inspiratory and expiratory flows and thus much larger tidal volume compared to normal breaths. Sighs are an important feature of respiratory physiology as they prevent atelectasis, which is the occurrence of collapsed alveoli that create hypoventilated areas of the lungs (Nicholas *et al.*, 1982) and they therefore maintain lung compliance and efficacy of gas exchange. On the other hand, sighs have also been proposed to promote ventilatory instability in subsequent breathing cycles, because they tend to be followed by apnoea and temporarily alter respiratory frequency (Perez-Padilla *et al.*, 1983; Fleming *et al.*, 1984; Fukumizu & Kohyama, 2004; Yamauchi *et al.*, 2008). Normally respiratory rhythm is quickly restored, but sighs can be seriously disruptive for some individuals, for example those suffering from sleep-disordered breathing (Fleming *et al.*, 1984; Hoch *et al.*, 1998; Brown & Bates, 2000). The generation of sighs has been suggested to arise during embryogenesis within the preBötC immediately following the maturation of eupneic-like activity (Chapuis *et al.*, 2014). Hypoxia in the adult increases the frequency of sighs and this effect has been postulated to occur via catecholaminergic neurotransmission and β-adrenergic receptor stimulation within preBötC neurons. This appears to require the additional actions of the neuropeptides neuromedin B and gastrin-releasing peptide, as well as input from vagal pulmonary C fibres that innervate the caudal NTS (Xu *et al.*, 2003; Bell *et al.*, 2009; Burke *et al.*, 2014; Li *et al.*, 2016).

As mentioned above, sighs are commonly followed by an apnoea. Although thought to arise from the preBötC neuronal network, post-sigh apnoeas (PSA) were found to be modulated by glutamatergic signalling within the pons. However, this modulation was state-dependent, as it occurred during rapid eye-movement (REM) sleep, but not during non-REM sleep (Radulovacki *et al.*, 2001). In contrast, serotonin was found to modulate the frequency and duration of PSA during non-REM sleep (Saponjic *et al.*,

2007). One prominent hypothesis as to how PSA are generated relates to the Hering-Breuer reflex, whereby pulmonary stretch receptors activated during lung inflation (sighing) lead to afferent vagal activity that inhibits inspiration and thus results in apnoea (Breuer, 1868). Importantly, the duration of the PSA appears to be directly related to the magnitude of vagal inhibition, and the counter balance delivered through increasing inspiratory excitatory input from central and peripheral chemosensors. Therefore, a stronger vagal inhibition will increase PSA duration, whereas increasing levels of CO_2 during apnoeas will terminate PSA and re-initiate inspiration (Younes *et al.*, 1974). Spontaneous apnoeas (SA) on the other hand appear to be generated by different mechanisms. The frequency of SA but not PSA has been correlated to the expression levels of TASK-1 potassium channels within the respiratory networks of the pons and medulla (Wang *et al.*, 2008), and peripheral administration of serotonin was found to increase the generation of SA but not PSA during REM sleep (Carley & Radulovacki, 1999a; Radulovacki *et al.*, 2001). Therefore, PSA and SA appear to have distinct origins.

5.1.2 AMPK deficiency in catecholaminergic cells augments the apnoeic phenotype during hypoxia

Recent work on the role of AMPK within the catecholaminergic respiratory network has shown that deletion of the catalytic AMPK-α1 and -α2 subunits within tyrosine hydroxylase (TH)-positive cells (TH AMPK-α1/α2 dKO) precipitated more frequent and prolonged apnoeas during hypoxia (Mahmoud *et al.*, 2016). Moreover, this response was found to be PO_2-dependent.

5.1.3 Aims

The work on TH AMPK-α1/α2 dKO mice described above only considered total changes in the apnoeic responses to hypoxia during 5min exposures. In this chapter, I investigated the ventilatory stability of control AMPK-α1/α2 Flx and TH AMPK-α1/α2 dKO mice during longer exposures to hypoxia.

Accordingly, mice were exposed to 10min of mild (12% O_2) and severe (8% O_2) hypoxia, as well as 60min of severe hypoxia and their ventilatory stability and apnoeic phenotype assessed using whole-body plethysmography. Moreover, I sought to determine whether AMPK deletion impacts on the balance of vagal and chemoafferent inputs that modulate respiratory stability. Therefore, sighs, post-sigh apnoeas and spontaneous apnoeas were separated and compared to each other in order to determine whether AMPK deletion preferentially impacts one type of apnoea over the other.

5.2 Results

5.2.1 AMPK deletion in catecholaminergic cells increases ventilatory instability and disorder throughout 10min exposures to hypoxia

Given the hypoventilation and highly disordered breathing pattern induced by hypoxia in TH AMPK-α1/α2 dKO mice described in section 3.2, it was of interest to assess and compare the overall breathing regularity and hence stability during 10min exposures to mild and severe hypoxia. This was achieved by plotting each inter-breath interval (BBn) against each subsequent inter-breath interval (BBn+1) for control AMPK-α1/α2 Flx and TH AMPK-α1/α2 dKO mice.

Ventilatory stability of controls Example plots from single 10min exposures are shown in Figure 5.1 A, which compare the breathing patterns of a control (black) and knockout (red) mouse during 12% (left panel) and 8% (right panel) hypoxia. It is quite clear that control AMPK-α1/α2 Flx mice had a regular breathing pattern with few apnoeas evident through increases in inter-breath interval during mild hypoxia, which increased in number proportionally to the severity of hypoxia. Notably, the occurrence of apnoeas has been described in wild-type mice and healthy humans and is consistent with previous observations from this mouse model (Stettner *et al.*, 2008; Ainslie *et al.*, 2013; Mahmoud *et al.*, 2016). These outcomes were analysed in more detail and quantified by comparing the standard deviations (SD) of BBn and BBn+1.

Mild hypoxia: During 12% O_2, the breathing variability of control AMPK-α1/α2 Flx mice (n = 55 exposures from 19 mice) increased slightly but significantly between the first and the second half of 10min exposures (Figure 5.1 B, left panels; 0-5min: 77 ± 2.3ms; 5-10min: 81.5 ± 2.2ms; $p<0.05$). A more detailed minute-by-minute analysis revealed that the higher SD of control mice during the second half of 10min exposures was due to a gradual increase in breathing variability over the course of the exposure to mild hypoxia (Figure 5.1 C, left panel; at 0-1min: 64.8 ± 2.7ms; at 5-6min: 75.9 ± 2.5ms; at 9-10min: 80.8 ± 2.5ms).

Severe hypoxia: Consistent with previous observations (Mahmoud, 2014; Mahmoud *et al.*, 2016), the SD of AMPK-α1/α2 Flx mice during the first 5min of hypoxia significantly increased from 12% O_2 to 8% O_2 (Figure 5.1 B, right panel; 0-5min: 98 ± 3.7ms, $p<0.0001$ relative to 12% O_2; n = 58 exposures from 25 mice). Interestingly though and contrary to mild hypoxia, the breathing variability of control AMPK-α1/α2 Flx mice significantly decreased during the second half of severe hypoxia (5-10min: 79.8 ± 3.8ms, $p<0.01$ relative to 0-5min) to a level that was comparable to the second half of exposures to mild hypoxia (not significant relative to 5-10min of 12% O_2). This overall decrease appeared to be due to a time-dependent decrease in the SD of the inter-breath intervals following a peak at 1-2min of 8% O_2 (Figure 5.1 C, right panel; at 1-2min: 108.4 ± 4.4ms; at 5-6min: 82.4 ± 4.4ms; at 9-10min: 77.9 ± 4.2ms).

Ventilatory stability of knockouts Example plots of TH AMPK-α1/α2 dKO mice presented with very similar breathing regularities – and irregularities – compared to controls during mild hypoxia, where the main cluster of "regular" inter-breath intervals was within the same range as those of AMPK-α1/α2 Flx mice. There were only a few breathing irregularities that could be attributed to the occurrence of apnoeas. In stark contrast to mild hypoxia, the response of TH AMPK-α1/α2 dKO mice to severe hypoxia was not only drastically more disordered with an overall increase in the number of prolonged inter-breath intervals, but individual inter-breath-intervals could be as long as 4s. Additionally, the main cluster of "regular" breath intervals had almost twice the range when compared to AMPK-α1/α2 Flx mice, indicative of disordered breathing and prolonged inter-breath intervals, consistent with the observed hypoventilation described in section 3.2.1.

Mild hypoxia: Regarding the SD of BBn and BBn+1, the breathing variability of TH AMPK-α1/α2 dKO mice during 12% O_2 (n = 35 exposures from 11 mice) was indeed comparable to controls during both the first half (SD of 73.5 ± 2.2ms, not significant) and the second half (SD of 75.1 ± 1.9ms, not significant relative to controls and relative to 0-5min) of 10min exposures. This comparable degree of breathing variability between controls and TH AMPK-α1/α2 dKO mice during mild hypoxia was also evident at each point

measured throughout the 10min exposures (at 0-1min: 56.6 ± 1.9ms, not significant; at 5-6min: 73.2 ± 2.6ms, not significant; at 9-10min: 73.7 ± 2.2ms, not significant).

Severe hypoxia: In contrast to mild hypoxia, exposures to 8% O_2 significantly increased the SD of TH AMPK-α1/α2 dKO mice (n = 46 exposures from 22 mice) compared to controls (0-5min: 174.9 ± 6.8ms, $p<0.0001$; 5-10min: 169.8 ± 10.9ms, $p<0.0001$; not significant relative to 0-5min), which was expected given the outcomes from the plots described above. The highest degree of breathing variability in TH AMPK-α1/α2 dKO mice was also observed during the second minute of severe hypoxia (1-2min: 207.7 ± 13.6ms, $p<0.0001$ compared to controls). However, unlike controls, there was no time-dependent reduction of the SD and breathing remained significantly more irregular compared to controls throughout the remainder of the exposure, with SD of 170.3 ± 15.5ms by 5-6min ($p<0.0001$) and 146 ± 11ms by 9-10min ($p<0.0001$).

From these plots it was obvious that increases in breathing irregularities were inversely related to the environmental concentration of O_2, and that loss of AMPK-α1 and -α2 subunits in catecholaminergic cells markedly augments these irregularities during severe hypoxia.

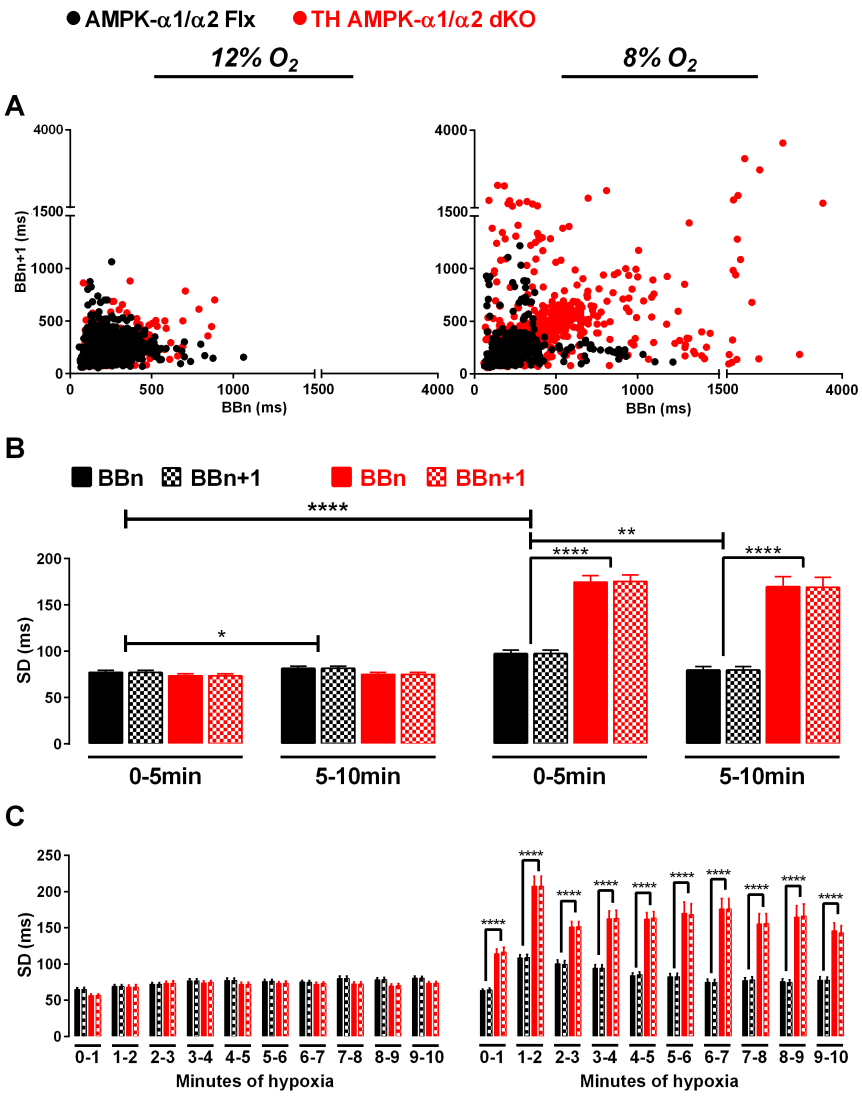

Figure 5.1: AMPK-α1/α2 catalytic subunit deletion in catecholaminergic cells precipitates breathing irregularities during severe hypoxia.

(A) Example Poincaré plots show the inter-breath interval (BBn) versus the subsequent interval (BBn+1) of AMPK-α1/α2 Flx floxed (AMPK-α1/α2 Flx, black) and TH-driven AMPK-α1 and -α2 double knockout (TH AMPK-α1/α2 dKO, red) mice during 10min exposures to to **(i)** mild hypoxia (12% O_2) and **(ii)** severe hypoxia (8% O_2). **(B+C)** Means ± SEM of the standard deviation (SD) of BBn and BBn+1 for AMPK-α1/α2 Flx mice (12% O_2: n = 55 exposures from 19 mice, 8% O_2: n = 58 exposures from 25 mice) and TH AMPK-α1/α2 dKO mice (12% O_2: n = 35 exposures from 11 mice, 8% O_2: n = 46 exposures from 22 mice) for **(B)** 5min averages and **(C)** 1min averages. * = p<0.05, ** = p<0.01, **** = p<0.0001. Significance tested by two-way ANOVA with Sidak post-hoc tests.

5.2.2 AMPK deletion in catecholaminergic cells increases the number and duration of apnoeas during 10min exposures to severe hypoxia

Previous analyses of raw box flow traces revealed that the conditional deletion of AMPK-α1 and -α2 subunits in catecholaminergic cells precipitated more frequent and prolonged apnoeas during 5min exposures to hypoxia (Mahmoud, 2014). Figure 5.2 illustrates these findings and highlights the PO_2-dependence of the response. Consistent with our previous study, apnoeas were defined as cessations of breathing ≥600ms (Mahmoud *et al.*, 2016), which corresponds to the duration of two normoxic breaths (Nakamura & Kuwaki, 2003; Voituron *et al.*, 2009; Peng *et al.*, 2011).

5.2.2.1 Apnoeic index

Mild hypoxia When exposed to 10min of 12% O_2, AMPK-α1/α2 Flx mice presented with apnoeas at a frequency of 0.8 ± 0.1 apnoeas/min (n = 55 exposures from 19 mice) for the first, and 1 ± 0.1 apnoeas/min for the second 5min of hypoxia (Figure 5.3 Ai). A constant number of apnoeas was also observed on a minute-by-minute basis, although there was a slight increase towards the end of the 10min exposure (Figure 5.3 Bi; apnoeas/min – at 1-2min: 0.6 ± 0.1; at 5-6min: 0.7 ± 0.1; at 9-10min: 1 ± 0.2).

Severe hypoxia During 8% O_2, the apnoea frequency in AMPK-α1/α2 Flx mice was increased compared to mild hypoxia, measuring 3.1 ± 0.2 apnoeas/min (n = 58 exposures from 25 mice) during the first half of 10min hypoxia, and 1.6 ± 0.2 apnoeas/min during the second half (Figure 5.3 Aii). Interestingly, the decline in apnoea frequency observed during the second half of the 10min exposure appeared to be time-dependent, as the number of apnoeas decreased from 4 ± 0.4 apnoeas/min by 1-2min to 2 ± 0.3 apnoeas/min by 5-6min and 1.9 ± 0.2 apnoeas/min by 9-10min (Figure 5.3 Bii). Thereafter, additional experiments in which the effect of 60min exposures to severe hypoxia (8% O_2; n = 6) was investigated allowed me to explore whether this decrease was limited to, or extended beyond the initial 10min measured. The 60min exposures revealed that this slow decline lasted until 20-25min (Figure 5.3 C; 20-25min: 1.1 ± 0.2 apnoeas/min).

Apnoea frequency then remained stable for about 10min (25-30min: 1.3 ± 0.2 apnoeas/min) before increasing slightly to 1.8 ± 0.1 apnoeas/min by 35-40min. This apnoeic index was then maintained at a steady level with some minor fluctuations until the end of the exposure (55-60min: 1.8 ± 0.4 apnoeas/min).

Effect of AMPK deletion on apnoea frequency during mild hypoxia In contrast to previous findings (Mahmoud *et al.*, 2016), the TH AMPK-α1/α2 dKO mice used here (n = 35 exposures from 11 mice) produced a comparable number of apnoeas relative to controls during the first (0.7 ± 0.1 apnoeas/min, not significant) and second half (0.7 ± 0.1 apnoeas/min, not significant) of the 10 min exposure to mild hypoxia. Further dissection of this response for each minute of hypoxia revealed that the numbers of apnoeas were indeed comparable between the genotypes throughout the hypoxic exposure (apnoeas/min – at 1-2min: 0.6 ± 0.1; at 5-6min: 0.9 ± 0.2; at 9-10min: 1 ± 0.2; not significant compared to controls at any time point).

Effect of AMPK deletion on apnoea frequency during severe hypoxia Consistent with previous observations, there was a much bigger increase in apnoea frequency in TH AMPK-α1/α2 dKO mice (n = 46 exposures from 22 mice) compared to controls, which measured 5.9 ± 0.4 apnoeas/min ($p<0.0001$) during the first half and 4.4 ± 0.4 apnoeas/min ($p<0.0001$) during the second half of 10min exposures. This significantly augmented apnoeic frequency was also apparent throughout the 10min exposure (apnoeas/min – at 1-2min: 9.3 ± 0.8, $p<0.0001$; at 5-6min: 4 ± 0.5, $p<0.0001$; at 9-10min: 5.5 ± 0.9, $p<0.0001$). In addition, not only was the frequency of apnoeas augmented in TH AMPK-α1/α2 dKO mice relative to controls, but the frequency at which apnoeas occurred oscillated with time, increasing and then decreasing over the course of the first 20-25min (n = 4). Thereafter, the frequency of apnoeas remained significantly augmented relative to controls between 30 and 60 min (10-15min: 7.1 ± 1.6 apnoeas/min, $p<0.05$; 25-30min: 4.2 ± 0.9 apnoeas/min, $p<0.05$). Curiously, for the last 30min of 60min exposures the averaged apnoeic index was generally comparable to controls (30-35min: 2.8 ± 0.7 apnoeas/min; 45-50min: 3 ± 1 apnoeas/min; 55-60min: 2.9 ± 0.7 apnoeas/min). Nevertheless, minute-by-minute

analyses revealed the presence periodic “apnoeic bursts”, which were characterised as time-dependent phasic increases in the number of apnoeas, that occurred at a frequency of every 3.3 to 4.2 mHz (once every 4-5min) and had a duration of 1min per burst. Strikingly, these bursts were present in each of the 4 TH AMPK-α1/α2 dKO mice analysed (Appendix 3.1) and were not lost upon averaging across the genotype.

Therefore, in TH AMPK-α1/α2 dKO mice the apnoeic index was greater than for controls, consistent with previous outcomes. However, while control AMPK-α1/α2 Flx mice were able to maintain a steady number of apnoeas throughout prolonged exposures to hypoxia, mice with dual deletion of AMPK-α1 and -α2 subunits in catecholaminergic cells retained a degree of ventilatory instability that presented as “apnoeic bursts” at regular intervals, indicative of phasic disturbances of the central pattern generators (rCPGs) during periods of prolonged hypoxia.

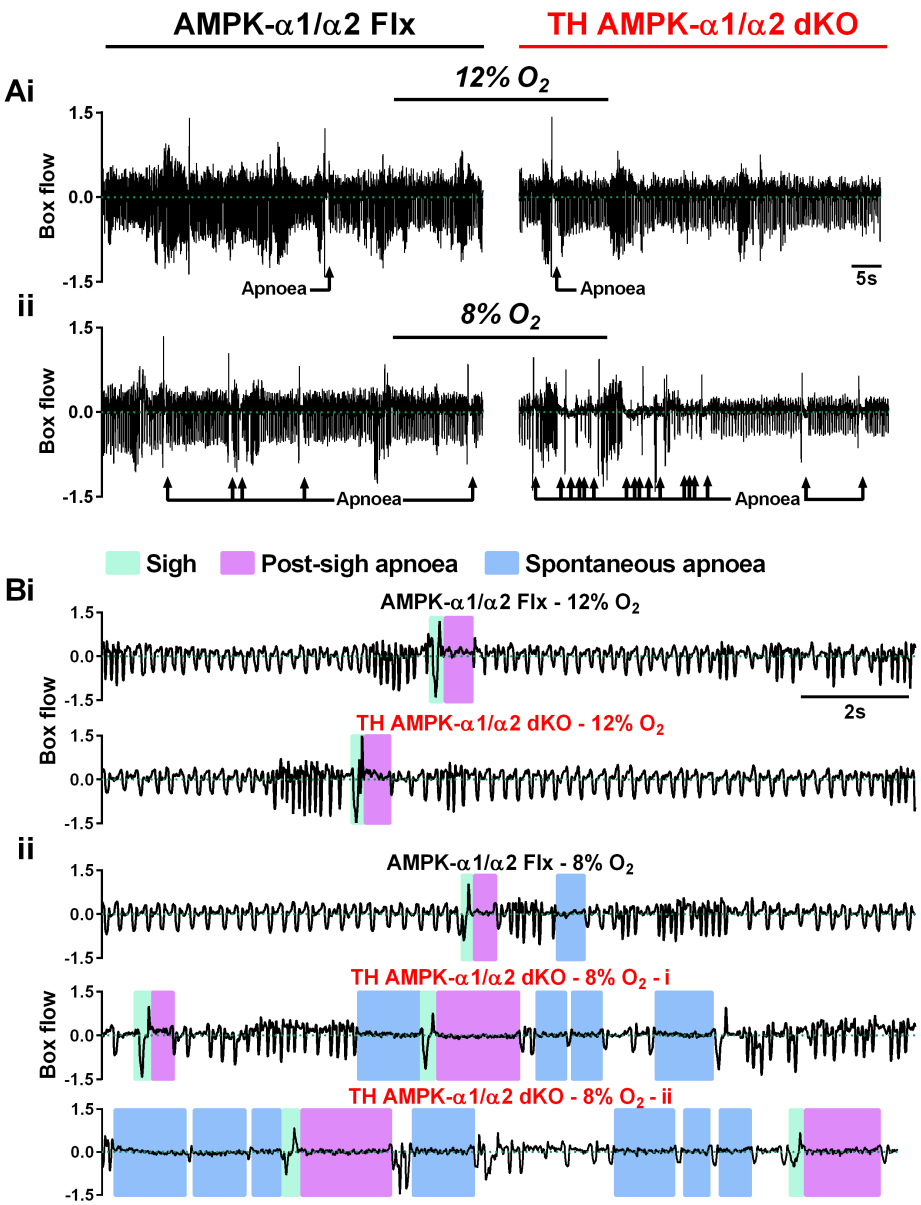

Figure 5.2: Conditional deletion of AMPK-α1/α2 catalytic subunits in catecholaminergic cells precipitates breathing instabilities that manifest as hypoventilation and apnoeas.

(A) Exemplary box flow records of ventilatory activity obtained by plethysmography from AMPK-α1 and -α2 floxed (AMPK-α1/α2 Flx, left panels) and TH-driven AMPK-α1 and -α2 double knockout mice (TH AMPK-α1/α2 dKO, right panels) during **(i)** mild hypoxia (12% O_2) and **(ii)** severe hypoxia (8% O_2). **(B)** Expanded box flow records from the same AMPK-α1/α2 Flx (top panel) and TH AMPK-α1/α2 dKO (bottom panel) mice used in **(A)** at an expanded time scale during **(i)** mild hypoxia (12% O_2) and **(ii)** severe hypoxia (8% O_2).

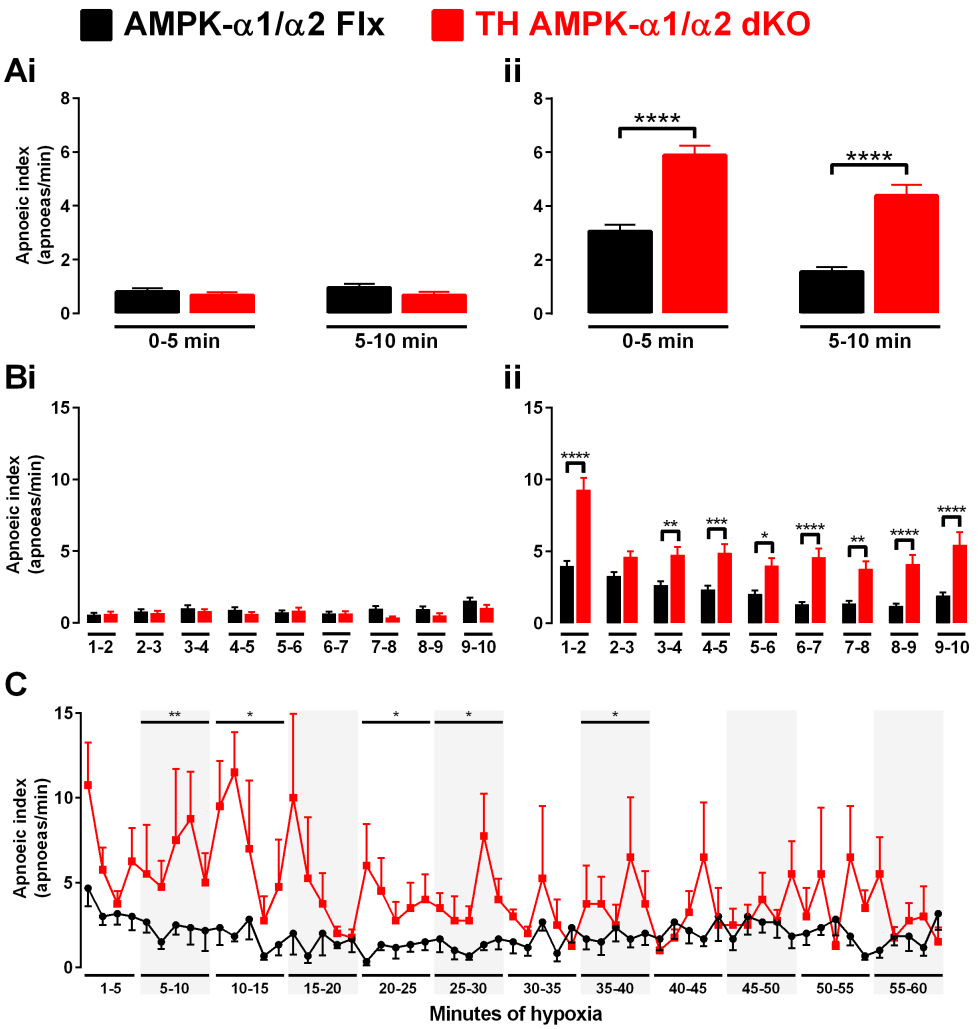

Figure 5.3: The precipitation of apnoeas in mice with conditional deletion of AMPK-α1/α2 catalytic subunits in catecholaminergic cells is PO_2-dependent.

Means ± SEM for the apnoeic index (apnoeas/min) during **(A)** the first and second half of 10 minute exposures and **(B)** for every 60 seconds of 10 minute exposures to **(i)** mild hypoxia (12% O_2) and **(ii)** severe hypoxia (8% O_2) in AMPK-α1 and -α2 floxed mice (AMPK-α1/α2 Flx, black, 12% O_2: n = 55 exposures from 19 mice, 8% O_2: n = 58 exposures from 25 mice) and TH-driven AMPK-α1 and -α2 double knockout mice (TH AMPK-α1/α2 dKO, red, 12% O_2: n = 35 exposures from 11 mice, 8% O_2: n = 46 exposures from 22 mice), as well as **(C)** every 60s of 60min exposures to severe hypoxia for AMPK-α1/α2 Flx (n = 6 mice) and TH AMPK-α1/α2 dKO (n = 4 mice). * = $p<0.05$, ** = $p<0.01$, *** = $p<0.001$, **** = $p<0.0001$. Significance tested by two-way ANOVA with Sidak post-hoc tests.

5.2.2.2 Apnoea duration

Mild hypoxia The duration of apnoeas for AMPK-α1/α2 Flx mice during mild hypoxia (12% O_2) was stable during both halves of 10min exposures to hypoxia (Figure 5.4 Ai; 742.5 ± 17.7ms and 781 ± 15.8ms, respectively). That said, when looking at the average durations of apnoeas during each minute a minor statistically insignificant increase over time was observed (Figure 5.4 Bi; at 1-2min: 750.6 ± 27.4ms; at 4-5min: 787.8 ± 30.6ms; at 9-10min: 837.6 ± 37ms).

Severe hypoxia During 8% O_2, apnoea durations were slightly greater relative to 12% O_2 in AMPK-α1/α2 Flx mice and measured 909.7 ± 21.4ms during the first, and 844.4 ± 26.1ms during the second half of 10min exposures to hypoxia (Figure 5.4 Aii). Moreover, the duration of apnoeas remained fairly stable throughout the exposure, measuring 870.6 ± 19.8ms by 1-2min, 918.6 ± 34.6ms by 5-6min, and 869.4 ± 37.4ms by 9-10min (Figure 5.4 Bii) and also remained constant during prolonged exposures of 60min hypoxia (Figure 5.4 C; 20-25min: 830 ± 20ms; 35-40min: 812 ± 28ms; 55-60min: 906 ± 66ms).

Effect of AMPK deletion on apnoea duration during mild hypoxia Unexpectedly, apnoea durations were significantly reduced in TH AMPK-α1/α2 dKO mice compared to controls during 12% O_2, measuring 693.7 ± 11.1ms ($p<0.05$) for the first and 726.5 ± 16.6ms ($p<0.05$) for the second half of 10min exposures. However, closer analyses of the durations for each minute revealed that apnoeas were only significantly shorter in TH AMPK-α1/α2 dKO mice compared to controls during the second and fifth minute of mild hypoxia (at 1-2min: 681.7 ± 13.9ms, $p<0.05$; at 4-5min: 703 ± 16.6ms, $p<0.05$).

Effect of AMPK deletion on apnoea duration during severe hypoxia Under these conditions, TH AMPK-α1/α2 dKO mice exhibited a marked increase in apnoea duration compared to controls (0-5min: 1139.4 ± 39.2ms, $p<0.0001$; 5-10min: 1143.6 ± 54.3ms, $p<0.0001$), consistent with previous observations. Importantly, this increase in apnoea duration was evident at each minute throughout 10min exposures to hypoxia (at 1-2min: 1031 ±

38.9ms, $p<0.0001$; at 5-6min: 1185.5 ± 47.3ms, $p<0.0001$; at 9-10min: 1064.2 ± 80.7ms, $p<0.05$). However, 60min exposures revealed that the significant augmentation only lasted until 25min (20-25min: 1126 ± 53ms, $p<0.01$), after which the apnoea durations decreased in TH AMPK-α1/α2 dKO mice to the same level observed for control AMPK-α1/α2 Flx mice (25-30min: 920 ± 70ms; 35-40min: 950 ± 56ms; 55-60min: 926 ± 99ms; not significant relative to controls for any 5min block).

Thus, deletion of AMPK-α1/α2 subunits in catecholaminergic cells precipitates prolonged apnoeas during severe, but not mild, hypoxia. Furthermore, the increase in apnoea duration observed in TH AMPK-α1/α2 dKO mice during hypoxia relative to controls declined in a time-dependent manner during prolonged exposures, suggesting that these mice are able to "recover" normal apnoea durations and thus re-initiate inspiratory activity within the same timeframe as control mice.

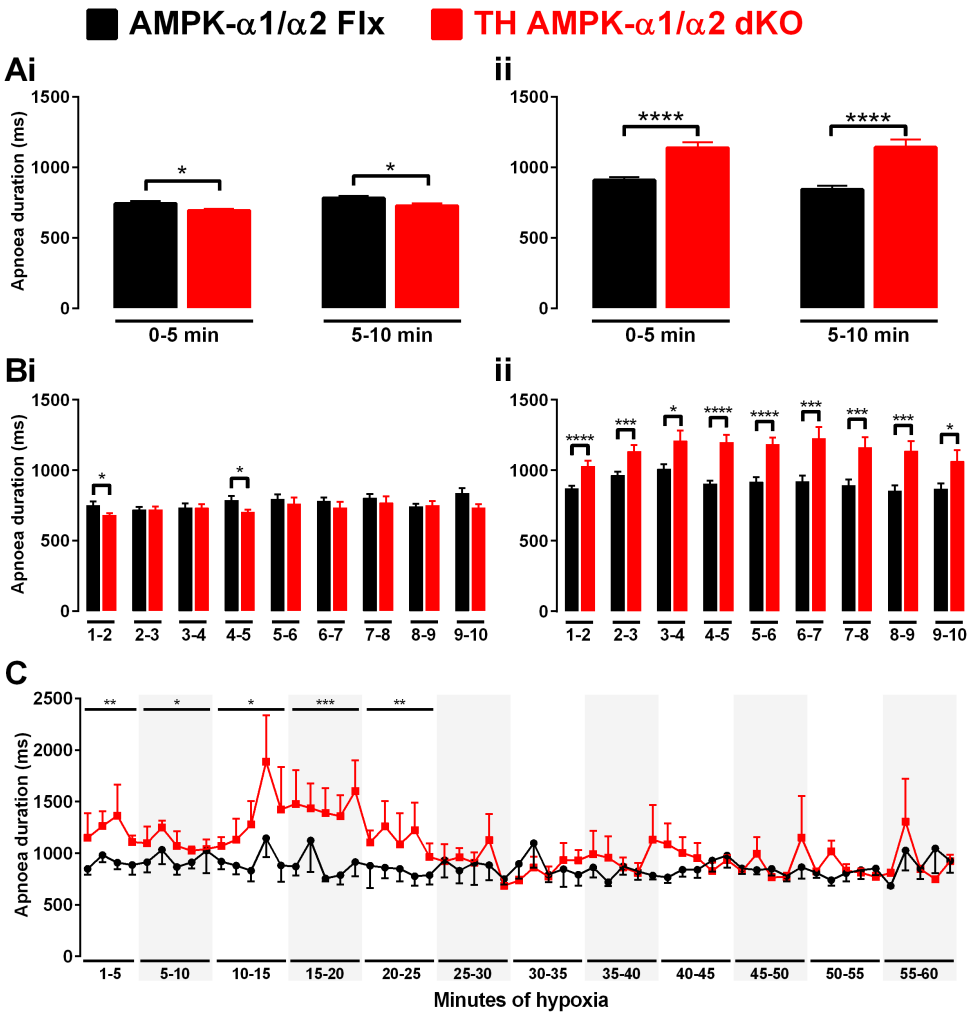

Figure 5.4: The increase in apnoea duration of mice with conditional deletion of AMPK-α1/α2 catalytic subunits in catecholaminergic cells is PO_2- and time-dependent.

Means ± SEM for the apnoea duration (ms) during **(A)** the first and second half of 10 minute exposures and **(B)** for every 60 seconds of 10 minute exposures to **(i)** mild hypoxia (12% O_2) and **(ii)** severe hypoxia (8% O_2) in AMPK-α1 and -α2 floxed mice (AMPK-α1/α2 Flx, black, 12% O_2: n = 55 exposures from 19 mice, 8% O_2: n = 58 exposures from 25 mice) and TH-driven AMPK-α1 and -α2 double knockout mice (TH AMPK-α1/α2 dKO, red, 12% O_2: n = 35 exposures from 11 mice, 8% O_2: n = 46 exposures from 22 mice), as well as **(C)** every 60s of 60min exposures to severe hypoxia for AMPK-α1/α2 Flx (n = 6 mice) and TH AMPK-α1/α2 dKO (n = 4 mice). * = p<0.05, ** = p<0.01, *** = p<0.001, **** = p<0.0001. Significance tested by multiple t-tests with Holm-Sidak post-hoc for apnoea duration.

5.2.2.3 Apnoea duration index

Mild hypoxia As would be expected from the outcomes for apnoea frequency and duration, the apnoea-duration index (ADI; frequency x duration), remained stable in AMPK-α1/α2 Flx mice for both halves of 10min exposures to mild hypoxia (Figure 5.5 Ai; 0.6 ± 0.1 and 0.8 ± 0.1, respectively), but showed a minor increase over time when analysed as minute-by-minute averages (Figure 5.5 Bi; at 1-2min: 0.4 ± 0.1; at 5-6min: 0.6 ± 0.1; at 9-10min: 1.2 ± 0.2).

Severe hypoxia Given the stable duration of apnoeas over time in AMPK-α1/α2 Flx mice it was not surprising that the time-dependent changes in the apnoea-duration index followed a similar pattern to apnoea frequency. Compared to mild hypoxia, the ADI of control mice was increased in response to 8% O_2 (Figure 5.5 Aii; 2.9 ± 0.2 and 1.5 ± 0.2, respectively) and showed a time-dependent decrease during 10min exposures of hypoxia (Figure 5.5 Bii; at 1-2min: 3.5 ± 0.3; at 5-6min: 1.9 ± 0.3; at 9-10min: 1.8 ± 0.3) that appeared to last until 20-25min (Figure 5.5 C; 1 ± 0.2), after which it remained stable for the remainder of prolonged 60min exposures to 8% O_2 (30-35min: 1.5 ± 0.2; 40-45min: 1.9 ± 0.2; 55-60min: 1.7 ± 0.3).

Effect of AMPK deletion on ADI during mild hypoxia The outcomes for apnoea frequency and duration translated into an ADI of TH AMPK-α1/α2 dKO mice that was comparable to controls in response to 12% O_2, both as averages over 5min (0-5min: 0.5 ± 0.08, not significant; 5-10min: 0.5 ± 0.1, not significant), and at each time point throughout the 10min exposure (at 1-2min: 0.4 ± 0.1; at 5-6min: 0 0.7 ± 0.2; at 9-10min: 0.8 ± 0.2; not significant compared to controls at any point).

Effect of AMPK deletion on ADI during severe hypoxia By contrast, during 8% O_2, the ADI of TH AMPK-α1/α2 dKO mice was augmented compared to controls during both halves of 10min exposures (0-5min: 6.4 ± 0.4, $p<0.0001$; 5-10min: 5.1 ± 0.5, $p<0.0001$) and throughout the duration when measured as 1min averages (at 1-2min: 9.5 ± 0.9, $p<0.0001$; at 5-6min: 4.9 ± 0.7, $p<0.001$; at 9-10min: 5.7 ± 0.9, $p<0.0001$). This significantly higher ADI of TH AMPK-α1/α2 dKO mice relative to controls was evident until

approximately 25min (20-25min: 4.3 ± 0.7, $p<0.05$). Thereafter, the ADI declined, on average, to a level similar to controls until the end of the exposure (30-35min: 2.4 ± 0.6; 40-45min: 2.7 ± 0.8; 55-60min: 2.6 ± 0.5). However, frequency-dependent “apnoeic bursts” were still evident every 3.3 to 4.2 mHz (once every 4-5min) when analysed on a minute-by-minute basis.

Overall, while TH AMPK-α1/α2 dKO mice presented with a severely augmented and prolonged apnoeic phenotype in response to acute hypoxia, they were able to regain some ventilatory stability during more prolonged hypoxic exposures, especially with respect to the re-initiation of inspiration following an apnoea (i.e. shortened apnoea duration). Nevertheless, a certain degree of instability clearly remained, which oscillated rhythmically throughout the exposures to prolonged hypoxia. These phasic periods of respiratory instability were driven by phasic “bursts” of increased apnoea frequency, and were present in every TH AMPK-α1/α2 dKO mouse (Appendix 3.3). This therefore points towards periodically disrupted signal integration within the central pattern generators following AMPK deletion in catecholaminergic cells.

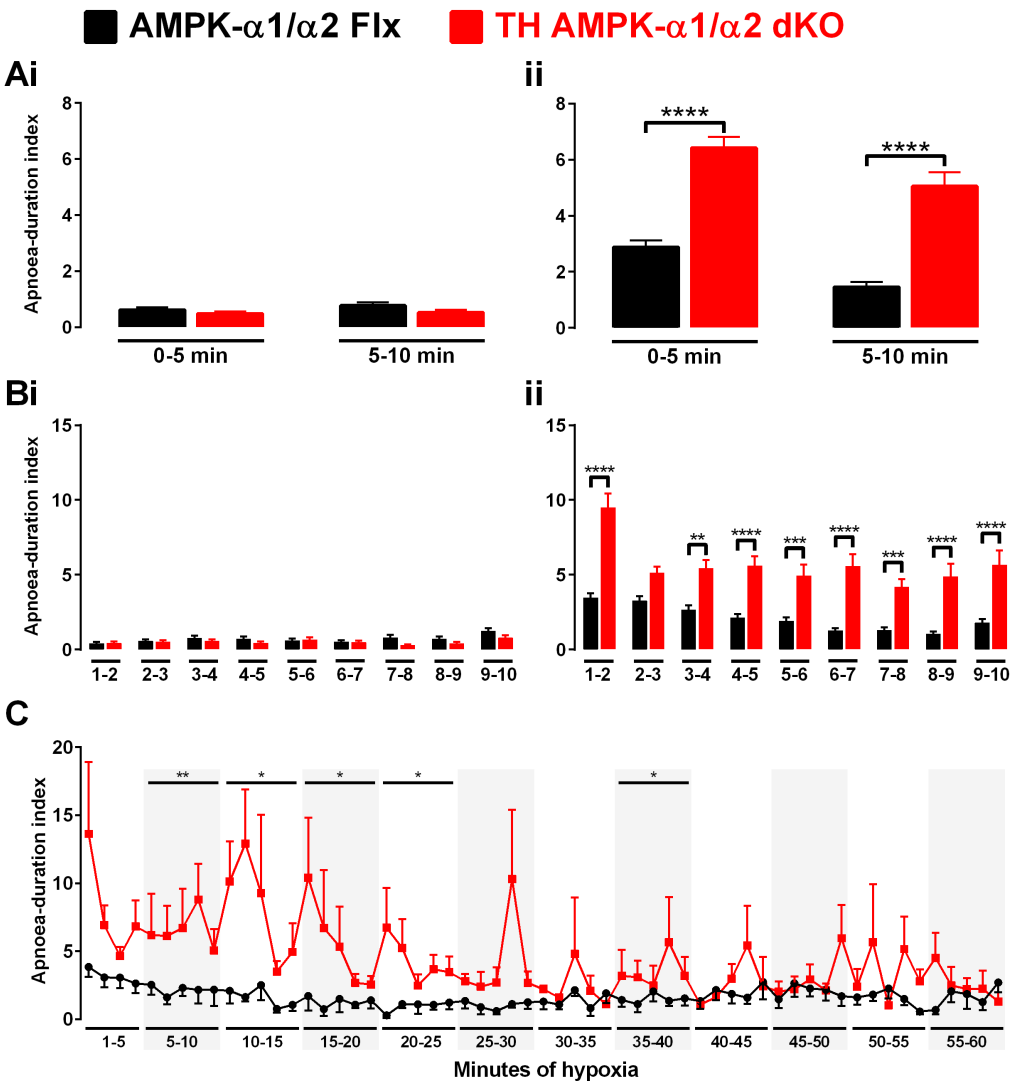

Figure 5.5: The augmentation of the apnoea-duration index in TH-driven AMPK-α1/α2 knockout mice is PO_2- dependent.

Means ± SEM for the apnoea-duration index (frequency x duration) during **(A)** the first and second half of 10 minute exposures and **(B)** for every 60 seconds of 10 minute exposures to **(i)** mild hypoxia (12% O_2) and **(ii)** severe hypoxia (8% O_2) in AMPK-α1 and -α2 floxed mice (AMPK-α1/α2 Flx, black, 12% O_2: n = 55 exposures from 19 mice, 8% O_2: n = 58 exposures from 25 mice) and TH-driven AMPK-α1 and -α2 double knockout mice (TH AMPK-α1/α2 dKO, red, 12% O_2: n = 35 exposures from 11 mice, 8% O_2: n = 46 exposures from 22 mice), as well as **(C)** every 60s of 60min exposures to severe hypoxia for AMPK-α1/α2 Flx (n = 6 mice) and TH AMPK-α1/α2 dKO (n = 4 mice). * = p<0.05, ** = p<0.01, *** = p<0.001, **** = p<0.0001. Significance tested by two-way ANOVA with Sidak post-hoc tests.

5.2.3 AMPK deletion in catecholaminergic cells increases the number of SA and the duration of PSA during 10min exposures to severe hypoxia

As mentioned in the introduction to this chapter, two types of apnoeas have been described, the generation of which is thought to be triggered by different mechanisms at the level of the brainstem (Radulovacki *et al.*, 2001; Wang *et al.*, 2008; Chapuis *et al.*, 2014). It was therefore of interest to see how deletion of AMPK-α1 and -α2 subunits in catecholaminergic cells impacts on the occurrence of spontaneous apnoeas (SA) and post-sigh apnoeas (PSA) during hypoxia.

5.2.3.1 Apnoeic index

Mild hypoxia - controls During 12% O_2, SA and PSA occurred at a comparable frequency in control AMPK-α1/α2 Flx mice (Figure 5.6 A). That said, there appeared to be a trend for SA to be slightly more frequent, but this only became statistically significant (compared to PSA) during the fifth and tenth minute of hypoxia (apnoeas/min for SA versus PSA – at 4-5min: 0.7 ± 0.2 versus 0.2 ± 0.1, $p<0.01$; at 9-10min: 1.2 ± 0.2 versus 0.4 ± 0.1, $p<0.0001$).

Severe hypoxia - controls Interestingly, there was a switch in apnoea frequency during severe hypoxia (Figure 5.6 B), whereby PSA were significantly more frequent in AMPK-α1/α2 Flx mice from the second to the seventh minute of 8% O_2 (apnoeas/min for SA versus PSA – at 1-2min: 0.8 ± 0.2 versus 3.1 ± 0.3, $p<0.001$; at 5-6min: 0.3 ± 0.1 versus 1.7 ± 0.2, $p<0.01$; at 9-10min: 0.5 ± 0.1 versus 1.4 ± 0.2, not significant). Moreover, it seemed that the PO_2-dependent increases of apnoea frequency of control mice mentioned in section 5.2.2.1 were primarily driven by increases in the frequency of PSA, but not SA. A closer inspection of the apnoeic profile during prolonged 60min exposures to 8% O_2 showed that over the last 30min the apnoea frequencies seemed to switch back to being comparable at each time point with, if anything, a slight predominance of SA (Figure 5.7 A;

apnoeas/min for SA versus PSA – at 30-31min: 1 ± 0.5 versus 0.5 ± 0.2; at 45-46min: 1.2 ± 0.5 versus 0.5 ± 0.2; at 59-60min: 2.8 ± 1 versus 0.3 ± 0.2).

Mild hypoxia - knockouts In TH AMPK-α1/α2 dKO mice, the numbers of SA and PSA were comparable to each other throughout the 10min exposures to mild hypoxia (apnoeas/min for SA versus PSA – at 1-2min: 0.2 ± 0.1 versus 0.5 ± 0.1, not significant; at 5-6min: 0.4 ± 0.1 versus 0.5 ± 0.2, not significant; at 9-10min: 0.7 ± 0.2 versus 0.3 ± 0.1, not significant).

Severe hypoxia - knockouts Unlike controls, the numbers of SA and PSA remained comparable in TH AMPK-α1/α2 dKO mice for most of the 10min of severe hypoxia. Significant differences were only seen during the second, third, and tenth minute of 8% O_2 (apnoeas/min for SA versus PSA – at 1-2min: 5.5 ± 0.7 versus 3.7 ± 0.3, $p<0.001$; at 2-3min: 1.6 ± 0.3 versus 3.1 ± 0.2, $p<0.01$; at 9-10min: 3.4 ± 0.8 versus 2.1 ± 0.2, $p<0.05$). Additionally, frequencies of SA and PSA also remained comparable throughout prolonged 60min exposures, even though it appeared that the "apnoeic bursts" described earlier were solely driven by periodic, oscillating increases in the spontaneous apnoeic index, while the numbers of PSA remained stable and possibly even declined over time (Figure 5.7 B; apnoeas/min for SA versus PSA during "apnoeic bursts" – at 28-29min: 6 ± 2 versus 1.8 ± 0.8; at 32-33min: 4 ± 4 versus 1.3 ± 0.5; at 38-39min: 5.3 ± 3 versus 1.3 ± 0.5; at 43-44min: 5 ± 3 versus 1.5 ± 0.3; at 49-50min: 4.8 ± 1.6 versus 0.8 ± 0.5; at 53-54min: 6 ± 2.9 versus 0.5 ± 0.3).

Therefore, it appears that the PO_2-dependent changes in apnoea frequency observed in AMPK-α1/α2 Flx mice were driven by increases in PSA, whereas the changes observed in TH AMPK-α1/α2 dKO mice were driven by increases in the frequencies of *both* PSA and SA. Additionally, periodic increases in apnoeas during prolonged exposures appeared to be due to an increased occurrence of SA, but not PSA, which indicates that over time TH AMPK-α1/α2 dKO mice are able to reduce their number of PSA to the level observed in control AMPK-α1/α2 Flx mice.

Effect of AMPK deletion on the frequency of *SA and PSA compared to controls* There were no significant differences in the frequencies of PSA

between AMPK-α1/α2 Flx and TH AMPK-α1/α2 dKO mice during either mild or severe hypoxia.

By contrast, SA were significantly *less* frequent in TH AMPK-α1/α2 dKO mice at certain points during exposures to mild hypoxia (at 4-5min: $p<0.01$; at 7-8min: $p<0.01$), but *augmented* throughout the entire exposure to 10min of severe hypoxia (at 1-2min: $p<0.0001$; at 5-6min: $p<0.01$; at 9-10min: $p<0.0001$). Importantly, during more prolonged 60min exposures SA remained augmented relative to controls, particularly during the "apnoeic bursts" which were solely driven by augmentations in the numbers of SA. Although significant differences in the apnoeic index of SA between controls and TH AMPK-α1/α2 dKO mice were not always reached (possibly due to the small cohort of animals tested and the high degree of variability within the numbers of SA), the average numbers of SA in TH AMPK-α1/α2 dKO mice were at least 3 times higher than in control AMPK-α1/α2 Flx mice (controls versus knockouts – at 15-16min: 1 ± 1 versus 8 ± 4.6, $p<0.0001$; at 28-29min: 0.2 ± 0.2 versus 6 ± 2, $p<0.01$; at 32-33min: 1.3 ± 0.6 versus 4 ± 4, $p>0.999$; at 38-39min: 1 ± 0.4 versus 5.3 ± 3.1, $p=0.266$; at 43-44min: 0.8 ± 0.5 versus 5 ± 3, $p=0.322$; at 49-50min: 1.2 ± 0.6 versus 4.8 ± 1.6, $p=0.829$; at 53-54min: 1 ± 0.4 versus 6 ± 2.9, $p<0.05$).

This shows that because both AMPK-α1/α2 Flx and TH AMPK-α1/α2 dKO mice had a comparable PO_2-dependent increase in the number of PSA, it was the additional PO_2-dependent increases in the number of SA in TH AMPK-α1/α2 dKO mice that resulted in the significantly augmented total apnoeic index described during acute hypoxia (section 5.2.2.1). Moreover, while TH AMPK-α1/α2 dKO mice appear to recover ventilatory stability during prolonged exposures to severe hypoxia with respect to the occurrence of PSA, they clearly still suffer from periodically oscillating disturbances of the rCPGs.

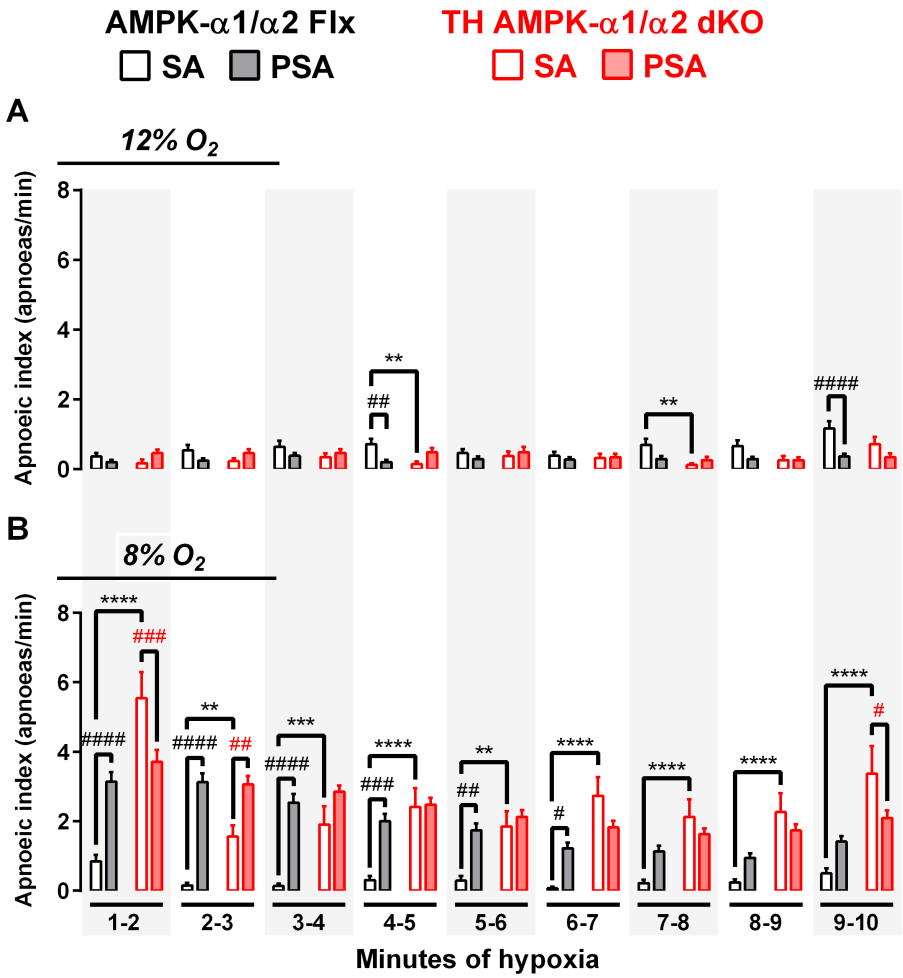

Figure 5.6: Conditional deletion of AMPK-α1/α2 catalytic subunits in catecholaminergic cells precipitates more frequent spontaneous apnoeas.

Means ± SEM for the apnoeic index (apnoeas/min) for every 60 seconds of 10 minute exposures to **(A)** mild hypoxia (12% O_2) and **(B)** severe hypoxia (8% O_2) in AMPK-α1 and -α2 floxed mice (AMPK-α1/α2 Flx, black, 12% O_2: n = 55 exposures from 19 mice, 8% O_2: n = 58 exposures from 25 mice) and TH-driven AMPK-α1 and -α2 double knockout mice (TH AMPK-α1/α2 dKO, red, 12% O_2: n = 35 exposures from 11 mice, 8% O_2: n = 46 exposures from 22 mice), separated into post-sigh apnoeas (PSA) and spontaneous apnoeas (SA). Between genotypes: ** = p<0.01, *** = p<0.001, **** = p<0.0001; between SA and PSA: # = p<0.05, ## = p<0.01, ### = p<0.001, #### = p<0.0001. Significance tested by two-way ANOVA with Sidak post-hoc tests for apnoeic index and apnoea-duration index, multiple t-tests with Holm-Sidak post-hoc for apnoea duration.

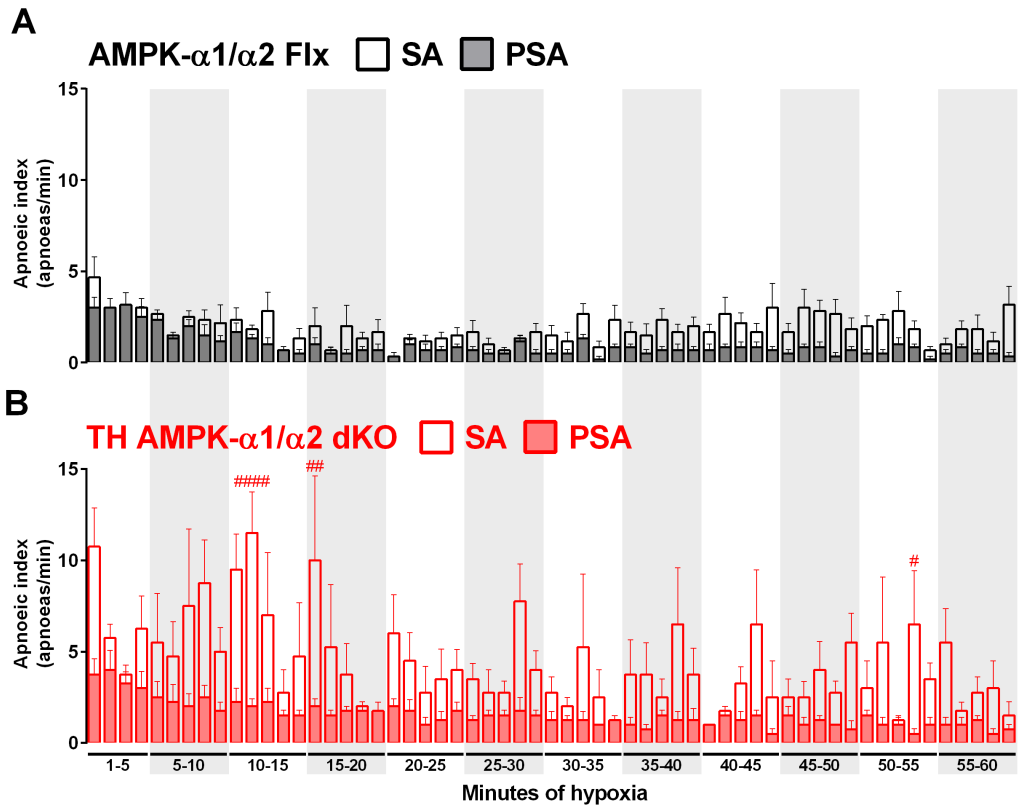

Figure 5.7: Conditional deletion of AMPK-α1/α2 catalytic subunits in catecholaminergic cells precipitates "apnoeic bursts" due to more frequent spontaneous apnoeas during prolonged exposures to severe hypoxia.

Means ± SEM for the apnoeic index (apnoeas/min) for every 60 seconds of 60 minute exposures severe hypoxia (8% O_2) in **(A)** AMPK-α1 and -α2 floxed mice (AMPK-α1/α2 Flx, black, n = 6) and **(B)** TH-driven AMPK-α1 and -α2 double knockout mice (TH AMPK-α1/α2 dKO, red, n = 4), separated into post-sigh apnoeas (PSA) and spontaneous apnoeas (SA). Between SA and PSA: # = $p<0.05$, ## = $p<0.01$, #### = $p<0.0001$. Significance tested by two-way ANOVA with Sidak post-hoc tests.

5.2.3.2 Apnoea duration

Mild hypoxia - controls Similar to apnoea frequency during 12% O_2, durations of SA and PSA were generally comparable to each other in control AMPK-α1/α2 Flx mice, but reached significance at the end of the 10 minutes with PSA being longer in duration than SA (Figure 5.8 A; SA versus PSA – at 8-9min: 720.3 ± 19.6ms versus 822.8 ± 47.5ms, $p<0.05$; at 9-10min: 759.3 ± 31.7ms versus 978.9 ± 66ms, $p<0.001$).

Severe hypoxia - controls During 8% O_2 (Figure 5.8 B), there was a trend for PSA durations of AMPK-α1/α2 Flx mice to be longer than those of SA, which reached significance during the second (SA: 702.5 ± 23.7ms, PSA: 923.2 ± 25.1ms, $p<0.0001$), fourth (SA: 716.3 ± 51.6ms, PSA: 1008.4 ± 31.2ms, $p<0.01$), fifth (SA: 745 ± 57.2ms, PSA: 939.4 ± 29.6ms, $p<0.01$), sixth (SA: 708.6 ± 41.4ms, PSA: 953.3 ± 36.2ms, $p<0.01$), and eighth (SA: 701.4 ± 33.1ms, PSA: 906.1 ± 48.2ms, $p<0.05$) minute. This trend, albeit generally statistically insignificant for the number of mice tested, was also present throughout prolonged 60min exposures to severe hypoxia (Figure 5.9 A; SA versus PSA – at 30-31min: 660 ± 30ms versus 1254 ± 55ms, $p<0.05$; at 44-45min: 780 ± 48ms versus 1290 ± 320ms, not significant; at 59-60min: 777 ± 40ms versus 1846 ± 0ms, not significant).

Mild hypoxia - knockouts Similar to controls, the durations of SA and PSA were also comparable to each other in TH AMPK-α1/α2 dKO mice throughout exposures to mild hypoxia (apart from the third minute, where SA: 661.1 ± 25.3, PSA: 762.1 ± 30.7, $p<0.05$).

Severe hypoxia - knockouts PSA durations were significantly longer than SA for TH AMPK-α1/α2 dKO mice throughout exposures to severe hypoxia (SA versus PSA – at 1-2min: 887.2 ± 62.4ms versus 1247.6 ± 100.8ms, $p<0.01$; at 5-6min: 882.2 ± 43.9ms versus 1359 ± 63.4ms, $p<0.001$; at 9-10min: 901.3 ± 67.7ms versus 1264.5 ± 99.1, $p<0.05$). However, as indicated in section 5.2.2.2, the average duration of apnoeas decreased throughout prolonged 60min exposures of hypoxia to a similar duration observed in controls. This reduction was driven by marked decreases in the duration of PSA with minimal changes in the durations of SA (Figure 5.9 B; SA versus

PSA – at 30-31min: 709 ± 77ms versus 752 ± 45ms; at 44-45min: 995 ± 0ms versus 882 ± 8ms; at 59-60min: 725 ± 0ms versus 989 ± 29ms).

This indicates that the PO_2-dependent increases of apnoea duration observed in both genotypes were mainly due to an augmentation in the durations of PSA. Moreover, deletion of AMPK in catecholaminergic cells further prolonged the duration of PSA during acute, but not prolonged hypoxia.

Effect of AMPK deletion on the duration of SA and PSA compared to controls

There were no differences in the durations of either SA or PSA between genotypes during mild hypoxia on the whole, but the durations of PSA were significantly shorter in TH AMPK-α1/α2 dKO mice compared to controls during the second ($p<0.01$) and tenth ($p<0.05$) minute of 12% O_2.

During severe hypoxia, the durations of SA were only significantly augmented in TH AMPK-α1/α2 dKO mice compared to controls during the second ($p<0.01$) and eighth ($p<0.01$) minute, whereas the durations of PSA were significantly longer during every minute of 8% O_2 (at 1-2min: $p<0.0001$; at 5-6min: $p<0.0001$; at 9-10min $p<0.001$). However, as mentioned above, a time-dependent reduction on PSA duration in TH AMPK-α1/α2 dKO mice resulted in apnoea durations that were similarly as long as those of controls during prolonged 60min exposures.

Therefore, deletion of AMPK-α1 and -α2 subunits in catecholaminergic cells appeared to increase the duration of apnoeas in a PO_2-dependent manner and predominantly through the prolongation of PSA, but not SA, during acute but not prolonged exposures to hypoxia.

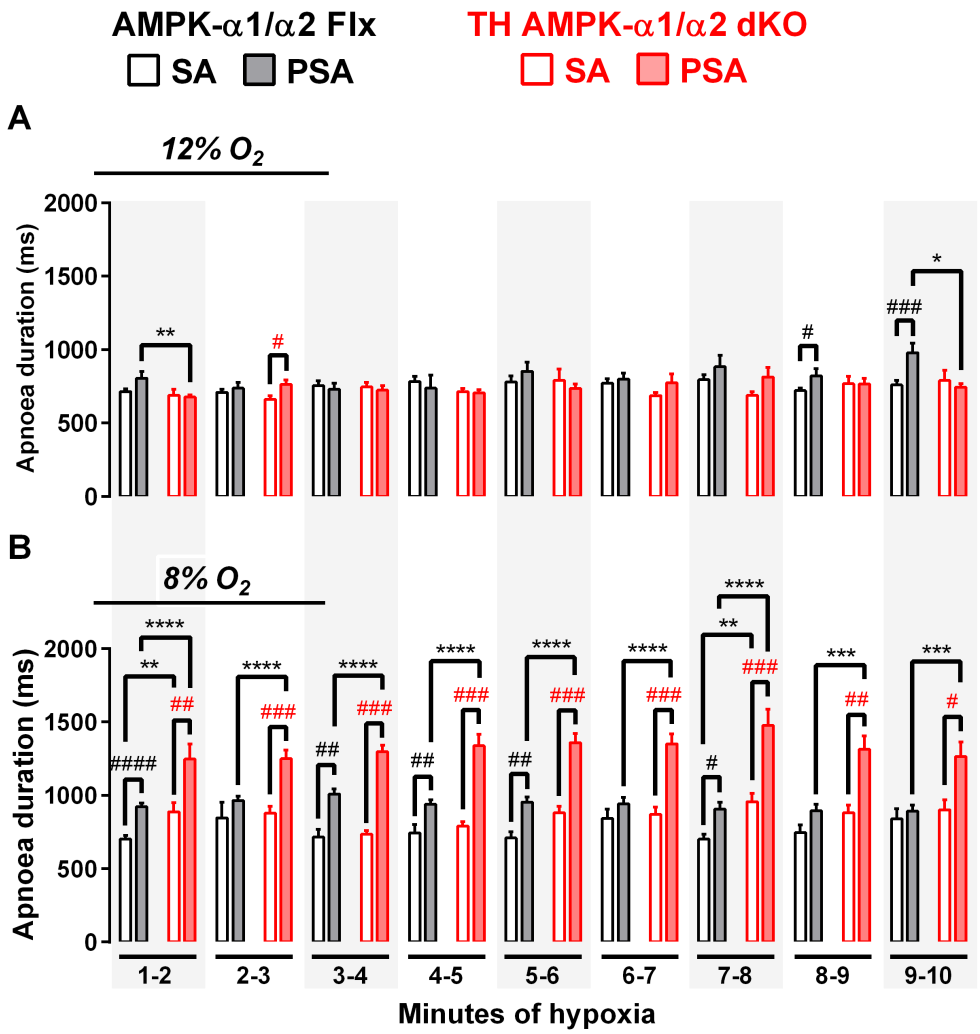

Figure 5.8: Conditional deletion of AMPK-α1/α2 catalytic subunits in catecholaminergic cells precipitates prolonged post-sigh apnoeas. Means ± SEM for the apnoea duration (ms) for every 60 seconds of 10 minute exposures to **(A)** mild hypoxia (12% O_2) and **(B)** severe hypoxia (8% O_2) in AMPK-α1 and -α2 floxed mice (AMPK-α1/α2 Flx, black, 12% O_2: n = 55 exposures from 19 mice, 8% O_2: n = 58 exposures from 25 mice) and TH-driven AMPK-α1 and -α2 double knockout mice (TH AMPK-α1/α2 dKO, red, 12% O_2: n = 35 exposures from 11 mice, 8% O_2: n = 46 exposures from 22 mice), separated into post-sigh apnoeas (PSA) and spontaneous apnoeas (SA). Between genotypes: * = p<0.05, ** = p<0.01, *** = p<0.001, **** = p<0.0001; between SA and PSA: # = p<0.05, ## = p<0.01, ### = p<0.001, #### = p<0.0001. Significance tested by two-way ANOVA with Sidak post-hoc tests for apnoeic index and apnoea-duration index, multiple t-tests with Holm-Sidak post-hoc for apnoea duration.

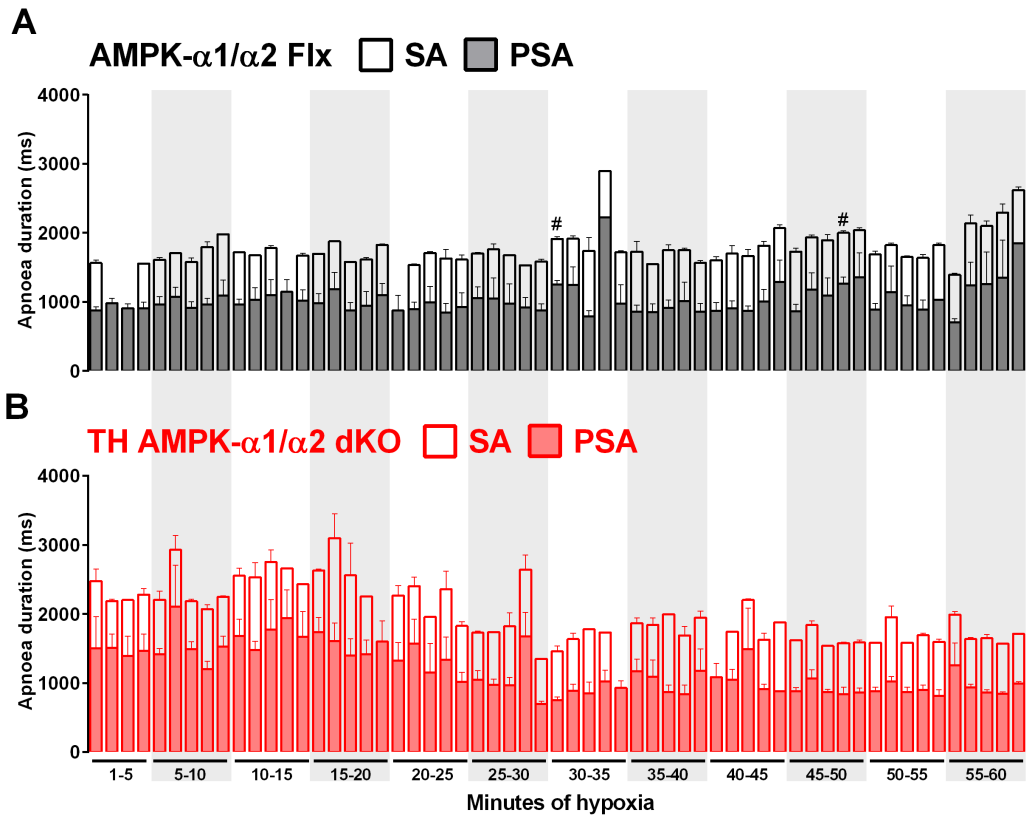

Figure 5.9: Conditional deletion of AMPK-α1/α2 catalytic subunits in catecholaminergic cells precipitates "apnoeic bursts" due to more frequent spontaneous apnoeas during prolonged exposures to severe hypoxia.

Means ± SEM for the apnoea duration (ms) for every 60 seconds of 60 minute exposures severe hypoxia (8% O_2) in **(A)** AMPK-α1 and -α2 floxed mice (AMPK-α1/α2 Flx, black, n = 6) and **(B)** TH-driven AMPK-α1 and -α2 double knockout mice (TH AMPK-α1/α2 dKO, red, n = 4), separated into post-sigh apnoeas (PSA) and spontaneous apnoeas (SA). Between SA and PSA: # = $p<0.05$. Significance tested by multiple t-tests with Holm-Sidak post-hoc.

5.2.3.3 Apnoea-duration index

Mild hypoxia - controls Together, measurements for apnoea frequency and duration during 12% O_2 (Figure 5.10 A) translated into an ADI that was generally comparable between SA and PSA for control AMPK-α1/α2 Flx mice (only significantly different at 4-5min and 9-10min, where SA: 0.6 ± 0.1, PSA: 0.2 ± 0.1, $p<0.01$ and SA: 0.9 ± 0.2, PSA: 0.4 ± 0.1, $p<0.0001$, respectively).

Severe hypoxia - controls During 8% O_2 (Figure 5.10 B), ADIs for PSA were significantly higher than for SA in control AMPK-α1/α2 Flx mice until the seventh minute of hypoxia (SA versus PSA – at 1-2min: 0.6 ± 0.1 versus 2.9 ± 0.3, $p<0.0001$; at 5-6min: 0.2 ± 0.1 versus 1.7 ± 0.2, $p<0.01$; at 9-10min: 0.4 ± 0.1 versus 1.3 ± 0.2, not significant) and comparable throughout prolonged exposures (Figure 5.11 A; SA versus PSA – at 30-31min: 0.68 ± 0.4 versus 0.62 ± 0.3; at 44-45min: 1.88 ± 1.1 versus 0.86 ± 0.3; at 59-60min: 2.16 ± 0.8 versus 0.31 ± 0.3; not significant at any point).

Mild hypoxia - knockouts No differences were found in the ADI of SA compared to PSA during exposures to 12% O_2 in TH AMPK-α1/α2 dKO mice.

Severe hypoxia - knockouts By contrast, exposures to 8% O_2 significantly augmented the ADI of PSA in TH AMPK-α1/α2 dKO mice compared to SA during the third (SA: 1.2 ± 0.3, PSA: 4 ± 0.4, $p<0.0001$), fourth (SA: 1.5 ± 0.4, PSA: 3.9 ± 0.3, $p<0.0001$), and sixth (SA: 1.5 ± 0.4, PSA: 3 ± 0.4, $p<0.001$) minute of hypoxia, but at no other time points during 10 or 60min exposures. That said, the time-dependent reduction of the number of PSA translated into a continued decline of the ADI over the course of the 60min exposure. By contrast, phasic oscillations of sudden increases in the ADI of SA, driven by periodic "bursts" in the number of SA, were still apparent throughout the duration of the exposure.

Effect of AMPK deletion on the ADI of SA and PSA compared to controls There were no overall differences in the ADIs of SA and PSA, respectively, between genotypes during exposures to mild hypoxia. The only significant frequency-dependent differences in SA between genotypes were at 4-5min

and 7-8min, where control mice measured 0.6 ± 0.1 and 0.6 ± 0.1, respectively, and TH AMPK-α1/α2 dKO mice only 0.1 ± 0.05 ($p<0.01$) and 0.1 ± 0.04 ($p<0.01$), respectively.

During severe hypoxia, TH AMPK-α1/α2 dKO mice had significantly augmented ADIs of SA and PSA, respectively, compared to AMPK-α1/α2 Flx mice at most time periods measured (SA – at 1-2min: $p<0.0001$; at 5-6min: $p<0.05$; at 9-10min: $p<0.0001$; PSA – at 1-2min: $p<0.001$; at 5-6min: $p<0.05$; at 9-10min: not significant). However, these differences declined over time so that by 20min the ADIs of both SA and PSA were generally comparable between controls and TH AMPK-α1/α2 dKO mice for the remainder of the 60min exposure (Figure 5.11 B). That said, the frequency-dependent "bursts" in the ADI of SA were still, on average, at least at least 3 times higher than in control AMPK-α1/α2 Flx mice, even though statistical significance was only reached twice (controls versus knockouts – at 15-16min: 0.7 ± 0.7 versus 7.2 ± 4.2, $p<0.001$; 28-29min: 0.1 ± 0.1 versus 6.7 ± 3.1, $p<0.0001$; at 32-33min: 1.1 ± 0.4 versus 3.7 ± 3.7, $p>0.999$; at 38-39min: 0.7 ± 0.3 versus 4.6 ± 2.9, $p=0.562$; at 43-44min: 0.7 ± 0.4 versus 4 ± 2.7, $p=0.944$; at 49-50min: 0.8 ± 0.4 versus 3.5 ± 1.2, $p>0.999$; at 53-54min: 0.7 ± 0.3 versus 4.7 ± 2.3, $p>0.999$).

In summary, these outcomes indicate that deletion of AMPK-α1 and -α2 subunits in catecholaminergic cells has a contrasting effect on the two types of apnoeas during acute hypoxia, whereby it augments the frequency of SA on one hand, and the duration of PSA on the other. This translated to a significantly increased apnoea-duration index of both SA and PSA in mice with deletion of AMPK-α1 and -α2 subunits in catecholaminergic cells. However, over time the frequencies and durations of both types of apnoeas decreased to match values obtained from control mice. That said, a certain level of instability within TH AMPK-α1/α2 dKO mice was retained, which lead to periodically oscillating augmentations of SA, a phenomenon that was not observed for PSA or either type of apnoea in controls. Therefore, while vagal afferent inhibition of ventilation may be enhanced upon AMPK deletion in catecholaminergic cells during the early phases of hypoxia, it appeared to normalise back to control levels during more prolonged exposures. By

contrast, AMPK deletion precipitates unforeseen phasic disturbances of the rCPGs that manifest as periodic oscillations or “bursts” in the numbers of SA.

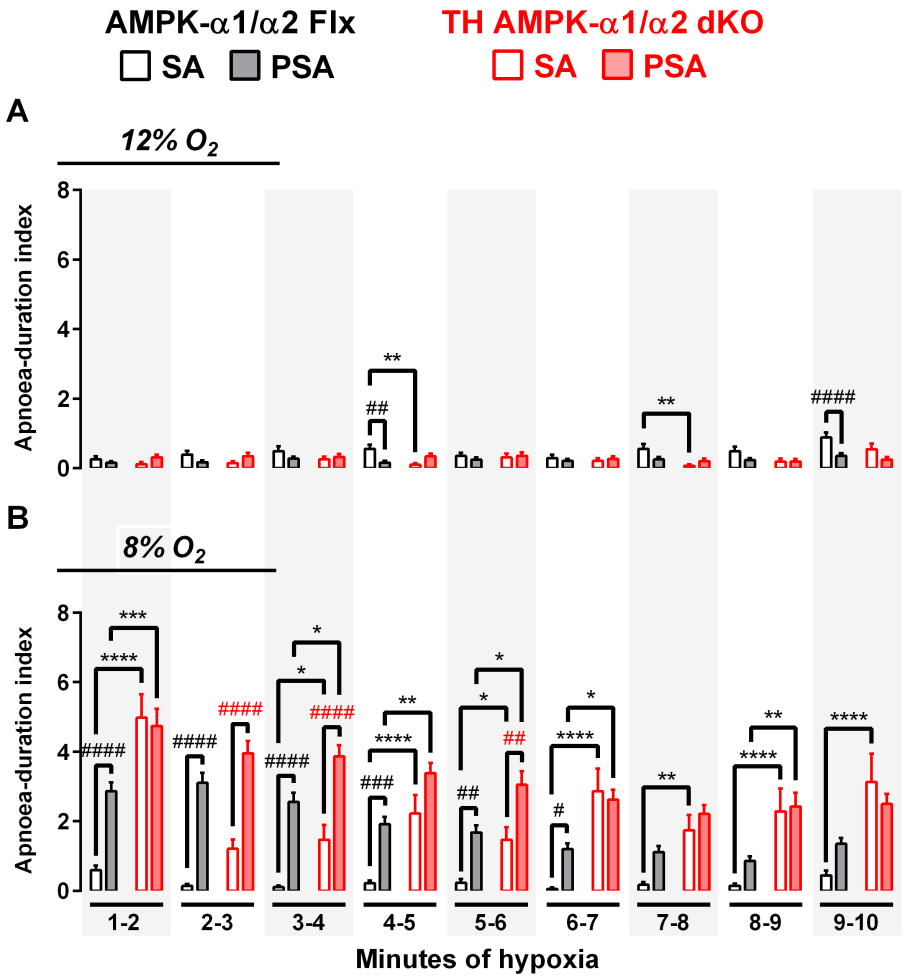

Figure 5.10: Conditional deletion of AMPK-α1/α2 catalytic subunits in catecholaminergic cells augments the spontaneous and post-sigh apnoea indexes.

Means ± SEM for apnoea-duration index for every 60 seconds of 10 minute exposures to **(A)** mild hypoxia (12% O_2) and **(B)** severe hypoxia (8% O_2) in AMPK-α1 and -α2 floxed mice (AMPK-α1/α2 Flx, black, 12% O_2: n = 55 exposures from 19 mice, 8% O_2: n = 58 exposures from 25 mice) and TH-driven AMPK-α1 and -α2 double knockout mice (TH AMPK-α1/α2 dKO, red, 12% O_2: n = 35 exposures from 11 mice, 8% O_2: n = 46 exposures from 22 mice), separated into post-sigh apnoeas (PSA) and spontaneous apnoeas (SA). Between genotypes: * = p<0.05, ** = p<0.01, *** = p<0.001, **** = p<0.0001; between SA and PSA: # = p<0.05, ## = p<0.01, ### = p<0.001, #### = p<0.0001. Significance tested by two-way ANOVA with Sidak post-hoc tests for apnoeic index and apnoea-duration index, multiple t-tests with Holm-Sidak post-hoc for apnoea duration.

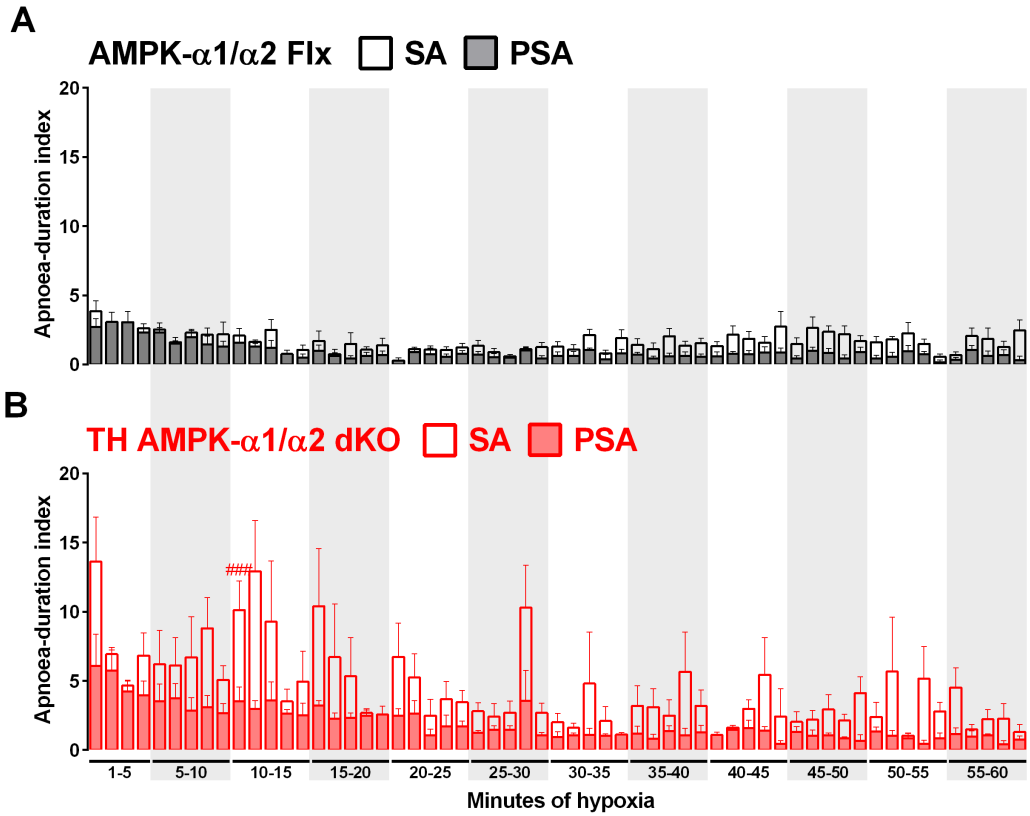

Figure 5.11: The ADI of PSA and SA in mice with conditional deletion of AMPK-α1/α2 catalytic subunits in catecholaminergic cells is comparable with controls during prolonged exposures to severe hypoxia.

Means ± SEM for the apnoea-duration index (frequency x duration) for every 60 seconds of 60 minute exposures severe hypoxia (8% O_2) in **(A)** AMPK-α1 and -α2 floxed mice (AMPK-α1/α2 Flx, black, n = 6) and **(B)** TH-driven AMPK-α1 and -α2 double knockout mice (TH AMPK-α1/α2 dKO, red, n = 4), separated into post-sigh apnoeas (PSA) and spontaneous apnoeas (SA). Between SA and PSA: ### = $p<0.001$. Significance tested by two-way ANOVA with Sidak post-hoc tests.

5.2.4 AMPK deletion in catecholaminergic cells attenuates PO_2-dependent increases in sigh frequency during 10min exposures to severe hypoxia

As described in the section above, the number of PSA increased in a PO_2-dependent manner in both AMPK-α1/α2 Flx and TH AMPK-α1/α2 dKO mice. However, sighs can also occur without a proceeding apnoea (Yamauchi *et al.*, 2008) and have been suggested to restore residual lung volume by reinflating collapsed alveoli (Chapuis *et al.*, 2014; Li *et al.*, 2016). Moreover, hypoxia has been found to increase sigh frequency dependent on vagal and carotid body chemoafferent activity (Bartlett, 1971). It was therefore of interest to compare the frequency of all sighs during hypoxia in control mice and those with catecholaminergic deletion of AMPK-α1 and -α2 subunits, given that CB afferent output during hypoxia is retained in TH AMPK-α1/α2 dKO mice (Mahmoud *et al.*, 2016).

Mild hypoxia The total frequency of sighs in control AMPK-α1/α2 Flx mice during the first half of 10min exposures to 12% O_2 measured 2.1 ± 0.07 sighs/min (Figure 5.12 Ai; n = 55 exposures from 19 mice), which declined to 1.4 ± 0.07 sighs/min during the second half. More detailed analyses of sigh frequencies for every minute of 12% O_2 revealed that this decrease was time-dependent (Figure 5.12 Bi), declining from 2.5 ± 0.1 sighs/min during the second minute, to 1.8 ± 0.1 sighs/min during the sixth minute and finally 1.5 ± 0.1 sighs/min during the tenth minute of hypoxia.

Severe hypoxia A very similar response was also observed during severe hypoxia, whereby sigh frequency declined from the first half (Figure 5.12 Aii; 4.7 ± 0.1 sighs/min; n = 58 exposures from 25 mice) to the second half (2.8 ± 0.1 sighs/min) of the 10min exposure. Once again, this decrease was clearly time-dependent (Figure 5.12 Bii), declining from 6.5 ± 0.2 sighs/min during the second minute, to 3.4 ± 0.1 sighs/min during the sixth minute and finally 2.8 ± 0.2 sighs/min during the tenth minute of hypoxia.

Effect of AMPK deletion on sigh frequency during mild hypoxia Compared to controls, the total number of sighs did not differ during exposures of TH AMPK-α1/α2 dKO mice to mild hypoxia. During the first half of 12% O_2, knockouts presented with 2.3 ± 0.1 sighs/min (n = 35 exposures from 11

mice; not significant compared to controls), which declined during the second half to 1.3 ± 0.1 sighs/min (not significant). A similar time-dependent decrease in sigh frequency was also observed, which measured 2.7 ± 0.2 sighs/min during the second minute, 1.4 ± 0.2 sighs/min during the sixth minute and finally 1.3 ± 0.2 sighs/min during the tenth minute of hypoxia (not significant compared to controls at any time).

Effect of AMPK deletion on sigh frequency during severe hypoxia In contrast, during severe hypoxia, clear differences between controls and knockouts were observed. Sigh frequency was significantly attenuated in TH AMPK-α1/α2 dKO mice (n = 46 exposures from 22 mice) compared to controls during both halves of 10min exposures to severe hypoxia (0-5min: 3.7 ± 0.2, $p<0.0001$; 5-10min: 2.3 ± 0.1, $p<0.05$). However, analysis of one minute periods revealed that although sigh frequency was on average lower in TH AMPK-α1/α2 dKO mice during every minute bar the last, the difference only reached significance during the first half of 8% O_2 compared to control AMPK-α1/α2 Flx mice (at 1-2min: 5.9 ± 0.3 sighs/min, $p<0.05$; at 5-6min: 2.5 ± 0.2 sighs/min, $p<0.01$; at 9-10min: 2.8 ± 0.2 sighs/min, not significant).

These outcomes were intriguing, given that PSA are thought to be coupled to sighs via the Hering-Breuer reflex. A significant reduction in sighs along with a significant augmentation of PSA in TH AMPK-α1/α2 dKO mice relative to controls might be plausible if control AMPK-α1/α2 Flx mice exhibit a significant number of sighs without a proceeding apnoea. Therefore, the relation between sighs and PSA needed to be addressed next.

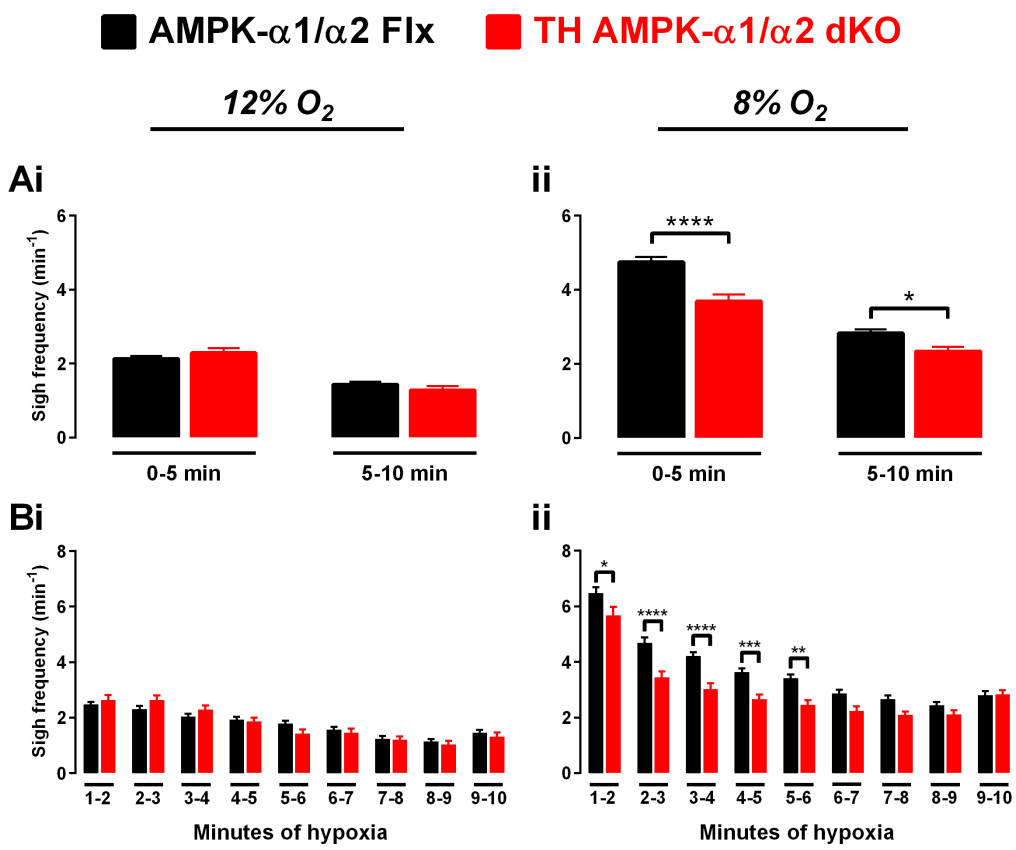

Figure 5.12: Conditional deletion of AMPK-α1/α2 catalytic subunits in catecholaminergic cells attenuates the number of sighs during the early hypoxic ventilatory response.

Means ± SEM for the sigh frequency during **(A)** the first and second half, and **(B)** every 60 seconds during 10 minute exposures to **(i)** mild hypoxia (12% O_2) and **(ii)** severe hypoxia (8% O_2) in AMPK-α1 and -α2 floxed mice (AMPK-α1/α2 Flx, black, 12% O_2: n = 55 exposures from 19 mice, 8% O_2: n = 58 exposures from 25 mice) and TH-driven AMPK-α1 and -α2 double knockout mice (TH AMPK-α1/α2 dKO, red, 12% O_2: n = 35 exposures from 11 mice, 8% O_2: n = 46 exposures from 22 mice). * = $p<0.05$, ** = $p<0.01$, *** = $p<0.001$, **** = $p<0.0001$. Significance tested by two-way ANOVA with Sidak post-hoc tests.

5.2.4.1 The relation between sighs and post-sigh apnoeas

Finally, in order to understand and clearly illustrate the nature of post-sigh breathing behaviour, the total number of sighs was compared against the number of PSA in the two genotypes.

Mild hypoxia - controls During exposures to 12% O_2 (Figure 5.13 A), sighs were rarely followed by an apnoea in AMPK-α1/α2 Flx mice, because the number of sighs was significantly higher than the number of PSA at every time point throughout the exposure (sighs/min versus PSA/min – at 1-2min: 2.5 ± 0.1 versus 0.2 ± 0.1, $p<0.0001$; at 5-6min: 1.8 ± 0.1 versus 0.3 ± 0.1, $p<0.0001$; at 9-10min: 1.5 ± 0.1 versus 0.4 ± 0.1, $p<0.0001$).

Severe hypoxia - controls During 8% O_2, the number of sighs remained significantly higher than PSA in control AMPK-α1/α2 Flx mice throughout the exposures (Figure 5.11 B, sighs/min versus PSA/min – at 1-2min: 6.5 ± 0.2 versus 3.1 ± 0.3, $p<0.0001$; at 5-6min: 3.4 ± 0.1 versus 1.7 ± 0.2, $p<0.0001$; at 9-10min: 2.8 ± 0.2 versus 1.4 ± 0.2, $p<0.0001$), indicating that a large number of sighs still occurs without a proceeding apnoea.

Mild hypoxia - knockouts During 12% O_2, sighs were also rarely followed by an apnoea in TH AMPK-α1/α2 dKO mice (sighs/min versus PSA/min – at 1-2min: 2.6 ± 0.2 versus 0.2 ± 0.1, $p<0.0001$; at 5-6min: 1.4 ± 0.2 versus 0.4 ± 0.1, $p<0.0001$; at 9-10min: 1.3 ± 0.2 versus 0.7 ± 0.2, $p<0.001$).

Severe hypoxia - knockouts However, during 8% O_2, sighs in TH AMPK-α1/α2 dKO mice were only significantly more frequent during the second minute of hypoxia. Thereafter, the number of sighs and PSA were comparable for the remainder of the exposure (sighs/min versus PSA/min – at 1-2min: 5.7 ± 0.3 versus 3.7 ± 0.3, $p<0.0001$; at 5-6min: 2.5 ± 0.2 versus 2.1 ± 0.2, not significant; at 9-10min: 2.8 ± 0.2 versus 2.1 ± 0.2, not significant), suggesting that almost every sigh was coupled to a PSA.

Effect of AMPK deletion on the frequency of sighs and PSA during mild hypoxia As expected, the numbers of sighs and PSA, respectively, were comparable between controls and TH AMPK-α1/α2 dKO mice throughout exposures to 12% O_2.

Effect of AMPK deletion on the frequency of sighs and PSA during severe hypoxia In agreement with outcomes from above, exposures to severe hypoxia revealed no differences in the numbers of PSA between genotypes, but a significant reduction in the numbers of sighs in TH AMPK-α1/α2 dKO mice compared to controls during the first half of 10min exposures to severe hypoxia (at 1-2min: $p<0.05$; at 5-6min: $p<0.01$; at 9-10min: not significant).

Therefore, these data suggest that in AMPK-α1/α2 Flx mice, sighs occur at a higher rate than PSA, regardless of the hypoxic intensity. In TH AMPK-α1/α2 dKO mice, however, the occurrence of sighing alone appears to be blocked with decreasing PO_2, because while a significant number of sighs without apnoeas was observed during mild hypoxia, almost every sigh was coupled to a PSA during severe hypoxia. Therefore, deletion of AMPK-α1 and -α2 subunits in catecholaminergic cells may alter signalling pathways within the brainstem respiratory network that ultimately blocks the generation of sighs that do not trigger subsequent apnoeas.

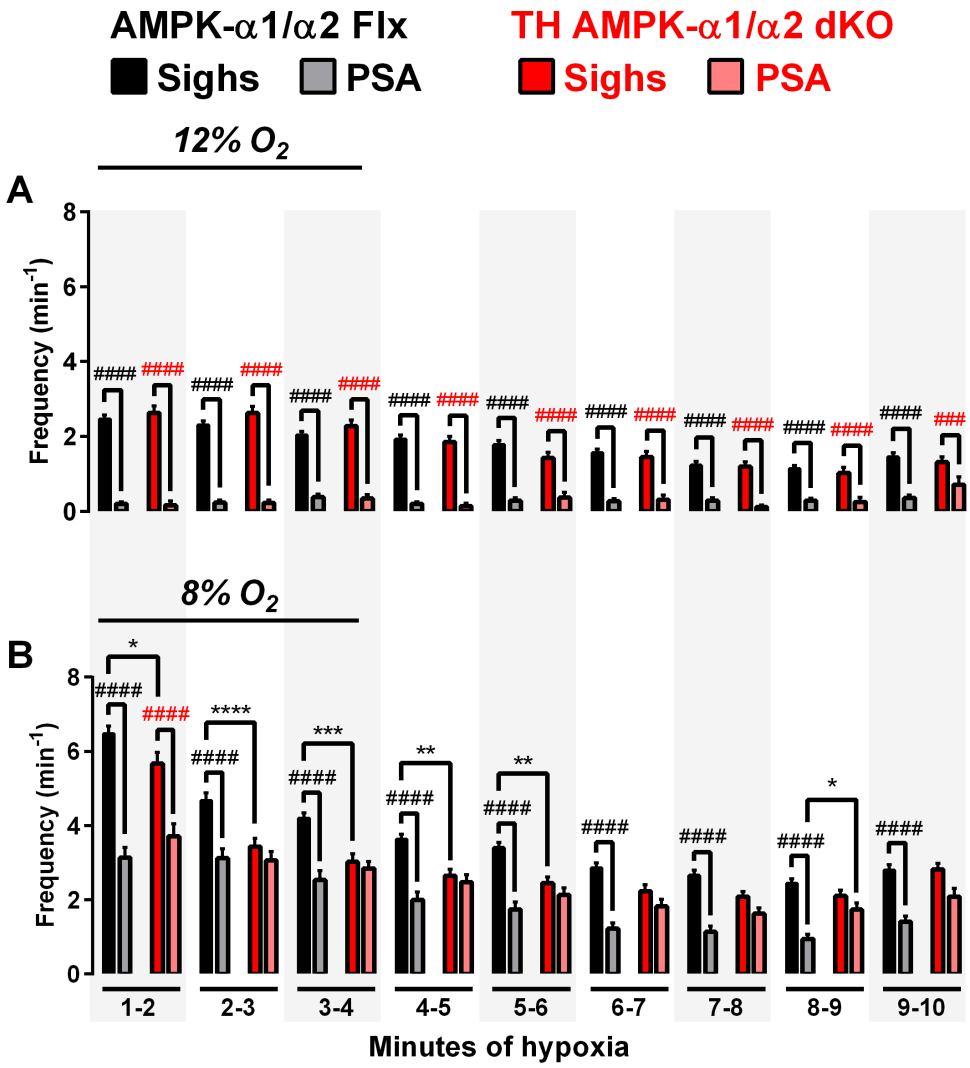

Figure 5.13: During severe hypoxia, sighs are followed by apnoeas in mice with conditional deletion of AMPK-α1/α2 catalytic subunits in catecholaminergic cells.

Means ± SEM for the frequency of sighs and post-sigh apnoeas (PSA) during 10 minute exposures to **(A)** mild hypoxia (12% O_2) and **(B)** severe hypoxia (8% O_2) in AMPK-α1 and -α2 floxed mice (AMPK-α1/α2 Flx, black, 12% O_2: n = 55 exposures from 19 mice, 8% O_2: n = 58 exposures from 25 mice) and TH-driven AMPK-α1 and -α2 double knockout mice (TH AMPK-α1/α2 dKO, red, 12% O_2: n = 35 exposures from 11 mice, 8% O_2: n = 46 exposures from 22 mice). Between genotypes: * = p<0.05, ** = p<0.01, *** = p<0.001, **** = p<0.0001; between sighs and PSA: ### = p<0.001, #### = p<0.0001. Significance tested by two-way ANOVA with Sidak post-hoc tests.

5.3 Discussion

5.3.1 Summary of findings

Chapter 5 shows that AMPK-dependent signalling pathways within the central respiratory network are required not only to support ventilatory drive during exposures to hypoxia, but also to support ventilatory stability. In this respect, loss of AMPK activity within catecholaminergic cells precipitated irregular breathing patterns, demonstrated by large standard deviations in the inter-breath intervals, as well as more frequent and prolonged apnoeas. Interestingly, loss of AMPK activity affected the two types of apnoeas differently, increasing the frequency of spontaneous apnoeas (SA) on one hand, and the duration of post-sigh apnoeas (PSA) on the other. Moreover, the occurrence of sighs without apnoeas appeared to be blocked during acute exposures to severe, but not mild hypoxia.

During more prolonged exposures, it appeared as though the severely apnoeic phenotype of TH AMPK-α1/α2 dKO observed during the initial phases of the response was partially compensated for by AMPK-independent reductions in the frequency of SA and the duration of PSA. Nevertheless, a clear phasic disturbance of the respiratory central pattern generators (rCPGs) remained apparent following AMPK deletion, which presented as periodic oscillations in the frequency of SA that were present at fairly regular intervals throughout the entire prolonged exposure to severe hypoxia.

5.3.2 AMPK activity in brainstem catecholaminergic cells promotes ventilatory stability during hypoxia

In addition to the marked reductions in respiratory drive during hypoxia described in Chapter 3, loss of AMPK activity in catecholaminergic cells also precipitated breathing irregularities associated with marked increases in the number and durations of apnoeas. Importantly, these were unlikely to be triggered by increases in catecholaminergic neurotransmission (Zanella *et al.*, 2014), as Chapter 4 identified no alterations in the number of TH-positive

cells or the total bioamine content in TH AMPK-α1/α2 dKO mice relative to controls. Therefore, it appears that loss of AMPK-dependent modulation of the rCPGs augments ventilatory instability and the precipitation of apnoeas.

Surprisingly, no differences in either the frequency or the duration of apnoeas during mild hypoxia were identified between the cohorts of controls and TH AMPK-α1/α2 dKO mice used here, which is in contrast to previous findings (Mahmoud, 2014; Mahmoud *et al.*, 2016). However, consistent with those previous reports, exposures to severe hypoxia significantly augmented both the frequency and the duration of apnoeas. Furthermore, it appears that the apnoeic threshold is determined, at least in part, by PO_2, and not solely by reductions in PCO_2 as has been suggested before (Dempsey, 2005). This was evident because the experimental mice used here received a constant supply of normocapnic hypoxia (8% O_2, 0.5% CO_2) and, paradoxically, hypoventilated rather than hyperventilated, which would further increase central PCO_2 levels. Therefore, these outcomes would be in agreement with other studies which have shown that the occurrence of periodic breathing and apnoea can be either resolved or eliminated by supplementation of PO_2, that blunting of the HVR increases the susceptibility to breathing irregularities and apnoeas, and that the degree of hypocapnia required to trigger apnoeas can be altered by the degree of hypoxia (Lahiri *et al.*, 1983; Xie *et al.*, 2001; Adachi *et al.*, 2006).

Importantly, consistent with reductions in the breathing variability over time, control AMPK-α1/α2 Flx mice displayed a clear time-dependent reduction in the number of apnoeas, both of which were blocked upon AMPK deletion. It is currently unclear which underlying mechanism led to this reduction of the apnoeic index in controls over time. Perhaps AMPK-dependent pathways are also able to integrate and coordinate inspiratory inhibition via vagal afferent input during hypoxia. In that sense, deletion of AMPK could allow vagal afferents to temporarily inhibit ventilation in a more frequent and stronger manner, thereby leading to the occurrence of more frequent and prolonged apnoeas (Younes *et al.*, 1974).

In spite of a reduction in the frequency of post-sigh apnoeas in TH AMPK-α1/α2 dKO mice, ventilatory stability was never fully regained

because AMPK deletion precipitated “apnoeic bursts” at regular intervals throughout the 60min exposure to hypoxia. These “bursts” are indicative of phasic disturbances of the central pattern generators during periods of prolonged hypoxia, which could have been affected via projections from the DAR to the rostral and caudal ventral respiratory groups, as well as the Bötzinger complex and pre Bötzinger complex (Alheid *et al.*, 2011). Notably, these phasic “bursts” of increased apnoea frequency were observed in every experimental TH AMPK-α1/α2 dKO mouse (Appendices 3.1 to 3.3), but not in any of the experimental control AMPK-α1/α2 Flx mice. The fact that these oscillations were still apparent after averaging apnoea frequencies across animals highlights the high degree of synchronicity regarding the periodic disruptions of the central pattern generators following AMPK deletion in catecholaminergic cells.

Therefore, AMPK activity in catecholaminergic cells supports ventilatory drive and protects against apnoea by maintaining respiratory stability during acute and prolonged exposures to hypoxia.

5.3.3 The differential impact of AMPK deletion on the occurrence of spontaneous and post-sigh apnoeas

Subdividing the two types of apnoeas into post-sigh (PSA) and spontaneous apnoeas (SA) revealed a differential impact of AMPK deletion, whereby it augmented the frequency of SA on one hand, and the duration of PSA on the other.

The underlying mechanism that leads to the generation of SA has still not been clearly identified. Consistently across the rodent literature it seems that SA arise during rapid eye movement (REM) sleep, but not during non-REM sleep (Radulovacki *et al.*, 1998; Carley & Radulovacki, 1999b; Radulovacki *et al.*, 2001; Nakamura *et al.*, 2003; Wang *et al.*, 2008). However, these findings are in contrast to human studies, where the generation of SA appears to be limited to non-REM sleep and their genesis excluded during REM sleep (Steffen *et al.*, 2010; Yuceege *et al.*, 2013) unless accompanied by co-pathologies or an increase in the ventilatory response-to-stimulus ratio

(loop gain) that can trigger central apnoeas subsequent to decreases in PCO_2 levels below the apnoeic threshold (Dempsey *et al.*, 2010; Jouett *et al.*, 2017). As mentioned earlier, however, this appears highly unlikely to be the case for TH AMPK-α1/α2 dKO mice, because their hypoventilatory phenotype would render them hypercapnic due to the reduced CO_2 blow-off. Clearly, further investigations into the pathogenesis of SA are eagerly awaited, but it seems apparent from the findings presented here that AMPK-dependent signalling pathways in catecholaminergic cells support rCPGs output and protect from increases in SA during acute and more prolonged exposures to hypoxia. Therefore, aberrant expression and/or loss of AMPK signalling leads to an augmented ventilatory instability that presents as oscillating increases in the frequency of SA.

Although still not fully elucidated, the genesis of sighs and PSA appears to be better understood. During hypoxia, an increased number of sighs is generated by the pre Bötzinger complex (Neubauer & Sunderram, 2004; Chapuis *et al.*, 2014), which is primarily determined by hypocapnia subsequent to hypoxia-induced hyperventilation (Bell *et al.*, 2009). Therefore, the time-dependent reduction in ventilation exhibited by control AMPK-α1/α2 Flx mice would have translated into gradual restoration of central CO_2 levels, which would reduce the sigh frequency over the course of the 10min exposure to hypoxia. By contrast, the ventilatory response of TH AMPK-α1/α2 dKO mice was significantly attenuated from the beginning of the exposure, which could very well explain the attenuated sigh frequency observed relative to controls. That said, in control AMPK-α1/α2 Flx mice about 40-60% of sighs occurred without apnoeas, whereas almost every sigh in TH AMPK-α1/α2 dKO mice was coupled to a PSA. Sighing was found to be dependent on afferent input from vagal pulmonary C fibres that innervate the caudal NTS (Xu *et al.*, 2003; Bell *et al.*, 2009; Burke *et al.*, 2014; Li *et al.*, 2016), and vagal activity has, at the same time, been proposed to temporarily inhibit inspiration due to activation of pulmonary stretch receptors during the augmented inspiration (Hering-Breuer reflex) (Breuer, 1868). Therefore, the question remains how AMPK-dependent signalling pathways may couple – or uncouple – sighs to apnoeas. Of note,

the overall number of PSA in TH AMPK-α1/α2 dKO mice was comparable to controls, even though their duration was significantly prolonged at the beginning of the exposure to hypoxia. Therefore, vagal inhibition of inspiration likely occurs at a similar frequency in controls and TH AMPK-α1/α2 dKO mice. Moreover, both genotypes displayed a time-dependent reduction in the number of PSA over the course of the 60min exposures. Therefore, it seems likely that vagal afferent inhibition of post-sigh inspiration occurs independently of AMPK activity. Nevertheless, because the duration of PSA has been positively correlated to the strength of the vagal afferent input (Younes *et al.*, 1974), it appears that AMPK-dependent circuit mechanisms may determine, at least temporarily, the susceptibility of the central respiratory network to vagal inhibition. In this regard, greater susceptibility conferred by AMPK deletion could explain the prolongation of PSA duration for TH AMPK-α1/α2 dKO mice. Apnoea-driven increases in PCO_2 were found to re-initiate inspiration after a PSA (Younes *et al.*, 1974), however it seems unlikely that AMPK deletion affected these pathways for two reasons: 1) as mentioned earlier, TH AMPK-α1/α2 dKO mice hypoventilate in response to hypoxia and therefore should exhibit increased PCO_2 levels, and 2) the hypercapnic response of TH AMPK-α1/α2 dKO mice is normal and hypercapnic hypoxia (8% O_2, 5% CO_2) rescues the hypoxic phenotype of these mice (Mahmoud, 2014; Mahmoud *et al.*, 2016). Therefore, loss of AMPK activity most likely renders the central respiratory network more susceptible to inspiratory inhibition via vagal afferent input.

Alternatively, sighs have been shown to be modulated in a state-dependent manner via ventral catecholaminergic C1 neurons (Burke *et al.*, 2014; Burke *et al.*, 2015) and β-adrenergic receptor stimulation within preBötC neurons (Viemari *et al.*, 2013). Looking back at the phenotype of control AMPK-α1/α2 Flx mice, a large proportion of sighs occurred on their own without preceding a PSA. This begs the question whether AMPK-dependent signalling pathways may, via adrenergic C1 neurons, determine the degree by which sighs trigger the Hering-Breuer reflex. In AMPK-α1/α2 Flx mice, sighs without apnoeas occur at a higher rate than PSA, regardless of the hypoxic intensity. In TH AMPK-α1/α2 dKO mice, however, the occurrence of sighing

alone appears to be blocked with decreasing PO_2, because while a significant number of sighs without apnoeas were observed during mild hypoxia, almost every sigh was coupled to a PSA during severe hypoxia with no effect on the total number of PSA. These findings could be explained *if* sighs consisted of two types: 1) 'weak' sighs, possibly of a smaller amplitude and/or duration which do not activate stretch receptors in the lungs and perhaps protect from atelectasis by re-inflating collapsed alveoli (Hartland *et al.*, 2014), and 2) 'strong' sighs of larger amplitude and/or duration which trigger the Hering-Breuer reflex subsequent to hyperventilation-induced hypocapnia. As of yet, this is the first indication of the existence of different types of sighs. Therefore, further experiments are critical to understand how AMPK-dependent signalling pathways in catecholaminergic neurons may impact the generation of sighs and how these are coupled to the induction of PSA.

5.3.4 Conclusion

In conclusion, AMPK-dependent circuit mechanisms protect against ventilatory instability subsequent to augmentation by hypoxia of the frequency of spontaneous apnoeas, and oppose prolongation of the duration of post-sigh apnoeas during the initial phases of the HVR. In addition, modulation of the respiratory network by AMPK activity appears to allow for the generation of sighs without apnoeas, which is blocked upon AMPK deletion in catecholaminergic cells. Furthermore, although there appears to be an AMPK-independent degree of stabilisation of ventilatory synchronicity over time, characterised by a reduction in apnoea frequency and duration, rhythmicity is still periodically lost upon AMPK deletion; which was evident from oscillating increases in the frequency of spontaneous apnoeas throughout prolonged exposures to hypoxia. Therefore, AMPK-dependent neural circuits are required to maintain ventilatory stability during acute and prolonged exposures to hypoxia in order to protect from whole-body hypoxia and hypercapnia induced by hypoventilation and apnoea.

Chapter 6: Characterisation of the hypoxic duty cycle in mice with AMPK deficiency in catecholaminergic cells

6.1 Introduction

6.1.1 Increased ventilatory drive during hypoxia is enabled through initiation of active expiration

In most mammals, alterations of breathing frequency during hypoxia are primarily determined by changes in the inter-breath-interval (Milsom, 1991; Jenkin & Milsom, 2014). In mammals, this is the result of accelerated expiration that reduces the expiratory pause with minimal, if any, changes in inspiration time (Harris & Milsom, 2001; Abdala *et al.*, 2009). Active expiration has several benefits: on the one hand it allows for an increased tidal volume by recruiting the expiratory reserve volume (Leith, 1976). On the other hand it creates a controllable and dynamic time constant that allows for a higher respiratory frequency by preventing hyperinflation of the lungs due to the longer time required for passive expiration (Mortola *et al.*, 1985).

As already mentioned in section 1.1.2, expiratory rhythm is generated through excitatory inputs to respiratory motorneurons from the pFRG/RTN and the BötC (Smith *et al.*, 2013), the former of which is associated with the production of active expiration (Feldman & Del Negro, 2006; Janczewski & Feldman, 2006; Pagliardini *et al.*, 2011; Pisanski & Pagliardini, 2018). During quiet breathing, where expiration occurs passively, the pFRG/RTN is silent with respect to its neuronal firing. During the transition from quiet to active expiration the pFRG/RTN becomes rhythmically active and transforms into an additional oscillator within the ventral brainstem that modulates breathing via recruitment of abdominal and intercostal muscles (Pagliardini *et al.*, 2011; Molkov *et al.*, 2014). Importantly, direct innervations of the RTN which influence the drive to breathe also arise from the catecholaminergic C1 cells of the ventrolateral medulla (Burke *et al.*, 2014). In support of a role of catecholaminergic neurotransmission to stimulate active expiration, selective depletion of C1 cells was found to attenuate active expiration during hypoxia, but not normoxia or hypercapnia (Malheiros-Lima *et al.*, 2015; Malheiros-Lima *et al.*, 2017).

On a molecular level, the pFRG/RTN remains silent during resting conditions by GABAergic and glycinergic neurotransmission that has been postulated to originate from the medullary BötC, preBötC and NTS, as well we the KF and LPBr in the pons (Pagliardini *et al.*, 2011). During metabolic demand and/or chemoreflex stimulation such as hypercapnia or hypoxia, the activity of the pFRG/RTN that generates active expiration has been suggested to depend on glutamatergic and serotonergic neurotransmission, because both of these neurotransmitters were shown to generate active expiration at rest and antagonists of their receptors blocked active expiration in response to their administration (Moraes *et al.*, 2012b; Lemes *et al.*, 2016; Lemes & Zoccal, 2016).

6.1.2 AMPK deficiency in catecholaminergic cells blocks active expiration during hypoxia

Previous investigations studying the effect of deleting AMPK-α1/α2 catalytic subunits in catecholaminergic cells on the HVR have shown that hypoventilation may result, in part, from a significant increase in the total breath time, due to prolongations in both inspiration time and expiration time. More importantly, the acceleration of expiration (active expiration) observed in control AMPK-α1/α2 Flx mice appeared to be blocked upon AMPK deletion, resulting in a significant increase in expiration time relative to normoxia and to controls (Mahmoud, 2014).

6.1.3 Aims

Following these previous outcomes on the blockage of active expiration during hypoxia in mice with AMPK deletion in catecholaminergic cells, I sought to extend these findings from 5min to 10min of exposures to mild and severe hypoxia in order to identify whether the augmentations of inspiration time and expiration time persisted, whether active expirations remained blocked, and how these changes impacted on the amount of air that was moved during inspiration and expiration.

6.2 Results

6.2.1 AMPK deletion in catecholaminergic cells prolongs breath duration throughout 10min exposures to hypoxia

In order to examine the nature of the response to hypoxia in TH AMPK-α1/α2 dKO mice compared to control AMPK-α1/α2 Flx mice in more detail, the inspiratory, expiratory, and total breath durations were analysed. Figures 6.1 to 6.3 show the mean ratiometric changes (hypoxia:normoxia) for various ventilatory parameters of both genotypes during 10min exposures to 12% O_2 and 8% O_2, with a 2s sampling frequency.

6.2.1.1 Inspiration time

Time-dependent changes in inspiration time (Ti) were observed in both AMPK-α1/α2 Flx and TH AMPK-α1/α2 dKO mice during exposures to mild and severe hypoxia.

Mild hypoxia 30s after the onset of 12% O_2 (Figure 6.1 Ai), control AMPK-α1/α2 Flx mice (n = 37 exposures from 14 mice) responded with an initial reduction in Ti (0.8 ± 0.03), which returned to normoxic values after approximately 1min. Thereafter, Ti reached a plateau that remained stable not only at the 5min mark (1 ± 0.04, $p<0.0001$ compared to 30s) as described previously (Mahmoud, 2014), but right through to the end of the 10min exposure (0.9 ± 0.04, $p<0.01$ compared to 30s, not significant compared to 5min).

Severe hypoxia In response to 8% O_2, AMPK-α1/α2 Flx mice (n = 54 exposures from 21 mice) also displayed a reduction of inspiration time 30s after the onset of the exposure (Figure 6.1 Bi; 0.9 ± 0.02) which returned to normoxic values at around 1min. However, before reaching a plateau there appeared to be a secondary increase after approximately 2 minutes, which prolonged Ti relative to normoxia. This slower inspiration time then remained stable until the 10min mark (at 5min: 1.2 ± 0.04, $p<0.0001$ compared to 30s;

at 10min: 1.3 ± 0.05, $p<0.0001$ compared to 30s, not significant compared to 5min).

Effect of AMPK deletion during mild hypoxia The overall effect of hypoxia on Ti in TH AMPK-α1/α2 dKO mice (n = 28 exposures from 11 mice) was very similar to controls. During mild hypoxia, knockouts displayed a comparable decrease in inspiratory duration relative to normoxia 30s following the onset of 12% O_2 (Figure 6.1 Aii; 0.9 ± 0.03; not significant compared to controls), which returned to normoxic values after approximately 1min and remained stable at a level comparable with controls until the end of the exposure (at 5min: 1 ± 0.04, not significant compared to controls; at 10min: 1 ± 0.04, not significant compared to controls).

Effect of AMPK deletion during severe hypoxia Similar to controls, severe hypoxia resulted in a decrease of inspiration time in TH AMPK-α1/α2 dKO mice (n = 37 exposures from 15 mice) at 30s (Figure 6.1 Bii; 0.9 ± 0.03, not significant compared to controls), which returned to normoxic measurements around 1min, followed by a secondary prolongation at around 2min that was maintained for the duration of the exposure to hypoxia. It should be pointed out that the response of the TH AMPK-α1/α2 dKO mice fluctuated slightly from 5min onwards, at which point Ti was significantly longer than that of controls (1.4 ± 0.05, $p<0.05$ compared to controls). However, by 10min the duration of inspiration was once again comparable between the genotypes (1.4 ± 0.07, not significant compared to controls).

Thus, TH AMPK-α1/α2 dKO mice displayed comparable changes in inspiration time during 12% O_2 when compared to controls, but exhibited a significantly prolonged Ti between 5min and 10min during exposures to severe hypoxia.

Overall, these data show that while both AMPK-α1/α2 Flx and TH AMPK-α1/α2 dKO mice responded to hypoxia with a comparable initial shortening of inspiration time relative to normoxia, measurements quickly recovered back to and remained at normoxic levels during mild hypoxia. During severe hypoxia, however, inspiration time was extended relative to normoxia, leading to a maintained prolongation of inspiration time for the

duration of the exposure. This prolongation was significantly greater for AMPK-α1/2 dKO mice relative to controls at 5min only, returning to control values by the end of 10min.

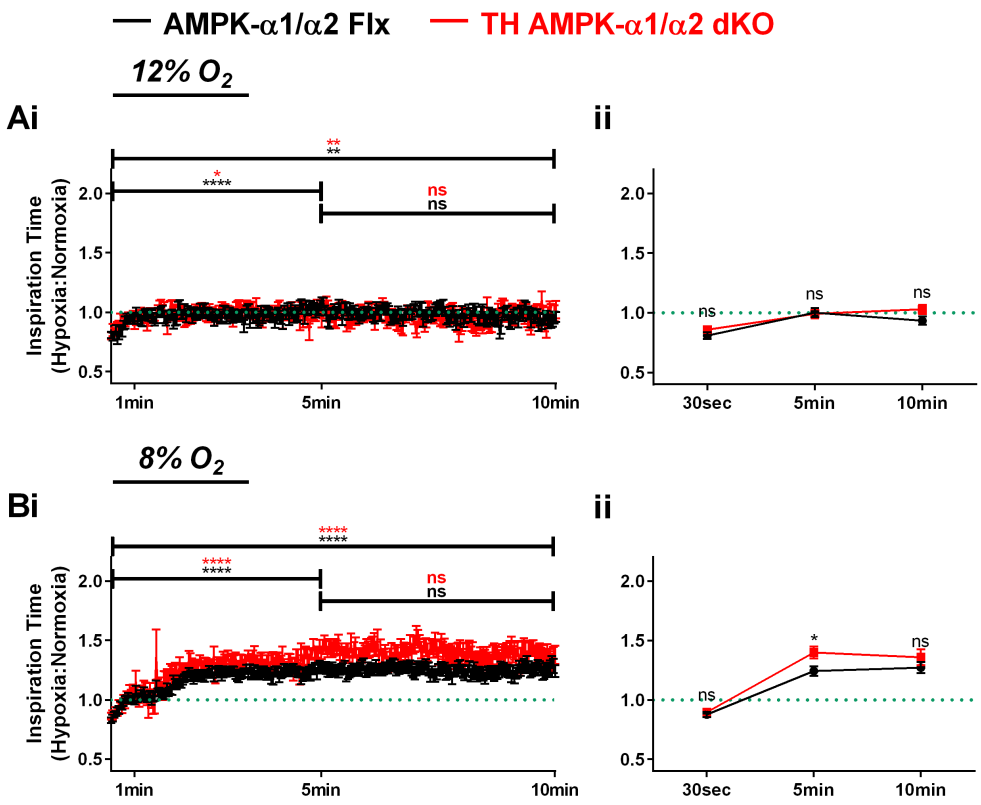

Figure 6.1: AMPK-α1/α2 catalytic subunit deletion in catecholaminergic cells temporarily prolongs inspiration time during severe, but not mild hypoxia.

The ratiometric changes relative to normoxia (green dotted line) of inspiration time during 10min exposures to **(A)** mild hypoxia (12% O_2) and **(B)** severe hypoxia (8% O_2) in AMPK-α1 and -α2 floxed mice (AMPK-α1/α2 Flx, black, 12% O_2: n = 37 exposures from 14 mice, 8% O_2: n = 54 exposures from 21 mice) and TH-driven AMPK-α1 and -α2 double knockout mice (TH AMPK-α1/α2 dKO, red, 12% O_2: n = 28 exposures from 11 mice, 8% O_2: 8% O_2: n = 37 exposures from 15 mice) are shown as means ± SEM **(i)** over time as 2s averages and **(ii)** at three selected time points to clearly illustrate differences between genotypes. ns = not significant, * = $p<0.05$, ** = $p<0.01$, **** = $p<0.0001$. Significance tested by two-way ANOVA with Sidak post-hoc tests.

6.2.1.2 Expiration time

Similar to Ti, AMPK-α1/α2 Flx and TH AMPK-α1/α2 dKO mice exhibited time-dependent changes in expiration time (Te).

Mild hypoxia At the onset of 12% O_2 Te was markedly shortened in control AMPK-α1/α2 Flx mice (Figure 6.2 Ai; at 30s: 0.4 ± 0.02). This shortening was followed by a gradual increase in expiration time until approximately 1-2min, after which Te plateaued. In contrast to Ti, however, Te remained shortened relative to normoxia, measuring 0.6 ± 0.02 after 5min ($p<0.0001$ compared to 30s), and 0.6 ± 0.03 after 10min ($p<0.0001$ compared to 30s, not significant compared to 5min).

Severe hypoxia During 8% O_2 exposures Te also displayed a marked reduction 30s after the onset of hypoxia (Figure 6.2 Bi; 0.5 ± 0.02). Thereafter, a lengthening of Te occurred until approximately 2min followed by a secondary minor decrease and plateau, measuring 0.8 ± 0.02 by 5min ($p<0.0001$ compared to 30s) and 0.8 ± 0.03 by 10min ($p<0.0001$ compared to 30s, not significant compared to 5min).

Effect of AMPK deletion during mild hypoxia The expiration time in TH AMPK-α1/α2 dKO mice also shortened initially, peaking at 30s after the onset of mild hypoxia, but failed to accelerate to the level that was observed in controls, resulting in a significantly longer Te at this time point (Figure 6.2 Ai; 0.5 ± 0.02, $p<0.01$ compared to controls). As with controls, Te then lengthened slightly until approximately 2min, where it plateaued at a level that remained faster relative to normoxia. However, expiration in TH AMPK-α1/α2 dKO mice remained significantly prolonged when compared to control mice (at 5min: 0.7 ± 0.03, $p<0.05$ compared to controls; at 10min: 0.7 ± 0.03, $p<0.05$ compared to controls).

Effect of AMPK deletion during severe hypoxia A reduction of Te in response to 8% O_2 was also observed in TH AMPK-α1/α2 dKO mice, measuring 0.7 ± 0.03 at 30s following the onset of hypoxia. However, as with mild hypoxia, the degree of acceleration was significantly lower than observed for controls (Figure 6.2 Bii; $p<0.05$). Following the nadir at 30s, Te of TH AMPK-α1/α2 dKO mice also proceeded to lengthen over time, but unlike control mice the

prolongation of expiration time plateaued close to normoxic values. This means that TH AMPK-α1/α2 dKO mice failed to maintain an accelerated expiration time and instead returned to and remained at Te values measured during normoxia, which were significantly lengthened compared to controls at 5min (1.1 ± 0.04; $p<0.0001$) and 10min (1 ± 0.04; $p<0.001$).

Therefore, during mild and severe hypoxia both AMPK-α1/α2 Flx and TH AMPK-α1/α2 dKO mice exhibited an initial shortening of expiration time relative to normoxia, which slightly lengthened but generally remained below normoxic values throughout the duration of the exposures. Importantly, Te was significantly prolonged in TH AMPK-α1/α2 dKO mice and reached normoxic values during severe hypoxia.

Thus, deletion of AMPK-α1 and -α2 subunits in catecholaminergic cells appears to block active expiration during hypoxia, in a PO_2-dependent manner.

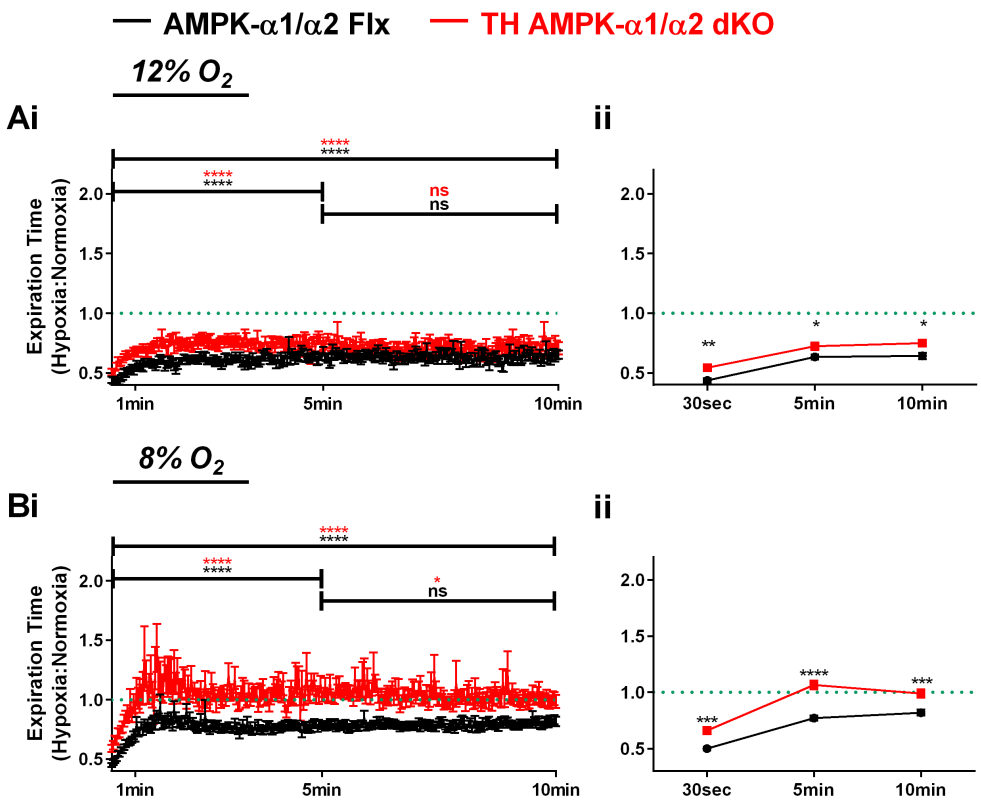

Figure 6.2: AMPK-α1/α2 catalytic subunit deletion in catecholaminergic cells prolongs expiration time and blocks active expiration during hypoxia.

The ratiometric changes relative to normoxia (green dotted line) of expiration time during 10min exposures to **(A)** mild hypoxia (12% O_2) and **(B)** severe hypoxia (8% O_2) in AMPK-α1 and -α2 floxed mice (AMPK-α1/α2 Flx, black, 12% O_2: n = 37 exposures from 14 mice, 8% O_2: n = 54 exposures from 21 mice) and TH-driven AMPK-α1 and -α2 double knockout mice (TH AMPK-α1/α2 dKO, red, 12% O_2: n = 28 exposures from 11 mice, 8% O_2: 8% O_2: n = 37 exposures from 15 mice) are shown as means ± SEM SEM **(i)** over time as 2s averages and **(ii)** at three selected time points to clearly illustrate differences between genotypes. ns = not significant, * = p<0.05, ** = p<0.01, *** = p<0.001, **** = p<0.0001. Significance tested by two-way ANOVA with Sidak post-hoc tests.

6.2.1.3 Total breath time

Mild hypoxia As one might expect, given the outcomes for Ti and Te, total breath time (To) of control AMPK-α1/α2 Flx mice was shortened relative to normoxia at the onset of mild hypoxia (Figure 6.3 Ai; 0.5 ± 0.02), before lengthening slightly and plateauing after approximately 2min. Predominantly driven by time-dependent reductions in Te, total breath time during mild hypoxia remained accelerated compared to normoxia and measured 0.7 ± 0.02 by 5min ($p<0.0001$ compared to 30s) and 0.7 ± 0.03 by 10min ($p<0.0001$ compared to 30s; not significant compared to 5min).

Severe hypoxia During severe hypoxia, total breath time was markedly reduced 30s following the onset of hypoxia (Figure 6.3 Bi; 0.6 ± 0.02), after which it increased slightly and plateaued below normoxic values, measuring 0.9 ± 0.02 by 5min ($p<0.0001$ compared to 30s) and 0.9 ± 0.02 at 10min ($p<0.0001$ compared to 30s; not significant compared to 5min).

Effect of AMPK deletion during mild hypoxia Similar to measurements obtained for Te, reductions in To during 12% O_2 were attenuated in TH AMPK-α1/α2 dKO mice. Initially To fell to 0.6 ± 0.02 after 30s hypoxia, which once again was significantly less rapid when compared to controls (Figure 6.3 Aii; $p<0.01$). Thereafter, the time-dependent prolongation and plateau of To was comparable to controls by 5min (0.8 ± 0.03; not significant), but this was not maintained until the end of the 10 min exposure, at which point To was significantly prolonged once more (10min: 0.8 ± 0.02; $p<0.01$ compared to controls).

Effect of AMPK deletion during severe hypoxia During severe hypoxia, To initially fell to 0.7 ± 0.03 at 30s, but the prolongation of Ti and, more importantly, the attenuation of active expiration (Te acceleration) resulted in a To that plateaued slightly above normoxic values (at 5min: 1.1 ± 0.03; at 10min: 1.1 ± 0.04). Importantly, and perhaps not surprising given the outcomes for Ti and Te described above, the total breath time of TH AMPK-α1/α2 dKO mice was significantly augmented compared to controls from the beginning of the exposure (Figure 6.3 Bii; at 30s: $p<0.05$) right through to the end (at 5min: $p<0.0001$; at 10min: $p<0.0001$).

Taken together, these data suggest that initiation of active expiration during hypoxia (Moraes *et al.*, 2012a) is the main driver of the reduced breath time observed in control AMPK-α1/α2 Flx mice that allows for increases in breathing frequency. This aspect of the HVR appears to be blocked upon conditional deletion of AMPK-α1 and -α2 subunits in catecholaminergic cells, leading to an overall increase in total breath time and a subsequent reduction in respiratory frequency.

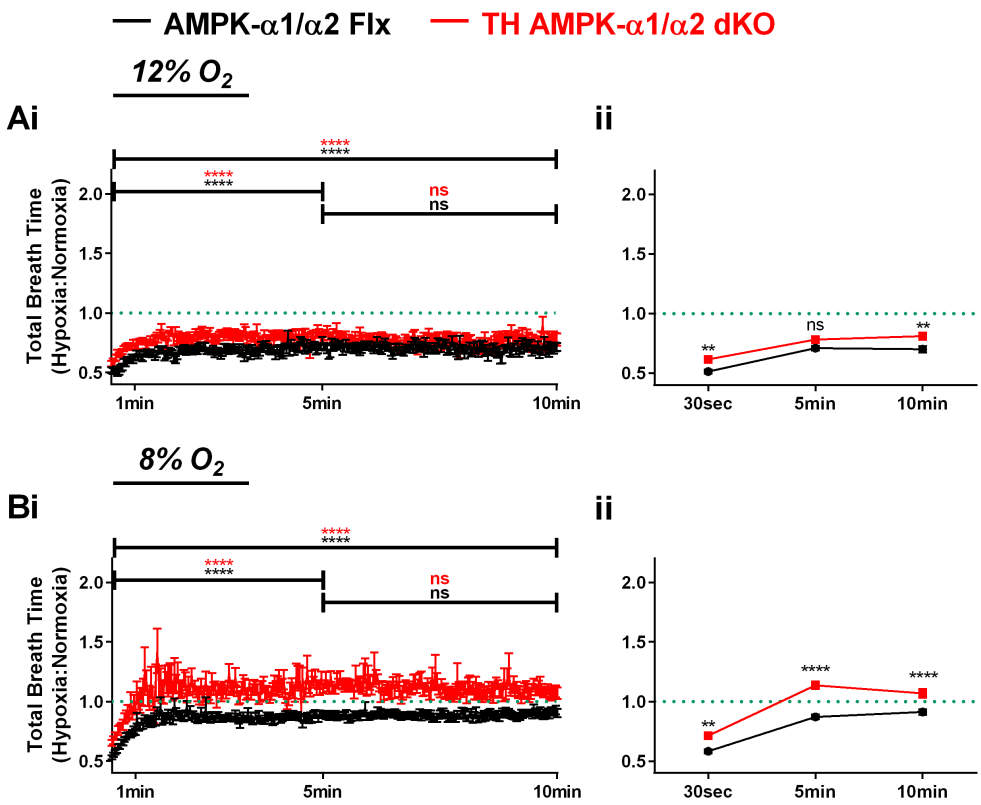

Figure 6.3: AMPK-α1/α2 catalytic subunit deletion in catecholaminergic cells prolongs total breath time during hypoxia.

The ratiometric changes relative to normoxia (green dotted line) of total breath time during 10min exposures to **(A)** mild hypoxia (12% O_2) and **(B)** severe hypoxia (8% O_2) in AMPK-α1 and -α2 floxed mice (AMPK-α1/α2 Flx, black, 12% O_2: n = 37 exposures from 14 mice, 8% O_2: n = 54 exposures from 21 mice) and TH-driven AMPK-α1 and -α2 double knockout mice (TH AMPK-α1/α2 dKO, red, 12% O_2: n = 28 exposures from 11 mice, 8% O_2: 8% O_2: n = 37 exposures from 15 mice) are shown as means ± SEM SEM **(i)** over time as 2s averages and **(ii)** at three selected time points to clearly illustrate differences between genotypes. ns = not significant, * = p<0.05, ** = p<0.01, *** = p<0.001, **** = p<0.0001. Significance tested by two-way ANOVA with Sidak post-hoc tests.

6.2.2 AMPK deletion in catecholaminergic cells attenuates the ratio of tidal volume to the duration of inspiration and expiration throughout 10min exposures to hypoxia

In the sections above it became apparent that TH AMPK-α1/α2 dKO mice displayed both a reduction in tidal volume during severe hypoxia (see Chapter 3.2.1.2) and an increase in inspiratory and expiratory duration. In order to further investigate which phase(s) of the breath cycle might predominantly result in the attenuation of air movement, the ratios of tidal volume and inspiration time (Tv/Ti), expiration time (Tv/Te), and total breath time (Tv/To) were analysed in relation to normoxia.

6.2.2.1 Tv/Ti

As with the durations of inspiration and expiration, similar time-dependent changes in the Tv/Ti ratio were observed in both AMPK-α1/α2 Flx and TH AMPK-α1/α2 dKO mice during exposures to mild and severe hypoxia.

Mild hypoxia 30s after the onset of 12% O_2 (Figure 6.4 Ai), control AMPK-α1/α2 Flx mice responded with an increase in Tv/Ti from normoxia (1.3 ± 0.05) that slowly declined for approximately 1-2min. Thereafter, Tv/Ti reached a plateau slightly above normoxia that was stable not only until the 5min mark (1.1 ± 0.05, $p<0.0001$ compared to 30s) (Mahmoud, 2014), but until the end of the exposure at 10min (1.2 ± 0.05, $p<0.01$ compared to 30s, not significant compared to 5min).

Severe hypoxia An initial increase in Tv/Ti was also observed at 30s following the onset of 8% O_2 (Figure 6.4 Bi; 1.2 ± 0.04), which was followed by a decline for approximately 2min before reaching a plateau below normoxic values at ≈3min. From then on, Tv/Ti remained stable until the 5min mark (0.8 ± 0.03, $p<0.0001$ compared to 30s) and until the end of the exposure at 10min (0.8 ± 0.03, $p<0.0001$ compared to 30s, not significant compared to 5min).

Effect of AMPK deletion during mild hypoxia For TH AMPK-α1/α2 dKO mice, Tv/Ti was also comparably increased 30s after the onset of mild hypoxia

(Figure 6.4 Aii; 1.2 ± 0.05, not significant compared to controls) before slowly declining. As with controls, Tv/Ti reached a plateau that was not only stable until the 5min mark (1 ± 0.05, not significant compared to controls), but until the end of the exposure at 10min (0.9 ± 0.04). However, even though both genotypes displayed a comparable response after 30s and 5min of 12% O_2, TH AMPK-α1/α2 dKO mice had an attenuated Tv/Ti relative to controls by the end of the exposure at 10min that reached significance ($p<0.05$ compared to controls).

Effect of AMPK deletion during severe hypoxia 30s following the onset of severe hypoxia Tv/Ti was also initially increased in TH AMPK-α1/α2 dKO mice to a level that was comparable to controls (Figure 6.4 Bii; 1.1 ± 0.03, not significant). Unlike controls however, Tv/Ti during 8% O_2 did not reach a plateau and continued to decline until the 5min mark (0.6 ± 0.02), after which values remained stable until the end of the 10min exposure (0.6 ± 0.03). The comparable level of ventilation observed at 30s could not be maintained over time and due to the delayed plateau, the remainder of the response was significantly attenuated when compared to AMPK-α1/α2 Flx mice (at 5min: $p<0.0001$; at 10min: $p<0.0001$).

This suggests that while both AMPK-α1/α2 Flx and TH AMPK-α1/α2 dKO mice responded to hypoxia with a comparable initial increases of the amount of air moved during inspiration relative to normoxia, AMPK-α1/α2 dKO mice were not able to maintain a level of ventilation that is comparable to controls until the end of 10min exposures, resulting in less volume being moved per unit time, and with more inspiration time required per volume of air moved.

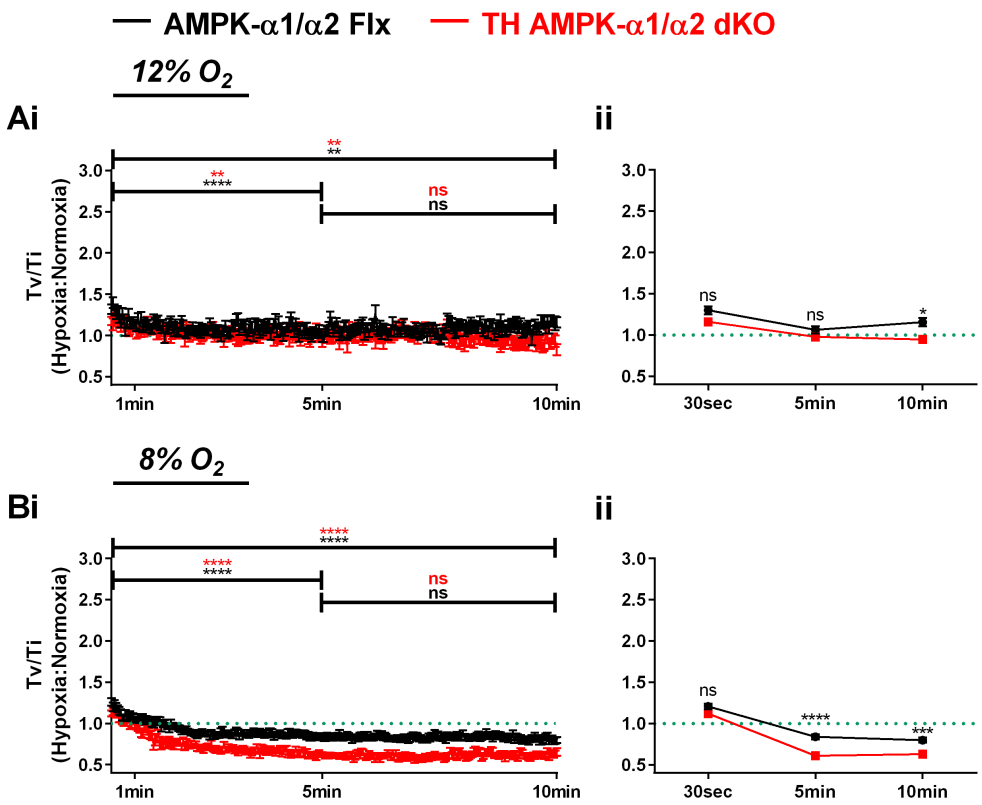

Figure 6.4: AMPK-α1/α2 catalytic subunit deletion in catecholaminergic cells reduces tidal volume over inspiration time during hypoxia in a time- and PO_2-dependent manner.

The ratiometric changes relative to normoxia (green dotted line) of tidal volume over inspiration time during 10min exposures to **(A)** mild hypoxia (12% O_2) and **(B)** severe hypoxia (8% O_2) in AMPK-α1 and -α2 floxed mice (AMPK-α1/α2 Flx, black, 12% O_2: n = 37 exposures from 14 mice, 8% O_2: n = 54 exposures from 21 mice) and TH-driven AMPK-α1 and -α2 double knockout mice (TH AMPK-α1/α2 dKO, red, 12% O_2: n = 28 exposures from 11 mice, 8% O_2: 8% O_2: n = 37 exposures from 15 mice) are shown as means ± SEM **(i)** over time as 2s averages and **(ii)** at three selected time points to clearly illustrate differences between genotypes. ns = not significant, * = p<0.05, ** = p<0.01, *** = p<0.001, **** = p<0.0001. Significance tested by two-way ANOVA with Sidak post-hoc tests.

6.2.2.2 Tv/Te

Similar to Tv/Ti described above, Tv/Te in AMPK-α1/α2 Flx and TH AMPK-α1/α2 dKO mice was highest at the onset of mild and severe hypoxia (Figure 6.5 Ai and Bi, respectively), followed by a time-dependent decrease and plateau until the end of the exposures.

Mild hypoxia During exposures to 12% O_2, Tv/Te of control AMPK-α1/α2 Flx mice was robustly increased to 2.5 ± 0.1 at 30s. Following a decline that lasted for approximately 2min, Tv/Te remained stably augmented relative to normoxia by 5min (1.7 ± 0.06; $p<0.0001$ compared to 30s), and 10min (1.8 ± 0.09; $p<0.0001$ compared to 30s, not significant compared to 5min).

Severe hypoxia A robust increase in Tv/Te relative to normoxia was also evident during exposures to severe hypoxia, where measurements for control mice were 2.2 ± 0.08 at 30s, which then decreased to a nadir around 2min before slightly increasing again and levelling at 1.4 ± 0.04 by 5min ($p<0.0001$ compared to 30s) and 1.2 ± 0.04 at 10min ($p<0.0001$ compared to 30s, not significant compared to 5min).

Effect of AMPK deletion during mild hypoxia Similar to controls, Tv/Te of TH AMPK-α1/α2 dKO mice was highest 30s after the onset of mild hypoxia (1.9 ± 0.06). Unlike Tv/Ti however, the degree to which the movement of each volume of air was initially accelerated during expiration in TH AMPK-α1/α2 dKO mice was significantly reduced when compared to AMPK-α1/α2 Flx mice (Figure 6.5 Aii; $p<0.0001$). This significantly attenuated Tv/Te relative to controls was retained throughout the exposure, measuring 1.3 ± 0.05 after 5min ($p<0.05$) and 1.3 ± 0.06 after 10min ($p<0.01$).

Effect of AMPK deletion during severe hypoxia As for mild hypoxia, the peak at 30s after the onset of severe hypoxia was significantly attenuated in TH AMPK-α1/α2 dKO mice compared to controls, measuring only 1.6 ± 0.09 (Figure 6.5 Bii; $p<0.0001$). Thereafter, Tv/Te of TH AMPK-α1/α2 dKO mice quickly dropped for 2min and, unlike controls, plateaued below baseline values. Notably, the reduction of Tv/Te was more severe than for control AMPK-α1/α2 Flx mice, resulting in a slowing of air movement during

expiration relative to normoxia by 5min (0.8 ± 0.04, $p<0.0001$ compared to controls) and 10min (0.9 ± 0.03, $p<0.001$ compared to controls).

Therefore, during mild and severe hypoxia both AMPK-α1/α2 Flx and TH AMPK-α1/α2 dKO mice exhibited an initial increase in the volume transferred per unit time during expiration relative to normoxia, which then decreased but generally remained accelerated relative to normoxia throughout the duration of the exposure. Crucially, TH AMPK-α1/α2 dKO mice were unable to reach full capacity of air movement during expiration compared to controls and failed to maintain an elevated Tv/Te relative to normoxia during 8% O_2.

Thus, in catecholaminergic cells AMPK supports active acceleration of air movement during hypoxic expiration.

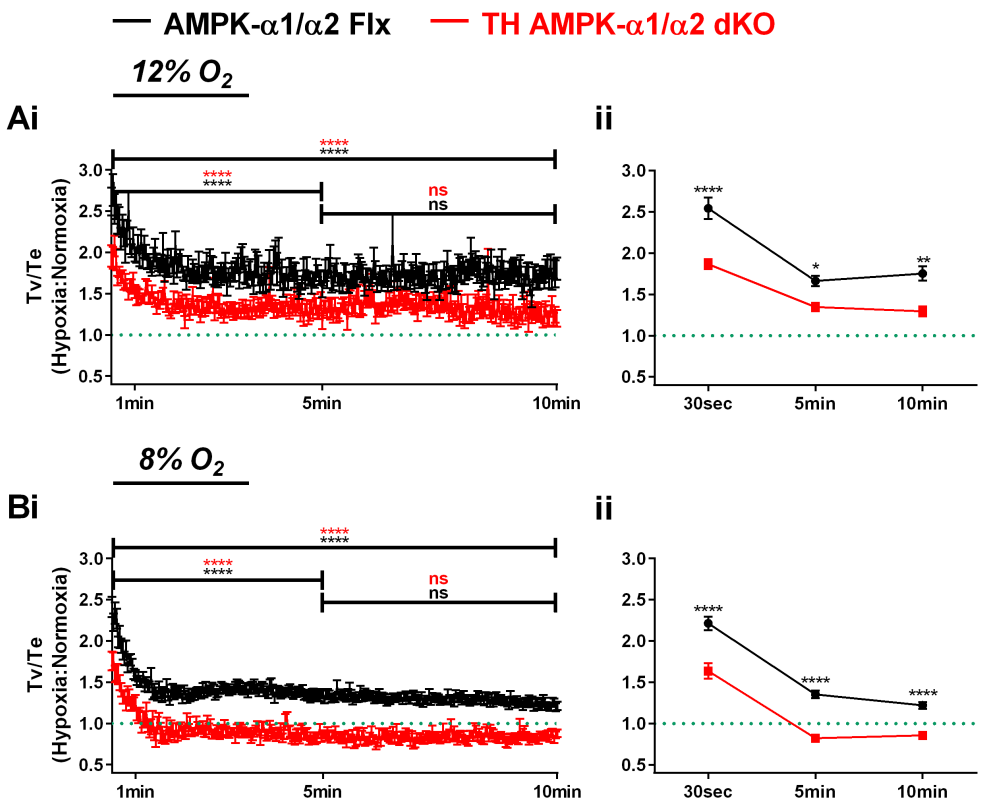

Figure 6.5: AMPK-α1/α2 catalytic subunit deletion in catecholaminergic cells reduces tidal volume over expiration time during hypoxia.

The ratiometric changes relative to normoxia (green dotted line) of tidal volume over expiration time during 10min exposures to **(A)** mild hypoxia (12% O_2) and **(B)** severe hypoxia (8% O_2) in AMPK-α1 and -α2 floxed mice (AMPK-α1/α2 Flx, black, 12% O_2: n = 37 exposures from 14 mice, 8% O_2: n = 54 exposures from 21 mice) and TH-driven AMPK-α1 and -α2 double knockout mice (TH AMPK-α1/α2 dKO, red, 12% O_2: n = 28 exposures from 11 mice, 8% O_2: 8% O_2: n = 37 exposures from 15 mice) are shown as means ± SEM **(i)** over time as 2s averages and **(ii)** at three selected time points to clearly illustrate differences between genotypes. ns = not significant, * = p<0.05, ** = p<0.01, **** = p<0.0001. Significance tested by two-way ANOVA with Sidak post-hoc tests.

6.2.2.3 Tv/To

As one might expect, given the outcomes for Tv/Ti and Tv/Te, the volume moved per total breath time (Tv/To) was highest at the onset of mild and severe hypoxia (Figure 6.6 Ai and Bi, respectively), and decreased to a plateau thereafter.

Mild hypoxia For control AMPK-α1/α2 Flx mice the peak of Tv/To after 30s of 12% O_2 measured 2.1 ± 0.09. Following this, Tv/To decreased and reached a plateau around 2min. Driven by increases in Tv/Te relative to normoxia, Tv/To remained above normoxic values by 5min (1.5 ± 0.05, $p<0.0001$ compared to 30s) and 10min (1.6 ± 0.07, $p<0.0001$ compared to 30s, not significant compared to 5min).

Severe hypoxia During 8% O_2, Tv/To in control AMPK-α1/α2 Flx mice was increased to 1.8 ± 0.06 by 30s, followed by a decrease until the 2min mark. Thereafter it plateaued at a level just above normoxia for the remainder of the exposure (at 5 min: 1.2 ± 0.03, $p<0.0001$ compared to 30s; at 10min: 1.1 ± 0.03, $p<0.0001$ compared to 30s, not significant compared to 5min).

Effect of AMPK deletion during mild hypoxia Similar to controls, Tv/To was highest in TH AMPK-α1/α2 dKO mice 30s after the onset of mild hypoxia (1.6 ± 0.04), after which Tv/To also decreased, plateaued around 2min and remained stable for the remainder of the exposure. However, the significant attenuation observed for Tv/Te at 30s also translated into a significantly lower Tv/To compared to controls (Figure 6.6 Aii; $p<0.0001$). Although TH AMPK-α1/α2 dKO mice were able to increase their Tv/Te relative to normoxia, the response remained significantly reduced compared to controls, measuring 1.2 ± 0.04 by 5min ($p<0.05$) and 1.2 ± 0.05 by 10min ($p<0.001$).

Effect of AMPK deletion during severe hypoxia Once again, Tv/To in TH AMPK-α1/α2 dKO mice initially rose relative to normoxia during exposures to 8% O_2, measuring 1.5 ± 0.06 at 30s and then declined below normoxic values where a plateau was quickly reached. The fact that TH AMPK-α1/α2 dKO blocked acceleration of air movement through active expiration during severe hypoxia at 30s translated to a decreased overall movement of air per

unit time (Figure 6.6 Bii; $p<0.0001$ compared to controls). Additionally, the significant attenuations of Tv/Ti (and Tv/Te) relative to controls meant that overall TH AMPK-α1/α2 dKO mice shifted significantly less volume of air during each breath throughout the exposures, reaching values of only 0.7 ± 0.03 by 5min ($p<0.0001$ compared to controls) and 0.8 ± 0.03 by 10min ($p<0.0001$ compared to controls).

Taken together, these data suggest that less air is moved per unit time during every phase of the breath cycle upon deletion of AMPK-α1 and -α2 subunits in catecholaminergic cells. This indicates that these knockout mice do not only breathe slower due to blocked active expiration, but also that each breath is shallower.

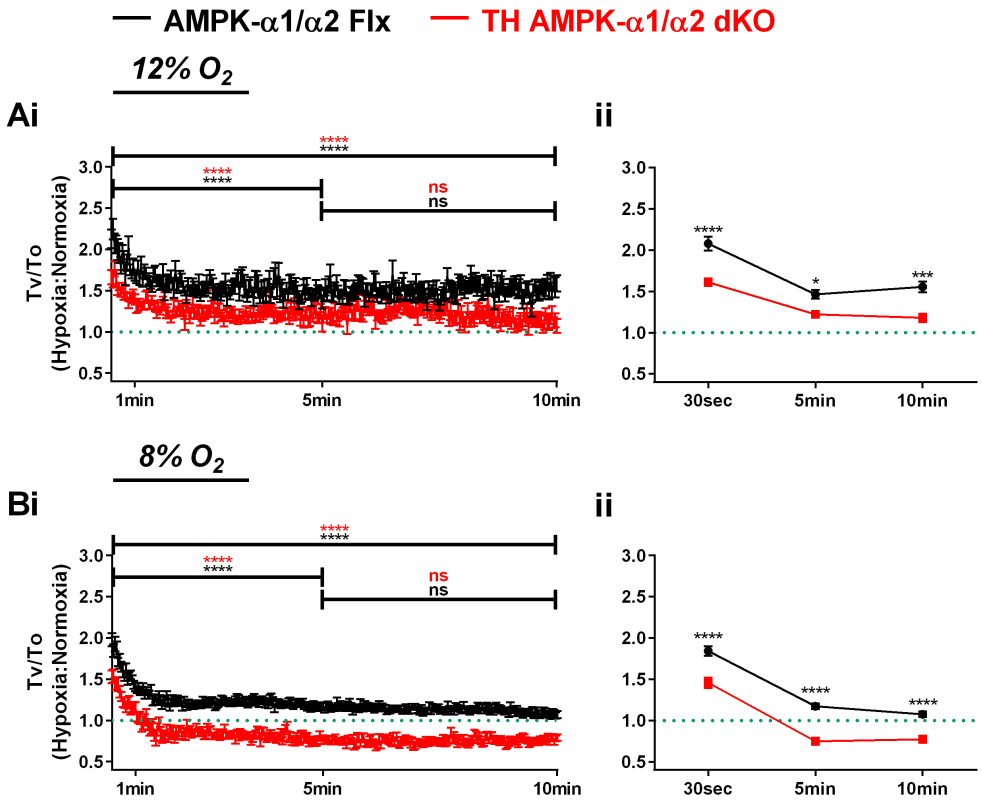

Figure 6.6: AMPK-α1/α2 catalytic subunit deletion in catecholaminergic cells reduces tidal volume over total breath time during hypoxia.

The ratiometric changes relative to normoxia (green dotted line) of tidal volume over total breath time during 10min exposures to **(A)** mild hypoxia (12% O_2) and **(B)** severe hypoxia (8% O_2) in AMPK-α1 and -α2 floxed mice (AMPK-α1/α2 Flx, black, 12% O_2: n = 37 exposures from 14 mice, 8% O_2: n = 54 exposures from 21 mice) and TH-driven AMPK-α1 and -α2 double knockout mice (TH AMPK-α1/α2 dKO, red, 12% O_2: n = 28 exposures from 11 mice, 8% O_2: 8% O_2: n = 37 exposures from 15 mice) are shown as means ± SEM **(i)** over time as 2s averages and **(ii)** at three selected time points to clearly illustrate differences between genotypes. ns = not significant, * = $p<0.05$, *** = $p<0.001$, **** = $p<0.0001$. Significance tested by two-way ANOVA with Sidak post-hoc tests.

6.3 Discussion

6.3.1 Summary of findings

Chapter 6 shows that the loss of both AMPK-α1 and -α2 catalytic subunits in catecholaminergic cells attenuates the ventilatory response to hypoxia by blocking acceleration of expiration time (i.e. active expiration), and reduces the overall volume of air that is moved during each breath, thus resulting in shallow breathing with an overall reduction of breathing frequency and tidal volume. Therefore, AMPK activity in catecholaminergic cells governs the maintenance of whole-body O_2 supply throughout periods of acute mild and severe hypoxia by continuously supporting appropriate ventilatory changes that are aimed to restore blood PO_2 levels.

6.3.2 The engagement of active expiration and acceleration of air movement during inspiration and expiration require AMPK activity in catecholaminergic cells

The attenuation of the HVR in TH AMPK-α1/α2 dKO mice described in Chapter 3 was mainly precipitated by significant PO_2-dependent attenuation of increases in breathing frequency and tidal volume. The findings in this chapter illustrate that such attenuation was elicited by a significant prolongation, relative to controls, of total breath time (To), which occurred due to significant increases in expiration time (Te) with minimal differences in inspiration time (Ti). This suggests that following the Augmenting phase of the HVR, the respiratory central pattern generators (rCPGs) in the ventrolateral medulla were unable to appropriately modulate the expiratory phase of respiration in the manner required to promote an overall increase in ventilation in response to hypoxia. Important in this context, modulation of the rCPGs via the RTN has been suggested to depend on glutamatergic and serotonergic neurotransmission (Moraes *et al.*, 2012a; Lemes *et al.*, 2016; Lemes & Zoccal, 2016), and catecholaminergic neurons were shown to use glutamate as a neurotransmitter (Fung *et al.*, 1994a; Fung *et al.*, 1994b; Stornetta *et al.*, 2002; Rinaman, 2011; DePuy *et al.*, 2013). Moreover,

selective inhibition of C1 cells was found to attenuate active expiration during hypoxia, but not during normoxia or hypercapnia (Malheiros-Lima *et al.*, 2017), which is entirely consistent with the retained hypercapnic response of Ti, Te and To in TH AMPK-α1/α2 dKO mice (Mahmoud, 2014).

Therefore, AMPK-dependent afferent inputs from catecholaminergic cells – which likely encompass the ventrolateral C1 cell group but may also arise from the dorsolateral A2/C2 cell groups – appear to act on the rCPG via the RTN in order to engage active expiration, thus reducing the total breath time to accommodate increases in ventilatory frequency (Moraes *et al.*, 2012a; Burke *et al.*, 2014; Malheiros-Lima *et al.*, 2015; Pisanski & Pagliardini, 2018).

Additionally, loss of AMPK activity resulted in a reduction of tidal volume during hypoxia, which was the result of marked attenuation of the amount of air that was moved during every phase of the breath cycle. This indicates that mice with conditional deletion of the AMPK-α1 and -α2 subunits in catecholaminergic cells do not only breathe slower, but also that each breath is shallower. Therefore, AMPK-dependent signalling pathways appear to also be required to increase tidal volume by active expiration via recruitment of the expiratory reserve volume (Leith, 1976).

6.3.3 Conclusion

In conclusion, active expiration during the HVR is supported by AMPK-dependent signalling pathways in catecholaminergic cells. Therefore, AMPK activity leads to an overall decrease in the total breath time and increases of air movement. Thus, AMPK activity in catecholaminergic cells prompts increases in respiratory frequency and tidal volume in an attempt to optimise whole-body O_2 supply during periods of hypoxia.

Chapter 7: AMPK-α1 or AMPK-α2 deletion in smooth muscle cells does not affect the hypoxic ventilatory response or systemic arterial blood pressure regulation during hypoxia

The majority of the data presented in this Chapter have been published:

MacMillan S & Evans AM. (2018). AMPK-alpha1 or AMPK-alpha2 Deletion in Smooth Muscles Does Not Affect the Hypoxic Ventilatory Response or Systemic Arterial Blood Pressure Regulation During Hypoxia. *Frontiers in Physiology* 9, 655.

7.1 Introduction

As described previously, it was demonstrated that the role of AMPK in metabolic homeostasis is not limited to cell autonomous pathways of energy supply (Ross *et al.*, 2011), but extends to the HVR (Teppema & Dahan, 2010; Mahmoud *et al.*, 2016; Wilson & Teppema, 2016) and thus O_2 and energy (ATP) supply to the body as a whole. In doing so AMPK acts to oppose central respiratory depression during hypoxia and thus resists hypoventilation and apnoea.

However, the HVR could well be affected by AMPK deficiency in cell systems other than catecholaminergic neurons due to off-target AMPK deletion through "leakage" of Cre beyond those cells targeted by the conditional deletion strategy that was employed. This possibility is highlighted by the fact that transient developmental expression of TH occurs in disparate cell groups that do not express TH in the adult (Lindeberg *et al.*, 2004), including, for example, a subset of heart wall cells. Therefore, there remains the possibility that AMPK deficiency might somehow affect ventilatory control mechanisms through myogenic rather than neurogenic mechanisms. This is evident from the fact that systemic arteries dilate in response to tissue hypoxemia in order to match local perfusion to local metabolism (Roy & Sherrington, 1890), and evidence suggests a role for AMPK in this response (Goirand *et al.*, 2007; Schneider *et al.*, 2015). With "leakage" of Cre, off-target deletion of AMPK in arterial myocytes could attenuate arterial dilation and thus impact O_2 supply to the brain during hypoxia and the HVR. Moreover, the sympathetic outflow that regulates these cardiovascular responses to hypoxia is determined by neuronal activity within the catecholaminergic cells that were targeted by our TH-driven AMPK deletion (King *et al.*, 2012; Guyenet *et al.*, 2013; King *et al.*, 2013; Burke *et al.*, 2014; King *et al.*, 2015) and shown to project to the dorsal motor nucleus of the vagus (10N), which was proposed to contribute to the bradycardia and mild hypertension associated with the diving reflex (Panneton *et al.*, 2014) and displayed a significant reduction of cFos expression in response to hypoxia described in Chapter 4. Therefore, AMPK deletion may also impact on myogenic influences on the HVR.

A further implication for off-target AMPK deficiency in cardiac myocytes induced by TH-Cre lies in the fact that AMPK expression in the heart has a protective role in the development of cardiac hypertrophy and delays the onset and severity of cardiac contracture during ischaemia. This in turn will impact on heart rate, systolic and diastolic functions and hence blood and O_2 supply to vital organs such as the brain (Zarrinpashneh *et al.*, 2006; Carvajal *et al.*, 2007; Zarrinpashneh *et al.*, 2008; Sung *et al.*, 2015).

7.1.1 Aims

In order to determine whether AMPK contributes to the HVR and blood pressure control during severe hypoxia (8% O_2) through neurogenic and/or myogenic mechanisms, the impact of AMPK deficiency in smooth muscles and catecholaminergic cells was assessed in relation to the HVR and blood pressure control.

7.2 Results

7.2.1 AMPK deletion in smooth muscle cells does not attenuate the hypoxic ventilatory response

Mice with conditional deletion of AMPK-α1 or AMPK-α2 subunits in smooth muscle cells (SM AMPK-α1 KO or SM AMPK-α2 KO) exhibited no obvious phenotype and no ventilatory dysfunction or deficiency was evident during normoxia (see Appendix 5.1). Most significantly in the context of the present investigation, no significant attenuation of the HVR relative to controls (AMPK-α1/α2 Flx) was identified during exposures to severe hypoxia (8% O_2). That said, subtle differences were observed between genotypes.

Breathing frequency Figure 7.1 A shows that both SM AMPK-α1 KO (n = 16 exposures from 4 mice) and SM AMPK-α2 KO mice (n = 16 exposures from 4 mice) produced increases in breathing frequency during the Augmenting phase (A) of the HVR that were comparable to control AMPK-α1/α2 Flx mice (SM AMPK-α1 KO: 61.7 ± 4%; SM AMPK-α2 KO: 68.3 ± 4.6% ; AMPK-α1/α2 Flx: 60.8 ± 6.6%, n = 45 exposures from 12 mice). However, for SM AMPK-α1 KO mice alone there appeared to be an insignificant yet noticeable lowering, relative to controls, of breathing frequency during "Roll-Off" (RO; -13 ± 4.1% and 10.7 ± 4.3%, respectively) that was maintained for the duration of the Sustained Phase (SP; -2.2 ± 7.2% and 11.7 ± 3.9%, respectively) of the HVR. This attenuation was not observed in SM AMPK-α2 KO mice which retained breathing frequencies above those measured during hypoxia at a level that was comparable to controls (RO: 7.5 ± 5.6%; SP: 20 ± 4.2%).

Tidal volume By contrast, in both SM AMPK-α1 KO and SM AMPK-α2 KO mice larger increases in tidal volume were observed relative to controls (Figure 7.1 B), which were comparable across all three genotypes during the Augmenting phase (AMPK-α1/α2 Flx: -3.2 ± 2.3%; SM AMPK-α1 KO: 11.6 ± 1.4%; SM AMPK-α2 KO: 10.3 ± 2.2%), but reached significance for SM AMPK-α1 KO mice relative to controls at the peak of "Roll-Off" (AMPK-α1/α2 Flx: -0.8 ± 2.7%; SM AMPK-α1 KO: 17.1 ± 5.8%, $p<0.05$; SM

AMPK-α2 KO: 10.3 ± 2.2%, not significant). This significance was lost again during the sustained phase, where tidal volume responses were comparable across the three genotypes tested (AMPK-α1/α2 Flx: -2.1 ± 9%; SM AMPK-α1 KO: 21.5 ± 5.3%; SM AMPK-α2 KO: 11.4 ± 1.2%).

Minute ventilation Increases in minute ventilation during hypoxia also showed a tendency to be greater for SM AMPK-α1 KO and SM AMPK-α2 KO mice than for control AMPK-α1/α2 Flx mice. However, this only reached significance during the initial Augmenting Phase of the HVR (Figure 7.1 C; AMPK-α1/α2 Flx: 53.2 ± 5.9%; SM AMPK-α1 KO: 79.1 ± 6.6%; SM AMPK-α2 KO: 84.3 ± 7.3%, $p<0.05$ compared to controls), which primarily results from increases in carotid body afferent input responses (Day & Wilson, 2007; Teppema & Dahan, 2010; Wilson & Teppema, 2016). Thereafter, minute ventilation was comparable across the three genotypes both at the peak of "Roll-Off" (AMPK-α1/α2 Flx: 8.5 ± 5.6%; SM AMPK-α1 KO: -0.5 ± 3.6%; SM AMPK-α2 KO: 19.3 ± 5.8%) and during the Sustained Phase (AMPK-α1/α2 Flx: 7.8 ± 5.1%; SM AMPK-α1 KO: 15.9 ± 5.4%; SM AMPK-α2 KO: 32.6 ± 3.9%).

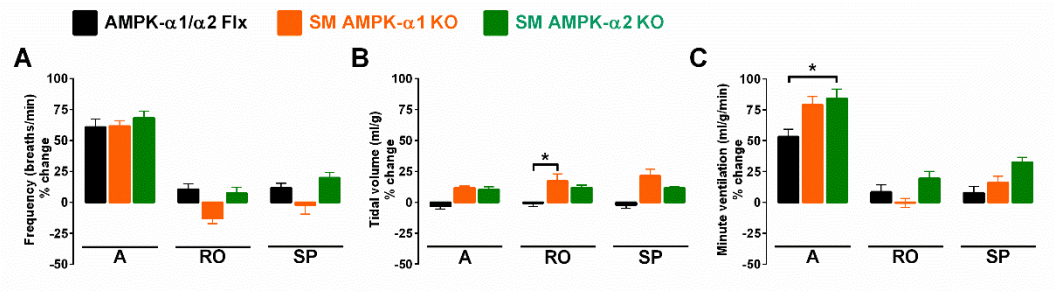

Figure 7.1: The hypoxic ventilatory response is not attenuated by conditional deletion of AMPK-α1 or AMPK-α2 catalytic subunits in smooth muscle cells.

Bar charts show mean ± SEM for changes in **(A)** respiratory frequency, **(B)** tidal volume, and **(C)** minute ventilation for AMPK-α1/α2 floxed mice (Flx; black, n = 45 exposures from 12 mice), and for mice with AMPK-α1 (orange; n = 16 exposures from 4 mice) and AMPK-α2 (green; n = 16 exposures from 4 mice) deletion in smooth muscles (transgelin expressing cells) during the peak of the Augmenting phase (A), after approximately 100s of Roll Off (RO) and the plateau of the Sustained Phase (SP) of the response to severe hypoxia (8% O_2). * = $p<0.05$. Significance tested by two-way ANOVA with Sidak post-hoc tests.

7.2.2 AMPK deletion in smooth muscle cells has no effect on the apnoeic phenotype during severe hypoxia

Perhaps most striking was the fact that deletion of neither AMPK-α1 nor AMPK-α2 catalytic subunits in smooth muscle cells had any discernible effect on hypoxia-evoked apnoeas (Figure 7.2), when compared to controls (AMPK-α1/α2 Flx). This was evident from the fact that there were no difference in either the apnoea frequency (Figure 7.2 A; AMPK-α1/α2 Flx: 3.1 ± 0.5 apnoeas/min; SM AMPK-α1 KO: 3.4 ± 0.6 apnoeas/min; SM AMPK-α2 KO: 2.4 ± 0.8 apnoeas/min), duration (Figure 7.2 B; AMPK-α1/α2 Flx: -928.9 ± 38.5ms; SM AMPK-α1 KO: 1021 ± 64.6ms; SM AMPK-α2 KO: 863.9 ± 92.4ms) or apnoea duration index (Figure 7.2 C; AMPK-α1/α2 Flx: 2.9 ± 0.4; SM AMPK-α1 KO: 3.4 ± 0.6; SM AMPK-α2 KO: 2.3 ± 0.9) in mice lacking the AMPK-α1 or AMPK-α2 subunits in smooth muscle cells.

The aforementioned findings are therefore in complete contrast to previous observations on mice with AMPK-α1 deletion in catecholaminergic neurons (driven by TH-Cre), which exhibited marked attenuation of the HVR and pronounced increases in apnoea frequency, duration and apnoea duration index (Mahmoud *et al.*, 2016).

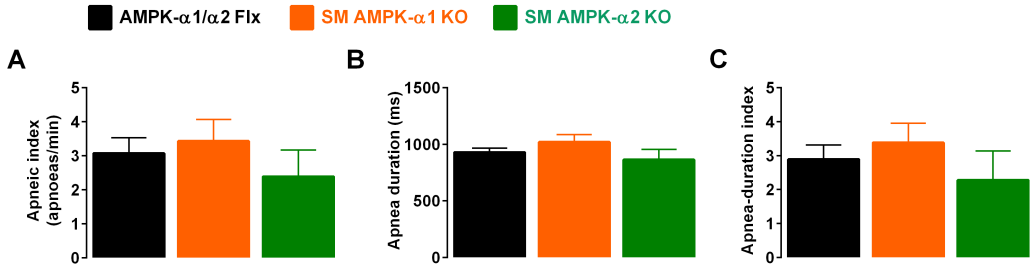

Figure 7.2: Deletion of AMPK-α1 or AMPK-α2 catalytic subunits in smooth muscle cells does not affect apnoea frequency or duration during hypoxia.

Bar charts show mean ± SEM for the **(A)** apnoeic index (per minute), **(B)** apnoea duration (ms), and **(C)** apnoea duration index (frequency x duration) of AMPK-α1/α2 floxed mice (Flx; black, n = 45 exposures from 12 mice), and for mice with AMPK-α1 (orange; n = 16 exposures from 4 mice) and AMPK-α2 (green; n = 16 exposures from 4 mice) deletion in smooth muscles (transgelin expressing cells). Significance tested by t-tests between genotypes.

7.2.3 Cardiovascular responses to hypoxia remain unaltered following deletion of AMPK-α1 and AMPK-α2 in smooth muscle or catecholaminergic cells

Next, the effect of AMPK deficiency on cardiovascular function was assessed during severe hypoxia by monitoring changes in systemic blood pressure. Deleting either AMPK-α1 KO or SM AMPK-α2 KO subunits in smooth muscle (SM) cells or both AMPK-α1/α2 subunits in catecholaminergic (TH) cells had little or no effect on resting blood pressure (Fig 7.3 A, Table 7.1). Furthermore, neither smooth muscle AMPK-α1 nor -α2 deficiency affected hypoxia-evoked falls in systemic blood pressure in mice (Fig 7.3 B and C), which were comparable to the range of responses reported previously (Mahmoud *et al.*, 2016). By contrast, hypoxia-evoked falls in blood pressure appeared to be significantly larger in TH AMPK-α1/α2 dKO mice than for control AMPK-α1/α2 Flx mice (mean: $p<0.01$; systolic: $p<0.05$; diastolic: $p<0.05$). This could, however, be caused by the higher pre-hypoxic blood pressures of TH AMPK-α1/α2 dKO mice measured during normoxia on the experimental days. In fact, all measures of systemic blood pressure responses during 8% O_2 were comparable between controls and TH AMPK-α1/α2 dKO mice (Figure 7.3 B), showing that dual AMPK-α1/α2 deletion in TH-positive cells did not lead to hypoxic hyper- or hypotension that could explain the hypoventilatory phenotype observed in Chapter 3.

Additional analyses of heart rates during hypoxia showed no differences between any of the genotypes tested (Figure 7.4). That said, the heart rate of SM AMPK-α1 KO mice was significantly lower compared to controls both during normoxia (controls: 702 ± 16 beats/min; SM AMPK-α1 KO: 628 ± 24 beats/min, $p>0.05$) and 8% O_2 (controls: 718 ± 21 beats/min; SM AMPK-α1 KO: 638 ± 37 beats/min, $p>0.05$). However, this was most likely be due to the small sample size, as measurements of 2 out of 3 SM AMPK-α1 KO mice were within the same range as controls and SM AMPK-α2 KO mice. Moreover, there was no difference observed during recovery and % changes between all genotypes were identical. It should, however, be pointed out that heart rate measurements were highly variable and that the manufacturer

advises against the use of tail pulse oximetry to obtain heart rate measurements (Kent, 2012).

That comparable levels of arterial hypoxia were achieved in all mice was confirmed by pulse oximetry, which demonstrated significant and similar falls in SpO_2 for all genotypes (Figure 7.5, Table 7.1). Moreover, there were no differences with respect to post-hypoxic recovery of arterial SpO_2 upon return to room air.

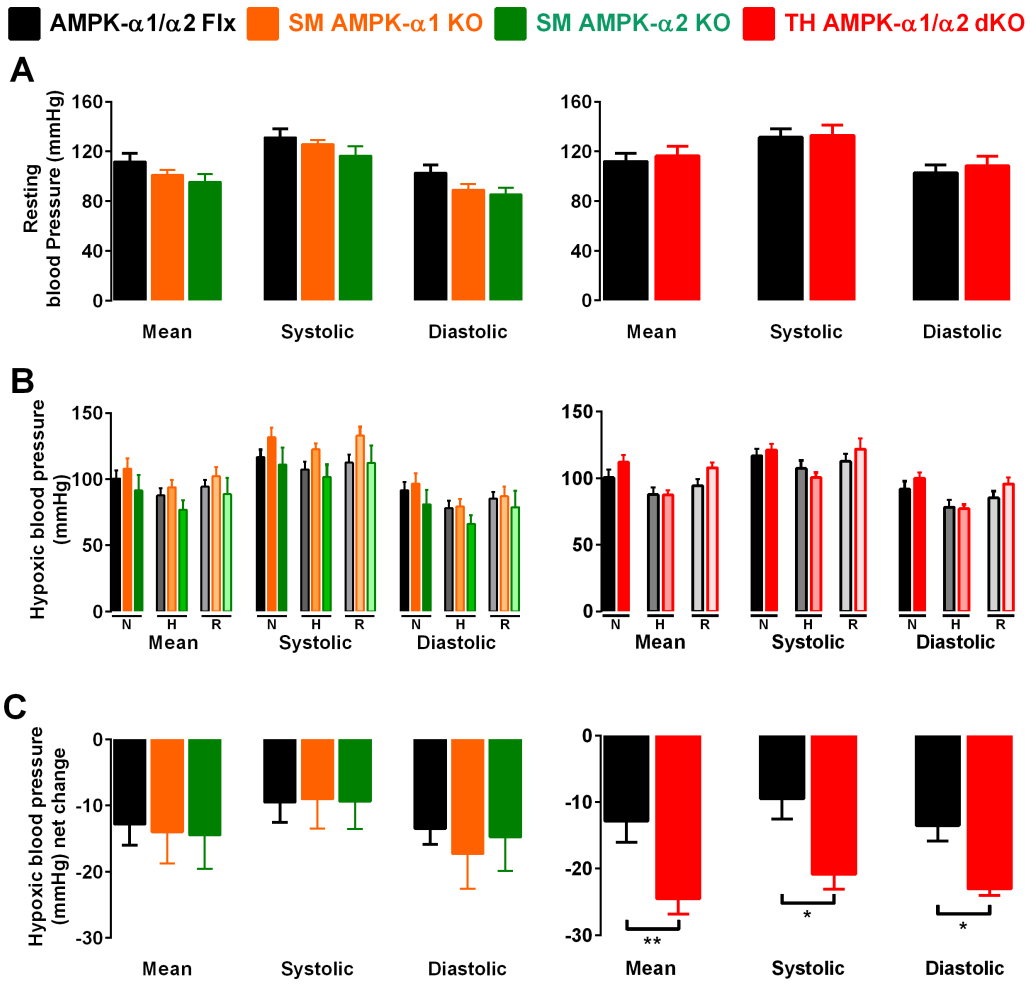

Figure 7.3: Deletion of AMPK-α1 and AMPK-α2 subunits in smooth muscle cells or catecholaminergic cells has no effect on systemic arterial blood pressure during normoxia or hypoxia.

(A) Bar charts show (mean ± SEM) the mean, systolic and diastolic blood pressure of control AMPK-α1/α2 floxed (Flx; black; n = 6) mice, those with AMPK-α1 (orange; n = 4) and AMPK-α2 (green; n = 4) deletion in smooth muscles (transgelin expressing cells) and AMPK-α1/α2 double KO in catecholaminergic cells (TH AMPK-α1/α2 dKO, red, n = 5). **(B)** Bar charts show the same measures of blood pressure during normoxia (N), after 10min of hypoxia (H; 8% O_2) and following recovery to normoxia (R). **(C)** Bar charts show the percentage change in blood pressure measured during hypoxia. Significance tested by one-way ANOVA with Sidak post-hoc tests.

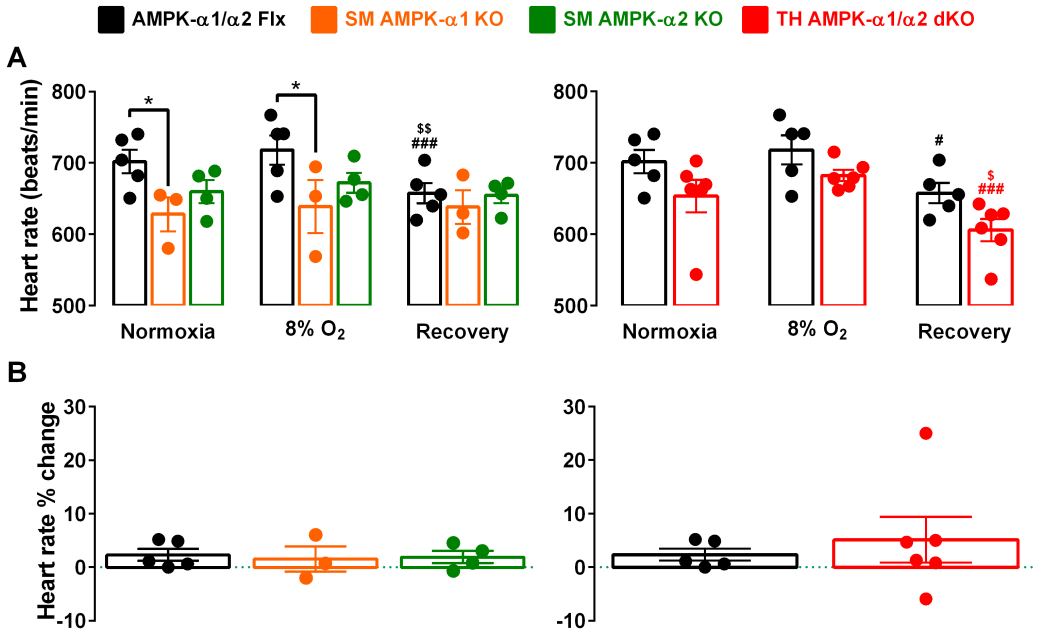

Figure 7.4: Heart rate during hypoxia was unaffected by AMPK-α1/α2 catalytic subunit deletion in smooth muscle or catecholaminergic cells.

(A) Bar charts show mean ± SEM for the heart rate (beats/min) during normoxia (room air), after 10 min of hypoxia (8% O_2) and following recovery to normoxia, and **(B)** shows mean ± SEM for percentage change in heart rate in AMPK-α1/α2 floxed (Flx; black, n = 12 exposures from 5 mice), smooth muscle AMPK-α1 KO (orange, n = 8 exposures from 3 mice), smooth muscle AMPK-α2 KO mice (green, n = 15 exposures from 4 mice) and catecholaminergic AMPK-α1/α2 double KO (TH AMPK-α1/α2 dKO, red, n = 12 exposures from 6 mice). Between genotypes: * = $p<0.05$; compared to normoxia: $ = $p<0.05$, $$ = $p<0.01$; compared to hypoxia: ## = $p<0.01$; ### = $p<0.001$. Significance tested by two-way ANOVA with Sidak post-hoc tests.

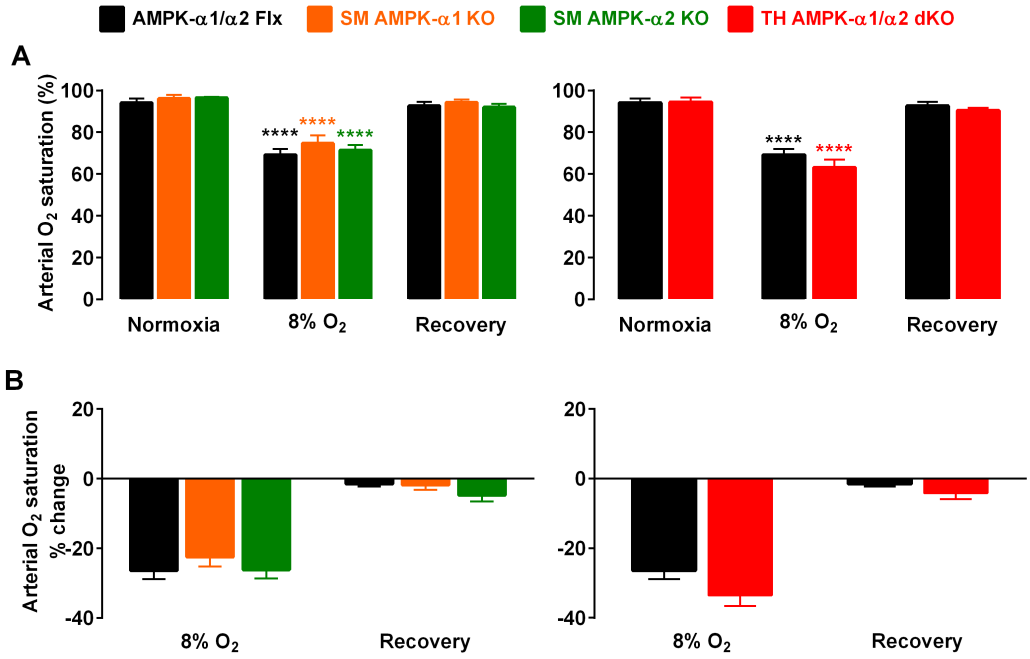

Figure 7.5: Deletion of AMPK-α1/α2 catalytic subunit deletion in smooth muscle or catecholaminergic cells did not affect falls in arterial oxygen saturation during exposures to severe hypoxia.

(A) Bar charts show mean ± SEM for the arterial oxygen saturation (SpO_2) during normoxia (room air), after 10 min of hypoxia (8% O_2) and following recovery to normoxia, and **(B)** shows mean ± SEM for percentage change in SpO_2 in AMPK-α1/α2 floxed (Flx; black, n = 12 exposures from 5 mice), smooth muscle AMPK-α1 KO (orange, n = 8 exposures from 3 mice), smooth muscle AMPK-α2 KO mice (green, n = 15 exposures from 4 mice) and catecholaminergic AMPK-α1/α2 double KO (TH AMPK-α1/α2 dKO, red, n = 12 exposures from 6 mice). **** = $p<0.001$. Significance tested by two-way ANOVA with Sidak post-hoc tests.

Table 7.1: Means ± SEM of values obtained by tail cuff blood pressure measurements and percentage changes in arterial SpO_2 before, during, and after exposures to hypoxia (8%O_2) across all genotypes.

Genotype	Resting BP (mmHg)	Mean BP (mmHg)	Sys BP (mmHg)	Dias BP (mmHg)	*Sp* O_2
AMPK-α1/α2 floxed	M 112±6 Sys 131±7 Dias 103±6	N 101±6 H 88±4.5 R 94±5	N 117±5 H 107±6 R 113±6	N 92±6 H 78±6 R 85±5	N 94±2% H 69±3% R 93±2%
SM AMPK-α1 knockouts	M 101±4 Sys 126±3 Dias 89±4	N 108±8 H 94±5 R 89±12	N 132±7.5 H 123±5 R 133±7	N 97±8 H 79±6 R 87±7.5	N 96±2% H 75±4% R 94±1%
SM AMPK-α2 knockouts	M 96±6 Sys 117±8 Dias 86±5	N 91±12 H 77±7 R 102±7	N 111±13 H 102±9.5 R 112±13	N 81±11 H 66±6.5 R 79±12	N 97±0.5% H 71±3% R 92±2%
TH AMPK-α1/α2 knockouts	M 116±8 Sys 133±8 Dias 108±8	N 112±5 H 87±3.5 R 108±4	N 121±4.5 H 100±4 R 122±8	N 100±4 H 77±3 R 96±5	N 94±2% H 63±4% R 90±1%

7.3 Discussion

7.3.1 Summary of findings

In this chapter I demonstrated that deletion of AMPK-α1 or AMPK-α2 subunits in smooth muscle cells had very little to no effect on the control of the cardiorespiratory system. Firstly, there were no differences in minute ventilation or blood pressure during normoxia. However, increases in minute ventilation during severe hypoxia (8% O_2) were, if affected at all, augmented by smooth muscle cell AMPK-α1 and AMPK-α2 deletion – despite the fact that hypoxia (8% O_2) evoked falls in arterial SpO_2 comparable with controls. Moreover, these mice exhibited no differences in heart rate or in systolic, diastolic or mean arterial blood pressure during hypoxia. In addition, cardiovascular responses to hypoxia were also unaffected by dual deletion of AMPK-α1 and AMPK-α2 subunits in catecholaminergic (TH) cells, therefore supporting our hypothesis that neurogenic mechanisms dependent on AMPK activity in TH-positive cells support the HVR.

7.3.2 AMPK activity within catecholaminergic cells modulates respiratory, but not cardiovascular responses to hypoxia

In previously reported findings, AMPK-α1 deficiency in catecholaminergic neurons (driven by TH-Cre) markedly attenuated the HVR and precipitated hypoventilation and apnoea during hypoxia (Mahmoud *et al.*, 2016). These outcomes led to the proposed model of central oxygen-sensing by catecholaminergic neurons of the brainstem respiratory network (see section 3.1.1). Outcomes presented in this chapter provide further detail for this model, given the consideration that the modulation of sympathetic outflow during hypoxia is supposedly orchestrated by the same catecholaminergic network within the brainstem that adjusts ventilatory responses (King *et al.*, 2012; Guyenet *et al.*, 2013; King *et al.*, 2013; Burke *et al.*, 2014; King *et al.*, 2015). So far, studies have shown that activation of dorsal A2/C2 and ventral A1/C1 neurons modulates both ventilatory and cardiovascular responses to hypoxia simultaneously. By contrast, deletion

of AMPK within the catecholaminergic network (driven by TH-Cre) which affects all of these neuronal groups was found to *only* alter the respiratory responses (see also Chapter 3), and *not* those of the cardiovascular system. This suggests that we may have uncovered a split in the dependency of AMPK activity within the catecholaminergic network that might separate these two systems, which could be anatomically inseparable and therefore so difficult to isolate and identify. Furthermore, there is a possibility that this effect could be co-dependent on serotonergic signalling, because serotonin receptor activation within the commissural (SolC) and medial (SolM) subnuclei of the NTS has been shown to decrease central respiratory output via phrenic nerve activity with no alteration of heart rate, arterial pressure, or sympathetic nerve activity (Ostrowski *et al.*, 2014). This is highly relevant, as the anatomical location of SolM is adjacent to the area of cFos deficiency uncovered in Chapter 4, and serotonin has been found to inhibit neuronal AMPK activity in other model organisms (Cunningham *et al.*, 2012; Cunningham *et al.*, 2014). By contrast, the proposed role of 10N to contribute to the bradycardia and mild hypertension associated with the diving reflex (Panneton *et al.*, 2014) appears to not translate to the modulation of cardiovascular responses to hypoxia. Despite exhibiting a bilateral deficiency in hypoxia-induced cFos expression within 10N, which was proposed to receive afferent input from the adrenergic subset of brainstem catecholaminergic neurons (Hokfelt *et al.*, 1973; Abbott *et al.*, 2013; DePuy *et al.*, 2013; Guyenet *et al.*, 2013), the systemic cardiovascular responses to hypoxia remained unaltered upon deletion of AMPK-α1/α2 catalytic subunits in catecholaminergic cells.

Therefore, AMPK activity may modulate signalling pathways within catecholaminergic neurons that stimulate respiratory, but not sympathetic, outflow.

7.3.3 AMPK-dependent hypoxic vasodilation is system-specific and does not translate to systemic blood pressure responses or the HVR

Additional significance of the present findings lies in the fact that reduced cerebral arterial dilation could affect O_2 supply to the brain during hypoxia and thus the HVR through consequent respiratory depression, because the activity of brainstem respiratory networks is ultimately reliant on O_2 delivery via the vasculature that could be modulated systemically and locally through myogenic responses. Such system-specific responses could well be affected by a number of mechanisms through which AMPK has been proposed to regulate myocyte function, rendering outcomes susceptible to off-target AMPK deletion due to "leakage" of Cre beyond those cells targeted by conditional deletion strategies. This was a distinct possibility, given that transient developmental expression of TH occurs in disparate cell groups that do not express TH in the adult (Lindeberg *et al.*, 2004), including, for example, a subset of heart wall cells. However, the data presented here showed that TH-driven deletion of AMPK did not affect heart rate during normoxia or hypoxia.

The outcomes of this investigation further indicate that while AMPK has been shown to mediate *ex vivo* arterial dilation in some circumstances (Goirand *et al.*, 2007; Schneider *et al.*, 2015), neither the expression of AMPK-α1 nor AMPK-α2 catalytic subunits in smooth muscles is a pre-requisite for *in vivo* arterial dilation during hypoxia sufficient enough to impact systemic arterial blood pressures. These findings do not, however, rule out a role for AMPK in maintaining resting vascular tone locally, or in governing organ- and/or tissue-specific perfusion and oxygen supply. Indeed, studies on other vascular beds have already revealed that AMPK might adjust local perfusion during hypoxia. For example, AMPK may mediate hypoxic pulmonary vasoconstriction (Evans *et al.*, 2005a; Evans, 2006; Moral-Sanz *et al.*, 2018), and thus assist ventilation-perfusion matching by diverting blood from oxygen deprived to oxygen rich areas of the lung (Bradford & Dean, 1894; von Euler & Liljestrand, 1946). Furthermore, evidence suggests that AMPK supports dilation of systemic arteries, such as the aorta and mesenteric

arteries, at the level of smooth muscles that may counter tissue hypoxaemia (Schneider *et al.*, 2015; Moral-Sanz *et al.*, 2016). Accordingly, AMPK has also been implicated in the regulation of uterine artery reactivity during hypoxia (Skeffington *et al.*, 2016), perhaps linking maternal metabolic and cardiovascular responses during pregnancy and governing oxygen and nutrient supply to the foetus.

The mechanisms involved in systemic arterial dilation during hypoxia include AMPK-dependent activation of SERCA and BK_{Ca} channels in systemic arterial myocytes (Schneider *et al.*, 2015), while AMPK exerts its effects on pulmonary smooth muscle cells, at least in part, through direct phosphorylation and inhibition of the voltage-gated potassium channel $K_V1.5$ (Moral-Sanz *et al.*, 2016). Significant to the context of this study, $K_V1.5$ availability has been proposed to impact cerebral myogenic responses (Koide *et al.*, 2018), which could equally well be affected by loss of capacity for AMPK-dependent activation of SERCA and BK_{Ca} channels. Either way, the data presented here argue strongly against the possibility that the HVR is influenced by AMPK-dependent mechanisms within smooth muscles that might affect local myogenic responses, irrespective of the tissue- and circulation-specific function they might impact. Nevertheless, it would be interesting to determine whether AMPK contributes to local autoregulatory mechanisms in the cerebral vasculature during hypoxia.

7.3.4 Conclusion

In conclusion, neither AMPK-α1 nor AMPK-α2 are required in smooth muscle or catecholaminergic cells for the regulation of systemic arterial blood pressure during hypoxia. Thus, AMPK likely supports the HVR through neurogenic but not myogenic mechanisms as previously proposed, by supporting increased respiratory drive (Mahmoud *et al.*, 2016) and perhaps functional hyperaemia (Bucher *et al.*, 2014), each of which may be coordinated by catecholaminergic neurons of the brainstem respiratory network.

7.3.5 Limitations of the study

The experiments described above compared outcomes of single AMPK-α1 and AMPK-α2 deletion in smooth muscle (SM) cells with those where both catalytic AMPK-α subunits were deleted in tyrosine hydroxylase-positive cells. Ideally, a double knockout of both AMPK-α1 and AMPK-α2 subunits in SM cells (SM AMPK-α1/α2 dKO) should be used for this comparison. However, such a genetic modification resulted in mice that were only viable for 8-10 weeks and therefore died before reaching a breeding age. Moreover, only very few SM AMPK-α1/α2 dKO could be generated from heterozygous breeding pairs which in other experiments carried out in our research group have not been observed to survive exposures to severe hypoxia for more than 2min, making comparisons of 5min and 10min exposures of hypoxia impossible. That said, blood pressure measurements taken under resting conditions showed no differences compared to control AMPK-α1/α2 Flx, SM AMPK-α1 KO, or SM AMPK-α2 KO mice (Appendix 4.1).

Chapter 8: Characterisation of the hypoxic ventilatory response in mice with AMPK deficiency in adrenergic cells

8.1 Introduction

8.1.1 The control of cardiorespiratory responses to hypoxia by adrenergic neurons of the brainstem

Located within the caudal portions of the brainstem are the noradrenergic (dopamine β-hydroxylase-expressing) A1 and A2 cell groups, which are heavily implicated in the receipt of peripheral chemoafferent fibre input and the control of breathing, as well as the modulation of other emotional and cognitive processes such as satiation, behavioural stress responses, addictive drug dependence, or emotional learning (Finley & Katz, 1992; Rinaman, 2011). The rostral portion of the brainstem on the other hand contains the adrenergic (Phenylethanolamine N-methyltransferase (PNMT)-expressing) C1, C2, and C3 cell groups, which are best known for the control of sympathoexcitatory responses and the stimulation of breathing. The vast majority (>70%) of PNMT-positive neurons is made up of the neuronal C1 group, which are located bilaterally in the ventral medulla (Minson *et al.*, 1990). The primary synaptic connections made by the C1 neurons are glutamatergic and therefore excitatory, and projections have been found to innervate several higher brainstem structures (for example the paraventricular nucleus of the hypothalamus), the dorsal motor nucleus of the vagus (10N) and the respiratory centres of the brainstem, as well as sympathetic preganglionic neurons in the spinal cord (Guyenet *et al.*, 2013). The anatomical location of the adrenergic C1 neurons in close proximity to the respiratory central pattern generators (rCPG) and the “pressor and depressor areas” - which control changes in arterial pressure - of the rostral and caudal ventrolateral medulla (respectively) make the connections between C1 neurons and the control of cardiorespiratory responses immediately obvious (Willette *et al.*, 1983; Burke *et al.*, 2014). Indeed, the contribution of C1 neurons to the baroreflex has already been well established, whereby the regulatory influence of the arterial baroreceptors activates bulbospinal C1 neurons, which then modulate arterial blood pressure and heart rate via vaso- and cardiomotor sympathetic efferents (Ross *et al.*, 1984; Dampney *et al.*, 2002; Guyenet, 2006; Guyenet *et al.*,

2013). In this context, targeted optogenetic and hypoxic activation of exclusively C1 neurons provided conclusive evidence that it is indeed the adrenergic cell population of the ventral medulla that determines the cardiovascular changes in the rat (Burke *et al.*, 2014).

In addition to its control of cardiovascular responses, stimuli that activate C1 neurons such as nociception, hypoxia, and hypotension also activate breathing, and targeted optogenetic stimulation of C1 cells has been shown to increase breathing frequencies in conscious mice (Abbott *et al.*, 2013) and rats (Burke *et al.*, 2014). The effects of C1 cell activation on the control of breathing have been proposed to be mostly mediated through direct projections to the retrotrapezoid nucleus (RTN), which in turn modulates respiratory output through innervations of the rCPG (Abbott *et al.*, 2009; Burke *et al.*, 2014; Burke *et al.*, 2015). However, the hypoxia-induced modulation of breathing by the C1-RTN signalling pathways does not always translate to increases in ventilation. Hypoxia-evoked hyperventilation, which is primarily determined and maintained by excitatory input from the carotid bodies, leads to overall reductions of CO_2 levels known as respiratory alkalosis (Foster *et al.*, 2001). This in turn has been shown to silence neurons of the RTN, even during exposures to mild hypoxia (12% O_2). Silencing of the RTN reduces the ventilatory drive during hypoxia through reductions in breathing frequency and tidal volume. Notably, additional optogenetic inhibition of the RTN during hypoxia did not lead to further reductions in breathing frequency unless the hypoxic stimulus was supplemented with 3% CO_2 or pharmacological agents that led to blood re-acidification (Basting *et al.*, 2015). Although the involvement of the adrenergic C1 neurons in the response to respiratory alkalosis was deemed unlikely, it could not be excluded. Therefore, the possibility remains that the release of inhibitory neuropeptides (such as enkephalin or neuropeptide Y) or signalling pathways involving GABAergic interneurons could, at least in part, involve the ventral adrenergic C1 neurons in the response hypoxia-induced respiratory alkalosis (Stornetta *et al.*, 1999; Pilowsky *et al.*, 2008).

8.1.2 Aims

Insofar, it has been demonstrated that loss of AMPK-α1/α2 catalytic subunits in catecholaminergic cells precipitates hypoventilation and apnoea during hypoxia (Mahmoud, 2014; Mahmoud *et al.*, 2016). Because the deletion strategy employed by TH Cre-driven AMPK deletion encompassed both the noradrenergic and adrenergic cell groups of the brainstem, it was impossible to determine whether the effect of AMPK deletion was synergistic or cell-type specific.

In this chapter, I aimed to further investigate the circuit mechanism by which AMPK deficiency impacts the HVR. More specifically, I sought to identify whether the attenuation of the HVR and augmentation of the apnoeic phenotype observed in TH AMPK-α1/α2 dKO mice was predominantly precipitated by AMPK deficiency in noradrenergic cells, adrenergic cells, or the combined effect of both cell types. Accordingly, AMPK-α1/α2 Flx mice were crossed with mice that express Cre recombinase under the control of the *Pnmt* gene. From these crosses, mice with dual deletion of the AMPK-α1/α2 catalytic subunits in PNMT-expressing cells were generated and exposed to 10min of severe hypoxia. Their ventilatory and apnoeic phenotype was then assessed using whole-body plethysmography.

8.2 Results

8.2.1 The generation of mice with dual deletion of the AMPK-α1/α2 catalytic subunits in adrenergic cells

As a result of a generous donation from Prof Steven Ebert (University of Central Florida), mice expressing Cre recombinase under the PNMT promoter (Ebert *et al.*, 2004) were crossed with AMPK-α1/α2 Flx mice, thereby generating PNMT-driven AMPK-α1/α2 dKO mice. However, a couple of limitations needed to be considered in advance of any experimental work and interpretation of outcomes.

Firstly, the insertion of Cre recombinase was targeted to exon 1 of the *Pnmt* gene, and homozygous insertion of Cre disrupted the functional expression of the PNMT protein. As might be expected, the absence of the enzyme that converts noradrenaline to adrenaline led to undetectable levels of adrenaline and increases in the concentration of noradrenaline in adrenal extracts. However, mice with heterozygous insertions of PNMT Cre did not exhibit any changes of noradrenaline and adrenaline concentrations, respectively (Ebert *et al.*, 2004). Therefore, in order to avoid any phenotypic side effects due to the absence of adrenaline, all experimental mice used in this chapter were exclusively heterozygous for the expression of Cre. Importantly, heterozygous Cre expression was shown to be sufficient for the cell-specific excision of both of the floxed AMPK-α1 and -α2 subunits (Mahmoud, 2014).

The second limitation was that the gifted PNMT Cre mice were bred on a CD1 background strain, whereas all our previously assessed catecholaminergic and smooth muscle AMPK knockout mice were bred on a C57Bl6 background strain. Genetic differences between background strains of mice are known to influence the ventilatory responses to hypoxia (Tankersley *et al.*, 1994; Tankersley *et al.*, 2000; Adachi *et al.*, 2006; Ward *et al.*, 2007; Ivy & Scott, 2017). Therefore, the donated CD1 PNMT Cre mice had to be back-crossed onto a C57Bl6 background to allow for comparisons with our previous mouse models. In order to determine whether the experimental mice used for this chapter still exhibited any mixed

background-specific differences in their ventilatory responses to hypoxia, all outcomes from the newly bred control PNMT Cre mice were also directly compared to control AMPK-α1/α2 Flx mice.

8.2.2 AMPK deletion in adrenergic cells augments ventilation throughout 10min exposures to hypoxia

Deletion of AMPK-α1/α2 catalytic subunits in adrenergic cells (PNMT AMPK-α1/α2 dKO) was found to have no effect on normoxic baseline breathing relative to control PNMT Cre mice (Appendix 5.1), but augmented the HVR during severe hypoxia. Example records of changes in breathing frequency (Figure 8.1 Ai and Aii), tidal volume (Figure 8.1 Bi and Bii) and minute ventilation (Figure 8.1 Ci and Cii) illustrate the responses of PNMT Cre and PNMT AMPK-α1/α2 dKO mice to 10min exposures of 8% O_2. Whereas control PNMT Cre mice responded to hypoxia with robust increases in ventilation which later stayed slightly above or returned to baseline values, PNMT AMPK-α1/α2 dKO mice retained an augmented ventilatory phenotype which appeared not only to have a more regular inter-breath interval, but also contained slightly fewer apnoeas.

8.2.2.1 Breathing frequency

5min exposures – controls As depicted in Figure 8.1 Aiii, control PNMT Cre mice responded to hypoxia (8% O_2) with robust increases in breathing frequency. Following the onset of hypoxia, values reached 66.5 ± 4.6% relative to normoxia (n = 32 exposures from 8 mice) during the peak of the Augmenting phase (A) and then declined during ventilatory Roll-Off (RO) to 4.2 ± 2.6%. On average, this level of ventilation was slightly increased during the Sustained Phase (SP), where breathing frequency measured 13.6 ± 2.9%. Importantly, each of these responses was comparable to outcomes from control AMPK-α1/α2 Flx mice described in Chapter 3.

10min exposures – controls Comparable breathing frequencies between control genotypes were also obtained during more prolonged 10min

exposures to hypoxia (Figure 8.2 Ai). Measures taken at each full minute of hypoxia showed that breathing frequencies of PNMT Cre mice during severe hypoxia were increased relative to normoxia to a level that was comparable to AMPK-α1/α2 Flx mice at each time point measured (Figure 8.2 A; at 1min: 19.1 ± 2.7%; at 5min: 13.6 ± 2.9%; at 10min: 11.1 ± 3.4%).

Effect of AMPK deletion during 5min exposures PNMT AMPK-α1/α2 dKO mice (n = 32 exposures from 8 mice) also responded with robust increases in breathing frequency during the Augmenting phase of 5min exposures to severe hypoxia (8% O_2, 64.2 ± 3.4% relative to normoxia), which were comparable to the responses of both AMPK-α1/α2 Flx and PNMT Cre mice. However, breathing frequencies of PNMT AMPK-α1/α2 dKO mice remained slightly elevated at a level that was significantly increased relative to PNMT Cre mice during RO (20.5 ± 3.8%, $p<0.05$ relative to PNMT Cre, not significant relative to AMPK-α1/α2 Flx), and relative to AMPK-α1/α2 Flx mice during the SP (25.8 ± 4.4%, not significant relative to PNMT Cre, $p<0.05$ relative to AMPK-α1/α2 Flx).

Effect of AMPK deletion during 10min exposures Analyses of breathing frequencies at each full minute of hypoxia revealed that PNMT AMPK-α1/α2 dKO mice displayed, on average, an augmentation of breathing frequency relative to both AMPK-α1/α2 Flx and PNMT Cre mice at each time point measured. However, this only became statistically significant during the fifth minute of hypoxia relative to AMPK-α1/α2 Flx mice (at 1min: 29.3 ± 3.4%, not significant relative to either control; at 5min: 25.9 ± 4.4%, $p<0.05$ relative to AMPK-α1/α2 Flx, not significant relative to PNMT Cre; at 10min: 15.1 ± 3.2%, not significant relative to either control). Given this on average augmented response in PNMT AMPK-α1/α2 dKO mice relative to either control, the entire 10min exposure was also analysed as a whole. This showed that the breathing frequency was significantly augmented in PNMT AMPK-α1/α2 dKO mice (Figure 8.2 Aii; 23.4 ± 1.6%) relative to both PNMT Cre mice (13.4 ± 0.9%; $p<0.0001$) and AMPK-α1/α2 Flx mice (13.9 ± 1.9%; $p<0.001$).

Therefore, changes in breathing frequencies of PNMT AMPK-α1/α2 dKO mice during severe hypoxia were in marked contrast to those observed in

TH AMPK-α1/α2 dKO mice, which exhibited significant attenuations of breathing frequency relative to controls during both 5min and 10min exposures to severe hypoxia (see Chapter 3). By contrast, PNMT AMPK-α1/α2 dKO mice retained a hyperventilatory phenotype and did not show any signs of a ventilatory deficit. In fact, it appeared as if deletion of AMPK in adrenergic cells augmented breathing frequencies relative to controls.

Therefore, the opposite effects of AMPK-α1 and -α2 catalytic subunit deletion in catecholaminergic cells compared to only adrenergic cells indicate that AMPK-dependent modulations of noradrenergic signalling pathways protect from hypoventilation by supporting hypoxia-induced increases in ventilatory frequency, whereas AMPK-dependent modulations of adrenergic signalling pathways appear to provide a mild inhibitory input to the central pattern generators that reduces ventilatory frequency during hypoxia. These reductions may help to reduce the degree of respiratory alkalosis that occurs through hypoxia-induced hyperventilation (Foster *et al.*, 2001).

8.2.2.2 Tidal volume

5min exposures – controls In marked contrast to the hypoxia-induced increases in breathing frequency, only marginal changes in tidal volume were observed. During severe hypoxia (Figure 8.1 Biii), measurements for tidal volume of PNMT Cre mice were -2.7 ± 2.4% relative to normoxia during the Augmenting phase, 4.5 ± 2.4% during RO, and -3.3 ± 1.7% during the SP. Importantly, these values were similar to those obtained in AMPK-α1/α2 Flx mice at each point measured.

10min exposures – controls During slightly longer exposures to hypoxia, tidal volume of control PNMT Cre mice was also slightly attenuated relative to normoxia and showed a mild reduction over time, which was comparable to AMPK-α1/α2 Flx mice at every time point measured (Figure 8.2 Bi; at 1min: 6 ± 2.1%; at 5min: -3.3 ± 1.7%; at 10min: -5.4 ± 1.9%).

Effect of AMPK deletion during 5min exposures Compared to both controls, highly similar outcomes for tidal volume in response to hypoxia were observed in PNMT AMPK-α1/α2 dKO mice, measuring (relative to normoxia) -0.9 ± 2.6% during the Augmenting phase, 3.1 ± 2.5% for RO, and -0.3 ± 1.9% during the SP (not significant compared to either control at any point).

Effect of AMPK deletion during 10min exposures Changes in tidal volume of PNMT AMPK-α1/α2 dKO mice measured at each full minute of hypoxia were minimal compared to normoxia and did not differ significantly from the changes in tidal volume observed in either cohort of control mice (at 1min: 6.3 ± 2.5%; at 5min: -0.2 ± 1.9%; at 10min: -0.5 ± 2.2%; not significant compared to either control at any time point). However, when considering the entire 10min exposure as a whole, the smaller reduction of tidal volume relative to normoxia in PNMT AMPK-α1/α2 dKO mice translated into a significantly attenuated change (i.e. reduction) in tidal volume relative to AMPK-α1/α2 Flx mice (Figure 8.2 Bii; PNMT AMPK-α1/α2 dKO: 0.4 ± 0.7%; AMPK-α1/α2 Flx: -2.9 ± 1%, $p<0.01$; PNMT Cre: -1.3 ± 1%, not significant).

Therefore, the minimal changes in tidal volume of PNMT AMPK-α1/α2 dKO mice during severe hypoxia were once again in marked contrast to those observed in TH AMPK-α1/α2 dKO mice, which exhibited significant attenuations of tidal volume relative to normoxia and controls during 5min and 10min exposures to severe hypoxia. By contrast, PNMT AMPK-α1/α2 dKO mice exhibited minimal reductions in tidal volume relative to normoxia that only on the whole were augmented relative to controls.

Therefore, AMPK-dependent modulation of noradrenergic signalling pathways also supports the HVR through maintenance of tidal volume, whereas AMPK-dependent modulation of adrenergic signalling pathways does not appear to make a significant contribution to the changes in tidal volume in response to hypoxia.

8.2.2.3 Minute ventilation

5min exposures – controls Adjustments of minute ventilation in PNMT Cre mice followed a similar trend to breathing frequency. During hypoxia (Figure 8.1 Ciii), control PNMT Cre mice responded similar to control AMPK-α1/α2 Flx mice by increasing minute ventilation to 60.6 ± 6.6% relative to normoxia during the Augmenting phase, which then declined to 7.7 ± 3.2% during RO and 8.8 ± 3.3% for the SP (not significant relative to AMPK-α1/α2 Flx at any point).

10min exposures – controls Not surprisingly perhaps, given the 10min outcomes for breathing frequency and tidal volume during hypoxia described above, minute ventilation of control PNMT Cre mice was increased relative to normoxia and similar to control AMPK-α1/α2 Flx mice at each time point measured during 10min exposures to hypoxia (Figure 8.2 Ci; at 1min: 25.3 ± 3.3%; at 5min: 8.8 ± 3.3%; at 10min: 4.1 ± 3.7%, not significant at any point).

Effect of AMPK deletion during 5min exposures Relative to controls, measurements of minute ventilation in PNMT AMPK-α1/α2 dKO mice during hypoxia were highly comparable to both PNMT Cre and AMPK-α1/α2 Flx mice during the Augmenting phase (61.6 ± 5.4%, not significant relative to either control). However, despite not reaching statistical significance, PNMT AMPK-α1/α2 dKO mice displayed a reduced ventilatory decline that lead to higher averages of minute ventilation during RO (22.9 ± 4.9%, $p=0.17$ relative to PNMT Cre and $p=0.27$ relative to AMPK-α1/α2 Flx) and the SP (24.2 ± 4.7%, $p=0.16$ relative to PNMT Cre and $p=0.09$ relative to AMPK-α1/α2 Flx).

Effect of AMPK deletion during 10min exposures In addition to the findings described above, the changes in minute ventilation of PNMT AMPK-α1/α2 dKO mice were, on average, augmented relative to both controls at every time point measured throughout 10min exposures to 8% O_2. However, this only reached significance relative to AMPK-α1/α2 Flx mice alone during the fifth and ninth minute of hypoxia (at 1min: 36.4 ± 4.6%, not significant relative to either control; at 5min: 24.4 ± 4.7%, $p<0.05$ relative to AMPK-α1/α2 Flx,

not significant relative to PNMT Cre; at 9min: 17.1 ± 4.5%, $p<0.05$ relative to AMPK-α1/α2 Flx, not significant relative to PNMT Cre; at 10min: 14.9 ± 4.1%, not significant relative to either control). Nevertheless, as might be expected, considering the 10min exposure as a whole revealed a significantly augmented minute ventilation in PNMT AMPK-α1/α2 dKO mice (Figure 8.2 Cii; 22.8 ± 2.2%) relative to both PNMT Cre mice (10.9 ± 1.9%; $p<0.0001$) and AMPK-α1/α2 Flx mice (10.3 ± 3%; $p<0.0001$).

Overall, the outcomes for breathing frequency and tidal volume of PNMT AMPK-α1/α2 dKO mice during severe hypoxia translated into changes of minute ventilation that were again in marked contrast to those observed in TH AMPK-α1/α2 dKO mice, which exhibited significant attenuations of minute ventilation relative to controls during 5min and throughout 10min exposures. By contrast, PNMT AMPK-α1/α2 dKO mice retained a breathing frequency-driven hyperventilatory phenotype and did not show signs of a ventilatory deficit at any point. Instead, deletion of AMPK in adrenergic cells appeared to augment the HVR relative to controls. Therefore, AMPK-α1 and -α2 catalytic subunit deletion in adrenergic cells did not contribute the ventilatory deficit observed in TH AMPK-α1/α2 dKO mice in response to severe hypoxia, which in light of these findings was most likely precipitated by loss of AMPK-dependent signalling pathways in the noradrenergic subset of catecholaminergic cells. Accordingly, these findings are in agreement with and further support the conclusions drawn in Chapter 4, which predicted the location of a hypoxia-responsive neuronal circuit within the noradrenergic population of catecholaminergic cells that supports the HVR via AMPK-dependent pathways.

Thus, whereas AMPK-dependent modulation of noradrenergic signalling pathways lead to increases in the ventilatory drive that shape the classical HVR, AMPK-dependent modulations of adrenergic signalling pathways may provide an inhibitory input to the central pattern generators during hypoxia that aim to protect from hyperventilation-induced hypocapnia (respiratory alkalosis) (Foster *et al.*, 2001; Basting *et al.*, 2015).

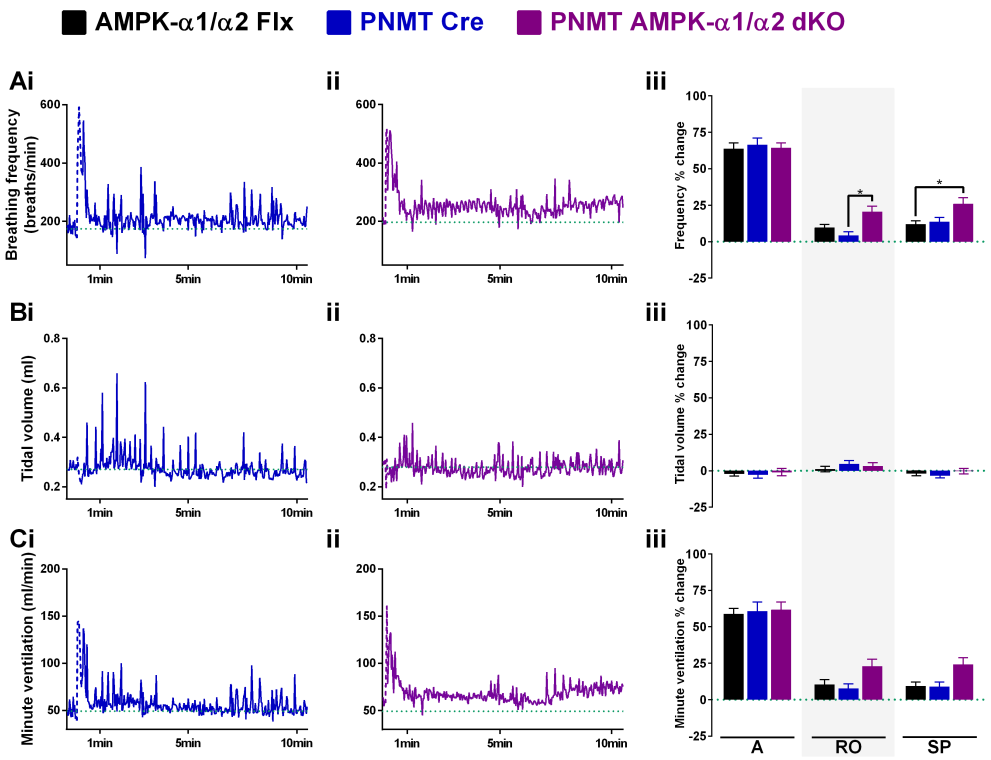

Figure 8.1: AMPK-α1/α2 catalytic subunit deletion in adrenergic cells augments the hypoxic ventilatory response to 5min exposures of severe hypoxia through increases in breathing frequency.

Left and middle panels show raw example records of breathing **(A)** frequencies (breaths/min), **(B)** tidal volume (ml) and **(C)** minute ventilation (ml/min) during 10 minute exposures to severe hypoxia (8% O_2) from **(i)** a mouse expressing Cre under the Phenylethanolamine N-methyltransferase reporter (PNMT Cre) and **(ii)** a PNMT-driven AMPK-α1 and -α2 double knockout (PNMT AMPK-α1/α2 dKO) mouse with a 2s sampling frequency. Dotted green lines indicate pre-hypoxic baseline frequency, dashed lines the artefacts induced by gas exchange. Right panels **(iii)** show means ± SEM for percentage changes of minute ventilation during the peak of the augmenting phase (A, approximately 30s), the nadir of the Roll-Off (RO, approximately 100s), and the plateau of the sustained phase (SP, at 300s) of the HVR in AMPK-α1 and -α2 floxed mice (AMPK-α1/α2 Flx, black, n = 54 exposures from 21 mice), PNMT Cre mice (blue, n = 32 exposures from 8 mice) and PNMT AMPK-α1/α2 dKO mice (purple, n = 32 exposures from 8 mice). * = $p<0.05$. Significance tested by two-way ANOVA with Sidak post-hoc tests.

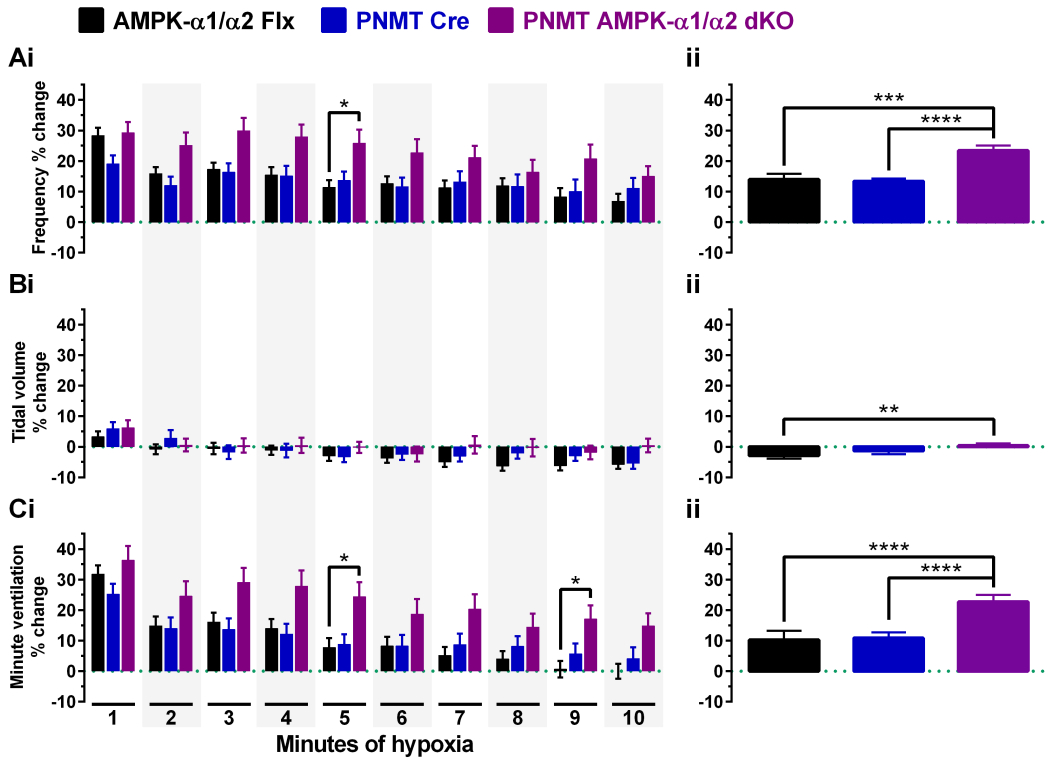

Figure 8.2: AMPK-α1/α2 catalytic subunit deletion in adrenergic cells augments the hypoxic ventilatory response to 10min exposures of severe hypoxia.

Means ± SEM for percentage changes relative to normoxia (green dotted line) of **(A)** breathing frequency (breaths/min), **(B)** tidal volume (ml), and **(C)** minute ventilation (ml/min) during **(i)** every 60s of and **(ii)** the entirety of 10 minute exposures to severe hypoxia (8% O_2) in AMPK-α1 and -α2 floxed mice (AMPK-α1/α2 Flx, black, n = 58 exposures from 21 mice), mice expressing Cre under the Phenylethanolamine N-methyltransferase reporter (PNMT Cre, blue, n = 32 exposures from 8 mice) and PNMT-driven AMPK-α1 and -α2 double knockout mice (PNMT AMPK-α1/α2 dKO, purple, n = 32 exposures from 8 mice) measured at each full minute of hypoxia. * = $p<0.05$, ** = $p<0.01$. Significance tested by two-way ANOVA with Sidak post-hoc tests.

8.2.3 AMPK deletion in adrenergic cells increases ventilatory stability throughout 10min exposures to hypoxia

Given the augmented hypoxic ventilatory phenotype of PNMT AMPK-α1/α2 dKO mice relative to controls it was of interest to further assess and compare the overall breathing regularity and hence stability during 10min exposures to severe hypoxia. As before, this was achieved by plotting each inter-breath interval (BBn) against each subsequent inter-breath interval (BBn+1) for PNMT Cre and PNMT AMPK-α1/α2 dKO mice.

Example plots from single 10min exposures are shown in Figure 8.3 A, which compare the inter-breath intervals of a control (blue) and knockout (purple) mouse during 8% hypoxia. It is quite clear that control PNMT Cre mice had a regular breathing pattern with some apnoeas, evident through increases in inter-breath interval. In comparison, it appeared that apnoeas were slightly less prevalent in PNMT AMPK-α1/α2 dKO mice, indicated by the smaller and possibly fewer increases in the inter-breath intervals. These outcomes were further analysed by comparing the standard deviations (SD) of BBn and BBn+1.

Ventilatory stability of controls Minute-by-minute analyses revealed that increases in the SD of the breathing pattern in control PNMT Cre mice (n = 32 exposures from 8 mice) were most prevalent during the second and third minutes of hypoxia (Figure 8.3 B; at 0-1min: 69.5 ± 3.4ms; at 1-2min: 104.2 ± 4.4ms; at 2-3min: 97.5 ± 8.7ms). Thereafter, breathing became more regular again and the SD declined back to the level observed during the first minute of hypoxia, which then remained constant throughout the remainder of the exposure (at 3-4min: 74.6 ± 4ms; at 5-6min: 72.4 ± 4.5ms; at 9-10min: 70.7 ± 3.6ms). Importantly, these time-dependent changes are similar to observations from control AMPK-α1/α2 Flx mice (see Chapter 5).

Ventilatory stability of knockouts Consistent with the observations from the plots described above, the breathing pattern of PNMT AMPK-α1/α2 dKO mice (n = 32 exposures from 8 mice) did indeed exhibit a less variable SD of the inter-breath intervals relative to controls during the first three minutes of hypoxia (at 0-1min: 52.1 ± 2.6ms, $p<0.05$; at 1-2min: 75.8 ± 3.8ms, $p<0.0001$; at 2-3min: 67.5 ± 4.3ms, $p<0.0001$) of 10min exposures.

Thereafter, the SD of PNMT AMPK-α1/α2 dKO mice was on average slightly lower but statistically comparable to control PNMT Cre mice for the remainder of the exposure (at 3-4min: 59.9 ± 3.4ms; at 5-6min: 63 ± 4.1ms; at 9-10min: 63.8 ± 3.8ms; not significant relative to PNMT Cre mice at any time point).

From these plots it was apparent that loss of AMPK-α1 and -α2 subunits in adrenergic cells did not precipitate increases in breathing irregularities, which is in stark contrast to the results obtained following AMPK deletion in all catecholaminergic cells, inclusive of the adrenergic population. In fact, adrenergic AMPK deletion appeared to do the opposite and stabilised breathing patterns during the first few minutes of hypoxia by reducing variabilities within the inter-breath intervals (see also Appendix4.2).

Therefore, AMPK-dependent modulations of noradrenergic signalling pathways seem to support ventilatory stability during periods of increased hypoxia-induced ventilatory drive, whereas the earlier suggested inhibitory input from AMPK-dependent modulations of adrenergic signalling pathways likely leads to disruptions of ventilatory rhythmicity at the beginning of the hypoxic exposure, possibly until respiratory drive from the carotid bodies and mild respiratory inhibition through silencing of the RTN may have reached an equilibrium of hyperventilation and protection from respiratory alkalosis.

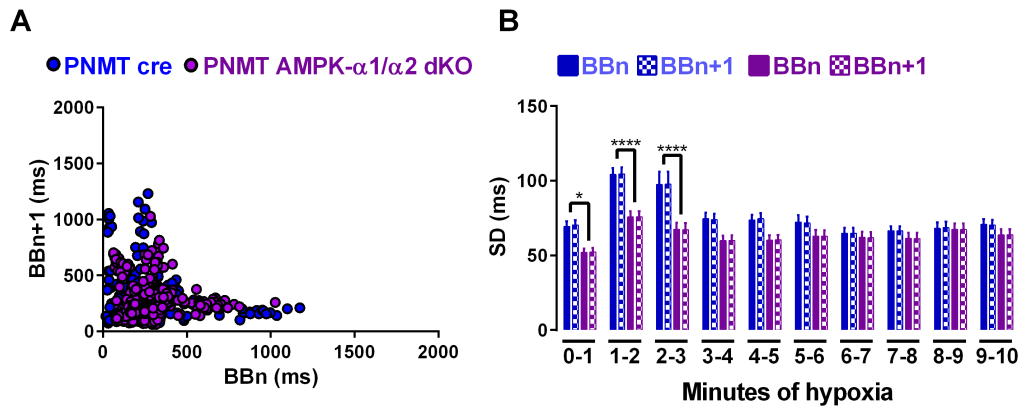

Figure 8.3: Mice with deletion of AMPK-α1/α2 catalytic subunits in adrenergic cells exhibit reduced breathing variability.

(A) Example Poincaré plots show the inter-breath interval (BBn) versus the subsequent interval (BBn+1) of mice expressing Cre under the Phenylethanolamine N-methyltransferase reporter (PNMT Cre, blue) and PNMT-driven AMPK-α1 and -α2 double knockout mice (PNMT AMPK-α1/α2 dKO, purple) mice during 10min exposures to severe hypoxia (8% O_2). **(B)** Means ± SEM of the standard deviation (SD) of BBn and BBn+1 for PNMT Cre mice (n = 32 exposures from 8 mice) and PNMT AMPK-α1/α2 dKO mice (n = 32 exposures from 8 mice) for 1min averages of 10min exposures to hypoxia. * = $p<0.05$, **** = $p<0.0001$. Significance tested by two-way ANOVA with Sidak post-hoc tests.

8.2.4 AMPK deletion in adrenergic cells reduces apnoeas throughout 10min exposures to hypoxia

The above described augmentation of ventilation and the reduction in breathing variability during hypoxia opened the possibility that deletion of AMPK-α1 and -α2 subunits in adrenergic cells may also have an effect on the number of apnoeas during 10min exposures to hypoxia. Accordingly, the apnoeic phenotype of control PNMT Cre PNMT AMPK-α1/α2 dKO mice was assessed.

8.2.4.1 Apnoeic index

Control mice When exposed to 10min of 8% O_2, control PNMT Cre mice presented with apnoeas at a frequency of 2.7 ± 0.3 apnoeas/min (n = 32 exposures from 8 mice) for the first, and 1.6 ± 0.2 apnoeas/min for the second 5min of hypoxia (Figure 8.4 Ai), which was comparable to the number of apnoeas observed in AMPK-α1/α2 Flx mice. Furthermore, a time-dependent decline in apnoea frequency was observed in PNMT Cre mice during minute-by-minute analyses of apnoea frequency, which measured 3.3 ± 0.4 apnoeas/min by 1-2min, 1.8 ± 0.3 apnoeas/min by 5-6min, and 1.9 ± 0.3 apnoeas/min by 9-10min (Figure 8.4 Aii). This reduction in apnoea frequency over time was entirely consistent with outcomes observed in AMPK-α1/α2 Flx mice at each time point measured.

Effect of AMPK deletion on apnoea frequency Interestingly, the apnoea frequency measured in PNMT AMPK-α1/α2 dKO mice (n = 32 exposures from 8 mice) was, on average, lower during the first half of hypoxia compared to both controls (1.9 ± 0.3 apnoeas/min) and reached significance relative to AMPK-α1/α2 Flx mice ($p<0.01$). During the second half of hypoxia, only a minor reduction in the apnoea frequency was observed in PNMT AMPK-α1/α2 dKO mice relative to the first half, measuring 1.2 ± 0.2 apnoeas/min. As just stated above, both controls exhibited a higher number of apnoeas during the first half of hypoxia. However, a pronounced decrease over time in controls and a minor decrease in PNMT AMPK-α1/α2 dKO mice

over time meant that during the second half of 10min exposures, the average numbers of apnoeas were comparable between the three genotypes.

However, an on average reduced apnoeic frequency relative to controls was still apparent throughout the 10min exposure, but this became only significant during the second and third minute of hypoxia (apnoeas/min – at 1-2min: 1.8 ± 0.4, $p<0.0001$ compared to AMPK-α1/α2 Flx, $p<0.01$ compared to PNMT Cre; at 2-3min: 2.5 ± 0.4, $p<0.05$ compared to PNMT Cre only; at 5-6min: 1.5 ± 0.2, not significant relative to either control; at 9-10min: 1.3 ± 0.2, not significant relative to either control). Despite exhibiting an attenuated number of apnoeas per minute relative to controls, PNMT AMPK-α1/α2 dKO mice still presented with a time-dependent decrease of the apnoeic index following a peak at 2-3min. However, given the already low number of apnoeas at the beginning of the exposure, this decrease was not as pronounced as it was for AMPK-α1/α2 Flx or PNMT Cre mice.

Overall, the effect of PNMT-driven deletion of AMPK is once again entirely opposite to the effect of TH-driven deletion of AMPK. Whereas TH AMPK-α1/α2 dKO mice exhibited marked and sustained increases in the apnoeic index relative to controls throughout exposures to severe hypoxia (see Chapter 5), PNMT AMPK-α1/α2 dKO mice presented with a slight reduction in the number of apnoeas relative to controls. Moreover, while the time-dependent decline of apnoea frequency was absent in TH AMPK-α1/α2 dKO mice, it was retained in PNMT AMPK-α1/α2 dKO mice. Therefore, AMPK-dependent modulation of noradrenergic signalling pathways appears to protect from apnoeas during hypoxia, whereas AMPK-dependent adrenergic signalling pathways may indirectly contribute to the generation of apnoeas.

8.2.4.2 Apnoea duration

Control mice The durations of apnoeas for PNMT Cre mice in response to 8% O_2 were fairly stable during both halves of 10min exposures to hypoxia (Figure 8.4 Bi; 834.3 ± 21.8ms and 781 ± 15.8ms, respectively). However,

apnoea durations were significantly shorter in PNMT Cre mice compared to AMPK-α1/α2 Flx mice during the first half of 10min exposures ($p<0.05$). Thereafter, the second half of hypoxia was comparable between the two control groups. Considering the average durations of apnoeas during each minute of hypoxia revealed minimal changes over time (Figure 8.4 Bii; at 1-2min: 850 ± 24.5ms; at 4-5min: 825.9 ± 30.8ms; at 9-10min: 798.1 ± 41.7ms). Each of these values was generally comparable to apnoea durations of AMPK-α1/α2 Flx mice, yet a significantly lower apnoea duration in PNMT Cre mice was observed during the fourth minute of hypoxia ($p<0.05$).

Effect of AMPK deletion on apnoea duration Like controls, apnoea durations of PNMT AMPK-α1/α2 dKO mice were significantly lower compared to AMPK-α1/α2 Flx mice during the first half of 8% O_2 (0-5min: 778.7 ± 35.7ms, $p<0.05$), but comparable to PNMT Cre mice. Furthermore, apnoea durations of PNMT AMPK-α1/α2 dKO mice remained stable during the second half of hypoxia (5-10min: 799.7 ± 27.5ms), during which period the durations were similar across all three genotypes. Closer analyses of the durations for each minute revealed that apnoeas were indeed stable throughout the 10min exposures (at 1-2min: 819.4 ± 52.5ms; at 4-5min: 760.4 ± 27.4ms; at 9-10min: 853.4 ± 43.8ms), and significant differences relative to controls were only found during the third (750.8 ± 24.6ms, $p<0.05$ relative to AMPK-α1/α2 Flx, $p<0.05$ relative to PNMT Cre), fourth (719.6 ± 25.5ms, $p<0.05$ relative to AMPK-α1/α2 Flx only), and fifth (760.4 ± 27.4ms, $p<0.05$ relative to AMPK-α1/α2 Flx only) minute of hypoxia.

Therefore, PNMT-driven deletion of AMPK did not appear to have a major effect on the overall duration of apnoeas relative to controls. However, minor differences between PNMT AMPK-α1/α2 dKO mice and controls did occasionally occur, where the average apnoea duration in knockouts was significantly decreased. Once again, this is entirely opposite to the effect of AMPK deletion in TH-positive cells, where apnoea durations were augmented relative to controls throughout the exposure to hypoxia. This suggests that AMPK-dependent modulation of noradrenergic signalling pathways may protect from apnoea prolongation during hypoxia by

re-initiating inspiration and hence terminating an apnoea, whereas AMPK-dependent modulations of adrenergic signalling pathways may indirectly contribute to the prolongation of apnoeas at the onset of the hypoxic exposure.

8.2.4.3 Apnoea duration index

Control mice Given the reduction of apnoea frequency over time with stable apnoea durations, it was not surprising that the apnoea-duration index (ADI) of PNMT Cre mice followed similar time-dependent changes to the apnoeic index. During the first half of hypoxia, the ADI measured 2.3 ± 0.3, which declined to 1.3 ± 0.2 during the second half of 10min exposures (Figure 8.4 Ci). Moreover, like apnoea frequency, the ADI of PNMT Cre mice was comparable to that of AMPK-α1/α2 Flx mice. A time-dependent decrease of the ADI driven by reductions in apnoea frequency was also observed during more detailed analyses of 10min exposures of hypoxia. In that respect, the ADI of PNMT Cre mice measured 2.8 ± 0.4 by 1-2min, 1.5 ± 0.2 by 5-6min, and 1.6 ± 0.3 by 9-10min (Figure 8.4 Cii). Importantly, each of these time points was comparable to the ADI of AMPK-α1/α2 Flx mice, even though the average ADI was often lower in PNMT Cre mice.

Effect of AMPK deletion on the apnoea duration index The outcomes for apnoea frequency and duration of PNMT AMPK-α1/α2 dKO mice translated into an ADI that was comparable to PNMT Cre during the first half of hypoxia, but significantly attenuated relative to AMPK-α1/α2 Flx mice (0-5min: 1.5 ± 0.2, $p<0.0001$). During the second half of 10min exposures, however, the ADI was once again comparable across the three genotypes (5-10min: 1 ± 0.1, not significant relative to either control). Minute-by-minute analyses revealed that attenuations of apnoea frequency and duration translated into a reduction of the ADI in PNMT AMPK-α1/α2 dKO mice relative to controls, which was significant during the second (1.4 ± 0.3, $p<0.0001$ relative to AMPK-α1/α2 Flx, $p<0.01$ relative to PNMT Cre), third (1.9 ± 0.3, $p<0.01$ relative to AMPK-α1/α2 Flx, $p<0.01$ relative to PNMT Cre), and fourth (1.3 ± 0.3, $p<0.01$ relative to AMPK-α1/α2 Flx, not significant relative to PNMT Cre)

minute of 8% O_2. In addition, following a peak at 2-3min of hypoxia, PNMT AMPK-α1/α2 dKO mice exhibited a time-dependent and apnoea frequency-driven decrease of the ADI, which apart from the third minute was comparable to both controls (5-6min: 1.2 ± 0.2; 7-8min: 0.9 ± 0.2; 9-10min: 1.1 ± 0.2).

Overall, PNMT-driven deletion of AMPK-α1 and -α2 subunits reduced the ADI relative to controls during 10min exposures to severe hypoxia (8% O_2). These findings are opposite to the effect of TH-driven AMPK deletion, which significantly increased the ADI relative to controls throughout the duration of the 10min exposure. Moreover, while a time-dependent decline of ADI was absent in TH AMPK-α1/α2 dKO mice, it was retained in PNMT AMPK-α1/α2 dKO mice. Therefore, AMPK-dependent modulations of noradrenergic signalling pathways protect from apnoeas during hypoxia, likely by supporting the generation of respiratory rhythm and re-initiation of inspiration during apnoea. By contrast, AMPK-dependent modulations of adrenergic signalling pathways may limit and indirectly periodically inhibit respiration in response to respiratory alkalosis triggered by hypoxic hyperventilation, and thus aid to restore CO_2 levels in the most rapid and efficient way (Basting *et al.*, 2015).

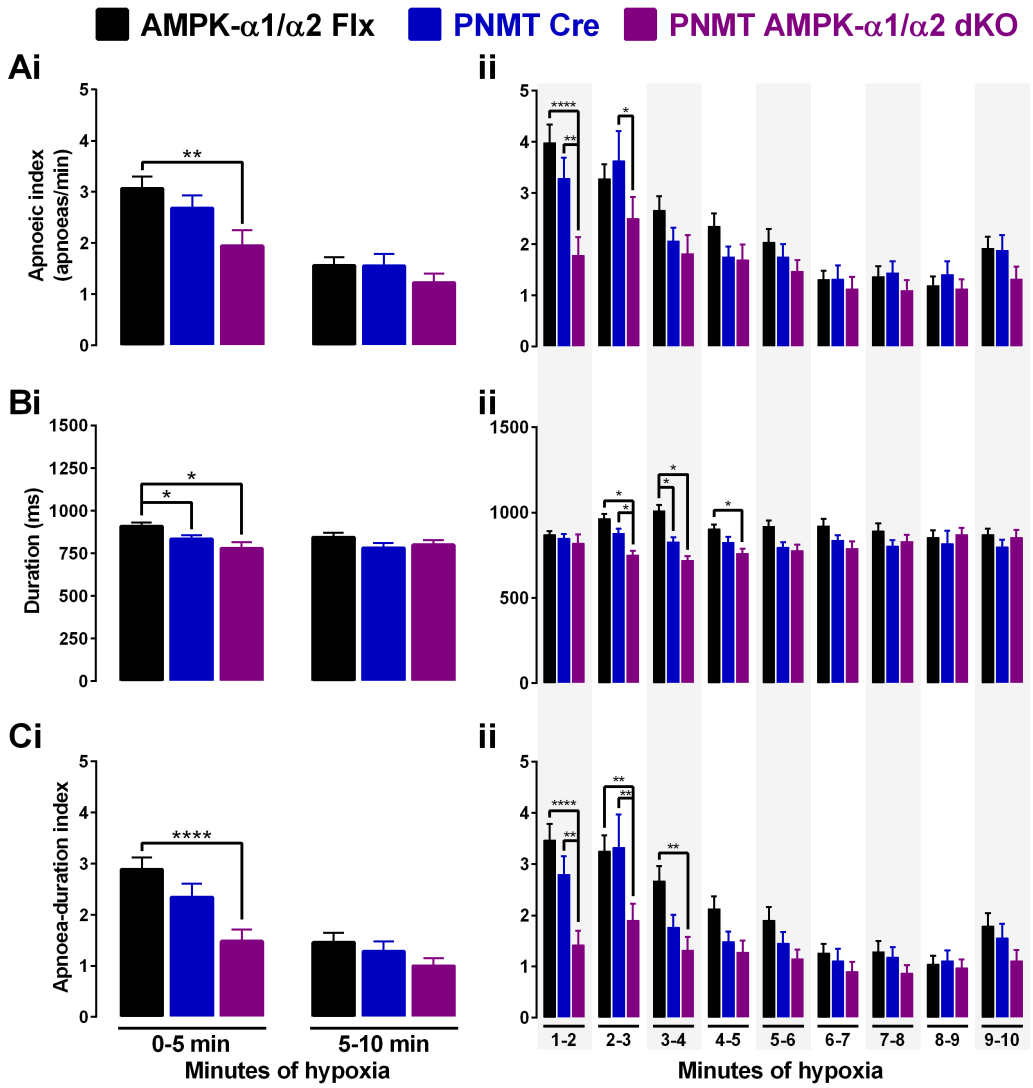

Figure 8.4: AMPK deletion in adrenergic cells reduces apnoeas during 10min exposures to severe hypoxia.

Means ± SEM for the **(A)** apnoeic index (apnoeas/min), **(B)** apnoea duration (ms), and **(C)** apnoea-duration index during **(i)** the first and second half and **(ii)** for every 60 seconds of 10 minute exposures to severe hypoxia (8% O_2) in AMPK-α1 and -α2 floxed mice (AMPK-α1/α2 Flx, black, n = 58 exposures from 25 mice), mice expressing Cre under the Phenylethanolamine N-methyltransferase reporter (PNMT Cre, blue, n = 32 exposures from 8 mice) and PNMT-driven AMPK-α1 and -α2 double knockout mice (PNMT AMPK-α1/α2 dKO, purple, n = 32 exposures from 8 mice). * = p<0.05, ** = p<0.01, **** = p<0.0001. Significance tested by two-way ANOVA with Sidak post-hoc tests for apnoeic index and apnoea-duration index, and multiple t-tests with Holm-Sidak post-hoc for apnoea duration.

8.3 Discussion

8.3.1 Summary of findings

Chapter 8 shows that AMPK activity within the adrenergic subset of catecholaminergic cells exerts completely opposing effects to the combined effect of all catecholaminergic cells regarding the respiratory response to hypoxia. Whereas loss of AMPK activity in all catecholaminergic cells precipitated severe hypoventilation, ventilatory instability and significant increases in the apnoeic phenotype, deletion of AMPK-α1 and -α2 catalytic subunits in the adrenergic subset of catecholaminergic cells mildly augmented the HVR, stabilised respiratory rhythmicity at the beginning of the hypoxic exposure, and mildly attenuated the apnoeic phenotype. Therefore, these findings are in complete contrast to those obtained in Chapter 3, and clearly point towards differential roles of noradrenergic and adrenergic input in the regulation of the HVR and thus the maintenance of whole-body O_2 supply.

8.3.2 AMPK activity in brainstem adrenergic cells likely protects from respiratory alkalosis during hypoxia-induced hyperventilation

Firstly, the ventilatory responses of control PNMT Cre mice were comparable to those of control AMPK-α1/α2 Flx mice. This shows that if any CD1 background strain-specific responses of the HVR remained after the back-crosses, then these were minimal and did not differ significantly from the inbred C57Bl6 background (see also Appendices 5.1 to 5.8). Therefore, outcomes obtained from PNMT AMPK-α1/α2 dKO mice could be reliably compared to both controls.

Strikingly, and in stark contrast to the HVR of TH AMPK-α1/α2 dKO mice, each component of the HVR of PNMT AMPK-α1/α2 dKO mice was augmented relative to controls. This was surprising at first, given that the adrenergic and thus PNMT Cre positive ventrolateral C1 neurons have been proposed to form an integral part of the neural circuit that drives increases in breathing frequency during hypoxia in mice and rats (Abbott *et al.*, 2013;

Burke *et al.*, 2014). Instead, the augmentation of the ventilatory responses to hypoxia following AMPK deletion in adrenergic cells was suggestive of the provision of an AMPK-dependent inhibitory input from the C1 and/or C2 neurons to the rCPGs. Given that AMPK deletion in all catecholaminergic cell types precipitated severe hypoventilation, this strongly suggests that noradrenergic signalling inputs act to increase ventilation to a degree that could quickly lead to reductions in central PCO_2 levels and thus respiratory alkalosis (Foster *et al.*, 2001). It seems quite plausible, therefore, that AMPK-dependent adrenergic inputs might act to limit the degree of hyperventilation and thus protect from severe hypocapnia. Respiratory alkalosis silences neurons of the RTN, and a role of C1 neurons in this pathway could not be excluded (Basting *et al.*, 2015). Thus, the possibility remains that silencing of the RTN could be mediated by AMPK-dependent release of inhibitory neuropeptides (such as enkephalin or neuropeptide Y) or signalling pathways involving GABAergic interneurons incorporating, at the very least, ventral adrenergic C1 neurons that are known to express inhibitory neurotransmitter (Stornetta *et al.*, 1999; Pilowsky *et al.*, 2008) and could therefore oppose hypoxia-induced respiratory alkalosis.

In this regard, it would also be interesting to determine whether selective deletion of AMPK in only noradrenergic cells would further exacerbate the ventilatory deficit observed in TH AMPK-α1/α2 dKO mice. If so, then such findings would provide additional, strong support for the predicted location of the hypoxia-responsive neuronal circuit called DAR (see Chapter 4) within the noradrenergic population of catecholaminergic cells that supports, in a manner dependent upon the expression of AMPK, the degree of the HVR.

Currently, the possibility remains that the DAR may encompass the adrenergic neuronal network to some extent, given the indication from our previous fMRI study that the DAR continues in Bregma that are rostral to the predicted boundaries of the noradrenergic neuronal network (Rinaman, 2011; Mahmoud *et al.*, 2016). However, if this was the case then clearly AMPK-dependent pathways in noradrenergic and adrenergic cells must act in concert but not in equal part, because noradrenergic ventilatory

stimulation must clearly outweigh adrenergic ventilatory inhibition during hypoxia.

Further indications of an inhibitory role of adrenergic inputs came from the fact that AMPK deletion decreased the variability of inter-breath intervals during the first three minutes of the hypoxic exposure. It is possible that during the Augmenting Phase of the HVR, respiratory drive from the carotid bodies and central hypoxia-responsive noradrenergic neurons may act in concert with a mild respiratory inhibition through silencing of the RTN in order to reach an equilibrium of optimal balance between O_2 intake through hyperventilation and protection from respiratory alkalosis. Consistent with this, AMPK deficiency in adrenergic cells appeared to reduce the frequency of apnoeas relative to controls at the beginning of the hypoxic exposure. Complete cessation of ventilation may thus be the most rapid and efficient way to restore central CO_2 levels during periods of intense respiratory effort (Dempsey, 2005). However, after approximately four minutes of hypoxia, which coincides with the Sustained Phase of the HVR, the balance of inspiratory drive from the carotid bodies and noradrenergic neurons, and inhibitory drive from the adrenergic neurons may keep hyperventilation and apnoea frequency at a level that maintains adequate CO_2 levels during periods of hypoxia. One question that remains is whether AMPK-dependent signalling pathways are the primary determinant of the increased frequency of spontaneous apnoeas observed in TH AMPK-α1/α2 dKO mice, or whether they impact on the duration of post-sigh apnoeas as well through modulation of inspiratory inhibition via vagal afferent input. However, vagal inhibition is received and interpreted by the caudal portion of noradrenergic cells (Kubin *et al.*, 2006), indicating that it is unlikely that rostral adrenergic cells contribute to the generation of post-sigh apnoeas.

8.3.3 Conclusion

In conclusion, it appears that AMPK-dependent signalling pathways within noradrenergic and adrenergic cells serve different roles in determining the ventilatory responses to hypoxia. While noradrenergic AMPK activity most likely prompts hyperventilation along with chemoafferent inputs from the

carotid bodies, activity of AMPK in adrenergic cells may instead limit the extent of respiratory frequency and protect from central hypocapnia and thus respiratory alkalosis. In this respect, adrenergic cells may induce ventilatory instability via increases in apnoea frequency during the Augmenting Phase of the HVR, which after a few minutes may normalise and reach an equilibrium with the ventilatory drive that come from the periphery and the caudal noradrenergic neurons. Overall, this delicate interplay may not only aim to restore and maintain whole-body O_2 supply, but may also protect from the hypocapnia-induced manifestation of 'pins and needles' in the extremities, chest discomfort, or light-headedness via reductions in cerebral blood flow that can lead to further tissue hypoxaemia (Madias & Adrogué, 2014).

8.3.4 Limitations and future directions

To date, the dual deletion of the AMPK-α1 and -α2 catalytic subunits in adrenergic cells has only been assumed following genotype analysis, which confirmed the presence of AMPK-α1$^{fl/fl}$, AMPK-α2$^{fl/fl}$, and PNMT Cre$^{+/-}$ alleles (Appendix 5.9). Unfortunately there is no homogeneous population of adrenergic cells within any tissue, but the adrenal medulla is reportedly made up of 50-98% adrenergic cells (Norris & Carr, 2013). Therefore, attempts have been made to use single cell laser microdissection in order to extract the nuclear content from individual nuclei of the adrenal medulla of PNMT Cre and PNMT AMPK-α1/α2 dKO mice. However, to this point the results have been inconclusive and could not definitively show that the AMPK-α1 and -α2 catalytic subunits have been successfully excised. Obtaining such evidence will be crucial in order to confirm the findings and support the conclusions drawn above. Nevertheless, laser microdissection of multiple adrenal medulla cells with subsequent RNA extraction and end-point qPCR indicated a reduced expression of the AMPK-α1 and -α2 catalytic subunits in PNMT AMPK-α1/α2 dKO mice relative to PNMT Cre controls (Appendix 5.10), which at the very least provides support for an AMPK knockdown. In any case, if AMPK deletion had not been achieved, a

significantly different ventilatory response to hypoxia relative to both controls would have been unlikely.

Further additional experiments on PNMT AMPK-α1/α2 dKO mice would be required to analyse the blood gas composition after 10min exposures to severe hypoxia in order to determine whether AMPK activity in adrenergic cells indeed protects from respiratory alkalosis. Moreover, analyses of the duty cycle would be beneficial to establish whether initiation of active expiration during hypoxia is mediated by glutamatergic signalling from noradrenergic, or indeed adrenergic cells, as was suggested in Chapter 6 (Fung *et al.*, 1994a; Fung *et al.*, 1994b; Stornetta *et al.*, 2002; Rinaman, 2011; DePuy *et al.*, 2013; Malheiros-Lima *et al.*, 2015).

As mentioned above, AMPK activity in adrenergic cells appeared to mildly increase the numbers of apnoeas. It was speculated that spontaneous apnoeas would be the main driver of the augmented apnoea index, due to the generation of post-sigh apnoeas via vagal inhibition of inspiration that terminates within the noradrenergic portion of catecholaminergic cells (see Chapter 5). Analyses of spontaneous versus post-sigh apnoeas would be required to corroborate or reject this hypothesis.

Another very important aspect of the response to hypoxia modulated by adrenergic neurons is that of the cardiovascular system. Ventrolateral C1 neurons have been heavily implicated in the control of the baroreflex, whereby the regulatory influence of the arterial baroreceptors activates bulbospinal C1 neurons, which then modulate arterial blood pressure and heart rate via vaso- and cardiomotor sympathetic efferents (Ross *et al.*, 1984; Dampney *et al.*, 2002; Guyenet, 2006; Guyenet *et al.*, 2013). Measurements of heart rate and blood pressure during exposures to hypoxia have been carried out by pulse oximetry and tail cuff, respectively, but results remained inconclusive. For both PNMT Cre and PNMT AMPK-α1/α2 dKO mice, the cardiovascular responses during hypoxia exhibited sometimes increases in blood pressure, sometimes decreases, and sometimes no response at all. Importantly, these outcomes were not sex-specific, as both male and female mice exhibited these variations between mice, as well as between exposures. Clearly a more sensitive

method of sampling blood pressure and heart rate is required, such as telemetry, in order to evaluate the effects of AMPK deletion in adrenergic cells on the cardiovascular system. However, given that no changes in heart rate or blood pressure during normoxia and hypoxia were identified upon AMPK deletion in all catecholaminergic cells (MacMillan & Evans, 2018), no adverse cardiovascular phenotype is currently expected in PNMT AMPK-α1/α2 dKO mice.

Chapter 9: General Discussion

9.1 Summary of findings

During periods of acute hypoxia, appropriate modulations of the drive to breathe are crucial in order to optimise O_2 uptake by increasing ventilation. Ventilatory drive is mediated by the respiratory central pattern generators (rCPGs) of the ventrolateral medulla, which are continuously modulated by specialised peripheral and central chemoreceptors to adjust ventilation according to changes in arterial PO_2, PCO_2, and pH levels. Regarding changes in arterial PO_2, catecholaminergic O_2-sensing cells of the carotid body and the brainstem are vital, as they are able to sense reductions in O_2 supply and trigger increases in ventilation. However, the underlying molecular mechanism(s) within O_2-sensing cells by which afferent output modulates respiratory adjustments during acute hypoxia still remain controversial. The findings presented in this thesis show that the ventilatory response to hypoxia requires the activity of AMPK within the central catecholaminergic neuronal network of the medulla oblongata, which likely forms a noradrenergic hypoxia-responsive neuronal circuit that integrates peripheral and central chemosensory information and determines – via projections to the rCPGs in the ventral medulla – the degree of ventilatory drive.

Initially, I set out to determine whether AMPK deficiency in catecholaminergic cells precipitates ventilatory deficits even during more prolonged exposures to acute hypoxia, or whether alternative AMPK-independent pathways would lead to an at least partial recovery of the HVR. By using the previously described mouse model of dual AMPK-α1 and -α2 catalytic subunit deletion targeted to catecholaminergic (tyrosine hydroxylase [TH]-expressing) cells (Mahmoud, 2014; Mahmoud *et al.*, 2016), I showed in Chapters 3, 5 and 6 that TH-driven AMPK-α1/α2 double knockout (dKO) mice were unable to recover ventilatory efforts and remained in a hypoventilatory state relative to normoxia, as well as relative to control AMPK-α1/α2 floxed (Flx) mice, for hypoxic durations that lasted up to an hour. Hypoventilation in TH AMPK-α1/α2 dKO mice was primarily driven by blocked active expiration and the inability to accelerate the movement of air in and out of the lungs during inspiration and expiration. In

addition, ventilatory instability was pronounced and retained throughout the exposure to hypoxia, which during more prolonged periods manifested as periodically oscillating “bursts” in the frequency of spontaneous apnoeas. Importantly, I have shown in Chapter 4 that the hypoxic ventilatory deficiencies of TH AMPK-α1/α2 dKO mice were not precipitated by loss of neuronal cell numbers or catecholaminergic neurotransmission *per se*, but rather resulted from a functional deficit subsequent to an attenuated neuronal activation within a specific area of the caudal dorsal brainstem. This area is likely to harbour a hypoxia-responsive neuronal circuit which, in an AMPK-dependent manner, may integrate and coordinate peripheral and central chemoafferent input with the modulation of the ventrolateral rCPGs and thus ventilation and O_2 supply at the level of the whole body. Moreover, the herein identified putative hypoxia-responsive neuronal circuit was consistent with the location of the DAR that was previously identified by fMRI, and proposed to be located within the noradrenergic population of brainstem catecholaminergic cells. Nevertheless, the possibility remains that this hypoxia-sensitive circuit may also encompass a subset of the adrenergic cell population.

In further support for a functional role of AMPK-dependent signalling pathways in specifically mediating the HVR, I showed in Chapter 7 that the cardiovascular responses to hypoxia were retained in TH AMPK-α1/α2 dKO mice. This was surprising, given that hypoxia appears to simultaneously activate the same neurons of the brainstem that subsequently determine the HVR and the cardiovascular response. Therefore, these findings may provide the first evidence of a separation of these two physiological responses in a manner that is determined by AMPK activity within central catecholaminergic neurons. In addition, Chapter 7 revealed that cardiorespiratory adjustments during hypoxic exposures were also unaffected by deletion of either AMPK-α1 or -α2 subunits targeted to arterial smooth muscle (SM) cells. The retention of a normal cardiorespiratory response to hypoxia in SM AMPK-α1 KO and SM AMPK-α2 KO mice thus further supported the conclusion that the ventilatory deficits observed in TH AMPK-α1/α2 dKO mice were precipitated by attenuations in neuronal

activity and function, rather than alterations in cerebral hypoxia-induced vasodilation and thus O_2 supply via the vasculature, or off-target effects via “leakage” of Cre.

Finally, in Chapter 8 my findings corroborated a role for AMPK activity within noradrenergic cells to deliver ventilatory drive, because when conditional dual deletion of AMPK-α1/α2 catalytic subunits was targeted to adrenergic (Phenylethanolamine N-methyltransferase [PNMT]-expressing) cells, an increased ventilatory phenotype during hypoxia relative to controls and stabilisation of ventilation subsequent to reductions in the apnoeic phenotype at the beginning of the hypoxic exposure were observed. Clearly, these outcomes were in stark contrast and completely opposite to the outcomes following deletion of AMPK-α1/α2 in all catecholaminergic cells. Therefore, it appeared that AMPK-dependent signalling pathways within the catecholaminergic network of the brainstem differentially modulate the HVR in noradrenergic and adrenergic cells, whereby it augments respiratory drive in the former, but mildly inhibits it in the latter.

9.2 The modulation of respiratory drive during hypoxia by AMPK activity within brainstem catecholaminergic cells

Within the majority of the scientific field, it is believed that the carotid body (CB) is the primary peripheral chemoreceptor which solely determines acute increases in ventilation during hypoxia through increased afferent discharge and modulation of the rCPGs via the catecholaminergic network of the dorsal brainstem (Guyenet, 2000; Prabhakar, 2000; Kumar, 2007; Guyenet, 2014). However, the responsiveness of central neurons to hypoxia has been suggested repeatedly over the decades (Dampney & Moon, 1980; Smith *et al.*, 1993; Sun & Reis, 1993; Curran *et al.*, 2000; Hill *et al.*, 2011) and a variety of mammalian animal studies have demonstrated that the HVR can be either partially or completely restored after either denervation or surgical removal of the CB (Davenport *et al.*, 1947; Miller & Tenney, 1975; Bisgard *et al.*, 1980; Martin-Body *et al.*, 1986; Daristotle *et al.*, 1991; Roux *et al.*, 2000a; Roux *et al.*, 2000b). Therefore, the search for a central O_2-sensing

site within the brainstem remains ongoing. Moreover, recent findings from our laboratory showed that targeted deletion of the AMPK-α1/α2 catalytic subunits in catecholaminergic cells attenuated the HVR and precipitated hypoventilation and apnoea during brief exposures to acute hypoxia, despite retaining normal increases in CB chemoafferent fibre discharge in response to hypoxia (Mahmoud, 2014; Mahmoud *et al.*, 2016). Therefore, it appears that a component of the HVR arises centrally within the catecholaminergic neurons of the brainstem, and that within this catecholaminergic network AMPK activity may govern the integration and onward relay of peripheral and possibly central chemoafferent input during periods of reduced O_2 availability.

9.2.1 The ongoing search for a central respiratory oxygen sensor

The search for a central O_2-sensitive site has been under investigation for several decades, but the continuous failure to concretely identify such a structure or cell population still generates considerable disagreement and doubt within the field. However, it now seems that the use of anaesthesia may have been a potential confounding factor in suppressing a central stimulatory component of the HVR, because the majority of studies that reported recovery of the HVR following CB denervation were undertaken in awake, and therefore unanaesthetised, animals (Davenport *et al.*, 1947; Miller & Tenney, 1975; Bisgard *et al.*, 1980; Martin-Body *et al.*, 1986; Daristotle *et al.*, 1991; Roux *et al.*, 2000a; Roux *et al.*, 2000b). Moreover, one particular study directly compared the HVR of CB denervated rats in the awake state and during urethane-induced general anaesthesia. It was found that during anaesthesia, the robust HVR observed in the awake state was dramatically reduced, therefore suggesting that anaesthetic agents inhibit the signalling mechanisms of central O_2-sensitive neurons (Angelova *et al.*, 2015). In this respect it is important to note that in response to hypoxia, a ~30% increase in respiratory frequency was also reported in CB denervated sleeping dogs, suggesting that a degree of central O_2-sensitivity is retained even in the subconscious state (Curran *et al.*, 2000).

Certain proponents of the central respiratory O_2 sensor hypothesis have recently suggested that this mechanism may not be neuronal in nature, but rather determined by ATP-releasing glial cells (Gourine & Funk, 2017). Hypoxia was found to induce exocytosis of ATP-containing vesicles in astrocytes, which was proposed to potently excite ATP-sensitive neurons of the pre-Bötzinger complex (preBötC) (Gourine *et al.*, 2005). However, at least within the human brainstem, glial numbers were estimated to outweigh neurons in a ratio of 11.35/1 (Azevedo *et al.*, 2009; Lent *et al.*, 2012; Herculano-Houzel, 2014), which means their high density and wide spread across the brainstem make them unlikely candidates to specifically activate the rCPGs. Rather, it would seem more likely that the increased and sustained activity of central O_2-sensitive neurons during hypoxia is supported by ATP-releasing astrocytes, and in direct support of this it was found that the metabolic stress-induced activity of catecholaminergic neurons in the murine brainstem is dependent on purinergic signalling from astrocytes via P2 receptors (Rogers *et al.*, 2018). In this respect, a role for catecholaminergic neurons has long been prominent (Roux *et al.*, 2000a; Neubauer & Sunderram, 2004), not at least because other O_2-sensing cells that are able to potently modulate ventilation are also catecholaminergic (Nurse, 2014; Nurse *et al.*, 2018).

9.2.2 The activation of a putative hypoxia-responsive neuronal network within the dorsal brainstem is dependent on AMPK activity in catecholaminergic cells

The first direct evidence showing that AMPK-dependent signalling pathways in catecholaminergic neurons support the HVR through central neuronal activation during hypoxia was obtained by examining the brainstem function of TH AMPK-α1/α2 dKO mice by functional magnetic resonance imaging. These experiments identified key areas within the dorsal and ventral brainstem that exhibited reduced O_2 consumption during hypoxia relative to controls, indicative of reduced neuronal activity. These regions were subsequently termed the ‘dorsal active region’ (DAR) and ‘ventral active region’ (VAR), respectively (Mahmoud *et al.*, 2016). Importantly, my analysis

of cFos expression corroborated these findings and revealed an area of significant right-side dominant reductions in neuronal cFos expression within the dorsal brainstem, which spanned three subnuclei of the NTS and was entirely consistent with the predicted shape, anatomical location and rostrocaudal extend of the DAR.

It seems entirely possible that the DAR forms a hypoxia-responsive neuronal circuit within the dorsal medulla through which ventilatory drive is increased during hypoxia in an AMPK-dependent manner. In support of this view, its anatomical location lies in very close proximity to the area postrema (AP), which is highly vascularised and shares blood-borne signals with the NTS via its unusual blood supply of highly fenestrated capillaries (Price *et al.*, 2008). In this respect, the DAR would be strategically placed to monitor arterial PO_2 centrally. Furthermore, the fenestrated capillaries of the AP create a relatively low O_2 saturation within the surrounding tissue (Fodor *et al.*, 2007; McGinnis *et al.*, 2013), which means that within the neuronal population that forms the DAR, this mildly hypoxic environment could result in increased afferent output in response to even minor reductions in the arterial O_2 saturation. Additional O_2-sensitivity could be conferred via expression of COX4I2 (as has been observed in other O_2-sensitive cells such as pulmonary arterial smooth muscle cells and CB type I cells) (Huttemann *et al.*, 2001; Zhou *et al.*, 2016), consequent susceptibility to deficits in mitochondrial ATP production during hypoxia, and thus activation of AMPK-dependent signalling pathways to increase O_2 uptake via enhanced ventilatory effort. However, future analyses of responses to hypoxia in TH AMPK-α1/α2 dKO mice and COX4I2 expression within the NTS will be required to confirm the nature and capacity for O_2-sensing by the DAR, and the role of signal integration by these neurons in mediating ventilatory output.

The position of the DAR is also consistent with the location of the rostral portion of the noradrenergic A2 cell group, but an involvement of the more rostrally located adrenergic C2 cell group could not be excluded at this point. Recent studies on laser microdissected A1/A2 and C1/C2 neurons have demonstrated that AMPK is indeed expressed in all four catecholaminergic

cell groups, and that its activity increases in response to metabolic stress (Shrestha *et al.*, 2014). Caudally, the A2 neurons receive chemoafferent input from the carotid body and relay these information to other brain regions that are involved in the control of breathing (Andresen & Kunze, 1994; Andresen & Mendelowitz, 1996; King *et al.*, 2015). Although these afferent inputs may not directly innervate the regions encompassing the DAR, relay pathways within the NTS lead to the activation of second-order NTS neurons in more rostral Bregmas (Andresen *et al.*, 2004), which includes the rostrocaudal extend of the DAR. Accordingly, AMPK availability in these catecholaminergic neurons may be of primary importance to mediate the appropriate response to 'applied metabolic stress' during exposures to acute hypoxia, and ultimately support the HVR and whole-body O_2 homeostasis. Moreover, signalling inputs to the DAR could also be received from the AP, which contains bidirectional projections to and from the dorsal portion of the NTS (van der Kooy & Koda, 1983; Shapiro & Miselis, 1985; Hermann *et al.*, 2005) and therefore allows for rapid communication between brainstem structures within and outside of the Blood-Brain-Barrier. In this respect, the DAR could form a 'central integration hub' which receives information from the periphery as well as the cerebral vasculature and could determine – in an AMPK-dependent manner – the degree to which a ventilatory response is initiated. Consistent with our proposed model of action (see Figure 9.1), the capacity of AMPK activation within the DAR may therefore be determined by the co-action of 'local hypoxic stress' within the brainstem that increases the AM(D)P:ATP ratio via decreases in ATP supply (Hardie, 2014), coupled to 'applied metabolic stress' via intense neuronal activation following inputs from peripheral and central afferent projections and thus increases in ATP usage.

The reception and relay of chemoafferent inputs aside, the neurons of the A2 cell group themselves have also been reported to be hypoxia-sensitive and able to potently modulate ventilation during hypoxia (Andresen & Kunze, 1994; Andresen & Mendelowitz, 1996; Buller *et al.*, 2008; Li *et al.*, 2008; Soliz *et al.*, 2008; McGinnis *et al.*, 2013). In light of the identification of the DAR, one could even speculate that this O_2-responsive circuit does not only

determine the degree of the HVR, but may also offer an explanation as to how in some species components of the HVR could be, at least partially, restored following CB resection (Davenport *et al.*, 1947; Miller & Tenney, 1975; Bisgard *et al.*, 1980; Martin-Body *et al.*, 1986; Daristotle *et al.*, 1991; Roux *et al.*, 2000a). A direct modulation of ventilation originating from hypoxia-responsive A2 neurons and/or the DAR is possible due to the afferent projections from the NTS that terminate within the respiratory compartments of the ventrolateral medulla and thus the respiratory central pattern generators (rCPGs). When taken as a whole, the NTS sends afferent projections to each distinct compartment of the ventral respiratory column (VRC). However, more detailed analyses of the dorsal to ventral innervations revealed that the projections from the individual nuclei of the NTS innervate the compartments of the VRC differentially (Alheid *et al.*, 2011). Importantly, the NTS subnuclei that I proposed to form the DAR appear to strongly innervate the rostral and caudal ventral respiratory groups which contain bulbospinal projections to motoneurons that facilitate inspiration and expiration, respectively, as well as the rostral and caudal ventrolateral medulla which contain pre-sympathetic catecholaminergic C1 neurons implicated in the control of the baroreflex (Ross *et al.*, 1984; Ross *et al.*, 1985; Aicher *et al.*, 1996; Dampney *et al.*, 2002; Guyenet, 2006; Guyenet *et al.*, 2013). Moreover, at least one of the anatomical nuclei that forms part of the DAR was also found to strongly innervate the preBötC and Bötzinger complex (BötC), which are important autonomic oscillators that are required and sufficient for the rhythmogenesis of inspiration and expiration, respectively (Janczewski & Feldman, 2006; Smith *et al.*, 2007; Koizumi *et al.*, 2013; Anderson & Ramirez, 2017). Therefore, the activity of O_2-responsive neurons within the DAR may be sufficient to elicit a ventilatory response to hypoxia, even in the absence of increased chemoafferent input.

Overall, this is the first proposal of an anatomically well-defined central hypoxia-responsive neuronal network, which is hypothesised to determine the degree of the HVR centrally and whose activity is dependent on catecholaminergic AMPK-dependent signalling pathways.

9.2.3 Ventilatory drive during the hypoxic ventilatory response is differentially regulated by AMPK activity within brainstem noradrenergic and adrenergic cells

Dual deletion of the AMPK-α1/α2 catalytic subunits in catecholaminergic cells of the brainstem, and thus loss of neuronal activity within the DAR, significantly impacted the ventilatory response to hypoxia in mice. When both noradrenergic and adrenergic cell groups were targeted by our deletion strategy that was dependent on the expression of TH, hypoxia evoked severe hypoventilation, ventilatory instability and increases in the frequency and duration of apnoeas. Importantly however, components of the classical biphasic HVR were retained in TH AMPK-α1/α2 dKO mice, albeit in an attenuated manner. These outcomes are consistent with the view that – despite the fact that carotid body chemoafferent input responses remained unaffected – AMPK-α1/α2 deletion in catecholaminergic neurons blocked the HVR beyond the initial ventilatory augmentation during hypoxia for which peripheral afferent inputs may be responsible (Teppema & Dahan, 2010; Mahmoud *et al.*, 2016; Wilson & Teppema, 2016). That said, the attenuation of the Augmenting phase, particularly at 8% O_2, indicates that while chemoafferent inputs were most likely received within the brainstem, the appropriate physiological responses could not be executed sufficiently in the absence of AMPK activity within central catecholaminergic cells. This is entirely consistent with the proposal that AMPK-dependent signalling pathways within brainstem catecholaminergic cells and/or the neuronal network of the DAR continuously support signal integration and thus modulation of ventilatory output during acute and more prolonged periods of hypoxia via modulation of the respiratory central pattern generators (rCPGs) (Evans *et al.*, 2016; Mahmoud *et al.*, 2016; Evans, 2018).

Initially, the possibility remained that TH AMPK-α1/α2 dKO mice could enter a hypometabolic state in order to, at least partially, compensate for the fall in O_2 supply (Guppy & Withers, 1999). This possibility was particularly evident from the fact that these mice enter a 'torpor-like state' during hypoxia, during which the animal lies down and exhibits minimal body movements. Similarly, neonatal mammals, whose O_2-sensing network

comprising the catecholaminergic cells of the peripheral carotid body and NTS are still immature at birth (Bissonnette, 2000; Teppema & Dahan, 2010; Koos & Rajaee, 2014), also exhibit a ventilatory response to hypoxia that is characterised by a reduced augmentation phase and a quick decline into hypoventilation – similar to the hypoxic ventilatory pattern of TH AMPK-α1/α2 dKO mice. However, the depressed neonatal HVR is, at least partially, compensated for by a rapid decrease in metabolism and hence O_2 demand (Mortola & Maskrey, 2011). In contrast, no differences in the metabolic status between TH AMPK-α1/α2 dKO mice and controls were identified, despite exhibiting severe ventilatory deficiencies and 'torpor-like behaviour' for up to 60min of hypoxia. Therefore, these animals truly enter a hypoventilatory state, from which AMPK-dependent signalling pathways within central catecholaminergic cells protect.

A crucial component in the postnatal adaptation to extra-uterine life has been suggested to be the release of adrenaline during birth (Padbury *et al.*, 1982; Padbury *et al.*, 1987; Hillman *et al.*, 2012), given that the peripheral chemoreceptors are poorly developed and initially silenced in the perinatal and neonatal periods (Wasicko *et al.*, 1999; Donnelly, 2000; Lavezzi & Matturri, 2008). If adrenaline secretion from neonatal adrenal medullary chromaffin cells (nAMCs) is truly the developmental trigger, then it appears that this event is not dependent on AMPK-dependent signalling pathways. This was clear from the fact that dual deletion of the AMPK-α1/α2 catalytic subunits in PNMT-expressing adrenergic cells – which includes nAMCs – had no effect on the ventilatory phenotype during normoxia and did not result in any attenuation of the HVR. In fact, ventilatory frequencies of PNMT AMPK-α1/α2 dKO mice were significantly *augmented* during exposures to 10min of severe hypoxia relative to controls, suggesting that AMPK-dependent signalling pathways in adrenergic cells may to contribute an inhibitory input to the HVR in the adult. This was surprising, given that adrenergic – and thus PNMT Cre-positive – ventrolateral C1 neurons have been proposed to form an integral part of the neural circuit that drives increases in breathing frequency during hypoxia in mice and rats (Abbott *et al.*, 2013; Burke *et al.*, 2014), and a severe ventilatory deficit was observed

upon AMPK-α1/α2 catalytic subunit deletion in both adrenergic and noradrenergic neurons. It may be possible, therefore, that AMPK-dependent signalling pathways within noradrenergic and adrenergic cells serve different roles in determining the ventilatory responses to hypoxia. While noradrenergic AMPK activity most likely supports hyperventilation along with chemoafferent inputs from the carotid bodies, activity of AMPK in adrenergic cells may instead indirectly limit the extent of respiratory frequency and thus protect from hyperventilation-induced central hypocapnia and therefore respiratory alkalosis (Foster *et al.*, 2001). Alternatively, several studies have demonstrated that afferent projections from the adrenergic C1 cell group also terminate within the thalamus and pons (Haselton & Guyenet, 1990; Phillipson & Bohn, 1994; Otake *et al.*, 1995; Abbott *et al.*, 2012; Burke *et al.*, 2014), which in turn provide an inhibitory input to the rCPGs (Martin-Body, 1988; Kramer *et al.*, 1999). Therefore, innervations from the C1 cells to the rCPGs and pons could determine respiratory drive and inhibition, respectively, whereby afferent input to the rCPGs dominates and is perhaps determined by the sub-cellular localisation and activity of AMPK (Ross *et al.*, 2016).

Further indications that support an inhibitory role of adrenergic signalling – be it direct or indirect – came from the fact that AMPK-dependent signalling pathways within adrenergic cells appear to contribute to the genesis of apnoeas and thus ventilatory instability during the initial Augmenting phase of the HVR. By contrast, AMPK-dependent signalling pathways within noradrenergic cells seemed to protect from frequent and prolonged apnoeas throughout the hypoxic exposure, because deletion of AMPK-α1/α2 catalytic subunits in all catecholaminergic cells precipitated highly irregular breathing patterns, as well as more frequent spontaneous and prolonged post-sigh apnoeas, the former of which were retained as periodically oscillating “bursts” evident throughout even prolonged exposures to hypoxia. This suggests that AMPK activity within the DAR is required to protect from phasic disturbances of the central pattern generators during periods of prolonged hypoxia via its projections to the rostral and caudal ventral

respiratory groups, as well as the Bötzinger complex and pre-Bötzinger complex (Alheid *et al.*, 2011).

On the whole, it is therefore possible that during the Augmenting Phase of the HVR respiratory drive is jointly determined by chemoafferent input from the carotid bodies, the DAR, and/or central hypoxia-responsive noradrenergic neurons that may act in concert with a mild respiratory inhibition originating from central adrenergic neurons which may reduce ventilation through silencing of the RTN until an equilibrium of optimal balance between O_2 intake through hyperventilation and protection from respiratory alkalosis has been reached (Basting *et al.*, 2015). In this respect, complete cessation of ventilation during the Augmenting phase may thus be the most rapid and efficient way to restore central CO_2 levels during periods of intense respiratory effort (Dempsey, 2005). However, after approximately four minutes of hypoxia, which coincides with the Sustained Phase of the HVR, the balance of inspiratory drive from the carotid bodies, the DAR and/or central hypoxia-responsive noradrenergic neurons, and inhibitory drive from the adrenergic neurons and/or pons may keep hyperventilation and apnoea frequency at a level that maintains adequate CO_2 levels during periods of hypoxia.

Roughly coinciding with the end of the Augmenting phase, expiration time remains accelerated during hypoxia relative to normoxia due to the initiation of active expiration, which is determined by the modulation of the rCPGs via activity of the RTN (Feldman & Del Negro, 2006; Janczewski & Feldman, 2006; Pagliardini *et al.*, 2011; Pisanski & Pagliardini, 2018). This modulation appears to be dependent on glutamatergic and serotonergic neurotransmission (Moraes *et al.*, 2012b; Lemes *et al.*, 2016; Lemes & Zoccal, 2016), and catecholaminergic neurons were shown to use glutamate as a neurotransmitter (Fung *et al.*, 1994a; Fung *et al.*, 1994b; Stornetta *et al.*, 2002; Rinaman, 2011; DePuy *et al.*, 2013). The fact that active expiration appeared to be blocked upon AMPK-α1/α2 catalytic subunit deletion in catecholaminergic cells may therefore not be entirely surprising. Importantly, selective inhibition of C1 cells was found to attenuate active expiration during hypoxia but not during normoxia or hypercapnia (Malheiros-Lima *et al.*,

2017). Moreover, each of the NTS nuclei identified as the DAR also project densely to the RTN (Alheid *et al.*, 2011). Together, this indicates that AMPK-dependent afferent inputs from catecholaminergic cells – which likely encompass the ventrolateral C1 cell group but may also arise from the DAR and/or dorsolateral A2/C2 cell groups – appear to act on the rCPG via the RTN in order to engage active expiration, thus reducing the total breath time to accommodate increases in ventilatory frequency (Moraes *et al.*, 2012a; Burke *et al.*, 2014; Malheiros-Lima *et al.*, 2017; Pisanski & Pagliardini, 2018).

9.2.4 Similarities between the breathing irregularities in the AMPK double knockouts and Rett syndrome

As observed in our TH-driven AMPK knockout model, patients with Rett syndrome also exhibit hypoventilation with PO_2-dependent increases in the frequency of apnoeas. In 60-90% of cases, Rett syndrome is caused by a loss-of-function mutation in the methyl-CpG binding protein 2 (MECP2) (Amir *et al.*, 1999; Shahbazian & Zoghbi, 2001), which has been strongly associated with the progressive degeneration of central catecholaminergic neuromodulatory systems (Ide *et al.*, 2005). As previously mentioned, A1/C1 and A2/C2 catecholaminergic neurons have been proposed to project and modulate the rCPGs during hypoxia in a manner dependent on chemoafferent input from the carotid body in order to maintain physiological PO_2 and PCO_2 at the whole-body level (Smith *et al.*, 1995; Li *et al.*, 2008; King *et al.*, 2012; King *et al.*, 2013). Thus, respiratory instability, hypoventilation and increased apnoea frequency appear to occur following reductions and loss of catecholaminergic neurotransmission from the A1/C1 and A2/C2 catecholaminergic neurons to the rCPGs, which could rely on AMPK-dependent signalling pathways.

By contrast, breathing irregularities and apnoeas during hypoxia were also shown to be triggered by *increases* in noradrenergic neurotransmission (Zanella *et al.*, 2014). Therefore, appropriate neuromodulation of the rCPGS appears to especially depend on precise noradrenergic signalling outputs from medullary A1/A2 cells – and possibly pontine A5/A6/A7 cells – whereby

subtle changes in synaptic transmission can have dramatic consequences at the whole respiratory network level.

Given that AMPK deletion was targeted to all catecholaminergic neurons and that these mice exhibit breathing irregularities similar to those manifested with Rett syndrome or increased noradrenergic neurotransmission, AMPK-dependent signalling pathways appear to be crucial within these neurons to determine catecholaminergic neuromodulation and therefore ventilatory responses during hypoxia. However, in contrast to the underlying pathology of Rett syndrome, TH AMPK-α1/α2 dKO mice did not appear to exhibit any alterations in the number of catecholaminergic neurons within the brainstem. As discussed previously, the success of TH-labelling may have been limited in my studies, however my overall cell counts were in line with those previously reported in the rabbit and rat (Hirooka *et al.*, 1997; Teppema *et al.*, 1997; King *et al.*, 2015). Moreover, analyses of brainstems and spinal cords of AMPK knockouts and controls identified no differences or alterations in the total bioamine contents. Therefore, ventilatory deficiencies subsequent to loss of catecholaminergic AMPK-dependent signalling pathways were not precipitated by alterations in the number of catecholaminergic neurons or their bioamine content, but the possibility remains that they could be affected by reductions or loss of AMPK-mediated exocytosis (Puljak *et al.*, 2008) and subsequent disturbances of onward signalling pathways to the rCPGs. For example, noradrenaline was shown to stabilise inspiratory rhythmogenesis of the preBötC by stimulation of both the strength and frequency of inspiratory bursts (Viemari & Ramirez, 2006; Viemari *et al.*, 2011). Thus, the possibility remains that hypoventilation was, at least in part, subsequent to loss of noradrenergic neuromodulation of the rCPGs following AMPK deletion in catecholaminergic cells.

9.3 AMPK activity in brainstem catecholaminergic neurons separates respiratory from cardiovascular responses to hypoxia

In concert with the modulation of respiratory effort, hypoxia also synergistically regulates well-defined responses of the cardiovascular system via activation of sympathetic efferents. While increased ventilation aims to maximise O_2 uptake, the cardiovascular response to hypoxia ensures that O_2 delivery and perfusion are optimised. Within the mouse, this translates to progressive decreases in heart rate and blood pressure (Campen *et al.*, 2004; Campen *et al.*, 2005a; Campen *et al.*, 2005b). The hypotensive effect of acute exposure to hypoxia in mice would be consistent with direct vasodilating effects of hypoxia on systemic vessels that may override sympathetically mediated increases in systemic vascular resistance (Prabhakar & Kumar, 2010; Kulandavelu *et al.*, 2015). In this respect, the cardiovascular responses of the mouse are in contrast to other species such as rats, cats, pigs, dogs and humans, where hypoxia either maintains or increases blood pressure (Bower & O'Donnell, 1991; Hedner *et al.*, 1992; Bao *et al.*, 1997; Chen *et al.*, 1998; Schneider *et al.*, 2000).

9.3.1 Cardiorespiratory signal integration at the level of the brainstem

Peripheral chemoafferent fibre inputs from the CB terminate within the caudal NTS, and the vast majority of NTS subnuclei that are innervated by these chemoafferents were shown to project to both the respiratory, as well as the cardiovascular centres of the ventrolateral medulla (see also Figure 4.1) (Finley & Katz, 1992; Alheid *et al.*, 2011). In addition, extensive overlap exists between the termination sites of chemoafferent input and baroreceptor feedback from the vasculature, because both of these peripheral sensors densely project to the medial subnucleus of the NTS (SolM) (Mendelowitz *et al.*, 1992). Therefore, the integration of these two peripheral inputs within the same anatomical structure of the dorsal brainstem and the simultaneous onward projections from SolM to the rCPGs as well as the ‘pressor and depressor areas’ of the rostral and caudal

ventrolateral medulla (RVL and CVL, respectively) directly or via 2nd-order NTS neurons make a separation of the individual signalling pathways mediating the cardiorespiratory responses to hypoxia nearly impossible. Moreover, recordings of sympathetic activity from pre-sympathetic neurons of the RVL and CVL have shown that the majority of them are subjected to rhythmic respiratory modulation (Numao *et al.*, 1987; Dick *et al.*, 2004; Moraes *et al.*, 2017), further highlighting that cardiorespiratory homeostasis is maintained and modulated by appropriate changes in both systems.

However, despite the synaptic connectivity and strong central convergence of the cardiorespiratory signalling pathways (Spyer & Gourine, 2009), my data supports the existence of an area within the dorsal brainstem where AMPK-dependent signalling pathways appear to separate the cardiorespiratory control by solely modulating the HVR, but not the cardiovascular responses to hypoxia.

9.3.2 Separation of respiratory and cardiovascular responses to hypoxia following AMPK deletion in catecholaminergic neurons

As previously stated, deletion of the AMPK-α1/α2 catalytic subunits in catecholaminergic cells resulted in a severely attenuated HVR and the identification of the DAR by means of fMRI and cFos expression analysis. Subsequently, the DAR was proposed to be crucial in supporting hypoxia-evoked increases in ventilation in an AMPK-dependent manner. However, the cardiovascular responses in mice with AMPK deletion were unaffected, as both changes in heart rate and blood pressure during hypoxia were comparable to controls, which means a role for the DAR in mediating the cardiovascular responses to hypoxia seems unlikely.

One possible explanation for this separation could be the existence of distinct 2nd-order NTS neuronal ‘integration hubs’ within the dorsal brainstem, which integrate and regulate the respiratory and cardiovascular responses to hypoxia, respectively, by different signalling pathways and/or receptor expression profiles. For example, in rhythmically active medullary brainstem slices, excitatory drive to both the respiratory and cardiac vagal

populations is delivered via serotonergic neuromodulation (Ramirez *et al.*, 1997; Telgkamp & Ramirez, 1999; Thoby-Brisson & Ramirez, 2000; Neff *et al.*, 2004; Evans *et al.*, 2005b; Pena & Ramirez, 2005; Hill *et al.*, 2011). However, while serotonin activates 5-HT_3 receptors on cardiac vagal efferents, neuromodulation of respiratory rhythmogenesis via neurons of the preBötC involves 5-HT_{2A} receptors (Pena & Ramirez, 2002; Tryba *et al.*, 2008; Dergacheva *et al.*, 2009). Similarly, variable receptor expression profiles of particular neurons within the NTS could lead to signal divergence following integration in the caudal portions of SolM and onward relay of cardiovascular activity by AMPK-independent pathways.

Alternatively, it may be possible that the activity and signalling output of a subset of catecholaminergic cells may be AMPK-independent. The involvement of the ventrolateral catecholaminergic C1 neurons in mediating the baroreflex during normoxia and exposures to hypoxia has been well established, whereby hypoxia activates bulbospinal C1 neurons, which then modulate arterial blood pressure and heart rate via vaso- and cardiomotor pre-sympathetic efferents (Ross *et al.*, 1984; Sun & Reis, 1994a; Dampney *et al.*, 2002; Guyenet, 2006; Guyenet *et al.*, 2013; Burke *et al.*, 2014). It may be possible that this pathway is, at least within a subset of C1 neurons, independent on AMPK activity, because fMRI analysis of TH AMPK-α1/α2 dKO mice during hypoxia revealed an area with significant reductions in ventral neuronal activity (i.e. the VAR) that was predominantly consistent with the anatomical location and rostrocaudal extend of the noradrenergic A1 cells (Mahmoud *et al.*, 2016). Importantly, while the rostral border of the VAR appeared to include caudal-most portion of the C1 cells, it appears as though the majority of more rostrally located ventral adrenergic cells were unaffected and thus retained their neuronal activity during hypoxia. Clearly, these assumptions still need to be corroborated by analysis of cFos expression. However, given the proposed direct contribution of the C1 cells to the ventilatory drive during hypoxia (Burke *et al.*, 2014), it seems likely that the sympathetic pathways that control cardiovascular responses to hypoxia may be independent of AMPK-mediated signalling pathways.

9.4 Future experiments

Clearly, a lot of questions about the role of AMPK signalling in mediating the HVR, but not the cardiovascular responses to hypoxia, still remain unresolved. Firstly, in order to determine the full anatomical shape and extent of the DAR, counts of nuclear cFos expression and TH-labelling need to be completed for the more rostral parts of the NTS that harbour the C2/C3 adrenergic cell populations. At the same time, assessment of the ventral regions of the brainstem encompassing the rCPGs and A1/C1 neuronal network are crucial to determine the degree by which ventilations during hypoxia might be compromised by the VAR, and could give further insight into the cardiovascular control by the C1 neurons in relation to AMPK activity. Moreover, extending these counts to the pontine regions will address whether AMPK activity within noradrenergic A5/A6/A7 neurons affected signalling outputs from the pontine respiratory group.

Once the areas with reduced neuronal activation following AMPK deletion have been anatomically defined, their individual and joint contributions to the HVR could be tested by means of viral injections into the target regions. This can be achieved by injecting a fluorescently tagged recombinant Cre-recombinase carrying virus vector into the target brainstem regions of AMPK-α1/α2 Flx mice. Accordingly, AMPK deletion will only be targeted to the injected region and the mice can be examined for their ventilatory phenotype during hypoxia. Immunofluorescent studies on perfused and fixed brain sections can then be performed to identify the injection site and viral spread, and hence the ratio of infected catecholaminergic versus non-catecholaminergic neurons. Alternatively, brain slices could be freshly dissected and neuronal activity and/or neurotransmitter release of the identified target regions recorded *ex vivo* during normoxic and hypoxic conditions by whole-cell patch clamping. However, it is very important to consider the local PO_2 of various regions within the brainstem, because the physiologically normoxic PO_2 of certain brainstem areas can be very low and perfusion of a higher O_2 concentration could therefore lead to silencing of hypoxia-responsive neurons and therefore impact on data interpretation of neuronal activity during hypoxia.

In addition to the electrophysiological experiments during exposures to normoxia and hypoxia, the proposed hypoxia-sensitivity of the DAR and other putative hypoxia-responsive sites could be tested by expression analysis of genes that confer O_2-sensitivity in other cells types. Accordingly, quantitative PCR or RNA sequencing could be carried out to test for the expression of NDUFA4L2 and, more importantly, COX4I2, which would confirm whether or not the mitochondria within these neuronal circuits are exquisitely sensitive to reductions in O_2 availability or not.

9.5 Conclusion

In conclusion, AMPK-dependent signalling pathways in central catecholaminergic neurons are not only critical for appropriate ventilatory adjustments during acute hypoxia, but also during prolonged periods of low O_2 availability in order to protect against hypoventilation, respiratory instability, and apnoeas. Crucially, AMPK is required to continuously deliver increases in the drive to breathe via activation of a putative hypoxia-responsive neuronal circuit located in the dorsal brainstem called the DAR. Within this neuronal network, the activation of AMPK may be determined by peripheral chemoreceptor inputs and brainstem hypoxia, and couples those inputs to increased ventilatory drive via signalling outputs to the respiratory central pattern generators (Figure 9.1). Therefore, AMPK-dependent signalling pathways are not only important to maintain cellular energy homeostasis, but have also evolved to regulate O_2, and thus energy supply, at the whole-body level. Given these indications, it seems plausible that aberrant expression levels of AMPK may underlie ventilatory pathophysiologies such as sleep-disordered breathing related to the metabolic syndrome (Chau *et al.*, 2012; Ruderman *et al.*, 2013), high altitude sickness (Ainslie *et al.*, 2013), or sudden infant death syndrome (Nakamura & Kuwaki, 2003) and could therefore offer new opportunities for the development of therapeutic strategies.

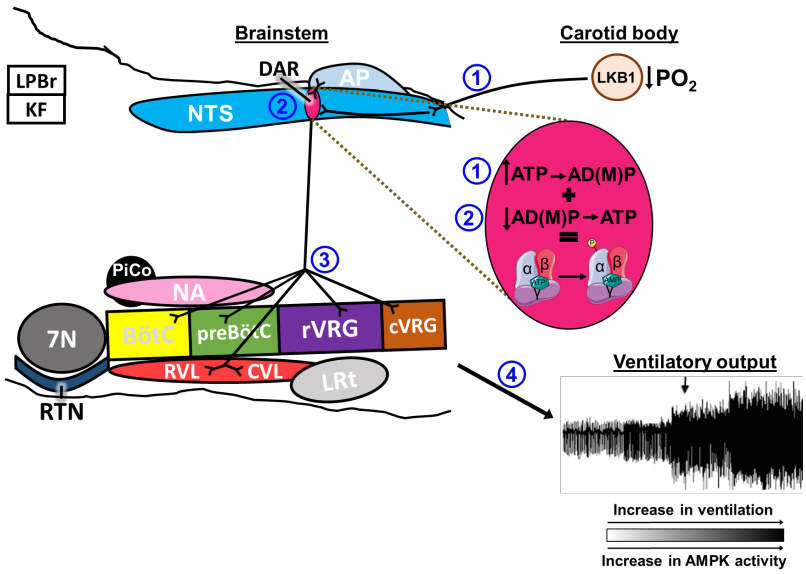

Figure 9.1: Proposed model for the delivery of respiratory drive during hypoxia mediated by AMPK dependent signalling pathways in central catecholaminergic neurons of the brainstem.

Ventilatory output during hypoxia, and therefore the degree of HVR, is proposed to be mediated by AMPK-dependent signalling pathways within, at the very least, dorsal noradrenergic cell of the brainstem which underpin the hypoxia-responsiveness of the DAR. During periods of reduced O_2 availability, AMPK activity is hypothesised to be determined by the coaction of (1) applied metabolic stress via increased neuronal activity (increased ATP consumption) from peripheral and central afferent inputs, and (2) the central effect of hypoxia (decreased ATP production). (3) Signalling outputs from the DAR innervate and modulate the ventral respiratory central pattern generators of the ventrolateral medulla, which in concert provide the efferent signals for (4) increased ventilatory output to optimise O_2 uptake. Omitted for clarity are projections from and to the pons, between the rCPGs, additional projections from the NTS to the rCPGs, and neuronal circuits regulating cardiovascular responses to hypoxia. AP = area postrema; NTS = nucleus tractus solitarius; 7N: facial nucleus, RTN: retrotrapezoid nucleus, NA: nucleus ambiguus, BötC: Bötzinger complex, preBötC: pre Bötzinger complex, rVRG: rostral ventral respiratory group, cVRG: caudal ventral respiratory group, RVL: rostral ventrolateral medulla, CVL: caudal ventrolateral medulla, LRt: lateral reticular nucleus.

Appendix 1

Supplementary material for Chapter 3

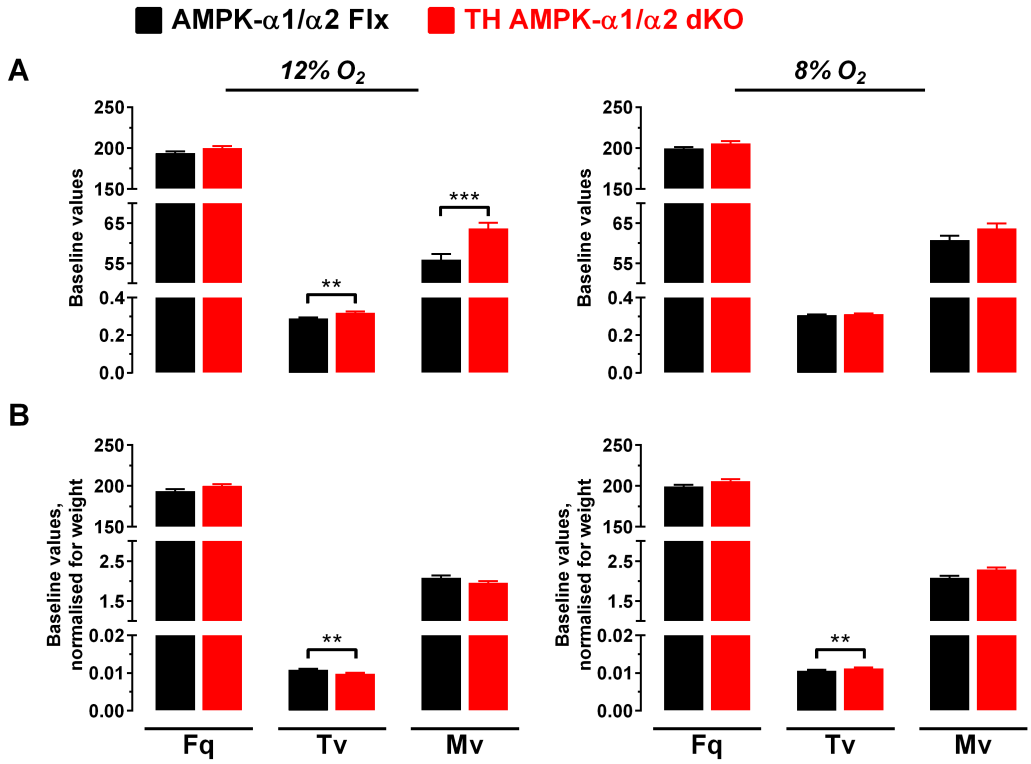

Appendix 1.1: Differences in the pre-hypoxic baselines between experimental mice.

Bar charts show mean ± SEM for **(A)** 'raw' baselines and **(B)** baselines normalised for weight that were selected prior to exposures to mild hypoxia (12% O_2, left panels) or severe hypoxia (8% O_2, right panels) for AMPK-α1 and -α2 floxed (AMPK-α1/α2 Flx, black, 12% O_2: n = 37 exposures from 14 mice, 8% O_2: n = 54 exposures from 21 mice) and TH-driven AMPK-α1 and -α2 double knockout mice (TH AMPK-α1/α2 dKO, red, 12% O_2: n = 28 exposures from 11 mice, 8% O_2: n = 49 exposures from 21 mice). ** = $p<0.01$, **** = $p<0.0001$. Significance tested by t-tests between genotypes for each ventilatory parameter.

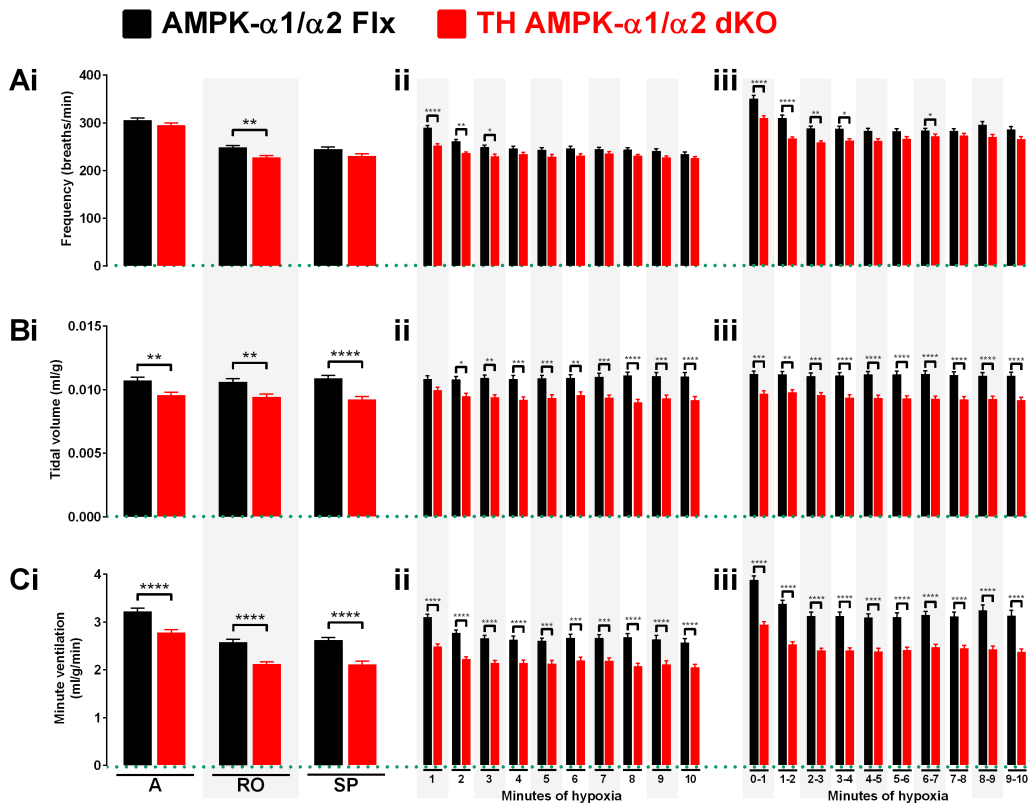

Appendix 1.2: Ventilatory deficiency of mice with dual deletion of AMPK α1/α2 catalytic subunits in catecholaminergic cells in response to mild hypoxia is also apparent in the 'raw' experimental data.

Bar charts show mean ± SEM of values computed by the FinePointe software for **(A)** breathing frequency, **(B)** tidal volume (normalised for weight), and **(C)** minute ventilation (normalised for weight) during 10 minute exposures to mild hypoxia (12% O_2) for analysis **(i)** of the HVR at the peak of the augmenting phase (A), the nadir of Roll-Off (RO), and the plateau of the sustained phase (SP), **(ii)** at each full minute of hypoxia, and **(iii)** whole minute averages in AMPK-α1 and -α2 floxed mice (AMPK-α1/α2 Flx, black, n = 37 exposures from 14 mice) and TH-driven AMPK-α1 and -α2 double knockout mice (TH AMPK-α1/α2 dKO, red, n = 28 exposures from 11 mice). * = p<0.05, ** = p<0.01, *** = p<0.001, **** = p<0.0001. Significance tested by two-way ANOVA with Sidak post-hoc tests.

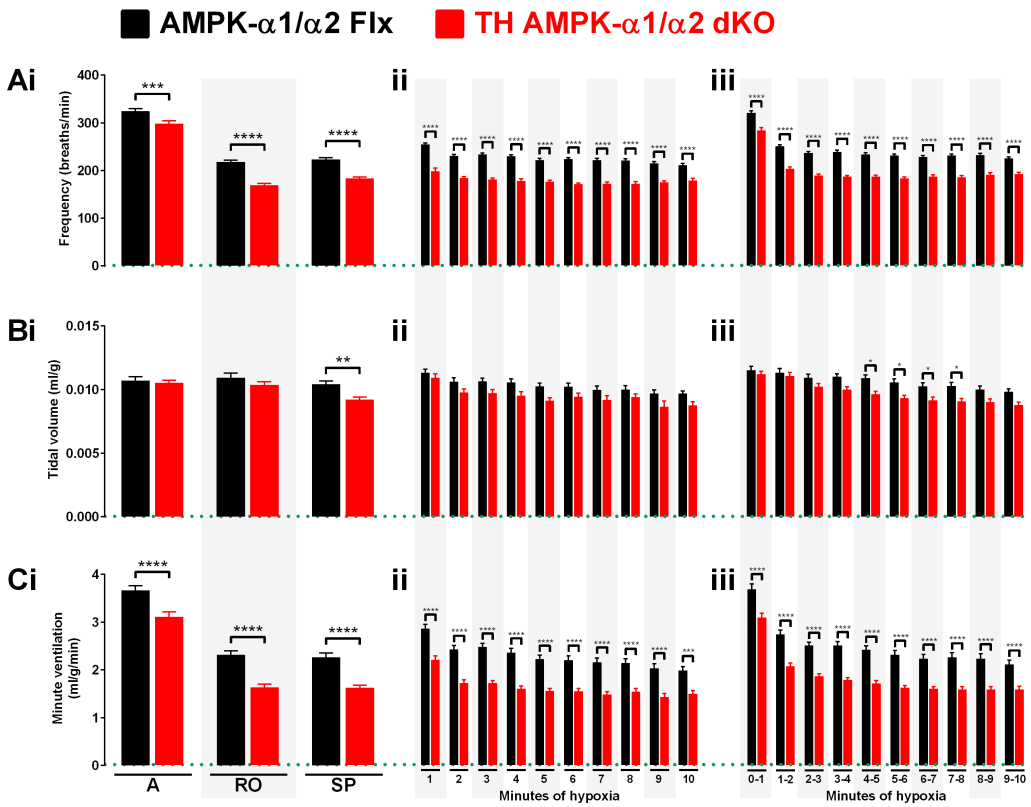

Appendix 1.3: Ventilatory deficiency of mice with dual deletion of AMPK α1/α2 catalytic subunits in catecholaminergic cells in response to severe hypoxia is also apparent in the 'raw' experimental data.

Bar charts show mean ± SEM of values computed by the FinePointe software for **(A)** breathing frequency, **(B)** tidal volume (normalised for weight), and **(C)** minute ventilation (normalised for weight) during 10 minute exposures to severe hypoxia (8% O_2) for analysis **(i)** of the HVR at the peak of the augmenting phase (A), the nadir of Roll-Off (RO), and the plateau of the sustained phase (SP), **(ii)** at each full minute of hypoxia, and **(iii)** whole minute averages in AMPK-α1 and -α2 floxed mice (AMPK-α1/α2 Flx, black, n = 55 exposures from 21 mice) and TH-driven AMPK-α1 and -α2 double knockout mice (TH AMPK-α1/α2 dKO, red, n = 40 exposures from 18 mice). * = p<0.05, ** = p<0.01, *** = p<0.001, **** = p<0.0001. Significance tested by two-way ANOVA with Sidak post-hoc tests.

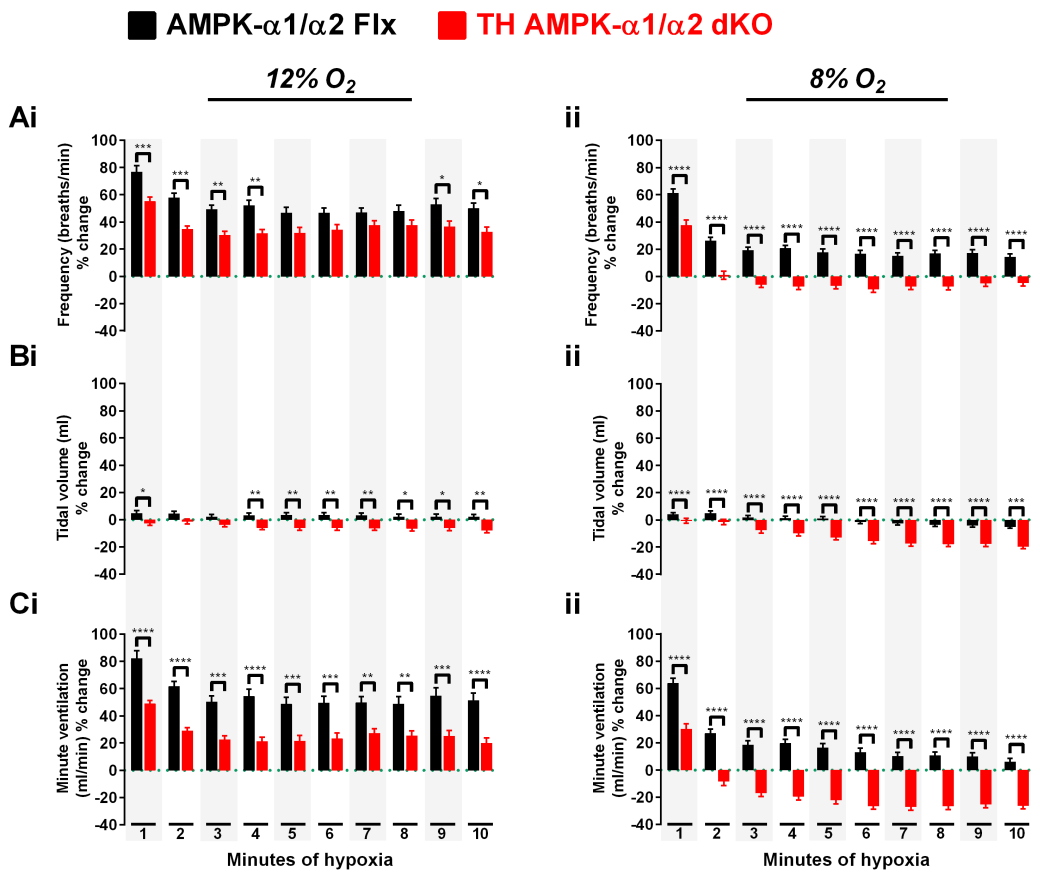

Appendix 1.4: The hypoxic ventilatory response to mild and severe hypoxia is significantly attenuated in mice with dual deletion of AMPK α1/α2 catalytic subunits in catecholaminergic cells when analysed as whole minute averages.

Bar charts show mean ± SEM for the % changes of 60 second averages in **(A)** breathing frequency, **(B)** tidal volume, and **(C)** minute ventilation during 10 minute exposures to **(i)** mild hypoxia (12% O_2) and **(ii)** severe hypoxia (8% O_2) for AMPK-α1 and -α2 floxed mice (AMPK-α1/α2 Flx, black, 12% O_2: n = 37 exposures from 14 mice, 8% O_2: n = 55 exposures from 21 mice) and TH-driven AMPK-α1 and -α2 double knockout mice (TH AMPK-α1/α2 dKO, red, 12% O_2: n = 28 exposures from 11 mice, 8% O_2: n = 40 exposures from 18 mice). * = p<0.05, ** = p<0.01, *** = p<0.001, **** = p<0.0001. Significance tested by two-way ANOVA with Sidak post-hoc tests.

Appendix 2

Supplementary material for Chapter 4

Appendix 2.1: Means ± SEM of dorsal (counts per 1000µm^3) and ventral (counts per sections) tyrosine hydroxylase (TH)-positive cells for the whole brainstem of AMPK-α1/α2 Flx (n = 16) and TH AMPK-α1/α2 dKO (n = 11) mice.

	AMPK-α1/α2 Flx	TH AMPK-α1/α2 dKO	p-value
Both sides			
Dorsal	0.0023 ± 0.00035	0.0016 ± 0.00027	ns
Ventral	16 ± 1.1	17 ± 0.99	ns
Right side			
Dorsal	0.001 ± 0.00016	0.0009 ± 0.0001	ns
Ventral	8.3 ± 0.58	8.5 ± 0.6	ns
Left side			
Dorsal	0.0009 ± 0.00015	0.0007 ± 0.0001	ns
Ventral	7.9 ± 0.73	8.45 ± 0.63	ns

ns = not significant; significance tested by unpaired t-test between genotypes.

Appendix 2.2: Means ± SEM of dorsal (counts per 1000µm^3) tyrosine hydroxylase (TH)-positive cells for the whole NTS of AMPK-α1/α2 Flx and TH AMPK-α1/α2 dKO mice at each Bregma.

	Both sides			Right side			Left side		
	AMPK-α1/α2 Flx	TH AMPK-α1/α2 dKO	p-value	AMPK-α1/α2 Flx	TH AMPK-α1/α2 dKO	p-value	AMPK-α1/α2 Flx	TH AMPK-α1/α2 dKO	p-value
- 7.76 mm	0.001 ± 0.0003 n = 10	0.001 ± 0.0002 n = 10	ns	0.001 ± 0.0003 n = 10	0.002 ± 0.0003 n = 10	ns	0.001 ± 0.0003 n = 10	0.001 ± 0.0002 n = 10	ns
- 7.70 mm	0.002 ± 0.0004 n = 6	0.001 ± 0.0001 n = 4	ns	0.002 ± 0.0005 n = 6	0.001 ± 0.0002 n = 4	ns	0.002 ± 0.0005 n = 6	0.001 ± 0.0002 n = 4	ns
- 7.64 mm	0.001 ± 0.0002 n = 15	0.001 ± 0.0002 n = 11	ns	0.001 ± 0.0003 n = 15	0.001 ± 0.0002 n = 11	ns	0.001 ± 0.0002 n = 15	0.001 ± 0.0002 n = 11	ns
- 7.60 mm	0.001 ± 0.0001 n = 4	0.001 ± 0.0001 n = 4	ns	0.001 ± 0.0004 n = 4	0.001 ± 0.0002 n = 4	ns	0.0008 ± 0.0003 n = 4	0.0008 ± 0.0002 n = 4	ns
- 7.56 mm	0.0008 ± 0.0001 n = 13	0.0006 ± 0.0001 n = 11	ns	0.0007 ± 0.0001 n = 13	0.0006 ± 0.0001 n = 11	ns	0.0009 ± 0.0001 n = 13	0.0007 ± 0.0001 n = 11	ns
- 7.50 mm	0.0009 ± 0.0002 n = 11	0.0005 ± 0.0001 n = 8	ns	0.001 ± 0.0002 n = 11	0.001 ± 0.0001 n = 8	ns	0.0007 ± 0.0002 n = 10	0.0004 ± 0.0001 n = 8	ns
- 7.48 mm	0.0006 ± 0.0001 n = 16	0.0005 ± 0.0001 n = 11	ns	0.0006 ± 0.0001 n = 16	0.0007 ± 0.0001 n = 8	ns	0.0007 ± 0.0001 n = 16	0.0005 ± 0.0001 n = 11	ns
- 7.44 mm	0.0001 ± 0.0001 n = 8	0.0006 ± 0.0003 n = 4	ns	0.0002 ± 0.0002 n = 8	0.0009 ± 0.0005 n = 4	ns	0.00008 ± 0.00006 n = 8	0.0002 ± 0.0001 n = 4	ns

ns = not significant; significance tested by multiple t-tests with Holm-Sidak post-hoc test.

Appendix 2.3: Means ± SEM of dorsal (counts per 1000µm^3) tyrosine hydroxylase (TH)-positive cells for the whole brainstem of AMPK-α1/α2 Flx (n = 16) and TH AMPK-α1/α2 dKO (n = 11) mice for each subnucleus of the NTS.

	Both sides			Right side			Left side		
	AMPK-α1/α2 Flx	TH AMPK-α1/α2 dKO	p-value	AMPK-α1/α2 Flx	TH AMPK-α1/α2 dKO	p-value	AMPK-α1/α2 Flx	TH AMPK-α1/α2 dKO	p-value
SubP	0.0002 ± 0.00007	0.00002 ± 0.00002	ns	0.0002 ± 0.00009	0 ± 0	ns	0.0001 ± 0.00006	0.0001 ± 0.00005	ns
10N	0.0004 ± 0.0001	0.0016 ± 0.00027	ns	0.0005 ± 0.0002	0.0005 ± 0.0002	ns	0.0003 ± 0.00008	0.0003 ± 0.00008	ns
SolC	0.00008 ± 0.00003	0.00012 ± 0.00006	ns	/	/	/	/	/	/
SolM	0.0006 ± 0.0001	0.0007 ± 0.0001	ns	0.0006 ± 0.0001	0.0007 ± 0.0001	ns	0.0006 ± 0.0001	0.0006 ± 0.0001	ns
SolDM	0.0002 ± 0.0001	0.0001 ± 0.0001	ns	0.00009 ± 0.00006	0 ± 0	ns	0.0002 ± 0.0001	0.0002 ± 0.0001	ns
SolDL	0.0003 ± 0.00007	0.0002 ± 0.00005	ns	0.0003 ± 0.00009	0.0003 ± 0.00008	ns	0.0002 ± 0.00008	0.0002 ± 0.00005	ns
SolI	0.0009 ± 0.0003	0.0006 ± 0.0001	ns	0.001 ± 0.0005	0.001 ± 0.0003	ns	0.0005 ± 0.0002	0.0002 ± 0.0001	ns
SolIM	0.003 ± 0.0004	0.002 ± 0.0004	ns	0.003 ± 0.0005	0.002 ± 0.0004	ns	0.002 ± 0.0004	0.002 ± 0.0005	ns
SolV	0.002 ± 0.0003	0.002 ± 0.0003	ns	0.002 ± 0.0003	0.001 ± 0.0003	ns	0.002 ± 0.0004	0.002 ± 0.0004	ns
SolVL	0.002 ± 0.0004	0.001 ± 0.0002	ns	0.002 ± 0.0005	0.001 ± 0.0003	ns	0.002 ± 0.0004	0.001 ± 0.0002	ns
SolL	0.0005 ± 0.0002	0.0003 ± 0.0001	ns	0.0007 ± 0.0003	0.0003 ± 0.0002	ns	0.0001 ± 0.00008	0.0002 ± 0.00011	ns
SolCe	0.003 ± 0.0004	0.002 ± 0.0003	ns	0.002 ± 0.0006	0.003 ± 0.0005	ns	0.002 ± 0.0005	0.002 ± 0.0003	ns

ns = not significant; significance tested by two-way ANOVA with Sidak post-hoc test.

Appendix 2.4: Means ± SEM of ventral (counts per sections) tyrosine hydroxylase (TH)-positive cells in AMPK-α1/α2 Flx (n = 16) and TH AMPK-α1/α2 dKO (n = 11) mice. ns = not significant, * = p<0.05; significance tested by unpaired t-test between genotypes.

	AMPK-α1/α2 Flx	TH AMPK-α1/α2 dKO	p-value
Both sides			
A1	18 ± 1.1	20.1 ± 1.2	ns
A1/C1	16.9 ± 1.3	16.6 ± 1.2	ns
C1	12.6 ± 1	15 ± 1.3	ns
Right side			
A1	9.4 ± 0.5	9.7 ± 0.8	ns
A1/C1	8.9 ± 0.8	8 ± 0.6	ns
C1	5.7 ± 0.6	8.3 ± 0.9	*
Left side			
A1	8.7 ± 0.7	10.4 ± 0.8	ns
A1/C1	8 ± 0.9	8.6 ± 0.9	ns
C1	6.9 ± 1.1	6.7 ± 0.9	ns

Appendix 2.5: Means ± SEM of bioamine contents in the brainstem and spinal cords of AMPK-α1/α2 Flx (n = 11) and TH AMPK-α1/α2 dKO (n = 12) mice.

	Brainstem			Spinal cord		
	AMPK-α1/α2 Flx	TH AMPK-α1/α2 dKO	p-value	AMPK-α1/α2 Flx	TH AMPK-α1/α2 dKO	p-value
L-DOPA	670 ± 97 ng/g	700.5 ± 110.5 ng/g	ns	1221 ± 138 ng/g	990 ± 198.5 ng/g	ns
NA	2399 ± 192 ng/g	2090 ± 162 ng/g	ns	1605 ± 185 ng/g	1662 ± 227 ng/g	ns
5-HT	826 ± 48 ng/g	790 ± 35 ng/g	ns	551 ± 35 ng/g	617 ± 46 ng/g	ns
5-HIAA	897 ± 93 ng/g	885 ± 71 ng/g	ns	398 ± 19 ng/g	436 ± 30 ng/g	ns

L-DOPA: L-3,4-dihydroxyphenylalanine, NA: noradrenaline, 5-HT: serotonin, 5-HIAA: 5-hydroxyindoleacetic acid. ns = not significant; significance tested by unpaired t-test between genotypes for each bioamine per preparation.

Appendix 2.6: Means ± SEM of total cFos counts (per 1000µm^3) for each Bregma of the total, right, and left NTS in AMPK-α1/α2 Flx mice following exposures to 21% O_2, 12% O_2, and 8% O_2.

	Both sides			Right side			Left side		
	21% O_2	12% O_2	8% O_2	21% O_2	12% O_2	8% O_2	21% O_2	12% O_2	8% O_2
- 7.76 mm	0.01 ± 0.001 n = 3	0.051 ± 0.018 n = 4	0.073 ± 0.008 n = 3	0.011 ± 0.001 n = 3	0.052 ± 0.017 n = 4	0.078 ± 0.01 n = 3	0.01 ± 0.002 n = 3	0.051 ± 0.018 n = 4	0.068 ± 0.008 n = 3
- 7.70 mm	/	0.059 ± 0.028 n = 2	0.073 ± 0.008 n = 4	/	0.056 ± 0.023 n = 2	0.067 ± 0.012 n = 4	/	0.063 ± 0.033 n = 2	0.074 ± 0.012 n = 4
- 7.64 mm	0.01 ± 0.001 n = 4	0.068 ± 0.022 n = 6	0.087 ± 0.012 n = 5	0.011 ± 0.002 n = 4	0.063 ± 0.019 n = 6	0.088 ± 0.013 n = 5	0.009 ± 0.001 n = 4	0.072 ± 0.025 n = 6	0.086 ± 0.013 n = 5
- 7.60 mm	0.011 n = 1	0.031 n = 1	0.07 ± 0.022 n = 2	0.011 n = 1	0.027 n = 1	0.072 ± 0.026 n = 2	0.011 n = 1	0.034 n = 1	0.067 ± 0.018 n = 2
- 7.56 mm	0.01 ± 0.001 n = 4	0.048 ± 0.01 n = 5	0.078 ± 0.011 n = 4	0.01 ± 0.002 n = 4	0.046 ± 0.008 n = 5	0.076 ± 0.012 n = 4	0.01 ± 0.002 n = 4	0.049 ± 0.012 n = 5	0.079 ± 0.009 n = 4
- 7.52 mm	0.01 n = 1	0.055 ± 0.014 n = 5	0.086 ± 0.013 n = 4	0.01 ± 0.002 n = 2	0.054 ± 0.014 n = 5	0.083 ± 0.015 n = 4	0.011 n = 1	0.057 ± 0.014 n = 5	0.089 ± 0.013 n = 4
- 7.48 mm	0.01 ± 0.0009 n = 4	0.048 ± 0.0114 n = 6	0.084 ± 0.0092 n = 6	0.011 ± 0.0003 n = 4	0.047 ± 0.0101 n = 6	0.081 ± 0.0097 n = 6	0.009 ± 0.002 n = 4	0.048 ± 0.013 n = 6	0.087 ± 0.009 n = 6
- 7.44 mm	0.01 n = 1	0.037 ± 0.006 n = 4	0.1 ± 0.007 n = 3	0.01 n = 1	0.039 ± 0.006 n = 4	0.101 ± 0.007 n = 3	0.011 n = 1	0.036 ± 0.006 n = 4	0.1 ± 0.007 n = 3

Appendix 2.7: Means ± SEM of total cFos counts (per 1000µm^3) for each subnucleus along the length of the total, right, and left NTS in AMPK-α1/α2 Flx mice following exposures to 21% O_2 (n = 4), 12% O_2 (n = 6), and 8% O_2 (n = 6).

	Both sides			Right side			Left side		
	21% O_2	12% O_2	8% O_2	21% O_2	12% O_2	8% O_2	21% O_2	12% O_2	8% O_2
AP	0.004 ± 0.002	0.037 ± 0.008	0.073 ± 0.014	/	/	/	/	/	/
SubP	0.002 ± 0.0006	0.023 ± 0.0078	0.052 ± 0.0069	0.002 ± 0.002	0.024 ± 0.008	0.059 ± 0.009	0.003 ± 0.001	0.021 ± 0.007	0.045 ± 0.008
10N	0.011 ± 0.002	0.052 ± 0.007	0.082 ± 0.009	0.012 ± 0.003	0.052 ± 0.006	0.076 ± 0.008	0.01 ± 0.002	0.052 ± 0.009	0.087 ± 0.011
SolC	0.003 ± 0.0005	0.021 ± 0.0051	0.039 ± 0.0044	/	/	/	/	/	/
SolM	0.006 ± 0.0007	0.058 ± 0.0149	0.09 ± 0.0102	0.004 ± 0.0006	0.058 ± 0.0152	0.085 ± 0.0082	0.007 ± 0.001	0.057 ± 0.015	0.094 ± 0.013
SolDM	0.003 ± 0.0008	0.034 ± 0.0128	0.061 ± 0.0105	0.003 ± 0.0004	0.036 ± 0.0179	0.068 ± 0.012	0.003 ± 0.002	0.033 ± 0.01	0.056 ± 0.01
SolDL	0.005 ± 0.001	0.045 ± 0.013	0.083 ± 0.009	0.005 ± 0.0009	0.041 ± 0.0117	0.09 ± 0.011	0.006 ± 0.001	0.048 ± 0.014	0.078 ± 0.009
SolI	0.011 ± 0.002	0.051 ± 0.009	0.118 ± 0.021	0.012 ± 0.002	0.049 ± 0.011	0.125 ± 0.029	0.009 ± 0.003	0.053 ± 0.013	0.111 ± 0.014
SolIM	0.016 ± 0.002	0.076 ± 0.017	0.126 ± 0.016	0.017 ± 0.005	0.075 ± 0.015	0.125 ± 0.015	0.014 ± 0.0009	0.077 ± 0.0191	0.128 ± 0.0174
SolV	0.024 ± 0.002	0.043 ± 0.009	0.086 ± 0.008	0.028 ± 0.004	0.049 ± 0.011	0.086 ± 0.011	0.02 ± 0.002	0.037 ± 0.009	0.086 ± 0.006
SolVL	0.013 ± 0.002	0.04 ± 0.01	0.079 ± 0.01	0.016 ± 0.005	0.04 ± 0.007	0.078 ± 0.013	0.01 ± 0.001	0.04 ± 0.013	0.08 ± 0.008
SolL	0.013 ± 0.004	0.034 ± 0.013	0.073 ± 0.007	0.012 ± 0.003	0.029 ± 0.009	0.069 ± 0.006	0.014 ± 0.005	0.039 ± 0.016	0.08 ± 0.01
SolCe	0.015 ± 0.002	0.077 ± 0.014	0.118 ± 0.016	0.016 ± 0.002	0.066 ± 0.011	0.118 ± 0.015	0.015 ± 0.003	0.087 ± 0.017	0.119 ± 0.018

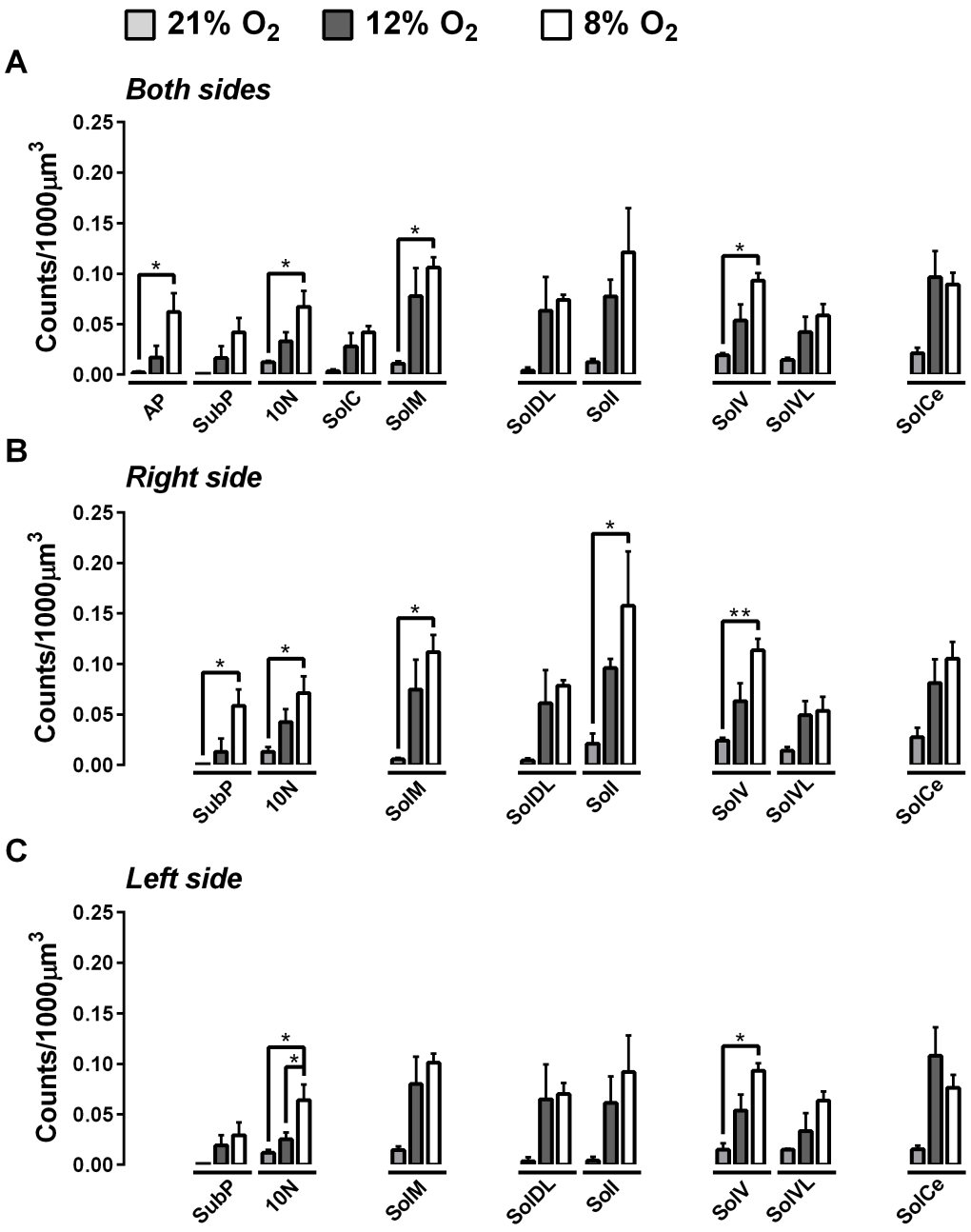

Appendix 2.8: cFos expression at Bregma -7.76mm increases with decreasing PO_2.

Means ± SEM of cFos-positive cell counts per 1000µm^3 in AMPK-α1/α2 floxed mice after 60min exposures to 21% O_2 (n = 4 mice), 12% O_2 (n = 6 mice), or 8% O_2 (n = 6 mice). * = $p<0.05$, ** = $p<0.01$; significance tested by one-way ANOVA with Tukey post-hoc tests.

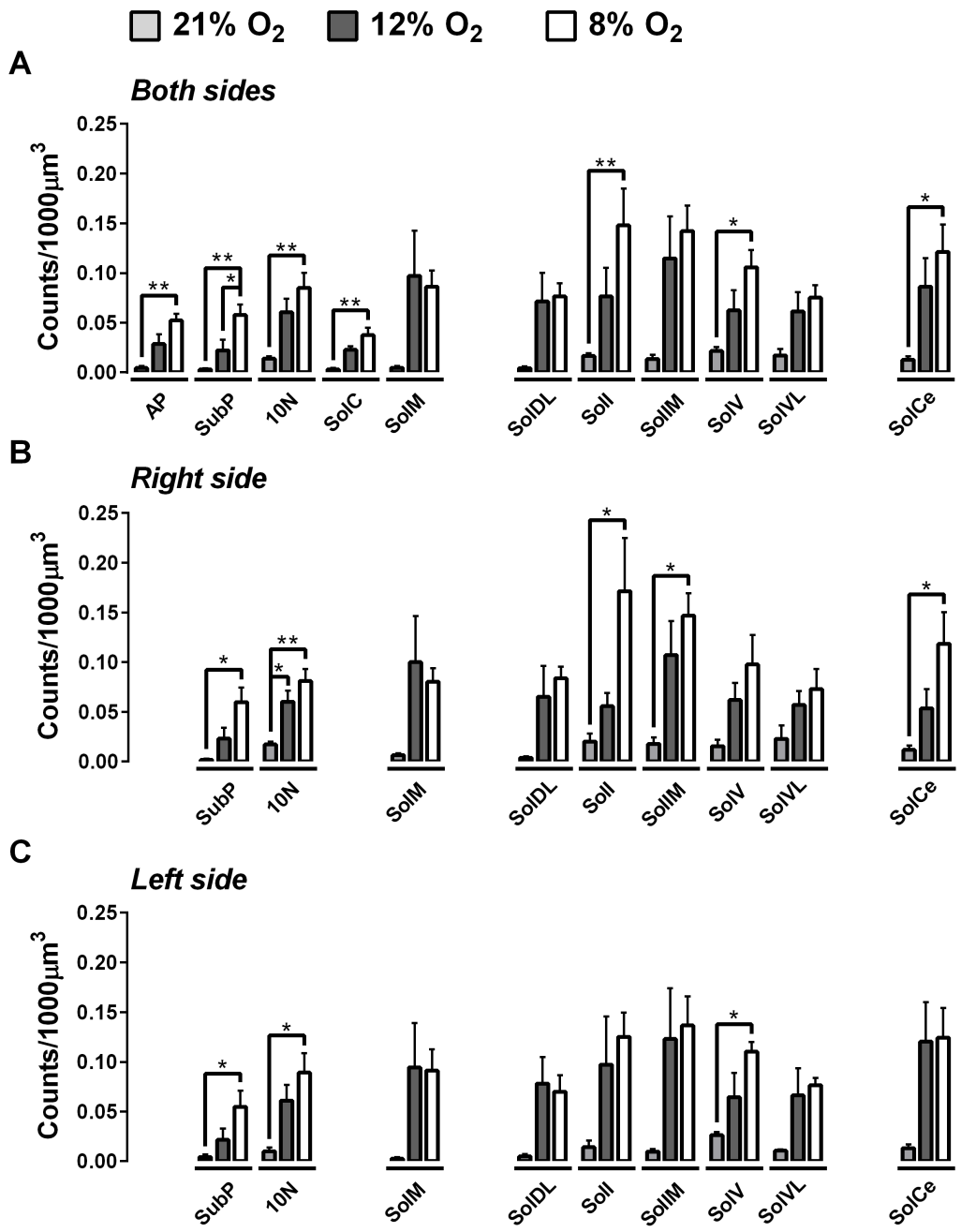

Appendix 2.9: cFos expression at Bregma -7.64mm increases with decreasing PO_2.

Means ± SEM of cFos-positive cell counts per 1000µm^3 in AMPK-α1/α2 floxed mice after 60min exposures to 21% O2 (n = 4 mice), 12% O2 (n = 6 mice), or 8% O2 (n = 6 mice). * = p<0.05, ** = p<0.01; significance tested by one-way ANOVA with Tukey post-hoc tests.

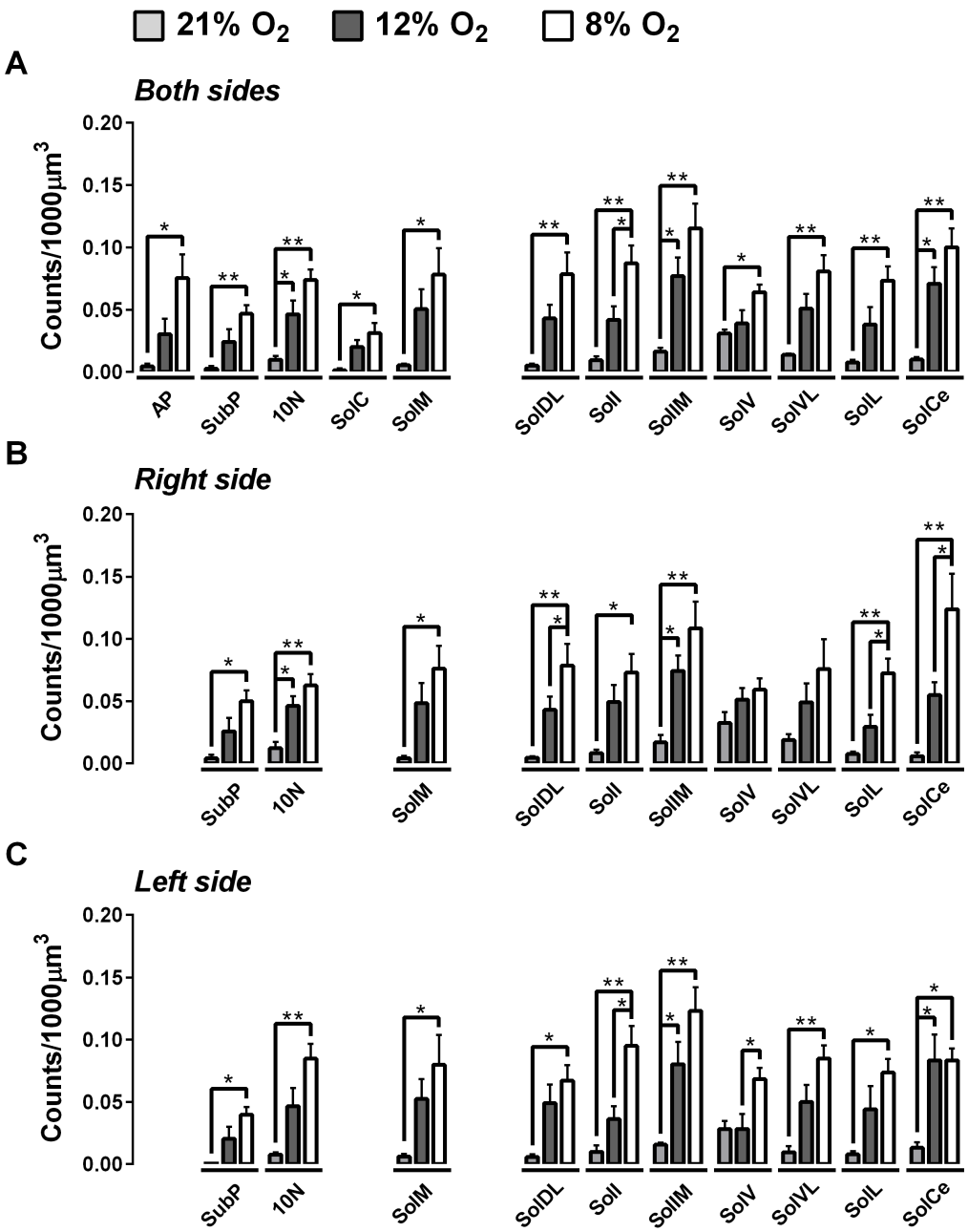

Appendix 2.10: cFos expression at Bregma -7.56mm increases with decreasing PO_2.

Means ± SEM of cFos-positive cell counts per 1000µm^3 in AMPK-α1/α2 floxed mice after 60min exposures to 21% O_2 (n = 4 mice), 12% O_2 (n = 6 mice), or 8% O_2 (n = 6 mice). * = $p<0.05$, ** = $p<0.01$; significance tested by one-way ANOVA with Tukey post-hoc tests.

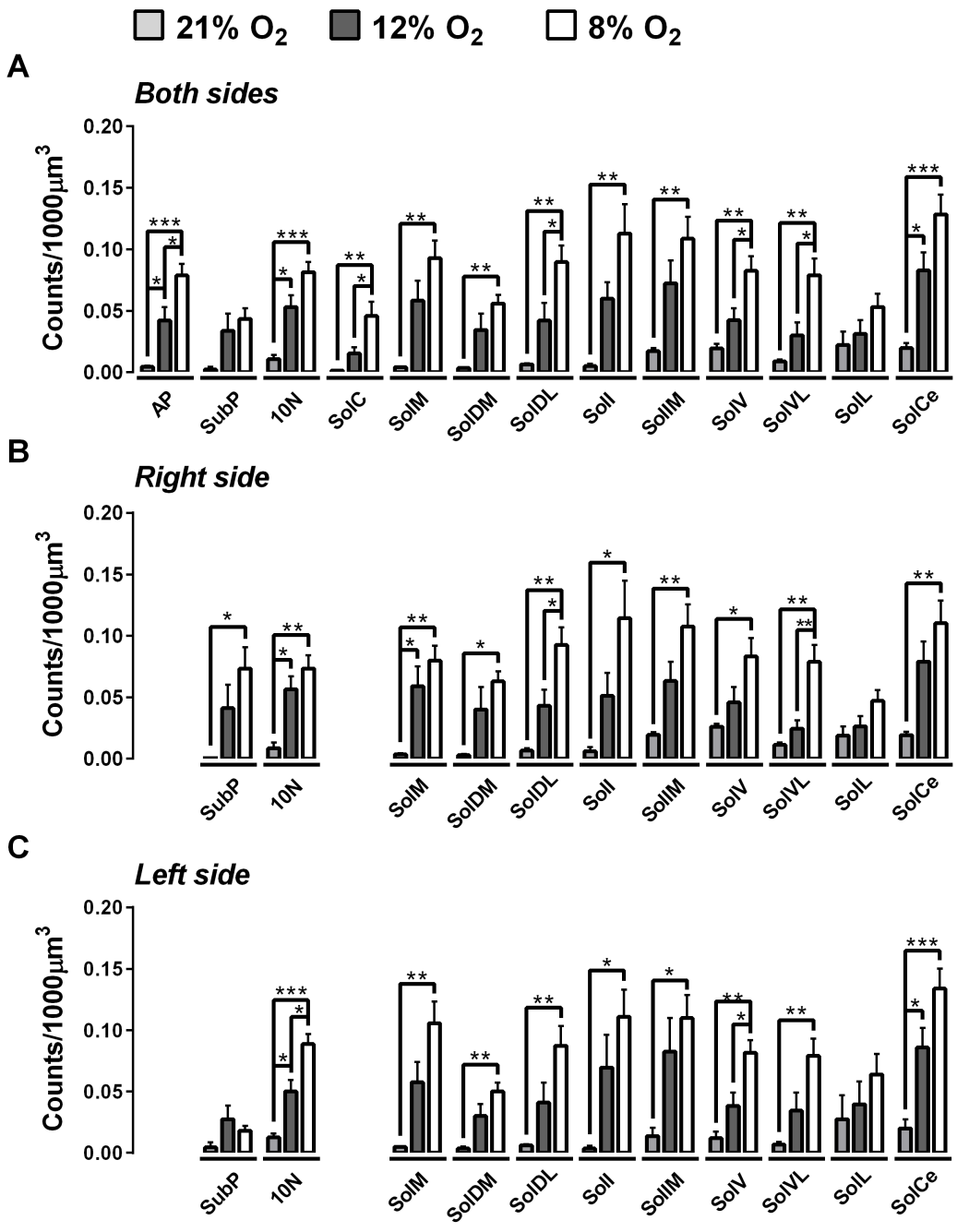

Appendix 2.11: cFos expression at Bregma -7.48mm increases with decreasing PO_2.

Means ± SEM of cFos-positive cell counts per 1000µm^3 in AMPK-α1/α2 floxed mice after 60min exposures to 21% O_2 (n = 4 mice), 12% O_2 (n = 6 mice), or 8% O_2 (n = 6 mice). * = $p<0.05$, ** = $p<0.01$, *** = $p<0.001$; significance tested by one-way ANOVA with Tukey post-hoc tests.

Appendix 2.12: Means ± SEM of cFos counts (per 1000µm^3) for each Bregma of the whole, right, and left side of the NTS in AMPK-α1/α2 Flx and TH AMPK-α1/α2 dKO mice.

	Both sides			Right side			Left side		
	AMPK-α1/α2 Flx	TH AMPK-α1/α2 dKO	p-value	AMPK-α1/α2 Flx	TH AMPK-α1/α2 dKO	p-value	AMPK-α1/α2 Flx	TH AMPK-α1/α2 dKO	p-value
- 7.76 mm	0.073 ± 0.008 n = 3	0.071 ± 0.012 n = 6	ns	0.078 ± 0.01 n = 3	0.072 ± 0.013 n = 6	ns	0.068 ± 0.008 n = 3	0.07 ± 0.011 n = 6	ns
- 7.70 mm	0.071 ± 0.011 n = 4	0.072 ± 0.017 n = 3	ns	0.067 ± 0.012 n = 4	0.071 ± 0.013 n = 3	ns	0.074 ± 0.012 n = 4	0.072 ± 0.021 n = 3	ns
- 7.64 mm	0.087 ± 0.012 n = 5	0.066 ± 0.013 n = 7	ns	0.088 ± 0.013 n = 5	0.068 ± 0.014 n = 7	ns	0.086 ± 0.013 n = 5	0.064 ± 0.012 n = 7	ns
- 7.60 mm	0.07 ± 0.022 n = 2	0.062 ± 0.037 n = 2	ns	0.072 ± 0.026 n = 2	0.061 ± 0.03 n = 2	ns	0.067 ± 0.018 n = 2	0.064 ± 0.043 n = 2	ns
- 7.56 mm	0.078 ± 0.011 n = 4	0.06 ± 0.012 n = 7	ns	0.076 ± 0.012 n = 4	0.062 ± 0.012 n = 7	ns	0.079 ± 0.009 n = 4	0.059 ± 0.012 n = 7	ns
- 7.52 mm	0.086 ± 0.013 n = 4	0.075 ± 0.016 n = 5	ns	0.083 ± 0.015 n = 4	0.073 ± 0.015 n = 5	ns	0.089 ± 0.013 n = 4	0.077 ± 0.017 n = 5	ns
- 7.48 mm	0.086 ± 0.009 n = 6	0.065 ± 0.013 n = 7	ns	0.081 ± 0.01 n = 6	0.065 ± 0.012 n = 7	ns	0.087 ± 0.009 n = 6	0.065 ± 0.014 n = 7	ns
- 7.44 mm	0.1 ± 0.007 n = 3	0.06 ± 0.014 n = 4	ns	0.101 ± 0.007 n = 3	0.065 ± 0.017 n = 4	ns	0.1 ± 0.007 n = 3	0.054 ± 0.011 n = 4	ns

ns = not significant; significance tested by multiple t-tests with Holm-Sidak post-hoc test.

Appendix 2.13: Means ± SEM of cFos counts (per 1000µm^3) for each subnucleus along the length of the total, right, and left NTS in AMPK-α1/α2 Flx (n = 6) and TH AMPK-α1/α2 dKO (n = 7) mice for each subnucleus of the NTS.

	Both sides			Right side			Left side		
	AMPK-α1/α2 Flx	TH AMPK-α1/α2 dKO	p-value	AMPK-α1/α2 Flx	TH AMPK-α1/α2 dKO	p-value	AMPK-α1/α2 Flx	TH AMPK-α1/α2 dKO	p-value
AP	0.073 ± 0.014	0.049 ± 0.009	ns	/	/	/	/	/	/
SubP	0.052 ± 0.007	0.03 ± 0.005	ns	0.059 ± 0.009	0.029 ± 0.005	ns	0.045 ± 0.008	0.03 ± 0.005	ns
10N	0.082 ± 0.009	0.06 ± 0.01	ns	0.076 ± 0.008	0.059 ± 0.011	ns	0.087 ± 0.011	0.062 ± 0.009	ns
SolC	0.039 ± 0.004	0.025 ± 0.006	ns	/	/	/	/	/	/
SolM	0.09 ± 0.01	0.074 ± 0.018	ns	0.085 ± 0.008	0.076 ± 0.018	ns	0.094 ± 0.013	0.072 ± 0.018	ns
SolDM	0.061 ± 0.01	0.037 ± 0.01	ns	0.068 ± 0.012	0.042 ± 0.014	ns	0.056 ± 0.01	0.034 ± 0.008	ns
SolDL	0.083 ± 0.009	0.056 ± 0.012	ns	0.09 ± 0.011	0.061 ± 0.012	ns	0.078 ± 0.009	0.052 ± 0.013	ns
SolI	0.118 ± 0.021	0.086 ± 0.013	ns	0.125 ± 0.029	0.091 ± 0.012	ns	0.111 ± 0.014	0.081 ± 0.015	ns
SolIM	0.126 ± 0.016	0.111 ± 0.025	ns	0.125 ± 0.015	0.113 ± 0.026	ns	0.128 ± 0.017	0.108 ± 0.024	ns
SolV	0.086 ± 0.008	0.06 ± 0.012	ns	0.086 ± 0.011	0.061 ± 0.011	ns	0.086 ± 0.006	0.059 ± 0.013	ns
SolVL	0.079 ± 0.01	0.064 ± 0.008	ns	0.078 ± 0.013	0.065 ± 0.007	ns	0.08 ± 0.008	0.064 ± 0.01	ns
SolL	0.073 ± 0.007	0.062 ± 0.006	ns	0.069 ± 0.006	0.056 ± 0.004	ns	0.08 ± 0.01	0.069 ± 0.011	ns
SolCe	0.118 ± 0.016	0.1 ± 0.018	ns	0.118 ± 0.015	0.104 ± 0.018	ns	0.119 ± 0.018	0.096 ± 0.019	ns

ns = not significant; significance tested by two-way ANOVA with Sidak post-hoc test.

Appendix 2.14: Means ± SEM of cFos counts (per 1000µm^3) for subnuclei of the NTS at each Bregma between AMPK-α1/α2 Flx and TH AMPK-α1/α2 dKO mice.

Both	Bregma 1			Bregma 2			Bregma 3			Bregma 4		
	AMPK-α1/α2 Flx	TH AMPK-α1/α2 dKO	p-value	AMPK-α1/α2 Flx	TH AMPK-α1/α2 dKO	p-value	AMPK-α1/α2 Flx	TH AMPK-α1/α2 dKO	p-value	AMPK-α1/α2 Flx	TH AMPK-α1/α2 dKO	p-value
Nucleus A	0.077 ± 0.013 n = 3	0.052 ± 0.013 n = 4	ns	0.09 ± 0.013 n = 6	0.051 ± 0.006 n = 7	*	0.083 ± 0.015 n = 4	0.057 ± 0.014 n = 5	ns	0.078 ± 0.018 n = 4	0.055 ± 0.013 n = 7	ns
Nucleus B	0.063 ± 0.021 n = 3	0.033 ± 0.004 n = 4	ns	0.043 ± 0.009 n = 6	0.027 ± 0.009 n = 7	ns	0.06 ± 0.006 n = 4	0.036 ± 0.012 n = 5	ns	0.047 ± 0.007 n = 4	0.028 ± 0.008 n = 7	ns
Nucleus C	0.075 ± 0.023 n = 3	0.023 ± 0.008 n = 3	ns	0.056 ± 0.007 n = 6	0.039 ± 0.01 n = 7	ns	0.083 ± 0.031 n = 2	0.046 ± 0.015 n = 5	ns	/	/	/
Nucleus D	0.107 ± 0.007 n = 3	0.049 ± 0.010 n = 4	**	0.081 ± 0.008 n = 6	0.064 ± 0.01 n = 7	ns	0.084 ± 0.01 n = 4	0.068 ± 0.012 n = 5	ns	0.074 ± 0.008 n = 4	0.061 ± 0.01 n = 7	ns
Nucleus E	0.063 ± 0.022 n = 3	0.062 ± 0.024 n = 4	ns	0.046 ± 0.011 n = 6	0.025 ± 0.008 n = 7	ns	0.028 ± 0.006 n = 4	0.036 ± 0.013 n = 5	ns	0.031 ± 0.008 n = 4	0.015 ± 0.005 n = 7	ns
Nucleus F	0.088 ± 0.011 n = 3	0.061 ± 0.02 n = 4	ns	0.093 ± 0.014 n = 6	0.075 ± 0.019 n = 7	ns	0.09 ± 0.023 n = 4	0.83 ± 0.024 n = 5	ns	0.078 ± 0.021 n = 4	0.053 ± 0.013 n = 7	ns
Nucleus G	0.105 ± 0.013 n = 3	0.131 ± 0.041 n = 4	ns	0.113 ± 0.024 n = 6	0.08 ± 0.019 n = 7	ns	0.117 ± 0.028 n = 4	0.111 ± 0.028 n = 5	ns	0.087 ± 0.014 n = 4	0.072 ± 0.011 n = 7	ns
Nucleus H	0.15 ± 0.005 n = 3	0.103 ± 0.041 n = 4	ns	0.109 ± 0.018 n = 6	0.109 ± 0.027 n = 7	ns	0.126 ± 0.028 n = 4	0.125 ± 0.026 n = 5	ns	0.115 ± 0.02 n = 4	0.105 ± 0.022 n = 7	ns
Nucleus I	0.114 ± 0.015 n = 3	0.051 ± 0.012 n = 4	*	0.082 ± 0.012 n = 6	0.059 ± 0.013 n = 7	ns	0.083 ± 0.01 n = 4	0.075 ± 0.02 n = 5	ns	0.064 ± 0.006 n = 4	0.056 ± 0.013 n = 7	ns
Nucleus J	0.095 ± 0.011 n = 3	0.08 ± 0.019 n = 4	ns	0.079 ± 0.014 n = 6	0.063 ± 0.008 n = 7	ns	0.084 ± 0.008 n = 4	0.073 ± 0.008 n = 5	ns	0.081 ± 0.013 n = 4	0.058 ± 0.009 n = 7	ns
Nucleus K	0.083 ± 0.006 n = 3	0.063 ± 0.014 n = 4	ns	0.053 ± 0.011 n = 6	0.064 ± 0.009 n = 7	ns	0.078 ± 0.019 n = 4	0.075 ± 0.015 n = 5	ns	0.073 ± 0.011 n = 4	0.054 ± 0.007 n = 7	ns
Nucleus L	0.146 ± 0.015 n = 3	0.094 ± 0.023 n = 4	ns	0.129 ± 0.016 n = 6	0.109 ± 0.024 n = 7	ns	0.115 ± 0.028 n = 4	0.127 ± 0.028 n = 5	ns	0.1 ± 0.015 n = 4	0.09 ± 0.018 n = 7	ns
Nucleus M	0.103 ± 0.031 n = 3	0.061 ± 0.013 n = 4	ns	0.079 ± 0.009 n = 6	0.058 ± 0.013 n = 7	ns	0.077 ± 0.024 n = 4	0.054 ± 0.015 n = 5	ns	0.076 ± 0.019 n = 4	0.035 ± 0.008 n = 7	*

Both	Bregma 5			Bregma 6			Bregma 7			Bregma 8		
	AMPK-α1/α2 Flx	TH AMPK-α1/α2 dKO	p-value	AMPK-α1/α2 Flx	TH AMPK-α1/α2 dKO	p-value	AMPK-α1/α2 Flx	TH AMPK-α1/α2 dKO	p-value	AMPK-α1/α2 Flx	TH AMPK-α1/α2 dKO	p-value
Nucleus A	0.064 ± 0.026 n = 2	0.047 ± 0.038 n = 2	ns	0.077 ± 0.013 n = 5	0.064 ± 0.015 n = 7	ns	0.07 ± 0.01 n = 4	0.075 ± 0.028 n = 3	ns	0.074 ± 0.005 n = 3	0.064 ± 0.016 n = 6	ns
Nucleus B	0.045 ± 0.023 n = 2	0.039 ± 0.027 n = 2	ns	0.058 ± 0.011 n = 5	0.029 ± 0.005 n = 7	ns	0.039 ± 0.01 n = 4	0.04 ± 0.015 n = 3	ns	0.042 ± 0.014 n = 3	0.03 ± 0.004 n = 6	ns
Nucleus C	/	/	/	/	/	/	/	/	/	/	/	/
Nucleus D	0.066 ± 0.013 n = 2	0.065 ± 0.03 n = 2	ns	0.085 ± 0.015 n = 5	0.06 ± 0.012 n = 7	ns	0.074 ± 0.015 n = 4	0.06 ± 0.017 n = 3	ns	0.067 ± 0.016 n = 3	0.069 ± 0.009 n = 6	ns
Nucleus E	0.023 ± 0.011 n = 2	0.032 ± 0.009 n = 2	ns	0.037 ± 0.007 n = 5	0.025 ± 0.006 n = 7	ns	0.03 ± 0.007 n = 4	0.021 ± 0.006 n = 3	ns	0.042 ± 0.006 n = 3	0.031 ± 0.006 n = 6	ns
Nucleus F	0.074 ± 0.033 n = 2	0.049 ± 0.034 n = 2	ns	0.086 ± 0.016 n = 5	0.092 ± 0.022 n = 7	ns	0.082 ± 0.013 n = 4	0.102 ± 0.025 n = 3	ns	0.106 ± 0.01 n = 3	0.106 ± 0.023 n = 6	ns
Nucleus G	0.061 ± 0.005 n = 2	0.082 ± 0.033 n = 2	ns	0.148 ± 0.037 n = 5	0.074 ± 0.012 n = 7	ns	0.097 ± 0.024 n = 4	0.073 ± 0.024 n = 3	ns	0.121 ± 0.044 n = 3	0.104 ± 0.016 n = 6	ns
Nucleus H	0.104 ± 0.037 n = 2	0.102 ± 0.06 n = 2	ns	0.142 ± 0.026 n = 5	0.118 ± 0.028 n = 7	ns	0.092 ± 0.014 n = 3	0.124 ± 0.019 n = 3	ns	/	/	/
Nucleus I	0.073 ± 0.012 n = 2	0.046 ± 0.027 n = 2	ns	0.106 ± 0.018 n = 5	0.06 ± 0.009 n = 7	*	0.083 ± 0.02 n = 4	0.072 ± 0.008 n = 3	ns	0.093 ± 0.008 n = 3	0.089 ± 0.014 n = 6	ns
Nucleus J	0.065 ± 0.012 n = 2	0.092 ± 0.052 n = 2	ns	0.075 ± 0.013 n = 5	0.056 ± 0.009 n = 7	ns	0.073 ± 0.014 n = 4	0.068 ± 0.012 n = 3	ns	0.058 ± 0.011 n = 3	0.068 ± 0.07 n = 6	ns
Nucleus K	0.075 ± 0.01 n = 2	0.059 ± 0.026 n = 2	ns	/	/	/	/	/	/	/	/	/
Nucleus L	0.085 ± 0.031 n = 2	0.093 ± 0.067 n = 2	ns	0.121 ± 0.027 n = 5	0.093 ± 0.015 n = 7	ns	0.088 ± 0.025 n = 4	0.095 ± 0.011 n = 3	ns	0.089 ± 0.012 n = 3	0.103 ± 0.019 n = 6	ns
Nucleus M	0.101 ± 0.021 n = 2	0.045 ± 0.029 n = 2	ns	0.052 ± 0.007 n = 5	0.033 ± 0.008 n = 7	ns	0.05 ± 0.02 n = 4	0.038 ± 0.007 n = 3	ns	0.062 ± 0.019 n = 3	0.047 ± 0.009 n = 6	ns

ns = not significant, * = p<0.05, ** = p<0.01, *** = p<0.001; significance tested by unpaired t-test between genotypes.

Right	Bregma 1			Bregma 2			Bregma 3			Bregma 4		
	AMPK-α1/α2 Flx	TH AMPK-α1/α2 dKO	p-value	AMPK-α1/α2 Flx	TH AMPK-α1/α2 dKO	p-value	AMPK-α1/α2 Flx	TH AMPK-α1/α2 dKO	p-value	AMPK-α1/α2 Flx	TH AMPK-α1/α2 dKO	p-value
Nucleus A	0.089 ± 0.013 n = 3	0.066 ± 0.014 n = 4	ns	0.093 ± 0.014 n = 6	0.051 ± 0.008 n = 7	*	0.091 ± 0.026 n = 4	0.049 ± 0.009 n = 5	ns	0.088 ± 0.022 n = 4	0.06 ± 0.014 n = 7	ns
Nucleus B	0.056 ± 0.028 n = 3	0.031 ± 0.009 n = 4	ns	0.073 ± 0.017 n = 6	0.025 ± 0.01 n = 7	*	0.074 ± 0.022 n = 4	0.035 ± 0.015 n = 5	ns	0.05 ± 0.009 n = 4	0.027 ± 0.005 n = 7	*
Nucleus C	0.092 ± 0.027 n = 3	0.029 ± 0.01 n = 3	ns	0.063 ± 0.008 n = 6	0.041 ± 0.014 n = 7	ns	0.089 ± 0.03 n = 2	0.059 ± 0.029 n = 5	ns	/	/	/
Nucleus D	0.105 ± 0.007 n = 3	0.049 ± 0.012 n = 4	*	0.073 ± 0.011 n = 6	0.064 ± 0.01 n = 7	ns	0.073 ± 0.01 n = 4	0.071 ± 0.01 n = 5	ns	0.062 ± 0.009 n = 4	0.057 ± 0.01 n = 7	ns
Nucleus E	/	/	/	/	/	/	/	/	/	/	/	/
Nucleus F	0.089 ± 0.01 n = 3	0.066 ± 0.024 n = 4	ns	0.08 ± 0.012 n = 6	0.077 ± 0.017 n = 7	ns	0.082 ± 0.022 n = 4	0.83 ± 0.024 n = 5	ns	0.076 ± 0.019 n = 4	0.057 ± 0.015 n = 7	ns
Nucleus G	0.106 ± 0.022 n = 3	0.142 ± 0.041 n = 4	ns	0.114 ± 0.031 n = 6	0.095 ± 0.02 n = 7	ns	0.122 ± 0.044 n = 4	0.099 ± 0.031 n = 5	ns	0.073 ± 0.015 n = 4	0.069 ± 0.014 n = 7	ns
Nucleus H	0.15 ± 0.015 n = 3	0.1 ± 0.045 n = 4	ns	0.108 ± 0.018 n = 6	0.1 ± 0.024 n = 7	ns	0.121 ± 0.03 n = 4	0.119 ± 0.035 n = 5	ns	0.109 ± 0.021 n = 4	0.114 ± 0.026 n = 7	ns
Nucleus I	0.113 ± 0.008 n = 3	0.054 ± 0.019 n = 4	ns	0.083 ± 0.015 n = 6	0.053 ± 0.012 n = 7	ns	0.082 ± 0.008 n = 4	0.072 ± 0.022 n = 5	ns	0.059 ± 0.009 n = 4	0.056 ± 0.013 n = 7	ns
Nucleus J	0.106 ± 0.022 n = 3	0.09 ± 0.021 n = 4	ns	0.079 ± 0.014 n = 6	0.063 ± 0.008 n = 7	ns	0.084 ± 0.009 n = 4	0.06 ± 0.006 n = 5	ns	0.076 ± 0.024 n = 4	0.059 ± 0.011 n = 7	ns
Nucleus K	0.082 ± 0.011 n = 3	0.049 ± 0.011 n = 4	ns	0.047 ± 0.009 n = 6	0.064 ± 0.009 n = 7	ns	0.071 ± 0.02 n = 4	0.06 ± 0.012 n = 5	ns	0.072 ± 0.012 n = 4	0.052 ± 0.005 n = 7	ns
Nucleus L	0.145 ± 0.008 n = 3	0.103 ± 0.036 n = 4	ns	0.11 ± 0.018 n = 6	0.105 ± 0.02 n = 7	ns	0.123 ± 0.037 n = 4	0.129 ± 0.023 n = 5	ns	0.124 ± 0.029 n = 4	0.091 ± 0.019 n = 7	ns

Right	Bregma 5			Bregma 6			Bregma 7			Bregma 8		
	AMPK-α1/α2 Flx	TH AMPK-α1/α2 dKO	p-value	AMPK-α1/α2 Flx	TH AMPK-α1/α2 dKO	p-value	AMPK-α1/α2 Flx	TH AMPK-α1/α2 dKO	p-value	AMPK-α1/α2 Flx	TH AMPK-α1/α2 dKO	p-value
Nucleus A	0.068 ± 0.037 n = 2	0.045 ± 0.035 n = 2	ns	0.084 ± 0.012 n = 5	0.067 ± 0.02 n = 7	ns	0.067 ± 0.014 n = 4	0.073 ± 0.026 n = 3	ns	0.079 ± 0.005 n = 3	0.084 ± 0.02 n = 6	ns
Nucleus B	0.039 ± 0.02 n = 2	0.049 ± 0.037 n = 2	ns	0.06 ± 0.015 n = 5	0.028 ± 0.006 n = 7	ns	0.044 ± 0.01 n = 4	0.039 ± 0.014 n = 3	ns	0.059 ± 0.016 n = 3	0.03 ± 0.005 n = 6	ns
Nucleus C	/	/	/	/	/	/	/	/	/	/	/	/
Nucleus D	0.059 ± 0.019 n = 2	0.07 ± 0.03 n = 2	ns	0.081 ± 0.012 n = 5	0.061 ± 0.016 n = 7	ns	0.076 ± 0.017 n = 4	0.056 ± 0.015 n = 3	ns	0.071 ± 0.016 n = 3	0.059 ± 0.012 n = 6	ns
Nucleus E	/	/	/	/	/	/	/	/	/	/	/	/
Nucleus F	0.075 ± 0.031 n = 2	0.049 ± 0.025 n = 2	ns	0.08 ± 0.013 n = 5	0.093 ± 0.023 n = 7	ns	0.073 ± 0.012 n = 4	0.096 ± 0.02 n = 3	ns	0.112 ± 0.017 n = 3	0.099 ± 0.022 n = 6	ns
Nucleus G	0.051 ± 0.004 n = 2	0.068 ± 0.008 n = 2	ns	0.171 ± 0.054 n = 5	0.069 ± 0.015 n = 7	ns	0.092 ± 0.03 n = 4	0.059 ± 0.02 n = 3	ns	0.158 ± 0.054 n = 3	0.138 ± 0.022 n = 6	ns
Nucleus H	0.112 ± 0.04 n = 2	0.085 ± 0.037 n = 2	ns	0.147 ± 0.023 n = 5	0.127 ± 0.031 n = 7	ns	0.09 ± 0.02 n = 3	0.131 ± 0.017 n = 3	ns	/	/	/
Nucleus I	0.072 ± 0.014 n = 2	0.053 ± 0.013 n = 2	ns	0.098 ± 0.03 n = 5	0.065 ± 0.008 n = 7	ns	0.078 ± 0.016 n = 4	0.081 ± 0.015 n = 3	ns	0.114 ± 0.011 n = 3	0.087 ± 0.023 n = 6	ns
Nucleus J	0.071 ± 0.011 n = 2	0.115 ± 0.06 n = 2	ns	0.073 ± 0.02 n = 5	0.061 ± 0.011 n = 7	ns	0.063 ± 0.018 n = 4	0.071 ± 0.003 n = 3	ns	0.054 ± 0.014 n = 3	0.065 ± 0.006 n = 6	ns
Nucleus K	0.101 ± 0.022 n = 2	0.04 ± 0.015 n = 2	ns	/	/	/	/	/	/	/	/	/
Nucleus L	0.105 ± 0.032 n = 2	0.084 ± 0.061 n = 2	ns	0.118 ± 0.032 n = 5	0.092 ± 0.016 n = 7	ns	0.07 ± 0.021 n = 4	0.11 ± 0.01 n = 3	ns	0.105 ± 0.016 n = 3	0.127 ± 0.028 n = 6	ns

Left	Bregma 1			Bregma 2			Bregma 3			Bregma 4		
	AMPK-α1/α2 Flx	TH AMPK-α1/α2 dKO	p-value	AMPK-α1/α2 Flx	TH AMPK-α1/α2 dKO	p-value	AMPK-α1/α2 Flx	TH AMPK-α1/α2 dKO	p-value	AMPK-α1/α2 Flx	TH AMPK-α1/α2 dKO	p-value
Nucleus A	0.074 ± 0.015 n = 3	0.038 ± 0.02 n = 4	ns	0.087 ± 0.016 n = 6	0.05 ± 0.012 n = 7	ns	0.081 ± 0.012 n = 4	0.062 ± 0.019 n = 5	ns	0.067 ± 0.013 n = 4	0.049 ± 0.013 n = 7	ns
Nucleus B	0.07 ± 0.02 n = 3	0.036 ± 0.009 n = 4	ns	0.018 ± 0.004 n = 6	0.03 ± 0.01 n = 7	ns	0.055 ± 0.012 n = 4	0.037 ± 0.009 n = 5	ns	0.04 ± 0.006 n = 4	0.03 ± 0.007 n = 7	ns
Nucleus C	0.063 ± 0.029 n = 3	0.029 ± 0.006 n = 3	ns	0.05 ± 0.007 n = 6	0.035 ± 0.009 n = 7	ns	0.079 ± 0.032 n = 2	0.041 ± 0.013 n = 5	ns	/	/	/
Nucleus D	0.11 ± 0.013 n = 3	0.048 ± 0.009 n = 4	*	0.089 ± 0.008 n = 6	0.064 ± 0.011 n = 7	ns	0.096 ± 0.02 n = 4	0.065 ± 0.015 n = 5	ns	0.085 ± 0.012 n = 4	0.064 ± 0.01 n = 7	ns
Nucleus E	/	/	/	/	/	/	/	/	/	/	/	/
Nucleus F	0.088 ± 0.013 n = 3	0.056 ± 0.017 n = 4	ns	0.105 ± 0.018 n = 6	0.074 ± 0.022 n = 7	ns	0.097 ± 0.027 n = 4	0.83 ± 0.026 n = 5	ns	0.08 ± 0.024 n = 4	0.05 ± 0.012 n = 7	ns
Nucleus G	0.105 ± 0.003 n = 3	0.099 ± 0.052 n = 4	ns	0.111 ± 0.022 n = 6	0.063 ± 0.02 n = 7	ns	0.112 ± 0.018 n = 4	0.12 ± 0.031 n = 5	ns	0.095 ± 0.016 n = 4	0.072 ± 0.013 n = 7	ns
Nucleus H	0.15 ± 0.016 n = 3	0.106 ± 0.038 n = 4	ns	0.11 ± 0.019 n = 6	0.12 ± 0.034 n = 7	ns	0.131 ± 0.028 n = 4	0.129 ± 0.023 n = 5	ns	0.123 ± 0.02 n = 4	0.095 ± 0.02 n = 7	ns
Nucleus I	0.114 ± 0.024 n = 3	0.046 ± 0.011 n = 4	*	0.082 ± 0.01 n = 6	0.066 ± 0.017 n = 7	ns	0.084 ± 0.013 n = 4	0.062 ± 0.019 n = 5	ns	0.068 ± 0.009 n = 4	0.056 ± 0.016 n = 7	ns
Nucleus J	0.086 ± 0.002 n = 3	0.072 ± 0.021 n = 4	ns	0.079 ± 0.014 n = 6	0.063 ± 0.01 n = 7	ns	0.085 ± 0.009 n = 4	0.084 ± 0.01 n = 5	ns	0.085 ± 0.01 n = 4	0.058 ± 0.009 n = 7	ns
Nucleus K	0.085 ± 0.003 n = 3	0.086 ± 0.02 n = 4	ns	0.064 ± 0.017 n = 6	0.065 ± 0.011 n = 7	ns	0.086 ± 0.017 n = 4	0.094 ± 0.018 n = 5	ns	0.073 ± 0.011 n = 4	0.055 ± 0.013 n = 7	ns
Nucleus L	0.174 ± 0.009 n = 3	0.085 ± 0.015 n = 4	**	0.134 ± 0.017 n = 6	0.113 ± 0.029 n = 7	ns	0.106 ± 0.029 n = 4	0.125 ± 0.034 n = 5	ns	0.083 ± 0.01 n = 4	0.09 ± 0.021 n = 7	ns

Left	Bregma 5			Bregma 6			Bregma 7			Bregma 8		
	AMPK-α1/α2 Flx	TH AMPK-α1/α2 dKO	p-value	AMPK-α1/α2 Flx	TH AMPK-α1/α2 dKO	p-value	AMPK-α1/α2 Flx	TH AMPK-α1/α2 dKO	p-value	AMPK-α1/α2 Flx	TH AMPK-α1/α2 dKO	p-value
Nucleus A	0.06 ± 0.013 n = 2	0.049 ± 0.041 n = 2	ns	0.07 ± 0.016 n = 5	0.061 ± 0.014 n = 7	ns	0.072 ± 0.016 n = 4	0.049 ± 0.041 n = 3	ns	0.07 ± 0.011 n = 3	0.046 ± 0.015 n = 6	ns
Nucleus B	0.059 ± 0.028 n = 2	0.022 ± 0.008 n = 2	ns	0.055 ± 0.016 n = 5	0.030 ± 0.008 n = 7	ns	0.034 ± 0.008 n = 4	0.041 ± 0.016 n = 3	ns	0.029 ± 0.013 n = 3	0.029 ± 0.006 n = 6	ns
Nucleus C	/	/	/	/	/	/	/	/	/	/	/	/
Nucleus D	0.073 ± 0.008 n = 2	0.061 ± 0.03 n = 2	ns	0.089 ± 0.02 n = 5	0.06 ± 0.009 n = 7	ns	0.072 ± 0.014 n = 4	0.064 ± 0.02 n = 3	ns	0.064 ± 0.015 n = 3	0.076 ± 0.01 n = 6	ns
Nucleus E	/	/	/	/	/	/	/	/	/	/	/	/
Nucleus F	0.072 ± 0.034 n = 2	0.049 ± 0.042 n = 2	ns	0.091 ± 0.021 n = 5	0.091 ± 0.022 n = 7	ns	0.09 ± 0.018 n = 4	0.111 ± 0.033 n = 3	ns	0.101 ± 0.009 n = 3	0.111 ± 0.025 n = 6	ns
Nucleus G	0.07 ± 0.012 n = 2	0.092 ± 0.067 n = 2	ns	0.125 ± 0.024 n = 5	0.078 ± 0.019 n = 7	ns	0.103 ± 0.023 n = 4	0.088 ± 0.027 n = 3	ns	0.092 ± 0.036 n = 3	0.077 ± 0.019 n = 6	ns
Nucleus H	0.095 ± 0.034 n = 2	0.122 ± 0.088 n = 2	ns	0.137 ± 0.029 n = 5	0.11 ± 0.026 n = 7	ns	0.093 ± 0.014 n = 3	0.118 ± 0.024 n = 3	ns	/	/	/
Nucleus I	0.073 ± 0.011 n = 2	0.042 ± 0.037 n = 2	ns	0.11 ± 0.01 n = 5	0.056 ± 0.012 n = 7	**	0.087 ± 0.025 n = 4	0.066 ± 0.021 n = 3	ns	0.078 ± 0.007 n = 3	0.09 ± 0.014 n = 6	ns
Nucleus J	0.06 ± 0.013 n = 2	0.073 ± 0.045 n = 2	ns	0.076 ± 0.007 n = 5	0.05 ± 0.01 n = 7	ns	0.083 ± 0.019 n = 4	0.065 ± 0.022 n = 3	ns	0.063 ± 0.009 n = 3	0.071 ± 0.009 n = 6	ns
Nucleus K	0.056 ± 0.001 n = 2	0.073 ± 0.03 n = 2	ns	/	/	/	/	/	/	/	/	/
Nucleus L	0.069 ± 0.03 n = 2	0.1 ± 0.072 n = 2	ns	0.124 ± 0.03 n = 5	0.095 ± 0.016 n = 7	ns	0.104 ± 0.029 n = 4	0.078 ± 0.013 n = 3	ns	0.076 ± 0.012 n = 3	0.085 ± 0.013 n = 6	ns

Appendix 2.15: Means ± SEM of cFos counts (per 1000µm^3) for three subnuclei of the NTS and combinations of them that showed hemisphere- and Bregma-specific differences between AMPK-α1/α2 Flx (n = 6) and TH AMPK-α1/α2 dKO (n = 7) mice.

	Both sides			Right side			Left side		
	AMPK-α1/α2 Flx	TH AMPK-α1/α2 dKO	p-value	AMPK-α1/α2 Flx	TH AMPK-α1/α2 dKO	p-value	AMPK-α1/α2 Flx	TH AMPK-α1/α2 dKO	p-value
Nucleus A	0.09 ± 0.013	0.051 ± 0.006	*	0.093 ± 0.014	0.051 ± 0.008	*	0.087 ± 0.016	0.05 ± 0.012	ns
Nucleus B	0.043 ± 0.009	0.027 ± 0.009	ns	0.073 ± 0.017 n = 6	0.025 ± 0.01 n = 7	*	0.018 ± 0.004 n = 6	0.03 ± 0.01 n = 7	ns

	Nucleus A			Nucleus B			Nucleus C		
	AMPK-α1/α2 Flx	TH AMPK-α1/α2 dKO	p-value	AMPK-α1/α2 Flx	TH AMPK-α1/α2 dKO	p-value	AMPK-α1/α2 Flx	TH AMPK-α1/α2 dKO	p-value
Bregma 1	0.089 ± 0.013 n = 3	0.066 ± 0.014 n = 4	ns	0.056 ± 0.028 n = 3	0.031 ± 0.009 n = 4	ns	0.092 ± 0.027 n = 3	0.029 ± 0.01 n = 4	ns
Bregma 2	0.093 ± 0.014 n = 6	0.051 ± 0.008 n = 7	*	0.073 ± 0.017 n = 6	0.025 ± 0.01 n = 7	*	0.063 ± 0.008 n = 6	0.041 ± 0.014 n = 7	ns
Bregma 3	0.091 ± 0.026 n = 4	0.049 ± 0.009 n = 5	ns	0.074 ± 0.022 n = 4	0.035 ± 0.015 n = 5	ns	0.089 ± 0.03 n = 2	0.059 ± 0.029 n = 5	ns
Bregma 4	0.088 ± 0.022 n = 4	0.06 ± 0.014 n = 7	ns	0.063 ± 0.014 n = 6	0.028 ± 0.006 n = 7	*	/	/	/
Bregma 1+2	0.092 ± 0.011 n = 6	0.054 ± 0.007 n = 7	*	0.065 ± 0.0169 n = 6	0.028 ± 0.009 n = 7	ns	0.067 ± 0.011 n = 6	0.041 ± 0.012 n = 7	ns
Bregma 2+3	0.088 ± 0.014 n = 6	0.053 ± 0.013 n = 7	ns	0.074 ± 0.014 n = 6	0.033 ± 0.014 n = 5	ns	0.066 ± 0.01 n = 6	0.041 ± 0.015 n = 7	ns
Bregma 3+4	0.092 ± 0.018 n = 6	0.064 ± 0.016 n = 7	ns	0.063 ± 0.014 n = 6	0.028 ± 0.006 n = 7	*	/	/	/
Bregma 1-3	0.091 ± 0.013 n = 6	0.053 ± 0.01 n = 7	*	0.071 ± 0.014 n = 6	0.031 ± 0.01 n = 7	*	0.068 ± 0.012 n = 6	0.042 ± 0.014 n = 7	ns
Bregma 2-4	0.094 ± 0.014 n = 6	0.057 ± 0.01 n = 7	ns	0.063 ± 0.012 n = 6	0.027 ± 0.006 n = 7	*	/	/	/
Bregma 1-4	0.093 ± 0.013 n = 6	0.057 ± 0.009 n = 7	*	0.063 ± 0.013 n = 6	0.028 ± 0.006 n = 7	*	/	/	/

	Combination 1			Combination 2			Combination 3		
	0.084 ± 0.01 n = 6	0.044 ± 0.006 n = 7	**	0.084 ± 0.01 n = 6	0.044 ± 0.006 n = 7	**	0.079 ± 0.008 n = 6	0.044 ± 0.007 n = 7	**

ns = not significant, * = p<0.05, ** = p<0.01; significance tested by unpaired t-test between genotypes.

Appendix 2.16: Means ± SEM of dorsal tyrosine hydroxylase (TH)-positive cell activation (in %) and total cell counts for each Bregma of the whole brainstem in AMPK-α1/α2 Flx mice.

	% activation	Counts per Bregma
- 7.76 mm	73.55 ± 12.9 n = 3	15.67 ± 3.93 n = 3
- 7.70 mm	83.6 ± 5.67 n = 4	17.25 ± 5.15 n = 4
- 7.64 mm	73.67 ± 7 n = 5	14.2 ± 5.62 n = 5
- 7.60 mm	83.15 ± 5.74 n = 2	24.5 ± 6.5 n = 2
- 7.56 mm	82.41 ± 12.17 n = 4	15.75 ± 5.48 n = 4
- 7.52 mm	67.66 ± 13.54 n = 5	14.17 ± 4.72 n = 6
- 7.48 mm	74.37 ± 9.27 n = 6	12.33 ± 3.34 n = 6
- 7.44 mm	100 n = 1	0.5 ± 0.5 n = 2

Appendix 2.17: Means ± SEM of PO_2-dependent changes in dorsal tyrosine hydroxylase (TH)-positive cell activation (in %) for each Bregma of the whole brainstem in AMPK-α1/α2 Flx mice.

	21% O_2	12% O_2	8% O_2
- 7.76 mm	84.26 ± 7.91 n = 3	84.09 ± 11.81 n = 4	73.55 ± 12.9 n = 3
- 7.70 mm		86.16 ± 7.59 n = 2	83.6 ± 5.67 n = 4
- 7.64 mm	77.73 ± 5.28 n = 4	64.74 ± 15.34 n = 6	73.67 ± 7 n = 5
- 7.60 mm	43.48 n = 1	81.25 n = 1	83.15 ± 5.74 n = 2
- 7.56 mm	71.07 ± 9.05 n = 4	69.79 ± 13.84 n = 5	82.41 ± 12.17 n = 4
- 7.52 mm	95 ± 5 n = 2	88.04 ± 6.38 n = 5	67.66 ± 13.54 n = 5
- 7.48 mm	70.98 ± 7.8 n = 4	70.4 ± 4.79 n = 4	74.37 ± 9.27 n = 6
- 7.44 mm	46.67 n = 1	100 n = 1	100 n = 1

Appendix 3

Supplementary material for Chapter 5

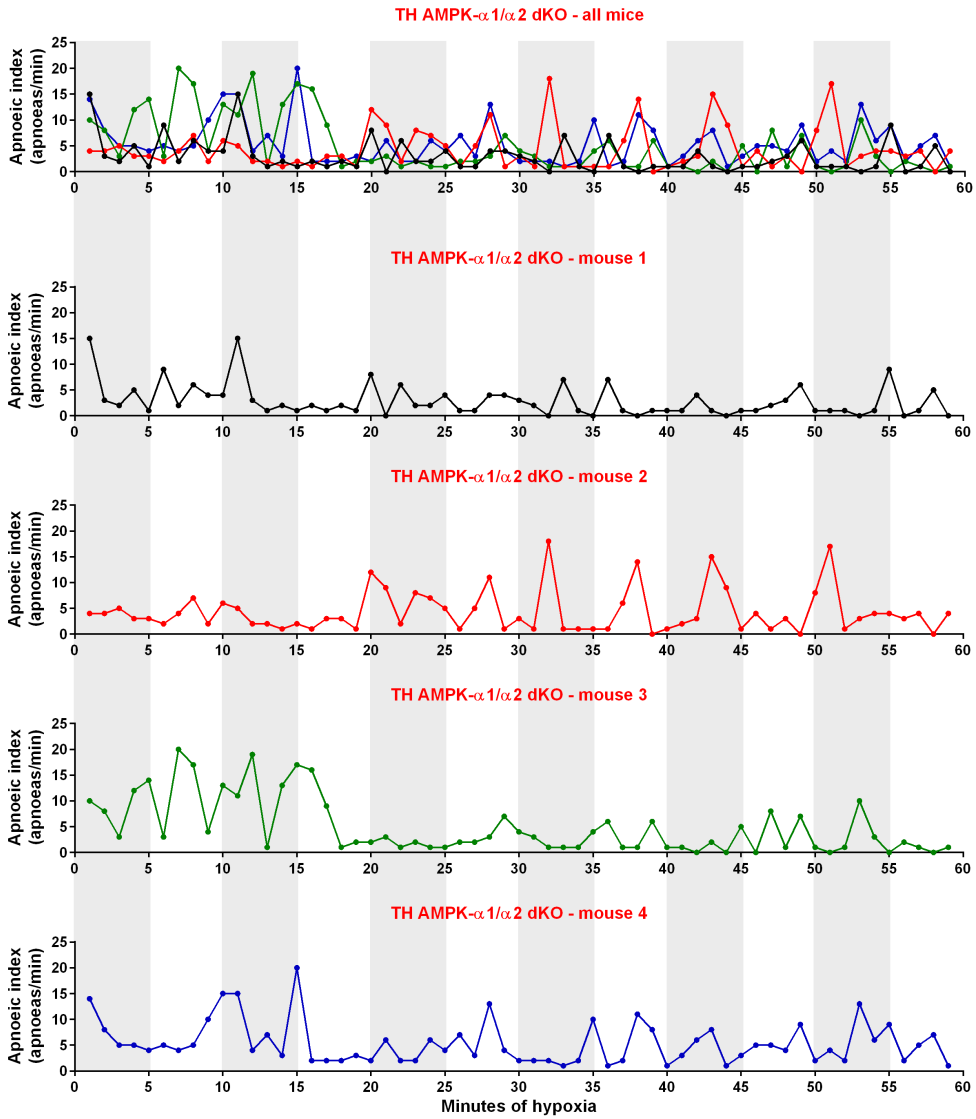

Appendix 3.1: Dual deletion of the AMPK-α1/α2 catalytic subunits in catecholaminergic cells precipitates "bursts" of apnoea frequency at regular intervals during prolonged 60min exposures to severe hypoxia.

Line charts show the mean apnoea index (AI, apnoeas/min) over a 60min period of severe hypoxia (8% O_2) of all experimental TH-driven AMPK-α1 and -α2 double knockout mice (TH AMPK-α1/α2 dKO, n = 4) at the top and each individual trace below.

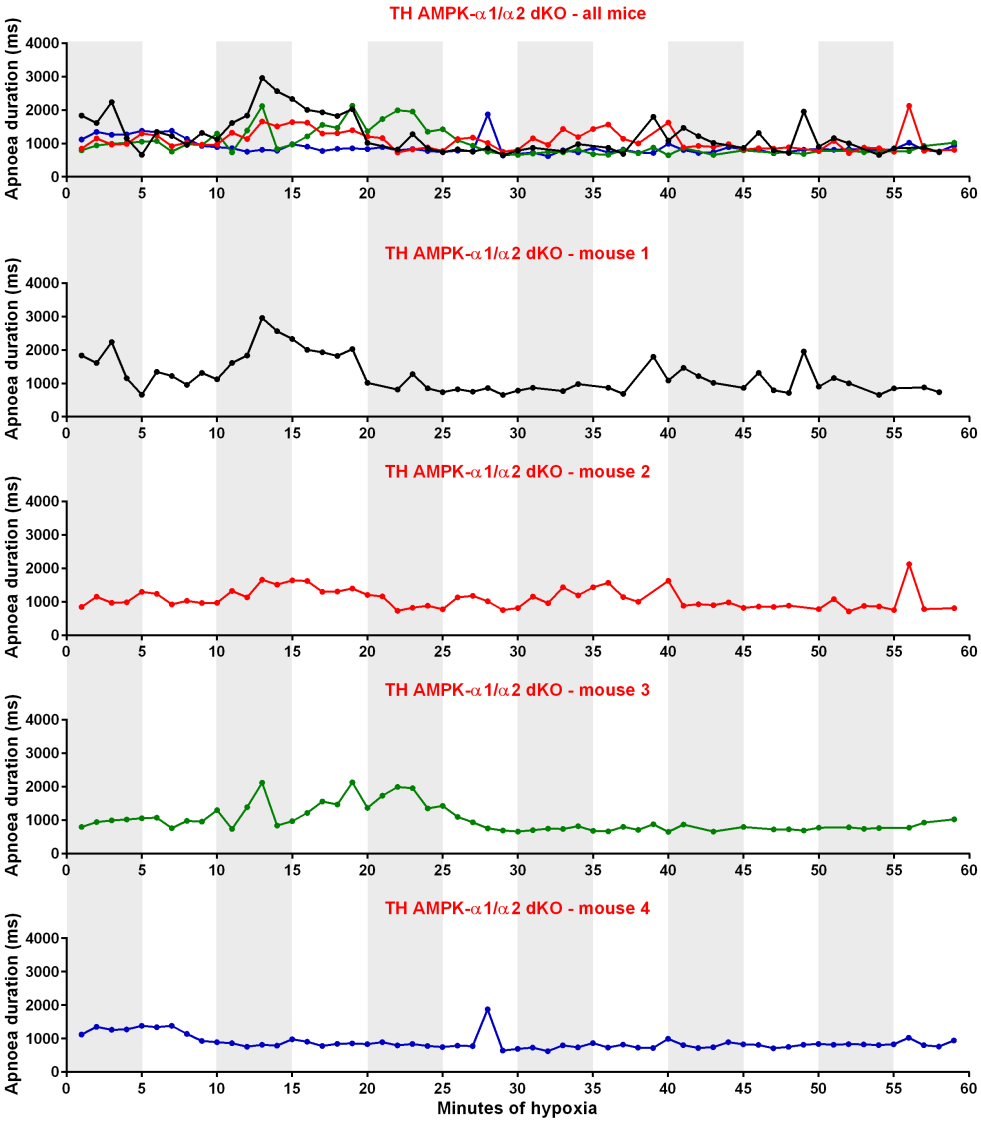

Appendix 3.2: The apnoea duration declines and stabilises over time in mice with dual deletion of the AMPK-α1/α2 catalytic subunits in catecholaminergic cells during prolonged 60min exposures to severe hypoxia.

Line charts show the mean apnoea duration (AD, ms) over a 60min period of severe hypoxia (8% O_2) of all experimental TH-driven AMPK-α1 and -α2 double knockout mice (TH AMPK-α1/α2 dKO, n = 4) at the top and each individual trace below.

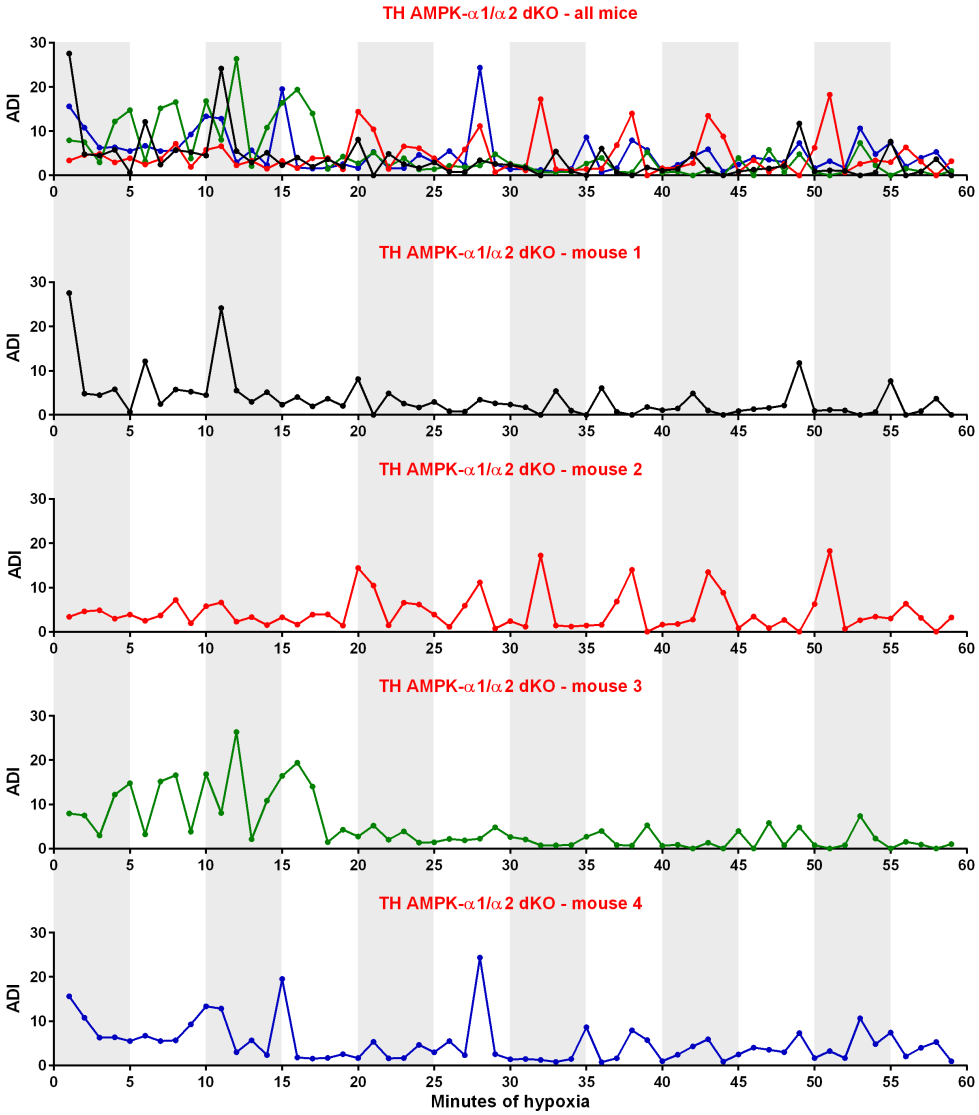

Appendix 3.3: Dual deletion of the AMPK-α1/α2 catalytic subunits in catecholaminergic cells precipitates "bursts" of the apnoea duration index at regular intervals during prolonged 60min exposures to severe hypoxia.

Line charts show the mean apnoea duration index (ADI, AI x duration) over a 60min period of severe hypoxia (8% O_2) of all experimental TH-driven AMPK-α1 and -α2 double knockout mice (TH AMPK-α1/α2 dKO, n = 4) at the top and each individual trace below.

Appendix 4

Supplementary material for Chapter 7

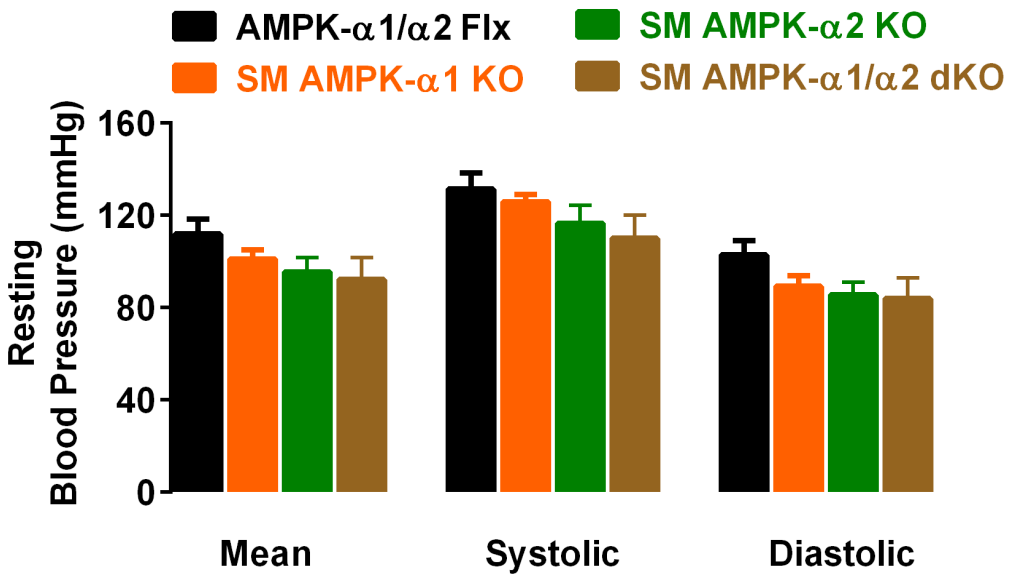

Appendix 4.1: Dual deletion of the AMPK-α1/α2 catalytic subunits in arterial smooth muscle cells does not alter resting blood pressure values.

Bar charts show mean ± SEM of the mean, systolic and diastolic blood pressures of control AMPK-α1/α2 floxed (Flx; black; n = 6) mice, those with AMPK-α1 (orange; n = 4) and AMPK-α2 (green; n = 4) deletion in arterial smooth muscles (transgelin expressing cells) and AMPK-α1/α2 double KO in arterial smooth muscle cells (SM AMPK-α1/α2 dKO, brown, n = 4).

Appendix 5

Supplementary material for Chapter 8

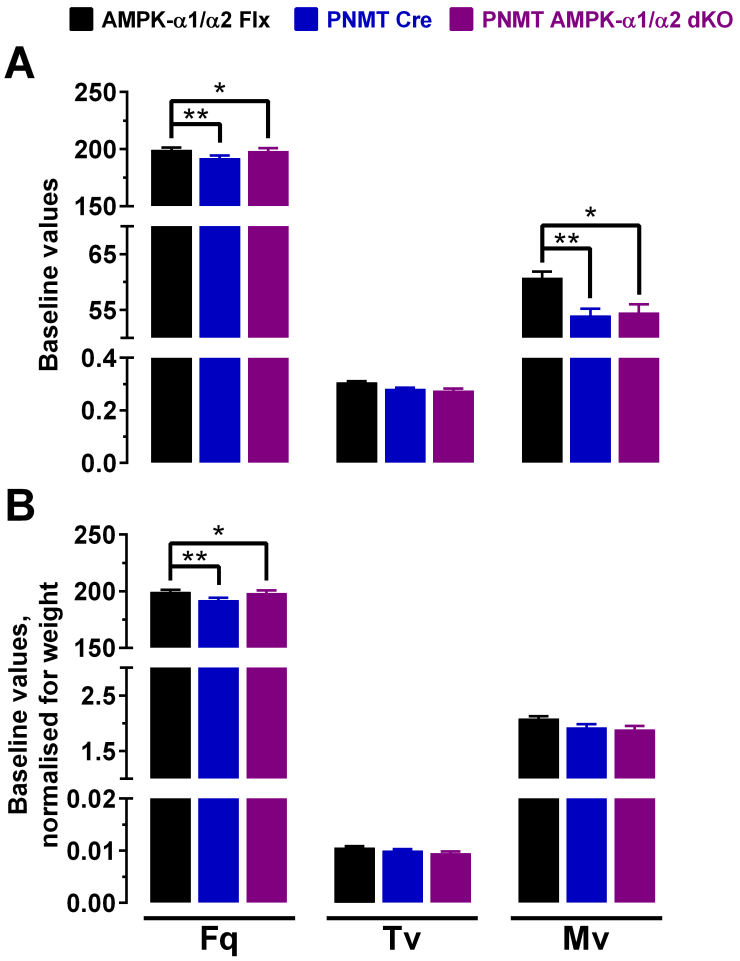

Appendix 4.1: Differences in the pre-hypoxic baselines between the genotypes tested.

Bar charts show mean ± SEM for **(A)** 'raw' baselines and **(B)** baselines normalised for weight that were selected prior to exposures to severe hypoxia (8% O_2) for AMPK-α1 and -α2 floxed (AMPK-α1/α2 Flx, black, n = 54 exposures from 21 mice), mice expressing Cre under the Phenylethanolamine N-methyltransferase reporter (PNMT Cre, blue, n = 32 exposures from 8 mice) and PNMT-driven AMPK-α1 and -α2 double knockout mice (PNMT AMPK-α1/α2 dKO, purple, n = 32 exposures from 8 mice). * = $p<0.05$, ** = $p<0.01$. Significance tested by one-way ANOVA between genotypes for each ventilatory parameter.

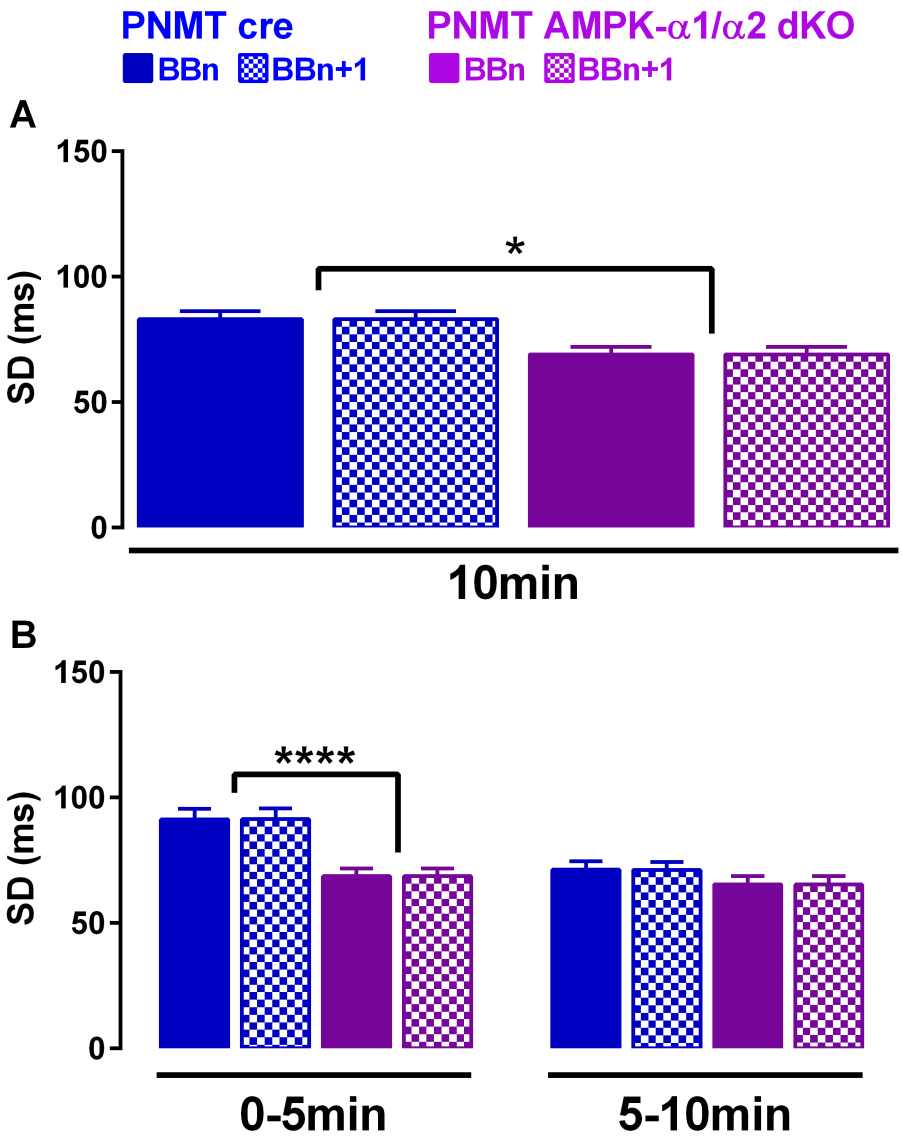

Appendix 4.2: The inter-breath intervals during exposures to severe hypoxia are attenuated in the first half of the exposure in mice with dual deletion of the AMPK α1/α2 catalytic subunits in adrenergic cells.

Bar charts show mean ± SEM for the standard deviations (SD) of the inter-breath intervals in mice expressing Cre under the Phenylethanolamine N-methyltransferase reporter (PNMT Cre, blue, n = 32 exposures from 8 mice) and PNMT-driven AMPK-α1 and -α2 double knockout mice (PNMT AMPK-α1/α2 dKO, purple, n = 32 exposures from 8 mice) for **(A)** the entire 10min and **(B)** the first and second half of 10min exposures to severe hypoxia (8% O_2). * = $p<0.05$, **** = $p<0.0001$. Significance tested by (A) t-test and (B) one-way ANOVA between genotypes.

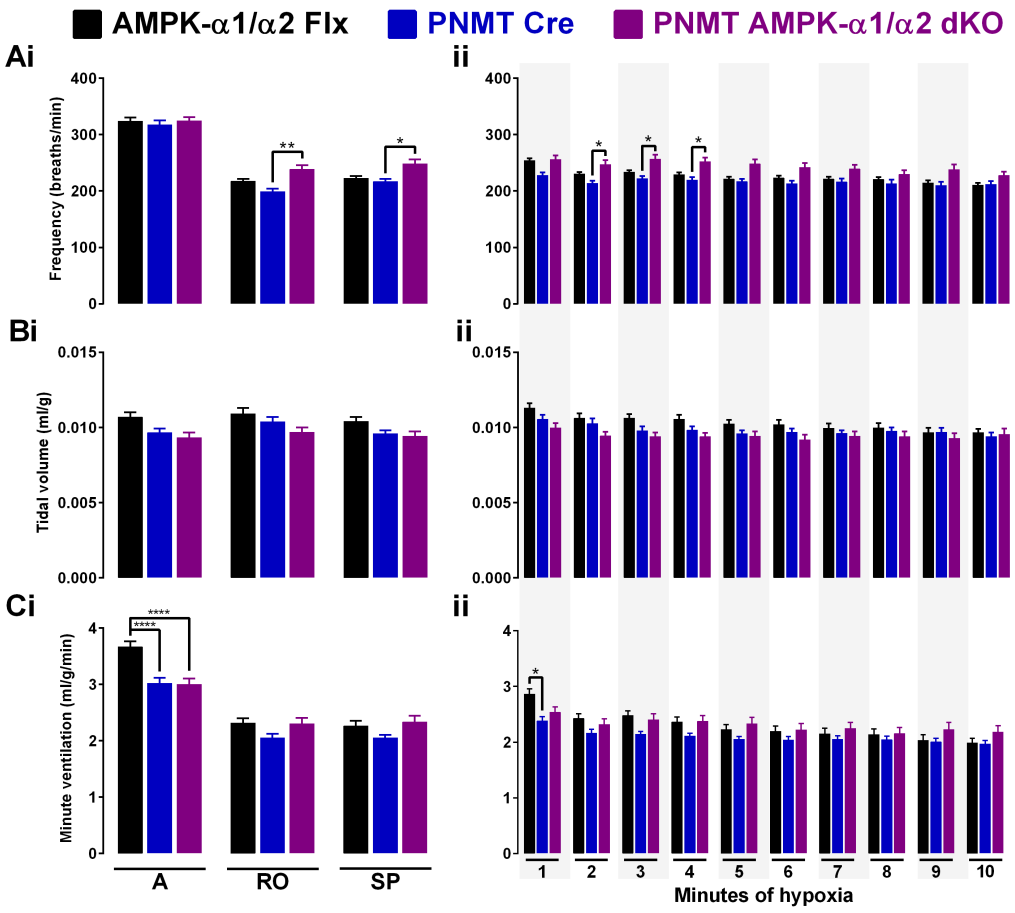

Appendix 4.3: Ventilatory differences in the response to severe hypoxia are also apparent in the 'raw' experimental data.

Bar charts show mean ± SEM of values computed by the FinePointe software for **(A)** breathing frequency, **(B)** tidal volume (normalised for weight), and **(C)** minute ventilation (normalised for weight) during 10 minute exposures to severe hypoxia (8% O_2) for analysis **(i)** of the HVR at the peak of the augmenting phase (A), the nadir of Roll-Off (RO), and the plateau of the sustained phase (SP), and **(ii)** as whole minute averages for AMPK-α1 and -α2 floxed mice (AMPK-α1/α2 Flx, black, 12% O_2: n = 37 exposures from 14 mice, 8% O_2: n = 55 exposures from 21 mice), mice expressing Cre under the Phenylethanolamine N-methyltransferase reporter (PNMT Cre, blue, n = 32 exposures from 8 mice) and PNMT-driven AMPK-α1 and -α2 double knockout mice (PNMT AMPK-α1/α2 dKO, purple, n = 32 exposures from 8 mice). * = p<0.05, ** = p<0.01, **** = p<0.0001. Significance tested by two-way ANOVA with Sidak post-hoc tests.

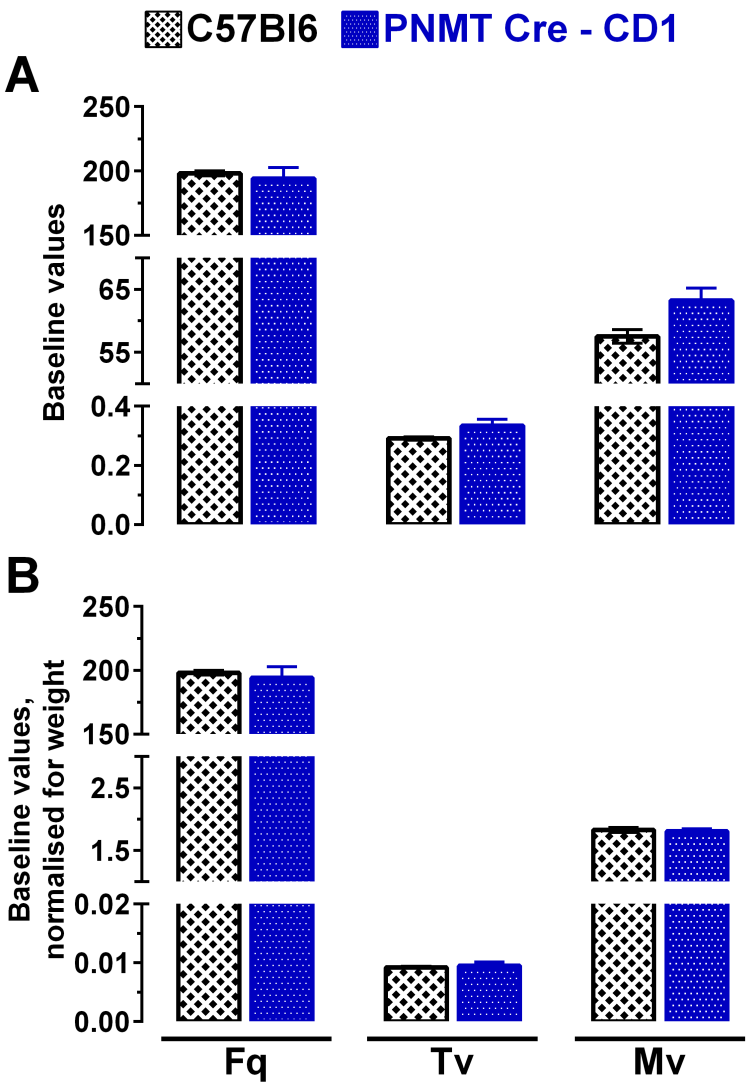

Appendix 4.4: Pre-hypoxic baselines are comparable for C57Bl6 and CD1 background controls.

Bar charts show mean ± SEM for **(A)** 'raw' baselines and **(B)** baselines normalised for weight that were selected prior to exposures to severe hypoxia (8% O_2) for wild-type C57Bl6 mice (black checked, n = 20 exposures from 5 mice), and CD1 mice expressing Cre under the Phenylethanolamine N-methyltransferase reporter (PNMT Cre – CD1, blue checked, n = 8 exposures from 2 mice). Significance tested by one-way ANOVA between genotypes for each ventilatory parameter.

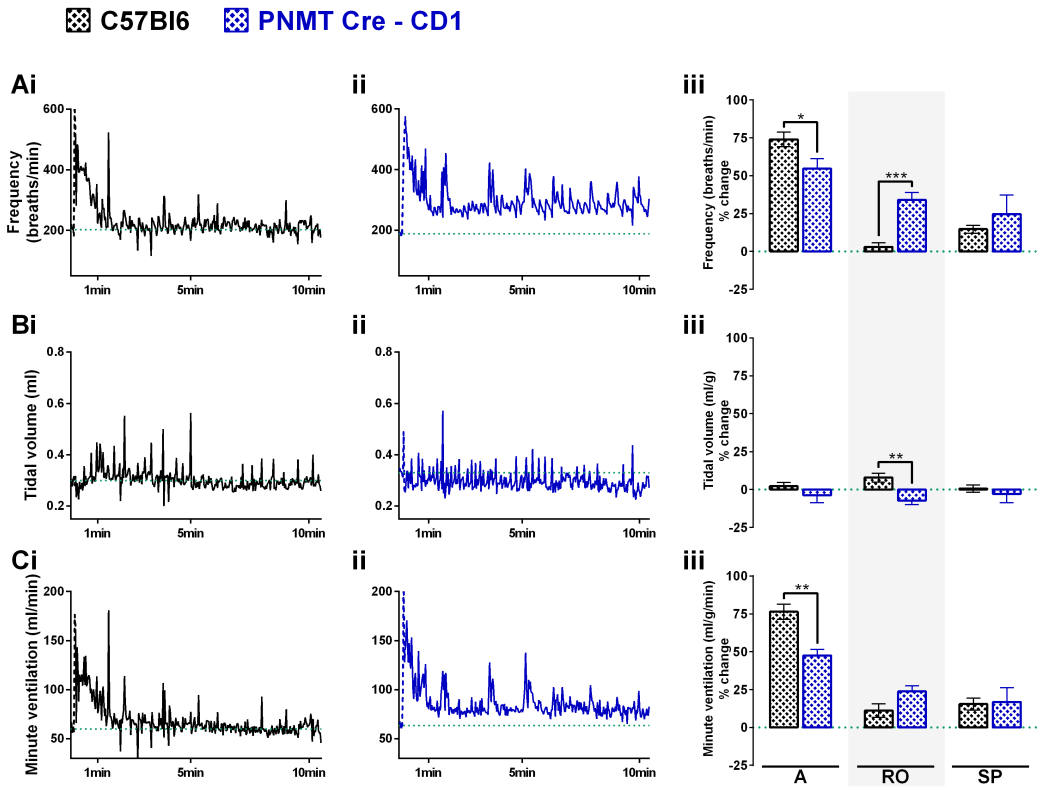

Figure 4.5: The hypoxic ventilatory response to 5min of severe hypoxia is background strain-specific.

Left and middle panels show raw example records of breathing **(A)** frequencies (breaths/min), **(B)** tidal volume (ml/min) and **(C)** minute ventilation (ml/g/min) during 10 minute exposures to severe hypoxia (8% O_2) from **(i)** a wild-type C57Bl6 mouse and **(ii)** a CD1 mouse expressing Cre under the Phenylethanolamine N-methyltransferase reporter (PNMT Cre – CD1) with a 2s sampling frequency. Dotted green lines indicate pre-hypoxic baseline frequencies, dashed lines the artefacts induced by gas exchange. Right panels **(iii)** show means ± SEM for percentage changes during the peak of the augmenting phase (A, approximately 30s), the nadir of the Roll-Off (RO, approximately 100s), and the plateau of the sustained phase (SP, at 300s) of the HVR in C57Bl6 mice (black checked, n = 20 exposures from 5 mice) and PNMT Cre – CD1 mice (blue checked, n = 8 exposures from 2 mice). * = p<0.05, ** = p<0.01, *** = p<0.001. Significance tested by two-way ANOVA with Sidak post-hoc tests.

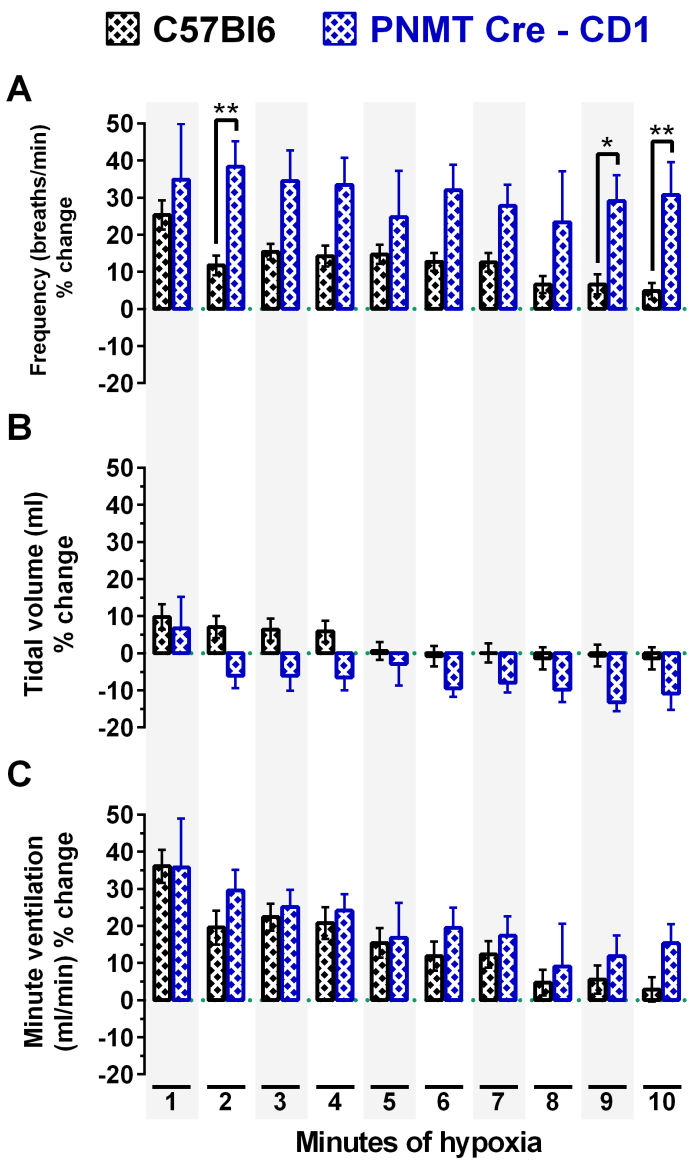

Figure 4.6: The hypoxic ventilatory response to 10min of severe hypoxia is background strain-specific.

Means ± SEM for percentage changes relative to normoxia (green dotted line) of **(A)** breathing frequency (breaths/min), **(B)** tidal volume (ml), and **(C)** minute ventilation (ml/min) during 10 minute exposures to severe hypoxia (8% O_2) in wild-type C57Bl6 mice (black checked, n = 20 exposures from 5 mice) and CD1 mice expressing Cre under the Phenylethanolamine N-methyltransferase reporter (PNMT Cre – CD1, blue checked, n = 8 exposures from 2 mice) measured at each full minute of hypoxia. * = $p<0.05$, ** = $p<0.01$. Significance tested by two-way ANOVA with Sidak post-hoc tests.

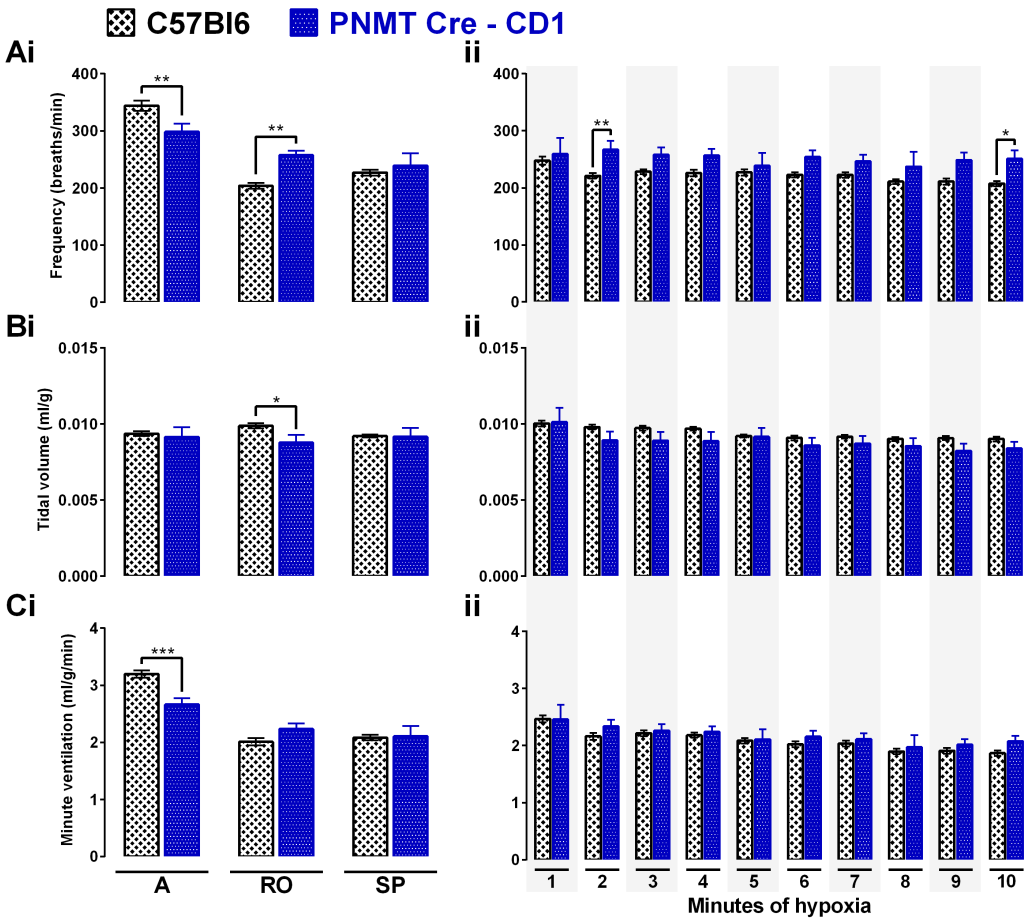

Appendix 4.7: Background strain-specific differences in the ventilatory response to severe hypoxia are also apparent in the 'raw' experimental data.

Bar charts show mean ± SEM of values computed by the FinePointe software for **(A)** breathing frequency, **(B)** tidal volume (normalised for weight), and **(C)** minute ventilation (normalised for weight) during 10 minute exposures to severe hypoxia (8% O_2) for analysis **(i)** of the HVR at the peak of the augmenting phase (A), the nadir of Roll-Off (RO), and the plateau of the sustained phase (SP), and **(ii)** as whole minute averages for wild-type C57Bl6 mice (black checked, n = 20 exposures from 5 mice) and CD1 mice expressing Cre under the Phenylethanolamine N-methyltransferase reporter (PNMT Cre – CD1, blue checked, n = 8 exposures from 2 mice) * = $p<0.05$, ** = $p<0.01$, *** = $p<0.001$. Significance tested by two-way ANOVA with Sidak post-hoc tests.

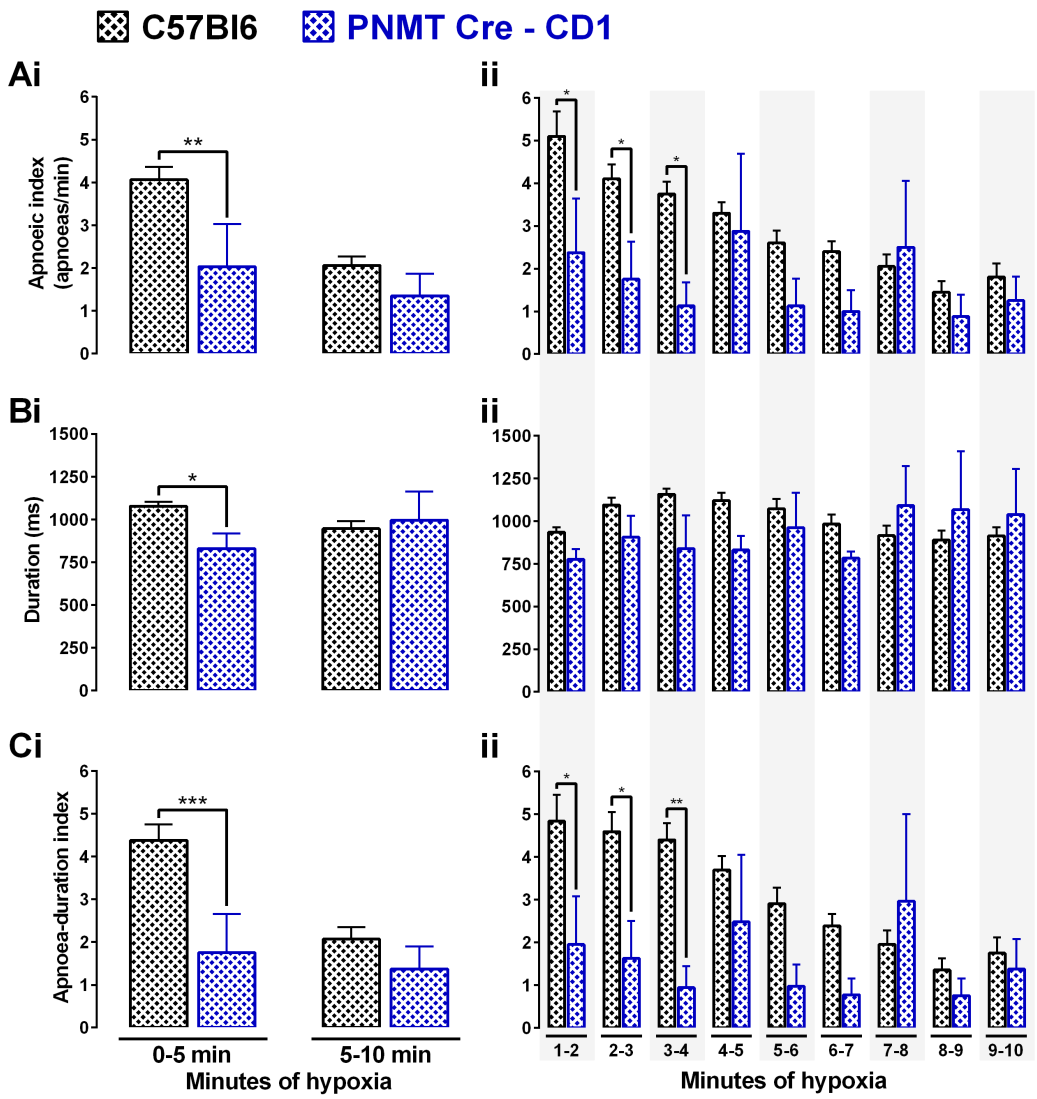

Appendix 4.8: The precipitation of apnoeas during 10min exposures to severe hypoxia is background strain-specific.

Means ± SEM for the **(A)** apnoeic index (apnoeas/min), **(B)** apnoea duration (ms), and **(C)** apnoea-duration index during **(i)** the first and second half and **(ii)** for every 60 seconds of 10 minute exposures to severe hypoxia (8% O_2) in wild-type C57Bl6 mice (black checked, n = 20 exposures from 5 mice) and CD1 mice expressing Cre under the Phenylethanolamine N-methyltransferase reporter (PNMT Cre – CD1, blue checked, n = 8 exposures from 2 mice). * = p<0.05, ** = p<0.01, *** = p<0.001. Significance tested by two-way ANOVA with Sidak post-hoc tests for apnoeic index and apnoea-duration index, and multiple t-tests with Holm-Sidak post-hoc for apnoea duration.

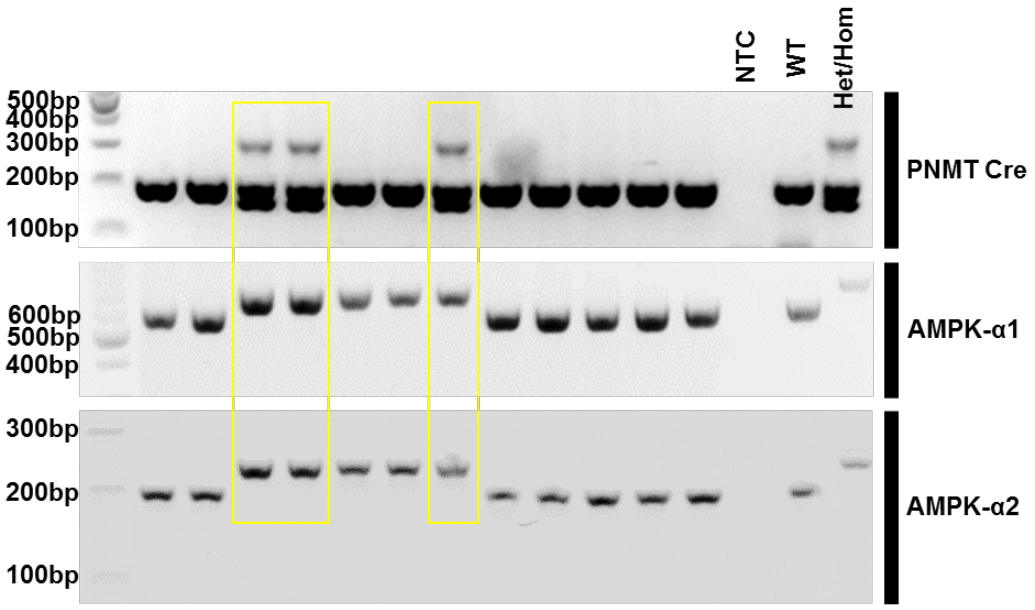

Appendix 4.9: Genotype analysis confirms the expression of PNMT Cre and AMPK-α1$^{fl/fl}$ and AMPK-α2$^{fl/fl}$ catalytic subunits.

The products of targeted gene amplification obtained by polymerase chain reaction were run on a 2% agarose gel and visualised. The first lane was loaded with a 1kb DNA ladder, followed by 12 ear clip samples obtained from PNMT AMPK-α1/α2 dKO pups. NTC contains a no-template control, WT an ear clip sample from a wild-type C57Bl6 mouse, and Het/Hom was loaded with a sample from a mouse with heterozygous genetic modification of the PNMT gene and a homozygous genetic modification of the AMPK-α1 and -α2 subunits. The yellow boxes highlight three mice that were confirmed as PNMT Cre-driven AMPK-α1 and -α2 double knockout mice.

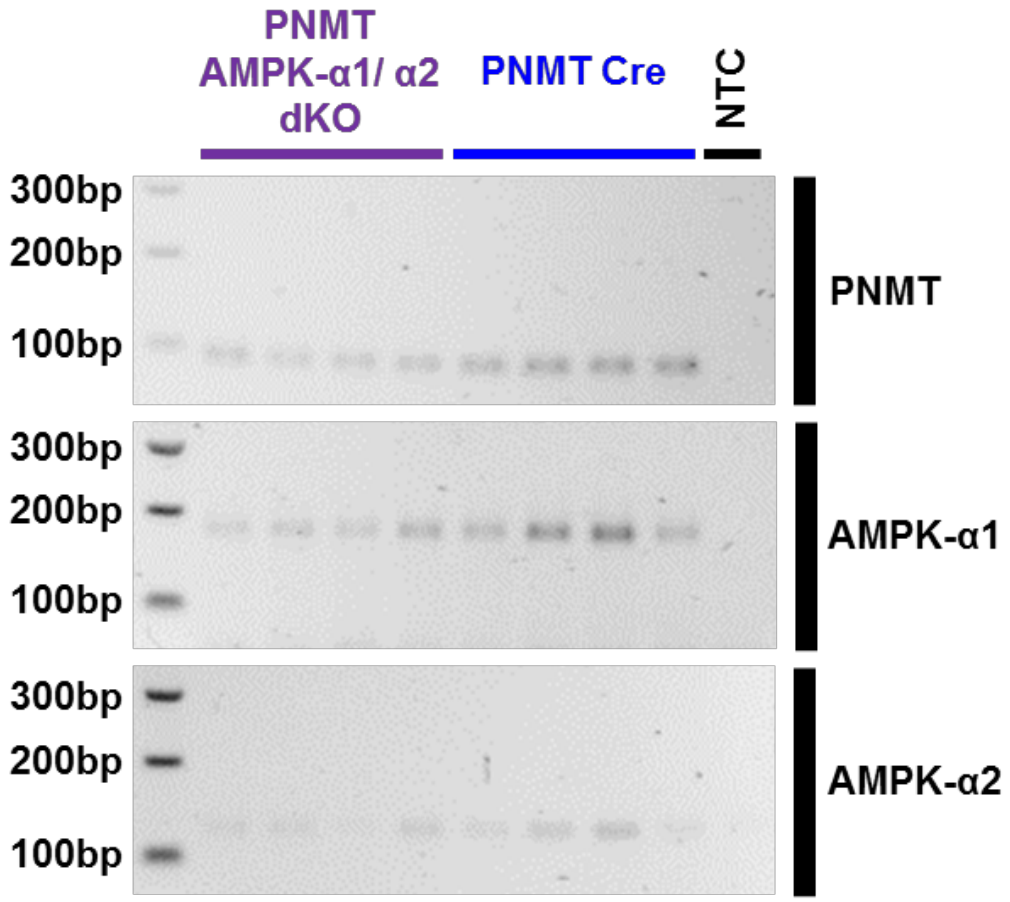

Appendix 4.10: End-point PCR analysis of RNA extracted from the adrenal medullae of PNMT AMPK-α1/α2 dKO mice indicates reduced expression of the AMPK-α1 and -α2 subunits relative to PNMT Cre mice.

The products of targeted gene amplification obtained by end-point quantitative polymerase chain reaction following RNA extraction and cDNA conversion from laser dissected adrenal medullae were run on a 2% agarose gel and visualised. The first lane was loaded with a 1kb DNA ladder, followed by 4 samples obtained from PNMT AMPK-α1/α2 dKO mice and 4 samples obtained from PNMT Cre mice. NTC contains a no-template control. The yellow boxes highlight three mice that were confirmed as PNMT Cre-driven AMPK-α1 and -α2 double knockout mice.

Bibliography

Abbott SB, DePuy SD, Nguyen T, Coates MB, Stornetta RL & Guyenet PG. (2013). Selective optogenetic activation of rostral ventrolateral medullary catecholaminergic neurons produces cardiorespiratory stimulation in conscious mice. *The Journal of neuroscience : the official journal of the Society for Neuroscience* **33,** 3164-3177.

Abbott SB, Kanbar R, Bochorishvili G, Coates MB, Stornetta RL & Guyenet PG. (2012). C1 neurons excite locus coeruleus and A5 noradrenergic neurons along with sympathetic outflow in rats. *J Physiol* **590,** 2897-2915.

Abbott SB, Stornetta RL, Coates MB & Guyenet PG. (2011). Phox2b-expressing neurons of the parafacial region regulate breathing rate, inspiration, and expiration in conscious rats. *The Journal of neuroscience : the official journal of the Society for Neuroscience* **31,** 16410-16422.

Abbott SB, Stornetta RL, Fortuna MG, Depuy SD, West GH, Harris TE & Guyenet PG. (2009). Photostimulation of retrotrapezoid nucleus phox2b-expressing neurons in vivo produces long-lasting activation of breathing in rats. *The Journal of neuroscience : the official journal of the Society for Neuroscience* **29,** 5806-5819.

Abdala AP, Rybak IA, Smith JC & Paton JF. (2009). Abdominal expiratory activity in the rat brainstem-spinal cord in situ: patterns, origins and implications for respiratory rhythm generation. *J Physiol* **587,** 3539-3559.

Adachi T, Ogawa H, Okabe S, Kitamuro T, Kikuchi Y, Shibahara S, Shirato K & Hida W. (2006). Mice with blunted hypoxic ventilatory response are susceptible to respiratory disturbance during hypoxia. *The Tohoku journal of experimental medicine* **209,** 125-134.

Ahmadi M & Roy R. (2016). AMPK acts as a molecular trigger to coordinate glutamatergic signals and adaptive behaviours during acute starvation. *eLife* **5**.

Aicher SA, Saravay RH, Cravo S, Jeske I, Morrison SF, Reis DJ & Milner TA. (1996). Monosynaptic projections from the nucleus tractus solitarii to C1 adrenergic neurons in the rostral ventrolateral medulla: comparison with input from the caudal ventrolateral medulla. *J Comp Neurol* **373,** 62-75.

Ainslie PN, Lucas SJE & Burgess KR. (2013). Breathing and sleep at high altitude. *Respir Physiol Neurobiol* **188,** 233-256.

Alheid GF, Jiao W & McCrimmon DR. (2011). Caudal nuclei of the rat nucleus of the solitary tract differentially innervate respiratory compartments within the ventrolateral medulla. *Neuroscience* **190,** 207-227.

Alheid GF & McCrimmon DR. (2008). The chemical neuroanatomy of breathing. *Respir Physiol Neurobiol* **164,** 3-11.

Amir RE, Van den Veyver IB, Wan M, Tran CQ, Francke U & Zoghbi HY. (1999). Rett syndrome is caused by mutations in X-linked MECP2, encoding methyl-CpG-binding protein 2. *Nature genetics* **23,** 185-188.

Andersen MN, Skibsbye L, Tang C, Petersen F, MacAulay N, Rasmussen HB & Jespersen T. (2015). PKC and AMPK regulation of Kv1.5 potassium channels. *Channels* **9,** 121-128.

Anderson TM, Garcia AJ, 3rd, Baertsch NA, Pollak J, Bloom JC & Wei AD. (2016). A novel excitatory network for the control of breathing. *Nature* **536,** 76-80.

Anderson TM & Ramirez JM. (2017). Respiratory rhythm generation: triple oscillator hypothesis. *F1000Research* **6,** 139.

Andresen MC, Doyle MW, Bailey TW & Jin YH. (2004). Differentiation of autonomic reflex control begins with cellular mechanisms at the first synapse within the nucleus tractus solitarius. *Brazilian journal of medical and biological research = Revista brasileira de pesquisas medicas e biologicas* **37,** 549-558.

Andresen MC & Kunze DL. (1994). Nucleus tractus solitarius--gateway to neural circulatory control. *Annual review of physiology* **56,** 93-116.

Andresen MC & Mendelowitz D. (1996). Sensory afferent neurotransmission in caudal nucleus tractus solitarius--common denominators. *Chemical senses* **21,** 387-395.

Angelova PR, Kasymov V, Christie I, Sheikhbahaei S, Turovsky E, Marina N, Korsak A, Zwicker J, Teschemacher AG, Ackland GL, Funk GD, Kasparov S, Abramov AY & Gourine AV. (2015). Functional Oxygen

Sensitivity of Astrocytes. *The Journal of neuroscience : the official journal of the Society for Neuroscience* **35,** 10460-10473.

Azevedo FA, Carvalho LR, Grinberg LT, Farfel JM, Ferretti RE, Leite RE, Jacob Filho W, Lent R & Herculano-Houzel S. (2009). Equal numbers of neuronal and nonneuronal cells make the human brain an isometrically scaled-up primate brain. *J Comp Neurol* **513,** 532-541.

Bain J, Plater L, Elliott M, Shpiro N, Hastie CJ, McLauchlan H, Klevernic I, Arthur JS, Alessi DR & Cohen P. (2007). The selectivity of protein kinase inhibitors: a further update. *The Biochemical journal* **408,** 297-315.

Bao G, Randhawa PM & Fletcher EC. (1997). Acute blood pressure elevation during repetitive hypocapnic and eucapnic hypoxia in rats. *J Appl Physiol (1985)* **82,** 1071-1078.

Bartlett D, Jr. (1971). Origin and regulation of spontaneous deep breaths. *Respir Physiol* **12,** 230-238.

Basting TM, Burke PG, Kanbar R, Viar KE, Stornetta DS, Stornetta RL & Guyenet PG. (2015). Hypoxia silences retrotrapezoid nucleus respiratory chemoreceptors via alkalosis. *The Journal of neuroscience : the official journal of the Society for Neuroscience* **35,** 527-543.

Bell HJ, Ferguson C, Kehoe V & Haouzi P. (2009). Hypocapnia increases the prevalence of hypoxia-induced augmented breaths. *Am J Physiol Regul Integr Comp Physiol* **296,** R334-344.

Biscoe TJ & Duchen MR. (1990a). Cellular basis of transduction in carotid chemoreceptors. *Am J Physiol* **258,** L271-278.

Biscoe TJ & Duchen MR. (1990b). Responses of type I cells dissociated from the rabbit carotid body to hypoxia. *J Physiol* **428,** 39-59.

Biscoe TJ & Silver A. (1966). The distribution of cholinesterases in the cat carotid body. *J Physiol* **183,** 501-512.

Biscoe TJ & Stehbens WE. (1966). Ultrastructure of the carotid body. *The Journal of cell biology* **30,** 563-578.

Bisgard GE, Forster HV & Klein JP. (1980). Recovery of peripheral chemoreceptor function after denervation in ponies. *Journal of*

applied physiology: respiratory, environmental and exercise physiology **49,** 964-970.

Bissonnette JM. (2000). Mechanisms regulating hypoxic respiratory depression during fetal and postnatal life. *Am J Physiol Regul Integr Comp Physiol* **278,** R1391-1400.

Bodineau L & Larnicol N. (2001). Brainstem and hypothalamic areas activated by tissue hypoxia: Fos-like immunoreactivity induced by carbon monoxide inhalation in the rat. *Neuroscience* **108,** 643-653.

Bower EA & O'Donnell CP. (1991). Mean circulatory filling pressure during splanchnic nerve stimulation and whole-body hypoxia in the anaesthetized cat. *J Physiol* **432,** 543-556.

Bradford JR & Dean HP. (1894). The Pulmonary Circulation. *J Physiol* **16,** 34-158 125.

Breuer J. (1868). *Die Selbststeuerung der Athmung durch den Nervus vagus*. Bayerische Staatsbibliothek, Wien.

Brizzee KR & Klara PM. (1984). The structure of the mammalian area postrema. *Federation proceedings* **43,** 2944-2948.

Brown K & Bates JH. (2000). Post sigh apnoea represents the majority of central apnoea in infants at risk for postoperative apnoea. *Paediatric anaesthesia* **10,** 696.

Bucci D, Busceti CL, Calierno MT, Di Pietro P, Madonna M, Biagioni F, Ryskalin L, Limanaqi F, Nicoletti F & Fornai F. (2017). Systematic Morphometry of Catecholamine Nuclei in the Brainstem. *Frontiers in neuroanatomy* **11,** 98.

Bucher ES, Fox ME, Kim L, Kirkpatrick DC, Rodeberg NT, Belle AM & Wightman RM. (2014). Medullary norepinephrine neurons modulate local oxygen concentrations in the bed nucleus of the stria terminalis. *Journal of cerebral blood flow and metabolism : official journal of the International Society of Cerebral Blood Flow and Metabolism* **34,** 1128-1137.

Buckler KJ. (1997). A novel oxygen-sensitive potassium current in rat carotid body type I cells. *J Physiol* **498 (Pt 3),** 649-662.

Buckler KJ. (2012). Effects of exogenous hydrogen sulphide on calcium signalling, background (TASK) K channel activity and mitochondrial function in chemoreceptor cells. *Pflugers Archiv : European journal of physiology* **463,** 743-754.

Buckler KJ. (2015). TASK channels in arterial chemoreceptors and their role in oxygen and acid sensing. *Pflugers Archiv : European journal of physiology* **467,** 1013-1025.

Buckler KJ & Turner PJ. (2013). Oxygen sensitivity of mitochondrial function in rat arterial chemoreceptor cells. *J Physiol* **591,** 3549-3563.

Buckler KJ & Turner PJ. (2015). Functional Properties of Mitochondria in the Type-1 Cell and Their Role in Oxygen Sensing. *Adv Exp Med Biol* **860,** 69-80.

Buckler KJ, Williams BA & Honore E. (2000). An oxygen-, acid- and anaesthetic-sensitive TASK-like background potassium channel in rat arterial chemoreceptor cells. *J Physiol* **525 Pt 1,** 135-142.

Buller KM, Wixey JA, Pathipati P, Carty M, Colditz PB, Williams CE & Scheepens A. (2008). Selective losses of brainstem catecholamine neurons after hypoxia-ischemia in the immature rat pup. *Pediatr Res* **63,** 364-369.

Bultot L, Guigas B, Von Wilamowitz-Moellendorff A, Maisin L, Vertommen D, Hussain N, Beullens M, Guinovart JJ, Foretz M, Viollet B, Sakamoto K, Hue L & Rider MH. (2012). AMP-activated protein kinase phosphorylates and inactivates liver glycogen synthase. *The Biochemical journal* **443,** 193-203.

Burke PG, Abbott SB, Coates MB, Viar KE, Stornetta RL & Guyenet PG. (2014). Optogenetic stimulation of adrenergic C1 neurons causes sleep state-dependent cardiorespiratory stimulation and arousal with sighs in rats. *Am J Respir Crit Care Med* **190,** 1301-1310.

Burke PG, Kanbar R, Viar KE, Stornetta RL & Guyenet PG. (2015). Selective optogenetic stimulation of the retrotrapezoid nucleus in sleeping rats activates breathing without changing blood pressure or causing arousal or sighs. *J Appl Physiol (1985)* **118,** 1491-1501.

Buttigieg J, Brown S, Zhang M, Lowe M, Holloway AC & Nurse CA. (2008). Chronic nicotine in utero selectively suppresses hypoxic sensitivity in neonatal rat adrenal chromaffin cells. *FASEB J* **22,** 1317-1326.

Campanucci VA, Zhang M, Vollmer C & Nurse CA. (2006). Expression of Multiple P2X Receptors by Glossopharyngeal Neurons Projecting to Rat Carotid Body O2-Chemoreceptors: Role in Nitric Oxide-Mediated Efferent Inhibition. *J Neurosci* **26,** 9482-9493.

Campen MJ, Shimoda LA & O'Donnell CP. (2005a). Acute and chronic cardiovascular effects of intermittent hypoxia in C57BL/6J mice. *Journal of Applied Physiology* **99,** 2028-2035.

Campen MJ, Tagaito Y, Jenkins TP, Balbir A & O'Donnell CP. (2005b). Heart rate variability responses to hypoxic and hypercapnic exposures in different mouse strains. *J Appl Physiol (1985)* **99,** 807-813.

Campen MJ, Tagaito Y, Li J, Balbir A, Tankersley CG, Smith P, Schwartz A & O'Donnell CP. (2004). Phenotypic variation in cardiovascular responses to acute hypoxic and hypercapnic exposure in mice. *Physiological genomics* **20,** 15-20.

Carley DW & Radulovacki M. (1999a). Mirtazapine, a mixed-profile serotonin agonist/antagonist, suppresses sleep apnea in the rat. *Am J Respir Crit Care Med* **160,** 1824-1829.

Carley DW & Radulovacki M. (1999b). Role of peripheral serotonin in the regulation of central sleep apneas in rats. *Chest* **115,** 1397-1401.

Carling D. (2004). The AMP-activated protein kinase cascade – a unifying system for energy control. *Trends in Biochemical Sciences* **29,** 18-24.

Carvajal K, Zarrinpashneh E, Szarszoi O, Joubert F, Athea Y, Mateo P, Gillet B, Vaulont S, Viollet B, Bigard X, Bertrand L, Ventura-Clapier R & Hoerter JA. (2007). Dual cardiac contractile effects of the alpha2-AMPK deletion in low-flow ischemia and reperfusion. *American journal of physiology Heart and circulatory physiology* **292,** H3136-3147.

Ceylan B, Khorshid L, Gunes UY & Zaybak A. (2016). Evaluation of oxygen saturation values in different body positions in healthy individuals. *Journal of clinical nursing* **25,** 1095-1100.

Chang AJ. (2017). Acute oxygen sensing by the carotid body: from mitochondria to plasma membrane. *J Appl Physiol (1985)* **123,** 1335-1343.

Chang AJ, Ortega FE, Riegler J, Madison DV & Krasnow MA. (2015). Oxygen regulation of breathing through an olfactory receptor activated by lactate. *Nature* **527,** 240-244.

Chang TJ, Chen WP, Yang C, Lu PH, Liang YC, Su MJ, Lee SC & Chuang LM. (2009). Serine-385 phosphorylation of inwardly rectifying K+ channel subunit (Kir6.2) by AMP-dependent protein kinase plays a key role in rosiglitazone-induced closure of the K(ATP) channel and insulin secretion in rats. *Diabetologia* **52,** 1112-1121.

Chapin JL. (1954). Ventilatory response of the unrestrained and unanesthetized hamster to CO2. *Am J Physiol* **179,** 146-148.

Chapuis C, Autran S, Fortin G, Simmers J & Thoby-Brisson M. (2014). Emergence of sigh rhythmogenesis in the embryonic mouse. *J Physiol* **592,** 2169-2181.

Chau EH, Lam D, Wong J, Mokhlesi B & Chung F. (2012). Obesity hypoventilation syndrome: a review of epidemiology, pathophysiology, and perioperative considerations. *Anesthesiology* **117,** 188-205.

Chen L, Jiao ZH, Zheng LS, Zhang YY, Xie ST, Wang ZX & Wu JW. (2009). Structural insight into the autoinhibition mechanism of AMP-activated protein kinase. *Nature* **459,** 1146-1149.

Chen L, Sica AL, Greenberg H & Scharf SM. (1998). Role of hypoxemia and hypercapnia in acute cardiovascular response to periodic apneas in sedated pigs. *Respir Physiol* **111,** 257-269.

Cheung PC, Salt IP, Davies SP, Hardie DG & Carling D. (2000). Characterization of AMP-activated protein kinase gamma-subunit isoforms and their role in AMP binding. *The Biochemical journal* **346 Pt 3,** 659-669.

Chou CL & Shirahata M. (1996). Two types of voltage-gated K channels in carotid body cells of adult cats. *Brain research* **742,** 34-42.

Comline RS & Silver M. (1961). The release of adrenaline and noradrenaline from the adrenal glands of the foetal sheep. *J Physiol* **156,** 424-444.

Conde SV & Monteiro EC. (2004). Hypoxia induces adenosine release from the rat carotid body. *J Neurochem* **89,** 1148-1156.

Conde SV, Monteiro EC, Obeso A & Gonzalez C. (2009). Adenosine in peripheral chemoreception: new insights into a historically overlooked molecule--invited article. *Adv Exp Med Biol* **648,** 145-159.

Conde SV, Monteiro EC, Rigual R, Obeso A & Gonzalez C. (2012). Hypoxic intensity: a determinant for the contribution of ATP and adenosine to the genesis of carotid body chemosensory activity. *J Appl Physiol (1985)* **112,** 2002-2010.

Cruz Jde C, Bonagamba LG, Stern JE & Machado BH. (2010). Fos expression in the NTS in response to peripheral chemoreflex activation in awake rats. *Autonomic neuroscience : basic & clinical* **152,** 27-34.

Culmsee C, Monnig J, Kemp BE & Mattson MP. (2001). AMP-activated protein kinase is highly expressed in neurons in the developing rat brain and promotes neuronal survival following glucose deprivation. *Journal of molecular neuroscience : MN* **17,** 45-58.

Cunningham KA, Bouagnon AD, Barros AG, Lin L, Malard L, Romano-Silva MA & Ashrafi K. (2014). Loss of a neural AMP-activated kinase mimics the effects of elevated serotonin on fat, movement, and hormonal secretions. *PLoS genetics* **10,** e1004394.

Cunningham KA, Hua Z, Srinivasan S, Liu J, Lee BH, Edwards RH & Ashrafi K. (2012). AMP-activated kinase links serotonergic signaling to glutamate release for regulation of feeding behavior in C. elegans. *Cell Metab* **16,** 113-121.

Curran AK, Rodman JR, Eastwood PR, Henderson KS, Dempsey JA & Smith CA. (2000). Ventilatory responses to specific CNS hypoxia in sleeping dogs. *J Appl Physiol (1985)* **88,** 1840-1852.

Cutz E & Jackson A. (1999). Neuroepithelial bodies as airway oxygen sensors. *Respir Physiol* **115,** 201-214.

Dampney RA, Coleman MJ, Fontes MA, Hirooka Y, Horiuchi J, Li YW, Polson JW, Potts PD & Tagawa T. (2002). Central mechanisms underlying short- and long-term regulation of the cardiovascular system. *Clinical and experimental pharmacology & physiology* **29,** 261-268.

Dampney RA & Moon EA. (1980). Role of ventrolateral medulla in vasomotor response to cerebral ischemia. *Am J Physiol* **239,** H349-358.

Daristotle L, Engwall MJ, Niu WZ & Bisgard GE. (1991). Ventilatory effects and interactions with change in PaO2 in awake goats. *J Appl Physiol (1985)* **71,** 1254-1260.

Daval M, Foufelle F & Ferré P. (2006). Functions of AMP-activated protein kinase in adipose tissue. *The Journal of Physiology* **574,** 55-62.

Davenport HW, Brewer G & et al. (1947). The respiratory responses to anoxemia of unanesthetized dogs with chronically denervated aortic and carotid chemoreceptors and their causes. *Am J Physiol* **148,** 406-416.

Davies SP, Carling D, Munday MR & Hardie DG. (1992). Diurnal rhythm of phosphorylation of rat liver acetyl-CoA carboxylase by the AMP-activated protein kinase, demonstrated using freeze-clamping. Effects of high fat diets. *European journal of biochemistry* **203,** 615-623.

Day TA & Wilson RJ. (2007). Brainstem PCO2 modulates phrenic responses to specific carotid body hypoxia in an in situ dual perfused rat preparation. *J Physiol* **578,** 843-857.

Deacon RM. (2006). Housing, husbandry and handling of rodents for behavioral experiments. *Nature protocols* **1,** 936-946.

Dempsey JA. (2005). Crossing the apnoeic threshold: causes and consequences. *Exp Physiol* **90,** 13-24.

Dempsey JA, Veasey SC, Morgan BJ & O'Donnell CP. (2010). Pathophysiology of sleep apnea. *Physiol Rev* **90,** 47-112.

Depuy SD, Kanbar R, Coates MB, Stornetta RL & Guyenet PG. (2011). Control of breathing by raphe obscurus serotonergic neurons in mice. *The Journal of neuroscience : the official journal of the Society for Neuroscience* **31,** 1981-1990.

DePuy SD, Stornetta RL, Bochorishvili G, Deisseroth K, Witten I, Coates M & Guyenet PG. (2013). Glutamatergic neurotransmission between the C1 neurons and the parasympathetic preganglionic neurons of the dorsal motor nucleus of the vagus. *The Journal of neuroscience : the official journal of the Society for Neuroscience* **33,** 1486-1497.

Dergacheva O, Kamendi H, Wang X, Pinol RM, Frank J, Jameson H, Gorini C & Mendelowitz D. (2009). The role of 5-HT3 and other excitatory receptors in central cardiorespiratory responses to hypoxia: implications for sudden infant death syndrome. *Pediatr Res* **65,** 625-630.

Dick TE, Hsieh YH, Morrison S, Coles SK & Prabhakar N. (2004). Entrainment pattern between sympathetic and phrenic nerve activities in the Sprague-Dawley rat: hypoxia-evoked sympathetic activity during expiration. *Am J Physiol Regul Integr Comp Physiol* **286,** R1121-1128.

Dobbins EG & Feldman JL. (1994). Brainstem network controlling descending drive to phrenic motoneurons in rat. *J Comp Neurol* **347,** 64-86.

Donnelly DF. (1997). Are oxygen dependent K+ channels essential for carotid body chemo-transduction? *Respir Physiol* **110,** 211-218.

Donnelly DF. (2000). Developmental aspects of oxygen sensing by the carotid body. *Journal of Applied Physiology* **88,** 2296-2301.

Dragunow M & Faull R. (1989). The use of c-fos as a metabolic marker in neuronal pathway tracing. *J Neurosci Methods* **29,** 261-265.

Drorbaugh JE & Fenn WO. (1955). A barometric method for measuring ventilation in newborn infants. *Pediatrics* **16,** 81-87.

Duchen MR & Biscoe TJ. (1992). Mitochondrial function in type I cells isolated from rabbit arterial chemoreceptors. *J Physiol* **450,** 13-31.

Dutschmann M & Herbert H. (2006). The Kolliker-Fuse nucleus gates the postinspiratory phase of the respiratory cycle to control inspiratory off-switch and upper airway resistance in rat. *The European journal of neuroscience* **24,** 1071-1084.

Dzeja P & Terzic A. (2009). Adenylate kinase and AMP signaling networks: metabolic monitoring, signal communication and body energy sensing. *International journal of molecular sciences* **10,** 1729-1772.

Dzeja PP & Terzic A. (2003). Phosphotransfer networks and cellular energetics. *J Exp Biol* **206,** 2039-2047.

Ebert SN, Rong Q, Boe S, Thompson RP, Grinberg A & Pfeifer K. (2004). Targeted insertion of the Cre-recombinase gene at the phenylethanolamine n-methyltransferase locus: a new model for studying the developmental distribution of adrenergic cells. *Developmental dynamics : an official publication of the American Association of Anatomists* **231,** 849-858.

Egan DF, Shackelford DB, Mihaylova MM, Gelino S, Kohnz RA, Mair W, Vasquez DS, Joshi A, Gwinn DM, Taylor R, Asara JM, Fitzpatrick J, Dillin A, Viollet B, Kundu M, Hansen M & Shaw RJ. (2011). Phosphorylation of ULK1 (hATG1) by AMP-activated protein kinase connects energy sensing to mitophagy. *Science* **331,** 456-461.

Ellenberger HH & Feldman JL. (1990). Brainstem connections of the rostral ventral respiratory group of the rat. *Brain research* **513,** 35-42.

Ellenberger HH & Feldman JL. (1994). Origins of excitatory drive within the respiratory network: anatomical localization. *Neuroreport* **5,** 1933-1936.

Endeward V, Gros G & Jürgens KD. (2010). Significance of myoglobin as an oxygen store and oxygen transporter in the intermittently perfused human heart: a model study. *Cardiovascular Research* **87,** 22-29.

Erickson JT & Millhorn DE. (1994). Hypoxia and electrical stimulation of the carotid sinus nerve induce fos-like immunoreactivity within catecholaminergic and serotoninergic neurons of the rat brainstem. *J Comp Neurol* **348,** 161-182.

Evans AM. (2006). AMP-activated protein kinase and the regulation of Ca2+ signalling in O2-sensing cells. *The Journal of Physiology* **574,** 113-123.

Evans AM. (2012). The LKB1-AMPK signalling pathway is required for regulation of breathing by hypoxia and thereby energy supply to the whole body. In *Physiology 2012*. Proc. Physiol. Soc., Edinburgh.

Evans AM. (2018). AMPK breathing and oxygen supply. *Respir Physiol Neurobiol*.

Evans AM, Lewis SA, Ogunbayo OA & Moral-Sanz J. (2015). Modulation of the LKB1-AMPK Signalling Pathway Underpins Hypoxic Pulmonary Vasoconstriction and Pulmonary Hypertension. In *Arterial Chemoreceptors in Physiology and Pathophysiology*, ed. Peers C,

Kumar P, Wyatt C, Gauda E, Nurse CA & Prabhakar N, pp. 89-99. Springer International Publishing.

Evans AM, Mahmoud AD, Moral-Sanz J & Hartmann S. (2016). The emerging role of AMPK in the regulation of breathing and oxygen supply. *The Biochemical journal* **473,** 2561-2572.

Evans AM, Mustard KJW, Wyatt CN, Peers C, Dipp M, Kumar P, Kinnear NP & Hardie DG. (2005a). Does AMP-activated Protein Kinase Couple Inhibition of Mitochondrial Oxidative Phosphorylation by Hypoxia to Calcium Signaling in O2-sensing Cells? *Journal of Biological Chemistry* **280,** 41504-41511.

Evans C, Wang J, Neff R & Mendelowitz D. (2005b). Hypoxia recruits a respiratory-related excitatory pathway to brainstem premotor cardiac vagal neurons in animals exposed to prenatal nicotine. *Neuroscience* **133,** 1073-1079.

Ezure K, Tanaka I & Kondo M. (2003). Glycine is used as a transmitter by decrementing expiratory neurons of the ventrolateral medulla in the rat. *The Journal of neuroscience : the official journal of the Society for Neuroscience* **23,** 8941-8948.

Faxelius G, Hägnevik K, Lagercrantz H, Lundell B & Irestedt L. (1983). Catecholamine surge and lung function after delivery. *Arch Dis Child* **58,** 262-266.

Feil S, Valtcheva N & Feil R. (2009). Inducible Cre mice. *Methods Mol Biol* **530,** 343-363.

Feldman JL & Del Negro CA. (2006). Looking for inspiration: new perspectives on respiratory rhythm. *Nat Rev Neurosci* **7,** 232-242.

Fernandez-Aguera MC, Gao L, Gonzalez-Rodriguez P, Pintado CO, Arias-Mayenco I, Garcia-Flores P, Garcia-Perganeda A, Pascual A, Ortega-Saenz P & Lopez-Barneo J. (2015). Oxygen Sensing by Arterial Chemoreceptors Depends on Mitochondrial Complex I Signaling. *Cell Metab* **22,** 825-837.

Finley JC & Katz DM. (1992). The central organization of carotid body afferent projections to the brainstem of the rat. *Brain research* **572,** 108-116.

Fitzgerald RS. (2000). Oxygen and carotid body chemotransduction: the cholinergic hypothesis - a brief history and new evaluation. *Respir Physiol* **120,** 89-104.

Fitzgerald RS, Shirahata M & Wang HY. (2000). Acetylcholine is released from in vitro cat carotid bodies during hypoxic stimulation. *Adv Exp Med Biol* **475,** 485-494.

Fleming PJ, Goncalves AL, Levine MR & Woollard S. (1984). The development of stability of respiration in human infants: changes in ventilatory responses to spontaneous sighs. *J Physiol* **347,** 1-16.

Fodor M, Palkovits M & Gallatz K. (2007). Fine structure of the area subpostrema in rat. Open gate for the medullary autonomic centers. *Ideggyogyaszati szemle* **60,** 83-88.

Foster GT, Vaziri ND & Sassoon CS. (2001). Respiratory alkalosis. *Respir Care* **46,** 384-391.

Franklin KBJ & Paxinos G. (2008). *The mouse brain in stereotaxic coordinates*. Elsevier, Amsterdam ; London.

Fukuda R, Zhang H, Kim JW, Shimoda L, Dang CV & Semenza GL. (2007). HIF-1 regulates cytochrome oxidase subunits to optimize efficiency of respiration in hypoxic cells. *Cell* **129,** 111-122.

Fukumizu M & Kohyama J. (2004). Central respiratory pauses, sighs, and gross body movements during sleep in children. *Physiology & behavior* **82,** 721-726.

Fung SJ, Reddy VK, Liu RH, Wang Z & Barnes CD. (1994a). Existence of glutamate in noradrenergic locus coeruleus neurons of rodents. *Brain Res Bull* **35,** 505-512.

Fung SJ, Reddy VK, Zhuo H, Liu RH, Wang Z & Barnes CD. (1994b). Anatomical evidence for the presence of glutamate or enkephalin in noradrenergic projection neurons of the locus coeruleus. *Microscopy research and technique* **29,** 219-225.

Gadalla AE, Pearson T, Currie AJ, Dale N, Hawley SA, Sheehan M, Hirst W, Michel AD, Randall A, Hardie DG & Frenguelli BG. (2004). AICA riboside both activates AMP-activated protein kinase and competes with adenosine for the nucleoside transporter in the CA1 region of the rat hippocampus. *J Neurochem* **88,** 1272-1282.

Geerling JC, Engeland WC, Kawata M & Loewy AD. (2006). Aldosterone target neurons in the nucleus tractus solitarius drive sodium appetite. *The Journal of neuroscience : the official journal of the Society for Neuroscience* **26,** 411-417.

Getsy PM, Davis J, Coffee GA, May WJ, Palmer LA, Strohl KP & Lewis SJ. (2014). Enhanced non-eupneic breathing following hypoxic, hypercapnic or hypoxic-hypercapnic gas challenges in conscious mice. *Respir Physiol Neurobiol* **204,** 147-159.

Goirand F, Solar M, Athea Y, Viollet B, Mateo P, Fortin D, Leclerc J, Hoerter J, Ventura-Clapier R & Garnier A. (2007). Activation of AMP kinase alpha1 subunit induces aortic vasorelaxation in mice. *J Physiol* **581,** 1163-1171.

Gonzalez C, Agapito MT, Rocher A, Gonzalez-Martin MC, Vega-Agapito V, Gomez-Nino A, Rigual R, Castaneda J & Obeso A. (2007). Chemoreception in the context of the general biology of ROS. *Respir Physiol Neurobiol* **157,** 30-44.

Gonzalez C, Almaraz L, Obeso A & Rigual R. (1994). Carotid body chemoreceptors: from natural stimuli to sensory discharges. *Physiological Reviews* **74,** 829-898.

Gourine AV & Funk GD. (2017). On the existence of a central respiratory oxygen sensor. *J Appl Physiol (1985)* **123,** 1344-1349.

Gourine AV, Llaudet E, Dale N & Spyer KM. (2005). Release of ATP in the ventral medulla during hypoxia in rats: role in hypoxic ventilatory response. *The Journal of neuroscience : the official journal of the Society for Neuroscience* **25,** 1211-1218.

Gowans GJ, Hawley SA, Ross FA & Hardie DG. (2013). AMP is a true physiological regulator of AMP-activated protein kinase by both allosteric activation and enhancing net phosphorylation. *Cell Metab* **18,** 556-566.

Gozal D, Gozal E & Simakajornboon N. (2000). Signaling pathways of the acute hypoxic ventilatory response in the nucleus tractus solitarius. *Respir Physiol* **121,** 209-221.

Gros G, Wittenberg BA & Jue T. (2010). Myoglobin's old and new clothes: from molecular structure to function in living cells. *J Exp Biol* **213,** 2713-2725.

Guppy M & Withers P. (1999). Metabolic depression in animals: physiological perspectives and biochemical generalizations. *Biological Reviews* **74,** 1-40.

Guyenet PG. (2000). Neural structures that mediate sympathoexcitation during hypoxia. *Respiration Physiology* **121,** 147-162.

Guyenet PG. (2006). The sympathetic control of blood pressure. *Nat Rev Neurosci* **7,** 335-346.

Guyenet PG. (2014). Regulation of breathing and autonomic outflows by chemoreceptors. *Compr Physiol* **4,** 1511-1562.

Guyenet PG, Bayliss DA, Stornetta RL, Ludwig MG, Kumar NN, Shi Y, Burke PG, Kanbar R, Basting TM, Holloway BB & Wenker IC. (2016). Proton detection and breathing regulation by the retrotrapezoid nucleus. *J Physiol* **594,** 1529-1551.

Guyenet PG, Sevigny CP, Weston MC & Stornetta RL. (2002). Neurokinin-1 receptor-expressing cells of the ventral respiratory group are functionally heterogeneous and predominantly glutamatergic. *The Journal of neuroscience : the official journal of the Society for Neuroscience* **22,** 3806-3816.

Guyenet PG, Stornetta RL, Bochorishvili G, DePuy SD, Burke PGR & Abbott SBG. (2013). C1 neurons: the body's EMTs. *American Journal of Physiology - Regulatory, Integrative and Comparative Physiology* **305,** R187-R204.

Gwinn DM, Shackelford DB, Egan DF, Mihaylova MM, Mery A, Vasquez DS, Turk BE & Shaw RJ. (2008). AMPK phosphorylation of raptor mediates a metabolic checkpoint. *Molecular cell* **30,** 214-226.

Hardie DG. (2007). AMP-activated/SNF1 protein kinases: conserved guardians of cellular energy. *Nat Rev Mol Cell Biol* **8,** 774-785.

Hardie DG. (2014). AMPK--sensing energy while talking to other signaling pathways. *Cell Metab* **20,** 939-952.

Hardie DG. (2015). Molecular Pathways: Is AMPK a Friend or a Foe in Cancer? *Clinical cancer research : an official journal of the American Association for Cancer Research* **21,** 3836-3840.

Hardie DG & Ashford ML. (2014). AMPK: regulating energy balance at the cellular and whole body levels. *Physiology (Bethesda)* **29,** 99-107.

Hardie DG, Carling D & Gamblin SJ. (2011). AMP-activated protein kinase: also regulated by ADP? *Trends in Biochemical Sciences* **36,** 470-477.

Hardie DG, Hawley SA & Scott JW. (2006). AMP-activated protein kinase – development of the energy sensor concept. *The Journal of Physiology* **574,** 7-15.

Hardie DG, Ross FA & Hawley SA. (2012). AMPK: a nutrient and energy sensor that maintains energy homeostasis. *Nat Rev Mol Cell Biol* **13,** 251-262.

Hardie DG, Schaffer BE & Brunet A. (2016). AMPK: An Energy-Sensing Pathway with Multiple Inputs and Outputs. *Trends in cell biology* **26,** 190-201.

Harris MB & Milsom WK. (2001). Vagal feedback is essential for breathing in unanesthetized ground squirrels. *Respir Physiol* **125,** 199-212.

Hartland BL, Newell TJ & Damico N. (2014). Alveolar recruitment maneuvers: are your patients missing out? *AANA journal* **82,** 307-314.

Haselton JR & Guyenet PG. (1990). Ascending collaterals of medullary barosensitive neurons and C1 cells in rats. *Am J Physiol* **258,** R1051-1063.

Hasenour CM, Ridley DE, Hughey CC, James FD, Donahue EP, Shearer J, Viollet B, Foretz M & Wasserman DH. (2014). 5-Aminoimidazole-4-carboxamide-1-beta-D-ribofuranoside (AICAR) effect on glucose production, but not energy metabolism, is independent of hepatic AMPK in vivo. *The Journal of biological chemistry* **289,** 5950-5959.

Hawley SA, Boudeau J, Reid JL, Mustard KJ, Udd L, Makela TP, Alessi DR & Hardie DG. (2003). Complexes between the LKB1 tumor suppressor, STRAD alpha/beta and MO25 alpha/beta are upstream kinases in the AMP-activated protein kinase cascade. *Journal of biology* **2,** 28.

Hawley SA, Davison M, Woods A, Davies SP, Beri RK, Carling D & Hardie DG. (1996). Characterization of the AMP-activated protein kinase kinase from rat liver and identification of threonine 172 as the major

site at which it phosphorylates AMP-activated protein kinase. *The Journal of biological chemistry* **271,** 27879-27887.

Hawley SA, Pan DA, Mustard KJ, Ross L, Bain J, Edelman AM, Frenguelli BG & Hardie DG. (2005). Calmodulin-dependent protein kinase kinase-beta is an alternative upstream kinase for AMP-activated protein kinase. *Cell Metab* **2,** 9-19.

Healy F & Marcus CL. (2011). Congenital central hypoventilation syndrome in children. *Paediatric respiratory reviews* **12,** 253-263.

Hedner JA, Wilcox I, Laks L, Grunstein RR & Sullivan CE. (1992). A specific and potent pressor effect of hypoxia in patients with sleep apnea. *Am Rev Respir Dis* **146,** 1240-1245.

Herculano-Houzel S. (2014). The glia/neuron ratio: how it varies uniformly across brain structures and species and what that means for brain physiology and evolution. *Glia* **62,** 1377-1391.

Hermann GE, Nasse JS & Rogers RC. (2005). Alpha-1 adrenergic input to solitary nucleus neurones: calcium oscillations, excitation and gastric reflex control. *J Physiol* **562,** 553-568.

Heymans J & Heymans C. (1927). Sur les modifications directes et sur la regulation reflexe de l'activite du centre respiratoire de la tete isolee du chien. *Arch Int Pharmacodyn Ther* **33,** 273-327.

Hilaire G, Monteau R & Errchidi S. (1989). Possible modulation of the medullary respiratory rhythm generator by the noradrenergic A5 area: an in vitro study in the newborn rat. *Brain research* **485,** 325-332.

Hill AA, Garcia AJ, 3rd, Zanella S, Upadhyaya R & Ramirez JM. (2011). Graded reductions in oxygenation evoke graded reconfiguration of the isolated respiratory network. *Journal of neurophysiology* **105,** 625-639.

Hillman NH, Kallapur SG & Jobe AH. (2012). Physiology of transition from intrauterine to extrauterine life. *Clinics in perinatology* **39,** 769-783.

Hirooka Y, Polson JW, Potts PD & Dampney RAL. (1997). Hypoxia-induced Fos expression in neurons projecting to the pressor region in the rostral ventrolateral medulla. *Neuroscience* **80,** 1209-1224.

Hoch B, Bernhard M & Hinsch A. (1998). Different patterns of sighs in neonates and young infants. *Biology of the neonate* **74,** 16-21.

Hokfelt T, Fuxe K, Goldstein M & Johansson O. (1973). Evidence for adrenaline neurons in the rat brain. *Acta physiologica Scandinavica* **89,** 286-288.

Holtwick R, Gotthardt M, Skryabin B, Steinmetz M, Potthast R, Zetsche B, Hammer RE, Herz J & Kuhn M. (2002). Smooth muscle-selective deletion of guanylyl cyclase-A prevents the acute but not chronic effects of ANP on blood pressure. *Proceedings of the National Academy of Sciences of the United States of America* **99,** 7142-7147.

Horn EM & Waldrop TG. (1997). Oxygen-sensing neurons in the caudal hypothalamus and their role in cardiorespiratory control. *Respir Physiol* **110,** 219-228.

Horner RL. (2009). Emerging principles and neural substrates underlying tonic sleep-state-dependent influences on respiratory motor activity. *Philosophical transactions of the Royal Society of London Series B, Biological sciences* **364,** 2553-2564.

Horvat S, Beyer C & Arnold S. (2006). Effect of hypoxia on the transcription pattern of subunit isoforms and the kinetics of cytochrome c oxidase in cortical astrocytes and cerebellar neurons. *J Neurochem* **99,** 937-951.

Hume C. (2017). Thesis: Behavioural and Neural Responses to the Consumption of Palatable, High-Sugar Food in Rats. University of Edinburgh, University of Edinburgh.

Hume C, Sabatier N & Menzies J. (2017). High-Sugar, but Not High-Fat, Food Activates Supraoptic Nucleus Neurons in the Male Rat. *Endocrinology* **158,** 2200-2211.

Huttemann M, Kadenbach B & Grossman LI. (2001). Mammalian subunit IV isoforms of cytochrome c oxidase. *Gene* **267,** 111-123.

Ide S, Itoh M & Goto Y. (2005). Defect in normal developmental increase of the brain biogenic amine concentrations in the mecp2-null mouse. *Neuroscience letters* **386,** 14-17.

Ikematsu N, Dallas ML, Ross FA, Lewis RW, Rafferty JN, David JA, Suman R, Peers C, Hardie DG & Evans AM. (2011). Phosphorylation of the

voltage-gated potassium channel Kv2.1 by AMP-activated protein kinase regulates membrane excitability. *PNAS* **108,** 18132-18137.

Iseli TJ, Walter M, van Denderen BJ, Katsis F, Witters LA, Kemp BE, Michell BJ & Stapleton D. (2005). AMP-activated protein kinase beta subunit tethers alpha and gamma subunits via its C-terminal sequence (186-270). *The Journal of biological chemistry* **280,** 13395-13400.

Iturriaga R & Alcayaga J. (2004). Neurotransmission in the carotid body: transmitters and modulators between glomus cells and petrosal ganglion nerve terminals. *Brain research Brain research reviews* **47,** 46-53.

Ivy CM & Scott GR. (2017). Ventilatory acclimatization to hypoxia in mice: Methodological considerations. *Respir Physiol Neurobiol* **235,** 95-103.

Izumizaki M, Pokorski M & Homma I. (2004). Role of the carotid bodies in chemosensory ventilatory responses in the anesthetized mouse. *Journal of Applied Physiology* **97,** 1401-1407.

Jager S, Handschin C, St-Pierre J & Spiegelman BM. (2007). AMP-activated protein kinase (AMPK) action in skeletal muscle via direct phosphorylation of PGC-1alpha. *Proceedings of the National Academy of Sciences of the United States of America* **104,** 12017-12022.

Janczewski WA & Feldman JL. (2006). Distinct rhythm generators for inspiration and expiration in the juvenile rat. *J Physiol* **570,** 407-420.

Jenkin SE & Milsom WK. (2014). Expiration: breathing's other face. *Progress in brain research* **212,** 131-147.

Jia X & Burggren W. (1997). Developmental changes in chemoreceptive control of gill ventilation in larval bullfrogs (Rana catesbeiana). II. Sites of O2-sensitive chemoreceptors. *J Exp Biol* **200,** 2237-2248.

Johnstone LE, Fong TM & Leng G. (2006). Neuronal activation in the hypothalamus and brainstem during feeding in rats. *Cell Metab* **4,** 313-321.

Jorgensen SB, Nielsen JN, Birk JB, Olsen GS, Viollet B, Andreelli F, Schjerling P, Vaulont S, Hardie DG, Hansen BF, Richter EA & Wojtaszewski JF. (2004a). The alpha2-5'AMP-activated protein

kinase is a site 2 glycogen synthase kinase in skeletal muscle and is responsive to glucose loading. *Diabetes* **53,** 3074-3081.

Jorgensen SB, Viollet B, Andreelli F, Frosig C, Birk JB, Schjerling P, Vaulont S, Richter EA & Wojtaszewski JF. (2004b). Knockout of the alpha2 but not alpha1 5'-AMP-activated protein kinase isoform abolishes 5-aminoimidazole-4-carboxamide-1-beta-4-ribofuranosidebut not contraction-induced glucose uptake in skeletal muscle. *The Journal of biological chemistry* **279,** 1070-1079.

Joubert F, Loiseau C, Perrin-Terrin AS, Cayetanot F, Frugiere A, Voituron N & Bodineau L. (2016). Key Brainstem Structures Activated during Hypoxic Exposure in One-day-old Mice Highlight Characteristics for Modeling Breathing Network in Premature Infants. *Frontiers in physiology* **7,** 609.

Jouett NP, Smith ML, Watenpaugh DE, Siddiqui M, Ahmad M & Siddiqui F. (2017). Rapid-eye-movement sleep-predominant central sleep apnea relieved by positive airway pressure: a case report. *Physiol Rep* **5**.

Kahlin J, Mkrtchian S, Ebberyd A, Hammarstedt-Nordenvall L, Nordlander B, Yoshitake T, Kehr J, Prabhakar N, Poellinger L, Fagerlund MJ & Eriksson LI. (2014). The human carotid body releases acetylcholine, ATP and cytokines during hypoxia. *Exp Physiol* **99,** 1089-1098.

Karobath M. (1971). Catecholamines and the hydroxylation of tyrosine in synaptosomes isolated from rat brain. *Proceedings of the National Academy of Sciences of the United States of America* **68,** 2370-2373.

Katz DM, Dutschmann M, Ramirez JM & Hilaire G. (2009). Breathing disorders in Rett syndrome: progressive neurochemical dysfunction in the respiratory network after birth. *Respir Physiol Neurobiol* **168,** 101-108.

Kemp PJ, Searle GJ, Hartness ME, Lewis A, Miller P, Williams S, Wootton P, Adriaensen D & Peers C. (2003). Acute oxygen sensing in cellular models: relevance to the physiology of pulmonary neuroepithelial and carotid bodies. *Anat Rec A Discov Mol Cell Evol Biol* **270,** 41-50.

Kent. (2012). PhysioSuiteTM Monitor for Mice and Rats Owner's Manual, 2.10.05 edn, ed. Corporation KS, pp. 52. Torrington.

Kim D, Kang D, Martin EA, Kim I & Carroll JL. (2014). Effects of modulators of AMP-activated protein kinase on TASK-1/3 and intracellular

Ca(2+) concentration in rat carotid body glomus cells. *Respir Physiol Neurobiol* **195,** 19-26.

King TL, Heesch CM, Clark CG, Kline DD & Hasser EM. (2012). Hypoxia activates nucleus tractus solitarii neurons projecting to the paraventricular nucleus of the hypothalamus. *American Journal of Physiology - Regulatory, Integrative and Comparative Physiology* **302,** R1219-R1232.

King TL, Kline DD, Ruyle BC, Heesch CM & Hasser EM. (2013). Acute systemic hypoxia activates hypothalamic paraventricular nucleus-projecting catecholaminergic neurons in the caudal ventrolateral medulla. *American Journal of Physiology - Regulatory, Integrative and Comparative Physiology* **305,** R1112-R1123.

King TL, Ruyle BC, Kline DD, Heesch CM & Hasser EM. (2015). Catecholaminergic neurons projecting to the paraventricular nucleus of the hypothalamus are essential for cardiorespiratory adjustments to hypoxia. *Am J Physiol Regul Integr Comp Physiol***,** ajpregu.00540.02014.

Klein H, Garneau L, Trinh NT, Prive A, Dionne F, Goupil E, Thuringer D, Parent L, Brochiero E & Sauve R. (2009). Inhibition of the KCa3.1 channels by AMP-activated protein kinase in human airway epithelial cells. *American journal of physiology Cell physiology* **296,** C285-295.

Kline DD, King TL, Austgen JR, Heesch CM & Hasser EM. (2010). Sensory afferent and hypoxia-mediated activation of nucleus tractus solitarius neurons that project to the rostral ventrolateral medulla. *Neuroscience* **167,** 510-527.

Koay A, Rimmer KA, Mertens HD, Gooley PR & Stapleton D. (2007). Oligosaccharide recognition and binding to the carbohydrate binding module of AMP-activated protein kinase. *FEBS letters* **581,** 5055-5059.

Koide M, Moshkforoush A, Tsoukias NM, Hill-Eubanks DC, Wellman GC, Nelson MT & Dabertrand F. (2018). The yin and yang of KV channels in cerebral small vessel pathologies. *Microcirculation* **25**.

Koizumi H, Koshiya N, Chia JX, Cao F, Nugent J, Zhang R & Smith JC. (2013). Structural-functional properties of identified excitatory and inhibitory interneurons within pre-Botzinger complex respiratory microcircuits. *The Journal of neuroscience : the official journal of the Society for Neuroscience* **33,** 2994-3009.

Koizumi H & Smith JC. (2008). Persistent Na+ and K+-dominated leak currents contribute to respiratory rhythm generation in the pre-Botzinger complex in vitro. *The Journal of neuroscience : the official journal of the Society for Neuroscience* **28,** 1773-1785.

Koos BJ & Rajaee A. (2014). Fetal breathing movements and changes at birth. *Adv Exp Med Biol* **814,** 89-101.

Koshiya N & Guyenet PG. (1996). NTS neurons with carotid chemoreceptor inputs arborize in the rostral ventrolateral medulla. *Am J Physiol* **270,** R1273-1278.

Kramer JM, Nolan PC & Waldrop TG. (1999). In vitro responses of neurons in the periaqueductal gray to hypoxia and hypercapnia. *Brain research* **835,** 197-203.

Kubin L, Alheid GF, Zuperku EJ & McCrimmon DR. (2006). Central pathways of pulmonary and lower airway vagal afferents. *J Appl Physiol (1985)* **101,** 618-627.

Kulandavelu S, Balkan W & Hare JM. (2015). Regulation of oxygen delivery to the body via hypoxic vasodilation. *Proceedings of the National Academy of Sciences of the United States of America* **112,** 6254-6255.

Kumar NN, Velic A, Soliz J, Shi Y, Li K, Wang S, Weaver JL, Sen J, Abbott SBG, Lazarenko RM, Ludwig M-G, Perez-Reyes E, Mohebbi N, Bettoni C, Gassmann M, Suply T, Seuwen K, Guyenet PG, Wagner CA & Bayliss DA. (2015). Regulation of breathing by CO2 requires the proton-activated receptor GPR4 in retrotrapezoid nucleus neurons. *Science* **348,** 1255-1260.

Kumar P. (2007). Sensing hypoxia in the carotid body: from stimulus to response. *Essays in biochemistry* **43,** 43-60.

Kumar P & Prabhakar NR. (2012). Peripheral chemoreceptors: function and plasticity of the carotid body. *Compr Physiol* **2,** 141-219.

Lagercrantz H. (1996). Stress, arousal, and gene activation at birth. *Age* **3**.

Lagercrantz H & Bistoletti P. (1977). Catecholamine Release in the Newborn Infant at Birth. *Pediatr Res* **11,** 889-893.

Lahiri S, Maret K & Sherpa MG. (1983). Dependence of high altitude sleep apnea on ventilatory sensitivity to hypoxia. *Respir Physiol* **52,** 281-301.

Lahiri S, Mokashi A, Mulligan E & Nishino T. (1981). Comparison of aortic and carotid chemoreceptor responses to hypercapnia and hypoxia. *Journal of applied physiology: respiratory, environmental and exercise physiology* **51,** 55-61.

LaManna JC, Haxhiu MA, Kutina-Nelson KL, Pundik S, Erokwu B, Yeh ER, Lust WD & Cherniack NS. (1996). Decreased energy metabolism in brain stem during central respiratory depression in response to hypoxia. *J Appl Physiol (1985)* **81,** 1772-1777.

Lantier L, Fentz J, Mounier R, Leclerc J, Treebak JT, Pehmoller C, Sanz N, Sakakibara I, Saint-Amand E, Rimbaud S, Maire P, Marette A, Ventura-Clapier R, Ferry A, Wojtaszewski JF, Foretz M & Viollet B. (2014). AMPK controls exercise endurance, mitochondrial oxidative capacity, and skeletal muscle integrity. *FASEB J* **28,** 3211-3224.

Larnicol N, Wallois F, Berquin P, Gros F & Rose D. (1994). c-fos-like immunoreactivity in the cat's neuraxis following moderate hypoxia or hypercapnia. *Journal of physiology, Paris* **88,** 81-88.

Lauweryns JM & Cokelaere M. (1973). Hypoxia-sensitive neuro-epithelial bodies. Intrapulmonary secretory neuroreceptors, modulated by the CNS. *Z Zellforsch Mikrosk Anat* **145,** 521-540.

Lauweryns JM, Cokelaere M, Deleersynder M & Liebens M. (1977). Intrapulmonary neuro-epithelial bodies in newborn rabbits. Influence of hypoxia, hyperoxia, hypercapnia, nicotine, reserpine, L-DOPA and 5-HTP. *Cell and tissue research* **182,** 425-440.

Lauweryns JM, Cokelaere M, Lerut T & Theunynck P. (1978). Cross-circulation studies on the influence of hypoxia and hypoxaemia on neuro-epithelial bodies in young rabbits. *Cell and tissue research* **193,** 373-386.

Lauweryns JM, Van Lommel AT & Dom RJ. (1985). Innervation of rabbit intrapulmonary neuroepithelial bodies. Quantitative and qualitative ultrastructural study after vagotomy. *J Neurol Sci* **67,** 81-92.

Lavezzi AM & Matturri L. (2008). Functional neuroanatomy of the human pre-Bötzinger complex with particular reference to sudden unexplained perinatal and infant death. *Neuropathology* **28,** 10-16.

Leith DE. (1976). Comparative mammalian respiratory mechanics. *The Physiologist* **19,** 485-510.

Lemes EV, Colombari E & Zoccal DB. (2016). Generation of active expiration by serotoninergic mechanisms of the ventral medulla of rats. *J Appl Physiol (1985)* **121,** 1135-1144.

Lemes EV & Zoccal DB. (2016). Active expiration and sympathetic excitation during hypercapnia require glutamatergic neurotransmission in the retrotrapezoid nucleus. In *Experimental Biology*. FASEB, San Diego.

Lent R, Azevedo FA, Andrade-Moraes CH & Pinto AV. (2012). How many neurons do you have? Some dogmas of quantitative neuroscience under revision. *The European journal of neuroscience* **35,** 1-9.

Leonard EM, Salman S & Nurse CA. (2018). Sensory Processing and Integration at the Carotid Body Tripartite Synapse: Neurotransmitter Functions and Effects of Chronic Hypoxia. *Frontiers in physiology* **9,** 225.

Levitsky KL & López-Barneo J. (2009). Developmental change of T-type Ca2+ channel expression and its role in rat chromaffin cell responsiveness to acute hypoxia. *The Journal of Physiology* **587,** 1917-1929.

Li A, Emond L & Nattie E. (2008). Brainstem Catecholaminergic Neurons Modulate both Respiratory and Cardiovascular Function. In *Integration in Respiratory Control*, ed. Poulin MJ & Wilson RJA, pp. 371-376. Springer New York.

Li P, Janczewski WA, Yackle K, Kam K, Pagliardini S, Krasnow MA & Feldman JL. (2016). The peptidergic control circuit for sighing. *Nature* **530,** 293-297.

Lindeberg J, Usoskin D, Bengtsson H, Gustafsson A, Kylberg A, Söderström S & Ebendal T. (2004). Transgenic expression of Cre recombinase from the tyrosine hydroxylase locus. *Genesis* **40,** 67-73.

Lipton AJ, Johnson MA, Macdonald T, Lieberman MW, Gozal D & Gaston B. (2001). S-nitrosothiols signal the ventilatory response to hypoxia. *Nature* **413,** 171-174.

Lizcano JM, Goransson O, Toth R, Deak M, Morrice NA, Boudeau J, Hawley SA, Udd L, Makela TP, Hardie DG & Alessi DR. (2004). LKB1 is a master kinase that activates 13 kinases of the AMPK subfamily, including MARK/PAR-1. *EMBO J* **23,** 833-843.

Llewellyn-Smith IJ, Gnanamanickam GJ, Reimann F, Gribble FM & Trapp S. (2013). Preproglucagon (PPG) neurons innervate neurochemically identified autonomic neurons in the mouse brainstem. *Neuroscience* **229,** 130-143.

Lopez-Barneo J, Lopez-Lopez JR, Urena J & Gonzalez C. (1988). Chemotransduction in the carotid body: K+ current modulated by PO2 in type I chemoreceptor cells. *Science* **241,** 580-582.

López-Barneo J, Ortega-Sáenz P, Pardal R, Pascual A & Piruat JI. (2008). Carotid body oxygen sensing. *Eur Respir J* **32,** 1386-1398.

Lopez-Lopez J, Gonzalez C, Urena J & Lopez-Barneo J. (1989). Low pO2 selectively inhibits K channel activity in chemoreceptor cells of the mammalian carotid body. *The Journal of general physiology* **93,** 1001-1015.

Lopez-Lopez JR, De Luis DA & Gonzalez C. (1993). Properties of a transient K+ current in chemoreceptor cells of rabbit carotid body. *J Physiol* **460,** 15-32.

Low MJ. (2016). Neuroendocrinology. In *Williams Textbook of Endocrinology*, 13th edn, pp. 109-175. Elsevier.

MacMillan S & Evans AM. (2018). AMPK-alpha1 or AMPK-alpha2 Deletion in Smooth Muscles Does Not Affect the Hypoxic Ventilatory Response or Systemic Arterial Blood Pressure Regulation During Hypoxia. *Frontiers in physiology* **9,** 655.

Madias NE & Adrogué HJ. (2014). Respiratory Acidosis and Alkalosis. In *National Kidney Foundation's Primer on Kidney Diseases*, 4th edn, ed. Gipson DS, Perazella MA & Tonelli M, pp. 144-150. Elsevier Inc.

Mahmoud AD. (2014). Thesis: The loss of LKB1 and the AMP-activated protein kinase in catecholaminergic cells and the effect on the ventilatory response to hypoxia and hypercapnia, pp. 1-273. University of Edinburgh, University of Edinburgh.

Mahmoud AD, Lewis S, Juricic L, Foretz M, Viollet B, Marshall I & Evans AM. (2015). AMPK couples oxygen to energy supply at the whole-body level by delivering increased drive to breathe during hypoxia and thus protects against apnoea. In *Physiology 2015*. Proc. Physiol. Soc., Cardiff.

Mahmoud AD, Lewis S, Juricic L, Udoh UA, Hartmann S, Jansen MA, Ogunbayo OA, Puggioni P, Holmes AP, Kumar P, Navarro-Dorado J, Foretz M, Viollet B, Dutia MB, Marshall I & Evans AM. (2016). AMPK Deficiency Blocks the Hypoxic Ventilatory Response and Thus Precipitates Hypoventilation and Apnea. *Am J Respir Crit Care Med* **193,** 1032-1043.

Malheiros-Lima M, Takakura A & Moreira T. (2015). Selective inhibition of the adrenergic C1 neurons reduces the hypoxic ventilatory response in unanesthetized rats. *FASEB J* **29,** 652.624.

Malheiros-Lima MR, Takakura AC & Moreira TS. (2017). Depletion of rostral ventrolateral medullary catecholaminergic neurons impairs the hypoxic ventilatory response in conscious rats. *Neuroscience* **351,** 1-14.

Martin-Body RL. (1988). Brain transections demonstrate the central origin of hypoxic ventilatory depression in carotid body-denervated rats. *J Physiol* **407,** 41-52.

Martin-Body RL, Robson GJ & Sinclair JD. (1986). Restoration of hypoxic respiratory responses in the awake rat after carotid body denervation by sinus nerve section. *J Physiol* **380,** 61-73.

McBryde FD, Hart EC, Ramchandra R & Paton JF. (2016). Evaluating the carotid bodies and renal nerves as therapeutic targets for hypertension. *Autonomic neuroscience : basic & clinical*.

McGinnis WR, Audhya T & Edelson SM. (2013). Proposed toxic and hypoxic impairment of a brainstem locus in autism. *International journal of environmental research and public health* **10,** 6955-7000.

Mendelowitz D, Yang M, Andresen MC & Kunze DL. (1992). Localization and retention in vitro of fluorescently labeled aortic baroreceptor terminals on neurons from the nucleus tractus solitarius. *Brain research* **581,** 339-343.

Merlen G, Gentric G, Celton-Morizur S, Foretz M, Guidotti JE, Fauveau V, Leclerc J, Viollet B & Desdouets C. (2014). AMPKalpha1 controls

hepatocyte proliferation independently of energy balance by regulating Cyclin A2 expression. *Journal of hepatology* **60,** 152-159.

Mia S, Munoz C, Pakladok T, Siraskar G, Voelkl J, Alesutan I & Lang F. (2012). Downregulation of Kv1.5 K channels by the AMP-activated protein kinase. *Cellular physiology and biochemistry : international journal of experimental cellular physiology, biochemistry, and pharmacology* **30,** 1039-1050.

Mifflin SW. (1992). Arterial chemoreceptor input to nucleus tractus solitarius. *Am J Physiol* **263,** R368-375.

Mihaylova MM & Shaw RJ. (2011). The AMPK signalling pathway coordinates cell growth, autophagy and metabolism. *Nature cell biology* **13,** 1016-1023.

Miller MJ & Tenney SM. (1975). Hypoxia-induced tachypnea in carotid-deafferented cats. *Respir Physiol* **23,** 31-39.

Mills E. (1972). Spectrophotometric and fluorometric studies on the mechanism of chemoreception in the carotid body. *Federation proceedings* **31,** 1394-1398.

Mills E & Jobsis FF. (1970). Simultaneous measurement of cytochrome a3 reduction and chemoreceptor afferent activity in the carotid body. *Nature* **225,** 1147-1149.

Mills E & Jobsis FF. (1972). Mitochondrial respiratory chain of carotid body and chemoreceptor response to changes in oxygen tension. *Journal of neurophysiology* **35,** 405-428.

Milsom WK. (1990). Mechanoreceptor modulation of endogenous respiratory rhythms in vertebrates. *Am J Physiol* **259,** R898-910.

Milsom WK. (1991). Intermittent breathing in vertebrates. *Annual review of physiology* **53,** 87-105.

Milsom WK & Burleson ML. (2007). Peripheral arterial chemoreceptors and the evolution of the carotid body. *Respir Physiol Neurobiol* **157,** 4-11.

Minson J, Llewellyn-Smith I, Neville A, Somogyi P & Chalmers J. (1990). Quantitative analysis of spinally projecting adrenaline-synthesising neurons of C1, C2 and C3 groups in rat medulla oblongata. *Journal of the autonomic nervous system* **30,** 209-220.

Mochizuki-Oda N, Takeuchi Y, Matsumura K, Oosawa Y & Watanabe Y. (1997). Hypoxia-induced catecholamine release and intracellular Ca2+ increase via suppression of K+ channels in cultured rat adrenal chromaffin cells. *J Neurochem* **69,** 377-387.

Molkov YI, Rubin JE, Rybak IA & Smith JC. (2017). Computational models of the neural control of breathing. *Wiley Interdiscip Rev Syst Biol Med* **9**.

Molkov YI, Zoccal DB, Baekey DM, Abdala AP, Machado BH, Dick TE, Paton JF & Rybak IA. (2014). Physiological and pathophysiological interactions between the respiratory central pattern generator and the sympathetic nervous system. *Progress in brain research* **212,** 1-23.

Moraes DJ, Dias MB, Cavalcanti-Kwiatkoski R, Machado BH & Zoccal DB. (2012a). Contribution of the retrotrapezoid nucleus/parafacial respiratory region to the expiratory-sympathetic coupling in response to peripheral chemoreflex in rats. *Journal of neurophysiology* **108,** 882-890.

Moraes DJ, Zoccal DB & Machado BH. (2012b). Sympathoexcitation during chemoreflex active expiration is mediated by L-glutamate in the RVLM/Botzinger complex of rats. *Journal of neurophysiology* **108,** 610-623.

Moraes DJA, Bonagamba LGH, da Silva MP, Paton JFR & Machado BH. (2017). Role of ventral medullary catecholaminergic neurons for respiratory modulation of sympathetic outflow in rats. *Scientific reports* **7,** 16883.

Moral-Sanz J, Lewis SA, MacMillan S, Ross FA, Thomson A, Viollet B, Foretz M, Moran C, Hardie DG & Evans AM. (2018). The LKB1-AMPK-alpha1 signaling pathway triggers hypoxic pulmonary vasoconstriction downstream of mitochondria. *Science signaling* **11**.

Moral-Sanz J, Mahmoud AD, Ross FA, Eldstrom J, Fedida D, Hardie DG & Evans AM. (2016). AMP-activated protein kinase inhibits Kv 1.5 channel currents of pulmonary arterial myocytes in response to hypoxia and inhibition of mitochondrial oxidative phosphorylation. *J Physiol* **594,** 4901-4915.

Morgan JI, Cohen DR, Hempstead JL & Curran T. (1987). Mapping patterns of c-fos expression in the central nervous system after seizure. *Science* **237,** 192-197.

Mortola JP, Magnante D & Saetta M. (1985). Expiratory pattern of newborn mammals. *J Appl Physiol (1985)* **58,** 528-533.

Mortola JP & Maskrey M. (2011). Metabolism, temperature, and ventilation. *Compr Physiol* **1,** 1679-1709.

Mouradian GC, Forster HV & Hodges MR. (2012). Acute and chronic effects of carotid body denervation on ventilation and chemoreflexes in three rat strains. *The Journal of Physiology* **590,** 3335-3347.

Mulligan E, Lahiri S & Storey BT. (1981). Carotid body O2 chemoreception and mitochondrial oxidative phosphorylation. *Journal of applied physiology: respiratory, environmental and exercise physiology* **51,** 438-446.

Murali S & Nurse CA. (2016). Purinergic signalling mediates bidirectional crosstalk between chemoreceptor type I and glial-like type II cells of the rat carotid body. *J Physiol* **594,** 391-406.

Murali S, Zhang M & Nurse CA. (2015). Paracrine Signaling in Glial-Like Type II Cells of the Rat Carotid Body. *Adv Exp Med Biol* **860,** 41-47.

Murphy BA, Fakira KA, Song Z, Beuve A & Routh VH. (2009). AMP-activated protein kinase and nitric oxide regulate the glucose sensitivity of ventromedial hypothalamic glucose-inhibited neurons. *American journal of physiology Cell physiology* **297,** C750-758.

Nakamura A, Fukuda Y & Kuwaki T. (2003). Sleep apnea and effect of chemostimulation on breathing instability in mice. *J Appl Physiol (1985)* **94,** 525-532.

Nakamura A & Kuwaki T. (2003). Sleep apnea in mice: a useful animal model for study of SIDS? *Early human development* **75 Suppl,** S167-174.

Neff RA, Simmens SJ, Evans C & Mendelowitz D. (2004). Prenatal nicotine exposure alters central cardiorespiratory responses to hypoxia in rats: implications for sudden infant death syndrome. *The Journal of neuroscience : the official journal of the Society for Neuroscience* **24,** 9261-9268.

Neubauer JA, Melton JE & Edelman NH. (1990). Modulation of respiration during brain hypoxia. *J Appl Physiol (1985)* **68,** 441-451.

Neubauer JA & Sunderram J. (2004). Oxygen-sensing neurons in the central nervous system. *Journal of Applied Physiology* **96,** 367-374.

Niane LM, Joseph V & Bairam A. (2012). Systemic blockade of nicotinic and purinergic receptors inhibits ventilation and increases apnoea frequency in newborn rats. *Exp Physiol* **97,** 981-993.

Nicholas TE, Power JH & Barr HA. (1982). The pulmonary consequences of a deep breath. *Respir Physiol* **49,** 315-324.

Norris DO & Carr JA. (2013). The Mammalian Adrenal Glands: Cortical and Chromaffin Cells. In *Vertebrate Endocrinology*, 5th edn, pp. 261-290. Elsevier Inc.

Numao Y, Koshiya N, Gilbey MP & Spyer KM. (1987). Central respiratory drive-related activity in sympathetic nerves of the rat: the regional differences. *Neuroscience letters* **81,** 279-284.

Nunez-Abades PA, Morillo AM & Pasaro R. (1993). Brainstem connections of the rat ventral respiratory subgroups: afferent projections. *Journal of the autonomic nervous system* **42,** 99-118.

Nurse CA. (2010). Neurotransmitter and neuromodulatory mechanisms at peripheral arterial chemoreceptors. *Exp Physiol* **95,** 657-667.

Nurse CA. (2014). Synaptic and paracrine mechanisms at carotid body arterial chemoreceptors. *J Physiol* **592,** 3419-3426.

Nurse CA, Buttigieg J, Brown S & Holloway AC. (2009). Regulation of Oxygen Sensitivity in Adrenal Chromaffin Cells. *Annals of the New York Academy of Sciences* **1177,** 132-139.

Nurse CA & Piskuric NA. (2013). Signal processing at mammalian carotid body chemoreceptors. *Seminars in cell & developmental biology* **24,** 22-30.

Nurse CA, Salman S & Scott AL. (2018). Hypoxia-regulated catecholamine secretion in chromaffin cells. *Cell and tissue research* **372,** 433-441.

Nurse CA & Zhang M. (1999). Acetylcholine contributes to hypoxic chemotransmission in co-cultures of rat type 1 cells and petrosal neurons. *Respir Physiol* **115,** 189-199.

Ortega-Saenz P, Pardal R, Garcia-Fernandez M & Lopez-Barneo J. (2003). Rotenone selectively occludes sensitivity to hypoxia in rat carotid body glomus cells. *J Physiol* **548,** 789-800.

Osanai S, Buerk DG, Mokashi A, Chugh DK & Lahiri S. (1997). Cat carotid body chemosensory discharge (in vitro) is insensitive to charybdotoxin. *Brain research* **747,** 324-327.

Ostrowski TD, Ostrowski D, Hasser EM & Kline DD. (2014). Depressed GABA and glutamate synaptic signaling by 5-HT1A receptors in the nucleus tractus solitarii and their role in cardiorespiratory function. *Journal of neurophysiology* **111,** 2493-2504.

Otake K, Ruggiero DA & Nakamura Y. (1995). Adrenergic innervation of forebrain neurons that project to the paraventricular thalamic nucleus in the rat. *Brain research* **697,** 17-26.

Padbury J, Agata Y, Ludlow J, Ikegami M, Baylen B & Humme J. (1987). Effect of fetal adrenalectomy on catecholamine release and physiologic adaptation at birth in sheep. *Journal of Clinical Investigation* **80,** 1096.

Padbury JF, Roberman B, Oddie TH, Hobel CJ & Fisher DA. (1982). Fetal catecholamine release in response to labor and delivery. *Obstet Gynecol* **60,** 607-611.

Pagliardini S, Janczewski WA, Tan W, Dickson CT, Deisseroth K & Feldman JL. (2011). Active expiration induced by excitation of ventral medulla in adult anesthetized rats. *The Journal of neuroscience : the official journal of the Society for Neuroscience* **31,** 2895-2905.

Palmer LA, May WJ, deRonde K, Brown-Steinke K, Gaston B & Lewis SJ. (2013). Hypoxia-induced ventilatory responses in conscious mice: Gender differences in ventilatory roll-off and facilitation. *Respir Physiol Neurobiol* **185,** 497-505.

Pamenter ME & Powell FL. (2016). Time Domains of the Hypoxic Ventilatory Response and Their Molecular Basis. *Compr Physiol* **6,** 1345-1385.

Panayiotou C, Solaroli N & Karlsson A. (2014). The many isoforms of human adenylate kinases. *The international journal of biochemistry & cell biology* **49,** 75-83.

Pang T, Xiong B, Li JY, Qiu BY, Jin GZ, Shen JK & Li J. (2007). Conserved alpha-helix acts as autoinhibitory sequence in AMP-activated protein kinase alpha subunits. *The Journal of biological chemistry* **282,** 495-506.

Panneton WM, Anch AM, Panneton WM & Gan Q. (2014). Parasympathetic preganglionic cardiac motoneurons labeled after voluntary diving. *Frontiers in physiology* **5,** 8.

Panossian L & Daley J. (2013). Sleep-disordered breathing. *Continuum* **19,** 86-103.

Pascual O, Morin-Surun M-P, Barna B, Denavit-Saubié M, Pequignot J-M & Champagnat J. (2002). Progesterone reverses the neuronal responses to hypoxia in rat nucleus tractus solitarius in vitro. *The Journal of Physiology* **544,** 511-520.

Pattinson KT, Governo RJ, MacIntosh BJ, Russell EC, Corfield DR, Tracey I & Wise RG. (2009a). Opioids depress cortical centers responsible for the volitional control of respiration. *The Journal of neuroscience : the official journal of the Society for Neuroscience* **29,** 8177-8186.

Pattinson KT, Mitsis GD, Harvey AK, Jbabdi S, Dirckx S, Mayhew SD, Rogers R, Tracey I & Wise RG. (2009b). Determination of the human brainstem respiratory control network and its cortical connections in vivo using functional and structural imaging. *NeuroImage* **44,** 295-305.

Peers C. (1990). Hypoxic suppression of K+ currents in type I carotid body cells: selective effect on the Ca2(+)-activated K+ current. *Neuroscience letters* **119,** 253-256.

Peers C & Buckler KJ. (1995). Transduction of chemostimuli by the type I carotid body cell. *The Journal of membrane biology* **144,** 1-9.

Pehmoller C, Treebak JT, Birk JB, Chen S, Mackintosh C, Hardie DG, Richter EA & Wojtaszewski JF. (2009). Genetic disruption of AMPK signaling abolishes both contraction- and insulin-stimulated TBC1D1 phosphorylation and 14-3-3 binding in mouse skeletal muscle. *American journal of physiology Endocrinology and metabolism* **297,** E665-675.

Pena F & Ramirez JM. (2002). Endogenous activation of serotonin-2A receptors is required for respiratory rhythm generation in vitro. *The*

Journal of neuroscience : the official journal of the Society for Neuroscience **22,** 11055-11064.

Pena F & Ramirez JM. (2005). Hypoxia-induced changes in neuronal network properties. *Molecular neurobiology* **32,** 251-283.

Peng YJ, Nanduri J, Khan SA, Yuan G, Wang N, Kinsman B, Vaddi DR, Kumar GK, Garcia JA, Semenza GL & Prabhakar NR. (2011). Hypoxia-inducible factor 2alpha (HIF-2alpha) heterozygous-null mice exhibit exaggerated carotid body sensitivity to hypoxia, breathing instability, and hypertension. *Proceedings of the National Academy of Sciences of the United States of America* **108,** 3065-3070.

Peng YJ, Nanduri J, Raghuraman G, Souvannakitti D, Gadalla MM, Kumar GK, Snyder SH & Prabhakar NR. (2010). H2S mediates O2 sensing in the carotid body. *Proceedings of the National Academy of Sciences of the United States of America* **107,** 10719-10724.

Perez-Garcia MT, Colinas O, Miguel-Velado E, Moreno-Dominguez A & Lopez-Lopez JR. (2004). Characterization of the Kv channels of mouse carotid body chemoreceptor cells and their role in oxygen sensing. *J Physiol* **557,** 457-471.

Perez-Padilla R, West P & Kryger MH. (1983). Sighs during sleep in adult humans. *Sleep* **6,** 234-243.

Perrin-Terrin AS, Jeton F, Pichon A, Frugiere A, Richalet JP, Bodineau L & Voituron N. (2016). The c-FOS Protein Immunohistological Detection: A Useful Tool As a Marker of Central Pathways Involved in Specific Physiological Responses In Vivo and Ex Vivo. *Journal of visualized experiments : JoVE*.

Phillipson OT & Bohn MC. (1994). C1-3 adrenergic medullary neurones project to the paraventricular thalamic nucleus in the rat. *Neuroscience letters* **176,** 67-70.

Pilowsky PM, Abbott SB, Burke PG, Farnham MM, Hildreth CM, Kumar NN, Li Q, Lonergan T, McMullan S, Spirovski D & Goodchild AK. (2008). Metabotropic neurotransmission and integration of sympathetic nerve activity by the rostral ventrolateral medulla in the rat. *Clinical and experimental pharmacology & physiology* **35,** 508-511.

Pisanski A & Pagliardini S. (2018). The parafacial respiratory group and the control of active expiration. *Respir Physiol Neurobiol*.

Porteus C, Hedrick MS, Hicks JW, Wang T & Milsom WK. (2011). Time domains of the hypoxic ventilatory response in ectothermic vertebrates. *Journal of comparative physiology B, Biochemical, systemic, and environmental physiology* **181,** 311-333.

Prabhakar NR. (2000). Oxygen sensing by the carotid body chemoreceptors. *Journal of Applied Physiology* **88,** 2287-2295.

Prabhakar NR & Kumar GK. (2010). Mechanisms of sympathetic activation and blood pressure elevation by intermittent hypoxia. *Respir Physiol Neurobiol* **174,** 156-161.

Price CJ, Hoyda TD & Ferguson AV. (2008). The Area Postrema: A Brain Monitor and Integrator of Systemic Autonomic State. *Neuroscientist* **14,** 182-194.

Puljak L, Parameswara V, Dolovcak S, Waldrop SL, Emmett D, Esser V, Fitz JG & Kilic G. (2008). Evidence for AMPK-dependent regulation of exocytosis of lipoproteins in a model liver cell line. *Experimental cell research* **314,** 2100-2109.

Radulovacki M, Pavlovic S, Rakic A, Janelidze M, Shermulis L & Carley DW. (2001). Riluzole suppresses post-sigh, but not spontaneous apnoeas during sleep in rats. *The Journal of pharmacy and pharmacology* **53,** 1555-1559.

Radulovacki M, Trbovic SM & Carley DW. (1998). Serotonin 5-HT3-receptor antagonist GR 38032F suppresses sleep apneas in rats. *Sleep* **21,** 131-136.

Ramirez JM, Quellmalz UJ & Wilken B. (1997). Developmental changes in the hypoxic response of the hypoglossus respiratory motor output in vitro. *Journal of neurophysiology* **78,** 383-392.

Ramirez JM, Quellmalz UJ, Wilken B & Richter DW. (1998). The hypoxic response of neurones within the in vitro mammalian respiratory network. *J Physiol* **507 (Pt 2),** 571-582.

Ream MA, Chandra R, Peavey M, Ray AM, Roffler-Tarlov S, Kim HG, Wetsel WC, Rockman HA & Chikaraishi DM. (2008). High oxygen prevents fetal lethality due to lack of catecholamines. *Am J Physiol Regul Integr Comp Physiol* **295,** R942-953.

Rinaman L. (2010). Ascending projections from the caudal visceral nucleus of the solitary tract to brain regions involved in food intake and energy expenditure. *Brain research* **1350,** 18-34.

Rinaman L. (2011). Hindbrain noradrenergic A2 neurons: diverse roles in autonomic, endocrine, cognitive, and behavioral functions. *American Journal of Physiology - Regulatory, Integrative and Comparative Physiology* **300,** R222-R235.

Rogers RC, McDougal DH, Ritter S, Qualls-Creekmore E & Hermann GE. (2018). Response of catecholaminergic neurons in the mouse hindbrain to glucoprivic stimuli is astrocyte dependent. *Am J Physiol Regul Integr Comp Physiol* **315,** R153-R164.

Rosin DL, Chang DA & Guyenet PG. (2006). Afferent and efferent connections of the rat retrotrapezoid nucleus. *J Comp Neurol* **499,** 64-89.

Ross CA, Ruggiero DA, Park DH, Joh TH, Sved AF, Fernandez-Pardal J, Saavedra JM & Reis DJ. (1984). Tonic vasomotor control by the rostral ventrolateral medulla: effect of electrical or chemical stimulation of the area containing C1 adrenaline neurons on arterial pressure, heart rate, and plasma catecholamines and vasopressin. *The Journal of neuroscience : the official journal of the Society for Neuroscience* **4,** 474-494.

Ross CA, Ruggiero DA & Reis DJ. (1985). Projections from the nucleus tractus solitarii to the rostral ventrolateral medulla. *J Comp Neurol* **242,** 511-534.

Ross FA, MacKintosh C & Hardie DG. (2016). AMP-activated protein kinase: a cellular energy sensor that comes in 12 flavours. *The FEBS journal* **283,** 2987-3001.

Ross FA, Rafferty JN, Dallas ML, Ogunbayo O, Ikematsu N, McClafferty H, Tian L, Widmer H, Rowe ICM, Wyatt CN, Shipston MJ, Peers C, Hardie DG & Evans AM. (2011). Selective Expression in Carotid Body Type I Cells of a Single Splice Variant of the Large Conductance Calcium- and Voltage-activated Potassium Channel Confers Regulation by AMP-activated Protein Kinase. *Journal of Biological Chemistry* **286,** 11929-11936.

Roussin AT, D'Agostino AE, Fooden AM, Victor JD & Di Lorenzo PM. (2012). Taste coding in the nucleus of the solitary tract of the awake, freely licking rat. *The Journal of neuroscience : the official journal of the Society for Neuroscience* **32,** 10494-10506.

Roux J-C, Pequignot J-M, Dumas S, Pascual O, Ghilini G, Pequignot J, Mallet J & Denavit-Saubié M. (2000a). O2-sensing after carotid chemodenervation: hypoxic ventilatory responsiveness and upregulation of tyrosine hydroxylase mRNA in brainstem catecholaminergic cells. *European Journal of Neuroscience* **12,** 3181-3190.

Roux JC, Panayotis N, Dura E & Villard L. (2010). Progressive noradrenergic deficits in the locus coeruleus of Mecp2 deficient mice. *Journal of neuroscience research* **88,** 1500-1509.

Roux JC, Peyronnet J, Pascual O, Dalmaz Y & Pequignot JM. (2000b). Ventilatory and central neurochemical reorganisation of O2 chemoreflex after carotid sinus nerve transection in rat. *The Journal of Physiology* **522,** 493-501.

Roux JC & Villard L. (2010). Biogenic amines in Rett syndrome: the usual suspects. *Behavior genetics* **40,** 59-75.

Roy CS & Sherrington CS. (1890). On the Regulation of the Blood-supply of the Brain. *J Physiol* **11,** 85-158 117.

Ruderman NB, Carling D, Prentki M & Cacicedo JM. (2013). AMPK, insulin resistance, and the metabolic syndrome. *J Clin Invest* **123,** 2764-2772.

Ruppersberg JP, Stocker M, Pongs O, Heinemann SH, Frank R & Koenen M. (1991). Regulation of fast inactivation of cloned mammalian IK(A) channels by cysteine oxidation. *Nature* **352,** 711-714.

Sakamoto K, Goransson O, Hardie DG & Alessi DR. (2004). Activity of LKB1 and AMPK-related kinases in skeletal muscle: effects of contraction, phenformin, and AICAR. *American journal of physiology Endocrinology and metabolism* **287,** E310-317.

Sambucetti LC & Curran T. (1986). The Fos protein complex is associated with DNA in isolated nuclei and binds to DNA cellulose. *Science* **234,** 1417-1419.

Saponjic J, Radulovacki M & Carley DW. (2007). Monoaminergic system lesions increase post-sigh respiratory pattern disturbance during sleep in rats. *Physiology & behavior* **90,** 1-10.

Schneider H, Schaub CD, Chen CA, Andreoni KA, Schwartz AR, Smith PL, Robotham JL & O'Donnell CP. (2000). Neural and local effects of hypoxia on cardiovascular responses to obstructive apnea. *J Appl Physiol (1985)* **88,** 1093-1102.

Schneider H, Schubert KM, Blodow S, Kreutz CP, Erdogmus S, Wiedenmann M, Qiu J, Fey T, Ruth P, Lubomirov LT, Pfitzer G, Mederos YSM, Hardie DG, Gudermann T & Pohl U. (2015). AMPK Dilates Resistance Arteries via Activation of SERCA and BKCa Channels in Smooth Muscle. *Hypertension* **66,** 108-116.

Scott JW, Hawley SA, Green KA, Anis M, Stewart G, Scullion GA, Norman DG & Hardie DG. (2004). CBS domains form energy-sensing modules whose binding of adenosine ligands is disrupted by disease mutations. *J Clin Invest* **113,** 274-284.

Seeley RR. (2011). *Seeley's anatomy & physiology*. McGraw-Hill, New York.

Seidler FJ & Slotkin TA. (1985). Adrenomedullary function in the neonatal rat: responses to acute hypoxia. *The Journal of Physiology* **358,** 1-16.

Seidler FJ & Slotkin TA. (1986). Ontogeny of adrenomedullary responses to hypoxia and hypoglycemia: Role of splanchnic innervation. *Brain Research Bulletin* **16,** 11-14.

Shahbazian MD & Zoghbi HY. (2001). Molecular genetics of Rett syndrome and clinical spectrum of MECP2 mutations. *Current opinion in neurology* **14,** 171-176.

Shapiro RE & Miselis RR. (1985). The central neural connections of the area postrema of the rat. *J Comp Neurol* **234,** 344-364.

Sheng M, McFadden G & Greenberg ME. (1990). Membrane depolarization and calcium induce c-fos transcription via phosphorylation of transcription factor CREB. *Neuron* **4,** 571-582.

Shirahata M, Balbir A, Otsubo T & Fitzgerald RS. (2007). Role of acetylcholine in neurotransmission of the carotid body. *Respir Physiol Neurobiol* **157,** 93-105.

Shrestha PK, Tamrakar P, Ibrahim BA & Briski KP. (2014). Hindbrain medulla catecholamine cell group involvement in lactate-sensitive

hypoglycemia-associated patterns of hypothalamic norepinephrine and epinephrine activity. *Neuroscience* **278,** 20-30.

Sicard KM & Duong TQ. (2005). Effects of hypoxia, hyperoxia, and hypercapnia on baseline and stimulus-evoked BOLD, CBF, and CMRO2 in spontaneously breathing animals. *NeuroImage* **25,** 850-858.

Skeffington KL, Higgins JS, Mahmoud AD, Evans AM, Sferruzzi-Perri AN, Fowden AL, Yung HW, Burton GJ, Giussani DA & Moore LG. (2016). Hypoxia, AMPK activation and uterine artery vasoreactivity. *J Physiol* **594,** 1357-1369.

Slotkin TA & Seidler FJ. (1988). Adrenomedullary catecholamine release in the fetus and newborn: secretory mechanisms and their role in stress and survival. *Journal of developmental physiology* **10,** 1-16.

Smith CA, Engwall MJ, Dempsey JA & Bisgard GE. (1993). Effects of specific carotid body and brain hypoxia on respiratory muscle control in the awake goat. *J Physiol* **460,** 623-640.

Smith DW, Buller KM & Day TA. (1995). Role of ventrolateral medulla catecholamine cells in hypothalamic neuroendocrine cell responses to systemic hypoxia. *J Neurosci* **15,** 7979-7988.

Smith JC, Abdala AP, Koizumi H, Rybak IA & Paton JF. (2007). Spatial and functional architecture of the mammalian brain stem respiratory network: a hierarchy of three oscillatory mechanisms. *Journal of neurophysiology* **98,** 3370-3387.

Smith JC, Abdala APL, Borgmann A, Rybak IA & Paton JFR. (2013). Brainstem respiratory networks: building blocks and microcircuits. *Trends in Neurosciences* **36,** 152-162.

Smith PG & Mills E. (1980). Restoration of reflex ventilatory response to hypoxia after removal of carotid bodies in the cat. *Neuroscience* **5,** 573-580.

Soliz J, Soulage C, Borter E, van Patot MT & Gassmann M. (2008). Ventilatory responses to acute and chronic hypoxia are altered in female but not male Paskin-deficient mice. *Am J Physiol Regul Integr Comp Physiol* **295,** R649-658.

Souza G, Kanbar R, Stornetta DS, Abbott SBG, Stornetta RL & Guyenet PG. (2018). Breathing regulation and blood gas homeostasis after near complete lesions of the retrotrapezoid nucleus in adult rats. *J Physiol* **596,** 2521-2545.

Spyer KM & Gourine AV. (2009). Chemosensory pathways in the brainstem controlling cardiorespiratory activity. *Philosophical transactions of the Royal Society of London Series B, Biological sciences* **364,** 2603-2610.

St-John WM, Stornetta RL, Guyenet PG & Paton JF. (2009). Location and properties of respiratory neurones with putative intrinsic bursting properties in the rat in situ. *J Physiol* **587,** 3175-3188.

Stapleton D, Mitchelhill KI, Gao G, Widmer J, Michell BJ, Teh T, House CM, Fernandez CS, Cox T, Witters LA & Kemp BE. (1996). Mammalian AMP-activated protein kinase subfamily. *The Journal of biological chemistry* **271,** 611-614.

Steffen A, Hagenah J, Wollenberg B & Bruggemann N. (2010). A case of central sleep apnea strictly dependent upon REM-sleep. *Journal of neurology* **257,** 143-145.

Stettner GM, Huppke P, Brendel C, Richter DW, Gartner J & Dutschmann M. (2007). Breathing dysfunctions associated with impaired control of postinspiratory activity in Mecp2-/y knockout mice. *J Physiol* **579,** 863-876.

Stettner GM, Zanella S, Huppke P, Gartner J, Hilaire G & Dutschmann M. (2008). Spontaneous central apneas occur in the C57BL/6J mouse strain. *Respir Physiol Neurobiol* **160,** 21-27.

Stornetta RL, Akey PJ & Guyenet PG. (1999). Location and electrophysiological characterization of rostral medullary adrenergic neurons that contain neuropeptide Y mRNA in rat medulla. *J Comp Neurol* **415,** 482-500.

Stornetta RL, Moreira TS, Takakura AC, Kang BJ, Chang DA, West GH, Brunet JF, Mulkey DK, Bayliss DA & Guyenet PG. (2006). Expression of Phox2b by brainstem neurons involved in chemosensory integration in the adult rat. *The Journal of neuroscience : the official journal of the Society for Neuroscience* **26,** 10305-10314.

Stornetta RL, Sevigny CP & Guyenet PG. (2002). Vesicular glutamate transporter DNPI/VGLUT2 mRNA is present in C1 and several other

groups of brainstem catecholaminergic neurons. *J Comp Neurol* **444,** 191-206.

Sun MK & Reis DJ. (1993). Differential responses of barosensitive neurons of rostral ventrolateral medulla to hypoxia in rats. *Brain research* **609,** 333-337.

Sun MK & Reis DJ. (1994a). Central neural mechanisms mediating excitation of sympathetic neurons by hypoxia. *Progress in neurobiology* **44,** 197-219.

Sun MK & Reis DJ. (1994b). Hypoxia selectively excites vasomotor neurons of rostral ventrolateral medulla in rats. *Am J Physiol* **266,** R245-256.

Sunday Udoh U-A. (2015). Effects of AMPK deletion on the response to hypoxia. In *Centre for Integrative Physiology*, pp. 156. University of Edinburgh, University of Edinburgh.

Sung MM, Zordoky BN, Bujak AL, Lally JS, Fung D, Young ME, Horman S, Miller EJ, Light PE, Kemp BE, Steinberg GR & Dyck JR. (2015). AMPK deficiency in cardiac muscle results in dilated cardiomyopathy in the absence of changes in energy metabolism. *Cardiovasc Res* **107,** 235-245.

Tankersley CG, Elston RC & Schnell AH. (2000). Genetic determinants of acute hypoxic ventilation: patterns of inheritance in mice. *J Appl Physiol (1985)* **88,** 2310-2318.

Tankersley CG, Fitzgerald RS & Kleeberger SR. (1994). Differential control of ventilation among inbred strains of mice. *Am J Physiol* **267,** R1371-1377.

Telgkamp P & Ramirez JM. (1999). Differential responses of respiratory nuclei to anoxia in rhythmic brain stem slices of mice. *Journal of neurophysiology* **82,** 2163-2170.

Tello D, Balsa E, Acosta-Iborra B, Fuertes-Yebra E, Elorza A, Ordonez A, Corral-Escariz M, Soro I, Lopez-Bernardo E, Perales-Clemente E, Martinez-Ruiz A, Enriquez JA, Aragones J, Cadenas S & Landazuri MO. (2011). Induction of the mitochondrial NDUFA4L2 protein by HIF-1alpha decreases oxygen consumption by inhibiting Complex I activity. *Cell Metab* **14,** 768-779.

Teppema LJ & Dahan A. (2010). The ventilatory response to hypoxia in mammals: mechanisms, measurement, and analysis. *Physiol Rev* **90,** 675-754.

Teppema LJ, Veening JG, Kranenburg A, Dahan A, Berkenbosch A & Olievier C. (1997). Expression of c-fos in the rat brainstem after exposure to hypoxia and to normoxic and hyperoxic hypercapnia. *J Comp Neurol* **388,** 169-190.

Thoby-Brisson M, Karlen M, Wu N, Charnay P, Champagnat J & Fortin G. (2009). Genetic identification of an embryonic parafacial oscillator coupling to the preBotzinger complex. *Nat Neurosci* **12,** 1028-1035.

Thoby-Brisson M & Ramirez JM. (2000). Role of inspiratory pacemaker neurons in mediating the hypoxic response of the respiratory network in vitro. *The Journal of neuroscience : the official journal of the Society for Neuroscience* **20,** 5858-5866.

Thompson R, Farragher S, Nurse C & Cutz E. (2002). Developmental regulation of O2 sensing in neonatal adrenal chromaffin cells from wild-type and NADPH-oxidase-deficient mice. *Pflügers Archiv European Journal of Physiology* **444,** 539-548.

Thompson RJ, Jackson A & Nurse CA. (1997). Developmental loss of hypoxic chemosensitivity in rat adrenomedullary chromaffin cells. *The Journal of Physiology* **498,** 503-510.

Thornton C, Snowden MA & Carling D. (1998). Identification of a novel AMP-activated protein kinase beta subunit isoform that is highly expressed in skeletal muscle. *The Journal of biological chemistry* **273,** 12443-12450.

Timmers HJLM, Wieling W, Karemaker JM & Lenders JWM. (2003). Denervation of carotid baro- and chemoreceptors in humans. *The Journal of Physiology* **553,** 3-11.

Torres-Torrelo H, Ortega-Saenz P, Macias D, Omura M, Zhou T, Matsunami H, Johnson RS, Mombaerts P & Lopez-Barneo J. (2018). The role of Olfr78 in the breathing circuit of mice. *Nature* **561,** E33-E40.

Tryba AK, Pena F, Lieske SP, Viemari JC, Thoby-Brisson M & Ramirez JM. (2008). Differential modulation of neural network and pacemaker activity underlying eupnea and sigh-breathing activities. *Journal of neurophysiology* **99,** 2114-2125.

Tse A, Yan L, Lee AK & Tse FW. (2012). Autocrine and paracrine actions of ATP in rat carotid body. *Canadian journal of physiology and pharmacology* **90,** 705-711.

Turrens JF. (2003). Mitochondrial formation of reactive oxygen species. *J Physiol* **552,** 335-344.

van der Kooy D & Koda LY. (1983). Organization of the projections of a circumventricular organ: the area postrema in the rat. *J Comp Neurol* **219,** 328-338.

Varas R, Wyatt CN & Buckler KJ. (2007). Modulation of TASK-like background potassium channels in rat arterial chemoreceptor cells by intracellular ATP and other nucleotides. *J Physiol* **583,** 521-536.

Venkatraman A, Edlow BL & Immordino-Yang MH. (2017). The Brainstem in Emotion: A Review. *Frontiers in neuroanatomy* **11,** 15.

Viemari J-C, Roux J-C, Tryba AK, Saywell V, Burnet H, Peña F, Zanella S, Bévengut M, Barthelemy-Requin M, Herzing LBK, Moncla A, Mancini J, Ramirez J-M, Villard L & Hilaire G. (2005). Mecp2 Deficiency Disrupts Norepinephrine and Respiratory Systems in Mice. *J Neurosci* **25,** 11521-11530.

Viemari JC. (2008). Noradrenergic modulation of the respiratory neural network. *Respir Physiol Neurobiol* **164,** 123-130.

Viemari JC, Garcia AJ, 3rd, Doi A, Elsen G & Ramirez JM. (2013). beta-Noradrenergic receptor activation specifically modulates the generation of sighs in vivo and in vitro. *Frontiers in neural circuits* **7,** 179.

Viemari JC, Garcia AJ, 3rd, Doi A & Ramirez JM. (2011). Activation of alpha-2 noradrenergic receptors is critical for the generation of fictive eupnea and fictive gasping inspiratory activities in mammals in vitro. *The European journal of neuroscience* **33,** 2228-2237.

Viemari JC & Ramirez JM. (2006). Norepinephrine differentially modulates different types of respiratory pacemaker and nonpacemaker neurons. *Journal of neurophysiology* **95,** 2070-2082.

Viollet B, Andreelli F, Jorgensen SB, Perrin C, Geloen A, Flamez D, Mu J, Lenzner C, Baud O, Bennoun M, Gomas E, Nicolas G, Wojtaszewski

JF, Kahn A, Carling D, Schuit FC, Birnbaum MJ, Richter EA, Burcelin R & Vaulont S. (2003). The AMP-activated protein kinase alpha2 catalytic subunit controls whole-body insulin sensitivity. *J Clin Invest* **111,** 91-98.

Voituron N, Zanella S, Menuet C, Dutschmann M & Hilaire G. (2009). Early breathing defects after moderate hypoxia or hypercapnia in a mouse model of Rett syndrome. *Respir Physiol Neurobiol* **168,** 109-118.

von Euler C. (1983). On the central pattern generator for the basic breathing rhythmicity. *Journal of applied physiology: respiratory, environmental and exercise physiology* **55,** 1647-1659.

von Euler US & Liljestrand G. (1946). Observations on the Pulmonary Arterial Blood Pressure in the Cat. *Acta physiologica Scandinavica* **12,** 301-320.

Wakai J, Takamura D, Morinaga R, Nakamuta N & Yamamoto Y. (2015). Differences in respiratory changes and Fos expression in the ventrolateral medulla of rats exposed to hypoxia, hypercapnia, and hypercapnic hypoxia. *Respir Physiol Neurobiol* **215,** 64-72.

Wang J, Zhang C, Li N, Su L & Wang G. (2008). Expression of TASK-1 in brainstem and the occurrence of central sleep apnea in rats. *Respir Physiol Neurobiol* **161,** 23-28.

Wang X, Guo R & Zhao W. (2015). Distribution of Fos-Like Immunoreactivity, Catecholaminergic and Serotoninergic Neurons Activated by the Laryngeal Chemoreflex in the Medulla Oblongata of Rats. *PLoS One* **10,** e0130822.

Ward NL, Moore E, Noon K, Spassil N, Keenan E, Ivanco TL & LaManna JC. (2007). Cerebral angiogenic factors, angiogenesis, and physiological response to chronic hypoxia differ among four commonly used mouse strains. *J Appl Physiol (1985)* **102,** 1927-1935.

Wasicko MJ, Sterni LM, Bamford OS, Montrose MH & Carroll JL. (1999). Resetting and postnatal maturation of oxygen chemosensitivity in rat carotid chemoreceptor cells. *J Physiol* **514 (Pt 2),** 493-503.

Watson C, Paxinos G & Puelles L. (2012). *The mouse nervous system*. Elsevier Academic Press, Amsterdam ; Boston.

Weese-Mayer DE, Berry-Kravis EM & Marazita ML. (2005). In pursuit (and discovery) of a genetic basis for congenital central hypoventilation syndrome. *Respir Physiol Neurobiol* **149,** 73-82.

Weese-Mayer DE, Lieske SP, Boothby CM, Kenny AS, Bennett HL, Silvestri JM & Ramirez JM. (2006). Autonomic nervous system dysregulation: breathing and heart rate perturbation during wakefulness in young girls with Rett syndrome. *Pediatr Res* **60,** 443-449.

Willette RN, Barcas PP, Krieger AJ & Sapru HN. (1983). Vasopressor and depressor areas in the rat medulla. Identification by microinjection of L-glutamate. *Neuropharmacology* **22,** 1071-1079.

Wilson DF, Mokashi A, Chugh D, Vinogradov S, Osanai S & Lahiri S. (1994). The primary oxygen sensor of the cat carotid body is cytochrome a3 of the mitochondrial respiratory chain. *FEBS letters* **351,** 370-374.

Wilson RJ & Teppema LJ. (2016). Integration of Central and Peripheral Respiratory Chemoreflexes. *Compr Physiol* **6,** 1005-1041.

Woods A, Dickerson K, Heath R, Hong SP, Momcilovic M, Johnstone SR, Carlson M & Carling D. (2005). Ca2+/calmodulin-dependent protein kinase kinase-beta acts upstream of AMP-activated protein kinase in mammalian cells. *Cell Metab* **2,** 21-33.

Woods A, Johnstone SR, Dickerson K, Leiper FC, Fryer LG, Neumann D, Schlattner U, Wallimann T, Carlson M & Carling D. (2003). LKB1 is the upstream kinase in the AMP-activated protein kinase cascade. *Current biology : CB* **13,** 2004-2008.

Woods A, Salt I, Scott J, Hardie DG & Carling D. (1996). The alpha1 and alpha2 isoforms of the AMP-activated protein kinase have similar activities in rat liver but exhibit differences in substrate specificity in vitro. *FEBS letters* **397,** 347-351.

Wu Y, Jiji LM, Lemons DE & Weinbaum S. (1995). A non-uniform three-dimensional perfusion model of rat tail heat transfer. *Physics in medicine and biology* **40,** 789-806.

Wu Y, Song P, Xu J, Zhang M & Zou M-H. (2007). Activation of Protein Phosphatase 2A by Palmitate Inhibits AMP-activated Protein Kinase. *Journal of Biological Chemistry* **282,** 9777-9788.

Wyatt CN & Buckler KJ. (2004). The effect of mitochondrial inhibitors on membrane currents in isolated neonatal rat carotid body type I cells. *J Physiol* **556,** 175-191.

Wyatt CN, Mustard KJ, Pearson SA, Dallas ML, Atkinson L, Kumar P, Peers C, Hardie DG & Evans AM. (2007). AMP-activated Protein Kinase Mediates Carotid Body Excitation by Hypoxia. *Journal of Biological Chemistry* **282,** 8092-8098.

Xiao B, Heath R, Saiu P, Leiper FC, Leone P, Jing C, Walker PA, Haire L, Eccleston JF, Davis CT, Martin SR, Carling D & Gamblin SJ. (2007). Structural basis for AMP binding to mammalian AMP-activated protein kinase. *Nature* **449,** 496-500.

Xiao B, Sanders MJ, Carmena D, Bright NJ, Haire LF, Underwood E, Patel BR, Heath RB, Walker PA, Hallen S, Giordanetto F, Martin SR, Carling D & Gamblin SJ. (2013). Structural basis of AMPK regulation by small molecule activators. *Nat Commun* **4,** 3017.

Xiao B, Sanders MJ, Underwood E, Heath R, Mayer FV, Carmena D, Jing C, Walker PA, Eccleston JF, Haire LF, Saiu P, Howell SA, Aasland R, Martin SR, Carling D & Gamblin SJ. (2011). Structure of mammalian AMPK and its regulation by ADP. *Nature* **472,** 230-233.

Xie A, Skatrud JB & Dempsey JA. (2001). Effect of hypoxia on the hypopnoeic and apnoeic threshold for CO(2) in sleeping humans. *J Physiol* **535,** 269-278.

Xu F, Gu QH, Zhou T & Lee LY. (2003). Acute hypoxia prolongs the apnea induced by right atrial injection of capsaicin. *J Appl Physiol (1985)* **94,** 1446-1454.

Xu F, Xu J, Tse FW & Tse A. (2006). Adenosine stimulates depolarization and rise in cytoplasmic [Ca2+] in type I cells of rat carotid bodies. *American journal of physiology Cell physiology* **290,** C1592-1598.

Yamaguchi S, Lande B, Kitajima T, Hori Y & Shirahata M. (2004). Patch clamp study of mouse glomus cells using a whole carotid body. *Neuroscience letters* **357,** 155-157.

Yamauchi M, Ocak H, Dostal J, Jacono FJ, Loparo KA & Strohl KP. (2008). Post-sigh breathing behavior and spontaneous pauses in the C57BL/6J (B6) mouse. *Respir Physiol Neurobiol* **162,** 117-125.

Younes M, Vaillancourt P & Milic-Emili J. (1974). Interaction between chemical factors and duration of apnea following lung inflation. *J Appl Physiol* **36,** 190-201.

Youngson C, Nurse C, Yeger H & Cutz E. (1993). Oxygen sensing in airway chemoreceptors. *Nature* **365,** 153-155.

Yuan G, Vasavda C, Peng YJ, Makarenko VV, Raghuraman G, Nanduri J, Gadalla MM, Semenza GL, Kumar GK, Snyder SH & Prabhakar NR. (2015). Protein kinase G-regulated production of H2S governs oxygen sensing. *Science signaling* **8,** ra37.

Yuceege M, Firat H, Kuyucu M & Ardic S. (2013). Rapid eye movement dependent central apnea with periodic leg movements. *Annals of Indian Academy of Neurology* **16,** 154-156.

Zanella S, Doi A, Garcia AJ, 3rd, Elsen F, Kirsch S, Wei AD & Ramirez JM. (2014). When norepinephrine becomes a driver of breathing irregularities: how intermittent hypoxia fundamentally alters the modulatory response of the respiratory network. *The Journal of neuroscience : the official journal of the Society for Neuroscience* **34,** 36-50.

Zanella S, Roux JC, Viemari JC & Hilaire G. (2006). Possible modulation of the mouse respiratory rhythm generator by A1/C1 neurones. *Respir Physiol Neurobiol* **153,** 126-138.

Zarrinpashneh E, Beauloye C, Ginion A, Pouleur AC, Havaux X, Hue L, Viollet B, Vanoverschelde JL & Bertrand L. (2008). AMPKalpha2 counteracts the development of cardiac hypertrophy induced by isoproterenol. *Biochemical and biophysical research communications* **376,** 677-681.

Zarrinpashneh E, Carjaval K, Beauloye C, Ginion A, Mateo P, Pouleur AC, Horman S, Vaulont S, Hoerter J, Viollet B, Hue L, Vanoverschelde JL & Bertrand L. (2006). Role of the alpha2-isoform of AMP-activated protein kinase in the metabolic response of the heart to no-flow ischemia. *American journal of physiology Heart and circulatory physiology* **291,** H2875-2883.

Zhang J, Dong J, Martin M, He M, Gongol B, Marin TL, Chen L, Shi X, Yin Y, Shang F, Wu Y, Huang HY, Zhang J, Zhang Y, Kang J, Moya EA, Huang HD, Powell FL, Chen Z, Thistlethwaite PA, Yuan ZY & Shyy JY. (2018). AMP-activated Protein Kinase Phosphorylation of Angiotensin-Converting Enzyme 2 in Endothelium Mitigates Pulmonary Hypertension. *Am J Respir Crit Care Med* **198,** 509-520.

Zhang M, Zhong H, Vollmer C & Nurse CA. (2000). Co-release of ATP and ACh mediates hypoxic signalling at rat carotid body chemoreceptors. *J Physiol* **525 Pt 1,** 143-158.

Zhou T, Chien MS, Kaleem S & Matsunami H. (2016). Single cell transcriptome analysis of mouse carotid body glomus cells. *J Physiol* **594,** 4225-4251.

Zoccal DB, Furuya WI, Bassi M, Colombari DS & Colombari E. (2014). The nucleus of the solitary tract and the coordination of respiratory and sympathetic activities. *Frontiers in physiology* **5,** 238.

Publications

Oral communications

Hartmann S & Evans AM. (2016). Is AMPK required for acute acclimation to hypoxia? In *Proc Physiol Soc*, pp. 59.

Research publications

MacMillan S & Evans AM. (2018). AMPK-alpha1 or AMPK-alpha2 Deletion in Smooth Muscles Does Not Affect the Hypoxic Ventilatory Response or Systemic Arterial Blood Pressure Regulation During Hypoxia. *Frontiers in Physiology* 9, 655.

Moral-Sanz J, Lewis SA, **MacMillan S**, Ross FA, Thomson A, Viollet B, Foretz M, Moran C, Hardie DG & Evans AM. (2018). The LKB1-AMPK-alpha1 signaling pathway triggers hypoxic pulmonary vasoconstriction downstream of mitochondria. *Science Signaling* 11.

Mahmoud AD, Lewis S, Juricic L, Udoh UA, **Hartmann S**, Jansen MA, Ogunbayo OA, Puggioni P, Holmes AP, Kumar P, Navarro-Dorado J, Foretz M, Viollet B, Dutia MB, Marshall I & Evans AM. (2016). AMPK Deficiency Blocks the Hypoxic Ventilatory Response and Thus Precipitates Hypoventilation and Apnea. *Am J Respir Crit Care Med* 193, 1032-1043.

Review articles

Evans AM, Mahmoud AD, Moral-Sanz J & **Hartmann S**. (2016). The emerging role of AMPK in the regulation of breathing and oxygen supply. The Biochemical Journal 473, 2561-2572.